A.I.Ch.E. JOURNAL

CHEMICAL ENGINEERING RESEARCH AND DEVELOPMENT / SEPTEMBER, 1960

THE UNIVERSITY OF MICHIGAN

OCT - 5 1960

ENGINEERING LIBRARY

CONTENTS

Limiting Velocities, Holdup, and Pressure Drop at Flooding in Packed Extraction Columns	Gopal Venkataraman and G. S. Laddha
Radiological Study of Liquid Holdup and Flow Distribution in Packed Gas-Absorption Columns	C. S. Hwa and R. B. Beckmann
Ion Exchange Kinetics for Systems of Linear Equilibrium Relationships	Chi Tien and George Thodos
The Dual Nature of a Catalytic Reaction: The Dehydrogenation of sec-Butyl Alcohol to Methyl Ethyl Ketone at Elevated Pressures	Lawrence H. Thaller and George Thodos
A Study of Sieve-Tray Efficiencies	J. M. Hay and A. I. Johnson
Comparison of the Specific Resistances of Cakes Formed in Filters and Centrifuges	V. V. Valleroy and J. O. Maloney
Pressure Drop and Liquid Holdup in Concurrent Gas Absorption	W. S. Dodds, L. F. Stutzman, B. J. Sollami, and R. J. McCarter
Extractive Reaction: Batch and Continuous-Flow Chemical Reaction Systems Dilute Case	Edgar L. Piret, W. H. Penney, and P. J. Trambouze
Longitudinal Mixing in Fluidization	E. J. Cairns and J. M. Prausnitz
Mechanism of Drying Thick Porous Bodies During the Falling-Rate Period: III. Analytical Treatment of Macroporous Systems	A. H. Nissan, H. H. George, Jr., and T. V. Bolles
Mass Transfer in Laminar-Boundary-Layer Flows with Finite Interfacial Velocities	Andreas Acrivos
Liquid Viscosities Above the Normal Boiling Point for Methane, Ethane, Propane, and *n*-Butane	G. W. Swift, John Lohrenz, and Fred Kurata
Suspension of Slurries by Mechanical Mixers	Joel Weisman and L. E. Efferding
The Viscosity of Liquid Mixers	R. A. McAllister
Flow Patterns and Mixing Rates in Agitated Vessels	K. W. Norwood and A. B. Metzner
Liquid, Gas, and Dense-Fluid Viscosity of Propane	Kenneth E. Starling, Bert E. Eakin, and Rex T. Ellington
Effect of Radial Temperature Variation on Axial Mixing in Pipes	R. D. Hawthorn
General Short-cut Equation for Equilibrium Stage Processes	Buford D. Smith and W. K. Brinkley
Rigorous Solution of Multicomponent, Multistage Extraction Problems	Buford D. Smith and W. K. Brinkley
Effect of Uniformity of Fluidization On Catalytic Cracking of Cumene	Albert Gomezplata and W. W. Shuster
A Boundary-Layer Model of Fluid-Particle Mass Transfer in Fixed Beds	James J. Carberry
Entrainment and Pressure Drop in Concurrent Gas-Liquid Flow: I. Air-Water in Horizontal Flow	Moye Wicks, III, and A. E. Dukler
Performance of Packed Columns: VI. Mass Transfer Rates for Dehumidification at High Solute Concentrations	H. L. Shulman and R. G. Robinson
Transient Response Study of Gas Flowing Through Irrigated Packing	Francesco DeMaria and Robert R. White
Mass Transfer in Semifluidized Beds For Solid-Liquid System	Liang-Tseng Fan, Yung-Chia Yang, and Chin-Yung Wen
On the Steady State Activity Levels in a Reactor-Regenerator System	E. E. Petersen
The Kinetics of the Absorption of Phosgene into Water and Aqueous Solutions	W. H. Manogue and R. L. Pigford
Detonation Characteristics of Hydrogen-Oxygen Mixtures at High Initial Pressures	Roy L. Gealer and Stuart W. Churchill
A Scintillation Method for Determining Liquid-Liquid Interfacial Areas	George J. Mitsis, Richard R. Plebuch, and Kenneth F. Gordon
Heat Transfer and Kinetics in a Catalyst Bed of Rectangular Cross Section: Air Oxidation of Nitric Oxide with Silica Gel	J. H. Jaffer, Jr., and Harding Bliss
Multicomponent Diffusion Problems	Hsien-Wen Hsu and R. Byron Bird

STAND and be counted

for the SYMPOSIUM SERIES

A STANDING ORDER

ensures your not missing a needed book and saves you 10% on each book

Each book in the Series is a collection of papers in a specific field of chemical engineering. Some papers have been presented at A.I.Ch.E. symposia during national meetings; some have been submitted directly for publication. All are reviewed by experts in the particular fields and revised before publication.

During 1959 eight books were published—on heat transfer; nuclear engineering; computer techniques, chemical engineering education; reaction kinetics; adsorption, dialysis, and ion exchange.

At least six more are planned for 1960—on rockets and missiles, computer techniques, nuclear engineering, and heat transfer.

This Series is produced in an attractive but economical format—8½ x 11 inch volumes, paper covered, averaging 150 to 200 pages. It is priced as close to cost as possible for Members and about one-third higher for others.

MONOGRAPH & SYMPOSIUM SERIES

29-S. Heat Transfer—Chicago: The A.I.Ch.E.-sponsored papers presented at the Joint Heat Transfer Conference in 1958. $4.00 to members, $5.00 to nonmembers.

28-S. Nuclear Engineering, Part VIII: The A.I.Ch.E.-sponsored papers presented at the 1958 Nuclear Congress, together with additional papers from A.I.Ch.E. Symposia. $3.50 to members, $4.50 to nonmembers.

26-S. Chemical Engineering Education—Academic and Industrial: The new philosophies behind both graduate and undergraduate curricula, together with descriptions of successful programs held in industry. $3.00 to members, $4.00 to nonmembers.

25-S. Reaction Kinetics and Unit Operations: 23 surveys of the basic fields in chemical engineering, covering the most recent developments and future trends. $3.50 to members, $4.50 to nonmembers.

24-S. Adsorption, Dialysis, and Ion Exchange: Detailed discussion of the use of these operations in fractionation and other operations, with emphasis on the chemical viewpoint. $3.50 to members, $4.50 to nonmembers.

18-S. Heat Transfer—Louisville: Studies of vertical tubes, forced-circulation boiling, cross-flow cooling tower, burnout, boiling liquids, metal vapors, condensation, large temperature differences, single-baffle exchangers. Vol. 52; paper bound; about 125 pp.; $3.00 to members, $4.00 to nonmembers.

17-S. Heat Transfer—St. Louis: Data on surface boiling, liquid metals, gas-solid contact, convection; solids melting, immiscible liquids, nonisothermal flow, and jacketed agitated kettles. Vol. 51; paper bound; 125 pp.; $3.00 to members, $4.00 to nonmembers.

9-S. Heat Transfer—Research Studies: Data on fluidized systems, free convection between horizontal surfaces, temperature-level and radiation effects, liquid-solid suspensions, two-phase, two-component flow, pyrolisis-coil designs, and metal wetting and gas entrainment. Vol. 50; paper bound; 67 pp.; $1.50 to members, $2.25 to nonmembers.

5-S. Heat Transfer—Atlantic City: Studies of heated tubes, liquid metals, fluidized beds, three-fluid exchangers, etc. Vol. 49; paper bound; 162 pp.; $3.00 to members, $4.00 to nonmembers.

22-S, 23-S, and 27-S Nuclear Engineering—Parts V, VI, and VII: In all, 63 papers on the chemical engineering aspects of the nuclear field. Most of the A.I.Ch.E.-sponsored papers presented at the 1958 Nuclear Congress are included in Part VI. $3.50 each to members, $4.50 each to nonmembers.

19-S. Nuclear Engineering, Part IV: Containing papers sponsored by the A.I.Ch.E. at the second nuclear engineering and science congress, in Cleveland, this volume of 206 pages contains more on reactors, solvent extraction systems, economic design of power packages, neutron flux in critical assemblies, engineering design, reactor site selection, metallurgy, etc. Vol. 52; paper bound; $3.00 to members, $4.00 to nonmembers.

13-S. Nuclear Engineering, Part III: The third volume from the Ann Arbor meeting covers pulsed-column techniques; the breeder reactor; recovery of uranium from pitchblende; radiochemical processes; a series of articles on the impact of the atomic field on health, safety of individuals, education, etc.; materials testing reactor, radioisotope utilization. Vol. 50, 274 pp., paper bound; $3.00 to members, $4.00 to nonmembers.

12-S. Nuclear Engineering, Part II: The second volume from the first nuclear engineering congress, held at Ann Arbor, continues the technology of the first volume—reactors, analog computing techniques for reactor analysis, evaluation of reactor coolants, metallurgy, waste disposal, radiation damages and effects on structural materials. Vol. 50, 259 pp., paper bound; $3.00 to members, $4.00 to nonmembers.

(Continued on inside back cover)

A.I.Ch.E. JOURNAL

SEPTEMBER, 1960 • VOL. 6, NO. 3

The A.I.Ch.E. Journal, an official publication of the American Institute of Chemical Engineers, is devoted in the main to theoretical developments and research in chemical engineering and allied branches of engineering and science. Manuscripts should be submitted to the New York office.

PUBLISHER
F. J. Van Antwerpen

EDITOR
Harding Bliss

MANAGING EDITOR
Sylvia Fourdrinier

ADVERTISING MANAGER
P. A. Jolcuvar

ADVISORY BOARD

C. M. Cooper	R. H. Newton
O. E. Dwyer	R. L. Pigford
W. C. Edmister	E. L. Piret
E. R. Gilliland	J. M. Smith
A. N. Hixson	Theodore Vermeulen
H. F. Johnstone	R. R. White
W. R. Marshall, Jr.	R. H. Wilhelm

Publication Office, 215 Canal Street, Manchester, New Hampshire. Published quarterly in March, June, September, and December by the American Institute of Chemical Engineers, 25 West 45 Street, New York 36, New York. Manuscripts and other communications should be sent to the New York office. Correspondence with the editor may be addressed to him at Yale University, 225 Prospect Street, New Haven 11, Connecticut. Statements and opinions in the *A.I.Ch.E. Journal* are those of the contributors, and the American Institute of Chemical Engineers assumes no responsibility for them. Subscriptions: one year, member $6.00; nonmember $12.00; industrial libraries $25.00; additional yearly postage, Canada 50 cents, Pan American Union $1.50, other foreign $2.00 (foreign subscriptions payable in advance). Single copies: $4.00. Second-class mail. Postage paid at Manchester, New Hampshire. Copyright 1960 by the American Institute of Chemical Engineers. National headquarters of A.I.Ch.E. is concerned about nondelivery of copies of the *A.I.Ch.E. Journal* and urgently requests subscribers to give prompt notification of any change of address. Sixty days must be allowed for changes to be made in the records.

Postmaster: Please send form 3579 to A.I.Ch.E. Journal, 25 West 45 Street, New York 36, N. Y.

Conservation and Engineering V. 353
Limiting Velocities, Holdup, and Pressure Drop at Flooding in Packed Extraction Columns ..... *Gopal Venkataraman and G. S. Laddha* 355
Radiological Study of Liquid Holdup and Flow Distribution in Packed Gas-Absorption Columns ..... *C. S. Hwa and R. B. Beckmann* 359
Ion Exchange Kinetics for Systems of Linear Equilibrium Relationships *Chi Tien and George Thodos* 364
The Dual Nature of a Catalytic Reaction: The Dehydrogenation of *sec*-Butyl Alcohol to Methyl Ethyl Ketone at Elevated Pressures *Lawrence H. Thaller and George Thodos* 369
A Study of Sieve-Tray Efficiencies ..... *J. M. Hay and A. I. Johnson* 373
Comparison of the Specific Resistances of Cakes Formed in Filters and Centrifuges *V. V. Valleroy and J. O. Maloney* 382
Pressure Drop and Liquid Holdup in Concurrent Gas Absorption *W. S. Dodds, L. F. Stutzman, B. J. Sollami, and R. J. McCarter* 390
Extractive Reaction: Batch and Continuous-Flow Chemical Reaction Systems Dilute Case ..... *Edgar L. Piret, W. H. Penney, and P. J. Trambouze* 394
Longitudinal Mixing in Fluidization ..... *E. J. Cairns and J. M. Prausnitz* 400
Mechanism of Drying Thick Porous Bodies During the Falling-Rate Period: III. Analytical Treatment of Macroporous Systems *A. H. Nissan, H. H. George, Jr., and T. V. Bolles* 406
Mass Transfer in Laminar-Boundary-Layer Flows with Finite Interfacial Velocities *Andreas Acrivos* 410
Liquid Viscosities Above the Normal Boiling Point for Methane, Ethane, Propane, and *n*-Butane ..... *G. W. Swift, John Lohrenz, and Fred Kurata* 415
Suspension of Slurries by Mechanical Mixers .. *Joel Weisman and L. E. Efferding* 419
The Viscosity of Liquid Mixers ..... *R. A. McAllister* 427
Flow Patterns and Mixing Rates in Agitated Vessels *K. W. Norwood and A. B. Metzner* 432
Liquid, Gas, and Dense-Fluid Viscosity of Propane *Kenneth E. Starling, Bert E. Eakin, and Rex T. Ellington* 438
Effect of Radial Temperature Variation on Axial Mixing in Pipes ... *R. D. Hawthorn* 443
General Short-cut Equation for Equilibrium Stage Processes *Buford D. Smith and W. K. Brinkley* 446
Rigorous Solution of Multicomponent, Multistage Extraction Problems *Buford D. Smith and W. K. Brinkley* 451
Effect of Uniformity of Fluidization On Catalytic Cracking of Cumene *Albert Gomezplata and W. W. Shuster* 454
A Boundary-Layer Model of Fluid-Particle Mass Transfer in Fixed Beds *James J. Carberry* 460
Entrainment and Pressure Drop in Concurrent Gas-Liquid Flow: I. Air-Water in Horizontal Flow ..... *Moye Wicks, III, and A. E. Dukler* 463
Performance of Packed Columns: VI. Mass Transfer Rates for Dehumidification at High Solute Concentrations ..... *H. L. Shulman and R. G. Robinson* 469
Transient Response Study of Gas Flowing Through Irrigated Packing *Francesco DeMaria and Robert R. White* 473
Mass Transfer in Semifluidized Beds For Solid-Liquid System *Liang-Tseng Fan, Yung-Chia Yang, and Chin-Yung Wen* 482
On the Steady State Activity Levels in a Reactor-Regenerator System *E. E. Petersen* 488
The Kinetics of the Absorption of Phosgene into Water and Aqueous Solutions *W. H. Manogue and R. L. Pigford* 494
Detonation Characteristics of Hydrogen-Oxygen Mixtures at High Initial Pressures *Roy L. Gealer and Stuart W. Churchill* 501
A Scintillation Method for Determining Liquid-Liquid Interfacial Areas *George J. Mitsis, Richard R. Plebuch, and Kenneth F. Gordon* 505
Heat Transfer and Kinetics in a Catalyst Bed of Rectangular Cross Section: Air Oxidation of Nitric Oxide with Silica Gel ... *J. H. Jaffer, Jr., and Harding Bliss* 510
Multicomponent Diffusion Problems ..... *Hsien-Wen Hsu and R. Byron Bird* 516
Communications to the Editor
H. L. Toor 525
Peter Harriott 528
C. A. Sleicher, Jr. 529
Abstracts
Symposium Series 3S
Computer Interchange Program 2S

new... **HEVI-DUTY**

CIRC-O-THERM OVEN

Temperatures to 250° C. (480° F.)

Improved Temperature Uniformity. With Hevi-Duty's "circle-of heat" design, there are *no cold corners.*

Fast Heat-Up. To 200° C. in less than one hour.

Low-Cost Operation on either 115 or 230 volts. Selector switch permits high or low input to enclosed heating elements.

Durable Double-Wall Construction. Steel outer shell is prime coated on both sides to prevent corrosion.

Accurate Temperature Control by sensitive bulb-type thermostat permits little lag or overshoot.

For complete information, write for Bulletin 458.

Model	Price	Chamber Size		Watts	Volts	Overall Dimensions			Shipping Weight
		Diameter	Depth			Width	Depth	Height	
HK	$169.	15	13	600	115/230	20	18	23	80
HL	$265.	20	18	1000	115	25	23	28	100

FOR GENERAL AND SPECIALIZED LABORATORY APPLICATIONS

HEVI-DUTY "Multiple Unit"
TUBE TYPE COMBUSTION FURNACES
in Two Temperature Ranges, 1850° F. or 2200° F.

Hevi-Duty Combustion Tube Furnaces are available in either the split* (illustrated) or solid type and can be used horizontally or modified for vertical operation. Long-life "Multiple Unit" brand heating units offer fast heat-up because the heat is radiated directly into the heating chamber. The heated length may be divided for zone temperature control which gives greater temperature uniformity over a specified length. A few of the standard furnaces are shown below. Many sizes are in stock. Special sizes with diameters up to 16 inches can be built to your specifications.

*5-in. and smaller diameters are hinged.

HINGED-TYPE TUBE FURNACE FOR 1850° F.					
TYPE	CHAMBER		RATING WATTS	SHIPPING WEIGHT	PRICE
	DIA.	LENGTH			
70	1¼"	12"	750	35	$ 75.00
M-2012	2⅜"	12"	1400	90	$ 165.00
M-3024	3"	24"	3400	135	$ 250.00
M-5036	5"	36"	7500	325	$ 650.00
M-8040	8"	40"	14500	520	$1180.00

HEVI-DUTY

Write for Bulletin 552 for complete details.

A DIVISION OF BP C BASIC PRODUCTS CORPORATION

HEVI-DUTY ELECTRIC COMPANY, MILWAUKEE 1, WISCONSIN

Industrial Furnaces and Ovens, Electric and Fuel • Laboratory Furnaces • Dry Type Transformers • Constant Current Regulators

Computer Program Abstracts

Readers of the *A.I.Ch.E. Journal* who are interested in programming for machine computation of chemical engineering problems will find in each issue of *Chemical Engineering Progress* abstracts of programs submitted by companies in the chemical process industries. Collected by the Machine Computation Committee of the A.I.Ch.E., these programs will be published as manuals where sufficient interest is indicated. The following abstracts have appeared this year:

CEP (May, 1960), p. 86

Flue Gas Enthalpy (011)
Thermodynamic Functions of Polyatomic Gases (049)
Numerical Solution for Certain Systems of Differential Equations (051)

CEP (June, 1960), p. 88

Liquid-Liquid Heat Exchanger Design (052)
Automatic Computational Procedure for the Thermodynamic Correlation and Prediction of Vapor-Liquid Equilibria (055)
Design of Isothermal Batch Chemical Reactors (058)

CEP (July, 1960), p. 80

Color Properties from Bausch and Lomb Spectronic 20 Colorimeter Data (036)
Equilibrium Constants from the Benedict-Webb-Rubin Equation of State (044)
Selective Curve Set (053)

CEP (August, 1960), p. 86

Polynominal Equation Fitting (033)
Circulation of Zimm Plot for Determination of Polymer Molecular Weight from Light Scattering Data (046)
Polymer Molecular Weight Distribution from Weight Average and Number Average Molecular Weights of Fractions (056)

A.I.Ch.E. JOURNAL

Conservation and Engineering

V. Energy Sources

The uses of energy for transportation, space heating, lighting, and the operation of machinery are enormous. The growth in the amount and variety of such uses seems to be almost boundless. Fifteen years ago, thoughtful persons were quite justifiably concerned with the possible exhaustion of our primary energy sources which were and are coal, oil, and natural gas. Such energy sources are not inexhaustible, and the principal disagreements were as to when the well would go dry rather than whether or not it would.

The advent of nuclear fission has, of course, changed all that. Recent estimates indicate that uranium and thorium reserves are equivalent to, perhaps, twenty times the known reserves of all fossil fuels. While energy thus supplied may never be as cheap as that from fossil fuels, it will certainly be available. The prospect of energy from nuclear fission, if fulfilled, makes idle any worry about energy sources. The certainty of fission and the promise of fusion delay important new uses of solar energy and the applications of the winds and tides. Thus, another unhappy prospect is deferred; the necessity of solving the problem of energy storage, since sunlight, wind, and tides are highly irregular in supply. The storage of energy on the scale required for full development of these uneven sources is a long way from a satisfactory solution. Anyone who has ever computed the number of storage batteries or the height of a dam for a given storage job will agree. There will be problems, of course. The disposal of radioactive byproducts is not easy; therefore the absence of this problem in fusion processes is one of their most appealing features.

Since it is difficult, though not impossible, to imagine a nuclear-powered automobile or truck, it is probable that there will be a demand for liquid fuels for many years. Coal, oil, and natural gas (and shale and tar sands as they are required) will be available for a long time if they are conserved for this purpose. One can foresee a vast chemical engineering development for the conversion of gaseous and solid fuels to liquids.

One may also foretell that probably the best use of our fossil fuels is a chemical raw materials for a large array of synthetic chemical products. It should be much easier to make synthetic fibers and possibly paper and wood substitutes for structural materials from coal, oil, and gas than it would be to do so from carbon dioxide at 400 p.p.m. in the air. It probably will be easier to make such things than to grow them, and it certainly can relieve a great drain on our forests.

Conservation of fossil materials for automobile fuels and for chemical raw materials should become an important concern for all of us. The conservation of our fossil fuels for their best possible uses should be a great factor in accelerating the development of nuclear energy for electric ultilities and marine transportation. It would be tragic if such fossil materials were wasted as fuels when nuclear energy can supplant them.

DYSTAC*

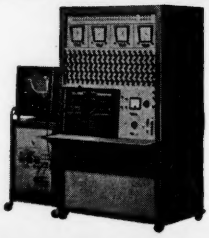

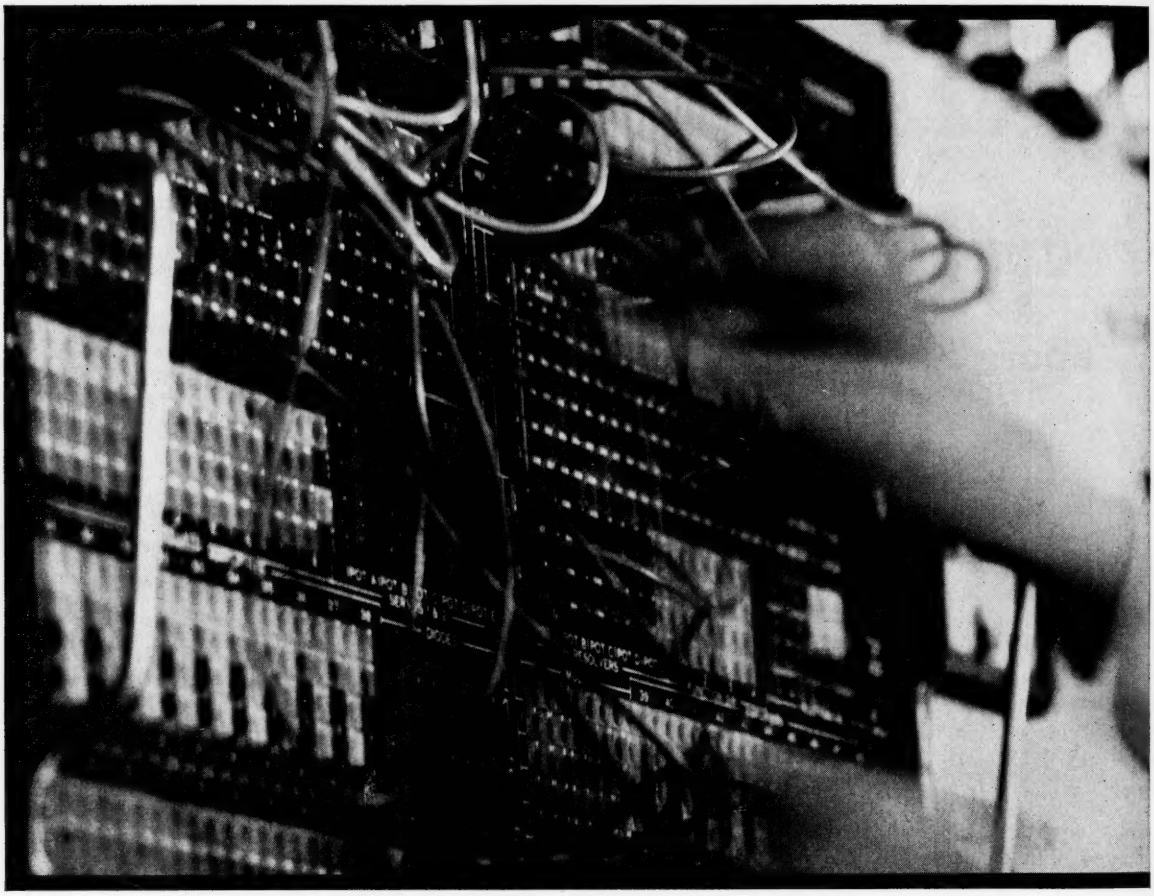

A MAJOR BREAKTHROUGH IN PROBLEM SOLVING

*DYSTAC: Dynamic Storage Analog Computer, developed by CSI, incorporates high-speed repetitive capabilities with dynamic storage of analog data to an accuracy of 0.01% and with a time-base accuracy of ±0.5 microsecond. This development has tremendously increased the versatility, economy, and speed of solution associated with analog computers.

DYSTAC provides unique time-sharing of computer components and high speed reiterations. These features make possible economic and rapid solution of complex problems that have required too many computer components or too long a solution time to be considered practical for either digital or analog techniques. Different combinations of this new development readily solve problems in four broad categories.

- Sequential calculation, as encountered in the distillation problem. Here, successive solutions to algebraic matrices are obtained from cycle to cycle at a repetitive speed of 60 cps until the problem is solved.
- Definite integral calculations. Varying definite integrals are evaluated from one cycle to another and held in memory for the successful solution of optimization problems.
- Rapid evaluation of multiple integrals. This technique can be employed for the solution of partial differential equations.
- Transient problems and difference-differential equations are solved with continuous memory.

For complete information or to arrange for a demonstration write, phone, or wire:

COMPUTER SYSTEMS, INC., Culver Road, Monmouth Junction, N. J. • DAvis 9-2351

A Schlumberger Subsidiary • formerly Mid-Century Instrumatic Corp.

Limiting Velocities, Holdup, and Pressure Drop at Flooding in Packed Extraction Columns

GOPAL VENKATARAMAN and G. S. LADDHA

University of Madras, Madras, India

Criterion for flooding which was found to be reproducible in packed columns has been described. Limiting velocities, holdup, and pressure drop at flooding have been experimentally determined for binary liquid systems in a countercurrent extraction column packed with Raschig rings, Berl saddles, Lessing rings, and spheres. Generalized correlations have been suggested, with the experimental data taken into account along with, published data of other workers for the estimation of limiting velocities, holdup, and pressure drop at flooding.

The operation of liquid-liquid extraction columns ordinarily involves the countercurrent flow of two immiscible liquids in a tower usually packed with materials specially designed to give a large surface area with the minimum amount of resistance to the flow of liquids. For a given flow rate of one of the phases in a column it has long been recognized that there will be a maximum flow rate of the other phase, which if exceeded will result in accumulation of one of the phases in the column and failure of the column operation. Further, in the operation of these columns it is observed that a definite amount of the dispersed phase is always present in the interstices of the packing and the amount of the dispersed phase thus held up is dependent upon the flow rates of the two phases and other physical variables. It is also noticed that there is always a pressure drop between any two sections of the packed column and that the holdup of the dispersed phase and the pressure drop attain a maximum value at flooding. Empirical correlations relating flooding velocities in extraction columns have been suggested by a number of authors (*2, 5, 7, 13, 15*). Elgin and Browning (*9*) made a theoretical study of spray-column operation giving an explanation of the familiar square-root plots. Minard and Johnson (*14*) gave an improved theoretical analysis of spray-column operation by extending the theory proposed by Bertitti (*3*) for gas-liquid absorption towers. Dell and Pratt (*8*) have reported theoretical correlations for flooding rates in packed columns. Very little information has appeared in literature on the determination of holdup in extraction columns. Appel and Elgin (1) gave some data of holdup in the course of their work on the rate of extraction of benzoic acid from water with toluene. Pratt and co-workers have suggested theoretical correlations for the estimation of holdup in packed columns (*15, 16*).

It has been the aim of the present investigation to determine the three important column characteristics: flooding rates, holdup, and pressure drop at flooding for various conditions of flow, and to correlate these in terms of the known variables of flow, physical properties of the liquid systems, and the packing characteristics.

EXPERIMENTAL

Apparatus

In many of the descriptions of packed columns used for liquid-liquid extraction studies (*1, 6, 16, 17*), much attention has been focused on the design of headers and the distributor. Dell and Pratt (*8*) indicate that there is no justification for increasing the diameter of the column at the dispersed-phase entry by more than 30 to 40%. However in the present study enlarged endpieces were used to obviate any reduction in the free cross-section due to the presence of the packing support at the bottom.

The column used in the investigation was a 2-in. I.D. Pyrex-glass tube, 3 ft. in length fitted with expanded endpieces 6-

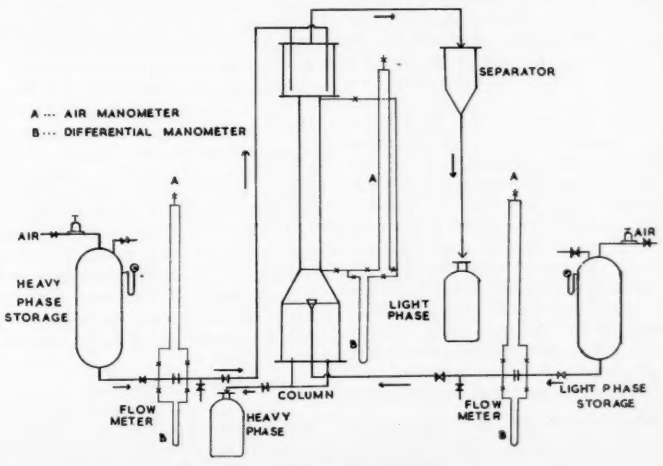

Fig. 1. Experimental set up.

in. I.D. at the bottom and 4½-in. I.D. at the top. The bottom endpiece was made of a truncated cone mounted on a cylindrical endpiece. The cylindrical portions of the endpieces were provided with a pair of sight glasses at diametrically opposite ends and also with outlet and inlet connections. Pressure tappings were made in the endpieces. The conical section at the bottom was also fitted with sight glasses for observation of the column behavior near the packing support and distributor. A distributor having 40 holes of 1/16-in. diameter was used to disperse the lighter phase liquid. The schematic flow diagram of the experimental setup is shown in Figure 1.

Packing Used

Two sizes of Raschig rings ⅜ and ¼-in.; three sizes of Lessing rings 3/16, ⅜, and ¼-in.; ¼-in. Berl saddles; and three sizes of glass balls, ½-in. 5 mm and 8 mm. were used in this investigation. The physical properties of the packings are listed in Table 1.* In the calculation of a the wetted area of the column has also been included.

Liquid Systems Studied

The different liquid systems studied were water–methyl *i*-butyl ketone, 10 and 20% glycerol with methyl *i*-butyl ketone, water-kerosene, 10 and 20% glycerol with kerosene, water-toluene, and nitrobenzene-water. The heavier phase was always made the continuous phase and the lighter the dispersed phase. Before the experiment was started each phase was saturated with respect to the other, and the physical properties of the saturated phases were determined. The values are recorded in Table 2.*

Experimental Procedure

Each time a new liquid system was used, the phases were circulated through the column until saturation was attained. Samples were taken out, and their physical properties were determined. The orifice meters were then calibrated by direct measurement.

The procedure for making a run was as follows. At first the continuous phase was let in and rate of flow maintained constant at a desired value. The dispersed phase was then let in and its rate gradually increased. After each change in the dispersed-phase flow rate some time was allowed for the column operation to reach equilibrium, indicated by the interface at the top separating section being constant and the manometer readings also remaining constant. The dispersed-phase flow rate was steadily increased until the flooding point was reached. The flooding point has been described in various ways by many workers. In the present work the approach of the flooding point could easily be judged by the rapid increase in the manometer recording of the pressure drop. It was observed that at the flooding point a thin layer of dispersed phase collected and tended to move below the packing support.

* Tabular material has been deposited as document No. 6258 with the American Documentation Institute, Photoduplication Service, Library of Congress, Washington 25, D. C., and may be obtained for $2.50 for photoprints or $1.75 for 35-mm. microfilm.

TABLE 4

System: Methyl isobutyl ketone–water
Dispersed phase: Methyl isobutyl ketone
Continuous phase: Water

Packing: ⅜-in. Raschig rings.
$a = 159.3$ $e = 0.616$ $a/e^3 = 676$
Temperature: 28°C.

Expt.	V_o	V_d	x	Δp	$\phi_1\phi_2 \cdot 10$	$\frac{a\hat{e}\gamma}{\rho_o V_o^2}$	$\frac{\Delta p}{\Delta\rho/\rho_o}$	$\frac{V_d^2 a}{ge^3}\frac{\rho_d}{\Delta\rho}\cdot 10^4$
136	15.52	48.98	0.590	0.131	5.08	1655.0	0.664	158.0
140	30.06	35.08	0.540	0.119	5.42	440.0	0.605	81.0
143	40.83	30.9	0.473	0.102	5.77	238.5	0.518	62.7
147	61.38	22.18	0.455	0.109	6.17	128.2	0.551	32.4

System: Nitrobenzene-water
Dispersed phase: Water
Continuous phase: Nitrobenzene

Packing: 8-mm. glass beads
$a = 154.1$ $c = 0.463$ $a/e^3 = 1{,}552$
Temperature: 28°C.

232	13.25	58.80	0.644	0.136	6.75	2313.0	0.821	650.0
234	20.70	43.80	0.533	0.105	6.80	954.0	0.627	361.0
236	32.20	33.30	0.441	0.115	7.10	393.0	0.698	207.5
239	50.00	18.65	0.388	0.082	7.26	164.0	0.496	65.2

System: Kerosene–water
Dispersed phase: Kerosene
Continuous phase: Water

Packing: ¼-in. Berl saddles:
$a = 227.2$ $e = 0.649$ $a/e^3 = 831.4$
Temperature: 27°C.

328	25.81	41.3	0.179	5.54	2065	0.814	119.6
330	37.4	29.31	0.175	5.66	983	0.794	60.3
332	44.14	23.12	0.175	5.72	707	0.694	37.45
335	55.05	15.52	0.120	5.76	453	0.545	16.93

This was found to be exactly reproducible. The first appearance of the dispersed phase below the packing support was therefore taken as the criterion for flooding. Simultaneously the readings of all manometers were taken, and all flow valves were closed. It was found desirable to close the dispersed-phase supply valve first so that no dispersed phase was allowed to enter the column after the flooding point. As soon as the flow of the liquids was stopped to the column, the interface at the top descended, owing to the accumulation of the dispersed phase held inside the column. When no more movement of phases inside the column was observed, the continuous-phase supply was turned on gradually, and the discontinuous-phase liquid flowing out was collected in a weighed beaker until the interface regained its original level and the weight of the dispersed phase collected was determined. This was then used to determine percentage or fractional holdup of the dispersed phase in the column.

Column Performance

In the case of all systems with water as the continuous phase the dispersed phase could be seen flowing upward through the interstices of the packing in well-defined droplets of almost spherical shape. Considerable amount of channeling was observed particularly with larger sizes of packing. At higher dispersed-phase flow rates there was a tendency for the droplets to become bigger and to cling to packing interstices, especially with smaller packings. Holdup and pressure drop were found to increase gradually with increase in dispersed-phase flow, but close to flooding region holdup and pressure drop increased rapidly, attaining a maximum at flooding. Very near the flooding point much coalescence of the droplets particularly at the base of the column was observed.

Results

The experimental data on limiting flow rates, holdup of dispersed phase, and pressure drop at flooding in 2-in. I.D. column for a few runs are given in Table 3.* Table 4 gives sample data.*

CORRELATION OF RESULTS

Dell and Pratt (8) had derived the following relationship for flooding in packed liquid-liquid extraction columns:

* See footnote in column 1.

$$\left[\ 1 + 0.835\left(\frac{\rho_d}{\rho_c}\right)^{1/4}\left(\frac{V_d}{V_c}\right)^{1/2}\ \right] = C_2\left[\left(\frac{V_c^2 a}{ge^3}\right)\left(\frac{\rho_c}{\Delta\rho}\right)\right]^{-1/4} \quad (1)$$

In order to take into account the effect of interfacial tension, a term γ was included within the bracket on the right-hand side of the correlation.

The above correlation was tested with published data (*7*, *8*) and the data collected in this investigation. It was found that the plot of

$$\left[\ 1 + 0.835\left(\frac{\rho_d}{\rho_c}\right)^{1/4}\left(\frac{V_d}{V_c}\right)^{1/2}\right] \text{ vs. } \left[\left(\frac{V_c^2 a}{ge^3}\right)\left(\frac{\rho_c}{\Delta\rho}\right)\ \right]$$

did not give straight lines properly placed when γ was taken as the parameter. Likewise the plot of

$$\left[\ 1 + 0.835\left(\frac{\rho_d}{\rho_c}\right)^{1/4}\left(\frac{V_d}{V_c}\right)^{1/2}\ \right] \text{ vs. } \left(\left[\frac{V_c^2 a}{ge^3}\right)\left(\frac{\rho_c}{\Delta\rho}\right)\gamma^{1/4}\right]$$

did not give properly oriented straight lines when the packing size was the parameter. This observation has also been made by Ghosal and Dutt (*12*).

In the light of these results it was necessary to modify the equation to a generalized correlation. An attempt was made to express C_2 as a function of such dimensionless groups, for example $(V_c \rho_c)/(a u_c)$, $\gamma/(V_c u_c)$, and $(\gamma \rho_c)/(u_c^2 a)$, but no satisfactory correlation was obtained. A resort was then made to the application of dimensional analysis.

The expression

$$\left[\ 1 + 0.835\left(\frac{V_d}{V_c}\right)^{1/2}\left(\frac{\rho_d}{\rho_c}\right)^{1/4}\right]$$

denoted by ϕ_1 is dimensionless and may be assumed to vary with V_c, a, ρ_c, density difference, and γ. Thus

$$\phi_1 = f(V_c, a, \rho_c, \Delta\rho, g, \gamma) \quad (2)$$

It can be shown that the following equation results from dimensional analysis:

$$\phi_1 = C\left[\left(\frac{\rho_c}{\Delta\rho}\right)^l\left(\frac{V_c^2 a}{g}\right)^m\left(\frac{a\gamma}{V_c^2\rho_c}\right)^n\right] \quad (3)$$

The actual velocity of the continuous phase through the interstices of the packing is V_c/e and the equivalent diameter e/a. The group $(V_c^2 a)/g$ will then become $(V_c^2 a)/(ge^3)$, and the group $(a\gamma)/(V_c^2\rho_c)$ becomes $(ae\gamma)/(\rho_c V_c^2)$. When one substitutes these in the correlation, it becomes

$$\left[1 + 0.835\left(\frac{\rho_d}{\rho_c}\right)^{1/4}\left(\frac{V_d}{V_c}\right)^{1/2}\right] = C\left[\left(\frac{V_c^2 a}{ge^3}\right)^m\left(\frac{\rho_c}{\Delta\rho}\right)^l\left(\frac{ae\gamma}{\rho_c V_c^2}\right)^n\right] \quad (4)$$

With the value of l and m taken as $-\lambda$ ¼ as in Pratt's correlation, a study was made to determine the effect of the modified Weber group $(ae\gamma)/(\rho_c V_c^2)$ by plotting

$$\left[\ 1 + 0.835\left(\frac{\rho_d}{\rho_c}\right)^{1/4}\left(\frac{V_d}{V_c}\right)^{1/2}\right]\left[\left(\frac{V_c^2 a}{ge^3}\right)\left(\frac{\rho_c}{\Delta\rho}\right)\right]^{1/4} \text{ vs. } \frac{ae\gamma}{\rho_c V_c^2}$$

on logarithmic coordinates.

The data obtained from more than 250 runs of the present investigation along with the published data of other authors (*4*, *5*, *8*, *16*) can be represented by the following correlation:

$$\left[\ 1 + 0.835\left(\frac{\rho_d}{\rho_c}\right)^{1/4}\left(\frac{V_d}{V_c}\right)^{1/2}\right]\left[\left(\frac{V_c^2 a}{ge^3}\right)\left(\frac{\rho_c}{\Delta\rho}\right)\right]^{1/4} = C\left[\frac{ae\gamma}{\rho_c V_c^2}\right]^n$$

The values of c and n as obtained by the method of least squares for the various types of packings are given below:

Type of packing	c	n
Raschig rings	0.894	−0.078
Berl saddles	0.882	−0.052
Lessing rings	0.853	−0.046
Spheres	0.839	−0.029

It is obvious that though the magnitude of n is not large, n varies significantly with the packing type. If the respective values of c and n are used in the flooding correlation for different packings, the average deviation of all points from those predicted by the correlation for Raschig rings, Berl saddles, Lessing rings, and spheres is 7.6, 8.8, 3.7, and 5.0% respectively. However if all the data of the present investigation along with data of other workers are subjected to statistical analysis, with all the types and sizes of packing, different tower diameters, and different liquid systems taken into account, the values of c and n are found to be 0.812 and 0.048 respectively. With these values of c and n the average deviation of all the points is 12.6%, and maximum deviations are +32 and −29% from those predicted by the correlation. It may be observed that introduction of the modified Weber Group $(ae\gamma)/(\rho_c V_c^2)$ brings together data for various liquid systems, different types and shapes of packings, and tower diameters ranging from 2 to 22-in. under one generalized correlation. It may be observed here that the percentage of average deviation of data is greater for the generalized correlation, and hence it may be preferable to use the values of c and n as obtained for each packing for estimation of limiting velocities wherever greater accuracy is desired for design purposes.

The correlation for flooding is shown in Figure 2*, where the data of Crawford and Wilke for a 12-in. column, data of Dell and Pratt for 3- and 6-in. columns, and data of the authors for 12-in. column have been plotted for Raschig rings. It may be mentioned that modified Weber group ranges from a value of 30 to 15,000. In Figure 3* the published data obtained by Breckenfeld and Wilke (*5*); Blanding and Elgin (*4*); and Row, Koffolt, and Withrow (*16*) are compared with the results of the present investigation. Figure 4* shows a similar correlation for Berl saddles, where the data of Dell and Pratt for 3- and 6-in. diam. column have been presented. The data of Dell and Pratt and those of the authors for Lessing rings are plotted in Figure 5*. The correlation for the spheres, including the data of Blanding and Elgin (*4*) is presented in Figure 6*. In Figures 2 through 6, ϕ_1 ϕ_2 is plotted vs. the modified Weber group.

HOLDUP OF DISPERSED PHASE AT FLOODING

Gayler and Pratt (*10*) have derived the following theoretical correlation for estimation of holdup at flooding:

$$x_f = C'\left[\left(\frac{V_d^2 a}{ge^3}\right)\left(\frac{\rho_d}{\Delta\rho}\right)\right]^{1/4} \quad (6)$$

Figure 7* shows a plot of holdup x_f at flooding vs. the group $[(V_d^2 a)/(ge^3)](\rho_d/\Delta\rho)$ on logarithmic coordinates for the various systems and packing under investigation. This correlation may be represented by the following equation derived by mathematical analysis of all the data:

$$x_f = 0.753\left[\left(\frac{V_d^2 a}{ge^3}\right)\left(\frac{\rho_d}{\Delta\rho}\right)\right]^{0.11} \quad (7)$$

The average deviation of all the points is 15.7%. The maximum deviations are +36 and −35%. As this equation brings under one generalized correlation all data for various systems and for shapes and sizes of various packings, the correlation may be regarded as satisfactory for design purposes. It

* See footnote on page 356.

may be noted here that the exponent 0.11 is the same as that obtained by Gayler and Pratt (*10*), but they obtained a value of 0.62 for the constant C'. Whereas the data reported here represent values taken exactly at flooding, Gayler and Pratt prepared their plot by extrapolation.

PRESSURE DROP AT FLOODING

Dell and Pratt (*8*) in their work have indicated that when the column is operating close to flooding, Bernoulli's theorem can be applied separately to the continuous- and discontinuous-phase channels in the column. In the case of the continuous phase the pressures P_1 and P_2 at two points separated by an arbitrary distance h are related as follows:

$$P_2 = P_1 + \rho_c h - \Delta P_c \qquad (8)$$

Similarly for the dispersed phase assumed to be flowing upwards

$$P_1 = P_2 - \rho_d h - \Delta P_d \qquad (9)$$

where ΔP_c and ΔP_d are due to flow of the continuous and discontinuous phase.

If Equation (8) is multiplied by $(1-x)$ and (9) by (x), one gets

$$(1-x)P_2 = (1-x)P_1 + \rho_c h(1-x) - (1-x)\Delta P_c \qquad (10)$$

and

$$xP_1 = xP_2 - x\rho_d h - x\Delta P_d \qquad (11)$$

Subtracting (11) from (10) one gets

$$P_2 = P_1 + \rho_c h(1-x) + \rho_d hx + x\Delta P_d - (1-x)\Delta P_c \qquad (12)$$

It may be observed that the term $[x\,\Delta P_d - (1-x)\Delta P_c]$ measures the net thrust. If at flooding the net thrust is assumed to be negligible (inasmuch as the dispersed phase is not allowed to go up in the column), Equation (12) simplifies to

$$P_1 - P_2 + \rho_c h = hx\Delta p$$

or

$$\Delta p' = \frac{P_1 - P_2 + \rho_c h}{\rho_c} = hx\,\Delta\rho/\rho_c \qquad (13)$$

The expression on the left side represents the actual pressure drop measured in terms of head of the continuous phase for the height. If Δp represents head loss per foot length of the column for the continuous phase, the following relationship

$$\frac{\Delta p'/h}{\Delta\rho/\rho_c} = \frac{\Delta p}{\Delta\rho/\rho_c} = x \qquad (14)$$

suggests that plot of $\Delta p/(\Delta\rho/\rho_c)$ vs. holdup should give a straight line. However it may be observed that at flooding there is always some net thrust present, and the values of holdup and pressure drop at flooding do not change appreciably. It is therefore not desirable to have a plot of two quantities which do not change appreciably for obtaining a generalized correlation. Since it has been shown that x is a function of the group $[(V_d^2 a)/(ge^3)]\,(\rho_d/\Delta\rho)$, $\Delta p/(\Delta\rho/\rho_c)$ may be plotted against this group on logarithmic coordinates. It may be noticed that the range of the experimental values of the group $[(V_d^2 a)/ge^3](\rho_d/\Delta\rho)$ is quite large, from about 5 to 1,000.

Such plots for each type of packings give fairly good correlations. Figure 8* shows the composite plot for all the packings and systems studied. The over-all relationship obtained for the combined correlation for all packings and systems by mathematical analysis of the data following the method of least squares may be expressed as

$$\frac{\Delta p}{\Delta\rho/\rho_c} = 0.83\left[\left(\frac{V_d^2 a}{ge^3}\right)\left(\frac{\rho_d}{\Delta\rho}\right)\right]^{0.061} \qquad (15)$$

The average deviation of all the points is 23.2%. The maximum deviations are +55 and −58%.

Data show an appreciable amount of scatter due partly to representing data of many liquid system and packings of different shapes and sizes by one generalized correlation and also due to a larger experimental error involved in the accurate measurement of pressure drop at flooding in liquid-liquid extraction columns. In view of the fact that the exponent on the group $[(V_d^2 a)/ge^3](\rho_d/\Delta\rho)$ is small, one may assume that the pressure drop at flooding is nearly independent of the dispersed-phase velocity, a condition reminiscent of constant pressure drop at flooding in gas-liquid absorption towers (*18*).

ACKNOWLEDGMENT

The authors wish to express their gratitude to the Government of India for the award of a research fellowship for this investigation and to J. M. Smith, Chairman, Technological Institute, Northwestern University, for encouragement and help in preparing this article.

NOTATION

a = superficial area of packing, sq.ft./cu.ft.
C, C', C_2 = constants
f = functional operator
g = gravitational acceleration
h = height of the column
l, m, n = constants
P = pressure, lb./sq.ft.
Δp = actual pressure drop measured at ft. of continuous phase/ft. height of packing
ΔP = differential pressure lb./sq.ft.
V = superficial velocity of the phase (empty tower), ft. hr.
x = fractional holdup of dispersed phase in column free space

Greek Letters

ρ = density of phase, lb./cu.ft.
$\Delta\rho$ = density difference, lb./cu.ft.
γ = interfacial tension, dynes/cm. (lb./hr.^{2} in modified Weber group)
ϕ = functional operator
ϕ_1 = $\left[1+0.835\left(\frac{\rho_d}{\rho_c}\right)^{1/4}\left(\frac{V_d}{V_c}\right)^{1/2}\right]$ dimensionless
ϕ_2 = $\left[\left(\frac{V_c^2 a}{ge^3}\right)\left(\frac{\rho_c}{\Delta\rho}\right)\right]$ dimensionless
e = fractional voids, dimensionless
u = viscosity of phase, lb./(hr.)(ft.)

Subscripts

c = continuous phase
d = dispersed phase
f = flooding state

LITERATURE CITED

1. Appel, F. J., and J. C. Elgin, *Ind. Eng. Chem.*, **29**, 451 (1927).
2. Ballard, J. H., and E. L. Piret, *ibid.*, **42**, 1088 (1950).
3. Bertetti, J. W., *Trans. Am. Inst. Chem. Engrs.*, **38**, 1023 (1942).
4. Blanding, F. H., and J. C. Elgin, *ibid.*, **33**, 305 (1942).
5. Breckenfeld, R. R., and C. R. Wilke, *Chem. Eng. Progr.*, **46**, 187 (1950).
6. Colburn, A. P., *Trans. Am. Inst. Chem. Engrs.*, **35**, 211 (1939).
7. Crawford, J. W., and C. R. Wilke, *Chem. Eng. Progr.*, **47**, 423 (1951).
8. Dell, F. R., and H. R. C. Pratt, *Trans. Inst. Chem. Engrs. (London)*, **29**, 89 (1951).
9. Elgin, J. C., and F. M. Browning, *Trans. Am. Inst. Chem. Engrs.*, **31**, 639 (1935); **32**, 105 (1936).
10. Gayler, R., and H. R. C. Pratt, *Trans. Inst. Chem. Engrs. (London)*, **29**, 110 (1951).
11. Gayler, R., N. W. Roberts, and H. R. C. Pratt, *ibid.*, **31**, 57 (1954).
12. Ghosal, S. R., and D. K. Dutt, *Trans. Ind. Inst. Chem. Engrs.*, **8**, 36 (1955-56).
13. Hoffing, E. M., and F. J. Lockhart, *Chem. Eng. Progr.*, **50**, 94 (1954).
14. Minard, G. W., and A. I. Johnson, *ibid.*, **48**, 62 (1952).
15. Rae, H. K., *ibid.*, **47**, 431 (1951).
16. Row, S. B., J. H. Koffolt, and J. R. Withrow, *Trans. Am. Inst. Chem. Engrs.*, **37**, 559 (1941).
17. Varteressian, K. A., and N. R. Fenske, *Ind. Eng. Chem.*, **28**, 928, 1153 (1936).
18. Zenz, F. A., *Chem. Eng. Progr.*, **43**, 415 (1947).

Manuscript received October 23, 1958; revision received August 25, 1959; paper accepted August 31, 1959.

* See footnote on page 356.

Radiological Study of Liquid Holdup and Flow Distribution in Packed Gas-Absorption Columns

C. S. HWA and R. B. BECKMANN

Carnegie Institute of Technology, Pittsburgh, Pennsylvania

A radiological method has been developed to study the local flow characteristics in two-phase contacting equipment. The method presented permits the evaluation of both the vertical and horizontal components of the liquid holdup and flow distribution and can also be used to study the performance of a wide variety of two-phase contacting apparatus. An external source of radiation is used, and hence neither phase is contaminated by the radioactive material.

The application of this method is illustrated in the specific case of air-water contact in a countercurrent packed column.

Knowledge of the local flow phenomena in two-phase contacting equipment will yield important information for a better understanding of its performance. The radiological method with a radioactive isotope used as an external energy source has been found to be capable of measuring the local holdup of liquid inside any two-phase contacting device. From such holdup data, the residence time and the flow distribution can be directly calculated.

For the purpose of verification and demonstration, the water-air system flowing countercurrently in packed columns has been investigated. Packed columns were chosen, since they represent a major class of the two-phase contacting device.

THEORETICAL BACKGROUND

The method of using an electromagnetic wave to detect or measure certain physical properties of matter on the basis of its nature of absorbing such electromagnetic energy is called the *radiological method.*

A high-energy electromagnetic wave, because of its short wave length, can penetrate substances to a great extent. If such a wave consists of only one wave length, then the absorption, through a homogeneous media, can be calculated by an equation similar to that of Lambert's law for the absorption of parallel monochromatic light:

$$I = I_o\, e^{-k_\lambda t} \qquad (1)$$

where I_o is the source intensity of the parallel monenergetic radiation, I is the intensity after it has penetrated a homogeneous material of thickness t, and k_λ is the absorption coefficient which is a function of the wave length and the physical properties of the absorber.

An X-ray generator and similar equipment can be used to produce the high-energy electromagnetic waves required by the radiological study. However the use of a radioisotope is much more convenient and economical.

In the selection of an appropriate radiation source the energy level and the half life of the isotope are two primary factors to be considered. The energy level of an isotope, according to Planck's law, is inversely proportional to the wave length, which in turn is related to the absorption coefficient in Equation (1). The half life is a measure of the decay rate of the radioactive isotope.

$$I_o = I_o \left(\frac{1}{2}\right)^{\theta/\gamma} \qquad (2)$$

Gamma radiation is electromagnetic in nature and is highly penetrating; therefore gamma emitters are most suitable for use as the energy source in a radiological study. The intensity of the gamma radiation can be easily measured. The high-frequency electromagnetic pulses emitted by the gamma source, when inpinging on a phosphor crystal, cause molecular excitation and ionization, and part of the energy dissipated in this form is reemitted as visible or ultraviolet photons. These light scintillations, when converted to electrical pulses, can be magnified, scaled, and recorded. The resultant rate of impulse expressed in terms of the number of counts per minute is a direct measure of the radiation intensity.

Theoretically Equation (1) holds true for only the parallel monoenergetic radiation. For a point source, therefore, the objects which are closer to the source will absorb or intercept more radiation than the objects which are farther away; if one assumes that the electromagnetic wave has the property of reflection, then the same is true for objects close to the viewing port of the sensing device. Figure 1 illustrates this relationship, the numbers at the bottom indicating the relative position.

This complication, however, can be eliminated if the cross-sectional area of the absorbing object is greater than the projected area of the cone formed by the radiation wave. In the case of a packed column this requirement can be fulfilled by properly shielding the radiation source so that the maximum

C. S. Hwa is with Esso Research and Engineering Company, Linden, New Jersey.

projected area of the radiation cone is smaller than the diameter of the packed bed.

It is assumed that in a packed bed the column wall, the randomly filled packing ring, and the water and air streams can be approximated by hypothetical layers. T, P, and A denote the thicknesses of the steel, ceramics, water, and air layers respectively; also the consecutive layers of the same material are identified by numeral subscripts. This schematic representation is shown in Figure 2. Furthermore the absorption coefficients for steel, ceramics, water, and air are k_t, k_p, k_l, and k_a respectively. Then by applying Equation (1) to each layer in Figure 2 consecutively one can calculate the radiation intensity behind each layer as follows:

$$\begin{aligned} I_1 &= I_0\, e^{-k_t t_1} \\ I_2 &= I_1\, e^{-k_p p_1} \\ I_3 &= I_2\, e^{-k_l l_1} \\ I_4 &= I_3\, e^{-k_a a_1} \\ &\cdots \\ I_{n-2} &= I_{n-3}\, e^{-k_l l_m} \\ I_{n-1} &= I_{n-2}\, e^{-k_a a_m} \\ I_n &= I_{n-1}\, e^{-k_t t_2} \end{aligned} \tag{3}$$

Eliminating I_{n-1} from the last equation and so on, one obtains

$$I = I_n = I_0 e^{-k_t t_1 \; -k_p p_1 \; -k_l l_1 \; -k_a a_1 \; - \; - \; - \; -k_t t_2}$$

or

$$I = I_0\, e^{-k_t \Sigma t \; -k_p \Sigma p \; -k_l \Sigma l \; -k_a \Sigma a} \tag{4}$$

Assuming that air absorbs gamma radiation much less than does steel, water, and ceramics and also assuming that the column wall thickness and the cumulative thickness of the ceramic packing rings across a specific segment of the column are constant, one can reduce the above equation to

$$I = (I_0 e^{-k_t T - k_p P})\, e^{-k_l \Sigma l}$$

or

$$I = I'_0\, e^{-k_l \Sigma l} \tag{5}$$

Equation (5) reduces to

$$I_F = I'_0\, e^{-k_l L} \tag{6}$$

when the packed column is filled with water; L is the over-all "thickness" of the water layers, equal to the void space within the column. Similarly, when the column without packing, is filled with water,

$$I^\circ{}_F = I''_0\, e^{-k_l D} \tag{7}$$

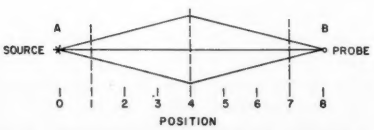

Fig. 1. Geometric configuration of nonparallel radiation source.

If I in Equation (5) is measured while the column is under operating condition, then Σl is the thickness of the running-water layers.

In Equations (5) and (6) I'_o is the radiation intensity of the packed column when $\Sigma l = 0$, or when the column is completely dry, if one lets

$$I_E = I'_o \tag{8}$$

for the packed column, and

$$I^\circ{}_E = I''_o \tag{9}$$

for the unpacked column, and notes that the ratio L/D is actually the void fraction, and $\Sigma lm/L$ is the local liquid holdup. Then

$$\frac{\Sigma l}{L} = \text{holdup} = \frac{\log\,(I/I_e)}{\log\,(I_f/I^\circ{}_e)} \tag{10}$$

and

$$\frac{L}{D} = \text{void fraction} = \frac{\log\,(I_e/I_e)}{\log\,(I^\circ{}_f/I^\circ{}_e)} \tag{11}$$

Consequently if the radiation intensities (I, $I^\circ{}_e$, I_e, $I^\circ{}_f$, and I_f) across a specific segment of the packed column are known, then the liquid holdup and the void fraction of that segment can be calculated. The holdup and the void fraction measured by this method refer only to a specific section within the column, and therefore they are called the local holdup and the local void fraction.

Three types of liquid holdups actually exist, which are defined as follows

1. *Total Holdup*: The total amount of liquid held within the apparatus under operating conditions is defined as the total holdup. It is determined by measuring the radiation intensities while the column is in operation.

2. *Static, or Permanent, Holdup*: The amount of the stagnant liquid which does not flow freely through the apparatus is defined as the static holdup. This part of the liquid either adheres to the surface or is trapped within the interstitial pockets of the packing rings. It can be determined by measuring the radiation intensities across the column after the supply of the influent liquid is discontinued.

3. *Operating Holdup*: The amount of liquid which flows freely through the apparatus under the operating conditions is defined as the operating holdup. It is the algebraic difference of the total holdup and the static holdup. Through this part of the liquid, which represents the constantly moving fresh fluid masses within the column, the mass transfer takes place.

These definitions of holdups are similar to those in the literature (*4*, *5*, *8*) except that they are expressed as the percentage of the dry void space which is occupied by the liquid. They are so defined because the fractional volume of the void space which is taken up by the liquid is of actual interest. To convert the holdups from percentage void space to percentage over-all volume of the column, the local holdups should be multiplied by the corresponding local void fraction.

In a randomly packed column the packing rings form a certain configuration; consequently the liquid inside the column follows certain channels and the local holdups within the various segments of the column differ considerably from one place to another. To determine the actual flow distribution, the local holdups within the various segments must be measured separately. In Figure 3 the packed column is divided into three concentric rings. The liquid holdups within each of the rings are determined by placing the measuring device at the appropriate lateral and transverse positions. Measurements at several positions are necessary for a representative average.

From similar measurements made at various vertical levels the liquid distribution along the column height can also be studied. The following equation is used to give the average liquid holdup inside a concentric ring and at a particular vertical level:

$$(\text{average holdup})_i = \frac{1}{4n} \sum_{j=1}^{n} (H_{n,i,j} + H_{e,i,j} + H_{w,i,j} + H_{s,i,j}) \tag{12}$$

where i denotes the specific concentric ring, j denotes each of the n vertical levels in the region of interest, and N, E, W, and S denote the circumferential positions.

REVIEW OF PREVIOUS WORK

Liquid holdup in packed gas-liquid contacting columns has been studied extensively. Jeber and Elgin (*4*) made a comprehensive study of the operating holdup for various packing materials; Otake and Okada (*6*) correlated most of the available literature data on liquid holdup and recommended an empirical formula for calculating the liquid holdup

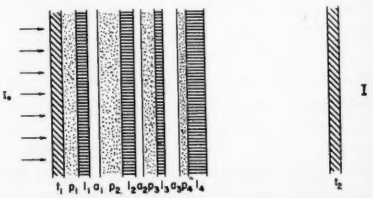

Fig. 2. Hypothetical layers of the packed column.

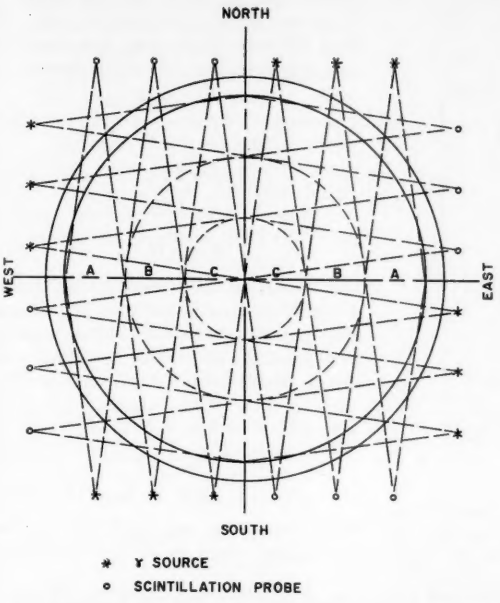

Fig. 3. Three concentric rings and corresponding lateral and traverse positions for scanning.

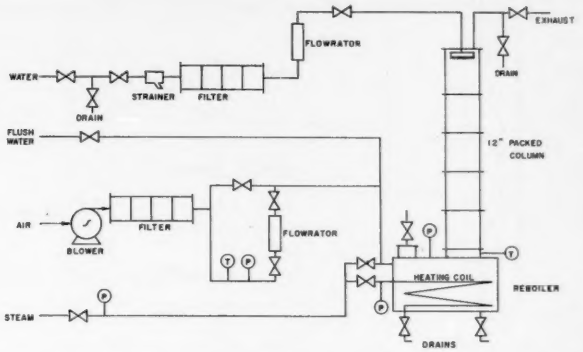

Fig. 4. Schematic flow diagram for the 12-in. packed-column system.

from the flow rates and the fluid properties. Most recently Schulman *et al.* (*7, 8*) measured the total static and operating holdups in a packed column using both aqueous and nonaqueous systems.

The principle of using a radiation-absorption method has been applied successfully to the study of other two-phase problems by earlier investigators. Isbin, Sher, and Eddy (*3*) recently used this technique to study the two-phase steam-water flow in a circular pipe, with selenium-75 as the energy source. These authors cited that Zmola and Bailey (*9*) have used iridium-192 to measure the densities of a boiling liquid; Anson, Belin, and Horlor (*1*) used a beta-ray absorption technique to measure the density of a steam-water mixture at the throat of a circular flow nozzle.

EXPERIMENTATION

Two columns were used in this investigation; one was 6 and the other 12 in. in diameter. The smaller column was used to gain preliminary knowledge of this new technique and to study the effect of the packing size and the flooding condition on the liquid holdup. The larger column was mainly used to investigate the flow distribution, both radially and vertically.

The schematic flow diagram is shown in Figure 4. The accessory equipment used for each of the columns was of the conventional type. Only the liquid distributors were specially made. They were designed to assure initial uniform distribution of the liquid at the top of the tower packing (Figure 5). The detailed description of the equipment is available in reference 2.

The 6-in. column was made from a section of Pyrex-glass pipe, 4 ft. long. Three sizes of unglazed ceramic Raschig packing rings were used (½, ¾, and 1 in.), corresponding to the diameter ratios of 12:1, 8:1, and 6:1 respectively. These ratios represent above, at, and below the critical of 8:1 (*5*). In Addition, the unpacked-column operation was also studied. The water rate was varied from 1,000 to 10,000 lb./(hr.)(sq. ft.), and the air, flowing countercurrently to the water, was varied from 0 to 400 lb./(hr.)(sq. ft.). Thirteen millicuries of mercury-203 were used as the energy source. Mercury-203 has a single-energy level of 0.279 mev. and a half life of 45.8 days.

The experimental results obtained from this column show that the total liquid holdup increases with the liquid rate (Figure 6), whereas the gas rate has negligible effect below the loading point

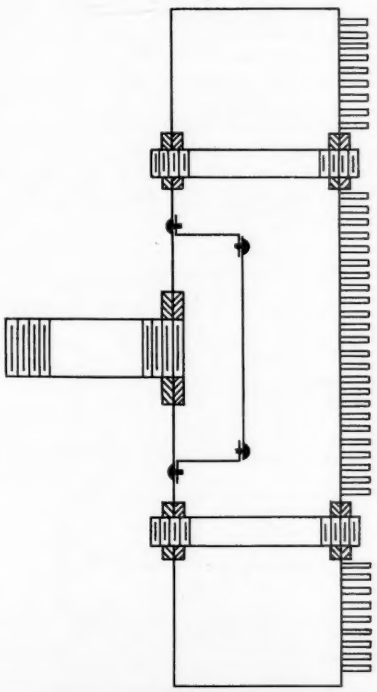

Fig. 5. Liquid distributor for the 12-in. column.

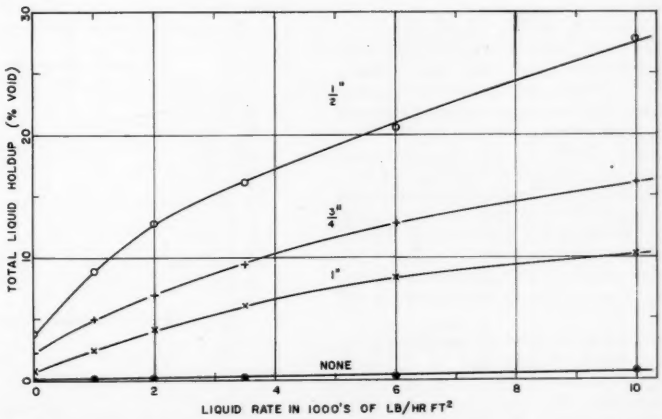

Fig. 6. Effect of liquid rate on total liquid holdup for the unpacked and Raschig-ring packed 6-in. column.

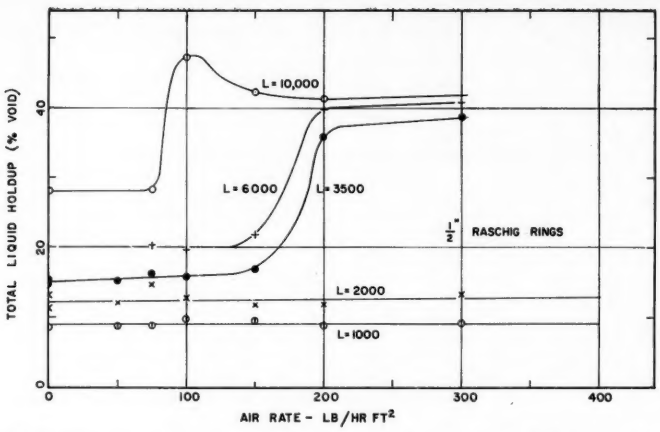

Fig. 7. Effect of gas rate on total holdup in the 6-in. column packed with ½-in. Raschig rings.

(Figure 7). Each of the experimental points is the average value of two separate runs. In each run measurements were made at four circumferential positions and three vertical levels, symmetrically located around the center of the column.

Although the gas rate has negligible effect on the liquid holdup below the loading point, the liquid holdup shows a rapid increase beyond this point (Figure 7). It is believed that at the loading point the water droplets start to stay afloat, since the upward drag force caused by the high air rate balances the gravitational force at this point. This ascending trend continues until the flooding point is reached. Further increase of the air rate, instead of keeping the liquid droplets afloat, carries the droplets away, hence reducing the liquid holdup. This explains the maximum dome appearing in the top curve of Figure 7.

The effect of the packing size and the void fraction was found to be as follows; under the same operating conditions the larger packings always give a lower liquid holdup, and for various sections of the column a lower holdup is always observed at regions where the local void fraction is higher. Figures 8 and 9 show these relationships and the entrance effect when the column is under the normal operating conditions, as well as when it is operated at flooding.

For the study of flow distribution a 20-ft. 12-in. steel column packed with 1-in. Raschig rings was used. This larger column allowed a much more complete scanning procedure for the study of various localized holdup phenomena. Two liquid rates, 1,300 and 13,000 lb./(hr.)(sq. ft.), and two gas rates, 0 and 530 lb./(hr.)(sq. ft.), were investigated. Twenty-three millicuries of thulium-170 were used as the energy source. Thulium-170 has a lower energy level (0.0842 mev.) than mercury-203; hence it yields a more sensitive measuring system. The half life of thulium-170 is 127 days.

The local liquid holdups measured in the 12-in. column, summarized in Table 1, correspond to the average values calculated by Equation (12) with $n = 4$. These results indicate that for the packed column with a column to packing diameter ratio of 12:1 the distribution of liquid remains uniform across the cross section of the column to the entire depth of its 18 ft. of packing. The strong variation of local holdup indicates that the channeling effect exists. Moderate changes of liquid and gas rates do not alter the general fluid-distribution pattern.

The radiation-absorption measuring device used for the 12-in. column consisted of a gamma source and a scintillation-detecting probe. They were shielded and mounted on a set of parallel tracks; the geometric layout is shown in Figure 10, and A and B are such that the intersection of the two cones is located at the center of the column. The tracks were rotated on a steel ring which had been properly grooved and mounted on a platform, and the platform moved vertically along the column, thus allowing the measuring device to scan at any part of the column. The detecting device used for the 6-in. column was similar in nature but somewhat less elaborate.

COMPARISON OF RESULTS WITH PREVIOUS INVESTIGATORS

Shulman, Ullrich, and Wells (*8*) made an extensive study of liquid holdup on a 10-in. packed column. They correlated their results with the data of several previous investigators and presented the following equations:

$$h_t = \frac{\alpha l^\beta}{D_p^2} \tag{13}$$

$$h_s = \delta D_p^{-x} \tag{14}$$

$$h_o = h_t - h_s \tag{15}$$

$$\beta = \gamma D_p^{\nu} \tag{16}$$

The values of the constants are given in Table 2. To convert these equations from percentage of the column volume to percentage of the void volume, one should divide by the void fraction:

$$H_t = h_t/\epsilon = (\alpha L^\beta)(\epsilon D_p^2) \tag{17}$$

$$H_s = h_s/\epsilon = (\delta/\epsilon) D_p^{-x} \tag{18}$$

$$H_o = H_t - H_s \tag{19}$$

These equations are applicable below the loading point only.

Table 2. For Porcelain Rashig Rings

	½	1 in.
D · ft.	0.0582	0.1167
α	2.25×10^{-5}	2.25×10^{-5}
γ	0.965	0.965
δ	0.00104	0.00104
x	1.21	1.21
v	0.376	0.376

Figure 11 shows the results of the present study in comparison with the experimental data of Shulman *et al.* and the results calculated from their equations.

The data obtained for the ½-in. rings are shown at the top of the graph. The experimental results of this study are in fair agreement with Shulman's, but they deviate from the calculated results beyond 2,000 lb./(hr.)(sq.ft.). For the 1-in. raschig rings, results are available on both 6 and 12-in. columns from this study. The data on the 6-in.

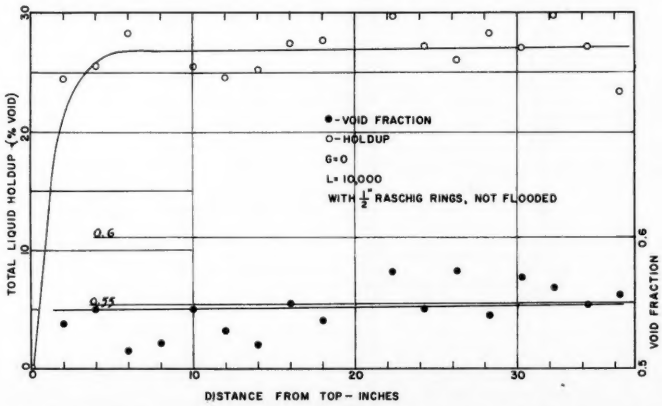

Fig. 8. Longitudinal variation of holdup and void fraction from the top of the packing under normal operating conditions in the 6-in. column.

column are not in good agreement with Shulman's because of the low column-to-packing diameter ratio (6:1), which may have caused excessive channeling. The data obtained on the 12-in. column indicate very good agreement with Shulman's experimental data. Since the 1-in. packing has a much higher loading point than the ½-in. packing, the experimental data follow the calculated results of the correlating equation to a higher liquid rate.

It should be noted in the consideration of this comparison, particularly with regard to the 12-in. column, that the data of the current investigation represent an average of the lateral and vertical scannings which in themselves show considerable variation throughout the column; yet the summation shows good agreement with the cumulative values obtained by other methods.

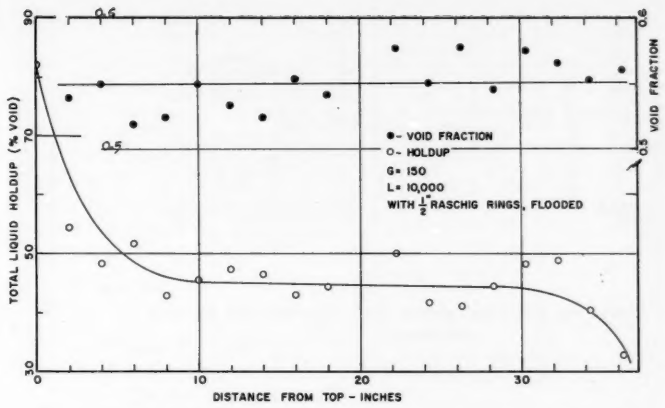

Fig. 9. Longitudinal variation of holdup and void fraction for the top of the packing under flooded conditions in the 6-in. column.

CONCLUSIONS

1. The radiological method described in this paper presents a new simple method of studying the local hydrodynamic characteristics of the packed column or other similar two-phase contacting equipment.

2. This method does not contaminate or disturb the system in any fashion.

3. The liquid-holdup data and the void fraction determined by the radiological method can be calculated by the following equations, which are derived by applying Lambert's law for the absorption of parallel monochromatic light to the radiological system:

$$H_t = \frac{\log I/I_e}{\log I_f/I_e}$$

$$\text{void} = \frac{\log I_f/I_e}{\log I_f^\circ/I_e^\circ}$$

4. By scanning the packed column in a systematic manner, one can obtain the local liquid holdups and the flow distribution.

5. The good agreement of the experimental results from this study and the corresponding data obtained by other methods prove the validity of this new technique.

ACKNOWLEDGMENT

The authors wish to express their gratitude for the Texas Company Fellowship which made this study possible.

Table 1. Local Operating Liquid Holdup in the 12-in. Column

H_o, percentage of void volume operating conditions	From wall to 2 in. from the wall	From 2 to 4 in. from the wall	From 4 in. from the wall of the column
L = 13000, G = 0 lb./(hr.)(sq. ft.)			
0-5	15.04	14.05	14.95
5-9	9.98	12.61	15.18
9-13	12.11	12.42	12.02
13-18	15.46	14.21	16.05
L = 13000, G = 530 lb./(hr.)(sq. ft.)			
0-5	18.60	15.90	14.36
5-9	13.76	13.38	15.03
9-13	12.56	11.89	13.65
13-18	17.58	14.45	17.31
Average void fraction			
0-5	0.719	0.732	0.717
5-9	0.750	0.724	0.680
9-13	0.748	0.749	0.689
13-18	0.701	0.724	0.716

NOTATION

a = thickness of air layer
D = inside diameter of the column
D_p = equivalent diameter of the packing
e = 2.7183
h = liquid holdup, percentage column volume
h_t = total holdup
h_s = static holdup
h_o = operating holdup
H = liquid holdup percentage column void
H_t = total holdup
H_s = static holdup
H_o = operating holdup
I = intensity of the parallel monoenergetic radiation
I_e = intensity when the column is dry
I_f = intensity when the column is filled with water
I_n = intensity after penetrating the R_{th} layer
I_o = source intensity, or at time O
I_θ = intensity at time θ
I° = intensity without packing
I' = $I_o e^{-k_t t - k_p p}$
I'' = same as $'$ except $p = 0$
k^λ = absorption coefficient for Equation (1)
l = thickness of water layer
L = liquid rate, lb./(hr.)(sq.ft.); cumulative length of the void space
m = number of hypothetical layers
n = number of vertical levels
p = thickness of ceramic layer
t = thickness of the homogeneous absorbing media, the column wall
x = constant
v = constant

Greek Letters

α = constant
γ = constant
δ = constant

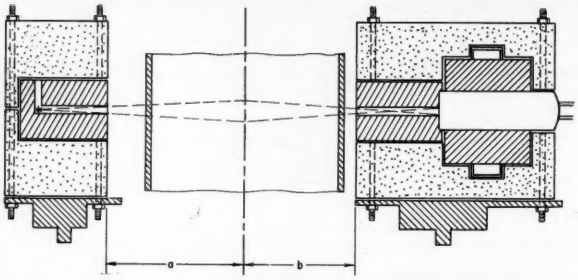

Fig. 10. Scintillation probe and gamma source assembly with the lead shieldings.

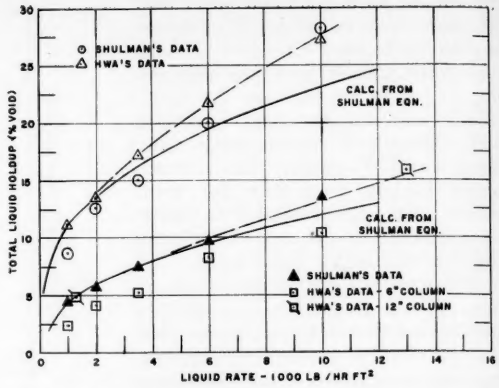

Fig. 11. Comparison of results at $G = 0$ (top two curves for ½-in. packing, lower two curves for 1-in. packing, solid lines for calculated results).

Γ = half life
ϵ = void fraction
λ = wave length
θ = time
Σ = summation

LITERATURE CITED

1. Anson, D., R. E. Belin, and M. L. Horlor, *Dominion Physical Lab. Rept. r239*, Lower Hutt, New Zealand (Feb., 1955).
2. Hwa, C. S., Ph.D. thesis, Carnegie Inst. Technol., Pittsburgh, Pa. (1958).
3. Isbin, H. S., N. C. Sher, and K. C. Eddy, *A.I.Ch.E. Journal*, **3**, 136 (1957).
4. Jesser, B. W., and J. C. Elgin, *Trans. Am Inst. Chem. Engrs.*, **39**, 277 (1943).
5. Markas, S. E., and R. B. Beckmann, *A.I.Ch.E. Journal*, **3**, 223 (1957).
6. Otake and Okada, *Chem. Engrs. (Japan)*, **17**, No. 5, 176 (1953).
7. Shulman, H. L., C. F. Ullrich, A. Z. Proulx, and J. O. Zimmerman, *A.I.Ch.E. Journal*, **1**, 253 (1955).
8. Shulman, H. L., C. F. Ullrich, and N. Wells, *ibid.*, p. 247.
9. Zmola, P. C., and R. V. Bailey, paper presented at December, 1954 meeting of Am. Soc. Mech. Engrs.

Manuscript received October 27, 1958; revision received September 2, 1959; paper accepted September 14, 1959. Paper presented at A.I.Ch.E. Atlantic City meeting.

Ion Exchange Kinetics for Systems of Linear Equilibrium Relationships

CHI TIEN and GEORGE THODOS

The Technological Institute, Northwestern University, Evanston, Illinois

The mathematical equations describing the kinetic behavior of ion exchange processes have been solved analytically for systems having linear equilibrium relationships of the type $q^* = K_1 + K_2C^*$. The concentration ratios of the effluent to the influent solution for these cases are found to depend on parameters involving time, position, and relative resistances of the liquid and resin phases. Numerical results have been obtained and are presented in tabular and graphical forms. Furthermore expressions for the constant pattern breakthrough curve for two special cases have also been worked out.

The mathematical equations describing the kinetic behavior of an ion exchange process with the rate-controlling mechanism represented by a combination of resistances for both the liquid and resin phases have been presented elsewhere (*5, 6*). These expressions consist of the equation of continuity, the rate of transfer, the equations describing the concentrations of the resin phase, and the relationship of surface concentrations:

$$\frac{\partial C}{\partial \xi} + \frac{\partial q}{\partial \tau} = 0 \qquad (1)$$

$$\frac{\partial q}{\partial \tau} = k_1 (C - C_s) \qquad (2)$$

$$q(\xi, \tau) = \frac{3}{b^3}\int_0^b q_i(r, \xi, \tau) r^2 dr \qquad (3a)$$

$$q_s(\xi, \tau) = q_i(b, \xi, \tau) \qquad (3b)$$

$$q_i(r, \xi, \tau) = \int_0^\tau q_s(\xi, \tau) \frac{\partial}{\partial \tau} H(r, \tau - \lambda) d\lambda \qquad (3c)$$

and

$$q_s = f(C_s) \qquad (4)$$

where

$$\xi = \frac{\rho}{u} z, \quad \tau = t - \frac{\phi}{u} z$$

$$H(r, \tau) = 1 - 2\sum_{n=1}^{\infty} \frac{(-1)^{n+1}}{\left(\frac{n\pi}{b}\right) r} e^{-D\left(\frac{n\pi}{b}\right)^2 \tau} \cdot \sin \frac{n\pi}{b} r$$

and the following initial and boundary conditions exist:

Chi Tien is at Essex College, Assumption University of Windsor, Windsor, Ontario, Canada.

$$\left.\begin{matrix} C = 0 \\ q = 0 \\ C_o = 0 \end{matrix}\right\} \text{for } \xi \geqq 0, \tau < 0$$

$$C = C_o \text{ at } \xi = 0, \tau \geqq 0$$

Equilibrium is assumed to exist at the interface, and consequently Equation (4) represents the equilibrium relationship of the system. It is obvious that the solution corresponding to this set of equations is dependent on the specific form of the equilibrium relationship.

Ion exchange equilibrium has been studied for many years, numerous theories having been proposed to correlate the experimental results. The various attempts to solve this problem fall essentially into two categories, one assuming a process of adsorption and the other applying the law of mass action. Most of the rigorous approaches require a knowledge of the true mechanism involved in the ion exchange process. Unfortunately, for most cases this information is not available. Furthermore the equilibrium relationship formulated on such a basis usually complicates the mathematical equations and gives additional difficulties to the solution of the problem. For this reason a simple empirical equation based directly on experimental data over a restricted concentration range probably would best serve this purpose.

A literature survey on ion exchange equilibrium indicates that if the equilibrium concentration in the resin phase is plotted against that of the liquid phase, several types of relationships result, as presented in Figure 1.

A simple linear relationship passing through the origin can be used to represent curve I. A nonlinear relationship of the Freundlich type is represented by curve II. Curve III can be approximated by a straight line having an intercept on the abscissa. For curve IV the equilibrium concentration in the resin phase increases very rapidly to a certain value and then becomes essentially constant. This relationship is too difficult to fit into a simple equation. However if the concentration range of the initial part of the curve is small, this can be neglected, thus making the concentration in the resin phase constant and independent of the liquid composition. The following expressions can approximate the various cases discussed:

$$q^* = K_1 + K_2 C^* \tag{5}$$

and

$$q^* = A(C^*)^a \tag{6}$$

Equation (5) represents the most general linear form and can be used with curves I, III, and IV; Equation (6) approximates curve II. This latter case is not discussed further inasmuch as it has been presented in detail elsewhere (5).

Numerical solutions of Equations (1), (2), (3*a*, *b*, *c*) with Equation (4) represented by Equation (5) with $K_1 = 0$, have already been presented in the literature (4). It is the object of this investigation to seek the solution when the equilibrium relationship is represented by Equation (5).

SOLUTION FOR GENERAL LINEAR CASE

When one substitutes Equation (5) into Equation (3*c*) and carries out the subsequent integration, the expression $q_i(r, \xi, \tau)$ thus obtained is substituted into Equation (3*a*) to give

$$q(\xi,\tau) = K_1 - \frac{6K_1}{b^2}\sum_{n=1}^{\infty}\frac{e^{-D\left(\frac{n\pi}{b}\right)^2\tau}}{\left(\frac{n\pi}{b}\right)^2} + \frac{6DK_2}{b^2}\sum_{n=1}^{\infty}\int_0^{\tau} C_s(\xi,\lambda)e^{-D\left(\frac{n\pi}{b}\right)^2(\tau-\lambda)}\,d\lambda \tag{7}$$

Differentiating Equation (7) with respect to τ and combining the resultant expression with Equations (1) and (2) follows:

$$\frac{\partial C}{\partial \xi} = -\frac{\partial q}{\partial \tau} = -\frac{6DK_1}{b^2}\sum_{n=1}^{\infty} e^{-D\left(\frac{n\pi}{b}\right)^2\tau} - \frac{6DK_2}{b^2}\sum_{n=1}^{\infty}\int_0^{\tau}\left[\frac{\partial C}{\partial \xi} + \frac{1}{k_1}\frac{\partial^2 C}{\partial \xi^2 \partial \lambda}\right]e^{-D\left(\frac{n\pi}{b}\right)^2(\tau-\lambda)}\cdot d\lambda \tag{8}$$

The solution of Equation (8) is obtained through the use of Laplace transforms (1). The transform of Equation (8) is found to be

$$\frac{\partial}{\partial \xi}c(\xi,s) = -\frac{6DK_1}{b_2}\sum_{n=1}^{\infty}\frac{1}{s+D\left(\frac{n\pi}{b}\right)^2} - \frac{6DK_2}{b^2}\left[\sum_{n=1}^{\infty}\frac{sc(\xi,s)}{s+D\left(\frac{n\pi}{b}\right)^2} + \sum_{n=1}^{\infty}\frac{1}{k_i}\frac{s}{s+D\left(\frac{n\pi}{b}\right)^2}\frac{\partial}{\partial \xi}c(\xi,s)\right] = \frac{6DK_2}{b^2}\left[-\frac{K_1}{sK_2} - c(\xi,s) - \frac{1}{k_1}\frac{\partial}{\partial \xi}c(\xi,s)\right]\phi_1(s) \tag{9}$$

where

$$\phi_1(s) = \sum_{n=1}^{\infty}\frac{s}{s+D\left(\frac{n\pi}{b}\right)^2} \tag{10}$$

By rearrangement one obtains

$$\frac{\partial}{\partial \xi}c(\xi,s)\left[\frac{b^2}{6DK_2\phi_1(s)} + \frac{1}{k_1}\right] + c(\xi,s) = -\frac{K_1}{sK_2} \tag{11}$$

The solution of this first-order linear differential equation can easily be found to be

$$c(\xi,s) = Be^{-\phi_2(s)\xi} - \frac{K_1}{sK_2} \tag{12}$$

where

$$\phi_2(s) = \frac{\left[\frac{6DK_2}{b^2}\right]\phi_1(s)}{1 + \frac{1}{k_1}\frac{6DK_2}{b^2}\phi_1(s)} \tag{13}$$

For the boundary condition of Equation (12)

$$\frac{c(\xi,s)}{C_o} = \frac{1}{s} \text{ at } \xi = 0$$

$$B = \frac{C_o}{s}\left[1 + \frac{K_1}{sK_2}\right]$$

Therefore Equation (12) becomes

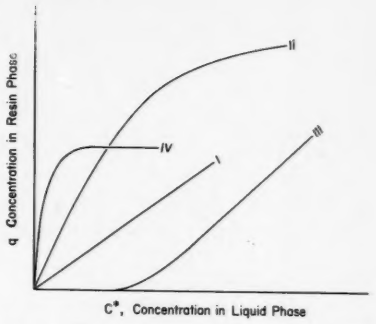

Fig. 1. Graphical representation of typical equilibrium relationships.

TABLE 1. NUMERICAL VALUES OF C/C_o RESULTING FROM EQUATION (15)*

$$\frac{C}{C_o} = -\frac{K_1}{K_2C_o} + \left[1 + \frac{K_1}{K_2C_o}\right]\Phi(\gamma\xi, \sigma\tau, N)$$

for $N = 0$ and $\dfrac{K_1}{K_1L_o} = 0.10$

$\gamma\xi=1$		$\gamma\xi=2$		$\gamma\xi=5$		$\gamma\xi=10$		$\gamma\xi=20$		$\gamma\xi=40$	
$\sigma\tau$	C/C_o	$\sigma\tau$	C/C_o	$\sigma\tau$	C/C_o	$\sigma\tau$	C/C_o	$\sigma\tau$	C/C_o	$\sigma\tau$	C/C_o
0.5	—	0.4	—	1.75	—	4.0	—	1.00	—	20.00	—
0.35	0.172	0.8	0.105	2.50	0.111	5.0	0.056	11.6	0.006	23.20	0.001
0.45	0.306	1.0	0.261	3.00	0.336	6.0	0.261	12.6	0.302	25.20	0.230
0.57	0.452	1.24	0.453	3.25	0.456	6.6	0.460	13.34	0.472	26.68	0.465
0.70	0.584	1.40	0.568	3.50	0.569	7.0	0.686	14.00	0.621	28.00	0.771
0.90	0.771	1.80	0.783	4.50	0.875	8.0	0.826	15.00	0.797	30.00	0.880
1.50	0.946	3.00	0.985	6.00	0.990	9.0	0.944	17.00	0.963	34.00	0.993

* Numerical values of $\Phi(\gamma\xi, \sigma\tau, N)$ are taken from Rosen's work (4).

$$\frac{c(\xi,s)}{C_o} = \left[1 + \frac{K_1}{K_2C_o}\right] e^{-\phi_2(s)\xi} - \frac{K_1}{sK_2} \tag{14}$$

The inverse transform, obtained through the use of the inversion integral formula, is given as

$$\frac{C(\xi,\tau)}{C_o} = \frac{1}{2\pi i}\int_{a-i\infty}^{a+i\infty} \frac{K_1}{K_2C_o}\frac{1}{s} e^{s\tau}\, ds +$$

$$\frac{1}{2\pi i}\int_{a+i\gamma}^{a+i\infty}\left[1 - \frac{K_1}{K_2}\right]\frac{1}{s} e^{-\phi_1(s)\xi + s\tau}\, ds =$$

$$-\frac{K_1}{K_2C_o} + \left[1 + \frac{K_1}{K_2C_o}\right]\Phi(\gamma\xi,\sigma\tau,N) \tag{15}$$

$$\Phi(\gamma\xi,\sigma\tau,N) = \frac{1}{2\pi i}\int_{a+i\infty}^{a-i\infty} \frac{1}{s} e^{-\phi_2(s)\xi + s\tau}\, ds \tag{16}$$

It is obvious that $\Phi(\gamma\xi,\sigma\tau,N)$ becomes the same as C/C_o when K_1 vanishes, a situation corresponding to the equilibrium case I. This case represented by Equation (16) has been solved by Rosen (3, 4). The numerical values of Φ, as given by Rosen, are dependent on three dimensionless groups, namely $\gamma\xi$, $\sigma\tau$, and N. In view of these conditions, the expression C/C_o defined by Equation (15) is a function of the parameters K_1/K_2C_o, $\gamma\xi$, $\sigma\tau$, and N. Numerical values for C/C_o corresponding to a special case when $N=0$ and $K_1/K_2C_o=0$ are presented in Table 1 and Figure 2.

CASE OF CONSTANT SURFACE CONCENTRATION

For the special case where $K_2=0$ Equation (5) reduces to $q^*=K_1$. This case corresponds to a situation where the surface concentration of the resin particles is kept constant. Analytical solutions for this special case can be obtained as follows. Referring to Equation (9) one gets

$$\frac{\partial}{\partial\xi} c(\xi,s) = -\frac{6DK_1}{b^2}\sum_{n=1}^{\infty}\frac{1}{s + D\left(\frac{n\pi}{b}\right)^2} \tag{17}$$

The solution of Equation (17) is

$$c(\xi,s) = -\frac{6DK_1}{b^2}\sum_{n=1}^{\infty}\frac{1}{s + D\left(\frac{n\pi}{b}\right)^2}\xi + \text{constant} \tag{18}$$

When one applies the boundary condition, $c(\xi,s)/C_o = 1/s$ at $\xi = 0$, Equation (18) becomes

$$c(\xi,s) = -\frac{6DK_1}{b^2}\sum_{n=1}^{\infty}\frac{1}{s + D\left(\frac{n\pi}{b}\right)^2}\xi + \frac{1}{s} \tag{19}$$

The inverse transform gives

$$\frac{C(\xi,\tau)}{C_o} = 1 - \frac{6DK_1}{C_ob^2}\xi\sum_{n=1}^{\infty} e^{-D\left(\frac{n\pi}{b}\right)^2\tau} = 1 - \nu\xi\sum_{n=1}^{\infty} e^{-D\left(\frac{n\pi}{b}\right)^2\tau} \tag{20}$$

The numerical values of C/C_o as given by Equation (20) depend on two parameters, $(6DK_1)/(C_ob^2)\xi$ and $D\tau/b^2$. The first parameter can be considered to be the product of $\gamma\xi$ and K_1/K_2C_o, while the second parameter is equal to $\sigma\tau/2$. For this case the absence of N can be accounted for, since the surface concentration of the resin phase is constant. Numerical values of C/C_o as expressed by Equation (20) have been computed (6) and are presented in Figure 3.

It can easily be shown that C/C_o as expressed by Equations (15) and (20) could become negative. This corresponds to a physical situation that is impossible. A rationalization for this case is given as follows.

The general linear relationship used for the solutions indicates that there is a definite concentration on the solid surface, even though the liquid phase is free of solute. This condition requires a transfer of material from the liquid phase into the resin phase as long as the resin particles remain unsaturated. Under the restriction of the material balance a transfer of solute from a solute-free solution would give the solution a negative concentration, a situation which is physically impossible. The breakthrough time as predicted with Equations (15) and (20) will be less than the actual case because the resin becomes hypothetically saturated at an earlier time. This effect will become more pronounced with increasing bed height. For this reason a different approach is employed to derive the expressions necessary to predict the breakthrough curve for cases of high values of $\gamma\xi$.

CONSTANT PATTERN BREAKTHROUGH CURVE

It has been shown experimentally that for certain instances the breakthrough curve approaches a constant pattern as the height of the bed increases. This behavior is commonly experienced for systems possessing an equilibrium relationship of the type represented by curve IV. When this condition is established, the breakthrough curve retains a definite shape on a linear plot, subject only to a constant displacement in total elapsed time which is proportional to the bed height. From the material balance one has

$$C_o u\int_o^{\infty}\left[1 - \frac{C}{C_o}\right] dt - z\phi C_o = (z\rho)\, q_{max} \tag{21}$$

The left-hand side of Equation (21) represents the material transferred from the solution; while the right-hand side gives the ultimate capacity of the column.

By rearranging Equation (21) and utilizing the conditions that $(C/C_o), \approx 0$ for $t < t_b$ one obtains

$$\int_{t_b}^{\infty}\left[1 - \frac{C}{C_o}\right] dt = \frac{z\rho}{uC_o}\, q_{max} - \left[t_b - \frac{\phi}{u}z\right]$$

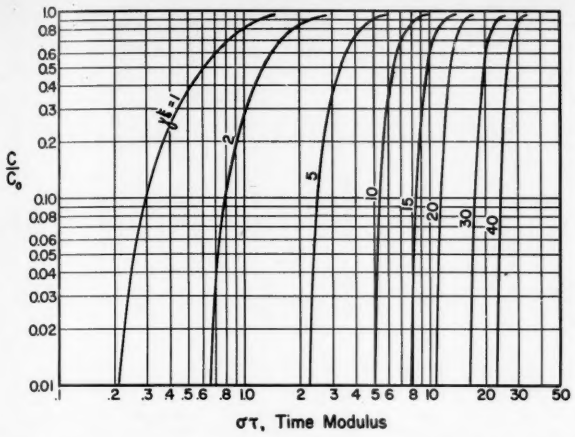

Fig. 2. Concentration ratio C/C_o for the general linear case $N = 0.00$ and $K_1/K_2C_o = 0.10$.

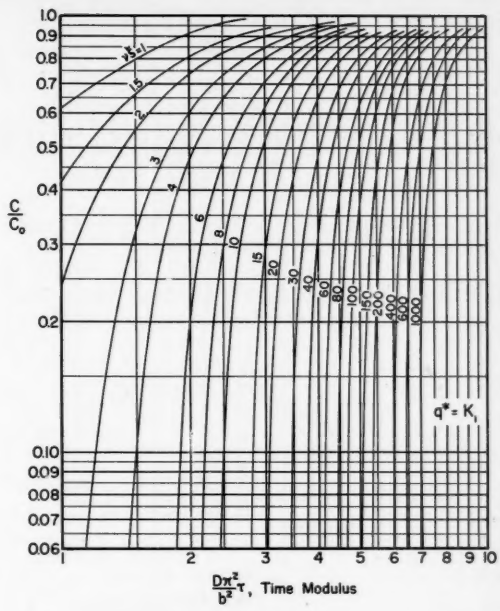

Fig. 3. Concentration ratio C/C_o for the case of constant concentration at the surface ($q^* = K_1$).

or

$$\int_{t_b}^{z}\left[1-\frac{C}{C_o}\right]d\tau=\frac{z\rho}{uC_o}q_{max}-\tau_b$$

and

$$\tau_b=\frac{q_{max}}{C_o}\xi-\int_{\tau_b}^{z}\left[1-\frac{C}{C_o}\right]d\tau \quad (22)$$

Equation (22) provides a relationship between the breakthrough curve and the breakthrough time from the consideration of a material balance.

It can be shown that for constant values of C/C_o a plot of t vs. z will yield a straight line, and the slope $[\partial t/\partial Z]_{C/C_o}$ is the same for all values of C/C_o, or

$$\left(\frac{\partial t}{\partial z}\right)_{\frac{C}{C_o}}=\left(\frac{\partial t}{\partial Z}\right)_{\frac{C}{C_o}}=\left(\frac{\partial t_b}{\partial Z}\right)_{\frac{C}{C_o}=0} \quad (23)$$

By transformation Equation (23) becomes

$$\left(\frac{\partial \tau}{\partial \xi}\right)=\left(\frac{\partial \tau_b}{\partial \xi}\right) \quad (24)$$

The value of $dt_b/\partial\xi$ is evaluated by differentiating Equation (22) to give

$$\frac{\partial \tau_b}{\partial \xi}=\frac{q_{max}}{C_o}=\frac{\partial \tau}{\partial \xi} \quad (25)$$

When the constant-pattern condition is established,

$$\frac{\partial(C/C_o)}{\partial \xi}d\xi+\frac{\partial(C/C_o)}{\partial \tau}d\tau=0 \quad (26)$$

which becomes

$$\frac{\partial(C/C_o)}{\partial \xi}=-\frac{\partial(C/C_o)}{\partial \tau}\frac{d\tau}{d\xi}=-\frac{q_{max}}{C_o}\frac{\partial(C/C_o)}{\partial \tau} \quad (27)$$

Also from Equation (1)

$$\frac{\partial(q/q_{max})}{\partial \tau}=-\frac{C_o}{q_{max}}\frac{\partial(C/C_o)}{\partial \xi}=\frac{\partial(C/C_o)}{\partial \tau} \quad (28)$$

Equation (27) gives the obvious conclusion that

$$\frac{q}{q_{max}}=\frac{C}{C_o} \quad (29)$$

for the constant-pattern period.

CONSTANT PATTERN, CONSTANT SURFACE CONCENTRATION, ALL RESISTANCES IN SOLID PHASE

When, the transformation $\chi=\tau-\tau_b$ for the constant-pattern period is introduced, Equation (7) becomes

$$q(\xi,\chi)=K_1-\frac{6K_1}{\pi^2}\sum_{n=1}^{\infty}\frac{e^{-D\left(\frac{n\pi}{b}\right)^2\chi}}{n^2}+\frac{6DK_2}{b^2}\sum_{n=1}^{\infty}\int_o^{\chi}C_s(\xi,\lambda)e^{-D\left(\frac{n\pi}{b}\right)^2(\chi-\lambda)}d\lambda \quad (30)$$

$$\frac{q}{K_1}=\frac{q}{q_{max}}=\frac{C}{C_o}=1-\frac{6}{\pi^2}\sum_{n=1}^{\infty}\frac{e^{-D\left(\frac{n\pi}{b}\right)^2\chi}}{n^2} \quad (31)$$

Substituting Equation (31) into Equation (22), one obtains the expression for τ_b:

$$\tau_b=\frac{q_{max}}{C_o}\xi-\frac{b^2}{15D} \quad (32)$$

Equations (31) and (32) completely define the constant-pattern breakthrough curve for the case where the surface concentration is constant. This solution agrees with that obtained by Vermeulen (7) for a similar case.

CONSTANT PATTERN, GENERAL CASE, ALL RESISTANCES IN SOLID PHASE

For the general case where $q_s = K_1 + K_2C_s$, the following expression is obtained by a combination of Equation (7) and Equation (2) and the utilization of the conditions postulated by Equation (29), as well as the definition of χ:

$$\frac{q}{q_{max}}=\frac{C}{C_o}=f(\chi)=\frac{K_1}{q_{max}}\left[1-\frac{6}{\pi^2}\sum_{n=1}^{\infty}\frac{e^{-D\left(\frac{n\pi}{b}\right)^2\chi}}{n^2}\right]+\frac{6DK_2L_o}{b^2q_{max}}\int_o^{\chi}f(\lambda)\sum_{n=1}^{\infty}e^{-D\left(\frac{n\pi}{b}\right)^2(\chi-\lambda)}d\lambda-\frac{6DK_2}{b^2k_l}\int_o^{\chi}\frac{\partial f(\lambda)}{\partial\lambda}\sum_{n=1}^{\infty}e^{-D\left(\frac{n\pi}{b}\right)^2(\chi-\lambda)}d\lambda \quad (33)$$

The solution of Equation (33) is obtained by successive approximations (2) as used for the solution of the second integral equation. This is accomplished by the following procedure. When one assumes an arbitrary function $f_o(\chi)$

$$f_1(\chi) = \frac{K_1}{q_{max}}\left[1 - \frac{6}{\pi^2}\sum_{n=1}^{\infty}\frac{e^{-D\left(\frac{n\pi}{b}\right)^2\chi}}{n^2}\right] + \frac{6DK_2C_o}{b^2q_{max}}\int_o^{\chi} f_0(\lambda)\sum_{n=1}^{\infty} e^{-D\left(\frac{n\pi}{b}\right)^2(\chi-\lambda)}\,d\lambda$$

$$- \frac{6DK_2}{b^2k_1}\int_o^{\chi}\frac{\partial f_0(\lambda)}{\partial\lambda}\sum_{n=1}^{\infty} e^{-D\left(\frac{n\pi}{b}\right)^2(\chi-\lambda)}\,d\lambda$$

$$f_2(\chi) = \frac{K_1}{q_{max}}\left[1 - \frac{6}{\pi^2}\sum_{n=1}^{\infty}\frac{e^{-D\left(\frac{n\pi}{b}\right)^2\chi}}{n^2}\right] + \frac{6DK_2L_o}{b^2q_{max}}\int_o^{\chi} f_1(\lambda)\sum_{n=1}^{\infty} e^{-D\left(\frac{n\pi}{b}\right)^2(\chi-\lambda)}\,d\lambda$$

$$- \frac{6DK_2}{b^2k_1}\int_o^{\chi}\frac{\partial f_1(\lambda)}{\partial\lambda}\sum_{n=1}^{\infty} e^{-D\left(\frac{n\pi}{b}\right)^2(\chi-\lambda)}\,d\lambda$$

$$f_n(\chi) = \frac{K_1}{q_{max}}\left[1 - \frac{6}{\pi^2}\sum_{n=1}^{\infty}\frac{e^{-D\left(\frac{n\pi}{b}\right)^2\chi}}{n^2}\right] + \frac{6DK_2C_o}{b^2q_{max}}\int_o^{\chi} f_{n-1}(\lambda)\sum_{n=1}^{\infty} e^{-D\left(\frac{n\pi}{b}\right)^2(\chi-\lambda)}\,d\lambda$$

$$- \frac{6DK_2}{b^2k_1}\int_o^{\chi}\frac{\partial f_{n-1}(\lambda)}{\partial\lambda}\sum_{n=1}^{\infty} e^{-D\left(\frac{n\pi}{b}\right)^2(\chi-\lambda)}\,d\lambda$$

if it is assumed that

$$\lim_{n\to\infty} f_n(\chi) = f(\chi) \qquad (34)$$

It is apparent that this procedure becomes tedious; however for the special case where diffusion in the resin phase is dominant, $N \to 0$, the second integral of Equation (33) vanishes, and under these conditions the approximate expression for $f(\chi)$ is found to be

$$\frac{C}{C_o} \approx 1 - \frac{6}{\pi^2}\sum_{n=1}^{\infty}\frac{e^{-D\frac{\pi^2}{b^2}\left[n^2 - \frac{6K_2L_o}{\pi^2q_{max}}\right]\chi}}{n^2} \qquad (35)$$

Furthermore the expression for τ_b is

$$\tau_b = \frac{q_{max}}{C_o}\xi - \frac{6b^2}{D\pi^4}\sum_{n=1}^{\infty}\frac{1}{n^2\left[n^2 - \frac{6K_2C_o}{\pi^4q_{max}}\right]} \qquad (36)$$

Similar to the previous case, Equations (36) and (38) predict the breakthrough curve for the general case when diffusion in the resin phase controls.

The infinite series of Equation (36) can be obtained by the following expression:

$$\sum_{n=1}^{\infty}\frac{1}{n^2\left[n^2 - \frac{6K_2L_o}{\pi^2q_{max}}\right]} = \sum_{n=1}^{\infty}\frac{1}{n^4} + a^2\sum_{n=1}^{\infty}\frac{1}{n^6} + a^4\sum_{n=1}^{\infty}\frac{1}{n^8} + a^6\sum_{n=1}^{\infty}\frac{1}{n^{10}} + \ldots \qquad (37)$$

where $a^2 = (6K_2C_o)/(\pi^2q_{max})$. The sum of the series $\Sigma\,(1/n^{2r})$, where r is a positive integer, is presented in Table 2.

The developments of this investigation make possible the establishment of the breakthrough curve for systems having linear equilibrium relationships. For small values of $\gamma\xi$ Equations (14) and (20) apply. For larger values the equations for the constant-pattern breakthrough curve would give better results should such a curve exist.

NOTATION

b = radius of particle, cm.
c = Laplace transform of C
C = concentration of solution, meq./cc.
C_o = concentration of influent solution, meq./cc.
C_s = concentration of solution at surface, meq./cc.
D = diffusion coefficient in resin phase, sq. cm./sec.
k_1 = mass transfer coefficient for liquid film, meq./(sec.)(g. of dry resin)(meq./cc.)
K_1, K_2 = constants for Equation (5)

Table 2. Numerical Values of the Infinite Series, $\sum_{n=1}^{\infty}\frac{1}{n^{2r}}$

$$\sum_{n=1}^{\infty}\frac{1}{n^2} = \frac{\pi^2}{6} \qquad \sum_{n=1}^{\infty}\frac{1}{n^8} = \frac{2^6}{9!}\cdot\frac{3}{5}\pi^8$$

$$\sum_{n=1}^{\infty}\frac{1}{n^4} = \frac{\pi^4}{90} \qquad \sum_{n=1}^{\infty}\frac{1}{n^{10}} = \frac{2^8}{11!}\cdot\frac{5}{3}\pi^{10}$$

$$\sum_{n=1}^{\infty}\frac{1}{n^6} = \frac{2^4}{7!}\cdot\frac{\pi^6}{3} \qquad \sum_{n=1}^{\infty}\frac{1}{n^{12}} = \frac{2^{10}}{13!}\cdot\frac{691}{105}\pi^{12}$$

N = $(3DK_2)/(b^2k_1)$
q = average concentration in resin, meq./g. of dry resin
q_i = point concentration in resin, meq./g. of dry resin
q_{max} = concentration in resin phase in equilibrium with influent solution, meq./g. of dry resin
q_s = concentration on resin surface, meq./g. of dry resin
t = time, sec.
t_b = breakthrough time, sec.
u = superficial velocity, cm./sec.
z = bed height, cm.

Greek Letters

γ = $(3DK_2)/(b^2)$
ν = $(6DK)/(C_ob^2)$
ξ = $(\rho z)/u$
ρ = bulk density of resin, g. of dry resin/cc.
σ = $(2D)/(b^2)$
τ = $t - (\phi z)/u$
τ_b = $t_b - (\phi z)/u$
ϕ = porosity
χ = $\tau - \tau_b$

LITERATURE CITED

1. Churchill, R. V., "Modern Operational Mathematics in Engineering," McGraw-Hill, New York (1944).
2. Lovitt, W. V., "Linear Integral Equations," 1 ed., Dover Publications (1950).
3. Rosen, J. B., *J. Chem. Phys.*, **20**, 387 (1952).
4. ———, *Ind. Eng. Chem.*, **46**, 1590 (1954).
5. Tien, Chi, and George Thodos, *A.I.Ch.E. Journal*, **5**, 373 (1959).
6. Tien, Chi, Ph.D. thesis, Northwestern Univ., Evanston, Illinois (1958).
7. Vermeulen, Theodore, *Ind. Eng. Chem.*, **45**, 1665 (1953).

Manuscript received January 26, 1959; revision received July 7, 1959; paper accepted July 10, 1959.

The Dual Nature of a Catalytic Reaction: The Dehydrogenation of *sec*-Butyl Alcohol to Methyl Ethyl Ketone at Elevated Pressures

LAWRENCE H. THALLER and GEORGE THODOS
The Technological Institute, Northwestern University, Evanston, Illinois

A detailed analysis of initial rate data obtained for the catalytic dehydrogenation of *sec*-butyl alcohol to methyl ethyl ketone in the presence of brass reveals that the controlling step of the reaction changes and depends on the operating conditions. To take advantage of the unique characteristics of initial rate equations, the experimental phase of this work has been carried out with a differential reactor and covered the temperature range 550° to 700°F. for pressures up to 15 atm. Feed compositions containing sec-butyl alcohol and mixtures with methyl ethyl ketone and hydrogen were used.

These studies show that the desorption of molecularly adsorbed hydrogen ceases to be the controlling step in favor of a dual-site surface reaction depending on the operating variables. In view of these observations it now becomes necessary to calculate reaction rates with both over-all rate equations and to select the lower rate as representative of the controlling step of the reaction.

Previous dehydrogenation studies for the production of methyl ethyl ketone from *sec*-butyl alcohol by means of a brass catalyst (*3*) were limited to atmospheric pressure and temperatures ranging from 650° to 750°F. These initial studies involved the dehydrogenation of *sec*-butyl alcohol in an integral reactor and necessitated extrapolation of conversion data into the region where the resistance to mass transfer became negligible. The resulting data were then subjected to a least-squares analysis involving a number of hyperplanes (*1*). The hyperplane represented only by positive coefficients was selected as representative of the most probable over-all rate equation. In this connection it was concluded that the desorption of hydrogen involving a single-site surface reaction was the controlling step.

The present investigation has been undertaken to extend the study of this reaction. To avoid the potential source of error associated in the extrapolation of data in the earlier studies (*3*), it was decided that a differential reactor would produce initial rate data directly without recourse to extrapolation. The use of initial reaction rates offers definite advantages in processing data and planning future experimental studies that would assist in the selection of a suitable rate equation. For over-all reaction rates representing a single controlling step the rate equation can be reduced to a hyperplane of the following general form:

$$y = a + bx_b + cx_c + dx_d + \ldots \quad (1)$$

where y, x_b, x_c, x_d, ... are quantities that can be obtained from the experimental data, and a, b, c, d, ... are constants to be established by the method of least squares. For the selection of a proper controlling step all these constants must be positive. Equation (1) is uniquely adaptable to initial rate data and permits the study of the effect of a single variable when the other variables are held constant. Through this approach it becomes possible to trace the effect of each variable on the over-all rate equation.

RESTRICTIONS OF REACTION RATES TO INITIAL CONDITIONS

For the dehydrogenation of *sec*-butyl alcohol to methyl ethyl ketone

$$\underset{\text{A}}{\textit{sec}\text{-}C_4H_9OH} \longrightarrow \underset{\text{K}}{CH_3COC_2H_5} + \underset{\text{H}}{H_2}$$

the following controlling steps give rise to the associated initial rate equations: (*a*) desorption of a product from the catalyst surface

$$r_{A_o} = A \quad (2)$$

(*b*) adsorption of a reactant on the catalyst surface

$$r_{A_o} = B\pi \quad (3)$$

(*c*) surface reaction (single sites)

$$r_{A_o} = \frac{C\pi}{1 + K_A\pi} \quad (4)$$

(*d*) surface reaction (dual sites)

$$r_{A_o} = \frac{D\pi}{[1 + K_A\pi]^2} \quad (5)$$

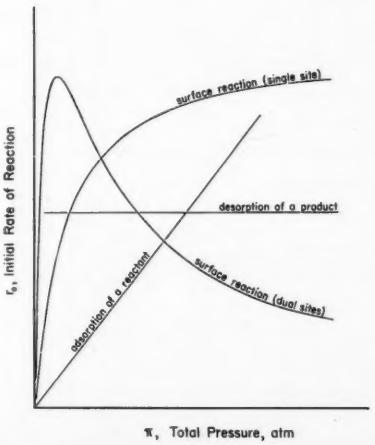
surface reaction (single site)
desorption of a product
surface reaction (dual sites)
desorption of a reactant
r_{A_o}, Initial Rate of Reaction
π, Total Pressure, atm

Fig. 1. Variation of initial rates with pressure for typical controlling steps.

Equations (2) through (5) result from the over-all rate equations for the controlling steps when no products are present in the feed. This condition is realized at the top differential thickness of a catalyst bed. With these equations it is possible to interpret experimental data directly. They may provide a method for substantiating the assumption that a single step controls the over-all rate of reaction.

With pressure as the operating variable the initial reaction rates can be represented for Equations (2) through (5) as indicated in Figure 1. The horizontal line representing Equation (2) shows the independence of pressure of the initial rate of reaction, and Equation (3) indicates a direct linear dependence on pressure. On the other hand the equations representative of the surface-reaction equations produce relations that are not linear. The one involving single sites gives rise to a continuous curve approaching an upper limit; the one involving dual sites reaches a maximum and then asymptotically approaches zero.

The straight-line relationships resulting from Equations (2) and (3) permit the direct establishment of the constants for these equations. The constants of Equations (4) and (5) can be obtained directly by rearranging

these equations into the following linear expressions:

$$\frac{\pi}{r_{A_o}} = \frac{K_A}{C}\pi + \frac{1}{C} \qquad (6)$$

$$\sqrt{\frac{\pi}{r_{A_o}}} = \frac{K_A}{\sqrt{D}} + \frac{1}{\sqrt{D}} \qquad (7)$$

When the quantities π/r_{A_o} or $\sqrt{\pi/r_{A_o}}$ are related to the pressure, a straight line will result, the slope and intercept of which enable the calculation of the constants of Equation (4) or (5).

Initial reaction-rate data and the use of Equations (2) through (5) give information regarding the rate equation but do not completely describe the state of the reactants and products occupying the active centers of the catalyst. In order to establish specifically which components are adsorbed and what state they exist in on the active centers, it becomes necessary to obtain additional information. In this connection initial rates resulting from mixed feeds give information that should completely describe the general behavior of reactants and products on a catalyst surface and thus enable the establishment of over-all reaction rates.

EXPERIMENTAL PROCEDURE

The experimental equipment with which the data were obtained is described elsewhere (3). In order to conduct this investigation at elevated pressures, a back-pressure valve was installed between the condenser and the gas separator. With this arrangement the pressure of the reaction in the course of a run was adequately controlled and varied a maximum of ± 2 lb./sq. in. at the highest pressure of 14.6 atm. Aside from this modification the steps utilized in operating this equipment were identical with those of the earlier work presented by Perona and Thodos (3).

To obtain initial rate data, a differential reactor was utilized. The catalyst was prepared from a brass stock having a composition of 65% copper and 35% zinc, by weight. In order to produce uniformity in size and shape of the catalyst to be used, coarse brass filings were dropped through a three-phase carbon arc, where these particles melted, assumed a spherical shape, and solidified soon after leaving the arc. These raw spherical particles were then screened, and only reasonably round particles which would roll off a smooth surface were used in these studies. Only those spheres which passed through a 50-mesh screen and were retained on a 60-mesh screen were used as the catalyst for this investigation.

The use of thin differential beds approximately 1/16 in. in depth raised questions regarding bed uniformity and possible channeling effects. To eliminate these possible sources of error, the brass spheres were thoroughly mixed with glass spheres of the same size in the approximate ratio of one volume of catalyst to twenty volumes of glass spheres.

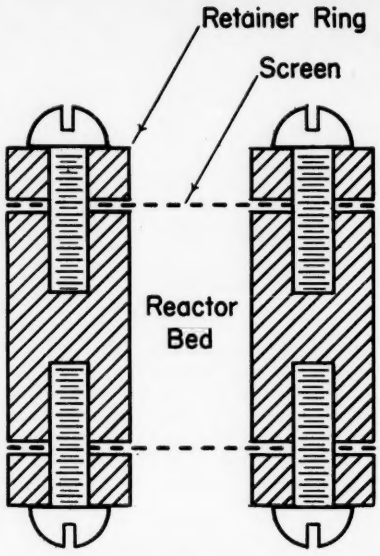

Fig. 2. Diagrammatic sketch of the cartridge type of differential bed reactor.

The differential reactor was confined in a hollow stainless steel cylinder, provided with stainless steel screens on the top and bottom. These screens were held securely in place with bolted-down retainer rings and confined the reactor bed within the cylindrical volume of the cartridge, which fitted snugly inside the reactor tube. A diagrammatic sketch of the reactor cartridge is presented in Figure 2. The catalyst charge was loaded into the reactor cartridge, which was then placed within the reactor tube.

Liquid samples resulting from this study were analyzed with an infrared spectrophotometer. Methyl ethyl ketone concentrations in *sec*-butyl alcohol were analyzed and ranged from 0.001 to 0.04 mole fraction.

QUALITATIVE INTERPRETATION OF RESULTS

Initial reaction rates were calculated from a material balance and the extent of conversion in the differential reactor. The initial reaction rates resulting from the experimental runs of this investigation were used to establish the rate equation for this dehydrogenation reaction. The majority of runs were conducted with pure *sec*-butyl alcohol as feed. To clarify certain aspects of the rate equation, it also became necessary to use mixed feeds. The operating temperature ranged from 550° to 700°F. and the pressure from subatmospheric conditions to 14.6 atm.

To obtain a preliminary background on the response of this reaction to pressure, five runs were conducted at 700°F. with the same catalyst charge

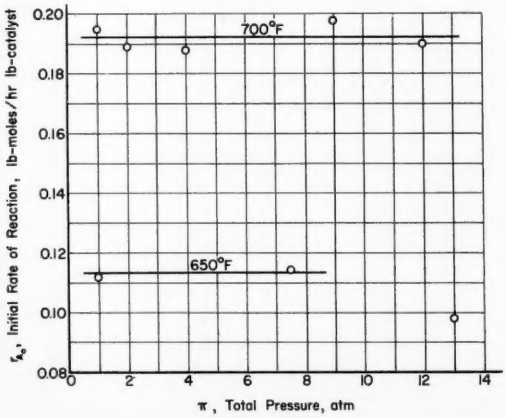

Fig. 3. Initial rates of reaction vs. total pressure for a feed of *sec*-butyl alcohol.

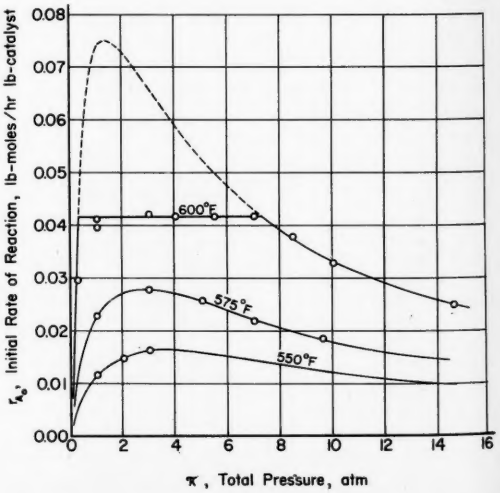

Fig. 4. Initial rate of reaction vs. pressure for a feed of *sec*-butyl alcohol.

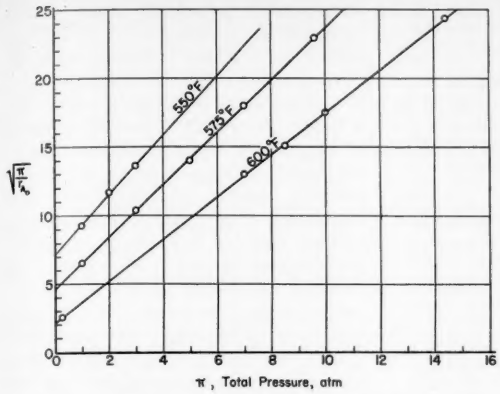

Fig. 5. Correlation of initial rate data with total pressure.

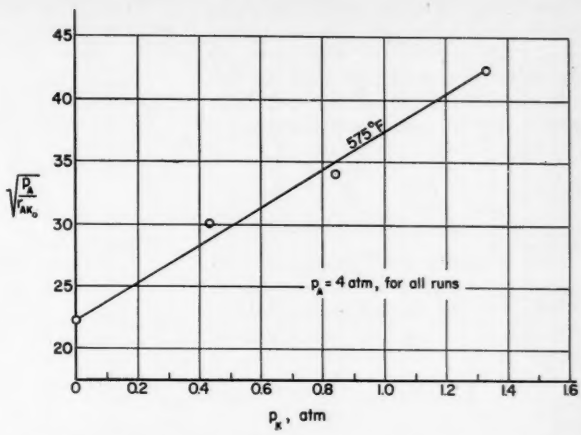

Fig. 7. Correlation of initial rate data for a mixed feed of alcohol and ketone.

of 1 g. and a feed rate of 0.0072 lb.-moles of alcohol/hr. For these runs the pressure was varied from 1 to 12 atm. The resulting initial rates presented in Figure 3 were found to be independent of pressure. This behavior suggests the possible existence of a controlling desorption step.

To take full advantage of the data obtained from a differential reactor, it is essential that the resistance to mass transfer be minimized. An exploratory set of runs was conducted to establish the existence of diffusional effects. The variation of the initial rate of reaction with feed rate was investigated at 600° and 650°F. and at several pressures. It was found that the initial rate of reaction increased to a leveling-off point beyond which the resistance to mass transfer became insignificant. Therefore in order to minimize the concentration gradients across the gas film and to relate the interfacial composition directly to the composition of the main gas stream, it became necessary to conduct the remaining runs of this study at high feed rates.

With this in mind and with a new batch of catalyst used the pressure dependence of this reaction was again investigated for three runs at 650°F. The resulting rates of reaction are presented in Figure 3. They were also found to be independent of pressure, except for the value at 13 atm., which happens to fall below the other two points. This decrease cannot be properly accounted for by means of experimental error. As was the case with the series of runs at 700°F., the first two points suggest a continuation of the probable desorption step exhibited at the higher temperature level. However the lower initial rate value at 13 atm. gives rise to the possibility of the existence of a controlling step other than the desorption of a product.

In order to investigate the possible cause for this lower initial rate, a series of runs was conducted to account for possible deviations from a desorption-controlling step. Since this rate decrease was completely absent at 700°F., it was assumed that this effect would become more pronounced with lower temperatures. Table 1 presents the experimental results obtained at 600°, 575°, and 550°F. from catalyst beds having the same level of activity. For these runs, feed rates of approximately 0.0139 lb.-moles of alcohol/hr. were used in the presence of a brass catalyst. This catalyst was diluted by glass spheres of the same size (50 to 60 mesh) in the proportions of twenty parts of glass to one part of catalyst in order to realize uniformity of flow throughout the differential reactor. These results have been plotted in Figure 4 and indicate that a definite plateau exists at the 600°F. temperature level, which completely disappears at 575° and 550°F.

The results presented at 600°F. are not only unusual but also unique in being able to account properly for the full length of the horizontal portion of the curve. The horizontal portion suggests the existence of a desorption-controlling step, whereas the remaining portions give a strong implication as to the existence of a possible dual-site surface-reaction rate equation.

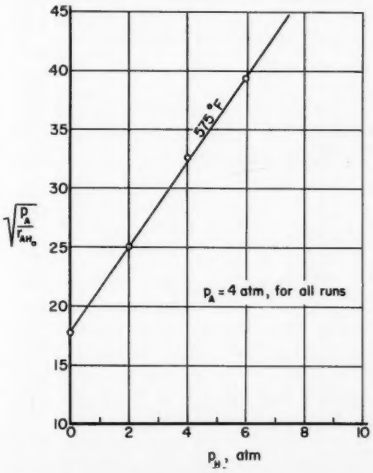

Fig. 6. Correlation of initial rate data for a mixed feed of alcohol and hydrogen.

ESTABLISHMENT OF REACTION RATES AND CONTROLLING STEPS

Surface Reaction

The general shape of the curves in Figure 4 at 575° and 550°F. and the nonhorizontal portions of the curve at 600°F. strongly suggest the existence of a dual-site surface-reaction controlling step. In view of this supposition these experimental data were fitted to Equation (7) by plotting $\sqrt{\pi/r_{A_0}}$ against π, as indicated in Figure 5. The resulting straight lines confirm this speculation and allow the calculation of $K_A/\sqrt{D}$ as the slope and $1/\sqrt{D}$ as the intercept. The rate constants resulting from Figure 5 are as follows:

t, °F.	D	K_A
550	0.0192	0.30
575	0.0430	0.412
600	0.202	0.689

and permit the calculation of the initial reaction rate for this temperature interval as

$$r_{A_0} = \frac{Dp_A}{[1 + K_A p_A]^2} \qquad (5)$$

Equation (5) is applicable for the dual-site surface reaction when it is the controlling step. These results establish the existence of a dual-site reaction that should continue to prevail when the surface-reaction step is no longer controlling.

The results obtained thus far establish the presence of a dual-site reaction in which alcohol is adsorbed on a single site and is involved with an adjacent

vacant site to produce the products ketone and hydrogen. Ketone should exist only in its molecular state. If hydrogen is assumed to exist on the surface in its molecular state, the following over-all rate equation applies

$$r = \frac{D\left[p_A - \frac{p_K p_H}{K}\right]}{[1+K_A p_A+K_K p_K+K_H p_H]^2} \quad (8)$$

For a mixed feed containing only hydrogen and alcohol, with the partial pressure of the alcohol held constant, Equation (8) can be rearranged to give

$$\sqrt{\frac{p_A}{r_{AH_o}}} = M + \frac{K_H}{\sqrt{D}} p_H \quad (9)$$

Experimental data obtained for a mixed feed of alcohol and hydrogen at 575°F. have been interpreted with the aid of Equation (9), and the results have been plotted in Figure 6. The linearity verifies the fact that the hydrogen on the catalyst surface exists in its molecular form. The slope $K_H/\sqrt{D}$ resulting from Equation (9) enables the establishment of the adsorption equilibrium constant for hydrogen once the value of D becomes known for the prevailing catalyst activity. This investigation was continued at 575°F. with a feed of alcohol and ketone in which the partial pressure of alcohol was held constant. As a result of these restrictions a relation comparable to Equation (9) was developed:

$$\sqrt{\frac{p_A}{r_{AK_o}}} = M + \frac{K_K}{\sqrt{D}} p_K \quad (10)$$

The resulting data, correlated with Equation (10), again produce a straight-line relationship when $\sqrt{p_A/r_{AK_o}}$ is plotted against p_K as shown in Figure 7. As for the case of hydrogen, the adsorption equilibrium constant can be calculated from the slope $K_K/\sqrt{D}$ once the constant D is determined for the prevailing catalyst activity.

A series of runs was made at a constant activity level that permitted the calculation of all the kinetic constants for Equation (8) at 575°F. The thermodynamic equilibrium constant was calculated from equilibrium studies (2) on this system. As a result the reaction rate at 575°F. becomes

$$r = \frac{0.0369\left[p_A - \frac{p_K p_H}{1.62}\right]}{[1+0.831p_A+2.91p_K+0.436p_H]^2} \quad (11)$$

Desorption of Hydrogen

The horizontal line of Figure 4 suggests the presence of a desorption-controlling step. For a constant alcohol-ketone composition the resulting initial rates were not independent of pressure, and on this premise the desorption step does not involve ketone. On the other hand it was found that for an alcohol-hydrogen feed the resulting initial rates remained constant and were independent of pressure. Since the addition of hydrogen in the feed gives rise to constant initial rates, it is reasonable to assume that the desorption of molecular hydrogen is the other controlling step. Therefore the following rate equation for hydrogen desorption control applies:

$$r = \frac{k_H K L\left[p_A - \frac{p_K p_H}{K}\right]}{p_K\left[1+K_A p_A+K_K p_K+KK_H\frac{p_A}{p_K}\right]} \quad (12)$$

The initial rate equation for the desorption of hydrogen follows from Equation (12) and is

$$r_{A_o} = r_{AH_o} = \frac{k_H K L p_A}{K K_H p_A} = \frac{k_H L}{K_H} = k'_H L = \text{constant}$$

Table 1. Initial Reaction Rates Resulting from the Dehydrogenation of *sec*-Butyl Alcohol

(feed: 100% *sec*-butyl alcohol)

Catalyst: 1 g. of brass spheres (50 to 60 mesh) mixed with glass spheres of the same size in the proportion of twenty parts of glass to one of catalyst.

Run	Temperature, °F.	Pressure, atm.	Feed rate, lb.-moles/hr.	r_{A_o}, initial rate lb.-moles of alcohol/(hr.)(lb.-catalyst)
5-30	600	1.0	0.01359	0.0392
6-1	600	7.0	0.01366	0.0416
6-2	600	4.0	0.01394	0.0416
6-3	600	10.0	0.01367	0.0326
6-4	600	14.6	0.01398	0.0247
6-6	600	5.5	0.01389	0.0415
6-7	600	8.5	0.01384	0.0376
6-9	600	3.0	0.01392	0.0420
6-11	600	0.22	0.01362	0.0295
7-14	600	1.0	0.01390	0.0410
7-16	550	1.0	0.01396	0.0115
7-17	550	3.0	0.01392	0.0161
7-18	575	1.0	0.01411	0.0227
7-19	575	3.0	0.01400	0.0277
7-20	575	5.0	0.01401	0.0255
7-21	575	7.0	0.01374	0.0217
7-23	575	9.6	0.01342	0.0183
7-26	550	2.0	0.01386	0.0146

GENERAL COMMENTS

The logarithmic values of the constants D and K_A established at 550°, 575°, and 600°F. were correlated against the reciprocal absolute temperature and failed to produce to conventional linear relationships commonly associated with kinetic studies. Instead the two resulting relationships exhibited curvatures, and both possessed positive temperature coefficients. From a thermodynamic consideration K_A should exhibit a negative temperature coefficient provided that the number of active sites on the catalyst surface remains constant. The deviations found to be present in these studies may be explained on the premise of an increasing number of active sites with increasing temperature. For metallic catalyst surfaces it is reasonable to expect that increasing temperatures will produce additional active sites. As a result of activation phenomena, inactive sites which could not participate in the reaction at lower temperatures became sufficiently energized to participate in the over-all reaction.

The existence of a model which exhibits different controlling steps at different reaction conditions poses a new concept in kinetic studies. For these dehydrogenation studies the dual-site surface reaction involving an adsorbed alcohol molecule and an adjacent vacant site changes to a surface-controlling step in which the adsorbed molecule and a vacant adjacent site react to produce adsorbed ketone and molecularly adsorbed hydrogen. The surface-controlling step is favored at the lower temperatures and is independent of pressure. With increasing temperature the rate of the dual-site surface reaction increases more rapidly than the rate of the desorption step, which becomes the controlling step in the over-all reaction. This behavior is apparent from the results of Figure 3, in which the data at 700°F. indicate that the desorption step controls throughout the entire pressure range investigated. With decreasing temperature the controlling desorption step continues to control over a limited pressure interval. Outside this interval the surface reaction controls, as shown in Figure 4, at 600°F. With continued temperature decrease the controlling desorption step disappears completely in favor of a surface-reaction controlling step. In view of these findings, it becomes necessary to consider the rate of reaction with two possibilities involving both steps and to select as limiting that step which produces the lower reaction rate.

NOTATION

a,b,c,d = constants for Equation (1)
A,B,C,D = over-all rate constants, Equations (2), (3), (4), and (5)
k_H = forward-reaction velocity constant for the adsorption of hydrogen
k'_H = reverse-reaction velocity constant for the adsorption of hydrogen
K = over-all thermodynamic equilibrium constant

K_A = adsorption equilibrium constant for alcohol

K_H = adsorption equilibrium constant for hydrogen

K_K = adsorption equilibrium constant for ketone

L = total molal adsorption sites per unit mass

M = parameter, $(1+K_A p_A)/\sqrt{D}$

p_A = partial pressure of alcohol, atm.

p_K = partial pressure of ketone, atm.

p_H = partial pressure of hydrogen, atm.

r = rate of reaction, lb.-moles/(hr.)(lb. of catalyst)

r_{A_0} = initial rate of reaction from a feed containing only alcohol

r_{AH_0} = initial rate of reaction from a feed containing alcohol and hydrogen

r_{AK_0} = initial rate of reaction from a feed containing alcohol and ketone

x_b, x_c, x_d = independent variables for Equation (1)

y = dependent variable for Equation (1)

π = total pressure, atm.

LITERATURE CITED

1. Hougen, O. A., and K. M. Watson, "Chemical Process Principles," pp. 902-926, Wiley, New York (1947).
2. Kolb, H. B., and R. L. Burwell, Jr., *J. Am. Chem. Soc.*, **67**, 1084 (1945).
3. Perona, J. J., and George Thodos, *A.I.Ch.E. Journal*, **3**, 230 (1957).

Manuscript received December 1, 1958; revision received October 19, 1959; paper accepted October 21, 1959.

A Study of Sieve-Tray Efficiencies

J.M. HAY and A. I. JOHNSON

University of Toronto, Toronto, Canada

The performance of sieve trays in the rectification of the methanol-water system without entrainment or leakage from the perforations was studied in an 8-in.–diameter five-tray column. The trays had a 2-in. weir height and 4-in. length of liquid path. Three tray geometries were studied: 1/4-in. diameter holes on 3/4-in. triangular spacing, 1/8-in. holes on 3/8-in. triangular spacing, and 3/16-in. on 7/16-in. triangular spacing. The superficial vapor velocity was varied from 2.2 ft./sec. to the limit of stable operation, which for this apparatus was 4.4 ft./sec. The ratio L_M/V_M within the column was varied from 1 to 0.5. The Murphree plate efficiency varied greatly from 105% at low concentration to 82% at high concentrations of methanol. Variations of 10 or 12 efficiency % were noted owing to changing velocities and tray geometries. Measurements of concentration gradients, foam heights, and gas pressure drops are also reported. This paper proposes a method of calculating the point efficiency and the number of individual-phase mass transfer units independent of the actual concentration gradient on the tray.

The method is applied to the methanol-water data, and calculated point efficiencies range from 50 to 65%. The value of $1/N_L$ for the methanol-water system is found to be small. The values of N_G and the effect of the velocity on N_G are believed to be the first in the literature for a tray in distillation operation. The effect of velocity is shown to be in agreement with the theory proposed by Gerster and co-workers. It is shown that $k_G' a_G$ decreases for increasing free area and increasing hole size. Finally variation in L_M/V_M is shown to have little effect on E_{MV}.

Fractionation in tray type of distillation columns is perhaps the most widely used means of separating the components of a liquid mixture. The calculation of the number of trays required for such a separation can be made readily (*31*) even for the most complicated separations. However only in recent years has much effort been directed toward analyzing the efficiency of operation of such trays in view of modern mass transfer theory (*1, 5, 6, 9, 14, 16, 17, 23, 27*). Any such analysis is complicated by the large number of variables involved in the properties of the gas and liquid phases, the conditions of operation, and the geometry of the system.

J. M. Hay is with Dow Chemical of Canada, Sarnia, Ontario, Canada.

This paper reports efficiency data obtained by operating an 8-in. sieve-tray column at total reflux on the system methanol-water and discusses the data in the light of recent theory. A special study is made of the number of gas-phase transfer units.

The definitions of the transfer unit terms, appearing in the notation, will be assumed known to the reader. The usual assumptions made in using them are that the driving forces are concentration difference for liquids and partial-pressure difference for vapors and that equilibrium exists at phase interfaces. In addition in this paper it will be assumed that the vapor composition below a tray is uniform, that there is no back mixing of the vapor in the vertical direction, and that there are no unusual end effects at either bubble formation or break.

THE ADDITION OF RESISTANCES

The basic equation for obtaining the individual gas-phase value depends on the well-known (*32*) equation describing the additivity of resistances:

$$\frac{1}{N_{OG}} = \frac{1}{N_G} + \frac{m_G V_M}{L_M}\frac{1}{N_L} \qquad (1)$$

Normally in using this equation one assumes N_G and N_L to be constant and plots $1/N_{OG}$ against $(m_G V_M)/L_M$ to obtain N_G from an intercept on such a plot. Using total-reflux sieve-tray plate-efficiency data, one must modify this direct approach in two ways.

First with total reflux data V_M/L_M has a value of unity, and $(m_G V_M/L_M$

Table 1. Tabulation of Tray Geometries

Tray type	Position in column	Hole diameter, in.	Triangular spacing, center to center, in.	No. of moles	Free area, sq. ft.	% free area based on Bubbling area	% free area based on Column area
I	1	1/8	3/8	216	0.0185	8.56	5.23
II	2	3/16	7/16	145	0.0278	12.87	8.02
III	3	1/4	3/4	49	0.0167	7.73	4.82
II	4	3/16	7/16	149	0.0286	13.21	8.23
I	5	1/8	3/8	218	0.0186	8.61	5.36
IIA	1	3/16	3/8	151	0.0290	13.41	8.34
IIIA	1	1/4	3/4	73	0.0249	11.51	17.37

Velocities used: Series *A* 5.8 moles/hr. *B* 6.8 moles/hr. *C* 9.4 moles/hr. *D* 11.3 moles/hr.

can be changed only by changing the concentration on the trays, which will affect the values of N_G and N_L. It is necessary, therefore, to introduce into Equation (1) correction factors similar to those used by Oliver and Watson (33), which allow for the effect of these variables:

$$\frac{1}{N_{OG}B} = \frac{1}{N_{GS}} + \frac{m_G V_M}{L_M}\frac{A}{B}\frac{1}{N_{LS}} \quad (2)$$

where, from the definitions of N_L and N_G

$$A = \frac{N_{LS}}{N_L} = \frac{k_{LS}}{k_L}\frac{a_{LS}}{a_L}\frac{\epsilon_S}{\epsilon}\frac{q}{q_S} \quad (3)$$

$$B = \frac{N_{GS}}{N_G} = \frac{k_{GS}'}{k_G}\frac{a_{GS}}{a_G}\frac{\beta_S}{\beta}\frac{U}{U_S} \quad (4)$$

An equation similar to (2) can be written for the liquid phase:

$$\frac{1}{N_{OL}A} = \frac{1}{N_{LS}} + \frac{1}{\dfrac{m_L V_M}{L_M}\dfrac{A}{B}N_{GS}} \quad (5)$$

The second factor to be considered, and one which still prevents the direct application of the revised Equation (2), is that the type of mixing on a sieve tray is not known. Thus N_{OG} applying at a point cannot be obtained directly from the observed tray efficiencies. It is proposed that a pseudo number of transfer units be defined as the N_{OG} value calculated from the composition change across the tray on the assumption that each of the following cases is applicable:

(*a*) The liquid may be completely mixed; then

$$N_{OG} = -\ln(1 - E_{MV}) \quad (6)$$

(*b*) As considered by Lewis (24), the liquid may be completely mixed in the vertical direction but not mixed in the direction of liquid flow; then

$$E_{OV} = \frac{1}{\dfrac{m_T V_M}{L_M}}\ln\frac{m_T V_M}{L_M}E_{MV} + 1 \quad (7)$$

where E_{OV} is related to the value of N_{OG} by an equation similar to (6).

(c) As described by Kamei and Takamatsu (23) there may be no mixing in the direction of either liquid or vapor flow. These authors presented graphically the relationship between E_{MV}, $(m_T'V_M)/L_M$, Z_V, Z_H, and N_{OG}.

To obtain N_{OL} for Equation (5) two special cases are applicable:

(a) If it is assumed that the liquid moves across the plate in plug flow and that the equilibrium concentration x^* remains constant on the tray, then

$$N_{OL} = -\ln(1 - E_{ML}) \quad (8)$$

(b) If it is assumed that the liquid on the tray is completely mixed and the equilibrium concentration remains constant, then

$$N_{OL} = \frac{E_{ML}}{1 - E_{ML}} \quad (9)$$

If there is no mixing on the tray in either phase, the Kamei and Takamatsu relationship between E_{ML}, N_{OL}, $(m_T'V_M)/L_M$, Z_H, and Z_V discussed above will apply.

In the case of extrapolation to $1/N_G$ all the special cases should have the same intercept since they all assume that there is no mixing of the vapor in the direction of vapor flow. This assumption is reasonable since, in general, vapor bubbles will rise through a liquid with little tendency for back mixing.

However for the case of extrapolation to $1/N_{LS}$ no such assumption is applicable, for it is exactly the variation among types of mixing that necessitates the theoretical approach proposed in this paper. Thus the intercept corresponding to Equation (8) will be different from that of Equation (9), and the Kamei and Takamatsu intercept would be expected to be the same as for Equation (8). The two intercepts should give the limits of N_{LS}. It may be added here that for most practical cases $1/N_{LS}$ will be small and will have little effect on the calculated point efficiency except for very large values of m_G.

Table 2. Concentration Gradients

(Concentration in mole per cent methanol)

Run	Location of sampler	Reflux sample Before	Reflux sample After	Sampler location 1	2	3	Liquid leaving plate Before	After	Reflux reading	Temperature, °C Top return		Production reading	Top plate L_M/V_M	Vapor flow top moles/hr.
31	Vapor above tray	90.5	89.4	86.4	85.6	82.6	75.2	73.2	45.5	68.7	30.5	—	—	12.45
	Foam liquid			—	78.4	74.6								
	Liquid on tray floor			77.4	73.4	69.3								
	Vapor below tray			79.4	76.4	73.7								
34	Vapor above tray			—	78.6	74.1								
	Foam liquid			—	65.1	55.7								
	Liquid on tray floor	79.9	77.4	51.6	49.1	48.1		60.7	40.9°	73.6	23.7	—	—	11.80°
	Liquid on tray floor	77.4	74.8	40.4	35.9	34.9		56.1						
	Vapor below tray			—	60.3	53.0								
36	Vapor above tray	52.9	51.1	59.1	54.4	50.6	17.7	14.4	30.0°	82.5	23.0	—	—	10.13°
	Foam liquid			35.0	25.4	21.2								
	Liquid on tray floor			16.3	11.4	7.0								
	Vapor below tray			27.1	23.0	19.4								

° Average values.

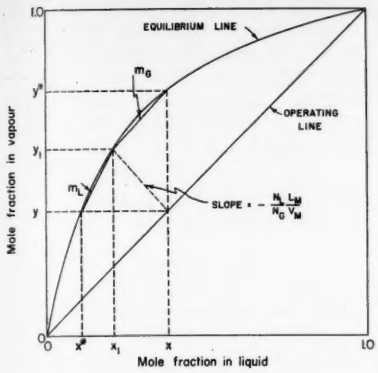

Fig. 1. Representation of mass transfer driving forces on x-y diagram.

It will be noted that N_{OG}' is calculated for a concentration change taking place across a whole tray, whereas m_G, A, and B refer to mass transfer taking place at particular liquid and vapor compositions.

Actually these quantities are calculated at the average liquid and vapor compositions across the tray, the concentration changes being small, and thus only a very small error is introduced.

The method as developed to this point could be used with data obtained from a number of systems each of which had a different constant value of m_G. However it seems more realistic at the present time to employ a single system having a variation in m_G. In this latter case the effect of the physical-property corrections is small. For boiling systems the equilibrium line will be curved, and it is necessary to calculate m_G, m_L, and m_T for the curved equilibrium line.

It is easily shown that the following define m_G and m_L exactly:

$$m_G = \frac{y^* - y_i}{x - x_i}; \; m_L = \frac{y_i - y}{x_i - x^*} \quad (10\,a,b)$$

where x_i and y_i are equilibrium values on the line of slope $-N_L/N_G$ passing through x, y. It is therefore necessary to determine x_i and y_i, which requires a trial-and-error solution. To do this the ratio N_{LS}/N_{GS} is first assumed and N_L/N_G calculated for other compositions. N_{LS} and N_{GS} are then determined by extrapolation, and the original assumption is checked.

For use in the Lewis equation, for a curved equilibrium line the following is assumed:

$$m_T = \frac{y^*_{x\,on} - y^*_{x_{off}}}{x_{on} - x_{off}} \quad (11)$$

Figure 1 has been included to illustrate the various slopes m_G, m_L, and m_T referred to in this paper.

For the special case of Kamei and Takamatsu it was assumed that m_T' could be approximated by Equation (11); this gave reasonable results.

EXPERIMENTAL APPARATUS

The experimental apparatus and the trays employed are illustrated in Figures 2 and 3. Table 1 lists the various tray geometries employed. A standard distillation circuit was used, the overhead product being recycled to the reboiler. A complete description is given in reference *19*. The top tray was located in a glass cylinder for visual observation of foam height and leakage.

Samples were taken from the downcomers as illustrated in Figure 4, by method similar to that of Garner *et al.* (*13*). The method of sampling and analysis must be as precise as possible mainly because of the apparent magnification of errors caused by taking differences in Equations (5) and (6).

The top tray was used for a study of concentration gradients. Samples were withdrawn from the floor of the tray, from the foam ½ in. above the floor, and from the vapor above and below the tray by means of fixed sampling probes in the floor (Figure 3) and a movable probe for the liquid and vapor.

Foam heights were measured visually by using the top tray. All tray types were installed in the top position during the course of the experimental work to obtain foam heights and concentration gradients.

Pressure drops across the trays were also measured. After correction for the dry-tray pressure drop these were used to obtain foam densities.

Thermometers were installed in the vapor above all trays. In addition the temperature above tray 4 was recorded. Only after all temperatures and flows had been steady for at least ½ hr. were the samplers closed off and samples taken; a steady temperature was defined as a temperature constant within ±0.25°C. Usually the apparatus required 2 to 5 hr. to reach steady conditions; during this time the column was operated manually.

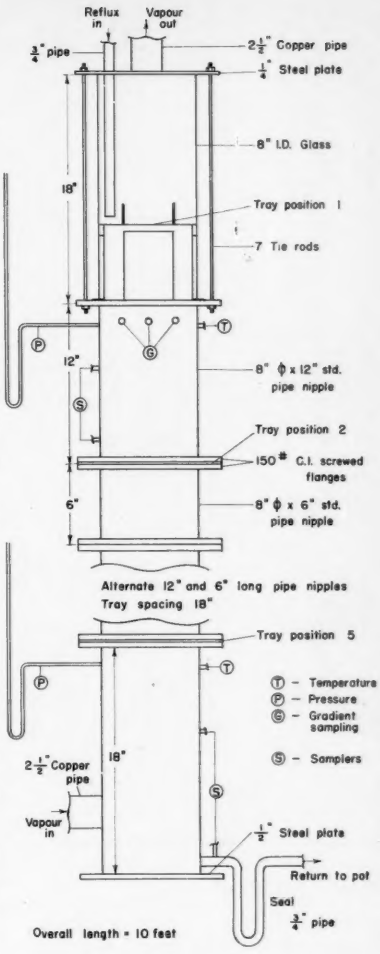

Fig. 2. Detail drawing of column.

DISCUSSION OF RESULTS

The column was operated at four vapor velocities, denoted on the graphs as series A, B, C, and D, ranging from 5.85 to 11.34 moles/hr. Data were taken on the three tray geometries. There was no entrainment at the highest velocity that could be detected by injecting dye on one of the intermediate trays and sampling the liquid from the tray above. Also there was no visible leakage from any of the tray types at the lowest velocity.

CONCENTRATION GRADIENTS

Table 2 shows some typical concentration gradients. In interpreting these measured concentrations, one should note that when vapor samples and samples are obtained from the foam, a slight amount of the undesirable phase may be sampled. This is more critical for the vapor than the liquid, since a small amount of entrained liquid could have a great effect on the measured concentration.

Vapor concentration gradients were evident for the runs where the total change in concentration across the tray was large. However the effect of these vapor gradients on tray performance must be small, since the same tray performs identically in positions 1 and 5 in the column; position 5 has of course a homogeneous vapor below it.

Examination of the liquid concentration gradients shows that in some runs the concentration of the liquid on the tray floor is lower than that of the liquid leaving the tray. Further, the concentration in the foam above the tray floor is always higher than on the floor. These data therefore suggest a vertical concentration gradient in the liquid worthy of further study.

It was felt that the trays in this column were too short to warrant any attempt to use the concentration gradients to study mixing theory.

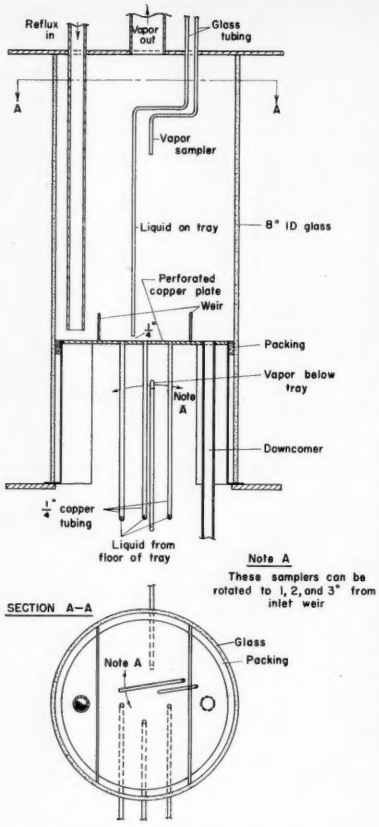

Fig. 3. Concentration-gradient sampling.

FOAM PROPERTIES

The volumetric gas holdup and clear liquid holdup on the tray are required for the calculation of contact time. Foam heights and pressure drops were measured at the four velocities and for the three tray geometries shown in Table 1. A typical plot of the data is shown in Figure 5. The scatter in the data is large at the low weir height used, and the two low-velocity curves A and B and the two high-velocity curves C and D cannot be separated. The foam pressure drop ΔP in centimeters of water is shown on the plots together with $\Delta P_f'$ in terms of the average liquid density on the tray.

The foam volume ratio is the ratio of clear liquid height to foam height. Although its accurate calculation is difficult because of the errors in measurement, a value of ϕ' is calculated by using Z_v and $\Delta P_f'$. Here ϕ' is proportional to ϕ provided that the difference between ΔP_f and the clear liquid head is constant (3, 22). Other effects such as the influence of interfacial tension have been neglected in the calculation of ϕ' in this paper.

The purpose of the foam study presented here was to determine the variation of foam density and foam height with gas rate, composition, and free area for the methanol-water system. The data are seen to support the assumption that the gas and liquid holdup do not vary significantly with composition for the system studied. Also ϕ is constant with varying gas velocity, but the foam height increases with increasing gas velocity. The effect of hole size is negligible. However for the tray with increased free area the foam density decreased, since the foam height was almost the same for all trays; β increased and ϵ decreased for this tray.

In a separate study Price (30) has reported increasing value of ϕ' as the weir height was increased.

It is recognized that these conclusions are debatable because of the scatter of the data. However they are also supported by other data in the literature (4, 27) (taken from nonboiling trays) with the notable exception of the data of Gerster and Foss (17). These latter authors reported decreasing ϕ values with increasing gas velocity, but it is not clear whether or not the effects of free-area change have been eliminated.

While the ϕ values calculated in this study are not sufficiently accurate to resolve controversies regarding the factors influencing them, it is believed that final values of β/U shown on Figure 11, which depend on the ϕ values, are accurate to $\pm$ 0.01.

TRAY-PERFORMANCE DATA AT TOTAL REFLUX

Because the calculation of efficiencies from experimental data magnifies errors, the authors would like to discuss their treatment of the data in detail. It should be noted that at total reflux the concentration of liquid leaving a tray is the same as the vapor entering it. It is postulated that the concentration change across a tray will be a unique, continuous function of the average concentration of the liquid on the plate. Therefore the experimental data were plotted as $Y_{off} - Y_{on}$ against the arithmetic average concentration Y_{avg}.

Here Y_{off} and Y_{on} are the average mole fractions of more volatile in the vapor leaving or entering a tray and are obtained from the liquid samples, since the column is operated at total reflux.

An average curved line was drawn through the data on such plots, as illustrated in Figure 6. Efficiencies were then calculated from those smoothed curves for all further calculations.

These curves were drawn for all plates for all vapor velocities. Complete data are given in reference 19. The method described above was then applied for each geometry and velocity with a standard state of 60 mole % methanol used. This reference concentration was chosen because $1/N_a$ was

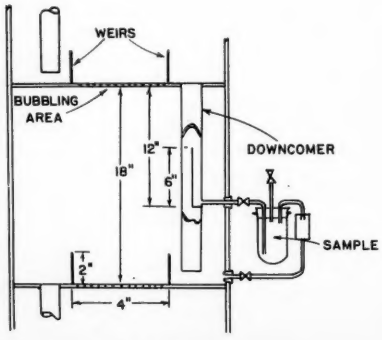

Fig. 4. Sketch of tray and sampler.

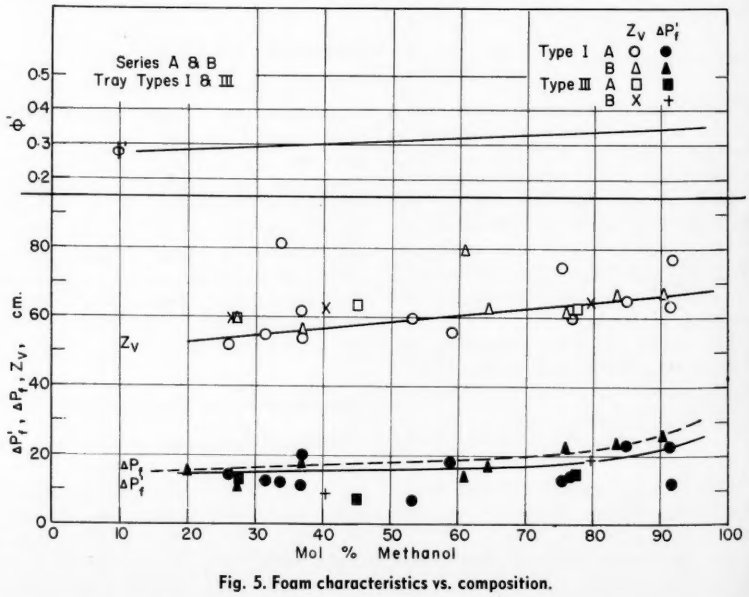

Fig. 5. Foam characteristics vs. composition.

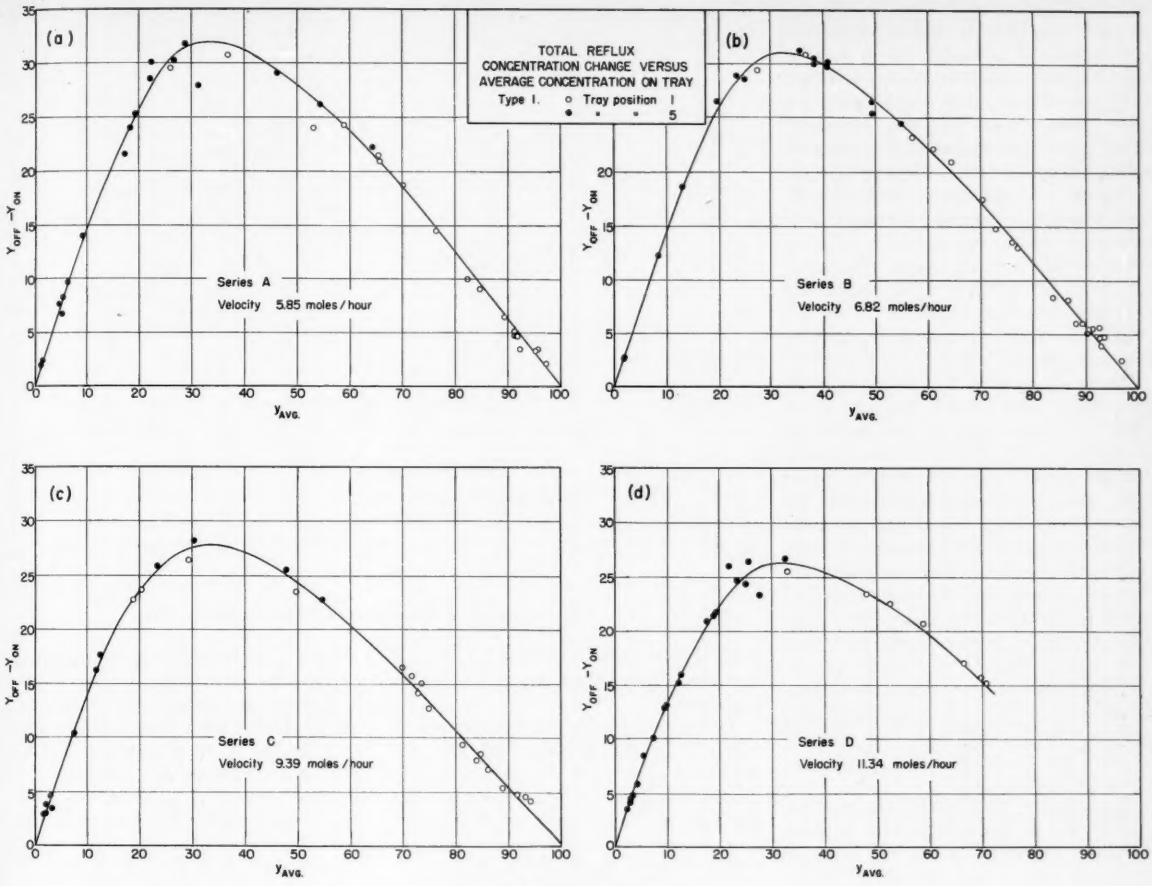

Fig. 6. Tray performance.

practically as large and $1/N_L$ was larger than at any other concentration.

The method of calculation uses the following steps:

(a) Using the smoothed data for average vapor compositions at 10, 20 . . . . 80 mole % calculate Y_{off} and Y_{on}. For example if $(Y_{off}+Y_{on})/2 = 10.0$ mole % and the corresponding $Y_{off}-Y_{on} = 15$ mole %, then $Y_{on} = 2.5$ mole % and $Y_{off} = 17.5$ mole %. Since the column is operated at total reflux, $X_{off} = Y_{on} = 2.5$ mole % and $Y_{x_{off}}{}^{*} = 17.0$ mole % from the equilibrium diagram for methanol-water.

(b) In order to find m_G and m_L for each composition, the corresponding values of x_i and y_i must be found as described above. Assumed values at the reference concentration, for example $N_L/N_{G\,\infty} = 3.0$, are taken, and N_L/N_G for the other compositions are calculated with the A and B factors defined basically in equations but modified as discussed in the following paragraphs.

The A.I.Ch.E. group report the effect of physical properties on N_G of

$$N_G = N_{G\,\infty}\frac{(D_v^{0.5}T\,\rho_G^{0.13}t_G)}{(D_v^{0.5}T\,\rho_G^{0.13}t_G)_\infty} \quad (12)$$

From measurements of ϕ reported previously, it appears that t_G is not a function of composition. Furthermore the effect of density is seen to be small, and the effect of viscosity (although not yet reported by the A.I.Ch.E. group) would be expected to vary inversely with density. Therefore for the system methanol-water

$$B = \left(\frac{T_\infty}{T}\right)^{1.75} \quad (13)$$

The A factor is calculated from Equation (3). The exact proportionality between k_L and D_v is not known for a foaming tray but here has been taken to be proportional to $N_{Sc}^{-0.5}$, primarily following the work of Danckwerts (*10*). The inclusion of ρ_L and μ_L in the Schmidt number is an assumption. It would be expected that a_L would be independent of composition, and in this work ϵ was found to be similarly independent. The volumetric flow rate is not constant but is inversely proportional to ρ_{ML}. From these arguments A is defined for the system methanol-water as

$$A = \left(\frac{\mu_L D_L}{\rho_{ML}}\right)_\infty^{0.5}\left(\frac{\rho_{ML}}{D_L\mu_L}\right)^{0.5}\frac{\rho_{ML\,\infty}}{\rho_{ML}} \quad (14)$$

The A and B correction factors are shown in Figure 7.

With the smoothed data (for example Figure 6) used, the calculations were made for the average tray compositions, at increments of 10% from 10 to 80 mole % methanol. Compositions below and above these values were not used because the concentration differences are so small and/or the slope of the equilibrium curve is so large that there is an undesirable magnification of errors.

(c) By means of the over-all concentration change and the smoothed data E_{MV}, E_{ML}, and m_T are calculated. Then N_{OG}', $1/N_{OG}'B$, N_{OL}', and $1/N_{OL}'A$ are calculated for each of the three special cases for the gas-phase driving force and for the two special cases for the liquid-phase driving force. Figures 8 and 9 show the plots of these curves and the extrapolations to $1/N_{G\,\infty}$ and $1/N_{L\,\infty}$ for these operating conditions. It should be noted that the $N_{L\,\infty}/N_{G\,\infty}$ calculated from these extrapolations must check the original assumption.

Now with $N_{G\,\infty}$ and $N_{L\,\infty}$ known, N_G and N_L at other compositions may be calculated by the use of B or A factors. In turn the point efficiency may be

calculated by combining these individual-phase transfer units by means of Equations (1) and (6). The values of E_{MV} and the calculated E_{OV} are shown in Figure 10 together with curves for other velocities for this tray geometry. This figure demonstrates the effect of the liquid gradients on the tray on E_{MV}.

Figure 10 indicates several interesting effects of changing methanol concentration upon E_{OV} and E_{MV}. E_{OV} is seen to decrease at lower concentration. This is believed to be caused by the corresponding increase in m_G resulting in the liquid-phase resistance becoming appreciable.

At the same time E_{MV} increases with decreasing methanol concentration. This is believed to be the result of increasing the liquid concentration change across a given tray at these lower concentrations. Thus it could be expected that this increased concentration change would increase the concentration gradient, decreasing the effects of mixing and therefore increasing E_{MV}. Presumably if reliable data were available at concentrations lower than those shown on Figure 10, it could be shown that E_{MV} approaches E_{OG} as the methanol concentration approaches zero and the liquid concentration change across the plate approaches zero.

It is obvious that the liquid concentration change across the tray is governed by the shape of the equilibrium curve for total reflux operations. Thus the plot of E_{MV} against concentration for any system under total reflux condition is dependent upon the shape of the equilibrium curve.

It is obvious from Figure 9 that the extrapolation to $1/N_{LS}$ is questionable because of the difficulty of extrapolation and because the actual degree of mixing is unknown. However $1/N_L$ is small and is significant only at high values of m_G. In this work the extrapolation of Equation (8) was used for N_L because, for the system used, increasing m_L in general corresponds to increasing values of $Y_{on} - Y_{off}$, and therefore the tray performance is approaching that for no liquid mixing. At the same time the extrapolation of $1/N_L$ is not considered sufficiently accurate to attempt a more fundamental analysis of N_L such as will be considered for N_G.

THE EFFECT OF GAS VELOCITY ON N_G

When one follows the mass transfer theory outlined above, the N_G values can be treated further. From the definition of N_G it is apparent that N_G is not a function of liquid rate, provided that β does not vary with liquid rate. The effect of liquid rate on Z_v has been shown to be very small (*1*), and therefore little effect on β would be expected.

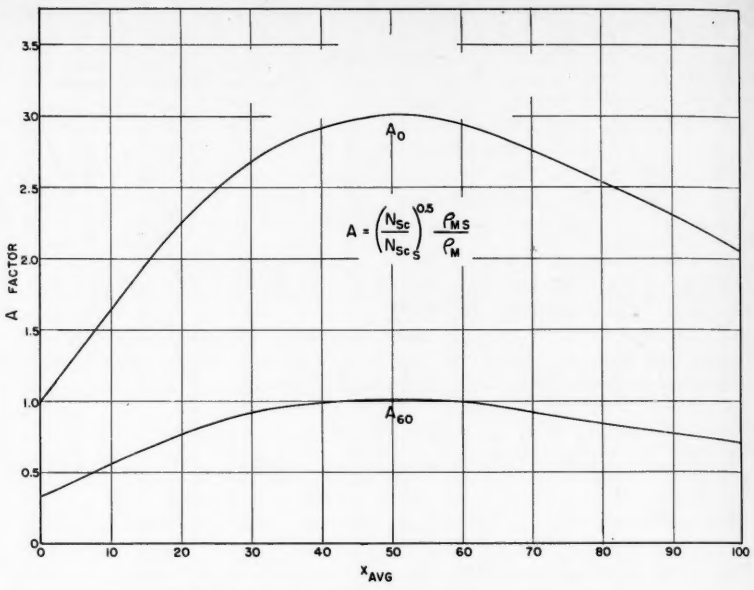

Fig. 7*a*. *A* factor vs. liquid composition for methanol-water.

Theoretically if the assumptions outlined in the introduction are applicable, a plot of N_G against β/U should yield a straight line passing through the origin with slope $k_G'a_G$, if $k_G'a_G$ is not a function of gas velocity. Such a plot is presented in Figure 11 for a bulk composition of vapor and liquid of 60 mole % methanol. Also included on the plot are the data of Price (*30*) for 3- and 4-in. weirs with the same apparatus, system, and calculation methods.

Some care must be taken in drawing conclusions from such a plot since it is difficult to measure β/U with accuracy. It has been shown that a given weir height ϕ is practically constant with gas velocity, and therefore the time of contact is proportional to Z_v. The foam height does increase with gas velocity, and therefore the time of contact does not decrease proportionately with increasing gas rate.

A DISCUSSION OF TIME OF CONTACT

It is evident that the effect on N_G of vapor velocity depends to a large ex-

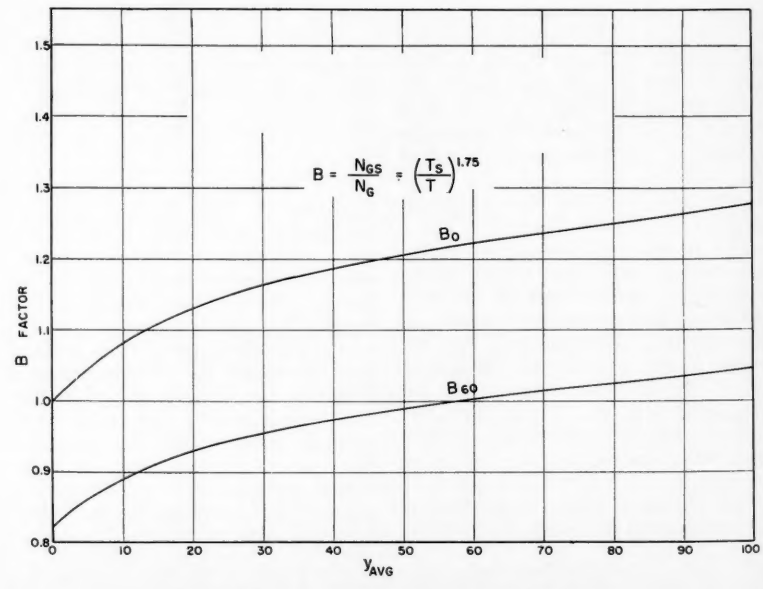

Fig. 7*b*. *B* factor vs. vapor composition for methanol-water.

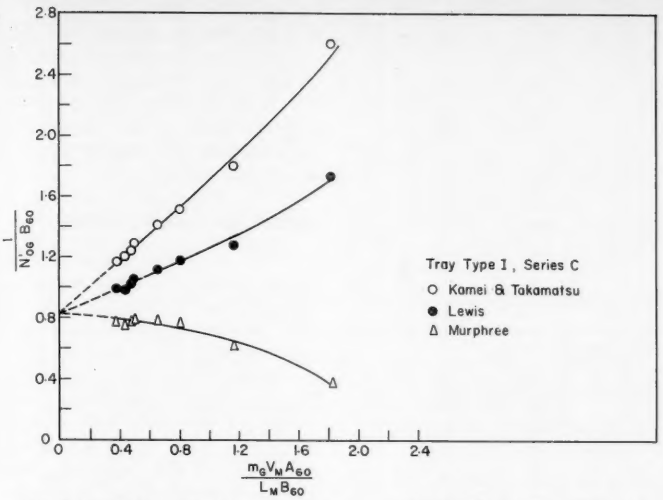

Fig. 8. Extrapolation to $(1/N_G)_{\infty}$, reference concentration 60 mole % methanol.

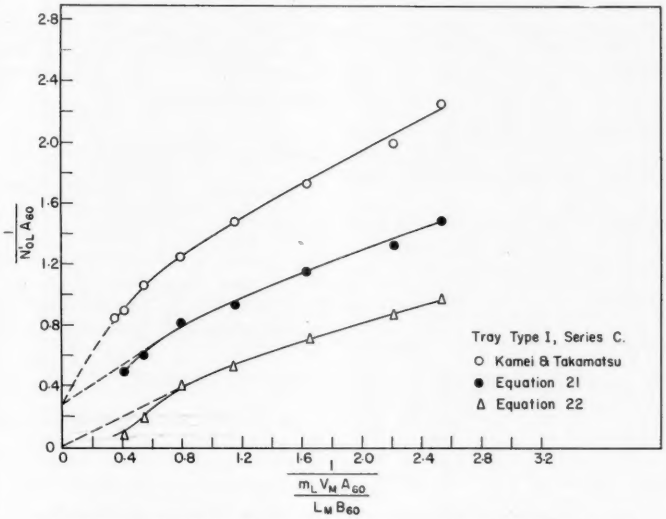

Fig. 9. Extrapolation to $(1/N_L)_{\infty}$, reference concentration 60 mole % methanol.

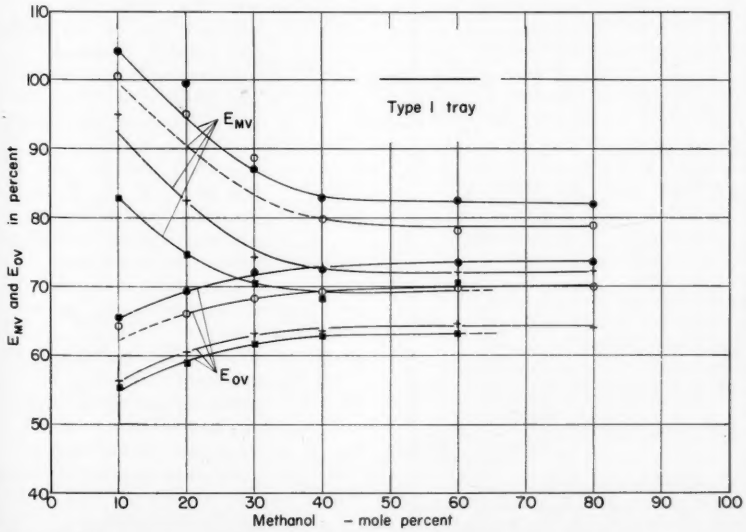

Fig. 10. Efficiency vs. composition, calculated E_{MV} and E_{OV} from smoothed data. • series A, o series B, + series C, ■ series D.

tent on the definition of the time of contact for which several relationships have been proposed. Geddes (*14*) suggested that bubbles rose through the foam at the terminal velocity of a freely rising bubble, and therefore the time of contact would be independent of vapor velocity. Several investigators (*7*, *12*) have supported this idea, but the data were taken on bubble-plate trays in which there might be relatively little interference between bubbles from adjacent slots.

Stone (*33*) has proposed that the bubbles actually push each other through the foam at a velocity proportional to the superficial gas velocity, and therefore the time of contact is proportional to Z_v/U. Using both bubble-cap and sieve trays operating at high gas velocity, he found support for this relationship. Anderson's data (*2*) on sieve trays also supported Stone's mechanism for weir heights of 2 in. In this paper the contact time proposed by Gerster is used:

$$t_G = \frac{\beta}{U} = (1-\phi)\frac{Z_v}{U} \qquad (15)$$

Except for the obvious difficulty of measuring ϕ at low seals, it provides an accurate definition of t_G over the range of interest.

t_G having been defined in this manner, the data reported here shows that $k_G' a_G$ is a function of tray geometry but not of gas velocity. This is different from the results of the A.I.Ch.E. group (*1*), which used bubble trays where $k_G' a_G$ is a function of gas velocity up to a limiting value. It is suggested here that the latter effect is due to increasing a_G; with increasing gas velocity the bubbles tend to break up until they reach a minimum average size at the limiting velocity. As a part of this study Price (*30*) has found that ϕ varies with weir height, and therefore the time of contact is not proportional to Z_v/U if a number of weir heights are to be considered. However on Figure 11 this effect does not appear when time of contact is defined as β/U; for each tray geometry a straight line through the origin is seen to represent the data adequately.

THE EFFECT OF TRAY GEOMETRY

The effect of tray geometry is reflected by the slopes of the lines on Figure 11. Type I trays have larger $k_G' a_G$ values than the other two types, but types II and III have almost indistinguishable slopes.

The experimental evidence that is available to support any explanation of mass transfer within the foam is restricted to foam density and foam heights, both of which are difficult to measure exactly. These data do not

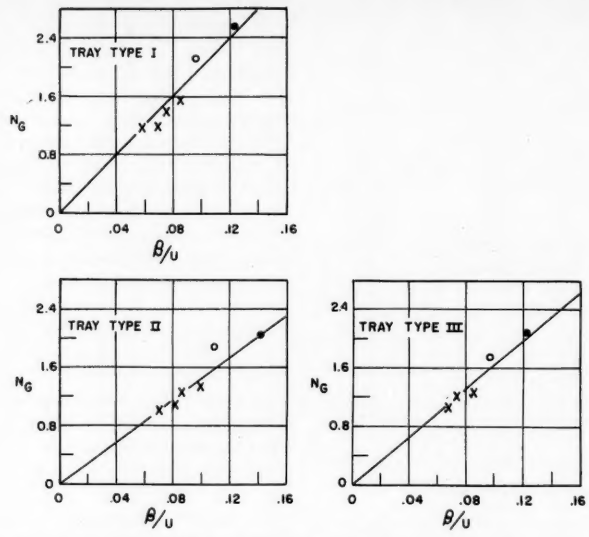

Fig. 11. Number of gas phase transfer units vs. time of contact. • 4-in. weirs, o 3-in. weirs, x 2-in. weirs.

indicate changes in interfacial area, since the number and size of bubbles could be changing without affecting foam density. The bubble shape also changes, but the assumption of essentially spherical bubbles is generally made to affect some simplification; photographic studies have indicated that this is reasonable (*11*).

The performance of type I and type III trays which have the same free area can be compared to indicate the effect of hole size. The foam density is seen to be constant for both trays, and $k_G' a_G$ decreases with increasing hole size. This decrease is believed to be due primarily to a decrease in a_G with increasing hole size rather than a decrease in the turbulence and therefore a decrease in k_G'.

With type II tray the free area was increased. It is possible that the time of contact was increased while $k_G' a_G$ was decreased.

END EFFECTS

Work with single bubbles (*9, 18, 31*) and the study of Anderson (*2*) have shown that k_G is probably higher at formation than during bubble rise. Anderson has noted that this effect is not apparent at higher seals, since the bubble a_G at formation is smaller than in the foam, probably owing to bubble breakup. The data on Figure 11 and the work of the A.I.Ch.E. group (*1*) support the assumption that end effects are small.

EFFECT OF REFLUX RATIO

A few runs were made at reflux conditions other than total reflux and are reported on Figure 12. For a given tray geometry and change in liquid concentration E_{MV} was found to be practically independent of reflux ratio. It was found empirically that less scatter of the data was obtained by using Y_{avg} than using X_{avg} in plotting the points on this graph, Y_{avg} and X_{avg} no longer being equal as for the total reflux runs. It is recommended that the point efficiency be calculated as for a total reflux run and that the appropriate mixing Equation (*24, 26*) be used to yield E_{MV} for a tray under any operating condition.

CONCLUDING REMARKS

This paper has provided new efficiency data for the operation of sieve plates in an 8-in.–diameter column on the system methanol-water. It is believed that the values of N_G are the first reported in the literature for a tray in distillation operation.

ACKNOWLEDGMENT

The authors would like to acknowledge the work of Price (*30*), who checked some of the original data and carried out the investigation of 3-and 4-in. weir heights.

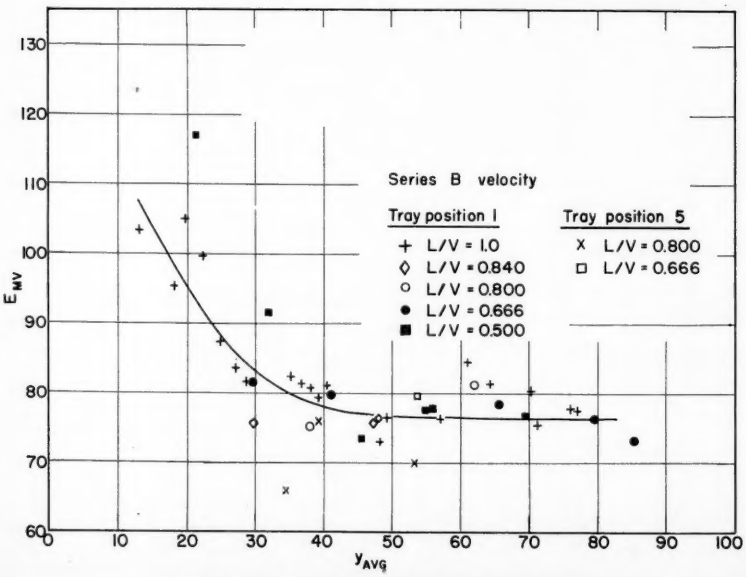

Fig. 12. E_{MV} vs. vapor composition for various L_M/V_M.

NOTATION

A = correction factor for N_L to standard set of conditions (60 mole % methanol)
a = interfacial area per unit volume of foam, sq. ft./cu. ft.
a_G = interfacial area per unit volume of vapor, sq. ft./cu. ft.
a_L = interfacial area per unit volume of liquid, sq. ft./cu. ft.
B = correction factor for N_G to standard set of conditions (60 mole % methanol)
b = constant
c = concentration, lb. moles/cu. ft.
D_L = diffusivity in the liquid, sq. cm./sec.
D_V = diffusivity in the vapor, sq. cm./sec.
E_{MV} = Murphree plate efficiency based on vapor driving force
E_{ML} = plate efficiency based on liquid driving force
E_{OV} = point or local efficiency based on vapor driving force

K_G = over-all mass transfer coefficient based on vapor driving force, lb.moles/(sq.ft.)(sec.)(atm.)

K_L = over-all mass transfer coefficient based on liquid driving force, lb. moles/(sec.)(sq. ft.)(lb. mole/cu.ft.)

k_G = individual gas-phase mass transfer coefficient, lb.moles/(sec.)(sq.ft.)(atm.)

k_G' = $k_G P/\rho_{MG}$ or $k_G RT$, ft./sec.

k_L = individual liquid-phase mass transfer coefficients, lb. moles/(sec.) (sq. ft.) (lb. mole/cu. ft.)

L_M = liquid molar flow, moles/sec.

L_{OY} = length of over-all gas phase transfer exit, ft.

M = molecular weight

m = slope of equilibrium line

m_G = slope of equilibrium line with calculations based on vapor driving force defined by Equation (15)

m_L = slope of equilibrium line with calculations based on liquid driving force defined by Equation (15)

m_T = slope of equilibrium line defined by Lewis to relate point and plate efficiencies on a tray

m_T' = slope of equilibrium line defined by Kamei and Takamatsu to relate N_{OG} and E_{MV} on a plate

N_G = number of individual vapor-phase mass transfer units = $\dfrac{k_G P a Z_V}{\rho_{MG} U} = k_G RT a_G \dfrac{\beta}{U} = k_G' a t_G$

N_L = number of individual liquid-phase mass transfer units = $k_L a\, \epsilon/q = k_L a_L t_L$

N_{OG} = number of over-all gas-phase mass transfer units = $K_G P a Z_V/\rho_{MG} U$

N_{OL} = number of over-all liquid-phase mass transfer units = $K_L \rho_{ML} a Z_V/L_M$

N_{SC} = Schmidt number $\mu_L/D_L\rho_L$

P = pressure, atm.

q = total volumetric flow of liquid across tray, cu. ft./sec.

T = absolute temperature

t_e = time of contact in general solution of unsteady state diffusion equation applied to liquid at interface of a bubble, sec.

t_G = time of contact of vapor with liquid on tray, sec.

t_L = time of contact of liquid with vapor on tray

U = linear velocity of vapor within the column based on the bubbling area, ft./sec.

V_M = molar vapor flow, moles/sec.

X = average mole fraction more volatile in the liquid entering or leaving the tray

x = mole fraction more volatile in the liquid at a particular point on the tray

Y = average mole fraction more volatile in vapor entering or leaving the tray

y = mole fraction more volatile in vapor at a particular point on the tray

Z_e = height of foam, ft.

Greek Letters

β = volumetric holdup of vapor in foam, cu. ft./sq. ft. of tray bubbling area

ϵ = total volumetric holdup of liquid on tray, cu. ft.

$\Delta P_f'$ = pressure drop through foam on tray corresponding to clear liquid head, cm. of liquid on tray

ΔP_f = total pressure drop through the tray cm. of water

ΔP_R = difference of pressure drop through foam and clear liquid head on tray

ρ = density, lb./cu. ft.

ρ_M = molar density, lb. moles/cu. ft.

ϕ = volume fraction of clear liquid on tray, cu. ft. of liquid/cu. ft. of foam

ϕ' = $\Delta P_f'/Z_V$

μ = viscosity of liquid

Subscripts

G = gas or vapor phase

i = concentrations at the interface

L = liquid phase

M = quantities on molar basis

on, off = compositions entering or leaving tray respectively

S = standard or reference concentration to which N_G and N_L at other concentrations and physical properties are corrected

$X_{on}, X_{off}, Y_{on}, Y_{off}$ = material to which the equilibrium refers; $Y^*_{X_{on}}$ = the mole fraction more volatile in a hypothetical vapor in equilibrium with the liquid entering the tray, used with superscript *

Superscript

* = phrase *mole fraction more volatile in a hypothetical liquid in equilibrium with;* material with which equilibrium occurs is denoted by the subscript

LITERATURE CITED

1. "Tray Efficiencies in Distillation Columns," Third Annual Progress Report, American Institute of Chemical Engineers (1955).
2. Anderson, J. E., Sc.D thesis, Mass. Inst. Technol., Cambridge (1954).
3. Arnold, D. S., C. A. Planck, and E. M. Schoenborn, *Chem. Eng. Progr.*, **48**, 633 (1952).
4. Bagnoli, E., thesis, Univ. Del., Newark (1950).
5. Bakowski, S., *Chem. Eng. Sci.*, **1**, 266 (1952).
6. Calderbank, P. H., *Trans. Inst. Chem. Engrs. (London)*, **34**, 31 (1956).
7. Carey, J. S., J. Griswold, W. K. Lewis, and W. H. McAdams, *Trans. Am. Inst. Chem. Engrs.*, **30**, 504 (1934).
8. Chilton, T. H., and A. P. Colburn, *Ind. Eng. Chem.*, **27**, 255 (1935).
9. Chu, J. C., John Forgrieve, and G. C. Papacosta, paper presented at A.I.Ch.E. meeting, St. Louis (1953).
10. Danckwerts, P. V., *Ind. Eng. Chem.*, **43**, 1460 (1951).
11. Furter, W. F., M.Sc. thesis, Mass. Inst. Technol., Cambridge (1955).
12. Cadwa, J. A., Sc.D. thesis, Mass. Inst. Technol., Cambridge (1936).
13. Garner, F. H., S. R. M. Ellis, and A. J. Hugill, *Trans. Inst. Chem. Engrs. (London)*, **31**, 13 (1953).
14. Geddes, R. L., *Trans. Am. Inst. Chem. Engrs.*, **42**, 79 (1946).
15. Gerster, J. A., A. P. Colburn, W. E. Bonnet, and T. W. Carmody, *Chem. Eng. Progr.*, **45**, 716 (1949).
16. Gerster, J. A., W. E. Bonnet, and Irwin Hess, *ibid.*, **47**, 523, 621 (1951).
17. Gerster, J. A. and A. S. Foss, *ibid.*, **52**, 28-J (1956).
18. Grossman, U., *Chem.-Ingr. Tech.*, **28**, 109 (1956).
19. Hay, J. M., Ph.D. thesis, Univ. Toronto, Canada (1957).
20. ———, film taken at Univ. Toronto, Canada.
21. Higbie, Ralph, *Trans. Am. Inst. Chem. Engrs.*, **31**, 365 (1935).
22. Hunt, Charles, D. N. Hanson, and C. R. Wilke, *A.I.Ch.E. Journal*, **1**, 441 (1955).
23. Kamei, S., and T. Takamatsu, *Mem. Fac. Eng. Kyoto Univ.*, **15**, No. 11 (1953).
24. Lewis, W. K., Jr., *Ind. Eng. Chem.*, **28**, 399 (1936).
25. ———, and W. G. Whitman, *ibid.*, **16**, 1215 (1924).
26. Marangozis, J., M.A.Sc. thesis, Univ. Toronto, Canada (1956).
27. Mayfield, F. D., W. L. Church, Jr., A. A. Green, D. C. J. Lee, and R. W. Rosmussena, *Ind. Eng. Chem.*, **44**, 2238 (1952).
28. Murphree, E. V., *ibid.*, **17**, 747 (1925).
29. Peavy, C. C., and E. M. Baker, *ibid.*, **29**, 1056 (1937).
30. Price, D., M.A.Sc. thesis, Univ. Toronto, Canada (1958).
31. Sherwood, T. K., and R. L. Pigford, "Absorption and Extraction," McGraw-Hill, New York (1952).
32. Stone, H. L., Sc.D. thesis, Mass. Inst. Technol., Cambridge (1953).
33. Watson, C. C., and E. D. Oliver, *A.I.Ch.E. Journal*, **2**, 18 (1956).

Manuscript received October 9, 1958; revision received November 10, 1958; paper accepted November 12, 1958.

Comparison of the Specific Resistances of Cakes Formed in Filters and Centrifuges

V. V. VALLEROY and J. O. MALONEY

University of Kansas, Lawrence, Kansas

Resistances to the flow of fluids through porous beds were determined in a compression-permeability cell, a vacuum test filter, and an experimental centrifugal filter. The study was made on nearly incompressible beds composed of Lucite spheres having a given size distribution. The results show that liquid flow through the cakes in all three kinds of equipment can be described by a common basic equation, the terms of which are modified to reflect the type of operation. The centrifugal-drainage data confirm the form of the centrifugal-filtration equation. The specific resistances deduced from vacuum-filtration and centrifugal-drainage tests agree with permeability-cell alphas within 16% at the same ΔP and within 2 to 3% at the same porosity.

The development of the principles and the experimental techniques for investigating filtration and centrifugal filtration in the last decade has encouraged studies of the two separate operations as a single one. Storrow and his co-workers (5) showed experimentally that the same type of equations applies to both types of filtration. Grace (4) demonstrated in several cases that there was a reasonably close agreement between the specific resistance measured in filtration and that measured in centrifugation apparatus. The objective of this work was to study further the degree of agreement which could be obtained between the specific resistances measured in permeability cells, in vacuum filters, and in a centrifuge. Also the authors wished to compare their results with those predicted from the Kozeny-Carman equation.

Centrifugal filtration is basically an operation in which a centrifugal-force field is substituted for the pressure-driving force encountered in normal pressure or vacuum filtration. There are, however, a number of differences, and these have been pointed out by workers in the field who have proposed equations to describe the operation.

Maloney (8) in the first of his annual reviews of centrifugation suggested that an analytical relationship for centrifugal filtration could be developed by extending the filtration equations to the centrifugal operation. Starting with the basic differential equation

$$\frac{dV}{d\theta} = \frac{A\,\Delta P\,g_c}{\mu\left[\dfrac{\alpha w V}{A} + R_m\right]} = \frac{A\,\Delta P\,g_c}{\mu\left[\dfrac{\alpha_v c V}{A} + R_m\right]} \qquad (1)$$

and neglecting the resistance associated with the filter septum, he proposed essentially this expression:

$$\frac{dV}{d\theta} = \frac{A_{avg}^2\,(\Delta P)_L\,g_c}{\mu\,\alpha_v c V} \qquad (2)$$

Storrow and co-workers (1, 5, 6, 7) developed and employed an equation which they wrote as

$$Q = \frac{K_s\,2\pi h}{g\,\mu \ln \dfrac{r_o}{r_c}}\left[\frac{1}{2}(2\pi N)^2\,(r_o^2 - r_i^2)\right] \qquad (3)$$

but which is equivalent to

$$\frac{dV}{d\theta} = \frac{A_{avg}\,A_{lm}\,(\Delta P)_L g_c}{\mu\,c\,V}\,\frac{K_s}{\rho_L g} \qquad (4)$$

Other than characterizing the bed by a permeability expression $K_s/\rho_L g$ instead of a specific resistance, Storrow's equation differs from Equation (2) only in the use of the product $A_{avg}\,A_{lm}$ instead of A_{avg}^2.

When the ratio $r_o/r_c = 2$, A_{avg} will be about 4% higher than A_{lm}, and when the ratio $r_o/r_c = 1.5$, A_{avg} is only 1.2% higher than A_{lm}. Therefore Equations (2) and (4) will give essentially the same answers for all cases except those of thick cakes in small-diameter machines.

Storrow and Haruni (6) confirmed the form of the equations and found satisfactory agreement in their tests of the Q, N^2, and $(r_o^2 - r_L^2)$ relationships. They varied the viscosity from 1 to 3 centipoises and used both 9- and 18-in. -diameter centrifuge baskets. Although these authors concluded that the cake layer next to the cloth offers a much higher resistance than the layers subsequently laid down, they did not include a separate term for the initial resistance.

Grace (4) developed rigorously the basic rate equation for centrifugal filtration. But the solution for the general case is not possible, since the point specific resistance and point porosity are not known as a function of basket radius. The average specific resistance cannot be computed directly from compression-permeability data alone as is possible for most pressure filtrations.

For the special case of a nearly incompressible cake and in the absence of kinetic-energy effects, Grace's general equation simplifies to

$$\frac{dV}{d\theta} = \frac{(\Delta P)_L\,g_c}{\mu\left[\dfrac{\alpha w V}{A_{lm}\,A_{avg}} + \dfrac{R_m}{A_o}\right]} \qquad (5)$$

The equation thus takes the initial resistance into account and associates A_o with it. The area-squared factor entering the cake-resistance term is made up of the product of the log mean area and the arithmetic mean area.

Grace's equation is seen to be similar to Storrow's except for the inclusion of the initial resistance term. The only additional difference from Equation (2) is the use of the log mean area as one of the factors in the A^2 term, this point having been discussed previously.

Grace obtained data on the flow rate of water through cakes of various thicknesses deposited in a laboratory centrifuge. In some of his runs he encountered difficulties with filter cakes developing cracks.; in other runs he apparently found good agreement (within 10%) for diatomaceous earth between centrifugal- and pressure-filtration average specific resistances and with permeability-cell data. Most unexpectedly Grace also found agreement within 25% for semicompressible cakes of cellulose and carbon filter aids and of titanium dioxide powder. Grace thought that the materials and the

V. V. Valleroy is with Jersey Production Research Company, Tulsa, Oklahoma.

method of testing may have allowed the expected discrepancies to be masked by the scatter of the experimental points. While recognizing the significant contributions made by Grace one should, because of the uncertainties mentioned, have further confirmation and comparison of the resistances of porous beds composed of spherical particles to liquid flow.

EXPERIMENTAL PROCEDURE

All the studies in this work were carried out on porous beds or filter cakes composed of Lucite spheres. Lucite 4F molding powder was used, as the particles have a remarkably uniform spherical shape which avoids the difficulties of trying to characterize a mixture of various shapes. For comparison purposes it also has the advantage of having a value of unity for the sphericity. The Lucite particles are solid and physically and chemically inert in water, neither softening nor swelling in it. Lucite 4F, however, is soluble in acetone, ethylene dichloride, and toluene, and these solvents may be used for removing embedded particles from screens and filter cloths. Owing to a specific gravity of only 1.18 the difficulty of maintaining Lucite particles in suspension prior to filtration is minimized.

A single size distribution of Lucite spheres was used in all experiments. The specific surface determined from microscopic counts was 890 sq. cm./cc. Half of the particles were below 40 μ in diameter.

The Lucite particles would not disperse in tap or distilled water. The contact angle between distilled water and a Lucite surface was measured as about 64 deg. by the shadowgraph technique. The addition of small amounts of certain wetting agents would, however, cause the particles to disperse readily. In effectiveness Dreft appeared equal to or better than any of the other surfactants tested, and a 0.05 wt. % solution of Dreft in water was used in making up the slurries from which the Lucite cakes were deposited. The 0.05% concentration was chosen because the surface-tension–concentration curve in this region was almost flat, the surface tension therefore being unaffected by small variations in Dreft concentration. Neither the density nor the viscosity of water was measurably altered by Dreft at this concentration.

Description of the Permeability Cell

The point porosity and specific resistance of a cake as a function of compressive stress can be determined most conveniently in a compression-permeability cell. This device allows a mechanical stress to be placed on a porous bed independently of the fluid head. The pressure drop caused by fluid flow can be made very small compared with the compressive stress which is imposed uniformly over the solid matrix of the cake.

A diagram of the compression-permeability cell is shown in Figure 1. and is similar to the one described by Grace (*4*). The brass cylinder in which the cakes

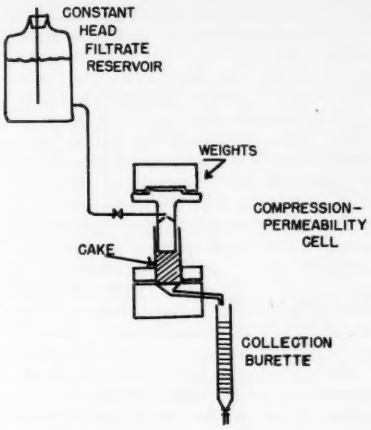

Fig. 1. Diagram of permeability-cell arrangement.

were deposited had an internal diameter of 1.133 in., and the sintered stainless steel disks between which the cake was confined were 0.185 in. thick.

In operation mechanical pressure was applied to the filter cake by loading the piston with calibrated weights. Filtrate flowed from a constant-head reservoir into the hollow piston, through the porous piston end plate and fllter paper, down through the filter cake, and thence through the bottom paper and drain plate into the drainage base. Movement of the piston was measured by a dial guage clamped to the cylinder and fitted against the piston flange. The flow rate at each value of compressive stress was found by timing with a stop watch the accumulation of a volume interval of filtrate in the collection burette.

The Lucite cakes of 6.65 g. each were deposited from 10% by weight suspensions of Lucite spheres in a 0.05 wt. % Dreft solution. A vacuum of 1 in. Hg was applied under the bottom disk to increase the rate of deposition so as to minimize the effects of differential settling. Addition filtrate added to the cylinder during the deposition of the cake kept the cake surface from becoming dry. It is of utmost importance in all studies, such as the ones described in this work, that the cake never be allowed to become dry. If it does, certain portions of the cake become airbound and the specific resistance changes.

The initial thickness and volume of the porous bed were found from micrometer measurements of the distance between piston and cylinder flanges. The filtrate prior to being placed in the reservoir was filtered through the same kind of filter paper as was used to confine the cake in the cell.

The first measurements were taken with only the weight of the piston to provide the compressive stress, the value being 3.28 lb./sq. in. After the first set of measurements a solid brass cylinder of known weight was placed on top of the piston to provide the compressive stress under which the next point was to be determined. Generally all the descent of the piston occurred within several minutes after the addition of the weight to the piston, but 15 to 20 min. was allowed between each set of measurements. Micrometer measurements between the piston and cylinder flanges were made often during a run, and they were always in good agreement with heights indicated by dial-gauge readings and initial height.

Description of the Vacuum Filter

The behavior of this Lucite-water system during filtration was established through tests with a small vacuum filter. Trials were made with other kinds of test filters, both pressure and vacuum types, but operation was not so satisfactory or convenient as with the vacuum filter shown in Figure 2.

The filter cell was made up of a cell body, a screen support ring which fit into the cell and upon which the stainless screen rested, and a sleeve which formed the cake space. The inside diameter of the sleeve was 1.065 in. and its length 2-9/64 in. Other than the screen all parts were machined from brass. A short length of standard ¼-in. galvanized pipe was screwed into the bottom of the cell body and served to transfer the filtrate to the ½-in. polyethylene delivery tubing. This line was made as large as convenience would allow, thereby making line pressure drop negligible.

The test filter was immersed in a Lucite-Dreft-water slurry, and in constant ΔP tests cakes about 1½ in. in diameter were deposited by applying vacua ranging from 6.4 to 24 in. Hg. The general arrangement of the filtration-test equipment is shown in the line diagram of Figure 2.

All water used in the vacuum-filtration runs was deaerated and boiled under 28 in. Hg vacuum before the slurry was made up. Weighed amounts of Lucite and Dreft were added to give a solids concentration of about 2% in a 0.05 wt. % Dreft solution.

In operation the filter cell and the filtrate delivery line were filled with distilled water first, and then the filter cell was immersed in the slurry facing upward. During filtration simultaneous readings of filtrate level and time were taken every 10 sec. After the cake had reached a thickness of approximately 1½ in. the run was concluded by raising the test filter out of the slurry, thus draining the filtrate line and dewatering the cake.

After a run the cake-containing sleeve was removed from the filter body by gently turning the sleeve. The cake was expelled with a flat plunger from the sleeve onto a weighed watch glass. The exact concentration of the slurry was computed from the weight of the dry cake and the volume (corrected) of the filtrate. The surfaces of the filter cakes at the end of the tests were always flat, and after dewatering the cakes were quite compact. Essentially complete recovery of the cakes was obtained. The only loss of cake consisted of those solids that remained embedded in the filter cloth after it had been scraped with a spatula.

A series of runs was made as rapidly as possible to minimize the amount of air dissolving in the slurry, and the runs were made in the order of decreasing pressure differences.

Different filter cloths were used in each run of a series, but the same set of cloths was used in successive series. These cloths were cut from preshrunk cotton drill. They were washed with Dreft solution and rinsed between runs but were not treated with toluene to dissolve out embedded Lucite spheres. Satisfactorily reproducible results for the value of the filter-cloth resistance were obtained without using the toluene wash.

Centrifugal-Filtration Equipment

The experimental centrifuge used in this portion of the work was a 12-in. diameter basket mounted on a horizontal shaft and driven by a variable-speed transmission coupled to an electric motor. Mounting a basket horizontally along its axis eliminated trouble with uneven cakes or cakes of varying thickness. This is a problem with vertically mounted baskets which has been reported by many investigators.

The filter cloth was made of the same material as was used in the filtration tests, and it was tailored to fit the basket. The portions of the cloth which covered the bottom and top lip of the basket were waterproofed with a rubber cement. Tests made with the cloth both in and out of the centrifuge showed that water could flow only through the sides of the cloth. Since the area for filtration must be accurately known, no filtration is permitted except through the fabric at the outer edge of the basket. A 4 by 8-mesh calendered stainless steel backing screen which fitted closely inside the basket provided support for the cloth.

Figure 3 is a sketch of the general arrangement of the equipment. The slurry was mixed in the 10-gal. galvanized tank at the upper right. A variable-speed mixer in combination with the corrugated sides of the container (acting as baffles) kept the slurry well agitated. At the centrifuge the Lucite slurry was directed downward at an angle toward the wall of the centrifuge through a feed nozzle made from a Bunsen burner wingtip. The wingtip, which was first used by Grace (*4*) for this purpose, was effective in spreading the slurry feed into a thin, flat stream across the filtering surface. The water was passed through a cartridge filter ahead of the rotameter, and a similar wing-tip nozzle was used for feeding the water to the cake during the drainage-rate runs. Drainage of the filtrate was by gravity from the outlet at the botton of the shell surrounding the basket. The shell was made from a short length of 20-in. diameter steel pipe. Cake thicknesses and liquid levels in the basket were measured by means of a probe which was movable from the basket wall toward the center along a radius. With this device cake thickness and liquid levels were measured to, and reproducible within 1/64 in. Rotational speeds were measured by a hand tachometer at the end of the shaft which passed through the middle of the basket. These readings were checked occasionally with a Strobotac and were always in good agreement.

The centrifugal tests which were conducted may be classified into several categories, of which the centrifugal-drainage studies are the first. In these the centrifuge speed and the fluid level in the basket were held constant. Under these conditions 1-lb. increments of cake solids were deposited up to a total cake weight of 5 lb., and the flow of filtrate through each weight cake was measured. The runs therefore, are analogous to constant-pressure filtration tests except that rate measurements were made at given increments instead of cumulative measurements being taken continuously. The second kind of centrifugal tests attempted consisted of regular centrifugal filtrations conducted under true constant-head conditions, for which cumulative filtrate volume was found as a function of time. The third set of centrifuge experiments, not treated in this paper, was made primarily for measurement of residual moisture in spun or wrungout centrifugal-filter cakes.

In all centrifugal experiments the filter cloth was fitted into the basket and spun in place at the highest speed of the centrifuge, 1,800 rev./min. approximately, while water was being fed into the basket. The location of the cloth surface was checked with the probe before the start of each run. In the drainage-rate tests the tip of the probe was then set where it was desired to maintain the liquid level.

For the drainage-rate runs the flow of feed slurry into the basket for deposition of filter cake was always started with water flowing through the basket, which had been brought up to desired speed. Filtration rates were very high with thin cakes, and the controlled addition of water ensured that the cake surface was always submerged and so could not become dry. The flow rate of extra water was reduced as the cake became thicker, and in the case of the constant-head drainage-rate studies both water and slurry rates were controlled to maintain the liquid level constant at the point of the probe. As the slurry tank emptied, it was washed down to make certain that all the weighed quantity of Lucite was fed to the centrifuge. When all the solids had been deposited, the water flow rate which would just keep the water level at the point of the probe was measured. In the drainage-rate runs the next increment of cake weight would be deposited from slurry and the procedure repeated at the same speed and liquid level.

At the conclusion of a run the water was shut off and the cake spun dry. When no more liquid was being wrung out at that speed, the centrifuge was stopped. The scale was read with the probe at the cake surface, and from this reading the thickness of the cake was computed. The thickness at various points also was measured directly with a depth gauge. Agreement within 1/64-in. usually was achieved. One or more samples of the cake were then removed for moisture analysis.

In the second type of centrifugal test, a regular centrifugal-filtration operation under constant-head conditions, no additional water was fed to the centrifuge during filtration. With the centrifuge rotating at a constant speed, cake deposition took place as rapidly as possible until the desired constant slurry level could be maintained. Filtration was then completed at a fixed speed, and liquid level and corresponding values of cumulative time and cumulative filtrate volume were obtained during the filtration.

EXPERIMENTAL RESULTS

Permeability-Cell Measurements

Compressive stresses applied to the Lucite beds in the compression-permeability cell ranged from about 3 to 56 lb./sq. in. The corresponding values of porosity and point specific resistance are found in Table 1 for two runs in which the Lucite beds were the same weight but furnished slightly different

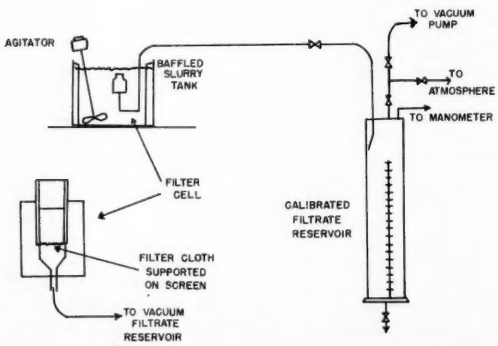

Fig. 2. Line diagram of vacuum-filter arrangement.

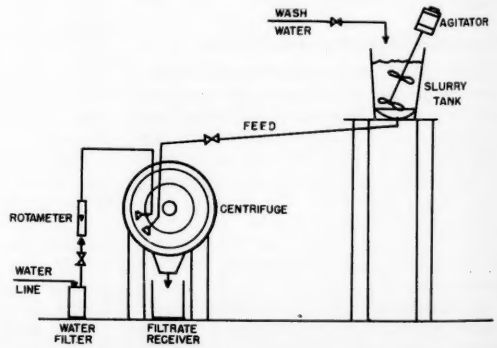

Fig. 3. Line diagram of arrangement of centrifugal filter.

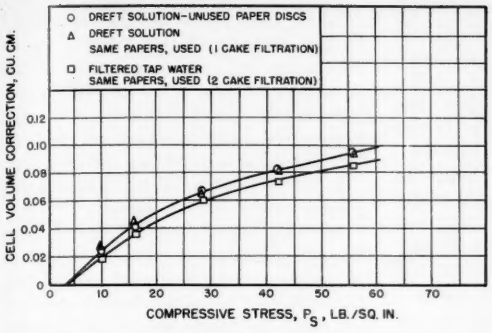
DREFT SOLUTION-UNUSED PAPER DISCS
DREFT SOLUTION
SAME PAPERS, USED (1 CAKE FILTRATION)
FILTERED TAP WATER
SAME PAPERS, USED (2 CAKE FILTRATION)
CELL VOLUME CORRECTION, CU. CM.
COMPRESSIVE STRESS, P_S, LB./SQ. IN.

Fig. 4. Cell-volume correction factor.

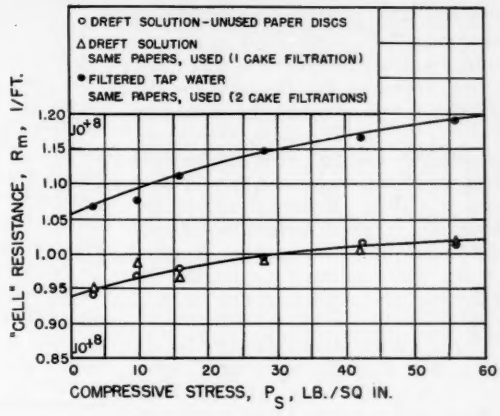
DREFT SOLUTION-UNUSED PAPER DISCS
DREFT SOLUTION
SAME PAPERS, USED (1 CAKE FILTRATION)
FILTERED TAP WATER
SAME PAPERS, USED (2 CAKE FILTRATIONS)
"CELL" RESISTANCE, R_m, 1/FT.
COMPRESSIVE STRESS, P_S, LB./SQ IN.

Fig. 5. Variation of cell resistance as a function of the compressive stress.

levels of porosity. A solution of 0.05 wt. % Dreft in distilled water constituted the filtrate in each of these tests. Another test was conducted however in which tap water was passed through the permeability cell containing a Lucite bed. These data are also shown in Table 1. This additional experiment was made because in the centrifugal-drainage–rate studies tap water was passed through the cakes.

Table 1 shows that the porosity and specific resistance change relatively little over the seventeen-fold range in compressive stress, thus indicating the incompressible nature of the cakes. In general the specific resistance falls in the range of 7 to 9 (10^8) ft./lb. These values are significantly lower than those usually encountered in filtration work. The specific resistance of most materials of importance in filtration is in the range of 10^{10} to 10^{13} ft./lb. The specific resistances of several commercial filter aids as reported by Grace (*4*) are between 10^{10} and 10^{11} ft./lb., an order of magnitude greater than for the Lucite beds.

The initial or cell resistance for the permeability tests was determined from blank cell runs, and from the results the cell-volume correction factors of Figure 4 also were derived. Each of the blank cell runs was made with the same two disks of filter paper inserted between the sintered stainless plates. CC-12 was made with 0.05 % Dreft solution and the previously unused filter papers. The filter papers were then used in the cake-permeability test CC-13, after which they were subjected to another blank-cell test CC-14 to learn how their filtration characteristics might have been changed. The papers were washed only with distilled water after the cake-permeability run. As the curve of Figure 5 shows, the cell resistance was found to be almost identical for these two tests. The same two filter papers then were used in run CC-16 with tap water to establish the cell-resistance values for run CC-17 to follow. As noted from Figure 5 the resistance to flow of tap water is 10 to 15 % greater than for Dreft solution, but the absolute change is not great.

It is of interest that the initial, or cell, resistance accounts for 5 to 7% of the total resistance measured in the cake permeability runs, and numerically it is equivalent to 12 to 16% of the specific cake resistance although the units are different. It had been learned in previous work that the resistance of filter papers from the same box showed a considerable variation in resistance, sometimes as much as twofold even when micrometer-measured thicknesses were almost identical. It was for this reason that where possible blank-cell data were obtained with the same papers used as employed in the cake tests.

The cell-resistance values are somewhat greater, but by coincidence are roughly in line with the filtration rule-of-thumb approximation that R_m ordinarily is numerically equal to about one tenth of the specific resistance. However this approximation usually is applied to a filter cloth suited to the operation. But here the filter medium was a double acid-washed paper having very fast filtering characteristics, and that the approximation still holds is another indication of the unusually low resistance exhibited by the Lucite beds.

For cake-permeability run CC-2 cell-resistance values for the particular filter papers used were not available, and the data were calculated by means of R_m values from Figure 5.

Table 1. Specific Resistance of Lucite Spheres as Measured in a Compression-Permeability Cell

Run	Compressive stress, p_s, lb./sq. in.	Porosity, ϵ	Specific-cake resistance, α, (ft./lb.)(10^{-8})
CC-17	3.28	0.387	6.88
CC-17	15.78	0.384	7.02
CC-17	42.16	0.380	7.34
CC-17	55.80	0.379	7.48
CC-13	3.28	0.397	8.0
CC-13	15.78	0.386	8.04
CC-13	42.16	0.379	7.71
CC-13	55.80	0.377	7.86
CC-2	3.28	0.371	7.60
CC-2	15.78	0.370	7.86
CC-2	27.62	0.368	8.11
CC-2	46.07	0.364	8.65
CC-2	52.32	0.364	8.92

Comparison of Results with the Kozeny-Carman Equation

One of the most useful relationships so far derived for the flow of fluids through granular beds is the Kozeny-Carman equation:

$$u = \frac{dV}{Ad\theta} = \frac{\epsilon^3 \Delta P\, g_c}{k(1-\epsilon)^2 S_o^2 \mu L} \qquad (6)$$

when one considers only the cake, and notes that

$$L = \frac{wV}{\rho_s (1-\epsilon) A} \qquad (7)$$

the Kozeny-Carman equation and the filtration expression of Equation (1) can be combined to show that

$$\alpha = \frac{k(1-\epsilon) S_o^2}{\rho_s \epsilon^3} \qquad (8)$$

Equation (8) predicts α to be linear in $[(1-\epsilon)/(\epsilon^3)]$ for a constant k and constant S_o. Any examination of permeability-cell data then should include a test of the relation between α and $[(1-\epsilon)/(\epsilon^3)]$. Figure 6 is a plot of corresponding values for the experimental points. A line expressing a rela-

tionship between the variables plotted must pass through the origin to be consistent with the fact that α is zero when $\epsilon = 1$. Therefore both the slope and the position are governed by the parameter $[(k S_o^2)/(\rho_s)]$. The data, which are admittedly meagre, align themselves fairly well except for the three points of run CC-13. Additional values are obviously needed before significant statements can be made. Further studies are underway; meanwhile the following are some tentative suggestions.

From the line drawn through the experimental data the value of $(k S_o^2)/(\rho_s)$ is 6.7 (10^7) ft./lb. The true solid density of Lucite was found to be 73.5 lb./cu. ft. When one takes this value and assumes $k = 5$, the specific surface turns out to be 31,000 sq. ft./cu. ft., or in metric units 1,019 sq. cm./cc. This value is 14.5% greater than the specific surface computed from the diameters microscopically measured. Another and perhaps more informative way of illustrating this discrepancy is to calculate the alphas predicted by Equation (8) when $k = 5$ and $S_o = 890$ sq. cm./cc. are used. This is shown by the lower line on Figure 6 which gives values for α which are 25 to 30% lower than the experimental alphas. The difference is too great to be accounted for by experimental error. The wall-effect correction suggested by Coulson (3) is minor in this case and reduces the difference by only 2%.

Now Carman suggested that $k=5 +$ 10%, and a larger value of k would reduce the difference. For spheres, though, recent published research (3, 9) confirms that k is close to 5 or perhaps slightly under. The specific surface from microscopic measurements also is believed to be correct. When this discrepancy was noted, additional microscopic counts were made with different sampling and counting techniques; the specific surface computed therefrom agreed well with the 890 sq. cm./cc. value.

The vacuum- and centrifugal-filtration results which follow give strong support to the experimental permeability data. The alphas from these other methods are in very close agreement with the permeability-cell alphas.

Carman (2) has written that the Kozeny-type of equation should be applied only to beds with reasonably uniform pore sizes. Yet in this investigation there was over a thirtyfold range in size of the particles, from 3.5 to 115 μ. The pore sizes no doubt varied widely, and perhaps it is this nonuniformity of pore structure that accounts for the disagreement between the measured surface and that calculated from the equation

$$k S_o^2/\rho_s = 6.7 \times 10^7$$

One can speculate also on the possibility that surface effects have influenced the experimental results. The addition of Dreft caused the Lucite spheres to be wetted and dispersed, but it did so by changing both the liquid-solid contact angle as well as the surface tension. Grace's work (4) has demonstrated the strong effect of electrolyte concentration on resistance and compressibility of filter cakes. Adsorption phenomena at the solid surface are no doubt involved, and research in this area might yield significant advances.

Vacuum-Filtration Results

The permeability-cell results discussed in the previous section constitute data on the point specific resistance of a porous bed under various compressive stresses. With the vacuum filter however it is the average specific resistance of a filter cake at a given ΔP that is measured in a constant-pressure filtration. Generally speaking therefore the point data must be integrated across the filter cake in order to arrive at the average resistance of the cake. But for an incompressible bed there is little or no variation in the point data, and the point and average specific resistances are the same. Since the cakes formed by the Lucite spheres are essentially incompressible, the specific resistances measured in the permeability cell and vacuum filter may be compared directly.

Filtration tests were made in the vacuum-filter cell in the manner described in the earlier section. Two types of runs were made: runs in which the slurry liquid was deaerated prior to filtration and runs in which the liquid was not degasified. While data from only the former runs are pertinent to the objective of this study, the effects of dissolved gases in the slurry of a vacuum filter are worthy of presentation.

The results of vacuum-filtration run F-7, presented in Figure 7, represent typical vacuum-filtration results for the deaerated slurries. The behavior of the system is in accord with filtration theory as shown by the straight-line plots of Figure 7. When θ/V is plotted against V for a constant ΔP filtration, a straight line should result whether the cake is compressible or incompressible.

For filtration runs F-3, F-4, F-5, and F-6 the water used in making up these slurries was not degasified prior to use. It was observed that the higher the vacuum applied, the greater the departure from linearity. Also the longer the filtration continues (the greater the volume of filtrate), the more pronounced the deviation becomes.

Since the plots of the deaerated slurries exhibit excellent linearity, these effects are believed due solely to the formation of gas or vapor within the cake. While runs F-3 through F-6 were in progress, large numbers of gas bubbles flowed in the filtrate delivery line, and the proportion of gas bubbles was greater at the higher vacua.

As the liquid enters and passes through the cake, it encounters regions of pressure progressively lower than atmospheric. Since the liquid was gas saturated or nearly so at atmospheric pressure, air or gas comes out of solution in these regions of lower pressure forming bubbles within the voids of the cake. Two-phase flow arises with both gas and liquid competing for the available flow channels. Effectively then the flow cross section for liquid is reduced. The effect is worse at higher vacua because more gas comes out of solution and also because at the lower absolute pressure the gas itself occupies a greater volume. In addition as the time of filtration lengthens, more and more of the flow channels would be expected to become vapor bound.

As pointed out earlier, the behavior of the deaerated slurries was in excellent agreement with theory, and the filtration constants were calculated from these runs. The concentration of the slurry was computed from the weight of the filter cake and the volume of filtrate collected. Well-used cotton-drill filter cloths were employed in these runs. The initial resistance and the average specific resistance computed from the intercept and slope appear in Table 2. The variation of values of α is less than 4.5%, and the maximum deviation from the mean value of 6.63 (10^8) ft./lb. is less than 2.3%. The initial resistance is numerically equal to about 36% of the value of α. All the filter cloths had been used in earlier filtrations of Lucite slurries, and very little change in initial resistance was exhibited.

Cake thickness was measured only for runs F-4, F-5, and F-6. Consequently information on cake porosity is available only on these three runs. The measurements and values of porosity calculated therefrom are given in Table 3.

The essential constancy of both the specific resistance and the porosity again confirm the incompressible nature of the cakes which was observed in the permeability tests.

Centrifugal-Filtration Results

From the preliminary experiments with the test centrifuge measurements were obtained to establish the relationship between the cake weight and thickness. A plot was made of dry-cake

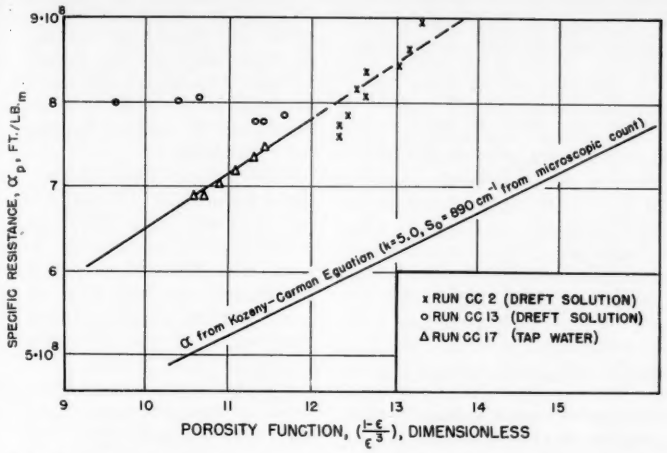
SPECIFIC RESISTANCE, α_p, FT./LB.$_m$
POROSITY FUNCTION, $(\frac{1-\epsilon}{\epsilon^3})$, DIMENSIONLESS
α from Kozeny-Carman Equation (k=5.0, S_o=890 cm^{-1} from microscopic count)
x RUN CC 2 (DREFT SOLUTION)
o RUN CC 13 (DREFT SOLUTION)
Δ RUN CC 17 (TAP WATER)

Fig. 6. Specific resistance as related to the porosity function of the Kozeny-Carman equation.

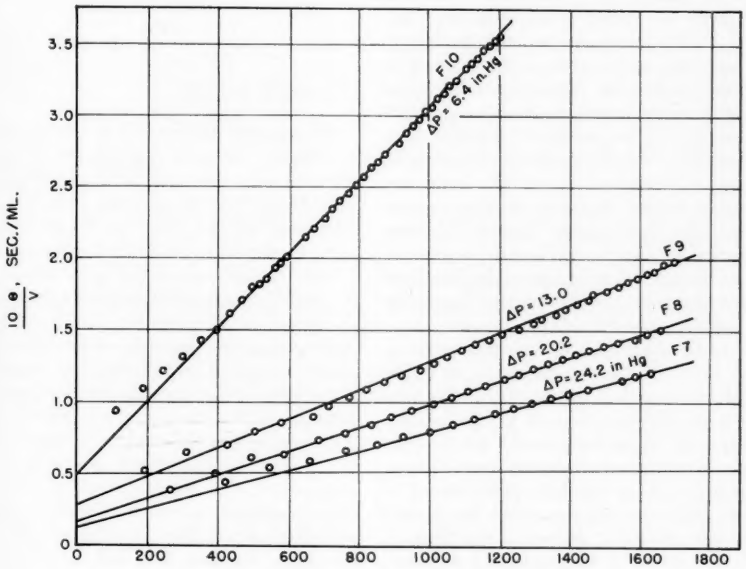

Fig. 7. Vacuum-filter data with degassed liquid used.

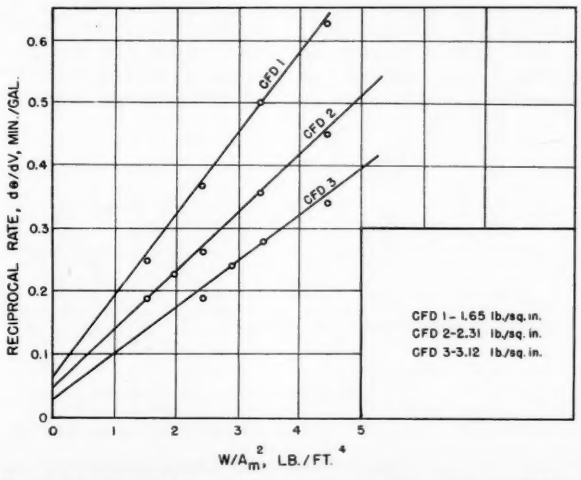

Fig. 8. Centrifugal-drainage rates under constant-pressure conditions.

Table 2. Filtration Constants Calculated from Vacuum-Filtration Tests

Run	ΔP, in. Hg	α, ft./lb.	R_m, 1/ft.
F-7	24.2	$6.48(10^8)$	$2.30(10^8)$
F-8	20.2	$6.52(10^8)$	$2.59(10^8)$
F-9	13.04	$6.76(10^8)$	$2.38(10^8)$
F-10	6.37	$6.76(10^8)$	$2.23(10^8)$

weight against $(r_o^2 - r_c^2)$, the difference of the squares of the outer and and inner radii respectively. The solids mass balance equation is

$$W = \pi\,(r_o^2 - r_c^2) h\,(1-\epsilon)\,\rho_s \quad (9)$$

Therefore from the slope of the line on the plot the porosity can be computed. The plot shows the line to be straight, thus implying a constant value for ϵ. In view of the earlier results this should be expected. The centrifuge cake porosity derived from the plot is 0.376.

When one allows for the initial resistance, the centrifugal-filtration rate equation, Equation (5), is written as

$$q = \frac{dV}{d\theta} = \frac{\Delta P\, g_c}{\mu\left[\dfrac{\alpha W}{A_m^2} + \dfrac{R_m}{A_o}\right]} = \frac{\frac{1}{2}(2\pi N)^2 \rho_L\,(r_o^2 - r_L^2)}{\mu\left[\dfrac{\alpha W}{A_m^2} + \dfrac{R_m}{A_o}\right]} \quad (10)$$

If this now be inverted to

$$\frac{d\theta}{dV} = \frac{\mu\,\alpha}{\Delta P\, g_c}\,\frac{W}{A_m^2} + \frac{\mu}{\Delta P\, g_c\, A_o} R_m \quad (11)$$

Table 3. Cake Porosities Measured in Vacuum-Filtration Study

Area of filtration (all runs) = 0.890 sq. in.

Run	ΔP, in. Hg	Weight of dry-cake solids, g.	Thickness, in.	Porosity
F-4	13.25	16.67	1.59	0.391
F-5	20.08	14.92	1.49	0.401
F-6	24.08	16.71	1.59	0.390
			Average	0.394

Table 4. Filtration Constants Calculated from Constant-Pressure Centrifugal-Drainage Rate Studies

Run	ΔP, lb./sq. in.	α, ft./lb.	R_m, 1/ft.
CFD-1	1.65	$7.58(10^8)$	$4.39(10^8)$
CFD-2	2.31	$7.52(10^8)$	$4.88(10^8)$
CFD-3	3.12	$8.04(10^8)$	$4.49(10^8)$

the equation shows that the reciprocal rate $d\theta/dV$ should plot as a straight line against W/A_m^2 for a constant-head centrifugal filtration and that α could be determined from the slope and R_m from the intercept.

Drainage-rate runs CFD-1, CFD-2, and CFD-3 each were made at a constant speed and constant liquid level. Flow rates were measured for various cake weights. These data therefore represent constant-head runs, and Figure 8 is a plot of the results. The arithmetic mean area was used as A_m^2 for the reasons advanced in the discussion of proposed centrifugal rate equations.

The relationship predicted by Equation (11) is confirmed and the values of α and R_m determined from the slope and intercept appear in Table 4.

The proportionality between the flow rate and the hydraulic pressure drop was checked by the plot of experimental data in Figure 9 and found to be validated.

The relationship between q and N, as well as q and $(r_o^2 - r_L^2)$ were tested by measuring corresponding values of drainage rate and liquid level, determined at various speeds for a 5-lb. Lucite filter cake. In Figure 11 $(r_o^2 - r_L^2)$ is plotted vs. $dV/d\theta$ on log-log coordinates, and Figure 10 is a log-log plot of N against $dV/d\theta$. The data points fit the theoretical relationship very well.

Although the system used in this study is so free filtering that R_m constitutes a sizable portion of the total resistance, there are many filter cakes for which R_m could be neglected. In these cases $d\theta/dV$ can be plotted against $\mu W/\Delta P g_c A_m^2$ to yield a straight line having a slope of α. Or, if $R_m/\Delta P$ were a constant, Equation (11) shows the data analysis still might be made by such a plot. These methods could not be expected to work however for compressible cakes or under any other conditions for which Equations (10) and (11) are invalid.

In the description of the centrifugal equipment and procedure reference

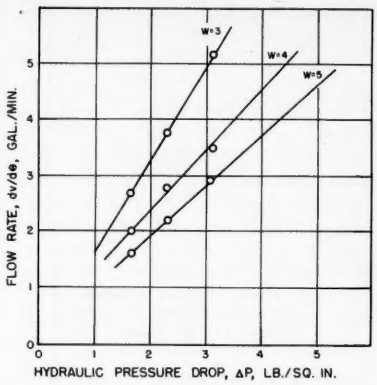

Fig. 9. Relationship between hydraulic pressure and flow rates in the centrifuge.

was made to a regular constant-pressure centrifugal filtration. Two attempts to obtain valid data in such runs were made during this investigation. The major obstacle to success in both trials was the impossibility of maintaining constant-head conditions over the entire portion of the run. At a specified rotational speed the restriction of constant hydraulic head requires a fixed liquid level. But because the cake must never become dry, the minimum height of liquid carried in the basket will be dictated by the level necessary to just cover the maximum thickness of cake.

In the first trial, designated as CF-1, a slurry of Lucite particles in Dreft solution was fed to the centrifuge. The rate of filtration was so great that the required liquid level could not be held until the run was almost over. Consequently, the valid data points were so few that no reliance could be placed on the constants derived from them.

In run CF-2 an attempt was made to overcome the fast filtration difficulties and still obtain valid measurements. This was done by making the filtrate a 65 wt. % glycerin-water solution which at the filtration temperature of 86°F. had a viscosity of 9.02 centipoises. The addition of 0.05% Dreft ensured the dispersion of the Lucite beads without affecting either the density or viscosity of the glycerin solution. The density of the solution was 1.15 g./ml., which being so close to the solid density of 1.18 minimized the settling tendency of the solid particles.

While these expediencies reduced the experimental difficulties, they did not eliminate them. The liquid height in the basket reached the prescribed level only after 130 sec.; therefore approximately the first 30% of the run could not be considered for the determination of the constants of the system.

Equation (11) can be formulated in terms of the mass rather than the volume of filtrate collected:

$$\frac{d\theta}{dM} = \frac{\mu \alpha x M}{\Delta P\, g_c\, \rho_L\, A_m^2} + \frac{\mu R_m}{\Delta P\, g_c\, \rho_L\, A_o} \qquad (12)$$

where $dM = \rho_L dV$.

The results of run CF-2 are plotted in Figure 12 with increments in reciprocal rate, $\Delta\theta/\Delta M$ as the ordinate, and M/A_m^2 as the abscissa. Graphical treatment of this kind in which raw-data increments are plotted constitutes a very severe test of the data because it emphasizes irregularities in the individual measurements. As readings were taken in this run only 10 sec. apart, a small difference in timing represents relatively a much larger fraction of the time interval. Moreover an error in any interval is reflected in the following increment as well; for example if the filtrate reading for a given interval is taken slightly early and the succeeding reading is taken correctly, the first ΔM will be smaller and the second ΔM larger than their true values.

The scatter exhibited by the plot is more or less typical of experimental filtration data treated in this manner. The straight line through the latter portion of the data was drawn by eye and without prejudice to any one point

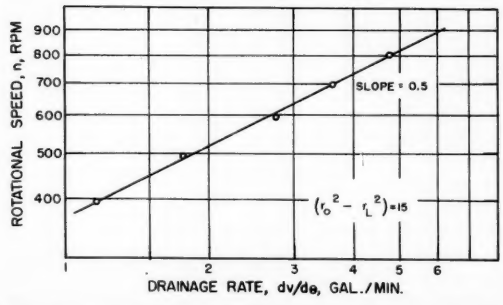

Fig. 10. Relationship between drainage rate and rotational speed.

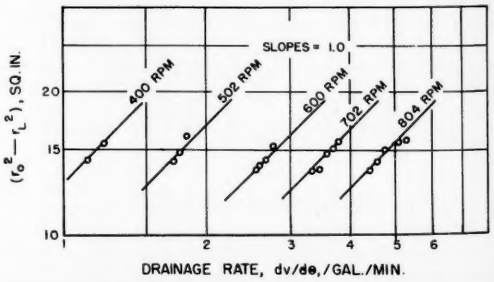

Fig. 11. Relationship between drainage rate and liquid-head function.

Table 5. Summary of Experimental Results for Comparative Purposes

Run	ΔP, lb./sq. in.	α, ft./lb.	R_m, 1/ft.
Vacuum filtration			
F-7	11.9	$6.48(10^8)$	$2.30(10^8)$
F-8	9.9	$6.52(10^8)$	$2.59(10^8)$
F-9	6.4	$6.76(10^8)$	$2.38(10^8)$
F-10	3.1	$6.76(10^8)$	$2.23(10^8)$
Average of runs		$6.63(10^8)$	$2.38(10^8)$
Centrifugal drainage rate			
CFD-1	1.65	$7.58(10^8)$	$4.39(10^8)$
CFD-2	2.31	$7.52(10^8)$	$4.88(10^8)$
CFD-3	3.12	$8.04(10^8)$	$4.49(10^8)$
Average of runs		$7.71(10^8)$	$4.58(10^8)$
Centrifugal filtration			
CF-2	4.24	$9.2(10^8)$	
Permeability cell			
General plot at			
$\epsilon = 0.376$		$7.64(10^8)$	
$\epsilon = 0.394$		$6.43(10^8)$	
Range of experimentally measured values		$6.8(10^8)$ to $9.2(10^8)$	

or group of points. From the slope of the line the value of α was determined by means of the experimentally measured properties of the system. This value of α was 9.2 (10^8) ft./lb.; it is about 19% greater than the average value of 7.71 (10^8) found in the drainage-rate runs. The agreement would be considered good in any case, but especially so in view of the conditions surrounding the runs under comparison.

COMPARISON OF PERMEABILITY-CELL, VACUUM-FILTRATION, AND CENTRIFUGAL-FILTRATION RESULTS

For comparative purposes the experimental results have been collected into a summary table, Table 5.

All values of α measured and reported in Table 5 are between 6.5 and 9.2 (10^8) ft./lb., which is a narrow range considering the methods and conditions employed. To examine the figures at approximately the same ΔP the data taken at about 3 lb./sq. in. were extracted and grouped together in Table 6. The correspondence in values is excellent, the total variation being less than 20%.

The Kozeny-Carman equation indicates the very great influence of porosity on specific resistance. A comparison of the vacuum-filtration and centrifugal-filtration alphas with the corresponding permeability-cell alphas then is of interest. Unfortunately porosity information of the vacuum-filtration tests F-7 through F-10 is lacking, but data are available on the cakes formed in runs F-4, F-5, and F-6, the ϵ's being 0.391, 0.401, and 0.390 respectively. These values do not differ much from one another, and it seems reasonable that the other vacuum-filtration cakes would not have a widely different porosity. Then if one assumes that the average porosity of 0.394 is representative of the vacuum-filtration cakes, the specific resistance of the filtration cakes can be compared to the permeability-cell value at this same porosity. Going through the α vs. $[(1-\epsilon)/(\epsilon^3)]$ plot one finds that the permeability-cell alpha at $\epsilon = 0.394$ is 6.43 (10^8), which is very close to the 6.63 (10^8) average for the filtration cakes.

Table 6. Comparison of Specific Resistances at the Same Pressure Drop Across the Cake

Method	Run	ΔP, lb./sq. in.	α, ft./lb.
Vacuum filtration	F-10	3.1	$6.76(10^8)$
Centrifugal drainage	CFD-3	3.12	$8.04(10^8)$
Permeability cell	CC-13	3.28	$^{\circ}8.0(10^8)$
	CC-17	3.28	$^{\circ\circ}6.88(10^8)$

° Dreft solution.
°° Tap water.

The porosity of the cakes deposited in the centrifugal drainage rate studies was 0.376. At this porosity the specific resistance indicated by the permeability cell is 7.64 (10^8), whereas the average of the centrifugal drainage-rate tests was 7.71 (10^8).

There is thus remarkable agreement between the permeability-cell values and the other tests when compared at the same porosities. This suggests strongly that the specific resistance of an incompressible filter cake (whether vacuum or centrifugal) can be predicted with greater accuracy from a laboratory permeability test at the same porosity rather than at the same compressive stress. This probably is not so surprising since the porosity is the basic parameter.

The Kozeny-Carman equation shows that the specific resistance is completely determined by the porosity if k and S_o are constant. While the fraction voids of an unconsolidated bed are determined mainly by the compressive stress, it is an experimental fact that uniform solid particles in random packing can form different porosities under the same compressive loading. However the range of porosity values generally is not large. Vibration or tapping of a porous cake can cause rearrangement of particles into a tighter mode of packing, and in some circumstances the possibility of bridging exists. Of even greater importance to mixtures of different sizes is the matter of segregation, either in the slurry prior to deposition or while a layer is being deposited.

Even though the results of this work are encouraging, much remains to be done in the combined areas of filtration and centrifugation. Studies are needed to explain the discrepancy between the specific resistance determined by three types of measurement and that predicted by the Kozeny-Carman equation. The behavior of compressible materials needs more complete investigation. The performance of large-scale

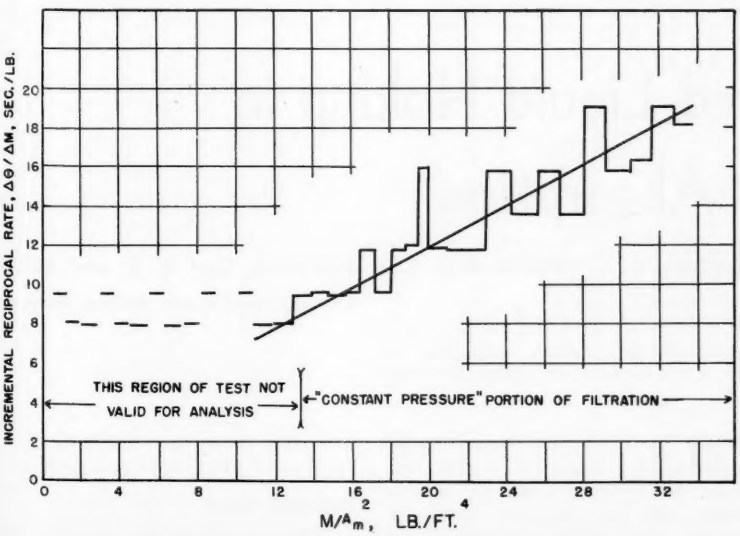

Fig. 12. Centrifugal-filtration data for calculating specific resistance.

centrifugal-filtering equipment needs to be compared with that of small-scale operations.

CONCLUSIONS

Three types of equipment, a permeability cell, a vacuum filter, and a centrifuge. were successfully used to measure the specific resistance of a bed of spherical particles. The specific resistances agreed among themselves within 20% at the same pressure drop and within 3% at the same cake porosity.

These results constitute the first known experimental data to be reported on the resistances offered by beds of incompressible spheres in all three methods of operation. It is only the third known study of its kind to be done on any sort of porous bed.

The Kozeny-Carman equation predicts specific resistances which are 25% lower than those measured in this work. The matter calls for further investigation.

ACKNOWLEDGMENT

The authors thank the Dow Chemical Company and the University of Kansas Research Grants Committee for funds which made this work possible.

NOTATION

A = area, sq. ft. or sq. cm.
A_{avg} = arithmetic mean area, sq. ft. or sq. cm.
A_{lm} = logarithmic mean area, sq. ft. or sq. cm.
A_o = area of the filter cloth, sq. ft. or sq. cm.
c = concentration of solids in the slurry expressed as volume of cake forming solids per unit volume of filtrate, dimensionless
D = diameter of particle, ft. or cm.
g = local acceleration of gravity, ft./(sec.)(sec.)
g_c = dimensional constant
h = height of centrifugal basket in centrifugal filtration equation, ft. or cm.
k = Kozeny-Carman constant
K_s = permeability in Storrow equation, $K_s = (\rho_L g)/\alpha_v$
L = length of porous bed in direction of flow, ft. or cm.
M = mass of filtrate, lb. or g.
N = rotational speed, rev./sec.
ΔP = pressure driving force or pressure drop, lb./sq. in. or lb./sq. ft.
q = volumetric flow rate, cu. ft./sec. or cc./sec.
Q = steady state volumetric flow rate in the Storrow equation, cu. ft./sec. or cc./sec.
r_c = radius to inside or exposed surface of centrifuge cake, ft.
r_L = radius to liquid level, ft.
r_o = radius to outside surface of centrifuge cake, ft.
R_m = initial or medium resistance, 1/(ft.)
S_o = solids surface area per unit volume of bed, sq. cm./cc.
V = volume of filtrate, cu. ft. or cc.
w = concentration of solids in slurry expressed as mass of solids per unit volume of filtrate, lb./cu. ft. or g./cc.
W = mass of solids in bed or cake, lb. or g.
x = mass fraction of cake solids deposited per unit mass of filtrate

Greek Letters

α = average specific resistance on a mass basis, ft./lb.
α_v = average specific resistance on a volume basis, ft./cu. ft., $\alpha_v = (1-\epsilon)(\rho_s)$
ϵ = cake porosity or fraction voids, dimensionless
θ = time, sec.
ρ_L = density of liquid, lb./cu. ft. or g./cc.
ρ_s = true density of solid particles, lb./cu. ft or g./cc.
μ = fluid viscosity, lb./(ft.)(sec.)

LITERATURE CITED

1. Burak, N., and J. A. Storrow, *J. Soc. Chem. Ind.*, **69**, 8 (1950).
2. Carman, P. C., *Discussion Faraday Soc.*, No. 3, 72 (1948).
3. Coulson, J. M., *Trans, Inst. Chem. Eng. (London)*, **27**, 237 (1949).
4. Grace, H. P., *Chem. Eng. Progr.*, **49**, 303, 367, 427 (1953).
5. Haruni, M. M., and J. A. Storrow, *Chem. Eng. Sci.*, **1**, 154 (1952).
6. ———, *Ind. Eng. Chem.*, **44**, 2751, 2756, 2764 (1952).
7. Inglesent, H., and J. A. Storrow, *Ind. Chemist*, **27**, 76 (1951).
8. Maloney, J. O., *Ind. Eng. Chem.*, **38**, 24 (1946).
9. Wyllie, M. R. J., and A. R. Gregory, *ibid.*, **47**, 1379 (1955).

Pressure Drop and Liquid Holdup in Concurrent Gas Absorption

W. S. DODDS, L. F. STUTZMAN, B. J. SOLLAMI, and R. J. McCARTER

Remington Rand Univac, St. Paul, Minnesota

This work presents initial information useful to concurrent gas-absorption design. Data are reported on the variation of pressure drop and liquid holdup obtained with various flow rates, packings, and liquids.

The advantages of concurrent operation for gas absorption were discussed earlier (*1*). Where applicable, this mode of operation may use uncommonly high flow rates, for which correlation and design information are unavailable. To supply such information on pressure drop and liquid holdup, the following work was performed.

Additional tables of data and literature references for contiguous countercurrent flow data, coded to type of packing, are filed with the American Documentary Institute, Photoduplication Service, Library of Congress, Washington 25, D. C., as document 6138. They may be obtained for $1.25 for photoprints or 35-mm. microfilm.

PRESSURE DROP

With concurrent gas absorption the main determinant of operating condi-

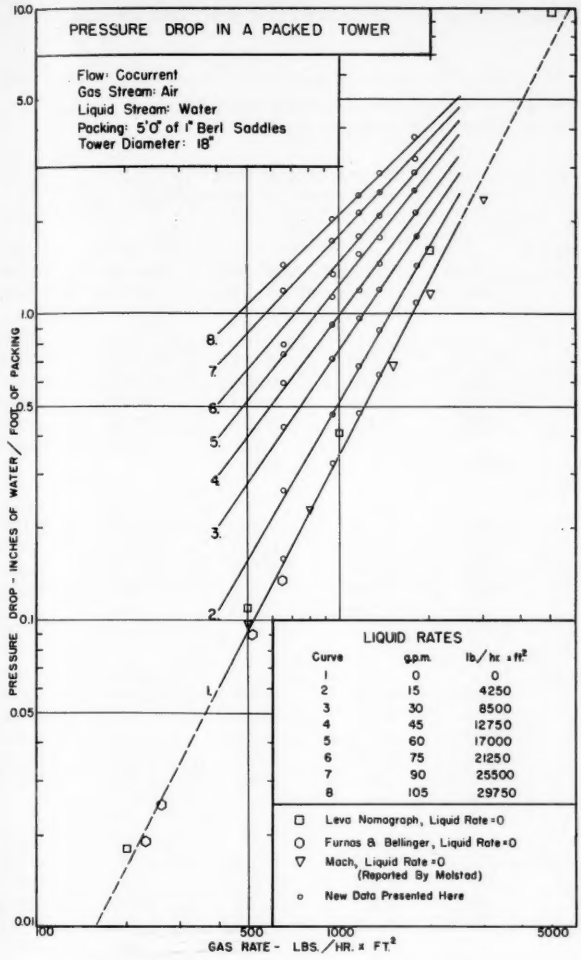
PRESSURE DROP IN A PACKED TOWER
Flow: Cocurrent
Gas Stream: Air
Liquid Stream: Water
Packing: 5'0" of 1" Berl Saddles
Tower Diameter: 18"
PRESSURE DROP - INCHES OF WATER / FOOT OF PACKING
GAS RATE - LBS. / HR. x FT.²
LIQUID RATES
Curve | g.p.m. | lb./hr. x ft.²
1 | 0 | 0
2 | 15 | 4250
3 | 30 | 8500
4 | 45 | 12750
5 | 60 | 17000
6 | 75 | 21250
7 | 90 | 25500
8 | 105 | 29750
Leva Nomograph, Liquid Rate = 0
Furnas & Bellinger, Liquid Rate = 0
Mach, Liquid Rate = 0 (Reported By Molstad)
New Data Presented Here

Fig. 1. Pressure drop in packed tower, concurrent flow.

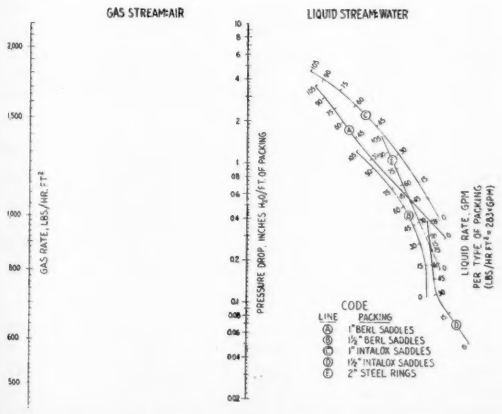
GAS STREAM: AIR
LIQUID STREAM: WATER
GAS RATE, LBS/HR. FT.²
PRESSURE DROP, INCHES H₂O/FT. OF PACKING
LIQUID RATE, GPM PER TYPE OF PACKING (LBS/HR. FT.² = 2.80 GPM)
CODE
LINE | PACKING
A | 1" BERL SADDLES
B | 1½" BERL SADDLES
C | 1" INTALOX SADDLES
D | 1½" INTALOX SADDLES
E | 2" STEEL RINGS

Fig. 2. Alignment chart, pressure drop in packed tower, concurrent flow.

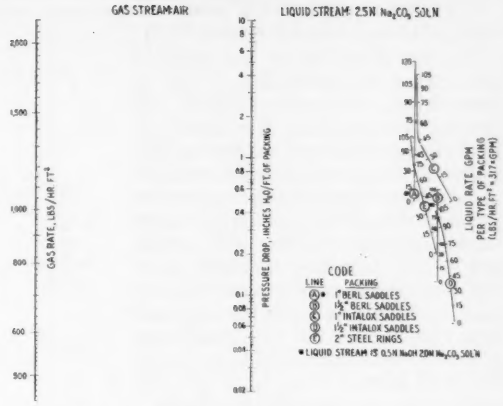
GAS STREAM: AIR
LIQUID STREAM: 2.5N Na₂CO₃ SOLN
GAS RATE, LBS/HR. FT.²
PRESSURE DROP, INCHES H₂O/FT. OF PACKING
LIQUID RATE, GPM PER TYPE OF PACKING (LBS/HR. FT.² = 3.17 GPM)
CODE
LINE | PACKING
A | 1" BERL SADDLES
B | 1½" BERL SADDLES
C | 1" INTALOX SADDLES
D | 1½" INTALOX SADDLES
E | 2" STEEL RINGS
* LIQUID STREAM IS 0.5N NaOH 2.0N Na₂CO₃ SOLN

Fig. 3. Alignment chart, pressure drop in packed tower, concurrent flow.

tions may be the power expended in tower pressure drop. Therefore, data on this drop are required to determine the most economical design. In these aspects the literature is limited to the more common countercurrent operation of absorption towers and includes data at rates only up to the loading or flooding points. Extrapolation of these data to high flow rates would be highly subject to error.

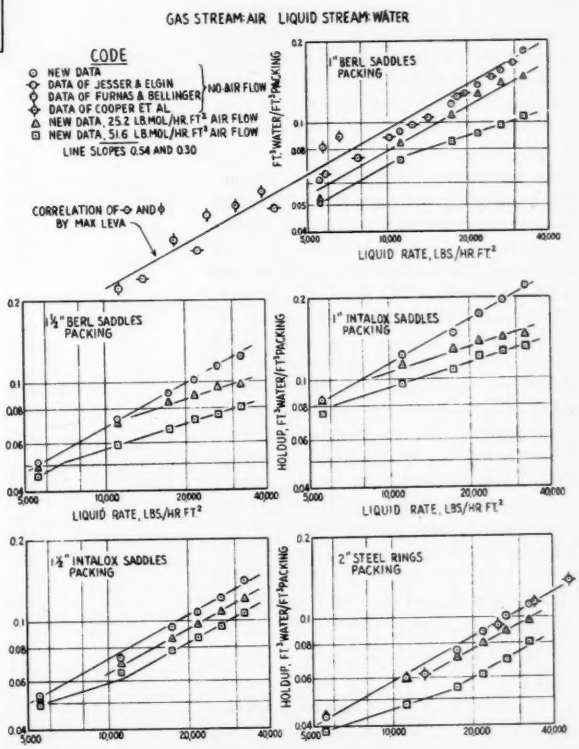
GAS STREAM: AIR
LIQUID STREAM: WATER
CODE
NEW DATA
DATA OF JESSER & ELGIN
DATA OF FURNAS & BELLINGER
DATA OF COOPER ET AL.
NO AIR FLOW
NEW DATA, 25.2 LB.MOL/HR.FT.² AIR FLOW
NEW DATA, 51.6 LB.MOL/HR.FT.² AIR FLOW
LINE SLOPES 0.54 AND 0.30
CORRELATION OF ◇ AND ϕ BY MAX LEVA
1" BERL SADDLES PACKING
1½" BERL SADDLES PACKING
1" INTALOX SADDLES PACKING
1½" INTALOX SADDLES PACKING
2" STEEL RINGS PACKING
HOLDUP, FT.³ WATER/FT.³ PACKING
LIQUID RATE, LBS/HR.FT.²

Fig. 4. Liquid holdup in packed tower, concurrent flow.

The same equipment was used as in a previous mass transfer study (*1*).

The variables under test included gas rate at six levels, liquid rate at seven levels, two types of liquid, and five types of packing. The data conformed to a statistical design, so that statistical interpretation might be facilitated. Operating procedure provided sufficient time before readings to ensure stable conditions: packing was settled and wetted, and the transients from resetting rates were dissipated. Checks were made to assure that the approach to any set of rates was immaterial, that is that no combination of a prior decrease or increase in liquid or gas rate would alter the pressure-drop result.

The experimental results are tabulated in Tables 1, and 2. The relationship between variables at any point of interest may be simply obtained by a log-log plot. An example is presented in Figure 1 which graphs one system (water-1-in. Berl saddles) with related correlations noted on the plot. For brevity the graphs for all results are condensed into the alignment charts of Figures 2 and 3, which offer quick but rough reference. In general for the carbonate-solution system the slopes of the correlating lines, hence the exponents to be attached to gas rate, were relatively constant. Conversely, the water systems yielded decreasing slopes with increasing liquid flow rates, hence a gas rate exponent influenced by liquid rate.* This complication and difference between the only two liquid systems tested precludes advancing a general correlation. Otherwise the data appeared amenable to correlation, albeit with interactions between variables.

A comparison with countercurrent flow relations may be adduced. The two flow systems are contiguous and similar at lower flow rates. In each case log plots of pressure drop vs. gas rate would yield similar parallel lines per liquid-rate parameter and hence the same exponent to be attached to gas rate. With countercurrent operation this exponent is sharply increased at the loading point and again at the flooding point. Conversely, with concurrent operation the exponent is not increased by higher flow velocities and may be decreased, as indicated in Figure 1. It would appear that at some higher range of gas velocity the lines of correlation would curve to converge with the extended line for zero liquid rate, as liquid holdup is progressively depressed under increasing gas pressure.

* The behavior of this system at higher gas rates would be of interest (Figure 1). Beyond the point where the lines of correlation converge would liquid rate be of no effect or would pressure drop be decreased by greater liquid flow, from additional liquid head?

TABLE 1. PRESSURE DROP IN CONCURRENT FLOW IN A PACKED TOWER

Air-water system in 18-in.-diameter tower at tower pressure 745 to 760 mm. Hg., tower temp. 85° to 90°F.

Liquid rate, lb./hr./ sq. ft.	Gas rate, lb./hr./ sq. ft.	Pressure drop in various packings in. water/ft. of packing height				
		1-in. Berl 5 ft.	1½-in. Berl 4 ft. 7 in.	2-in. rings 4 ft. 3 in.	1-in. Intalox 4 ft.	1½-in. Intalox 4 ft. 5 in.
0	461	—	—	—	0.091	0.030
	661	0.159	0.090	0.119	0.184	0.064
	953	0.323	0.182	0.234	0.364	0.131
	1178	0.471	0.269	0.350	0.546	0.197
	1362	0.629	0.354	0.478	0.728	0.273
	1745	—	0.549	0.747	1.150	0.474
	1810	1.075	—	—	—	—
4250	461	—	—	—	0.145	0.039
	661	0.265	0.126	0.148	0.263	0.080
	953	0.470	0.245	0.288	0.517	0.163
	1178	0.672	0.350	0.434	0.775	0.243
	1362	0.894	0.469	0.564	1.021	0.331
	1745	—	0.738	0.899	1.530	0.530
	1810	1.424	—	—	—	—
8500	461	—	—	—	0.203	0.043
	661	0.426	0.159	0.185	0.356	0.094
	953	0.716	0.303	0.352	0.709	0.185
	1178	0.960	0.424	0.516	1.025	0.275
	1362	1.178	0.561	0.681	1.296	0.372
	1745	—	0.863	1.061	1.867	0.592
	1810	1.766	—	—	—	—
12750	461	—	—	—	0.343	0.047
	661	0.594	0.168	0.228	0.558	0.109
	953	0.921	0.327	0.428	1.023	0.217
	1178	1.189	0.457	0.623	1.375	0.316
	1362	1.450	0.597	0.806	1.695	0.423
	1745	—	0.899	1.238	2.322	0.678
	1770	2.142	—	—	—	—
17000	461	—	—	—	0.517	0.060
	661	0.733	0.233	0.282	0.817	0.125
	953	1.125	0.410	0.502	1.385	0.243
	1178	1.550	0.578	0.743	1.809	0.365
	1362	1.760	0.731	0.969	2.171	0.485
	1745	—	1.069	1.450	2.815	0.762
	1770	2.570	—	—	—	—
21250	461	—	—	—	0.686	0.069
	661	0.782	0.273	0.329	1.083	0.140
	953	1.313	0.496	0.603	1.716	0.275
	1178	1.784	0.688	0.856	2.192	0.406
	1362	2.095	0.870	1.099	2.564	0.534
	1745	—	1.314	1.648	3.236	0.846
	1770	2.895	—	—	—	—
25500	461	—	—	—	0.972	0.079
	661	1.170	0.377	0.411	1.489	0.152
	953	1.705	0.637	0.736	2.202	0.298
	1178	2.134	0.861	1.035	2.708	0.432
	1362	2.470	1.058	1.290	3.101	0.566
	1745	—	1.531	1.932	3.866	0.961
	1770	3.375	—	—	—	—
29750	461	—	—	—	1.272	0.099
	661	1.422	0.484	0.525	1.881	0.193
	953	2.006	0.800	0.878	2.695	0.371
	1178	2.461	1.038	1.205	3.174	0.569
	1362	2.853	1.249	1.518	3.597	0.708
	1745	—	1.758	2.216	4.435	1.120
	1770	3.731	—	—	—	—

TABLE 2. PRESSURE DROP IN CONCURRENT FLOW IN A PACKED TOWER

Tower pressure 745 to 760 mm. Hg., tower temp. 85° to 90°F., 18-in. diameter tower

Air–2.0N Na_2CO_3, 0.5N NaOH system with 5 ft. of 1-in. Berl Saddles			Air-2.5N Na_2CO_3 system		Pressure drop in various packings in. water/ft. of packing height			
Liquid rate, lb./hr./ sq. ft.	Air rate, lb./hr./ sq. ft.	Pressure drop, in. H_2O/ft. pack. ht.	Liquid rate, lb./hr./ sq. ft.	Gas rate, lb./hr./ sq. ft.	1½-in. Berl 4 ft. 7 in.	2-in. rings 4 ft. 3 in.	1-in. Intalox 4 in.	1½-in. Intalox 4 ft. 5 in.
4730	516	0.169	4750	461	—	—	0.126	0.039
	749	0.323		661	0.117	0.160	0.256	0.084
	984	0.508		953	0.229	0.311	0.519	0.167
	1225	0.738		1178	0.336	0.457	0.767	0.247
	1491	1.040		1362	0.444	0.609	1.009	0.333
9540	515	0.198		1745	—	0.961	1.602	0.534
	741	0.375		1770	0.731	—	—	—
	950	0.559	9500	461	—	—	0.165	0.043
	1244	0.892		661	0.126	0.191	0.333	0.096
	1523	1.290		953	0.258	0.362	0.614	0.187
13940	516	0.227		1178	0.379	0.535	0.895	0.279
	749	0.440		1362	0.491	0.706	1.176	0.373
	986	0.705		1745	—	1.109	1.861	0.607
	1232	1.025		1770	0.827	—	—	—
	1500	1.449	14250	461	—	—	0.209	0.049
18920	504	0.235		661	0.150	0.222	0.395	0.103
	744	0.496		953	0.280	0.424	0.738	0.206
	1015	0.779		1178	0.415	0.634	1.069	0.303
	1223	1.191		1362	0.574	0.829	1.387	0.404
	1545	1.801		1745	—	1.288	2.161	0.657
23740	507	0.303		1770	0.904	—	—	—
	744	0.614	19000	461	—	—	0.248	0.056
	986	0.981		661	0.159	0.253	0.476	0.125
	1225	1.427		953	0.309	0.500	0.891	0.243
	1570	2.188		1178	0.475	0.732	1.274	0.365
28000	505	0.339		1362	0.632	0.965	1.658	0.485
	742	0.681		1745	—	1.494	2.737	0.772
	984	1.183		1770	1.036	—	—	—
	1230	1.813	23750	461	—	—	0.292	0.067
	1500	2.481		661	0.182	0.309	0.527	0.140
32800	513	0.435		953	0.347	0.584	1.003	0.275
	741	0.835		1178	0.520	0.852	1.501	0.410
	984	1.409		1362	0.690	1.117	1.977	0.549
	1229	2.054		1745	—	1.722	3.128	0.886
	1449	2.699		1770	1.132	—	—	—
37400	484	0.513	28500	461	—	—	0.345	0.083
	742	1.151		661	0.200	0.358	0.655	0.163
	985	1.852		953	0.390	0.687	1.259	0.333
	1221	2.493		1178	0.579	1.002	1.836	0.494
	1339	2.936		1362	0.762	1.298	2.349	0.655
				1745	—	1.973	3.467	1.047
				1770	1.256	—	—	—
			33250	461	—	—	0.387	0.099
				661	0.233	0.420	0.703	0.197
				953	0.466	0.778	1.307	0.395
				1178	0.695	1.134	2.053	0.590
				1362	0.942	1.454	2.655	0.779
				1745	—	2.212	3.992	1.223
				1810	1.513	—	—	—

LIQUID HOLDUP

Knowledge of the liquid holdup in an absorption tower can be useful in estimating the required surge capacity of a sump or the added weight that supports must carry or in correlating other properties such as pressure drop and mass transfer rates. Most published information on holdup pertains to countercurrent tower operation at conditions below the flooding point where the holdup is not affected by the gas rate. The following work was done to supply necessary data for the design of concurrent flow absorption towers, particularly at higher liquid and gas flow rates.

The variables tested include liquid rate at six levels, gas rate at three levels, and five types of packing; water was the only liquid used. The data were arranged in a statistical design to facilitate interpretation. Experimental procedure utilized an overflow drain to measure volumetric changes in the recycled liquid system. Each series of runs commenced at the highest liquid rate with the liquid at overflow level. Successive changes in holdup were measured by the liquid collected from overflow as liquid rates were decreased by increments down to zero flow. Appropriate corrections for liquid evaporation losses were calculated from inlet and outlet air humidities, air rates, and time intervals.

The data obtained are graphed in Figure 4. The values agree well with prior data, available only for 1-in. Berl saddles and 2-in. steel rings at zero air flow. The effects of variables and the presence of interactions between variables are apparent from an inspection of Figure 4.

In comparison with countercurrent operation, the relationships appear similar at low flow rates but diverge at higher rates. It might be generalized that with increasing flow velocities countercurrent operation tends toward the behavior of a liquid-filled tower and concurrent operation toward that of a tower empty of liquid. With concurrent flow higher gas rates flatten the holdup to liquid-rate relationship, and the relative increase of holdup lessens at higher liquid rates. Loading and flooding points are not obtained. These differences between the systems are expected and define the conditions where concurrent flow may be advantageous.

LITERATURE CITED

1. Dodds, W. S., L. F. Stutzman, B. J. Sollami, and R. J. McCarter, *A.I.Ch.E. Journal*, 6, No. 2, 197 (1960).

Manuscript received March 2, 1959; revision received June 1, 1959; paper accepted June 5, 1959.

Extractive Reaction: Batch and Continuous-Flow Chemical Reaction Systems Dilute Case

EDGAR L. PIRET, W. H. PENNEY, and P. J. TRAMBOUZE

University of Minnesota, Minneapolis, Minnesota

A reaction process occurring simultaneously with an extraction by an immiscible phase is referred to herein as *extractive reaction*.

Quantitative relations are developed which show how the rate of reaction, volumetric efficiency, and reactant conversion of a single-phase batch reaction can be enhanced by deliberately adding to the batch a second phase such as an immiscible solvent or an inert gas.

Analytical solutions are also obtained for continuous-flow extractive reactions of first order and of simple or complex stoichiometry occurring in single- or multistage stirred-tank reactors. The effect of recirculated or side streams is included.

Dilute systems and several types of reactions are considered. The equations are applicable, for instance, to liquid-liquid systems and solid-liquid or gas-liquid processes wherein reaction occurs in either the vapor or condensed phase.

The yield and rate of product formation for many reactions are affected, and often can be favorably increased, by the presence, or the deliberate, controlled addition to the reaction system, of an immiscible, extractive phase. Such operations, involving a simultaneous extraction and reaction process, will be herein referred to as *extractive reactions*.

The performance of such extractive reactions are compared herein to the yields and rate of the corresponding single-phase process. The developments are for batch and also for single- or multistage continuous-flow stirred-tank reactor installations operating on dilute, two-solvent, two-phase systems.

The term *extractive reaction* encompasses several unit operations, for example liquid-liquid extraction, gas absorption and desorption, leaching, distillation, and others wherein a reaction occurs simultaneously with the transfer processes. In the case of extractive reaction the emphasis is on affecting the conversion of a reaction process rather than on designing a unit to effect primarily an absorption, extraction, or separation operation. Related gas-absorption operations in which reactions occur in the gas or in the condensed phases simultaneously with mass transfer have in fact already received considerable attention in connection with the design of plate or packed columns.

Edgar L. Piret is at the American Embassy, Paris, France; W. H. Penney is with Minnesota Mining and Manufacturing Company, St. Paul, Minnesota; and P. J. Trambouze is at Institut Francais du Petrole, Rueil-Malmaison, France.

Of course many commercially important chemical reactions normally take place in multiphase systems, for example sulfonation, nitration, alkylation, esterification, etc., and the ratio of the phases can be varied for optimum results. The reactants enter the system in two or more immiscible phases, and two phases are normally present during the reaction; however in addition one should consider that some reactions which are carried out in a single-phase system or are normally followed by a solvent extraction, distillation, or other separation operation may be improved by deliberately introducing a second extractive phase to affect the rate of a reaction and conversion to a desired product and/or simultaneously to achieve the separation of the products.

In the following development, mixing of the phases will always be considered as being high and so effective that they will be in physical equilibrium with each other at all times. With mass transfer essentially instantaneous, it is the chemical-reaction step which controls the over-all rate of the process. The agitation is also sufficient to ensure that at all times the concentrations in either phase are uniform throughout the reactor contents. The simplifications will be made that reaction takes

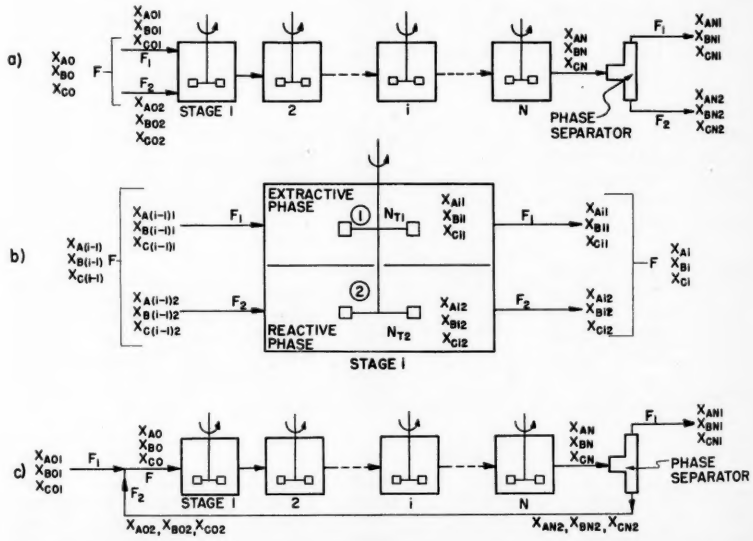

Fig. 1. Concurrent two-phase extractive-reaction systems, including separators and recirculation.

place in one phase only and that the presence of solvent has no effect upon the rate constants and reaction mechanism. No reaction occurs in the inert, solvent phase or at the interphase. However the equations are easily modified to include reaction in both phases. Isothermal conditions are assumed. The phase equilibrium partition coefficients and solubilities are considered as being independent of concentrations. Such conditions may obtain closely if the reacting components are present in low concentrations. As an example, the reactants are in a dilute aqueous phase, and a second immiscible liquid, such as benzene, is added to affect an extractive reaction process; this constitutes a dilute, two-solvent, two-phase system, the two solvents being in this case water and benzene. In another example an inert gas is caused to flow through a dilute, reactive liquid phase so as to strip a product or feed a reactant. A solid reactant might be present in the liquid, when a three-phase extractive reaction process is involved.

For simplicity of text, ideal solutions are assumed, and so activity coefficients are not written into the equations. For specific cases this simplification can be modified as needed. Concentrated solutions, higher order reactions, and single-solvent, two-phase systems will be considered in a later paper. Numerical examples will also be given.

TWO-PHASE BATCH PROCESSES

First-Order Reversible Reactions

A first-order reversible reaction of kinetics $A \underset{k'}{\overset{k}{\rightleftharpoons}} B$ and of stoichiometry $aA = bB$ is occurring in a two-phase extractive reaction batch process. The rate of decrease of concentration of A, that is $-(1/V)(dn_A/dt)$, in a homogeneous irreversible reaction system is set equal to $k(n_A/V)$. However since the partition coefficients are defined in terms of mole fractions, it is deemed convenient in the following sections to express the rate equations in terms of mole fractions rather than concentrations.

The rate equation in a single-phase system is

$$-\frac{dn_A}{V} = \frac{k}{V} x_A n_T\, dt - \frac{k'}{V} x_B n_T\, dt \tag{1}$$

Since the two-phase reaction occurs in dilute concentrations, the phase volumes and the ratio of the total moles in the extractive layer to that of the reactive layer may be considered constant throughout the reaction process.

Equation (1) becomes

$$-dn_A = k\, x_A\, n_T\, dt - k'\, x_B\, n_T\, dt \tag{2}$$

and since in a two-phase system

$$n_A = n_{A_1} + n_{A_2} \tag{3}$$

then from (2) and (3)

$$dn_{A_1} + dn_{A_2} = k'\, x_{B_2}\, n_{T_2}\, dt - k\, x_{A_2}\, n_{T_2}\, dt \tag{4}$$

The partition coefficient of a component is given by the ratio of its mole fractions in the two phases; thus

$$\alpha_A = \frac{x_{A_1}}{x_{A_2}} = \frac{n_{A_1}\, n_{T_2}}{n_{A_2}\, n_{T_1}} = \frac{n_{A_1}}{n_{A_2} R}$$

Upon substitution (4) becomes

$$(\alpha_A R + 1) dn_{A_2} + \alpha_A n_{A_2} dR = k' x_{B_2} n_{T_2}\, dt - k\, x_{A_2} n_{T_2}\, dt \tag{5}$$

and since R is constant

$$(\alpha_A R + 1)\, dn_{A_2} = k'\, x_{B_2}\, n_{T_2}\, dt - k\, x_{A_2}\, n_{T_2}\, dt \tag{6}$$

From stoichiometry

$$x_{B_2} = \frac{\dfrac{b}{a} n_{A_0 T} + n_{B_0 T}}{n_{T_2}} - \frac{b}{a} x_{A_2}(\alpha_A R + 1)}{(\alpha_B R + 1)} \tag{7}$$

Combining (6) and (7) yields

$$-\frac{dx_{A_2}}{dt} = \frac{bk'\, x_{A_2}}{a(\alpha_B R + 1)} + \frac{k x_{A_2}}{\alpha_A R + 1} - \frac{k'[b n_{A_0 T} + a n_{B_0 T}]}{a n_{T_2}(\alpha_A R + 1)(\alpha_B R + 1)} \tag{8}$$

Equation (8) relates dx_{A_2}/dt, the change in mole fraction of component A within the reactive phase only, with time.

$$x_{A_2} = \frac{[bk'(\alpha_A R + 1) + ak(\alpha_B R + 1)]\, n_{T_2}\, x_{A_{02}} - k'(b n_{A_0 T} + a n_{B_0 T})(1 - e^{\sigma})}{[bk'(\alpha_A R + 1) + ak(\alpha_B R + 1)] n_{T_2} e^{\sigma}} \tag{10}$$

where

$$\sigma = \frac{[bk'(\alpha_A R + 1) + ak(\alpha_B R + 1)]}{a(\alpha_A R + 1)(\alpha_B R + 1)} t$$

When $R = 0$, (10) becomes

$$x_A = \frac{[bk' + ak]\, n_T x_{A_0} - k'(b n_{A_0} + a n_{B_0})(1 - e^{\nu})}{[bk' + ak]\, n_T e^{\nu}} \tag{11}$$

where

$$\nu = \left(\frac{b}{a} k' + k\right) t$$

Combination of (8), (9), (10), and (11) yields

$$-\frac{dx_{A_2}}{dt} = \frac{[bk'(\alpha_A R + 1) + ak(\alpha_B R + 1)]\, n_{T_2} x_{A_{02}} - k'(b n_{A_0 T} + a n_{B_0 T})}{a\, n_{T_2}(\alpha_A R + 1)(\alpha_B R + 1) e^{\sigma}} \tag{12}$$

and

$$-\frac{dx_A}{dt} = \frac{[bk' + ak] n_T x_{A_0} - k'(b n_{A_0} + a n_{B_0})}{a\, n_T\, e^{\nu}} \tag{13}$$

Two-Phase Effect on Rate of Reaction, Time Ratio, Conversion Ratio, and Equilibrium Conversion

The development of expressions for the effect of an added phase on the rate of reaction, production per unit time, and equilibrium conversion of a single-phase system will now be illustrated for the above first-order reaction. Higher-order reactions can be treated in a similar manner.

The instantaneous over-all influence of the added phase on the reaction rate is expressed by the ratio of the total reactant consumption rate in a two-phase process to that in a single-phase operation at equal reaction times; that is $E_r = \dfrac{dn_{AT}}{dn_A}$ when $t = t_{ER}$.

A time ratio is defined as the ratio t/t_{ER} of the times required for equal fractional molar conversions in a two-phase and in an alternate single-phase system when the initial total number of moles of component A charged to the systems are the same; that is

$$\frac{\Delta n_{AT}}{n_{A_0 T}} = \frac{\Delta n_A}{n_{A_0}} \text{ and } n_{A_0 T} = n_{A_0}$$

The effect of the added phase on the equilibrium conversion is indicated by the ratio of the fractional conversions at equilibrium and for equal total number of moles of reactants charged to the systems; that is

$$E_e = \frac{(n_{A_0 T} - n^{\circ}_{AT}) / n_{A_0 T}}{(n_{A_0} - n^{\circ}_{A}) / n_{A_0}} = \frac{(n_{A_0 T} - n^{\circ}_{AT})}{(n_{A_0} - n^{\circ}_{A})} = \frac{\Delta n^{\circ}_{AT}}{\Delta n^{\circ}_{A}}$$

where $n_{A_0 T} = n_{A_0}$.

Reaction-Rate Ratio The single-phase reaction rate $-dx_A/dt$ is readily obtained from (8) by letting R be zero.

$$-\frac{dx_A}{dt} = \left(\frac{b}{a} k' + k\right) x_A - \frac{k'(b n_{A_0} + a n_{B_0})}{a n_T} \tag{9}$$

Also from (8) by integration

The ratio dx_{A2}/dx_A may be formed:

$$\frac{dx_{A2}}{dx_A} = \frac{e^{(\nu-\sigma)}\left[\frac{bk'}{\alpha_B R+1} + \frac{ak}{\alpha_A R+1}\right] x_{A02} - \frac{k'(bn_{AoT} + an_{BoT})}{n_{T2}(\alpha_A R+1)(\alpha_B R+1)}}{[bk' + ak]\ x_{Ao} - \frac{k'}{n_T}(bn_{Ao} + an_{Bo})} \quad (14)$$

An expression in terms of the total reactant consumption rate, dn_{AT}/dn_T, is obtained:

$$\frac{dx_{A2}}{dx_A} = \frac{dn_{AT}}{dn_A}\left[\frac{n_T}{n_{T2}(\alpha_A R+1)}\right] \quad (15)$$

Equations (14) and (15) give

$$E_r = \frac{dn_{AT}}{dn_A} = \frac{e^{(\nu-\sigma)}[bk'(\alpha_A R+1) + ak(\alpha_B R+1)]\, n_{T2}\, x_{A02} - k'(bn_{AoT} + an_{BoT})}{(\alpha_B R+1)[(bk' + ak)\, n_T\, x_{Ao} - k'(bn_{Ao} + an_{Bo})]} \quad (16)$$

Equation (16) describes the ratio of total reactant consumption rates for a first order reversible reaction as a function of time and the constants of the systems.

This relation can be advantageously applied for example to highly exothermic and autocatalytic reaction systems where the control of the rate of reaction for heat transfer or quality of product purposes is often of prime importance.

Time Ratio The integrated form of Equation (8) is

$$\frac{[bk'(\alpha_A R+1) + ak(\alpha_B R+1)]}{a(\alpha_A R+1)(\alpha_B R+1)}\, t_{ER} = \ln\left[\frac{[bk'(\alpha_A R+1) + ak(\alpha_B R+1)]\, n_{T2}\, x_{A02} - k'(bn_{AoT} + an_{BoT})}{[bk'(\alpha_A R+1) + ak(\alpha_B R+1)]\, n_{T2}\, x_{A2} - k'(bn_{AoT} + an_{BoT})}\right]$$

which when written for a single-phase system becomes

$$\left[\frac{bk' + ak}{a}\right] t = \ln\left[\frac{(bk' + ak)\, n_T\, x_{Ao} - k'(bn_{Ao} + an_{Bo})}{(bk' + ak)\, n_T\, x_A - k'(bn_{Ao} + an_{Bo})}\right]$$

If $\Delta n_{AT} = \Delta n_A$; that is, the moles of reactant converted in the extractive reaction and in the single-phase system are equal, then

$$n_{T2}x_{A2} = \frac{n_{AoT} - (n_{Ao} - n_A)}{(\alpha_A R+1)}$$

and molar balance requires

$$n_{T2}x_{A02} = n_{AoT}/(\alpha_A R+1)$$

From these relations a production time ratio t/t_{ER} is obtained:

$$\frac{t}{t_{ER}} = \frac{t[bk'(\alpha_A R+1) + ak(\alpha_B R+1)]}{a(\alpha_A R+1)(\alpha_B R+1)} \Big/ akn_{AoT}\left(\frac{\alpha_B R+1}{\alpha_A R+1}\right) - ak'(n_{BoT})$$

$$\ln\left[\frac{}{ak\left(\frac{\alpha_B R+1}{\alpha_A R+1}\right)[n_{AoT} - (n_{Ao} - n_A)] - k'[an_{BoT} + b(n_{Ao} - n_A)]}\right] \quad (17)$$

Equation (17) is the ratio of the times required to form equal moles of product for any initial concentrations or solvent ratios. If the ratio exceeds unity, the extractive reaction has the higher production per unit time.

When the initial total charges of component A are equal n_{AoT} is set equal to n_{Ao}, and (17) reduces to E_t, the ratio of times required to produce the same fractional conversion. E_t is a function of the molar phase ratio, the system properties, and the single-phase batch time.

Equilibrium Conversion Ratio. The value of the equilibrium constant, within the reactive phase of either a two- or a single-phase system, is a constant, and so

$$K_{eq} = k/k' = x^*_{B2}/x^*_{A2} = x^*_B/x^*_A = \frac{n^*_{B2}/n^*_{T2}}{n^*_{A2}/n^*_{T2}} = \frac{n^*_B/n^*_T}{n^*_A/n^*_T}$$

From a mass balance for a single-phase system

$$K_{eq.} = \frac{\frac{b}{a}(n_{Ao} - n^*_A) + n_{Bo}}{n^*_A} \quad (18)$$

From a mass balance for a two-phase system

$$K_{eq.} = \frac{(\alpha_A R+1)\left[\frac{b}{a}(n_{AoT} - (\alpha_A R+1)n^*_{A2}) + n_{BoT}\right]}{n^*_{AT}(\alpha_B R+1)} \quad (19)$$

From (8), when $-dx_{A2}/dt = 0$

$$n^*_{A2} = \frac{k'[bn_{AoT} + an_{BoT}]}{bk'(\alpha_A R+1) + ak(\alpha_B R+1)} \quad (20)$$

Likewise from (8), when $dx_{A2}/dt = 0$ and also $R = 0$

$$n^*_A = \frac{k'[bn_{Ao} + an_{Bo}]}{bk' + ak} \quad (21)$$

By equating (18) and (19) there results

$$\frac{\Delta n^*_{AT}}{\Delta n^*_A} = \frac{b(\alpha_B R+1)\ n^*_{AT}(n_{AoT} - n^*_{AT})}{n^*_A(\alpha_A R+1)[b(n_{AoT} - n^*_{AT}) + an_{BoT}] - [an_{Bo}\, n^*_{AT}(\alpha_B R+1)]} \quad (22)$$

If there is no initial component B present, n_{BoT} and n_{Bo} are zero, and with the substitution of Equations (20) and (21) Equation (22) reduces to

$$\frac{\Delta n^*_{AT}}{\Delta n^*_A} = \frac{n_{AoT}(\alpha_B R+1)\ (bk' + ak)}{n_{Ao}[bk'(\alpha_A R+1) + ak(\alpha_B R+1)]} \quad (23)$$

If $n_{AoT} = n_{Ao}$, then the equilibrium conversion ratio is obtained:

$$E_e = \frac{(\alpha_B R+1)(bk' + ak)}{bk'(\alpha_A R+1) + ak(\alpha_B R+1)} \quad (24)$$

This equation indicates an equilibrium-conversion advantage for the two-phase system when $\alpha_B > \alpha_A$.

TWO-PHASE CONTINUOUS STIRRED-TANK REACTOR SYSTEMS

The assumption of physical equilibrium between the phases in continuous extractive reaction processes can often best be achieved in continuous stirred-tank reactor (CSTR) systems, since it is in these installations that high levels of agitation can most readily be provided. In a CSTR chain the streams of the two phases can be arranged in several ways; hence the concurrent, crosscurrent, and countercurrent installations are of interest. Analytical solutions are illustrated herein for typical stoichiometrically simple as well as stoichiometrically complex first-order reaction systems.

Concurrent Arrangement

The kinetics and stoichiometry of the first-order reaction occurring in the system is taken as $A \xrightarrow{k} B \xrightarrow{k_1} C$. This is an example of a reaction which is kinetically and stoichiometrically complex (2).

In a concurrent arrangement the separation of the two phases need occur only at the end of the CSTR chain (Fig. 1*a*); however to facilitate the writing of the molar balances, an imagined separation of phases in stage i is schematized in Figure 1*b*.

$$F\,x_{A(i-1)} = F\,x_{Ai} + k\,n_{T_2}\,x_{Ai2} \quad (25a)$$

$$F\,x_{B(i-1)} = F\,x_{Bi} + k_1\,n_{T_2}\,x_{Bi2} - k\,n_{T_2}\,x_{Ai2} \quad (25b)$$

$$F\,x_{C(i-1)} = F\,x_{Ci} - k_1\,n_{T_2}\,x_{Bi2} \quad (25c)$$

with

$$F\,x_{Ai} = F_1\,x_{Ai1} + F_2\,x_{Ai2} \quad (26)$$

and identical relations for components B and C.

As in the batch case the two solvents are assumed completely immiscible or of partial miscibility not affected by the content of A, B, and C, which are present in low concentrations in either phase. Since the ratio of the phases within the reactors is not necessarily equal to the ratio of the flow rates,

$$\frac{F_1}{F_2} = \epsilon\,\frac{n_{T_1}}{n_{T_2}} = \epsilon R$$

where ϵ depends upon operating conditions and on the apparatus design, such for example as the position of baffles relative to the outlet tube (*1*). F_1, F_2, R, and ϵ can be assumed to remain constant along the reactor chain.

Then from (26)

$$x_{Ai2} = \frac{\epsilon R + 1}{\alpha_A\,\epsilon R + 1}\,x_{Ai} \quad (27)$$

Similar expressions are found for x_{Bi2} and x_{Ci2}.

Equations (25) become

$$x_{A(i-1)} = x_{Ai}\,(1 + A_1) \quad (28a)$$

$$x_{B(i-1)} = x_{Bi}\,(1 + A_2) - A_1\,x_{Ai} \quad (28b)$$

$$x_{C(i-1)} = x_{Ci} - A_2\,x_{Bi} \quad (28c)$$

where

$$A_1 = \frac{k\,n_{T_2}}{F}\,\frac{\epsilon R + 1}{\alpha_A\,\epsilon R + 1} \text{ and}$$

$$A_2 = \frac{k_1\,n_{T_2}}{F}\,\frac{\epsilon R + 1}{\alpha_B\,\epsilon R + 1}$$

From (28*a*) and (28*b*) a second-order difference equation is obtained:

$$x_{Bi}\,(1 + A_1)\,(1 + A_2) - x_{B(i-1)}\,(2 + A_1 + A_2) + x_{B(i-2)} = 0 \quad (29)$$

The roots of the characteristic equation are $\rho_1 = 1/1 + A_1$ and $\rho_2 = 1/1 + A_2$, and the general solution is, if $A_1 \neq A_2$:

$$x_{Bi} = G_1\,\rho_1^{\,i} + G_2\,\rho_2^{\,i} \quad (30)$$

By substituting (30) into (28*b*), one obtains

$$x_{Ai} = \frac{A_2 - A_1}{A_1}\,G_1\,\rho_1^{\,i} \quad (31)$$

and from (28*c*)

$$x_{Ci} = -\left[\frac{A_2}{A_1}\,G_1\,\rho_1^{\,i} + G_2\,\rho_2^{\,i}\right] + G_3 \quad (32)$$

The constants G_1, G_2, and G_3 are obtained from the boundary conditions, that is the feed compositions

$$x_{Ao} = \frac{F_1}{F}\,x_{Ao_1} + \frac{F_2}{F}\,x_{Ao_2}$$

with similar expressions for x_{Bo} and x_{Co}.

By equating these values of the feed to Equations (31), (30), and (32) when $i = 0$, one can obtain three equations in G_1, G_2, and G_3:

$$x_{Ao} = \frac{A_2 - A_1}{A_1}\,G_1,\; x_{Bo} = G_1 + G_2,$$

$$x_{Co} = G_3 - \frac{A_2}{A_1}\,G_1 - G_2$$

The composition of the final product of the reactor chain, x_{AN}, x_{BN}, and x_{CN}, is given by Equations (31), (30), and (32), with $i = N$. In some cases the residence time of the reactive phase in the phase separator will need to be taken into account to get the actual values of x_{AN_2}, x_{BN_2} and x_{CN_2}.

Recirculation of the reactive phase Recirculation of the reactive phase may result in better utilization of the reactants (Figure 1*c*). In this case $x_{Ao2} = x_{AN_2}$, $x_{Bo2} = x_{BN_2}$, and $x_{Co2} = x_{CN_2}$. Equations (30), (31), and (32) remain the same; only the boundary conditions are changed so that

$$x_{Ao} = \frac{F_1}{F}\,x_{Ao1} + \frac{F_2}{F}\,x_{Ao2}$$

$$= \frac{F_1}{F}\,x_{Ao1} + \frac{F_2}{F}\,x_{AN_2}$$

Using the value of x_{AN_2} given by Equation (31) one gets

$$x_{Ao} = \frac{\epsilon R\,x_{Ao1} + \dfrac{A_2 - A_1}{A_1}\,G_1\,\rho_1^{\,N}}{1 + \epsilon R}$$

$$= \frac{A_2 - A_1}{A_1}\,G_1$$

and similarly

$$x_{Bo} = \frac{\epsilon R\,x_{Bo1} + G_1\,\rho_1^{\,N} + G_2\,\rho_2^{\,N}}{1 + \epsilon R} = G_1 + G_2$$

$$x_{Co} = \frac{\epsilon R\,x_{Co1} + G_3 - \dfrac{A_2}{A_1}\,G_1\rho_1^{\,N} - G_2\rho_2^{\,N}}{1 + \epsilon R}$$

$$= G_3 - \frac{A_2}{A_1}\,G_1 - G_2$$

These equations allow the determination of G_1, G_2, and G_3 and the solution of the design problem.

Cross-current Arrangement

In this arrangement each reactor stage receives a stream of extractive phase, of the same composition for each stage, and also a stream of reactive phase coming from the phase separator of the preceding stage (Figure 2). If residence times in the phase separators are small compared with the holding times in the reactor stage, their effects may be neglected.

Crosscurrent operation may often be advantageous for reversible reactions; hence a first-order reversible reaction

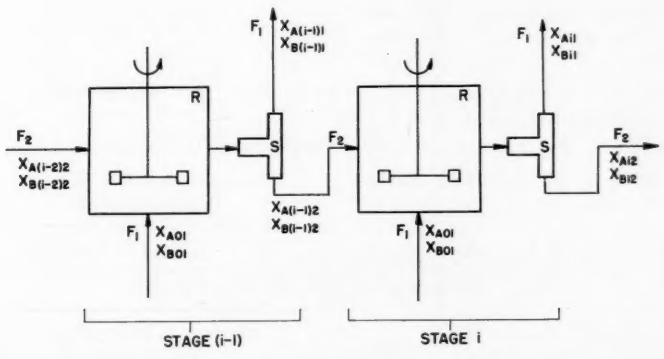

Fig. 2. Countercurrent two-phase extractive-reaction system with separators.

will be considered. Its stoichiometry is expressed by $aA = bB$ and kinetics by $A \underset{k_1}{\overset{k}{\rightleftharpoons}} B$, so that

$$-\frac{dn_A}{dt} = a\,k\,n_A - a\,k_1\,n_B \text{ and}$$

$$\frac{dn_B}{dt} = b\,k\,n_A - b\,k_1\,n_B$$

The case selected is stoichiometrically simple. Since the concentrations of A and B are assumed small, F_1 and F_2 will be taken as constant, even if $a \neq b$.

Molar balances around the ith stage result in

$$x_{A(i-1)2} + \epsilon R\, x_{Ao_1} = x_{Ai_2}\left[1 + \epsilon R\alpha_A + k\,a\frac{n\tau_2}{F_2}\right] - k_1\,a\frac{n\tau_2}{F_2}\,x_{Bi_2} \qquad (33a)$$

$$x_{B(i-1)2} + \epsilon R\, x_{Bo_1} = x_{Bi_2}\left[1 + \epsilon R\alpha_B + k_1\,b\frac{n\tau_2}{F_2}\right] - k\,b\frac{n\tau_2}{F_2}\,x_{Ai_2} \qquad (33b)$$

For simplicity of presentation set $x_{Ao_1} = x_{Bo_1} = 0$; that is each stage receives an extractive stream of pure solvent.

By letting

$$1 + \epsilon R\,\alpha_A = A_1,\ 1 + \epsilon R\,\alpha_B = A_2,$$

$$k\frac{n\tau_2}{F_2} = B_1 \text{ and } k_1\frac{n\tau_2}{F_2} = B_2$$

Equations (33) become

$$x_{A(i-1)2} = (A_1 + a\,B_1)\,x_{Ai_2} - a\,B_2 x_{Bi_2} \qquad (34a)$$

$$x_{B(i-1)2} = (A_2 + b\,B_2)\,x_{Bi_2} - b\,B_1 x_{Ai_2} \qquad (34b)$$

By combining (34a) and (34b) one obtains the second order difference equation:

$$x_{Ai_2}[(A_2 + b\,B_2)(A_1 + a\,B_1) - a\,b\,B_1\,B_2] - x_{A(i-1)2}[A_1 + A_2 + a\,B_1 + b\,B_2] + x_{A(i-2)2} = 0 \qquad (35)$$

The roots of the corresponding characteristic equation are

$$\rho_1;\ \rho_2 = \frac{(A_1 + A_2 + aB_1 + bB_2) \pm \sqrt{(A_1 + aB_1 - A_2 - bB_2)^2 + 4ab\,B_1\,B_2}}{2[(A_1 + aB_1)(A_2 + bB_2) - a\,b\,B_1\,B_2]}$$

and the solution of (35) is

$$x_{Ai_2} = G_1\rho_1^{\,i} + G_2\rho_2^{\,i} \qquad (36)$$

From (44)

$$x_{Bi_2} = \frac{1}{a\,B_2}\left[G_1\left(A_1 + a\,B_1 - \frac{1}{\rho_1}\right)\rho_1^{\,i} + G_2\left(A_1 + a\,B_1 - \frac{1}{\rho_2}\right)\rho_2^{\,i}\right] \qquad (37)$$

The constants G_1 and G_2 are obtained by expressing the feed composition x_{Ao2} and x_{Bo2} by the means of Equations (36) and (37) when $i = 0$:

$$x_{Ao2} = G_1 + G_2$$

$$x_{Bo2} = \frac{1}{a\,B_2}\left[G_1\left(A_1 + a\,B_1 - \frac{1}{\rho_1}\right) + G_2\left(A_1 + a\,B_1 - \frac{1}{\rho_2}\right)\right]$$

As in the concurrent arrangement, the effect of reactive-phase recirculation can also be calculated.

Countercurrent Arrangement

Figure 3 schematizes the chain under consideration. Again residence times in the phase separators will be considered small. Since the equations for countercurrent arrangements quickly become elaborate, the simple case of a first-order reversible reaction $A \underset{k_1}{\overset{k}{\rightleftharpoons}} B$ is chosen here. However more complex first-order reactions can be similarly treated.

The molal balances for components A and B around the ith stage are

$$F_2\,x_{A(i+1)2} - (\alpha_A F_1 + F_2 + k\,n\tau_2)\,x_{Ai_2} + k_1\,n\tau_2\,x_{Bi_2} + \alpha_A F_1\,x_{A(i-1)2} = 0 \qquad (38a)$$

$$F_2\,x_{B(i+1)2} - (\alpha_B F_1 + F_2 + k_1\,n\tau_2)\,x_{Bi_2} + k\,n\tau_2\,x_{Ai_2} + \alpha_B F_1\,x_{B(i-1)2} = 0 \qquad (38b)$$

By letting

$$A_1 = \alpha_A\,\epsilon R + 1 + \frac{k\,n\tau_2}{F_2},$$

$$B_1 = \frac{k_1\,n\tau_2}{F_2},\ C_1 = \epsilon R\,\alpha_A$$

$$A_2 = \epsilon R\,\alpha_B + 1 + k_1\frac{n\tau_2}{F_2},$$

$$B_2 = \frac{k\,n\tau_2}{F_2}, \text{ and } C_2 = \epsilon R\,\alpha_B$$

Equations (38) become

$$x_{A(i+1)2} - A_1\,x_{Ai_2} + B_1\,x_{Bi_2} + C_1\,x_{A(i-1)2} = 0 \qquad (39a)$$

$$x_{B(i+1)2} - A_2\,x_{Bi_2} + B_2\,x_{Ai_2} + C_2\,x_{B(i-1)2} = 0 \qquad (39b)$$

From (39a) and (39b) the fourth order difference equation is found to be

$$x_{A(i+3)2} - (A_1 + A_2)\,x_{A(i+2)2} + (C_1 + C_2 + A_1A_2 - B_1B_2)\,x_{A(i+1)2} - (A_2C_1 + A_1C_2)\,x_{Ai_2} + C_1C_2\,x_{A(i-1)2} = 0 \qquad (40)$$

Since $A_1 = 1 + C_1 + B_2$ and $A_2 = 1 + C_2 + B_1$, the characteristic equation is

$$(\rho - 1)[\rho^3 - (1 + C_1 + C_2 + B_1 + B_2)\,\rho^2 + (C_1 + C_2 + C_1C_2 + B_2C_2 + B_1C_1)\,\rho - C_1C_2] = 0$$

whose roots are 1, ρ_1, ρ_2, and ρ_3. The general solution may then be written, if the roots all differ, as

$$x_{Ai_2} = G_o + G_1\rho_1^{\,i} + G_2\rho_2^{\,i} + G_3\rho_3^{\,i} \qquad (41)$$

and from (39)

$$x_{Bi_2} = \frac{-1}{B_1}[G_o(1 - A_1 + C_1) + G_1(\rho_1^{\,2} - A_1\rho_1 + C_1)\,\rho_1^{\,i-1} + G_2(\rho_2^{\,2} - A_1\rho_2 + C_1)\,\rho_2^{\,i-1} + G_3(\rho_3^{\,2} - A_1\rho_3 + C_1)\,\rho_3^{\,i-1}] \qquad (42)$$

The constants G_o, G_1, G_2, and G_3 are determined from the knowledge of the inlet streams compositions, x_{Ao_1}, x_{Bo_1}, $x_{A(N+1)2}$, and $x_{B(N+1)2}$. Similarly if $i = N + 1$, other inlet compositions $x_{A(N+1)2}$ and $x_{B(N+1)2}$ are given by Equations (41) and (42). The resulting set of four equations allows the determination of G_o, G_1, G_2, and G_3.

In the case of recirculation of the reactive phase from the separator of the first stage to the last-stage reactor, the boundary conditions are different. The composition of the fresh feed entering the system x_{Ao_2} and x_{Bo_2} is of course usually known, but $x_{A(N+1)2}$ and $x_{B(N+1)2}$ are unknown. These however are respectively equal to x_{A12} and x_{B12}, and so again a set of four equations leads to the values of the constants.

REMARKS

In a chemical reacting system the total number of components taking part in the reaction can be distinguished from the number of components playing a role in the kinetics. If there are S independent stoichiometric relations between the M components and S' independent stoichiometric relations between the M' components, in the general case $M \geqq M'$, $S \geqq S'$, and $S \geqq 1$. As an example consider the following set of reactions:

$$A + B \leftrightharpoons C + D$$
$$C + D \rightarrow E + F$$
$$A + E \rightarrow G + J$$

Here $M = 8$ and $M' = 5$ (A, B, C, D, E). The independent stoichiometric relations are

$$\Delta n_G = \Delta n_J$$
$$\Delta n_A + \Delta n_B + \Delta n_C + \Delta n_D + \Delta n_E$$

$$+ \Delta n_F + \Delta n_G + \Delta n_J = 0$$
$$\Delta n_C = \Delta n_D$$

then

$$S = 3 \text{ and } S' = 1$$

In addition to the S stoichiometric relations, kinetic analysis yields M rate equations, which, when combined with material balances over the reactor, form the basis of design calculations. The mathematical problem is one of solving these M differential or difference equations with the boundary conditions, usually given by the feed, product, or recycle compositions.

The number of equations to be solved will be equal to the number of independent variables. In general (if phase-volume variations are neglected) this number is equal to the total number of components playing a role in the kinetics, minus the number of stoichiometric relations existing between these same components; that is $m = M' - S'$.

It is advantageous, as shown previously (2), to distinguish between kinetically simple reactions, that is where $m = 1$, and kinetically complex reactions, that is where $m > 1$. In the case of stoichiometrically simple reactions the use of the stoichiometric equation and of the initial conditions reduces the number of independent variables from M' to unity, and so in this case only one final equation has to be solved.

In a two-phase system, where physical equilibrium between the phases is assumed, the number of independent variables remains the same as in a single-phase system because additional relations, such as $a_1 = \alpha_A a_2$, give the composition of the phase when the composition of the other phase is known.

The available stoichiometric relations, however, can always be used to reduce the number of variables in conservative arrangements, that is where the total mass of reactants and products is the same in all portions of the system. Examples of conservative arrangements are batch, tubular, and single or multistage continuous stirred-tank reactors operating on single-phase reactions, and also batch and concurrent CSTR two-phase reaction systems. In such arrangements the boundary conditions may be given at any points of the system, without making impossible the use of the stoichiometric relations. In some cases, such as in a concurrent arrangement with recirculation, where boundary conditions are more complex, it can be more convenient for analytical purposes not to use the stoichiometric relations but rather to retain the original number of variables and to solve a larger number of simultaneous equations. Crosscurrent and countercurrent CSTR two-phase reaction arrangements are nonconservative; hence the S' stoichiometric relations cannot be used and $m = M'$. In a countercurrent arrangement the stoichiometric relations can be used only when the two necessary boundary conditions are given at the same end of the system.

If for any of the above listed nonconservative arrangements a stage-by-stage rather than an analytical solution is used, then, since a single stage is conservative, the stoichiometric relations can be applied.

The consequences of these remarks can be illustrated by considering first-order reaction systems. In such cases the simultaneous solution of the initial set of rate equations leads to one differential or difference equation, for example Equation (29) from (25), (35) from (33), and (40) from (38). In Table 1 the order p of the final equation to be solved is shown. It is seen how this order varies with the reactor type and arrangement used as well as with the reaction itself. The magnitude of p gives an idea of the complexity of the problem. It will be seen that for a countercurrent CSTR arrangement $p = 2M'$, because in the initial set the equations are of second order.

In a subsequent paper variations in volume will be considered. It will be seen that if the arrangement is conservative, $m = M - S$ and if nonconservative $m = M$.

Table 1. Order p of the Differential (D) or Difference (Δ) Equation Describing Homogeneous and Two-phase Processes with Negligible Phase-volume Changes

Reactor system	Reaction type: First order, stoichiometrically simple	Reaction type: First order, stoichiometrically complex
Single phase		
Batch or tubular	$Dp = 1$	$Dp = M' - S'$
Continuous stirred-tank reaction or	$\Delta p = 1$	$\Delta p = M' - S'$
Two-phase*		
Batch or tubular	$Dp = 1$	$Dp = M' - S'$
CSTR: Concurrent	$\Delta p = 1$	$\Delta p = M' - S'$
Concurrent with recirculation	$\Delta p = M'$	$\Delta p = M'$
Crosscurrent	$\Delta p = M'$	$\Delta p = M'$
Countercurrent	$\Delta p = 2M'$	$\Delta p = 2M'$

* When equilibrium is assumed between the phases.

ACKNOWLEDGMENT

This investigation was in part supported by a Minnesota Mining and Manufacturing Co. Fellowship and by an appointment of the International Cooperation Administration under a program administered by the National Academy of Sciences.

NOTATION

$A, B, C, D,$ = components A, B, C, D
a, b, c, d = stoichiometric coefficients
E_e = equilibrium conversion ratio
E_r = rate ratio

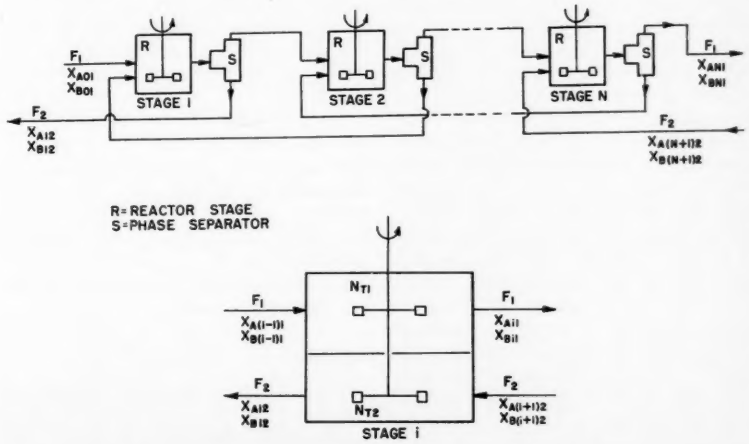

Fig. 3. Cross-current two-phase extractive-reaction system including separators.

F = molal flow rate of either or both phases, moles/min.
K = equilibrium constant
k, k_1 k_2 = reaction-rate constants
M = number of components taking part in the reaction
M' = number of components playing a role in the kinetics
m = number of independent variables
N = total number of stages in a chain
n = number of moles
N_{T1} = total number of moles in the extractive phase
n_{T2} = total number of moles in the reactive phase
p = order of differential or difference equation
R = ratio of the total number of moles in the extractive phase to the total number of moles in the reactive phase, n_{T_1}/n_{T_2}
S, S' = number of independent stoichiometric relations between the M or M' components
t = time
t_{ER} = time in an extractive reaction batch process
V = volume of the reactor
x_A = mole fraction of component A
x_{A1} = mole fraction of A in the extractive phase
$x_{A_{1_i}}$ = mole fraction of A in the extractive phase of the ith reactor stage
α_A = partition coefficient of the component A, x_{A_1}/x_{A_2}
ϵ = factor relating the phase ratio in a reactor to the effluent flow rates, $F_1/F_2 = \epsilon R$

Subscripts

$A, B, C \ldots$ = components $A, B, C \ldots$
i = any stage in a reactor chain
o = initial conditions
T = total moles in either or both phases
1, 2 = extractive and reactive phase respectively

Superscripts

$^\circ$ = chemical equilibrium conditions

LITERATURE CITED

1. Mattern, R. V., Olegh Bilous, and E. L. Piret, *A.I.Ch.E. Journal*, **3**, 497 (1957).
2. Trambouze, P. J., and E. L. Piret, *ibid.*, **5**, 384 (1959).

Manuscript received January 6, 1959; revision received January 4, 1960; paper accepted January 4, 1960.

Longitudinal Mixing in Fluidization

E. J. CAIRNS and J. M. PRAUSNITZ

University of California, Berkeley, California

Longitudinal mixing properties in liquid-solid fluidized beds were investigated by means of a salt-solution tracer technique. The electrical conductance breakthrough curves were measured with very small electrical conductivity probes for a step-function input of salt-solution tracer. Longitudinal eddy diffusivities were determined for 1.3- and 3.0-mm. lead spheres and 3.2-mm. glass spheres in 2- and 4-in.–diameter beds at a distance of 5 bed diam. from the injector and for various radial positions.

The longitudinal mixing properties are strongly affected by particle concentration; maximum mixing occurs at a fraction voids of 0.7. Longitudinal eddy diffusivity increases with particle density and with decreasing d_p/D ratio. Velocity profiles markedly influence the eddy-diffusivity profiles.

Fluidized systems have been of great interest in industry for the past decade or more and have come into prominence for use as chemical reactors. In most cases the yields of such reactors are highest when the radial mass transfer processes are maximized and the axial mass transfer processes minimized. The complicated hydrodynamic situation in fluidization defies theoretical analysis, except for very simplified and inexact approaches. Consequently there has been increased effort in the direction of definitive experimentation. A few radial-mixing studies have been conducted (*2, 10*), but data on longitudinal mixing in fluidized systems are rare. Gilliland, Mason, and Oliver (*9*) have presented a few data points for longitudinal diffusion in gas-solid fluidization, and these results yield longitudinal Peclet numbers (Ud_p/E) in the range of 0.0005 to 0.0015. Danckwerts *et al.* (*5*) investigated residence times in an industrial fluidized reactor, and their over-all Peclet number was of the order of 0.001.

The purpose of the present work was to determine and to investigate the important variables affecting the longitudinal mixing in liquid-solid fluidized systems. The mathematics of the model used here was originally presented by H. A. Einstein (*8*) in connection with the motion of pebbles in a water stream.

THEORY

The model applied to a packed bed assumes that the particles of packing material are stationary in space and that the fluid at the surface of the packing particles is stationary with respect to the main stream of fluid. If the assumption is made that the main fluid stream is moving rapidly with respect to the particles, then the model would be expected to be applicable to a fluidized bed. However if this assumption is only approximately valid, the mathematical results are still accurately applicable, owing to the central-limit theorem, provided that a large enough number of events is considered, that is, that the bed is of sufficient length.

The statistical model, which is discussed in detail elsewhere (*1, 11*), considers the motion of tracer corpuscles in the mainstream fluid. The corpuscles move according to a repeating pattern of a *motion phase* followed by a *rest phase*. A very small amount of time is required for the motion phase but the rest phase requires much longer. Thus the tracer corpuscles move, then rest, then move, etc. The rest phase may be thought of as taking place at the various stagnation points at each packing particle and in the eddies and the relatively stagnant points immediately downstream of the particles. The motion phase occurs during the rapid flow between particles.

E. J. Cairns is with General Electric Company, Schenectady, New York.

The probability density function for the position of the tracer corpuscle with respect to longitudinal distance and time after one double phase is

$$p(z,t')dzdt' = e^{-t'-z}dzdt' \quad (1)$$

By applying this probability density function to a consecutive set of motion and rest phases which result in the tracer corpuscle being found at the position $z = N$ at $t' = T$, and considering all possible paths for arriving at N at T, one arrives at the expression

$$F_{N(T)} = \int_0^T e^{-N-T}\, \mathbf{I}_0(2\sqrt{NT})\, dT \quad (2)$$

The definition of $F_{N(T)}$ in Equation (2) corresponds to a step function tracer input.

The important assumptions involved in the above derivation are that the velocity profile over the region of interest is flat, the probability of a corpuscle coming to rest is independent of longitudinal position, and the time lapse during the motion phase is short.

Equation (2) may well be approximated (*12*) by

$$F_{N(T)} = \frac{1}{2}\left[1 + \text{erf}\left(\sqrt{T} - \sqrt{N} - \frac{1}{8\sqrt{T}} - \frac{1}{8\sqrt{N}}\right)\right] \quad (3)$$

The parameters T and N are related to the more familiar parameters of eddy diffusivity and time by

$$N = \frac{ZU}{E} \quad (4)$$

$$T = \frac{U^2 t}{E} \quad (5)$$

$$T/N = \left(\frac{Ut}{Z}\right) \equiv \theta \quad (6)$$

Equation (4) is in essence a definition of the eddy diffusivity in terms of the Einstein statistical equations. If $F_{N(T)}$ is plotted against (T/N) for an assumed N, the familiar breakthrough type of curve is obtained.

A very convenient method of evaluating N (and hence the Peclet group which is equal to $N\, d_p/Z$) is to obtain the slope of the breakthrough curve at the point $T/N = 1$, since from Equation (2)

$$\left(\frac{\partial F}{\partial (T/N)}\right)_{T/N=1} = N\frac{I_0(2N)}{e^{2N}} \quad (7)$$

For large N one obtains

$$\left(\frac{\partial F}{\partial (T/N)}\right)_{T/N=1} = \frac{\sqrt{N}}{2\sqrt{\pi}} \quad (8)$$

$$N = 4\pi\left(\frac{\partial F}{\partial (T/N)}\right)^2_{T/N=1} \quad (9)$$

Equation (7) gives a very rapid method of determining Peclet groups from experimental data. Other methods (*4, 6, 7, 14, 15, 17, 20*) require considerably more extensive calculations.

EXPERIMENTAL

The discussion above indicates that it is desirable to use a tracer technique for studying longitudinal mixing behavior in fluidized beds. Since the fluid velocity is relatively high, ordinary sampling procedures are unsatisfactory; a continuous monitoring procedure would be very desirable, since transients in the system are to be followed. The electrical conductivity of an electrolytic solution is very nearly proportional to the concentration of the electrolyte, and the time lag of electrical conductivity measurements is negligible. Therefore the electrical conductivity method was chosen for continuously following the liquid-phase mixing behavior by injecting a sodium nitrate solution into an aqueous main stream.

General Flow Apparatus

A schematic flow diagram of the equipment is shown in Figure 1. Water is obtained from a constant-head tank, metered, and pumped by means of a regenerative type of turbine pump into the flow distributor, which causes the water to have a flat velocity profile. From the distributor the water passes up into the flow-development section, which is an 8-in. length of tube having the same diameter as the test section and packed with 2-mm. glass spheres. The injector head is mounted directly above the flow-development section, and the test section is immediately above the injector head.

The upper surface of the injector head supports a screen which in turn supports the fluidized bed. The space below the screen and above the flow-development section is also packed with spheres. Above the test section is a particle disengaging section, which is an open tube, 8 in. long, which overflows into a tank and drainage system.

The apparatus was designed in such a manner that various diameters and heights of test sections could be be employed. Two-and 4-in.–diameter test sections 2 ft. long were studied in this work. The diameters and specific gravities of the particles studied were 3.2 mm., $\rho = 2.45$; 3.0 mm., $\rho = 11.3$; 1.3 mm., $\rho = 11.3$.

Electrical Conductivity Probes

The probe tip which holds the electrodes was constructed from a Bakelite type of material in cylindrical form, 3 mm. in diameter. The rod contains a slot 7 mm. deep and 1 mm. wide. On each side of the slot a circular platinum electrode 1 mm. in diameter is mounted less than 1 mm. from the probe tip. Wires from the electrodes are passed through the tip and into the probe body of ⅛-in. diameter stainless steel tube. The leads are passed through the tube and connected to the electronic apparatus. These probes are able to measure the conductance of a very small volume of fluid (about 1 cu. mm.) and to trace that conductance with a negligible time lag. The stagnation point at the slot end is relatively far from the electrodes in order that there may be negligible stagnation or holdup effects on the conductance reading.

The mounting device for the probes was constructed such that the probes can monitor the conductance at any Z level in the bed and at any angular orientation around the axis. The radial positions can be obtained in multiples of $r_o/12$. The mounting device dips into the bed from above and fits snugly against the tube walls, causing a minimum of disturbance to the flow. The probe tips are at all times at least 4⅞ in. from the nearest portion of the probe support.

Electronics

The determination of the electrical conductance of the solution between the electrodes of the probe described above must be a continuous one, and hence standard bridge networks could not be used. Figure 2 schematically shows the basic network. The oscillator was voltage stabilized and supplied a 20-kc. voltage. A current-sensing resistor r was selected so that it would always be less than 0.01 R where R is the resistance of the solution in the conductivity probe. Therefore V_r is very nearly directly proportional to $(1/R)$, which is the conductance of the solution.

The signal V_r was then fed to an amplifier and demodulator network. The output of the amplifier demodulator was a varying d.c. voltage directly proportional to the conductivity of the solution in the probe.

The amplified signal was used to drive a mirror type of galvanometer in the Heiland type 906 Visicorder. The Visicorder had a flat frequency response up to about 300 cycles/sec. and hence could be used to study the transients of interest in this work.

The amplifier-demodulator network was able to accommodate six simultaneous signals from the probes and also delivered to the recorder these signals as well as a 60-cycle timing pip and a start pip, which was electronically placed on the chart when the step function of tracer solution was turned on or off. The start and timing pips are discussed in more detail elsewhere (*1*). The timing pip allows accurate calculation of the chart speed; the start pip allows calculation of time lapsed since the step-function injection.

Injection System

The tracer injection system consisted of a piston and cylinder driven by a geared-down variable-speed drive unit. The variable-speed drive was calibrated so that an accurately known volume of liquid was being delivered per unit of time for a given drive setting. The fluid from the cylinder could be delivered to either of two places, depending on the position of the solenoid-valve switch. The fluid could be fed back to the reservoir from which it originally came or to the injector head at the base of the test section.

The injector head for the 4-in.–diameter test section had one-hundred fifty-six hypodermic needles (18 gauge) placed on a square lattice having 9/32-in. spacing.

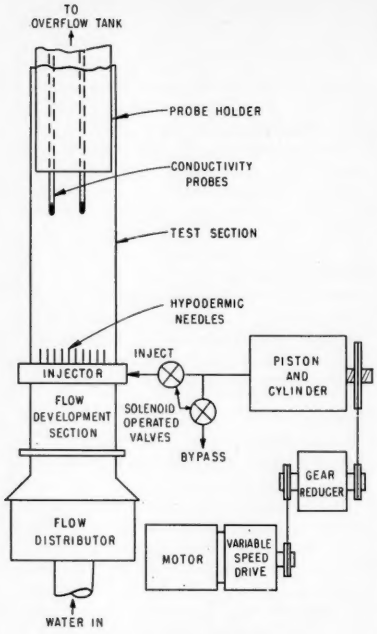

Fig. 1. Schematic flow diagram.

The head for the 2-in. test section had thirty-seven needles on the same arrangement. Calculations, which are described in detail elsewhere (*1*), showed that these injectors provide very nearly a plane source of tracer. At an axial distance of less than 5 particle diam. from the needle tips, the ripple in the concentration contour map for that Z level was only 9% of the average concentration.

The solenoid-valve arrangement mentioned above allowed a very sharp wave front of injectant to be sent into the test section or, conversely, the very rapid diversion of the injectant stream from the test section. This step-function property of the injection system allowed the use of the equations in the theory section for data analysis.

Procedure

During the time allowed for the fluidized bed to come to equilibrium the injector drive speed was determined in such a way that the linear injectant velocity at the needle tips was equal to the average main stream linear velocity (U_o/ϵ).

The injectant was fed into the test section until steady state was reached, as indicated by constant conductivity readings for all probes on the Visicorder. The amplifier gains were adjusted so that the traces on the chart were in certain relative positions that permitted each trace to be identified with the corresponding probe and probe position in the bed. The injectant stream was suddenly diverted from the column by activating the solenoid valve. At this same instant the start pip was electronically placed on the chart. The breakthrough curves for all the probes were traced to their final values, characteristic of tap water. The temperature of the water was recorded along with flow rate, injection rate, bed height and diameter,

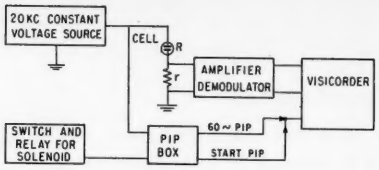

Fig. 2. Block diagram for one channel.

and weight, density, and diameter of the packing material.

Similar data were collected for various flow rates (or fraction voids) for each of the particle sizes in both 4- and 2-in. test sections.

REDUCTION OF DATA

For convenience and speed in the reduction of data it is advantageous to use an expression of the form of Equation (9). However from the raw data it is not possible to obtain the location of the point $T/N = 1$ without trial and error. For this reason it is convenient to take the slope of the breakthrough curve on the chart at some other point which can be located without trial and error; such a point is $F = 1/2$.

Knowing the slope at the point $F = 1/2$ one can calculate the slope at the point $T/N = 1$ by use of the derivative of Equation (2) with respect to (T/N). For an assumed N the corresponding T for $F = 1/2$ may be calculated from Equation (3), and then these values of T and N are inserted into the derivative of Equation (2) with respect to (T/N). The value of the slope for $(T/N) = 1$ is obtained from Equation (7) for this same assumed N. The ratio of the two slopes is defined as

$$\beta = \frac{\left(\frac{\partial F}{\partial \theta}\right)_{\theta=1}}{\left(\frac{\partial F}{\partial \theta}\right)_{F=1/2}} \qquad (10)$$

Therefore $(\partial F/\partial\theta)_{\theta=1}$ may be obtained from $(\partial F/\partial\theta)_{F=1/2}$.

Since Equation (9) is only approximate, it is desirable to have the relationship between the exact Equation (7) and the approximate Equation (9). This relationship is given in the form

$$N = 4\pi \left(\frac{\partial F}{\partial \theta}\right)^2_{\theta=1} \cdot \frac{1}{\alpha^2}$$

$$= 4\pi \left(\frac{\partial F}{\partial \theta}\right)^2_{\theta=1} \left[\frac{\exp(2N)}{I_o(2N) \cdot 2\sqrt{\pi N}}\right]^2 \qquad (11)$$

which also defines α for the case $T = N$.

Since the electrical conductivity of the sodium nitrate solution is not exactly proportional to the concentration of the sodium nitrate, an additional correction factor is needed. The form of the empirical equation relating C to L is

$$C = aL^b \qquad (12)$$

The correction factor takes the form

$$\left[b\left(\frac{L}{L_\infty}\right)^{b-1}\right]_{F=1/2} = \left[b\left(\frac{1}{2}\right)^{\frac{b-1}{b}}\right] \qquad (13)$$

which is a weak function of temperature. The final equation used in reducing the data is

$$N_{Pe'} = 4\pi\left\{\frac{dy}{dx}\ \frac{b}{1.02}\left(\frac{L}{L_\infty}\right)^{b-1}\left(\frac{Z}{U_i}\right)\left(\frac{dx}{dt}\right)\right\}^2_{F=1/2}\left(\frac{d_p}{Z}\right)\Delta^2 \qquad (14)$$

The term in the large brackets is $(dF/d\theta)_{F=1/2}$, where $\theta = T/N$ or $[(U_i t)/Z]$. The value of 1.02 is a correction factor for a slight nonlinearity in the Visicorder which must be incorporated in the determination of the slope of the breakthrough curve. This nonlinearity however is negligible in determining the point $F = 1/2$.

Equation (14) gives a rapid means for reducing data from the experimental step-function method. Details of its use and derivation have been previously presented, along with a plot of $(\Delta^2 - 1)$ vs. $(\partial F/\partial\theta)^2_{F=1/2}$ (*1*). The line velocity is found from the breakthrough curve. Since for $F = 1/2$, $\theta = U_i t/Z \approx 1$, $U_i = Z/t$ where t corresponds to the point $F = 1/2$. The error in this assumption is usually less than 1%.

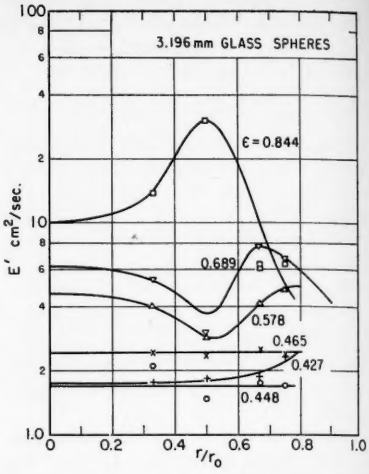

Fig. 3. Longitudinal eddy-diffusivity profile, 2-in. tube.

RESULTS

As discussed previously (*1, 2*), velocity profiles in packed and fluidized beds tend not to be flat. In a liquid-

solid fluidized bed the velocity distribution deviates from flatness much more than does the distribution for packed beds; these nonflat velocity profiles give rise to the corresponding nonflat eddy-diffusivity profiles shown in Figures 4 and 5.

The experiments described here indicate that under the conditions of greatest deviation from a flat velocity profile (±20%) the ratio of eddy diffusivities (E_z/E_r) is about 20 to 30. The longitudinal concentration gradients are one or two orders of magnitude steeper than any radial gradients that could develop, and hence the rate of longitudinal mass transfer is much greater than the rate of radial mass transfer; the ratio of axial to radial tracer flux is estimated as being at least 10^2. Thus the radial mass transfer is expected to have a negligible effect on the axial diffusivities reported here.

Figure 3 presents a sample set of eddy-diffusivity profiles showing the data points. The scatter is representative of the glass particle systems; the data for the lead particle systems scattered a little more. Figures 4 and 5 present the results for the various studies in terms of the eddy diffusivity as calculated from the Peclet group $E' = (U_t d_p)/N_{Pe}'$. The numbers in parentheses near each curve give the fraction voids as calculated from the bed height, weight and density of particles, and bed diameter. Tabulations of the data from which the curves were drawn are available elsewhere (*1*).

The left-hand portion of Figure 4 indicates that the 1.3-mm.–diameter lead spheres in the 4-in. tube yield eddy-diffusivity profiles very similar in shape to the velocity profiles reported previously (*2*). The impression given by these profiles is that the eddy diffusivity is not a function of radial position. The two profiles which deviate most from being flat are at fraction voids very near to one another (0.510 and 0.547). There is no special reason to believe that there is a sudden and extensive change in the eddy-diffusivity profile in this short range of fraction voids. Taken together these two curves would predict a resultant flat profile, consistent with the rest of the set. The very small d_p/D ratio (0.013) combined with the high particle-to-fluid density ratio (11.3) yields flat velocity profiles as well as flat eddy-diffusivity profiles. The eddy diffusivity reaches a maximum in the vicinity of $\epsilon = 0.66$.

The central portion of Figure 4 shows that there is an influence due to the wall and the nonflat velocity profile. When one starts with $\epsilon = 0.400$ (packed bed), the eddy diffusivity increases as the wall is approached. The

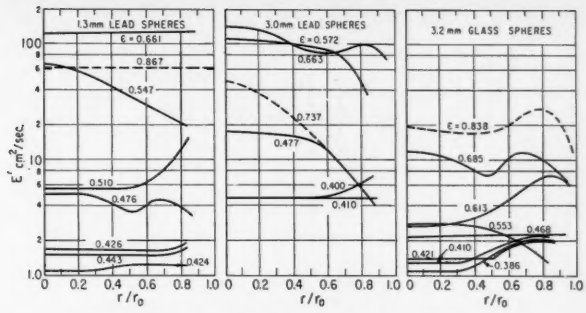

Fig. 4. Longitudinal eddy-diffusivity profiles in fluidization, 4-in. tube.

same is true for the velocity. This increase is undoubtedly due to a rise in the fraction voids as the wall is approached. As the bed is expanded to incipient fluidization ($\epsilon = 0.410$), the eddy-diffusivity profile becomes flat (corresponding to a flat velocity profile), and as the bed finally fluidizes ($\epsilon = 0.477$), there develops a well-defined nonflat eddy-diffusivity profile with a maximum at the center. An increase in the bed expansion changes the particle circulation pattern, velocity profile, scale and intensity of turbulence, and local fraction voids in such a manner that humps develop in the eddy-diffusivity profiles at $\epsilon = 0.572$ and $\epsilon = 0.663$.

The profiles in the right-hand portion of Figure 4 for glass particles of 3.2 mm. show the same general behavior at low fraction voids as those for the central portion for lead particles. However since lower velocities are required for the fluidization of the glass, and lower scales of turbulence are expected, lower eddy-diffusivity values would be expected than for the corresponding fraction voids in the case of lead. The humps caused by the particle circulation patterns are more predominant in the case of the glass particles; this is not surprising since the particle circulation is qualitatively different in the case of glass from that in the case of lead (*1*).

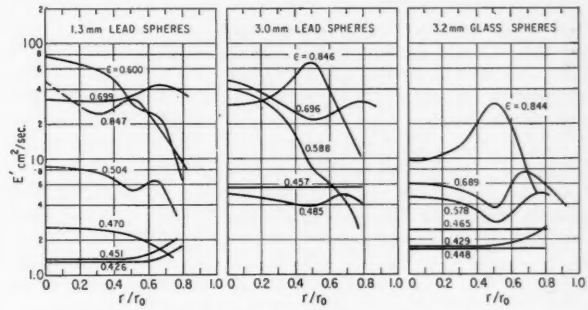

Fig. 5. Longitudinal eddy-diffusivity profiles in fluidization, 2-in. tube.

The left-hand portion of Figure 5 presents the results for the 1.3-mm. lead particles in the 2-in. test section at the corresponding distance from the injector in terms of Z/D. There are large deviations from flatness in the

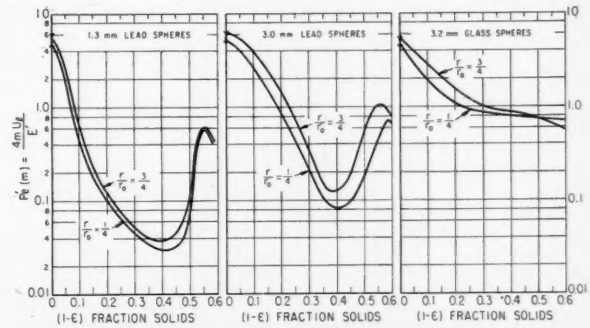

Fig. 6. Longitudinal Peclet numbers in fluidization, 4-in. bed.

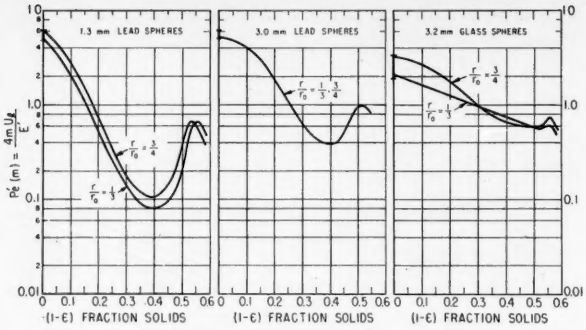

Fig. 7. Longitudinal Peclet numbers in fluidization, 2-in. bed.

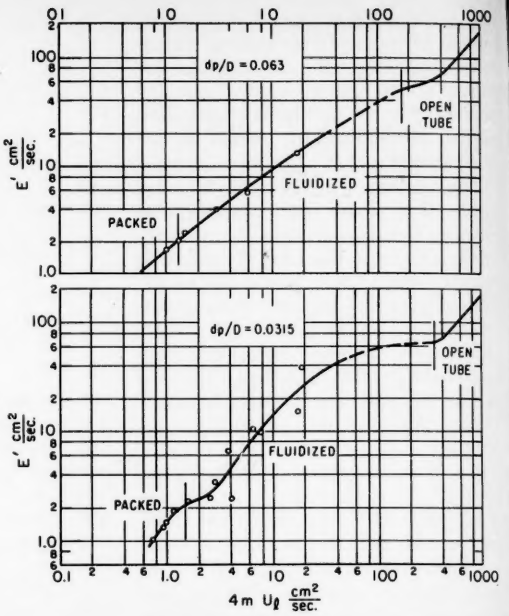

Fig. 9. Longitudinal eddy diffusivities in fluidization, glass spheres, d_p = 3.196 mm.

eddy-diffusivity profiles. Much better agreement between sets of profiles is obtained if they are compared on a basis of comparable d_p/D ratios rather than on the basis of particle diameter alone. When one uses this reasoning, the left-hand portion of Figure 5 agrees very well with the central portion of Figure 4. Again a maximum in eddy diffusivity occurs corresponding to fraction voids of 0.6 or 0.7.

The central portion of Figure 5, presenting results for 2.96-mm. lead spheres in the 2-in. test section, shows behavior similar to the other systems having comparable d_p/D ratios for the same bead density.

Finally the right-hand portion of Figure 5 shows the results for the 3.2-mm. glass beads in the 2-in. test section. These results show similarities to those for the same type of packing in the larger tube in that the humps occur at the same distance from the wall in terms of the number of bead diameters from the wall. Generally the eddy diffusivity is lower in the smaller tube owing to the more restricted circulation of the beads in the smaller tube.

To show the effects of fraction solids $(1-\epsilon)$ on the Peclet group $[N_{Pe'(m)} = (4mU_l)/E]$, Figures 6 and 7 were prepared. The symbol m refers to the hydraulic radius as extended by Wilhelm (*17, 21*) and is defined as m = volume of fluid/wetted area. If the characteristic length term is defined in this manner, the Peclet group may vary continuously from the packed-bed value, where m is determined primarily by the packing size to the open-tube value, where $4m$ is equal to the tube diameter.

When one considers Figure 6, it is apparent that there is slightly better mixing (lower Peclet group) toward the center of the tube for given average fraction voids. When compared with the fraction-voids effect, however, the effect of radial position is rather small in most cases, especially where ρ_p/ρ_f is large. The minimum in $N_{Pe'(m)}$, when present, occurs at $\epsilon = 0.6$. The effect of using $4m$ as a length term in $N_{Pe'(m)}$ tends to shift this minimum to the right, and if $N_{Pe'} = (U_l d_p)/E'$ were plotted against fraction solids, the minimum would occur at $\epsilon = 0.7$, where the corresponding minimum in radial Peclet group is situated (*1*).

Figure 7 contains plots similar to those of Figure 6; however these are for the 2-in. test section. There is a very good correspondence between the central portion of Figure 6 and the left-hand portion of Figure 7, again bringing out the importance of the d_p/D ratio in determining the mixing behavior in a fluidized bed.

All open-tube values $(1-\epsilon = 0)$ were obtained from Tichacek *et al.* (*19*) at velocities corresponding to the terminal velocity of the particle in question. The hydraulic radius is used

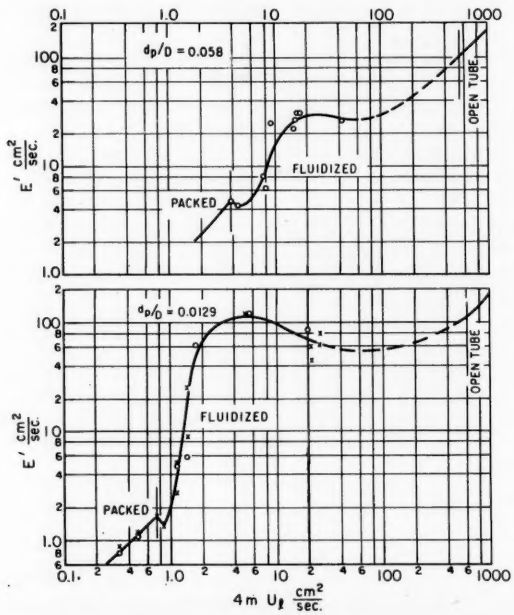

Fig. 8. Longitudinal eddy diffusivities in fluidization, lead spheres, d_p = 2.96 mm.

as the characteristic length because it is easily calculated from readily available data and provides a continuous function in going from the packed bed to the empty tube.

For comparing and summarizing the mixing behavior of various systems one may turn to the theories of turbulent mixing to suggest the characteristic parameters for correlating eddy-diffusion coefficients. The Einstein statistical model shows that the longitudinal eddy diffusivity is the product of a characteristic length term and a characteristic velocity term. Prausnitz (*18*), on the basis of a mixing-length model, comes to the same conclusion. The eddy diffusivity should therefore be expressed as a function of the product of a characteristic length term and a characteristic velocity term. The characteristic length term proposed here for simplicity is the hydraulic radius; the velocity term proposed is the line velocity discussed previously (*1, 2, 3*).

Figures 8 and 9 show representative results for some of the systems studied, plotted in the manner suggested by the above discussion. The remainder of the results are available elsewhere (*1*). The results for some of the lead particle systems as shown in Figure 8 indicate that there is a very rapid increase in the eddy diffusivity with increase in mU_l just after fluidization has set in. At mU_l values higher than those corresponding to fraction voids of about 0.7, there is a relatively small change in the eddy diffusivity for a given change in mU_l, until the open-tube value is approached. For the $d_p/D = 0.058$ curve there is a wall effect in restricting the particle motion causing the eddy diffusivity to be lower than that for the d_p/D ratio of 0.013 at the corresponding fraction voids (or corresponding mU_l).

Figure 9 shows similar results for the glass packing. There is a noticeable difference between Figures 8 and 9 in that the denser particles show a much more pronounced effect in increasing eddy diffusivity. For a d_p/D ratio of 0.063 and ρ_p of 2.45 g./cc. the line joining the packed- and open-tube values shows very little curvature. For d_p/D of 0.0315 the effect is increased somewhat but is not equivalent to that for lead packing for the same d_p/D ratio.

SUMMARY AND CONCLUSIONS

The longitudinal mixing properties in liquid-solid fluidized beds were investigated by means of a step function response technique. The longitudinal eddy diffusivities were determined for glass and lead particles in water at various d_p/D ratios, fraction voids, and radial positions at an axial level of about 5 bed diam.

The experimental results show that the eddy diffusivity is strongly affected by the density and concentration of the particles in the fluidized beds. The mixing results are consistent with the fact that the fluidized bed may be considered as a transition between a packed bed and an open tube.

NOTATION

a = constant in Equation (12)
b = constant in Equation (12)
C = salt concentration
d_p = packing-particle diameter
D = test-section diameter
E = eddy diffusivity (analogous to molecular diffusion constant), based on average velocity
E' = eddy diffusivity based on line velocity
F = dimensionless concentration $= C/C_\infty$
I_o = Bessel function of zero order and first kind of an imaginary argument
L = conductance
m = hydraulic radius = volume of fluid/wetted area
N = dimensionless longitudinal distance $= ZU/E$
p = probability density
N_{Pe} = longitudinal Peclet number $= U_o d_p/\epsilon E$
N_{Pe}' = longitudinal Peclet number based on line velocity $= U_l d_p/E'$
$N_{Pe(m)}$ = longitudinal Peclet number based on average velocity and hydraulic radius $= 4mU_o/E\epsilon$
$N_{Pe'(m)}$ = longitudinal Peclet number based on line velocity and hydraulic radius $= 4mU_l/E'$
r = radial position
r_o = radius of test section
t = time
t' = dimensionless time variable
T = dimensionless time unit $= U^2t/E$
$\frac{T}{N}$ = dimensionless time $= Ut/Z$
U = characteristic fluid velocity (general)
U_l = line velocity of fluid $= 1/Z \int_o^z U_p\, dZ$
U_o = superficial fluid velocity (based on open-tube cross section).
U_p = velocity of the fluid observed at a point
V = voltage of signal to recorder
x = distance on recorder chart parallel to time axis
y = displacement of recorder trace from its no-signal position
z = dimensionless longitudinal position
Z = distance of observation point from injection plane

Greek Letters

α = correction factor $= [2\sqrt{N}\, I_o(2N)]/[\exp\ (2N)]$ for $T = N$
β = $[\ (\partial F/\partial\theta)_{\theta=1}]/[(\partial F/\partial\theta)_{F=1/2}]$ = a correction factor
Δ = over-all correction factor $= \beta/\alpha$
ϵ = fraction voids
θ = dimensionless time $= T/N = Ut/Z$
ρ = density, g./cc.

Subscripts

∞ = value prevailing during steady state tracer injection
f = fluid
p = particle

Superscripts

'(prime) = based on line velocity

LITERATURE CITED

1. Cairns, E. J., dissertation, Univ. Calif., Berkeley (1959).
2. ———, and J. M. Prausnitz, *Ind. Eng. Chem.*, **51**, 1441 (1959).
3. ———, *Chem. Eng. Sci.*, to be published.
4. Carberry, J. J., and R. H. Bretton, *A.I.Ch.E. Journal*, **4**, 367 (1958).
5. Danckwerts, P. V., *et al.*, *Chem. Eng. Sci.*, **3**, 26 (1954).
6. Deisler, P. F., and R. H. Wilhelm, *Ind. Eng. Chem.*, **45**, 1219 (1953).
7. Ebach, E. A., and R. R. White, *A.I.Ch.E. Journal*, **4**, 161 (1958).
8. Einstein, H. A., dissertation, Eidgenossische Technische Hochschule, Zürich, Switzerland (1937).
9. Gilliland, E. R., E. A. Mason, and R. C. Oliver, *Ind. Eng. Chem.*, **45**, 1177 (1953).
10. Hanratty, T. J., George Latinen, and R. H. Wilhelm, *A.I.Ch.E. Journal*, **2**, 372 (1956).
11. Jacques, G. L., and Theodore Vermeulen, *A.I.Ch.E. Journal*, to be published.
12. Klinkenberg, Adrian, *Ind. Eng. Chem.*, **46**, 2285 (1954).
13. ———, and F. Sjenitzer, *Chem. Eng. Sci.*, **5**, 258 (1956).
14. Kramers, H., and G. Alberda, *ibid.*, **2**, 173 (1953).
15. Lapidus, Leon, and N. R. Amundson, *J. Phys. Chem.*, **56**, 984 (1952).
16. Levenspiel, Octave, and W. K. Smith, *Chem. Eng. Sci.*, **6**, 227 (1957).
17. McHenry, K. W., and R. H. Wilhelm, *A.I.Ch.E. Journal*, **3**, 83 (1957).
18. Prausnitz, J. M., *ibid.*, **4**, 14M (1958).
19. Tichacek, L. J., C. H. Barkelew, and Thomas Baron, *ibid.*, **3**, 439 (1957).
20. Van der Laan, E. T., *Chem. Eng. Sci.*, **7**, 187 (1958).
21. Wilhelm, R. H., *Chem. Eng. Progr.*, **49**, 150 (1953).

Manuscript received April 24, 1959; revision received September 18, 1959; paper accepted October 2, 1959.

Mechanism of Drying Thick Porous Bodies During the Falling-Rate Period: III. Analytical Treatment of Macroporous Systems

A. H. NISSAN, H. H. GEORGE, JR., and T. V. BOLLES

Rensselaer Polytechnic Institute, Troy, New York

The analysis of a drying process requires a knowledge of the temperature of the material as a function of time and position. Previous work (*1*, *2*) has shown the existence of a unique temperature obtained during the falling-rate period—the *pseudo-wet-bulb temperature*.

Figure 1 represents a generalized time-temperature plot for a porous body being dried in air. The curve A' B' C' represents the rate of drying; the other curves give the temperature distribution. The portion A' B' of the rate-of-drying curve is the constant-rate period during which the temperature of the bed tends toward the wet-bulb temperature of the air. When the critical moisture content is reached, that is point B', the drying rate decreases and the liquid surface recedes below the surface of the bed. During the falling-rate period the temperature of the wet portion of the bed tends toward the pseudo-wet-bulb temperature. The curve DD' portrays the temperature of the surface of the bed. Since the surface of the bed is dry at all times during the falling-rate period, its temperature immediately tends to equal the temperature of the air.

The curves DEE' and DFF' represent the temperature histories of internal points in the bed, showing how they first reach the pseudo-wet-bulb temperature and later, as the points pass into the dry portion, reach the air temperature. DGG' is the curve representing the temperature history of the bottom of the bed. When point G is reached, the bed is dry and all the temperature curves rise more sharply toward the air temperature, because the heat entering the bed is manifest entirely as sensible heat, whereas before dryness part of the heat went to supply the latent heat of vaporization.

In part I (*1*) an implicit equation was presented for determining the pseudo-wet-bulb temperature:

$$k_c(t_a - t_{pwb}) = 2.88 \times 10^{-4}(\epsilon D)_{pwb}\lambda_{pwb}\left(\frac{P_{pwb}}{T_{pwb}} - \frac{p_a}{T_a}\right) \quad (1)$$

in consistent c.g.s. units when water was the drying liquid.

In part II (*2*) it was shown that S, the pore liquid content or the degree to which pores are saturated with liquid in the wet portion, is not constant during the falling-rate period but decreases with time.

The intent of this paper is to show the generality of the pseudo-wet-bulb temperature, to present an explicit method of calculating the pseudo-wet-bulb temperature and the manner in which the bed rises to this new temperature, and finally to present equations suitable for predicting the rate of drying and the drying curves. These analyses apply, strictly, only to systems with relatively large pores—textiles or particulate systems like sand—since the exact behavior of gels and other collodial systems has not as yet been determined.

APPARATUS

The loop dryer was constructed of 8-by 12-in. by 21-gauge steel duct and was covered with 1 in. of asbestos insulation. The sample pan was 6 by 2 in. long dimension in the air direction, and 1-¼ in. deep. The pan was made from ¼-in. plywood and lined with polyethylene and epoxy resins to make it waterproof. Throughout the pan were located ten thermocouples at various depths.

The material that was dried was silica sand of — 16 + 20 mesh. The effective

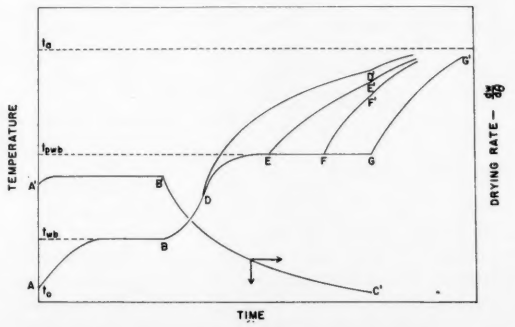

Fig. 1. Generalized time-temperature record.

thermal conductivity of the sand was determined to be 0.1645 Btu/(hr.)ft² (°F./ft.), and the void fraction was found to be 0.45.

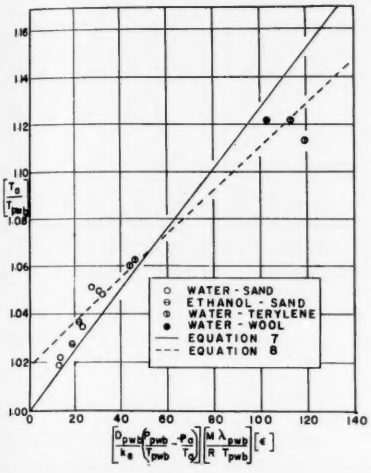

Fig. 2. Pseudo-wet-bulb temperature as a function of dimensionless groups.

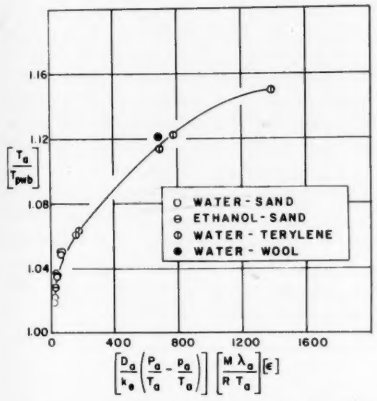

Fig. 3. Pseudo-wet-bulb temperature as a function of air temperature.

CALCULATION OF PSEUDO-WET-BULB TEMPERATURE

The drying of a wet material will be considered to have proceeded well into the falling-rate period and the evaporation to be taking place from a liquid surface well within the material. The liquid surface is a distance x from the surface of the bed, and the differential layer of bed just above the liquid surface through which must pass the entire heat required to vaporize the liquid will be considered. Hence

$$q = -k_e A_H \frac{dt}{dx} = -\frac{dW}{d\theta}\lambda_{pwb} \quad (2)$$

The rate of evaporation is assumed to be controlled by vapor diffusion. Then

$$-\frac{dW}{d\theta} = (\epsilon D)_{pwb} A_M \frac{dC}{dx} \quad (3)$$

$(\epsilon D)_{pwb}$ is the vapor diffusion coefficient at the temperature of the liquid surface corrected for the presence of the solid (assumed to have zero diffusion) by the void fraction ϵ.

The shapes of temperature and concentration curves are usually similar, and so it can be assumed that

$$\frac{\dfrac{dt}{dx}}{\dfrac{t_a - t_{pwb}}{x}} = \frac{\dfrac{dC}{dx}}{\dfrac{C_a - C_{pwb}}{x}} \quad (4)$$

and from the ideal gas law

$$C = \frac{M_L P}{RT} \quad (5)$$

Substituting Equations (3), (4), and (5) into Equation (2) yields

$$k_e(t_a - t_{pwb}) = 1.285 \times 10^{-3} (\epsilon D)_{pwb} \lambda_{pwb} \frac{M_L}{R}\left[\frac{P_{pwb}}{T_{pwb}} - \frac{p_a}{T_a}\right] \quad (6)$$

where $R = 1.98$ B.t.u./(lb.-mole) (°F.). Equation (6) can be rearranged to read

$$\frac{T_a}{T_{pwb}} = 1 + 1.285 \times 10^{-3} \left[\frac{D_{pwb}}{k_e}\left\{\frac{P_{pwb}}{T_{pwb}} - \frac{p_a}{T_a}\right\}\right]\left[\frac{M_L \lambda_{pwb}}{RT_{pwb}}\right][\epsilon] \quad (7)$$

The pseudo-wet-bulb temperature was calculated by means of Equation (6) for runs in which wool, terylene (British form of a polyester fiber), and sand were dried. In addition to drying water from all the materials, the ethanol-sand system was used for some runs.

The results were then plotted in the manner suggested by Equation (7) in Figure 2. A straight line was fitted through the points. The line of the form of Equation (7) is

$$\frac{T_a}{T_{pwb}} = 1.0185 + 1.111 \times 10^{-3} \left[\frac{D_{pwb}}{k_e}\left\{\frac{P_{pwb}}{T_{pwb}} - \frac{p_a}{T_a}\right\}\right]\left[\frac{M_L \lambda_{pwb}}{RT_{pwb}}\right][\epsilon] \quad (8)$$

Equation (7) is also shown in Figure 2.

The solution of Equation (8) for T_{pwb} still involves a trial-and-error procedure, since T_{pwb} appears on both sides of the equation. Since Equation (8) is dimensionally correct, the ratio T_a/T_{pwb} was calculated evaluating the properties of the liquid at the air temperature. These results are shown in Figure 3, which may be used to give T_{pwb} for the system directly from a knowledge of the air temperature and humidity. Thus the need for a trial-and-error method of calculating T_{pwb} is eliminated.

THE APPROACH TO PSUEDO-WET-BULB TEMPERATURE

With the pseudo-wet-bulb temperature rendered predictable, it is next

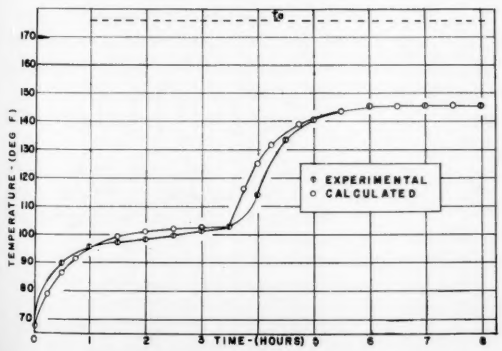

Fig. 4. Temperature of wet sand vs. time.

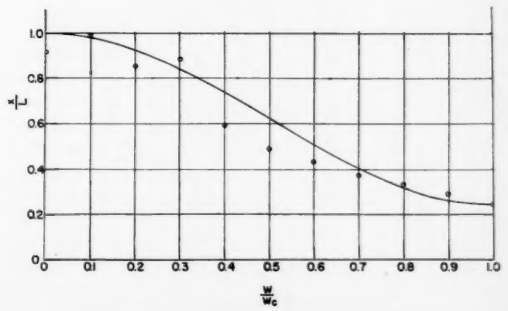

Fig. 5. Liquid distribution function.

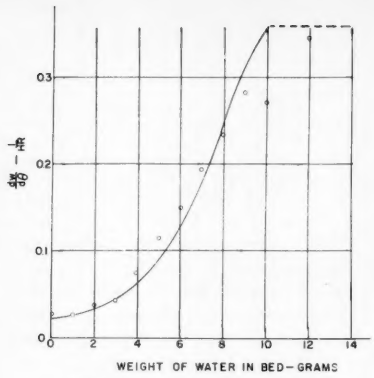

Fig. 6. Rate of drying curve.

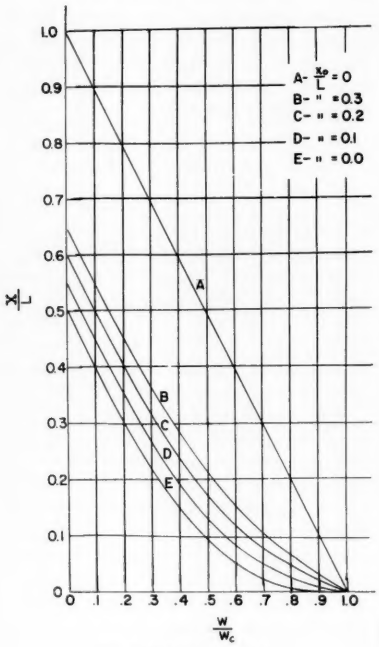

Fig. 7. Working plot 1.

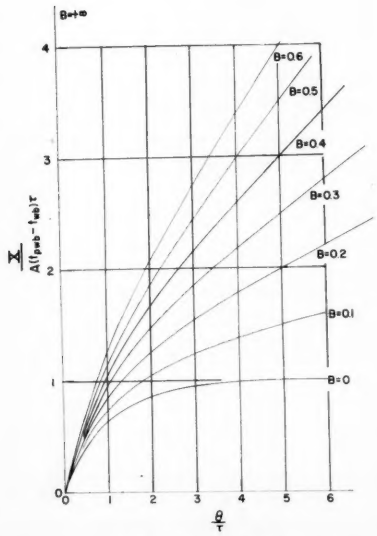

Fig. 8. Working plot 2.

necessary to describe the manner in which the bed approaches the pseudo-wet-bulb temperature once the critical moisture content is reached, that is point B' on Figure 1. Figure 1 suggests a first-order response to a step function of a resistance-capacitance complex. In other words the bed is behaving as if it were suddenly immersed, when it is at t_{wb}, into a bath at t_{pwb}. To simplify the analysis a flat bed will be assumed; for cylindrical or spherical bodies more complicated geometrical factors enter.

The wet portion of the bed is assume to be immersed in a virtual bath at the pseudo-wet-bulb temperature. (The excess temperature $t_a - t_{pwb}$ goes toward evaporating the liquid.) Then the sensible heat of the bed is given by

$$q = \frac{A_H}{R_H}(t_{pwb} - t) = V\bar{\rho}\bar{c}_P\frac{dt}{d\theta} \quad (9)$$

and the boundary condition at

$$t = t_{wb} \text{ at } \theta = 0 \quad (9a)$$

The solution to (9 and 9a) is known to be (3)

$$\frac{t - t_{pwb}}{t_{wb} - t_{pwb}} = e^{-\theta/(L-x_o)\bar{\rho}\bar{c}_P R_H} \quad (10)$$

$\theta = 0$ at critical moisture content One defines

$$R_H = \frac{(L - x_o)}{\bar{k}} \quad (11)$$

and then

$$\tau = \frac{L^2\bar{\rho}\bar{c}_P}{\bar{k}} = \frac{L^{(L-x_o)^2}[(1-\epsilon)\rho_s c_{Ps} + \epsilon S_c \rho_L c_{PL}]}{k_c + \epsilon S_c k_L} \quad (12)$$

or in terms of the critical moisture content Equation (12) may be expressed as

$$\tau = \frac{(L-x_o)^2\left[\rho_s c_{Ps}(1-\epsilon) + w_c\left(\frac{L}{L-x_o}\right)\rho_B c_{PL}\right]}{k_c + w_c\left(\frac{L}{L-x_o}\right)\frac{\rho_B}{\rho_L}k_L} \quad (12a)$$

Hence

$$t = t_{wb} + (t_{pwb} - t_{wb})(1 - e^{-\theta/\tau}) \quad (13)$$

Equation (13) is compared with an experimental run in Figure 4.

TABLE 1

Run	Experimental W_c	Calculated w_c	System
4	0.040	0.023	Sand, water
5	0.034	0.028	Sand, water
6	0.052	0.036	Sand, water
12	0.030	0.026	Sand, water
13	0.033	0.033	Sand, water

The temperature driving force for conduction through the dry portion of the bed is then given by

$$(t_a - t) = (t_a - t_{pwb}) + (t_{pwb} - t_{wb})e^{-\theta/\tau} \quad (14)$$

It is interesting to note that the rise from initial temperature to wet-bulb temperature at the beginning is given by the same τ value by the equation

$$t = t_o + (t_{wb} - t_o)(1 - e^{-\theta/\tau}) \quad (15)$$

LIQUID DISTRIBUTION

In order to derive a rate of drying equation, it is further necessary to know the location of the liquid surface as a function of time. Again only flat beds will be analyzed:

$$-k_c A_H\left(\frac{dt}{dx}\right) = -\lambda A_m L \rho_B\left(\frac{dw}{d\theta}\right) \quad (16)$$

Assuming a linear temperature gradient through the dry portion of the bed, one can use $(\Delta t/\Delta x)$ for (dt/dx) and $\Delta x = -x$. Thus

$$x = \frac{-k_c}{\lambda L \rho_B}\frac{(t_a - t_{pwb}) + (t_{pwb} - t_{wb})e^{-\theta/\tau}}{\frac{dw}{d\theta}} \quad (17)$$

As the liquid evaporates, two events take place: the surface of the liquid recedes into the bed, and the thickness of the liquid film covering the pore walls decreases. Thus very complex hydrodynamic and thermal forces come into play, resulting in complicated flows. An approximate but empirical solution was attained as follows. Experimental values of θ and $dw/d\theta$ were substituted into Equation (17) in order to determine the nature of $w = \phi(x)$ function. The results suggested, for a flat bed, a cosine relationship:

$$\cos\left(\frac{w}{w_c}\pi\right) = 2\left(\frac{x - x_o}{L - x_o}\right) - 1 \quad (18)$$

Equation (18) and some experimental points are presented in Figure 5. x_o in Equation (18) is obtained from Equation (17) by setting $\theta = 0$.

THE DRYING-RATE CURVE

Since $\Delta t = \Psi(\theta)$ and $x = \phi(w)$ are known, it is possible to write the drying rate equation. It is assumed that all

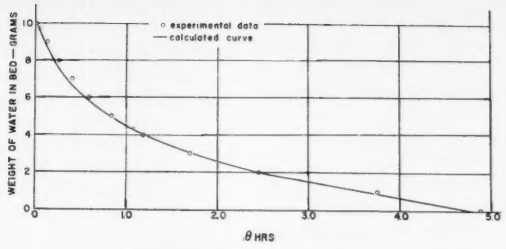

Fig. 9. Moisture-content vs. time curve.

faces except those for the drying surface of the bed are adiabatic, the area for heat transfer in the dry portion of the bed is equal to the area for mass transfer, and $(dt)/(dx) \cong (\Delta t)/(\Delta x)$ in the dry portion of the bed. In view of these assumptions Equation (16) may be written as

$$k_e \frac{\Delta t}{\Delta x} = \lambda L \rho_B \frac{dw}{d\theta} \qquad (16a)$$

Substituting Equations (14) and (18) into Equation (16*a*), one obtains

$$\frac{-k_e}{\lambda L \rho_B}\left[(t_a - t_{pwb}) + (t_{pwb} - t_{wb}) e^{-\theta/\tau} \right] d\theta = \left[\frac{L+x_o}{2} + \frac{L-x_o}{2} \cos\left(\frac{w}{w_c}\pi\right) \right] dw \qquad (19)$$

Equation (19) rearranges to give the drying rate explicitly:

$$\frac{dw}{d\theta} = \frac{-2k_e}{\lambda L \rho_B} \frac{(t_a - t_{pwb}) + (t_{pwb} - t_{wb}) e^{-\theta/\tau}}{(L+x_o) + (L-x_o)\cos\left(\frac{w}{w_c}\pi\right)} \qquad (20)$$

Figure 6 shows a comparison of Equation (20) with some experimental data.

On the basis that $dw/d\theta$ at time zero for the falling-rate period equals that for the constant-rate period, which can be independently evaluated, x_o can be calculated from Equation (17) by setting $\theta = 0$. Thus

$$x_o = \frac{-k_e (t_a - t_{wb})}{\lambda_{wb} L \rho_B \left(\frac{dw}{d\theta}\right)_{C.R.}} \qquad (21)$$

THE MOISTURE-CONTENT VS. TIME CURVE

The drying curve which gives the moisture content at different times is obtained by integration of Equation (20) with the limits of 0 to θ on $d\theta$ and w_c to w on dw. The resulting equation is

$$\frac{k_e}{\lambda L \rho_B W_c}\left[(t_a - t_{pwb})\theta + \tau(1 - e^{-\theta/\tau})(t_{pwb} - t_{wb}) \right] = \left\{ \left[\left(\frac{L+x_o}{2}\right)\left(1 - \frac{w}{w_c}\right) \right] - \left[\frac{L-x_o}{2\pi} \sin\left(\frac{w}{w_c}\pi\right) \right] \right\} \qquad (22)$$

In order to ease the use of Equation (22) it has been reduced to a graphical solution:

$$A = k_e/(\lambda L \rho_B W_c) \qquad (23)$$

$$B = \frac{t_a - t_{pwb}}{t_{pwb} - t_{wb}} \qquad (24)$$

$$X = \left(\frac{L+x_o}{2}\right)\left(1 - \frac{w}{w_c}\right) - \left(\frac{L-x_o}{2\pi}\right)\left(\sin\frac{w}{w_c}\pi\right) \qquad (25)$$

Substituting Equations (23), (24), and (25) into Equation (22) and rearranging, one gets

$$\frac{X}{A\tau(t_{pwb} - t_{wb})} = B\frac{\theta}{\tau} + (1 - e^{-\theta/\tau}) \qquad (26)$$

and

$$\frac{X}{L} = \left(\frac{1 + \frac{x_o}{L}}{2}\right)\left(1 - \frac{w}{w_c}\right) - \left(\frac{1 - \frac{X_o}{L}}{2\pi}\right)\left(\sin\frac{w}{w_c}\pi\right) \qquad (27)$$

Equation (27) is plotted in Figure 7 as a family of curves, X/L vs. w/w_c with x_o/L as the parameter. Equation (26) is plotted in Figure 8 as a family of curves θ/τ vs. $X/[A\tau(t_{pwb} - t_{wb})]$ with B as the parameter. To use Figures 7 and 8, one enters Figure 7 at a predetermined value of x_o/L and w/w_c and reads X/L. X/L is then multiplied by the group $L/[A\tau(t_{pwb} - t_{wb})]$ and entered into Figure 8 at the proper value of B; a value of θ/τ is obtained. τ is defined by Equation (12). Thus with a knowledge of t_a, t_{wb}, t_{pwb}, w_c, $(dw/d\theta)_{CR}$, and the thermal properties of bed and fluid, it is possible to calculate the drying curve. Figure 9 compares Equation (22) with experimental data.

DISCUSSION

The equations developed appear to define the drying process fairly well in spite of one arbitrary function imposed on the equations. This simplifying arbitrary function was imposed because a complete *a priori* derivation would demand the formulation of the laws of the fluid dynamics of nonisothermal flow through porous media. The present analysis was limited to heat and mass transfer considerations in the interests of simplicity. Hence a cosine function was adopted to describe the flow of the liquid inside the bed.

w_c is generally defined as the moisture content obtained by extrapolating the constant-rate curve and the falling-rate curve (*4, 5*). The calculated values of w_c were obtained by choosing the best values of w_c in Equation (22) which gave agreement between the calculated and the experimental time to dryness. The calculated and experimental values of w_c for some runs are shown in Table 1.

SUMMARY

The pseudo-wet-bulb temperature is found to exist in particulate as well as in fibrous materials. The equations for predicting the pseudo-wet-bulb temperature are the same, and its calculation is rendered explicit by the presentation of a chart.

An equation for the drying rate as a function of time is derived:

$$\frac{dw}{d\theta} = \frac{-2k_e}{\lambda L \rho_B} \frac{(t_a - t_{pwb}) + (t_{pwb} - t_{wb}) e^{-\theta/\tau}}{(L+X_o) + (L-X_o)\cos\left(\frac{w}{w_c}\pi\right)}$$

This is integrated to give the equation for the moisture content as a function of time:

$$\frac{k_e}{\lambda L \rho_B W_c}\left[(t_a - t_{pwb})\theta + \tau(1 - e^{-\theta/\tau})(t_{pwb} - t_{wb}) \right] = \left\{ \left[\left(\frac{L+x_o}{2}\right)\left(1 - \frac{w}{w_c}\right) \right]$$

$$-\left[\left(\frac{L-x_o}{2\pi}\right)\sin\left(\frac{w}{w_c}\pi\right)\right]\Bigg\}$$

Finally, to facilitate the use of this equation it is reduced to a graphical solution.

NOTATION

A = parameter defined by Equation (23)
A_H = heat transfer area, sq. ft.
A_M = mass transfer area, sq. ft.
B = parameter defined by Equation (24)
C = vapor concentration, lb./cu. ft.
C_P = specific heat at constant pressure, B.t.u./(lb.)(°F.)
D = volumetric diffusivity, sq. ft./hr.
k_e = effective thermal conductivity of solid, B.t.u./(hr.)(ft.)(°F.)
k_L = thermal conductivity of liquid, B.t.u./(hr.)(ft.)(°F.)
L = total depth of bed, ft.
M_L = molecular weight of liquid
P = vapor pressure, lb./sq. in.
p = partial pressure, lb./sq. in.
R = universal gas constant, B.t.u./lb. mole °F.
R_H = resistance to heat transfer, sq. ft. hr. °F./B.t.u.
S = pore liquid content or saturation, cu. ft. liquid/cu. ft. of void space in wet portion of bed
T = absolute temperature, °R.
t = temperature, °F.
V = bed volume, cu. ft.
W = total weight of bed, lb.
w = free moisture content, lb. liquid/lb. bed
x = depth of liquid surface from bed surface, ft.
X = parameter defined by Equation (25)

Greek Letters

ϵ = void fraction, volume voids/volume bed
λ = latent heat of vaporization, B.t.u./lb.
ρ_B = density of dry bed, lb./cu. ft.
ρ_L = density of liquid, lb./cu. ft.
τ = time constant for the system, hr.

Subscripts

o = property evaluated at initial bed temperature
wb = property evaluated at wet-bulb temperature of the air
pwb = property evaluated at pseudo-wet-bulb temperature
a = property evaluated at air temperature
c = indicates the property value at critical moisture content
$C.R.$ = property evaluated at the constant rate of drying condition

Superscripts

$-$ = average property for entire bed

LITERATURE CITED

1. Nissan, A. H., W. G. Kaye, and J. R. Bell, *A.I.Ch.E. Journal*, **5**, 103 (1959).
2. Bell, J. R., and Nissan, A. H., *ibid.*, **5**, 344 (1959).
3. Schneider, P. J., "Conduction Heat Transfer," Addison-Wesley, Reading, Mass. (1955).
4. McCabe, W. L., and J. C. Smith, "Unit Operations," McGraw-Hill, New York (1956).
5. Badger, W. L., and J. T. Banchero, "Introduction to Chemical Engineering," McGraw Hill, New York (1955).

Manuscript received August 18, 1959; revision received October 30, 1959; paper accepted November 17, 1959.

Mass Transfer in Laminar—Boundary-Layer Flows with Finite Interfacial Velocities

ANDREAS ACRIVOS

University of California, Berkeley, California

Asymptotic expressions are presented in this paper for the mass transfer Nusselt number in both forced- and free-convection laminar-boundary-layer flows with large interfacial velocities directed toward the surface. The analysis is valid for arbitrary surface geometries and includes transfer in a variable properties fluid. It is shown, in addition, how these asymptotic formulas may be used in conjunction with the Nusselt number for zero interfacial velocities to estimate the rate of mass transfer for the intermediate regions.

In mass transfer operations the surface past which the fluid moves has the additional property of acting as a source or a sink of material to the flowing stream. Strictly speaking, therefore, mass and heat transfer are not completely analogous phenomena, even under seemingly identical flow configurations; in the formal case the interfacial velocity is usually finite, rather than identically zero, owing to the material exchange on the surface. In particular, the breakdown of the analogy between mass and heat transfer is most pronounced when the mole fraction of the diffusing species is almost zero near the surface and almost unity in the main stream (or vice versa), for then the normal component of the hydrodynamic velocity at the surface is

no longer negligible and must be included in the analysis.

Therefore, owing to the importance of mass transfer in a great many operations—adsorption, sweat cooling, heterogeneous catalysis, to name but a few—it is of some interest to examine under what conditions the rate of mass transfer is affected by the finite interfacial velocity at the surface and how this effect can be predicted in those cases where it appears to be of importance.

The purpose of this article is then to attempt to answer these questions rigorously. The analysis will be limited to forced- and free-convection mass transfer in boundary-layer flows, under isothermal conditions, where the interfacial velocity is directed toward the surface. Further studies dealing with other aspects of this general problem will be considered in the future.

BASIC EQUATIONS FOR FORCED CONVECTION

For the flow of a mixture containing an inert and the diffusing component past the arbitrary two-dimensional surface of Figure 1, the problem is how to predict the rate of transfer of the diffusing substance from the bulk of the fluid to the surface, with which it may react. It will be shown below that for hydrodynamic conditions of the so-called "laminar–boundary-layer" type a simple solution to the problem may be obtained.

This phenomenon is governed by the basic laws of fluid mechanics, the Navier-Stokes and continuity equations, and in addition by the diffusion equation for convective mass transfer. This paper will deal only with laminar systems for which the standard boundary-layer simplifications (5, 2, 3) may be used. The basic equations are therefore the momentum balance

$$u_1 \frac{\partial u_1}{\partial x_1} + v_1 \frac{\partial u_1}{\partial y_1} = U_1 \frac{dU_1}{dx_1} + \frac{\partial^2 u_1}{dy_1^2} \qquad (1)$$

the mass balance

$$\frac{\partial u_1}{\partial x_1} + \frac{\partial v_1}{\partial y_1} = 0 \qquad (2)$$

and the diffusion equation

$$u_1 \frac{\partial \theta}{\partial x_1} + v_1 \frac{\partial \theta}{\partial y_1} = \frac{1}{N_{Sc}} \frac{\partial^2 \theta}{\partial y_1^2} \qquad (3)$$

where, for the moment, constant fluid properties have been assumed.

This system of equations is subject to the boundary conditions:

$$\text{At } y_1 = 0, \qquad u_1 = 0, \qquad \theta = 0 \qquad (4a)$$

$$\text{At } y_1 = \infty, \qquad u_1 = U_1, \qquad \theta = 1 \qquad (4b)$$

$$\text{At } x_1 = 0 \qquad u_1 = U_1, \qquad \theta = 1 \qquad (4c)$$

$$\text{At } y_1 = 0 \qquad v_1 = -\frac{n}{N_{Sc}} \left(\frac{\partial \theta}{\partial y_1} \right) \qquad (4d)$$

where

$$n = \frac{W_\infty - W_s}{1 - W_s}$$ (for mass transfer into the surface $W_s < W_\infty$ and therefore $0 < n < 1$)

The last restriction is obtained from the realization that the transfer rate of the inert into the surface is zero (1, 3, 7).

It is precisely this last boundary condition, Equation (4d), which is responsible for the breakdown of the analogy between heat and gas-phase mass transfer. When $n \to 0$, $v_1 = 0$ at the surface, and the velocity distribution may be calculated independently of the diffusion equation, which is of course what may be done for heat transfer in a constant properties fluid.

It is clear, however, that when n is appreciably different from zero, the momentum and diffusion equations are coupled and cannot, be solved independently of one another. In particular, if one recalls how difficult it is to calculate the velocity and the concentration distributions past a surface with a negligible interfacial velocity, it is rather surprising indeed that, when $n \to 1$, the present problem may be solved in a closed form for an arbitrary surface geometry.

A rigorous solution of Equations (1) to (4) is of course in general an impossible task. Exact analytic solutions are hard to come by unless one is dealing with wedgelike surfaces for which the standard similarity transformations of boundary-layer theory may be applied. On the other hand, approximate momentum integral methods, the von Kàrmàn-Pohlhausen technique for example, are cumbersome to use and may be inaccurate. A different approach is therefore needed.

It should be realized at this point now that the complete solution of Equations (1) to (4) is of little interest. What is required is not the complete velocity and mass fraction profiles but an expression for the local rate of mass transfer into the surface as a function of the parameters of the system: N_{Re}, N_{Sc}, n, and the surface geometry. This is normally accomplished by relating the Nusselt number to the above-mentioned variables, where

$$N_{Nu} \equiv -L \left(\frac{\partial \theta}{\partial y} \right)_{y=0} = -\sqrt{N_{Re}} \left(\frac{\partial \theta}{\partial y_1} \right)_{y_1=0} \qquad (5)$$

and since it is clear from Equations (1) to (4) that the quantity $(\partial\theta/\partial y_1)_{y_1=0}$ is a function only of x_1, n, and N_{Sc} for a given surface,

$$\frac{N_{Nu}}{\sqrt{N_{Re}}} = F(N_{Sc}, x_1, n) \qquad (6)$$

What happens to the function F as $n \to 0$ will not be considered here. This is the classical problem of mass transfer with zero interfacial velocity which has been studied in great detail by many investigators. Considerable information exists therefore about $F(N_{Sc}, x_1, 0)$ for various surface geometries, and a fair number of reliable approximate methods have been proposed for predicting this function.

It is clear then that since the behavior of F for $n \to 0$ may be assumed to be known, what is primarily needed is its asymptotic form for $n \to 1$. For it is found from experience with analogous physical setups that if the behavior of a phenomenon can be predicted

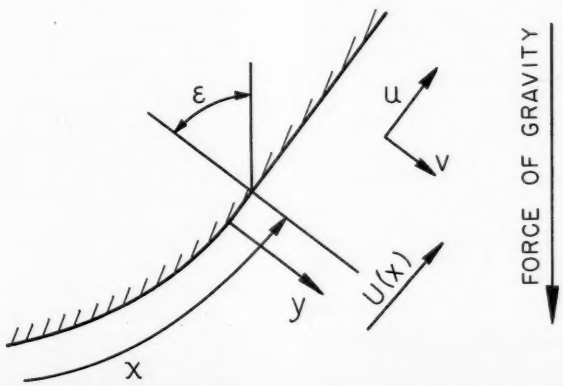

Fig. 1. The position directions of the coordinates x and y, the velocities u and v, and the angle ζ.

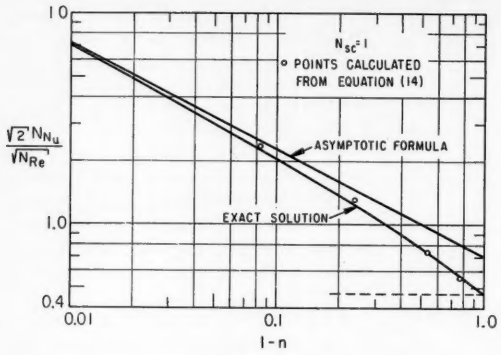

Fig. 2. Mass transfer for flow past a flat plate.

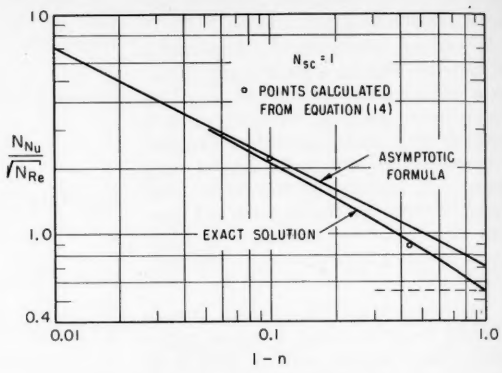

Fig. 3. Mass transfer for stagnation flow.

under the asymptotic conditions where a certain characteristic dimensionless group of the system may take on extreme values (very large or very small), it is a relatively easy matter to describe the process for intermediate values of this dimensionless group by the use of an interpolation formula. One is led to believe therefore that if the limiting form of $F(N_{Sc}, x_1, n)$ for $n \to 1$ were to be discovered, a simple interpolation between its two asymptotes would yield a reliable estimate of this function for all values of n. Experience has taught the author that this approach is far quicker, and the results thus obtained are at least as accurate as those arrived at by momentum integral methods.

ASYMPTOTIC SOLUTION FOR FORCED CONVECTION AS n → 1

Constant property fluids

Equations (1) to (4) admit of a simple solution when the parameter n is near unity. Following a well-established tradition, one begins by attempting to discover a similarity transformation which will reduce the partial differential equations into ordinary differential equations. This can fortunately be accomplished without too much difficulty.

Let

$$u_1 = U_1(x_1)F'(\eta) \text{ and } \theta = \theta(\eta) \quad (5)$$

where

$$\eta \equiv \frac{y_1 U_1}{\sqrt{2\int_0^{x_1} U_1 dx}} \quad (6)$$

which when substituted into the original equations reduce them to

$$F''' + FF'' = [(F')^2 - 1]\frac{2U'_1}{U_1^2}\int_0^{x_1} U_1 dx \quad (7a)$$

and

$$\theta'' + N_{Sc}F\theta' = 0 \quad (7b)$$

with the boundary conditions

$$\text{At } \eta = 0 \quad F = \frac{n}{N_{Sc}}\theta', \quad F' = 0, \quad \theta = 0$$
$$\text{At } \eta = \infty \quad F' = 1, \quad \theta = 1 \quad (8)$$

At this point, one readily perceives from Equation (7a) that, strictly speaking, similarity solutions for the original system of equations which would also satisfy all the imposed boundary conditions cannot generally be obtained unless the surface geometry is such that $\frac{2U'_1}{U_1^2}\int_0^{x_1} U_1 dx =$ a constant for all x_1 a condition which is satisfied only if U_1 is of the form

$$U_1 = x_1^m$$

This, as is well known (5), is the potential flow distribution past a wedge, and therefore similarity solutions for arbitrary values of n exist only for the wedge type of flow. The author will presently show, however, that as $n \to 1$, the right-hand side of Equation (7a) may be neglected and the similarity transformation given by Equation (6) may be applied to any surface geometry.

Physical intuition suggests now that as $n \to 1$ the thickness of the boundary layer will become vanishingly small and the rate of mass transfer, proportional to θ' at the surface, will increase beyond bound. Therefore let

$$\left(\frac{d\theta}{d\eta}\right)_{\eta=0} \equiv b \quad (9)$$

where $b \to \infty$ as $n \to 1$, and define

$$z \equiv b\eta \quad (10a)$$

$$F \equiv \frac{nb}{N_{Sc}} + \frac{1}{b}\phi(z) \quad (10b)$$

$$\theta = \theta(z) \quad (10c)$$

which, when substituted into Equations (7), becomes

$$\phi''' + \frac{n}{N_{Sc}}\phi'' = \frac{1}{b^2}\left\{-\phi\phi'' + [(F')^2 - 1]\frac{2U'_1}{U_1^2}\int_0^{x_1} U_1 dx\right\} \to 0 \text{ as } b \to \infty \quad (11a)$$

and

$$\theta'' + N_{Sc}\left[\frac{n}{N_{Sc}} + \frac{\phi}{b^2}\right]\theta' = 0 \quad (11b)$$

with the boundary conditions

$$\text{At } z = 0 \quad \phi = 0, \ \phi' = 0, \ \theta = 0, \ \theta' = 1$$
$$\text{At } z = \infty \quad \phi' = 1, \ \theta = 1 \quad (12)$$

Two things are immediately apparent: (1) as $n \to 1$, and therefore $b \to \infty$, the similarity transformation given by Equation (6) does indeed apply to surfaces of arbitrary geometry, since the right-hand side of Equation (11a) vanishes in the limit, and (2) the solution of Equations (11) and (12) is a classical eigenvalue problem for the unknown quantity b.

It can be shown now by direct integration, with careful use made of the fact that $b >> 1$, that

$$b = \sqrt{\frac{1}{1-n}\frac{N_{Sc}}{1+N_{Sc}}}$$

and therefore

$$N_{Nu} = \frac{U_1}{\sqrt{2\int_0^{x_1} U_1 dx}}\sqrt{\frac{N_{Re}\cdot N_{Sc}}{2(1-n)(1+N_{Sc})}}\{1 + O(1-n)\} \quad (13)$$

as $n \to 1$ for arbitrary two-dimensional surfaces. An identical result, restricted however to a flat-plate geometry with $U_1 \equiv 1$, was arrived at by Spalding (7) by means of a momentum-integral method.

As was pointed out earlier, Equations (1) to (4) may be reduced by a similarity transformation for all values of n only when the surface geometry is wedgelike. The resulting ordinary differential equations have been solved numerically for the velocity distribution past two simple surfaces, the flat plate and the stagnation region, when

the normal interfacial-velocity component is specified *a priori* (6, 4). The corresponding mass transfer problem has however not been worked out in such detail except for Schmidt numbers of 0.7 and 1.0 (2). Figures 2 and 3 show how the exact values for $N_{Nu}/\sqrt{N_{Re}}$ compare with the asymptotic formula, Equation (13), for the flow past a flat plate and in the stagnation region for $N_{Sc} = 1$. The curves labeled *exact* have been drawn on the basis of the numerical calculations of Schlichting and Bussman (6) and Emmons and Leigh (4) for the flat plate and those of Eckert and Hartnett (2) for the stagnation flow. A surprising result is that even for $n = 0$ the asymptotic expression is not too badly in error, 24% for the stagnation flow and 51% for the flat plate, which suggests that a simple interpolation formula between the two asymptotes, $n = 0$ and $n \to 1$, could be used for the whole range. As can be seen from Figures 2 and 3 the expression

$$N_{Nu} = \left[(N_{Nu})_0^{\frac{3}{2}} + (n(N_{Nu})_1)^{\frac{3}{2}} \right]^{\frac{2}{3}} \tag{14}$$

is in excellent agreement with the exact results for both the flat plate and the stagnation flow, and it is suggested therefore that Equation (14) be used for all surface geometries. $(N_{Nu})_0$ is the Nusselt number in the absence of an interfacial velocity ($n = 0$); $(N_{Nu})_1$ is given by Equation (13).

Variable property fluids

The analysis has dealt so far with a constant property fluid. For many physical systems however this may introduce a considerable error in the results, especially in the case where $W_s << W_\infty$ and $n \to 1$ owing to the large difference in the composition between the bulk and the region near the surface. This section, then, shows how problems involving a variable property fluid may be attacked.

The mass density ρ and the viscosity μ are undoubtedly the properties most sensitive to composition; the coefficient of ordinary diffusion D is, to a first approximation, independent of composition. The following analysis will however be made as general as possible. The basic equations are (3)

$$\rho' \left[u_1 \frac{\partial u_1}{\partial x_1} + v_1 \frac{\partial u_1}{\partial y_1} \right] = U_1 \frac{dU_1}{dx_1} + \frac{\partial}{\partial y_1} \left(\mu' \frac{\partial u_1}{\partial y_1} \right) \tag{15}$$

$$\frac{\partial}{\partial x_1} (\rho' u_1) + \frac{\partial}{\partial y_1} (\rho' v_1) = 0 \tag{16}$$

$$\rho' \left[u_1 \frac{\partial \theta}{\partial x_1} + v_1 \frac{\partial \theta}{\partial y_1} \right] = \frac{1}{N_{Sc}} \frac{\partial}{\partial y_1} \left(\rho' D' \frac{\partial \theta}{\partial y_1} \right) \tag{17}$$

with

$$v_1 = -\frac{nD'_s}{N_{Sc}} \left(\frac{\partial \theta}{\partial y_1} \right) \text{ at } y_1 = 0$$

where the symbols have the same meaning as before, except that the fluid properties are divided by their value in the bulk. Thus

$$N_{Re} \equiv \frac{U_\infty L}{\nu_\infty}, \quad N_{Sc} = \frac{\nu_\infty}{D_\infty}$$

$$\rho' = \frac{\rho}{\rho_\infty}, \quad D' = \frac{D}{D_\infty}, \quad \mu' = \frac{\mu}{\mu_\infty}$$

and D'_s is the value of D' at the surface. The discussion will be limited to the case where $n \to 1$, since it is believed that once the asymptotic expression for the Nusselt number has been calculated, the complete solution may again be approximated by Equation (14) with satisfactory accuracy.

Once more, the transformation given by Equations (5) and (6) may be used to reduce the equations in the limit as $n \to 1$. It is easy to show that the expressions corresponding to Equations (11) become

$$\frac{\mathrm{d}}{dz} \left(\mu' \frac{d^2\phi}{dz^2} \right) + \frac{n}{N_{Sc}} \rho'_s D'_s \frac{d^2\phi}{dz^2} = 0 \tag{18}$$

and

$$\frac{d}{dz} \left(\rho' D' \frac{d\theta}{dz} \right) + N_{Sc} \left[\frac{n}{N_{Sc}} D'_s \rho'_s + \frac{1}{b^2} \int_0^z \rho' \frac{d\phi}{dz} dz \right] \frac{d\theta}{dz} = 0 \tag{19}$$

$$\begin{aligned} \phi = \phi' = \theta = 0 \quad & \text{at } z = 0 \\ \phi' = \theta = 1 \quad & \text{at } z = \infty \\ \theta' = 1 \quad & \text{at } z = 0 \end{aligned}$$

This system may be solved in the limit $n \to 1$ by the following simple scheme. Equation (19) is first rearranged, after a transformation of variables from z to θ, into

$$\rho' D' \frac{d\theta}{dz} = \rho'_s D'_s - N_{Sc} \left[\frac{n\theta}{N_{Sc}} D'_s \rho'_s + \frac{1}{b^2} \int_0^\theta (\theta - \epsilon) \rho'(\epsilon) \frac{d\phi}{d\epsilon} d\epsilon \right] \tag{20}$$

However as $n \to 1$ $(b \to \infty)$

$$\frac{d\phi}{d\theta} \to \frac{D'\rho'}{D'_s \rho'_s (1-\theta)} \left[1 - e^{-\frac{\rho'_s D'_s}{N_{Sc}} \omega} \right] \tag{21}$$

where

$$\omega \equiv \int_0^\theta \frac{D'\rho'}{D'_s \rho'_s} \frac{d\epsilon}{\mu'(1-\epsilon)} \tag{21a}$$

and the eigenvalue problem, Equation (20), can therefore be solved by quadratures, since one of the boundary conditions requires that

$$\frac{d\theta}{dz} \to 0 \text{ as } \theta \to 1$$

The generalization to Equation (13) is then

$$N_{Nu} = \frac{U_1}{\sqrt{2(1-n) \int_0^{x_1} U_1 dx}} \frac{\sqrt{N_{Re} \cdot N_{Sc}}}{(D'_s \rho'_s)} \sqrt{\int_0^1 D'(\rho')^2 \left[1 - e^{-\frac{\rho'_s D'_s \omega}{N_{Sc}}} \right] d\theta} \tag{22}$$

where D', ρ', and μ' are known functions of θ.

ASYMPTOTIC SOLUTION FOR FREE CONVECTION AS n → 1

In free convection fluid motion is caused by the buoyancy forces and obeys, again for laminar–boundary-layer flows under isothermal conditions, the basic equations

$$u_2 \frac{\partial u_2}{\partial x_2} + v_2 \frac{\partial u_2}{\partial y_2} = (1-\theta) G(x_2) + \frac{\partial^2 u_2}{\partial y_2^2} \tag{23}$$

$$\frac{\partial u_2}{\partial x_2} + \frac{\partial v_2}{\partial y_2} = 0 \tag{24}$$

$$u_2 \frac{\partial \theta}{\partial x_2} + v_2 \frac{\partial \theta}{\partial y_2} = \frac{1}{N_{Sc}} \frac{\partial^2 \theta}{\partial y_2^2} \tag{25}$$

The boundary conditions are as before:

At $y_2 = 0$, $u_2 = 0$, $\theta = 0$,

$$\text{and } v_2 = -\frac{n}{N_{Sc}} \frac{\partial \theta}{\partial y_2}$$

At $x_2 = 0$ as well as

$$y_2 = \infty, \ u_2 = 0, \ \theta = 1 \tag{26}$$

It is again possible to arrive at an asymptotic solution for $n \to 1$ and for an arbitrary surface geometry. Let

$$\eta \equiv \left(\frac{3}{4} \right)^{1/4} \frac{y_2 G^{1/3}}{\left[\int_0^{x_2} G^{1/3} dx \right]^{1/4}} \tag{27}$$

and

$$u_2 = F'(\eta) \left(\frac{4}{3} \right)^{1/3} G^{1/3} \sqrt{\int_0^{x_2} G^{1/3} dx} \tag{28}$$

which transforms the original equations into

$$F''' + FF'' + (1-\theta) = (F')^2 \left(\frac{4}{3} \right)^{1/2} \frac{\sqrt{\int_0^{x_2} G^{1/3} dx}}{G^{2/3}} \frac{d}{dx_2} \left(\frac{4}{3} \right)^{1/2} G^{1/3} \sqrt{\int_0^{x_2} G^{1/3} dx} \tag{29}$$

and

$$\theta'' + N_{Sc} F\theta' = 0 \qquad (30)$$

with the boundary conditions

$$\text{At } \eta = 0,\ F = \frac{n}{N_{Sc}}\theta',\ F' = 0,\ \theta = 0$$

$$\text{At } \eta = \infty,\ F' = 0,\ \theta = 1 \qquad (31)$$

It is now obvious from Equation (29) that a similarity transformation cannot, strictly speaking, be assumed unless the surface geometry is such that

$$\frac{\sqrt{{}_0\int^{x_2} G^{1/3} dx}}{G^{2/3}} \frac{d}{dx_2} G^{1/3} \sqrt{{}_0\int^{x_2} G^{1/3} dx} = \text{a}$$

constant for all x_2 which is possible only if $G(x_2)$ is of the form

$$G(x_2) = x_2^{\,m}$$

It will be shown, however, that the transformation given by Equation (27) will apply to any surface as long as long as $n \to 1$. Let

$$\left(\frac{d\theta}{d\eta}\right)_{\eta=0} \equiv b_1 \qquad (32)$$

where $b_1 \to \infty$ as $n \to 1$, and define

$$z_1 \equiv b_1\eta \qquad (33a)$$

$$F \equiv \frac{n}{N_{Sc}} b_1 + \frac{\phi_1(z_1)}{b_1^{\,3}} \qquad (33b)$$

$$\theta \equiv \theta(z_1) \qquad (33c)$$

Therefore

$$\phi'''_1 + \frac{n}{N_{Sc}}\phi''_1 + (1-\theta)$$

$$= \bigcirc\left(\frac{1}{b_1^{\,4}}\right) \to 0 \text{ as } n \to 1 \qquad (34)$$

and

$$\theta'' + N_{Sc}\left[\frac{n}{N_{Sc}} + \frac{\phi_1}{b_1^{\,4}}\right]\theta' = 0 \qquad (35)$$

with the boundary conditions

$$\text{At } \eta = 0,\ \phi_1 = \phi'_1 = 0,\ \theta = 0, \theta' = 1$$

$$\text{At } \eta = \infty,\ \phi'_1 = 0,\ \theta = 1$$

One then is dealing again with an eigenvalue problem, which fortunately may be solved by direct integration. Thus in the limit as $n \to 1$

$$b_1 \to \left[\frac{N_{Sc}^{\,2}}{2(1-n)[1+N_{Sc}]}\right]^{1/4}$$

so that

$$N_{Nu} = \left[\frac{3}{8(1-n)} \frac{N_{Gr}(N_{Sc})^2}{1+N_{Sc}}\right]^{1/4} \frac{G^{1/3}}{\sqrt[4]{{}_0\int^{x_2} G^{1/3} dx}} \{1 + \bigcirc(1-n)\} \qquad (36)$$

It can also be shown that under similar conditions the asymptotic form of the Nusselt number for a variable property fluid is

$$N_{Nu} = \left[\frac{3N_{Gr}N_{Sc}}{8(1-n)}\right]^{1/4} \frac{G^{1/3}}{\sqrt[4]{{}_0\int^{x_2} G^{1/3} dx}} \sqrt[4]{\frac{{}_0\int^1 D'(\rho')^2 \Phi d\theta}{(D'_s\rho'_s)^2}} \qquad (37)$$

where

$$\Phi \equiv \frac{Z(\infty)N_{Sc}}{D'_s\rho'_s}\left[1 - e^{-\frac{\rho'_s D'_s}{N_{Sc}}\omega}\right]$$

$$-{}_0\int^{\omega} e^{-\frac{\rho'_s D'_s}{N_{Sc}}(\omega - x)} Z(x)\,dx$$

$$\omega \equiv {}_0\int^{\theta} \frac{D'\rho'}{D'_s\rho'_s} \frac{d\epsilon}{\mu'(1-\epsilon)}$$

and

$$Z(\omega) \equiv {}_0\int^{\theta(\omega)} \beta'(\theta) \frac{D'\rho'}{D'_s\rho'_s} d\theta;$$

$$Z(\infty) = {}_0\int^{1} \beta'(\theta) \frac{D'\rho'}{D'_s\rho'_s} d\theta$$

Again ρ', D', μ', and β' are the appropriate fluid properties divided by their value in the bulk.

Interestingly enough, the asymptotic expression for the Nusselt number, Equation (36), seems to hold with fair accuracy even for $n \sim 0$, exactly as was the case with the analogous forced-convection formula, Equation (13). For the vertical flat plate, for example, $G(x_1) = 1$, and

$$\frac{Nu}{(N_{Gr})^{1/4}} = 0.401 \text{ for } n = 0 \text{ and } N_{Sc} = 1$$

from reference 5 as compared with 0.66, which is predicted from Equation (36).

CONCLUSIONS

Asymptotic expressions were developed in this paper for the mass transfer Nusselt number in both forced- and free-convection laminar–boundary-layer flows with large interfacial velocities directed toward the surface. The analysis is valid for arbitrary surface geometries and includes transfer in a variable property fluid. It was shown in addition how these asymptotic formulas may be used in conjunction with the Nusselt number for zero interfacial velocities to estimate the rate of mass transfer for the intermediate regions.

The present development holds however, only for laminar–boundary-layer flows. This requires that in free convection $N_{Gr} >> 1$, and in forced convection $N_{Re} >> 1$; also, since it is assumed that the velocity distribution in the boundary layer does not affect the potential flow solution, it requires that

$$\frac{1}{N_{Re}(1-n)} << 1$$

which may be satisfied if N_{Re} is large enough.

ACKNOWLEDGMENT

This research was supported in part by a grant from the National Science Foundation and the Petroleum Research Fund administered by the American Chemical Society. Grateful acknowledgment is hereby made to the donors of these funds.

NOTATION

D	= diffusion coefficient
L	= characteristic length of the surface
u	= x component of the velocity vector
u_1	= u/U_∞
u_2	= $uL/\nu\ (1/N_{Gr})^{1/2}$
U_∞	= characteristic velocity of the bulk
U_1	= potential flow distribution outside the boundary layer, divided by U_∞
v	= y component of the velocity vector
v_1	= $v/U_\infty \sqrt{N_{Re}}$
v_2	= $vL/\nu\ (1/N_{Gr})^{1/4}$
x	= distance along the surface from the leading edge
x_1, x_2	= x/L
y	= distance along the surface from the leading edge
y_1	= $y/L \sqrt{N_{Re}}$
y_2	= $y/\text{L}\ (N_{Gr})^{1/4}$
W	= weight fraction of the diffusing species
W_s, W_∞	= weight fraction respectively at the surface and in the bulk
N_{Gr}	= Grashof number, $\beta g L^3/\nu^2$
N_{Nu}	= Nusselt number, $-L(\partial\theta/\partial y)_{y=0}$
N_{Re}	= Reynolds number, $U_\infty L/\nu$
N_{Sc}	= Schmidt Number, ν/D

Greek Letters

β	= expansion coefficient for the fluid which is defined by $\rho_s/\rho = 1 + \beta(1-\theta)(W_\infty - W_s)$
θ	$\equiv W - W_s/W_\infty - W_s$
ν	= kinematic viscosity
ρ	= mass density of the fluid
μ	= viscosity

LITERATURE CITED

1. Acrivos, Andreas, *Chem. Eng. Sci.*, **9**, 242 (1958).
2. Eckert, E. R. G., and J. P. Hartnett, *Trans. Am. Soc. Mech. Engrs.*, **79**, 247 (1957).
3. Eckert, E. R. G., and P. J. Schneider, *J. Aeronaut. Sci.*, **23**, Readers' Forum (April, 1956).
4. Emmons, H. W., and D. C. Leigh, *Aeronaut. Res. Council, Rept. FM1915* (June, 1953).
5. Schlichting, Hermann, "Boundary Layer Theory," McGraw-Hill, New York (1955).
6. ———, and K. Bussmann, *Schriften Deut. Akad. Luftfahrtforschung*, **7B**, No. 2 (1943).
7. Spalding, D. B., *Proc. Roy. Soc. (London)*, **A221**, 78 (1954).

Manuscript received June 12, 1959; revision September 9, 1959; paper accepted September 14, 1959.

Liquid Viscosities Above the Normal Boiling Point for Methane, Ethane, Propane, and *n*-Butane

G. W. SWIFT, JOHN LOHRENZ, and FRED KURATA

University of Kansas, Lawrence, Kansas

Viscosities, obtained with a falling-cylinder viscometer, are presented for liquid methane, ethane, and propane from their normal boiling points to their critical points and for *n*-butane from its normal boiling point to 100°C. The data of this study are compared with those of other investigators.

The experimental viscosities of this study are correlated within ± 5% over the reduced-temperature range from 0.65 to 0.95 by means of a modified Smith-Brown correlation. The Grunberg-Nissan equation for estimating the critical viscosity was tested with the experimentally determined critical viscosities of this study and was found satisfactory.

The importance of accurate viscosity data to the chemical engineer cannot be overemphasized. A knowledge of viscosity and its variation with temperature and pressure is required for the solution of many of the problems that confront him, for example heat transfer, mass transfer, and fluid flow. A study of the literature on viscosity will show that no systematic approach has been formulated for the collection of these data.

One reason for this lack appears to be caused by the limitations of the instruments used to measure viscosity. Instruments which give good results for gas viscosity, for example the Rankine viscometer, are often unsuited for liquid-viscosity measurement. Instruments which employ mercury drives are restricted to temperatures above the freezing point of mercury. The rolling ball viscometer is severely handicapped in regions where turbulent flow exists.

The problem of evaluating and correlating gas and liquid viscosities of a single substance over the range of temperature and pressure of interest is compounded when the data are not internally consistent. Thus it would be desirable to obtain all the pertinent data with one viscometer.

In the present research the materials investigated were methane, ethane, propane, and *n*-butane, and the falling-cylinder viscometer apparatus was developed to meet the needs of this research because it has the following advantages:

1. The design and construction of the falling-cylinder viscometer are simple.
2. It can be used at extremes of temperature and pressure.
3. The motion of the cylinder can be controlled to eliminate the undesirable components, for example spin and fishtailing.
4. Calibration is relatively simple.
5. All ranges of viscosity can be determined by using a series of bodies with different dimensions.

Since it has been shown that the falling-cylinder viscometer can measure fluid viscosities accurately, this instrument offers a method of determining internally consistent data for substances (in the gas or liquid phase) over wide ranges of temperature, pressure, and viscosity. This equipment can also be used to measure volumetric behavior concurrently with viscosity measurements.

EXPERIMENTAL APPARATUS

An article by Swift, Christy, Heckes, and Kurata (*21*) describes the basic experimental apparatus used in this investigation. Recent improvements in temperature control, viscometer falling-body design, and timing are discussed in detail by Swift (*20*).

Temperature in the viscometer bath was controlleed to within ± 0.01 °C. and was measured with a platinum resistance thermometer. The average uncertainty of temperature measurement was estimated to be ± 0.01°C. Experimental fall times were measured to four significant figures with a digital time-interval meter. A mean fall time was computed from ten consecutive experimental fall times at a given temperature and pressure. Percentage error for mean fall time, computed statistically for 98% probability, was about 0.1% on the average. Pressure was measured with a 0 to 2,000 lb./sq. in. Bourdon gauge with an uncertainty of ± 1 lb./sq. in.

EXPERIMENTAL RESULTS

Values of the viscosities of the different substances used for calibration

TABLE 1. PERCENTAGE OF ERRORS FOR THE VISCOMETER CALIBRATION DATA

Float number	Error in β_a, laminar region*, %	Maximum error in β_a, turbulent region, %	Average error in β_a, turbulent region, %
GCL-301	0.27	3.85	1.48
GCLO-304	0.76	1.72	0.74
MgSLO-303	0.49	3.20	1.20
MgSLO-305	0.21	2.00	1.08
MgSLO-307	0.63	2.39	1.09
MgSLO-309	0.93		

* Computed for 98% probability with t statistic used.

G. W. Swift is now with the Continental Oil Company, Ponca City, Oklahoma.

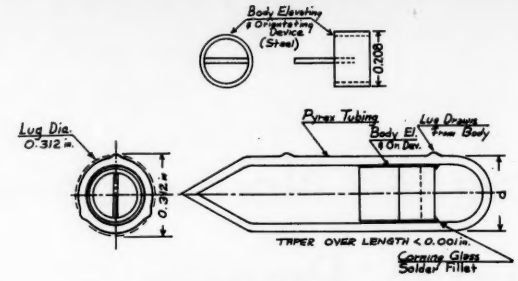

GLASS FALLING BODY

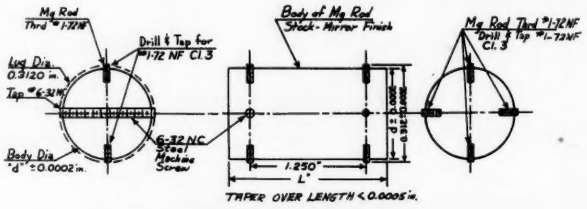
Mg Rod Thrd #1-72NF
Drill & Tap for #1-72 NF Cl 3
Lug Dia. 0.3120 in.
Tap #6-32NC
Body Dia "d" ±0.0002 in.
6-32 NC Steel Machine Screw
Body of Mg Rod Shock-Mirror Finish
1.250" L"
d ± 0.0005
0.312 ± 0.0005
Mg Rod Thrd #1-72NF Drill & Tap #1-72NF Cl. 3
TAPER OVER LENGTH < 0.0005 in.

MAGNESIUM FALLING BODY

Fig. 1. Schematic drawing of falling bodies.

of the viscometer were taken from Rossini (*14*); Comings, Mayland, and Egly (*3*); and Michels and Gibson (*12*). Liquid densities, vapor pressures, and critical properties were taken from Rossini (*14*); Matthews and Hurd (*11*); Barkelew, Valentine, and Hurd (*1*); Hanson (*8*); Deschner and Brown (*4*); Kay (*9*); and Eilerts, *et al.* (*5*).

Six viscometer falling bodies were used in this investigation. Two of these were fabricated from glass, the others from magnesium. The glass bodies were cylindrical with streamlined ends; the magnesium bodies were true cylinders. All the bodies were equipped with projections at either end to stabilize the motion of the bodies in the viscometer tube. Figure 1 shows sketches of the two types of falling cylinders used. Each body was identified by the following code system:

- *G* = material of construction, glass
- *Mg* = material of construction, magnesium
- *C* = closed or hollow construction
- *S* = solid construction
- *L* = lugs or projections on the body
- *O* = oriented

The three-digit number following the code group represents the diameter of the body in thousandths of an inch. (The internal diameter of the viscometer tube was 0.315 in.)

The viscometer was calibrated to account for the effects of temperature and turbulence. A linear coefficient of temperature for the viscometer constant was determined for each falling body. The effect of pressure on viscometer calibration was checked for *MgSLO*-309 and found to change the calibration constant by 2 to 3% at 1,000 lb./sq. in. abs. It was impossible to separate the effect of pressure from the turbulence effect for the other falling bodies; thus no correction for pressure effect on the calibration constant was made, since approximate methods for determining the pressure effect might compound an error of 2 to 3%, rather than correct it. The complete calibration procedure is discussed by Swift (*20*).

The accuracy of the calibration plots is given by the data of Table 1. Even in the region of turbulent flow the errors are quite low.

Phillips pure grade (99 mole % minimum) methane, propane, and *n*-butane and Phillips research grade (99.9 mole % minimum) ethane were used. Analyses by mass spectrometer made on these materials are given in Table 2.

Table 2. Purity Analyses for the Methane, Ethane, Propane, and *n*-Butane used in this Investigation
Mole %

	H_2	N_2	CH_4	C_2H_6	C_3H_6	C_3H_8	n-C_4H_{10}
Methane	0.06	0.95	98.99				
Ethane	0.09			99.91			
Propane			0.08	0.62	0.11	99.19	
n-Butane		0.80				1.33	97.87

Liquid viscosities were determined for methane, ethane, and propane over their respective temperature ranges from normal boiling point to critical point and for *n*-butane from below its normal boiling point to 100°C.

The computations for viscosity were made by the viscometric equation:

$$\mu = \beta_{t,p}(\sigma - \rho)\theta \qquad (1)$$

The original calibration plots of the type used by Sage and Lacey (*16*) were constructed on a scale such that four significant figures could be read for β_o for all bodies except *MgSLO*-307, where it was possible to read only

Table 3. Experimental Viscosities of Liquids

Temperature, °C.	Pressure, lb./sq.in.abs.	Viscosity, centipoise
	Methane	
-140	85	0.0742
	600	0.0762
-120	195	0.0531
	600	0.0544
-100	400	0.0376
	600	0.0396
-90	540	0.0301
	600	0.0303
-85	630	0.0262
-82.2	675	0.015
	Ethane	
-80	25	0.147
	600	0.149
-60	65	0.119
	600	0.121
-40	115	0.0959
-20	230	0.0755
	600	0.0786
0	370	0.0580
	595	0.0604
20	565	0.0418
	600	0.0428
25	625	0.0370
30	695	0.0327
32.3	716	0.0306
	Propane	
-30	50	0.173
-20	50	0.157
	600	0.159
0	100	0.124
20	150	0.105
	600	0.110
40	245	0.0819
	600	0.0881
60	330	0.0649
	600	0.0694
80	475	0.0481
	600	0.0511
90	545	0.0404
96.8	620	0.022
	n-Butane	
20	45	0.164
40	65	0.136
60	110	0.113
80	160	0.0950
100	250	0.0787

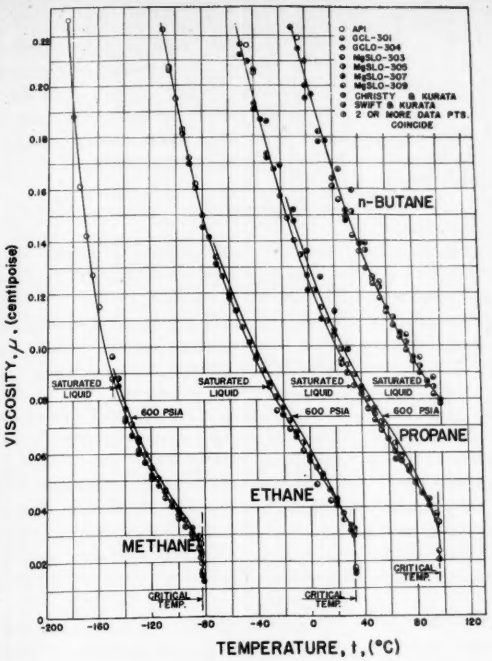

Fig. 2. Experimental viscosities of liquid methane, ethane, propane, and *n*-butane.

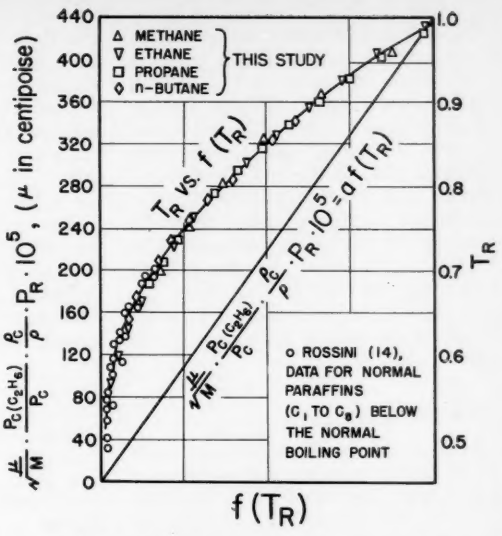

Fig. 3. Correlation for saturated-liquid normal paraffins.

three significant figures. The solution for viscosity in cases where turbulent flow existed was of a trial-and-error nature, since the viscosity had to be assumed before β_v could be determined. The solution converged rapidly however, and two, or at most three, trials were necessary to compute viscosity.

Some of the experimental data are tabulated in Table 3.* In the tabulated data the average value for viscosity for each temperature and pressure is reported. As this value was computed from experimental values determined by two or more falling bodies, bias from improper calibration of any one body is minimized. The precision of the experimental results, reported as average maximum error, was ± 4.0% for methane, ± 2.1% for ethane, ± 2.5% for propane, and ± 2.4% for *n*-butane.

Figure 2 gives a plot of viscosity as a function of temperature. The experimental data points are shown for each body on the saturated liquid curves. The data points which define the 600 lb./sq. in. abs. curves for methane, ethane, and propane were omitted to preserve the clarity of the plot.

The viscosity decreases quite rapidly with increasing temperature in the immediate vicinity of the critical point. Thus it is difficult to obtain accurate viscosity data in this region. This situation is aggravated by the sensitivity of the liquid phase to temperature and pressure in this region. In this investigation critical viscosities for methane and propane were obtained at the respective temperatures and pressures which gave the critical phenomena of opalescence. In the case of ethane the critical viscosity reported was interpolated from the data of a temperature traverse through the critical region.

COMPARISON OF EXPERIMENTAL DATA

An extensive survey of the literature was made for the purpose of comparing data. Table 4 lists data source, method, and approximate deviation of results of the different investigators.

The comparison of the experimental data strongly illustrates the need for a consistent set of viscosity data. The data of this study are consistent, and furthermore the agreement with the

Table 4. Results of Literature Survey

Source	Compound	Method	Approximate deviation from this study
(*2*)	Propane	Rolling ball	3% higher
(*6*)	Methane	Oscillating disk	20 to 25% higher
	Ethane		From 17% lower at low temperatures to 20% higher at high temperatures
(*10*)	Propane	Capillary	4 to 5% higher
	n-Butane		4 to 5% higher
(*13*)	Methane	Capillary	10 to 15% higher
(*14*)	Ethane	Compilation	Less than 1% higher
	Propane		4% higher
	n-Butane		2% higher
(*15*)	Methane	Oscillating disk	20 to 25% higher
(*16*)	Propane	Rolling ball	2% higher
(*17*)	*n*-Butane	Rolling ball	± 2%
(*18*)	Propane	Rolling ball	4% higher
(*19*)	Propane	Capillary	Less than ± 1%
(*22*)	Methane	Falling cylinder	6% lower
	Propane		10 to 12% higher at intermediate temperatures; ± 2% at higher temperatures
(*23*)	Propane	Falling cylinder	High-pressure data only; not directly comparable

* Tabular material has been deposited as document No. 6267 with the American Documentation Institute, Photoduplication Service, Library of Congress, Washington 25, D. C., and may be obtained for $3.75 for photoprints or $2.00 for 35-mm. microfilm.

data of Rossini (*14*) and Starling, Eakin, and Ellington (*19*) is good. In view of the precision of the data of this study, agreement with the data of all investigators save Pavlovich and Timrot (*13*); Gerf and Galkov (*6*); Rudenko (*15*); and Swift, Christy, and Kurata (*22*) is reasonable. The disagreement with the data of Swift, Christy, and Kurata is believed to be caused by improper low-temperature calibration on the part of those investigators. No explanation can be offered for the lack of agreement of the other data.

CORRELATION

A study of the literature was made to determine whether any satisfactory correlations had been made for saturated liquid hydrocarbons above their normal boiling points. A correlation by Smith and Brown (*18*) seemed most suitable. They plotted

$$\frac{\mu}{\sqrt{M}} \cdot \frac{P_{c(x)}}{P_c} \cdot P_R \text{ vs. } T_R$$

The purpose of the term $P_{c(x)}/P_c$ was to adjust all ordinate values to the common pressure basis of reference substance x. Data for saturated n-pentane and n-hexane were correlated by Smith and Brown for reduced temperatures up to 0.93.

The data of the present study were plotted in like manner and were fairly well correlated up to reduced temperatures of 0.8. For higher reduced temperatures the data scattered, but the data for each homologue followed an internally consistent trend. This behavior indicated that some correlation parameter, which was in effect primarily in the high reduced-temperature region, was not being considered. The inclusion of ρ_c/ρ in the ordinate group was found to correct the data scattering in the high reduced-temperature region.

The correlation presented graphically in Figure 3 is based upon the following equation:

$$\frac{\mu}{\sqrt{M}} \cdot \frac{P_{c(x)}}{P_c} \cdot \frac{\rho_c}{\rho} \cdot P_R \cdot (10^7) = af(T_R) \qquad (2)$$

For any T_R, $f(T_R)$ is represented by the curved line in Figure 3. To use the correlation, compute the reduced temperature and locate it on the right-hand ordinate scale. Draw a horizontal line through this value of T_R to intersect the T_R vs. $f(T_R)$ curve. The intersection on this curve defines the correct $f(T_R)$. Move vertically to the line representing Equation (2) and read the left-hand ordinate at the point of intersection. The saturated viscosity can then be computed, with $P_{c(x)}$, P_c, ρ, ρ, and M known.

The accuracy of the correlation is dependent upon the selection of critical constants. To obtain best results the values for T_c, P_c, and ρ_c given by Eilerts *et al.* (*5*) and used in this study are recommended.

The correlation is based on ethane as reference substance x. Smoothed data of this study and the compilation of Rossini (*14*) were used to construct Figure 3. Saturation pressures corresponding to actual temperatures were used.

The correlation predicts saturated liquid viscosities for normal paraffins from methane to n-octane within ± 5% over the reduced-temperature range from 0.65 to 0.95. The values computed from the Smith-Brown correlation for methane, ethane, propane, and n-butane at a T_R of 0.90 disagree with the experimental data of this study by as much as 30%.

A reduced temperature of 0.65 corresponds roughly to the normal boiling point for most paraffins and thus poses no restriction on the value of the correlation, since experimental viscosities for all paraffins are available at temperatures up to the normal boiling point (*14*). On the other hand the region of reduced temperature from 0.95 to 1.0 could be of considerable interest, and little experimental data are available in this region. Thus a method for extrapolating viscosity data in this region is required.

Grunberg and Nissan (*7*) proposed the following equation for the computation of critical viscosity:

$$\mu_c = K\left(\frac{\rho_c^{2/3}}{M^{1/6}}\right)T_c^{1/2} \qquad (3)$$

For the purposes of this discussion K will be defined in terms of Equation (3), where ρ_c is in grams per cubic centimeter, T_c in Kelvin degrees, and μ_c in centipoise. K was computed for methane, ethane, and propane, with the experimental critical viscosities of this study (Table 3) used. The calculated values for K were $K_{methane} = 0.00575$, $K_{ethane} = 0.00552$, and $K_{propane} = 0.00580$. The average value for K, with equal weight given to each of the three compounds was: $K_{avg} = 0.00569$.

By means of K_{avg}, the critical viscosities for straight-chain paraffins from C_1 through C_8 were calculated. As Grunberg and Nissan predicted, the computed critical values for n-butane through n-octane were constant at 0.023 centipoise with the exception of n-heptane, which had a computed critical viscosity of 0.024 centipoise.

When one assumes that the calculated values for critical viscosities are reasonable, saturated liquid viscosities in the region of reduced temperature for T_R's from 0.95 to 1.00 can be mapped using values from Figure 3 up to $T_R = 0.95$ and then extrapolating to the calculated critical viscosity.

CONCLUSIONS

1. The experimental apparatus used in this investigation employed a falling cylinder as a relative means of determining gas and liquid viscosities. The apparatus was operated within the temperature range from −185° to 100°C. and at pressures up to 1,000 lb./sq. in. abs. The performance of the falling cylinder was superior to the falling- or rolling-ball type of viscometer. Temperature was controlled and measured to within ± 0.01°C., pressure was measured to within ± 1 lb./sq. in., and fall times as low as 0.01 sec. were measured with a precision of ± 0.1%.

2. Experimental viscosity data were presented for liquid methane, ethane, and propane from their respective normal boiling points to their critical points, and for n-butane from its normal boiling point to 100°C.

3. Experimental values were determined for the critical viscosities of methane and propane, and the critical viscosity of ethane was estimated by interpolation.

4. The experimental data were correlated within ± 5% by a modified version of the Smith-Brown correlation for saturated hydrocarbon liquids over the reduced temperature range from 0.65 to 0.95. Estimates of saturated liquid viscosities for other normal paraffins can be made from this correlation.

5. The Grunberg-Nissan equation for estimating critical viscosities was tested with the experimentally determined values of critical viscosity for methane, ethane, and propane. The results may be used to estimate viscosities in the reduced temperature range from 0.95 to 1.00.

ACKNOWLEDGMENT

The Phillips Petroleum Company Fellowship Fund provided for the purchase of a major portion of the equipment used in this study and furnished all the hydrocarbons that were used.

The mass spectrometer analyses were performed by the Research and Development Department of the Continental Oil Company.

NOTATION

a = slope of Equation (2)
$f(T_R)$ = function of the reduced temperature in Equation (2)

K = universal constant in Equation (3)
M = molecular weight
P = pressure, lb./sq. in. abs.
P_c = critical pressure, lb./sq. in. abs.
$P_{c(x)}$ = critical pressure of reference substance x, lb./sq. in. abs.
P_R = reduced pressure, dimensionless
T_c = critical temperature, °K.
T_R = reduced temperature, dimensionless
t = temperature, °C.

Greek Letters

$\beta_{t,p}$ = viscometer constant at temperature and pressure, sq. cm./ sec.^{2}
β_o = viscometer constant corrected to 0°C. and 0 pressure, sq. cm./sec.^{2}
θ = fall time interval, sec.
μ = absolute viscosity, poise
ρ = density of fluid, g./cc.
ρ_c = critical density of fluid, g./cc.
σ = density of the falling body, g./cc.

LITERATURE CITED

1. Barkelew, C. H., J. L. Valentine, and C. O. Hurd, *Chem. Eng. Progr.*, **43**, 25 (1947).
2. Bicher, L. B., Jr., and D. L. Katz, *Ind. Eng. Chem.*, **35**, 754 (1943).
3. Comings, E. W., B. J. Mayland, and R. S. Egly, *Univ. Ill. Eng. Exp. Sta. Bull. Ser.*, No. 354 (1944).
4. Deschner, W. W., and G. G. Brown, *Ind. Eng. Chem.*, **32**, 836 (1940).
5. Eilerts, C. K., *et al.*, "Phase Relationships of Gas-Condensate Fluids," Vol. II, pp. 830-2, American Gas Association, New York (1959).
6. Gerf, S. F., and G. I. Galkov, *J. Tech. Phys. (U.S.S.R.)*, **11**, 801 (1941).
7. Grunberg, L., and A. H. Nissan, *Nature*, **161**, 170 (1948).
8. Hanson, G. H., *Trans. Am. Inst. Chem. Engrs.*, **42**, 959 (1946).
9. Kay, W. B., *Ind. Eng. Chem.*, **32**, 358 (1940).
10. Lipkin, M. A., J. A. Davison, and S. S. Kurtz, Jr., *ibid.*, **34**, 976 (1942).
11. Matthews, C. S., and C. O. Hurd, *Trans. Am. Inst. Chem. Engrs.*, **42**, 55 (1946).
12. Michels, A., and R. O. Gibson, *Proc. Roy. Soc. (London)*, **134A**, 288 (1931).
13. Pavlovich, N. V., and D. L. Timrot, *Teploenergetika*, **5**, No. 8, 61 (1958).
14. Rossini, F. D., "Am. Petrol. Inst. Research Proj. 44," Carnegie Press, Pittsburgh, Pa. (1958).
15. Rudenko, N. S., *J. Exp. Theoret. Phys. (U.S.S.R.)*, **9**, 1078 (1939).
16. Sage, B. H., and W. N. Lacey, *Ind. Eng. Chem.*, **30**, 829 (1938).
17. Sage, B. H., W. D. Yale, and W. N. Lacey, *ibid.*, **31**, 223 (1939).
18. Smith, A. S., and G. G. Brown, *ibid.*, **35**, 705 (1943).
19. Starling, K. E., B. E. Eakin, and R. T. Ellington, *A.I.Ch.E. Journal*, to be published.
20. Swift, G. W., Ph.D. thesis, Univ. Kansas, Lawrence (1959).
21. ———, J. A. Christy, A. A. Heckes, and Fred Kurata, *Chem. Eng. Progr.*, **54**, No. 6, 47 (1958).
22. Swift, G. W., J. A. Christy, and Fred Kurata, *A.I.Ch.E. Journal*, **5**, 98 (1959).
23. Van Wijk, W. R., J. H. Van der Veen, H. C. Brinkman, and W. A. Seeder, *Physica*, **7**, 45 (1940).

Manuscript received June 19, 1959; revision received November 6, 1959; paper accepted November 9, 1959. Paper presented at A.I.Ch.E. San Francisco meeting.

Suspension of Slurries by Mechanical Mixers

JOEL WEISMAN and L. E. EFFERDING

Westinghouse Electric Corporation, Pittsburgh, Pennsylvania

The production of essentially homogeneous slurries involves both initial solids suspension and expansion of the particle bed to fill the container. When geometry and solids concentration are held constant, both phenomena are found to be controlled by similar dimensionless groupings of power per unit volume, density, and relative velocity between the fluid and particle. The dimensionless group applicable to bed expansion is shown to be consistent with hydrodynamic theory. Design equations for use with the paddle type of impeller are presented.

Slurries have recently been used in an increasing number of industrial situations. An application of major interest is the proposed use of an aqueous thoria-urania slurry as a nuclear reactor fuel. Solving the problems associated with the use of this fuel in a large-sized power plant has been the subject of an extensive research and development program (*7, 8*).

Maintenance of an essentially homogeneous suspension is one of the prime requisites for successful operation of a slurry-fueled nuclear power plant. Therefore as part of the development program the problems of slurry suspension were investigated in several types of equipment. The mixing studies reported in this paper were one aspect of this investigation. The specific objectives of these mixing experiments were to determine for the turbulent region the factors controlling the production of essentially homogeneous suspensions of solid particles by mechanical mixers and to obtain the information necessary for the design of large mixers suitable for use in plant-sized slurry storage tanks.

Tabular material has been deposited as document No. 6268 with the American Documentation Institute, Photoduplication Service, Library of Congress, Washington 25, D. C., and may be obtained for $2.50 for photoprints or $1.75 for 35-mm. microfilm.

PREVIOUS STUDIES ON SLURRY AGITATION

Hixson and co-workers (*3* to *6*) in an extensive study of the agitation of slurries of soluble salts determined mass transfer coefficients as a function of mixing Reynolds number and system geometry.

White, Summerford, *et al.* (*14, 15*) and Raghavendra and Mukherji (*11*) studied the distribution of sand in unbaffled tanks using paddle agitators. White *et al.* found that with coarsely sized material the fines were suspended but the large particles remained at the tank bottom. Later studies with more closely sized material of various sizes (0.14 to 0.42 mm.) showed that it was not possible to achieve complete suspension of all the sand particles in

their system. They concluded that in an unbaffled system the vortex established at high speeds produces centrifugal forces which are sufficiently strong to combat the forces tending to produce a more uniform concentration.

The mixing of dilute suspensions of insoluble solids in highly viscous liquids was investigated by Hirsekorn and Miller (*2*). The particle size, liquid viscosity, and tank diameter were simultaneously varied so that both the mixing Reynolds number and particle settling rate were maintained approximately constant. The minimum power to achieve suspension was defined as the power input when all particles were lifted from the bottom of the tank. The authors' results can be expressed as

$$(P_s/V_l)\,(d/D) = \text{constant} \qquad (1)$$

It was noticed that just as complete suspension was obtained, the portion of the liquid nearest the surface was devoid of solids. The material below the slurry-fluid interface was however essentially uniform in concentration.

Zwietering (*16*) reported the results of an extensive investigation of stirrer speeds and dimensions required to suspend various slurries. He considered only the question of suspension and reported no quantitative information on the degree of homogeneity of the mixture. Zwietering did note that with rapidly settling particles just at their suspension point a layer of clean liquid exists adjacent to the surface. The investigation included studies with paddles, turbines, vaned disks, and propellers. When one uses Hirsekorn and Miller's (*2*) suspension criterion (no particles remaining on tank bottom), the conditions required for suspension could be correlated by

$$s = \frac{Nd^{0.85}}{\nu^{0.1}\delta^{0.2}(g\Delta\rho/\rho_l)^{0.45}B^{0.13}} = F\,[(D/d)\,(a/D)] \qquad (2)$$

The effect of D/d and D/a were presented graphically for each of the impeller types studied. For paddle type of impellers the dimensionless characterization group s increased with increasing values of D/d and a/D.

In studies of the rate of solution of salt crystals in an agitated tank Kneule (*9*) found that applied power inputs beyond those required just to suspend the particles had little effect on the rate of mass transfer. If the notation of Zwietering (*16*) is used to facilitate comparison, the suspension-power correlation presented by Kneule can be written as

$$A = \frac{B^{1/2}V_l[g(\Delta\rho)]^{3/2}\delta^{1/2}}{P_s g_c \rho_l^{1/2}} \qquad (3)$$

Values of A were not presented by Kneule. The correlations of Rushton *et al.* (*12*) show that the mixing power is given by

$$P = N_p\,\rho_m\,N^3\,d^5/g_c \qquad (4)$$

Since for a given geometry N_p is a constant in the fully turbulent region, one can rewrite Equation (3) as

$$K\left(\frac{D}{d}\right)A^{-1/3} = \left(\frac{g_c}{g}\right)\frac{Nd^{2/3}(\rho_l/\rho_m)^{1/6}}{\delta^{1/6}[g(\Delta\rho/\rho_m)]^{1/2}B^{1/6}} \qquad (5)$$

If one notes that for most of the systems tested ρ_m does not differ greatly from ρ_l, the marked similarity of Equations (2) and (5) is evident.

It is pointed out in the work of Hirsekorn and Miller (*2*) that the suspension of particulate solids involves two distinct problems: the initial suspension of the particles and the complete dispersion of the already suspended solids. At the beginning of this investigation the literature data on the former problem were not in complete agreement, and there was essentially no information applicable to the latter problem in the fully turbulent region.

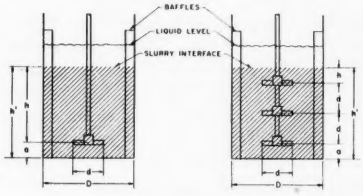

Fig. 1. Mixing-tank arrangements.

EXPERIMENTAL APPARATUS AND MATERIALS

Methods of producing slurry suspensions by rotating mixers were studied in transparent cylindrical tanks having diameters of 5½, 9⅜ and 11⅜ in. Figure 1 shows the arrangement of both single and multiple impeller systems. Each tank was fitted with four baffles extending to the tank bottom and having a baffle width to tank diameter ratio of 1/12. The tanks were mounted so that mixing phenomena might be observed visually through the walls and bottom of the vessel. In all cases studied, six-bladed paddle-type impellers with a width-to-diameter ratio of ⅛ were used. The impellers were 2, 3, and 4 in. in diameter. The mixing vessels were mounted in an adjustable frame so that the impeller height above the vessel bottom might be varied.

A ¼-hp. variable-speed motor was suspended vertically above the vessel by means of a thin wire. Lateral motion was restricted by a loosely fitted radial ball bearing. The power imput to the vessel was computed from measurement of the shaft torque and speed. Torque values were obtained from a calibrated spring scale of appropriate range acting upon a 2-in. lever arm. Speed measurements were obtained from an electronic frequency meter with a photoelectric pickup. An aluminum disk, integral with the motor chuck and painted in alternate dark and light bands, served as an intermittent reflector for the photoelectric pickup. During the course of the experiments the impeller power requirements varied from 0.001 to 0.17 hp., and impeller speeds ranged from 200 to 2,200 rev./min. It is estimated that the maximum error in the computed power was less than 10%.

The mixing studies were conducted with aqueous slurries of thorium oxide and both aqueous and nonaqueous slurries of spherical glass beads. A series of Tyler sieves were used to determine the average diameter of both sizes of glass beads which were studied. All particles of the small-size beads were between 37 and 53 μ in diameter. The average diameter was therefore taken as 45 μ. The large-sized glass beads were found to have the following size distributions:

Diameter range, (μ)	Weight, %
88 — 125	6.4
125 — 147	9.3
147 — 177	63.2
> 177	21.2
	100.0

Microscopic examination of the particles above 177 μ showed them to have an average diameter of about 185 μ. The average diameter of the large-sized beads was taken as

$$\delta_{avg} = \frac{\Sigma N_i\,\delta}{\Sigma N_i} \qquad (6)$$

By use of the mean diameter in each size range and the relative number of particles in each range δ_{avg} was computed as 140 μ.

The hindered settling rates of slurries of both the large and small beads were measured as a function of concentration. At any given concentration the ratio of settling rates was found to be in agreement with the ratio of the squares of the average particle diameters. This was taken as a good indication that the computations had given the correct relative values of the average diameters.

The problem of the determination of the average diameter (or free settling rate) of the thoria particles is more complex. Although the thoria is composed of very small particles (all under 4 μ, most under 1 μ), these particles agglomerate to form relatively large flocs. The mixing studies are concerned with the behavior of the flocs rather than the individual particles. Andreasen pipette measurements (without a dispersant) indicated the free

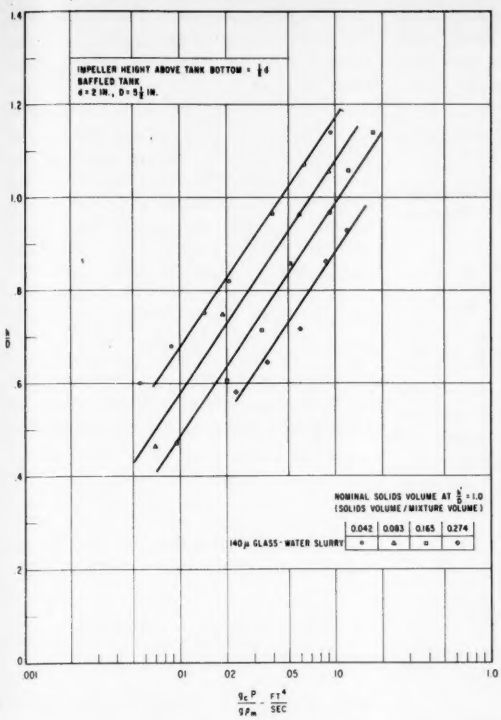

Fig. 2. Effect of concentration on height of the slurry interface.

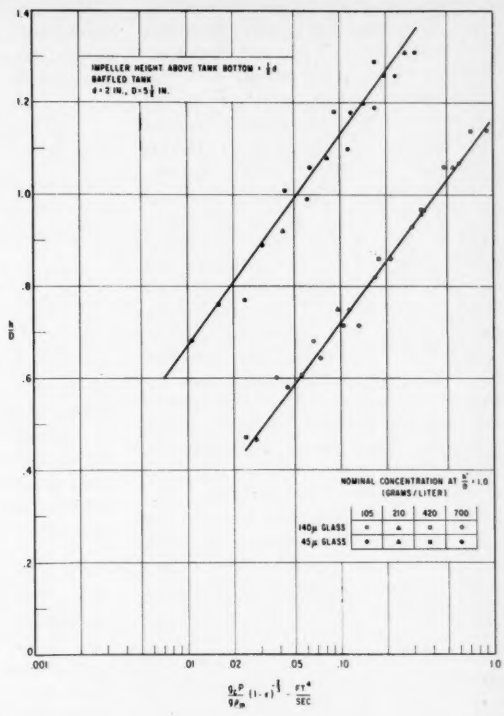

Fig. 3. Effect of particle size on power requirements and height of the slurry interface.

settling rate of the flocs to be of the order of 2 mm./sec. However with such a rapid settling rate the Andreasen pipette measurements are not accurate. The technique of using a substance such as glycerin to reduce the settling rate was not applicable in this case since another liquid would have changed the degree of flocculation. It will subsequently be shown that use of 2 mm./sec. for the free settling rate together with the assumption that the thoria flocs are half water allows the thoria data to be related to those obtained with glass beads. Additional support for this assumption is given by the work of Taylor and Biancheria (*1, 13*) in the correlation of room-temperature hindered settling rates with settled bed densities. They found that use of a 2 mm./sec. free settling rate and a 50% particle porosity in their equations resulted in a good correlation of the data for the thoria used in the present study.

DISPERSION OF AQUEOUS SLURRIES IN THE TURBULENT REGION

The first problem studied was that of dispersing already suspended solids throughout the vessel volume. Zwietering's (*16*) and Hirsekorn and Miller's (*2*) observations that areas devoid of solids may exist adjacent to the air-liquid interface although all particles are suspended were confirmed, and a range of power inputs was found for which no particles remain on the tank bottom but a definite slurry-water interface exists. As the power input is increased, the interface rises until the slurry finally occupies the entire tank. The variation in concentration with distance below the interface was investigated by measuring the change in pressure with liquid depth at a number of positions. The measurements were made with manometer dip tubes and a sensitive differential pressure cell with a porous-tipped probe. The porous tip served to exclude slurry from the instrument lead line. The pressure cell was capable of detecting a pressure differential equivalent to a concentration change of 40 g./liter persisting for a depth of 1 in. Velocity-head effects were eliminated by making measurements during and immediately after mixing. Provided that no particles remained on the tank bottom, no departure from the linear relationship between pressure and depth was observed except in the immediate vicinity of the slurry-water interface. Once all solids are suspended, the slurry concentration, averaged across any plane parallel to the tank bottom, appears to be essentially uniform below the slurry interface. (It should be noted that the measurement technique used would not detect local concentration variations such as might occur adjacent to the impeller, impeller shaft, or vessel walls.) It was therefore concluded that the height of the slurry-water interface could be used as an index of the degree of slurry dispersion.

Most of the data reported in this paper were obtained with the total liquid height 1.4 times the tank diameter. However a number of runs were made in which the liquid depth was varied from 1 to 2 tank diam. The interface location and impeller power requirements were found to be independent of the liquid level above the interface.

The slurry-water interface was more clearly defined with increasing solids concentration and with a decreasing variation in particle size. In the turbulent region interface height determinations at solids concentrations below 100 g./liter were not reproducible and were therefore omitted from the present study.

The initial dispersion studies were carried out with glass-bead–water slurries by means of single impellers placed one-half an impeller diameter above the tank bottom. Reynolds numbers ($Nd^2\rho_l/\mu_l$) varied from about 2×10^4 to 2×10^5. These tests established that the power input increases exponentially with the height of the slurry interface above the impeller midplane. It was

also found that at a given interface height the impeller power increases with increasing solids concentration. That this effect is not simply a matter of increasing mixture density is shown in Figure 2, where the interface height is plotted against $(g_c P)/(g\rho_m)$. It was found that the power varies directly with the volume fraction of solids to the 2/3 power $[(1-\epsilon)^{2/3}]$. The same variation was noted with the thoria slurries when $(1-\epsilon)$ was computed on the basis that the thoria flocs are half water. Application of the solids-fraction correction to a typical set of data is shown in Figure 3. This plot also shows the effect of particle size on power requirements. At a given interface level the data for the two particle sizes differ by a factor approximately equal to that of the ratio of the free-settling velocities of the particles.

The effects of both tank size and the ratio of impeller diameter to tank diameter were also evaluated. For geometrically similar systems compared at the same value of h/D the power requirements were found to be directly proportional to the vessel volume. For values of d/D between 0.176 and 0.426 it was found that the power per unit volume required to maintain the interface at a given value of h/D varied inversely with $(d/D)^{1/2}$.

It was found that for a given system the interface height increases by 25 to 35% if the baffles are lifted from the bottom by a distance equal to ½ an impeller diameter. Thus a vessel baffled to the bottom is less efficient in terms of the power requirement to expand a bed. This aspect of mixing was not pursued further because of the limited time available for this study. All curves and equations presented in this paper are based on the case where the baffles extend to the tank bottom.

ANALYSIS OF THE BEHAVIOR OF THE SLURRY INTERFACE

The experimental observations lead to the conclusion that the degree of mixing decreases with increasing distance from the impeller. It would seem reasonable to suppose that the region of the slurry-water interface is quiescent and therefore that laminar flow conditions prevail. In addition, at the slurry-water interface the suspending and settling forces must be in equilibrium. Making the above assumptions and noting that the particles just at the interface must be in a low concentration region, one can mathematically analyze the behavior of these particles. In so doing, the authors shall essentially follow the treatment developed by Langevin (*10*) for the analysis of Brownian motion.

For the interface region the partial differential equation describing the motion of a single particle in the vertical direction may be written as

$$\frac{m}{g_c}\left(\frac{\partial^2 x}{\partial t^2}\right) = -k\left(\frac{\partial x}{\partial t}\right) + X \quad (7)$$

Multiplying through by x and manipulating to incorporate x^2 as the dependent variable leads to

$$\frac{m}{2\,g_c}\left[\frac{\partial^2(x^2)}{\partial t^2}\right] - \frac{m}{2\,g_c}\left(\frac{\partial x}{\partial t}\right)^2 = -\frac{k}{2}\left(\frac{\partial(x^2)}{\partial t}\right) + Xx \quad (8)$$

If one applies this to the behavior of an average particle, the last term becomes zero owing to the random variation of collision forces and particle displacements. Equation (8) then becomes

$$\frac{m}{2g_c}\left[\frac{\overline{\partial^2(x^2)}}{\partial t^2}\right] + \frac{k}{2}\left(\frac{\overline{\partial(x^2)}}{\partial t}\right) = \frac{m}{g_c}\left(\frac{\overline{\partial x}}{\partial t}\right)^2 \quad (9)$$

where the bar denotes averaged conditions. The last term of Equation (9) represents twice the vertical component of the average kinetic energy of a particle. By replacing (m/g_c) $[(\overline{\partial x})/(\partial t)]^2$ by $2\overline{E}_x$ and noting that at equilibrium conditions t may be considered to be infinite, one may integrate Equation (9) to obtain

$$\overline{\Delta x}^2 = \frac{2\overline{E}_x}{k/2}\,t \quad (10)$$

where $\overline{\Delta x}$ is the average vertical displacement of a particle in the time interval t. If one now evaluates the friction factor in terms of Stokes's free-settling velocity, he obtains

$$(\overline{\Delta x})^2 = \frac{4\,g_c\,\overline{E}_x\,v_s}{g\,V_p(\Delta\rho)}\,t \quad (11)$$

Division by t^2 and replacement of $\overline{E}_x/t$ by $p'/3$ (this assumes the y and z components of kinetic energy of the particle are equal to the x component) yields

$$\frac{(\overline{\Delta x})^2}{t^2} = \frac{4\,g_c\,p'\,v_s}{3\,g\,V_p(\Delta\rho)} \quad (12)$$

The term $(\overline{\Delta x})^2/t^2$ is the square of the average velocity of a particle. Since the particle is in equilibrium at the slurry-liquid interface, the average velocity of a particle must be equal to the gravitational settling velocity. Therefore

$$p' = \frac{3\,g\,V_p(\Delta\rho)v_s}{4\,g_c} \quad (13)$$

It is now necessary to relate p' to the power input of the impeller. It has been shown by a number of investigations (*12*) of the fully turbulent region, and borne out by the data obtained in this study, that for a given system and impeller speed the power input of the impeller is directly proportional to the mixture density. Hence the ratio of the power required to agitate the slurry mixture to that required to agitate the suspending medium is given by

$$\frac{P_l}{P} = \frac{\rho_l}{\rho_m} \quad (14)$$

It seems reasonable to conclude that the difference between P and P_l is the total power input to the solid particles:

$$P_p = P\,\frac{\Delta\rho}{\rho_m}\,(1-\epsilon) \quad (15)$$

If one designates the average power input to an individual particle as p_{avg}, then

$$p_{avg} = \frac{V_p\,P_p}{V(1-\epsilon)} = \frac{V_p\,P(\Delta\rho)}{V\,\rho_m} \quad (16)$$

For agitation in geometrically similar systems the ratio p'/p_{avg} may be expected to be a function of h/D, $(1-\epsilon)$, and the mixing Reynolds number. However since in the fully turbulent region the Reynolds number does not affect the power number, it seems reasonable that for this restricted case N_{Re} will not affect p'/p_{avg}. Therefore

$$p' = p_{avg}\cdot F\,(1-\epsilon)\cdot F'\,(h/D) = \left(\frac{V_p\,P(\Delta\rho)}{V\,\rho_m}\right) F''\,(1-\epsilon)\,F'\,(h/D) \quad (17)$$

Substitution of the value of p' from Equation (13) and rearrangement gives

$$(h/D) = F'''\left(\frac{g_c P}{g\rho_m V v_s}\right)\cdot F'''(1-\epsilon) \quad (18)$$

CORRELATION OF INTERFACE BEHAVIOR AT MIXING REYNOLDS NUMBER IN THE TURBULENT REGION

The previously cited experimental data show that the power requirements in geometrically similar systems vary directly with $(1-\epsilon)^{2/3}$ and exponentially with h/D. Inserting these functions explicitly in Equation (18) gives

$$(h/D) = K_1 \ln\left[\left(\frac{g_c\,P}{g\,\rho_m\,V\,v_s}\right)(1-\epsilon)^{-2/3}\right] + K_2 \quad (19)$$

If one extends the above equation to include the effect of varying impeller-

diameter–to–tank-diameter ratios, one has

$$(h/D) = K'_1 \ln\left[\left(\frac{g_c P}{g\,\rho_m V v_s}\right)(1-\epsilon)^{-2/3}(d/D)^{1/2}\right] + K'_2 \quad (20)$$

Figure 4 shows the data for aqueous slurries agitated by a single impeller when correlated in this fashion. In this correlation the specific gravity of glass beads was taken as 2.25, and free-settling velocities in water of 18 and 1.85 mm./sec. were used for particle diameters of 140 and 45 μ respectively. As previously stated, the free-settling velocity of thoria particles was taken to be 2 mm./sec., and the porosity of thoria flocs was taken as ½ (specific gravity = 4.85). It can be seen that excellent agreement is obtained between the various systems tested. For h/D values above 0.5 the equation of the average line through the data is

$$h/D = 0.23 \ln\left[\left(\frac{g_c P}{g\,\rho_m V v_s}\right)(1-\epsilon)^{-2/3}(d/D)^{1/2}\right] + 0.1 \quad (21)$$

To check the above correlation with another fluid, a few runs were conducted where the 140-μ glass beads at a nominal concentration of 105 g./liter were agitated in carbon tetrachloride. When correlated in accordance with Equation (22), the limited data obtained fall within the scatter observed with the water data.

The effect of the height of the impeller from the tank bottom, was investigated for several different systems. It was found that this effect depended on the ratio a/d. The results can be expressed in terms of an empirical correction factor, where

$$\frac{h}{D} = f\left\{0.23 \ln\left[\left(\frac{g_c P}{g\,\rho_m V v_s}\right)(1-\epsilon)^{-2/3}(d/D)^{1/2}\right] + 0.1\right\} \quad (22)$$

Values of f as a function of a/d are presented graphically in Figure 5. It will be seen that for a/d values of ½ or more, f remains at 1; at values of a/d below ½, f increases slightly.

It would be expected that the power to expand a suspended bed in a long tank would be materially reduced by the use of several impellers. The effect of multiple impellers on the slurry water interface level was therefore investigated. It was found that the correlation developed for single-impeller systems applies provided that the power is divided by the number of impellers and the interface height is measured above the midplane of the uppermost impeller. As shown in Figure 6, the data for one-, two-, and three-impeller systems, arranged as illustrated in Figure 1, are well correlated by

$$\frac{h}{D} = 0.23 \ln\left[\left(\frac{g_c P}{gn\,\rho_m V v_s}\right)(1-\epsilon)^{-2/3}(d/D)^{1/2}\right] + 0.1 \quad (23)$$

or

$$h/D = 0.23 \ln \Psi + 0.1 \quad (24)$$

Equation (24) can be used to determine, for the fully turbulent region the number of impellers required to produce a fully dispersed suspension with the minimum power input. The authors will consider the situation where there are n equally spaced impellers; the lowest impeller is as close to the tank bottom as possible, and the distance of the liquid surface from the top impeller equals half the distance between impellers. It can be shown that the power is a minimum for

$$n = \frac{0.5 + 0.5\sqrt{1 + 0.92\,D/h'}}{-1 + \sqrt{1 + 0.92\,D/h'}} \quad (25)$$

For large values of h'/D Equation (25) simplifies to

$$n = 2.18\,(h'/D) \quad (26)$$

When h'/D is 5 or above, the value of n computed by Equation (26) is within 10% of that computed by Equation (25).

The optimum spacing predicted by Equations (25) and (26) must be considered as only approximate. Use of these equations involves extrapolation of the power-input relationship somewhat beyond the range of the data obtained.

DISPERSION STUDIES IN THE TRANSITION AND LAMINAR REGION

Although beyond the scope of the work originally contemplated, a number of runs were made outside the fully turbulent region. The work was restricted to studies of the 140/μ glass beads in the 5½-in. tank. Glycerol-water solutions having viscosities five and twenty-five times the viscosity of

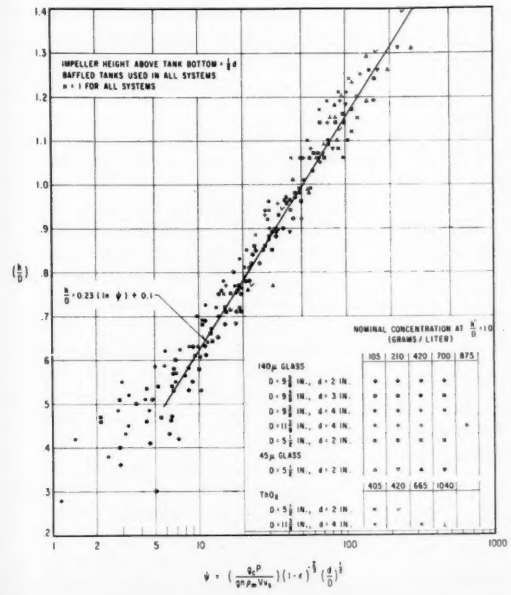
IMPELLER HEIGHT ABOVE TANK BOTTOM = ½ d
BAFFLED TANKS USED IN ALL SYSTEMS
n = 1 FOR ALL SYSTEMS
h/D = 0.23 (ln ψ) + 0.1
NOMINAL CONCENTRATION AT h/D = 1.0 (GRAMS / LITER)
105 | 210 | 420 | 700 | 875
140μ GLASS
D = 5½ IN., d = 2 IN.
D = 9½ IN., d = 3 IN.
D = 9½ IN., d = 4 IN.
D = 11½ IN., d = 4 IN.
D = 5½ IN., d = 2 IN.
45μ GLASS
D = 5½ IN., d = 2 IN.
405 | 420 | 665 | 1040
ThO2
D = 5½ IN., d = 2 IN.
D = 11½ IN., d = 4 IN.

Fig. 4. Generalized correlation of interface heights and power requirements for single impeller systems in the turbulent region.

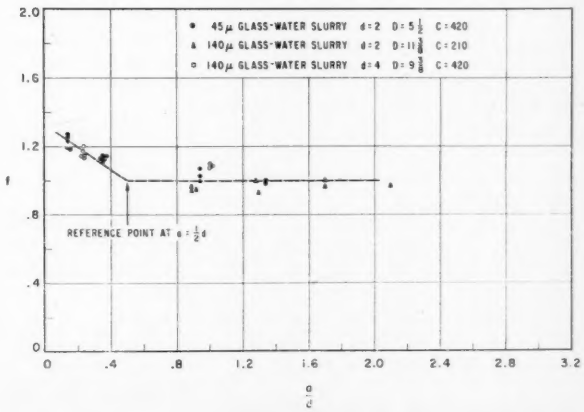
45μ GLASS-WATER SLURRY d = 2 D = 5½ C = 420
140μ GLASS-WATER SLURRY d = 2 D = 11½ C = 210
140μ GLASS-WATER SLURRY d = 4 D = 9½ C = 420
REFERENCE POINT AT a = ½ d

Fig. 5. Interface height-correction factor as a function of impeller height above tank bottom.

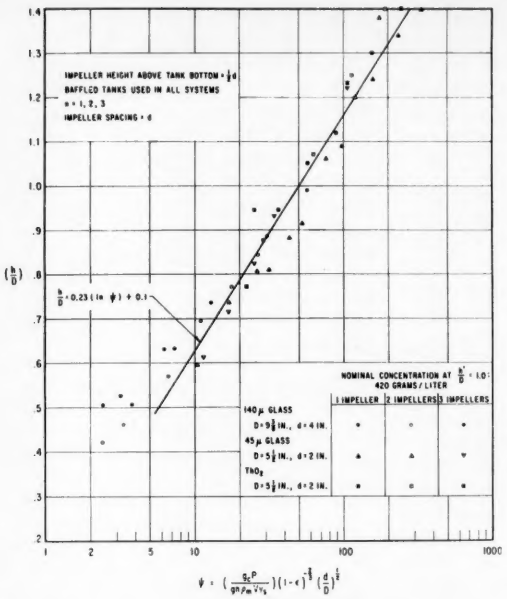
IMPELLER HEIGHT ABOVE TANK BOTTOM = ½d
BAFFLED TANKS USED IN ALL SYSTEMS
n = 1, 2, 3
IMPELLER SPACING = d
NOMINAL CONCENTRATION AT h/D = 1.0
420 GRAMS / LITER
1 IMPELLER
2 IMPELLERS
3 IMPELLERS
140μ GLASS
D = 9½ IN., d = 4 IN.
45μ GLASS
D = 5½ IN., d = 2 IN.
ThO2
D = 5½ IN., d = 2 IN.
h/D = 0.23 (ln ψ) + 0.1
h/D
ψ

Fig. 6. Correlation of interface heights and power requirements for multiple impeller systems in the turbulent region.

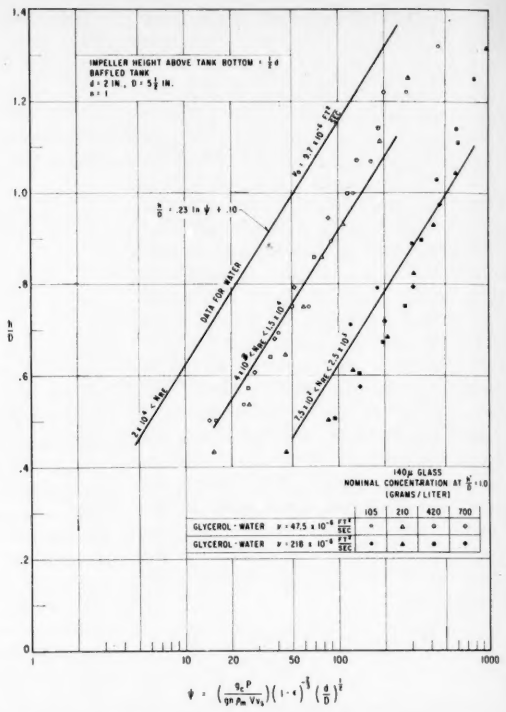

Fig. 7. Effect of Reynolds number on power requirements and interface heights.

room temperature water were used. Figure 7 compares the results with the data for the fully turbulent region. It is seen that the more viscous the suspending medium (lower Reynolds number), the more power is required. The supposition that the effect observed is a function of Reynolds number is also indicated by the fact that for a given fluid the increase in power is greatest at the lower interface heights and hence at the lowest agitator speeds and Reynolds numbers.

Figure 8 shows, as a function of Reynolds number, $Nd^2\rho_l/\mu_l$, the ratio of the actual power required to the power to maintain the same interface level computed from Equation (22). It would appear that this ratio is unity for values of N_{Re} above 2.5×10^4. For values of N_{Re} below 1.5×10^4 the data are fairly well correlated by

$$P/P_o = 4 \times 10^3 \, (N_{Re})^{-0.8} \quad (27)$$

The interface height data of Hirsekorn and Miller (2) for two-bladed paddles at N_{Re} values below 25 are also shown on Figure 9. These data are also correlated by Equation (27). It will be noted that the ratio of P/P_o begins to depart from unity at about $N_{Re} = 2 \times 10^4$. This is approximately the same Reynolds number at which the power number vs. N_{Re} curves for many impellers cease being horizontal lines (12). The power data obtained in this study also follow this pattern.

SUSPENSION-POWER REQUIREMENTS

The criterion used for full suspension is the same as that proposed by Hirsekorn and Miller (2) and Zwietering (16), namely that all particles are lifted from the vessel bottom. Since visual observation was required, it was necessary to rely solely on the glass-bead slurries for this portion of the investigation. All the thoria slurries studied were too milky to allow the point at which suspension occurred to be determined with any degree of accuracy.

Comparison of the data with the previously described correlations of Zwietering (16) and Kneule (9) showed that best agreement is obtained with Kneule's dimensionless group [Equation (3)]. If Equation (3) is rewritten with the notation of this paper used,

$$A' = \frac{V_t[g(\Delta\rho)]^{3/2}\delta^{1/2}}{P_s \, g_c \, \rho_l^{1/2}} \left(\frac{1-\epsilon_t}{\epsilon_t} \right)^{1/2} \quad (28)$$

Since in the turbulent region the relative velocity between the fluid and a particle is expressed by Newton's relation

$$u_s = 1.74 \left[\frac{g \, \delta(\Delta\rho)}{\rho_l} \right]^{1/2} \quad (29)$$

Equation (28) may be rewritten as

$$A' = \frac{g \, V_t \, u_s(\Delta\rho)}{1.74 \, g_c \, P_s} \left(\frac{1-\epsilon_t}{\epsilon_t} \right)^{1/2} \quad (30)$$

It will be noted that the dimensionless power group of Equation (30) is in the same form as the power group of Equations (18) through (23) but that $\Delta\rho$ replaces ρ_m and u_s replaces v_s. Use of a relative particle-fluid velocity calculated on the basis of Newton's law (u_s) rather than Stokes's law (v_s) seems reasonable since the particles on being removed from the tank bottom are in the turbulent region near the impeller.

The utility of Equation (31) in correlating the data from geometrically similar systems is shown in Figure 9. It will be noted that the data obtained with the glycerol-water solutions in the transition region are also correlated. It would appear that for mixing Reynolds numbers above about 10^3 the relative velocity between the fluid and a particle at the tank bottom is sufficiently high so that Newton's law may be used. As expected, the data of Hirsekorn and Miller (2) for Reynolds numbers below 30 are not well correlated. The suspension powers required were approximately seven times those which would be indicated by the results of the present investigation.

Figure 10 shows the effect of varying the D/d ratio as well as the height of the impeller above the tank bottom. For D/d ratios of 2.35 to 2.75 the data are represented by

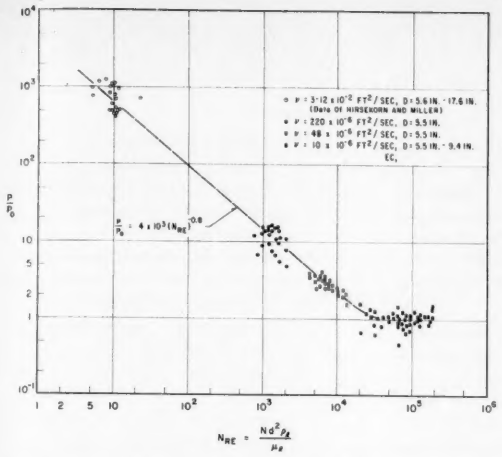

Fig. 8. Power requirement correction factor for the transition and laminar regions.

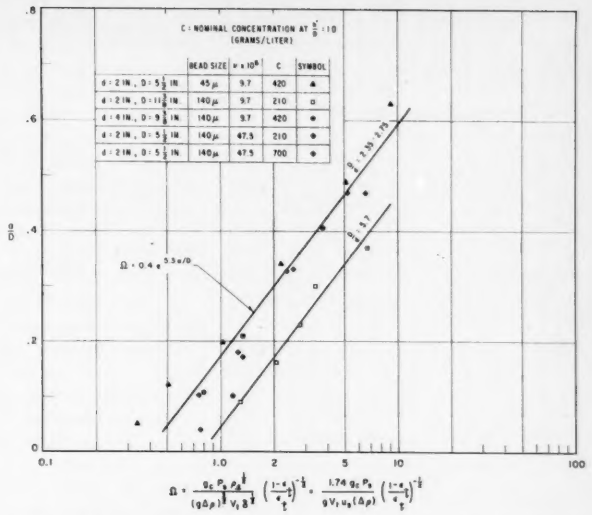
C = NOMINAL CONCENTRATION AT $\frac{a}{D}$ = 1.0 (GRAMS/LITER)
$\Omega = 0.4\, e^{5.3\, a/D}$
$\Omega = \frac{g_c P_s}{g V_t u_s(\Delta\rho)} \left(\frac{1-\epsilon_t}{\epsilon_t}\right)^{-1/2}$

Fig. 10. Effect of system geometry on suspension power requirements.

$$\Omega = \frac{1.74\, g_c P_s}{g V_t u_s(\Delta\rho)} \left(\frac{1-\epsilon_t}{\epsilon_t}\right)^{-1/2} = 0.4\, e^{5.3\, a/D} \qquad (31)$$

For a D/d ratio of 5.7, the data are represented by

$$\Omega = \frac{1.74\, g_c P_s}{g V_t u_s(\Delta\rho)} \left(\frac{1-\epsilon_t}{\epsilon_t}\right)^{-1/2} = 0.95\, e^{5.3\, a/D} \qquad (32)$$

Although a firm correlation cannot be advanced on the basis of the two D/d ratios studied, the following tentative equation is suggested:

$$\frac{1.74\, g_c P_s}{g V_t u_s(\Delta\rho)} \left(\frac{1-\epsilon_t}{\epsilon_t}\right)^{-1/2} (d/D) = 0.16\, e^{5.3\, a/D} \qquad (33)$$

This is in agreement with the (d/D) relationship observed by Hirsekorn and Miller [Equation (1)].

If Equation (32) is rewritten so that it is in the same form as Equation (21), one has

$$a/D = 0.19 \ln \left[\frac{1.74\, g_c P_s}{g V_t u_s(\Delta\rho)} \left(\frac{1-\epsilon}{\epsilon}\right)_t^{1/3} (d/D) \right] + 0.36 \qquad (34)$$

The similarity in the effect of distance from the impeller shown in these equations seems reasonable. One would expect that the rate of power dissipation per unit volume would decrease with distance in the same fashion both above and below the impeller.

It is of interest to compare the results of Zwietering (*16*) for two-bladed paddles with the data of the present investigation. The dimensionless grouping used in this paper can be related to that used by Zwietering by

$$s\left(\frac{2.33\, N_p^{1/3} \rho_m^{1/3} \rho_s^{1/6} \nu^{0.1} \delta^{0.034} d^{0.81}}{\rho_l^{0.45} (g\Delta\rho)^{0.05} B^{0.036} D}\right) = \Omega^{1/3} \qquad (35)$$

As those quantities describing slurry properties either do not change greatly or have low exponents, the quantity within the parenthesis varies little over the range of slurry properties investigated by Zwietering. If comparison is based on a 10 wt. % slurry in water with particles having a specific gravity of 2.3 and a diameter of 300 μ,

$$s\left(\frac{0.218\, N_p^{1/3} d^{0.81}}{D}\right) = \Omega^{1/3} \qquad (36)$$

A comparison of the values of $\Omega^{1/3}$ computed from the curves of Zwietering by means of Equation (36) and $\Omega^{1/3}$ computed by Equation (33) shows these to differ by a maximum of 30%. In addition while Zwietering had to use a separate set of curves for both paddle widths investigated, the present concept brings the curves for the two widths into close agreement.

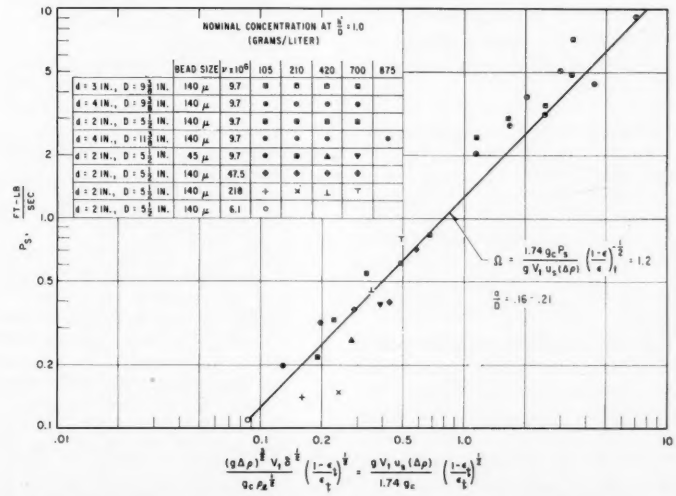
NOMINAL CONCENTRATION AT $\frac{a}{D}$ = 1.0 (GRAMS/LITER)
$\Omega = \frac{1.74\, g_c P_s}{g V_t u_s(\Delta\rho)} \left(\frac{1-\epsilon}{\epsilon}\right)_t^{-\frac{1}{2}} = 1.2$
$\frac{a}{D} = .16 - .21$

Fig. 9. Correlation of suspension power requirements for geometrically similar systems.

SUMMARY

This study has confirmed earlier observations that the production of an essentially homogeneous slurry by rotating mixers involves both the initial suspension of the particles and the expansion of the particle bed to occupy the desired volume. At constant system geometry the initial suspension of the particles was found to be controlled by the dimensionless grouping $(g_c P)\,[(1-\epsilon)/\epsilon]^{-1/2}/[g V_t u_s(\Delta\rho)]$ first published by Kneule (*9*). For mixing

Reynolds numbers above 10^3 Equation (33) can be used to predict suspension-power requirements when six-bladed paddles are used. The general agreement of Equation (33) with the results of Zwietering (*16*) indicates that suspension powers so calculated will also be approximately correct for paddles having fewer than six blades.

It was found that a range of power inputs existed where the slurry was fully suspended but where a definite slurry-fluid interface existed below the liquid level. The minimum power required to disperse a slurry in a given tank is thus determined by the conditions necessary just to maintain the slurry interface at the liquid level. The experimental results are consistent with the theoretical derivation which indicates that the interface level should be a function of the dimensionless group $(g_c P)/(g \rho_m V v_s)$. For a single six-bladed paddle located so that a/D is at least 0.5 and operating at Reynolds numbers above 2.5×10^3, the relationship between interface height and power input is given by Equation (21). The same relationship is applicable to multiple impellers provided the interface height is measured above the top impeller and the power input is divided by the number of impellers. When N_{Re} is below 2.5×10^4, the power required is greater than that computed by Equation (21) and the correction factor of Figure 8 is tentatively recommended.

Further work is needed in several areas. Additional studies with paddle type of impellers are needed to define more thoroughly behavior in the transition and laminar regions. Studies using solid-fluid systems with large density differences should be undertaken to establish definitely the density term appearing in the dimensionless power groups. These investigations should also be extended to other impeller types to determine whether similar relationships apply.

ACKNOWLEDGMENT

The authors appreciate the assistance received from many of the staff of the Westinghouse Atomic Power Department. In particular, the authors wish to acknowledge the contributions of D. H. Fax, who suggested this study, H. C. Chelemer, who assembled the apparatus and obtained part of the thoria data, and A. E. Biancheria, who suggested the theoretical approach used in treating the behavior of the slurry interface.

NOTATION

a = height of lowest impeller above vessel bottom, ft.

A = constant

B = weight ratio of solids to liquid times 100 (referred to tank volume V_t),%

c = solids concentration, g./liter of mixture

d = impeller diameter, ft.

D = vessel diameter, ft.

E_x = vertical component of kinetic energy of single particle, ft.-lb.-force

f = ratio of slurry interface height at given a/d to height at $a/d = \frac{1}{2}$, dimensionless

F = functional relationship

g = local gravitational acceleration, ft./sec.^{2}

g_c = mass acceleration/force conversion factor, (lb.-mass)(ft.)/(lb.-force)(sec.^{2})

h = interface height above midplane of top impeller, ft.

h' = interface height above vessel bottom, ft.

k = friction factor for individual particle, (lb.-force)(sec.)/ft.

K = constant

m = mass of individual particle, lb.-mass

n = number of impellers

N = impeller speed (rev./time)

N_p = power number $= P g_c/\rho_m N^3 d^5$, dimensionless

N_{Re} = mixing Reynolds number $= Nd^2 \rho_l/\mu_l$, dimensionless

N_i = number of particles in given size range

p_{avg} = average power input to individual particle, ft.-lb./sec.

p' = power input to a single particle in the region of the slurry water interface, ft.-lb.-force/sec.

P = total mixing power input, ft. lb.-force/sec.

P_l = power input to liquid, ft. lb.-force/sec.

P_m = mixing power computed from Equation (22), ft. lb.-force/sec.

P_p = power input to solid particles, ft. lb.-force/sec.

P_s = minimum mixing power required to suspend solids, ft. lb.-force/sec.

$s = \dfrac{N d^{0.85}}{\nu^{0.1} \delta^{0.2} (g\Delta\rho/\rho_l)^{0.45} B^{0.13}}$ dimensionless

t = time, sec.

u_s = relative vertical velocity between particle and fluid in turbulent region $= 1.74 \left(\dfrac{g\delta(\Delta\rho)}{\rho_l}\right)^{1/2}$, ft./sec.

v_s = free settling velocity calculated according to Stokes's law, ft./sec.

V = system volume below interface, cu. ft.

V_p = volume of individual particle, cu. ft.

V_t = volume of vessel 1 diam. in height, cu. ft.

X = force acting on particle owing to collisions, lb.-force

x = vertical distance, ft.

Greek Letters

δ = particle diameter, ft.

δ_{avg} = average diameter

ϵ = liquid fraction of system volume below interface, dimensionless

ϵ_t = liquid fraction based on vessel volume V_t, dimensionless

μ = size in μ (on figures)

μ_l = viscosity of suspending liquid, lb.-mass/sec. ft.

ν = kinematic viscosity, sq. ft./sec.

ρ_m = density of slurry mixture below interface, lb.-mass/cu. ft.

ρ_{mt} = density of slurry based on tank volume V_t, lb.-mass/cu. ft.

ρ_l = density of suspending liquid, lb.-mass/cu. ft.

ρ_s = density of solid, lb.-mass/cu. ft.

$\Delta\rho$ = $\rho_s - \rho_l$, lb.-mass cu. ft.

$\Psi = \left(\dfrac{g_c P}{gn \rho_m V v_s}\right)(1-\epsilon)^{-2/3} (d/D)^{1/2}$, dimensionless

$\Omega = \dfrac{1.74 g_c P_s}{g V_t u_s (\Delta\rho)} \left(\dfrac{1-\epsilon_t}{\epsilon_t}\right)^{-1/2}$, dimensionless

LITERATURE CITED

1. Garber, H. J., and G. R. Taylor, *WCAP*-1150, Westinghouse (1959).
2. Hirsekorn, F. S., and S. A. Miller, *Chem. Eng. Progr.*, **49**, 459 (1953).
3. Hixson, A. W., and S. J. Baum, *Ind. Eng. Chem.*, **33**, 478 (1941).
4. *Ibid.*, **34**, 120, 194 (1942).
5. Hixson, A. W., and J. H. Crowell, *ibid.*, **23**, 923, 1160 (1931).
6. Hixson, A. W., and G. A. Wilkens, *ibid.*, **25**, 1196 (1933).
7. Johnson, W. E., D. H. Fax, and S. C. Townsend, *Proc. Am. Power Conf.*, **19**, 640 (1957).
8. Johnson, W. E., and S. C. Townsend, *Nucleonics*, **17**, No. 2, 61 (1959).
9. Kneule, F., *Chem. Ing. Tech.*, **28**, 221 (1956).
10. Langevin, P., *Compt. Rend.*, **146**, 530 (1908).
11. Raghavendra, R. S., and B. K. Mukerji, *Trans. Indian Inst. Chem. Engrs.*, **7**, 63 (1954-55).
12. Rushton, J. H., E. W. Costich, and H. J. Everett, *Chem. Eng. Progr.*, **46**, 395, 467 (1950).
13. Taylor, G. R., and A.E. Biancheria, *WCAP*-1107, Westinghouse (1959).
14. White, A. M., and S. D. Summerford, *Ind. Eng. Chem.*, **25**, 1025 (1933).
15. ———, E. D. Bryant, and B. E. Lukens, *ibid.*, **24**, 1160 (1932).
16. Zwietering, T. N., *Chem. Eng. Sci.* **8**, 244 (1958).

Manuscript received March 31, 1959; revision received November 9, 1959; paper accepted November 11, 1959. Paper presented at A.I.Ch.E. St. Paul meeting.

The Viscosity of Liquid Mixtures

R. A. McALLISTER

Lamar State College of Technology, Beaumont, Texas

The theory of viscosity of liquid mixtures presented here is based on Eyring's theory of absolute reaction rates. The most important conclusions drawn are that for liquids the free energies of activation for viscosity are additive on a number fraction or mole fraction basis and that interactions of like and unlike molecules must be considered. Methanol-toluene, benzene-toluene, and cyclohexane-heptane systems were analyzed with a three-body model and found to fit within the accuracy of the experimental data. Acetone-water mixtures fit a four-body interaction much better. Indications are that to describe acetone-water mixtures well would require consideration of seven- or eight-body interactions.

The viscosity of liquid mixtures has attracted much attention in the literature (*3, 13, 14*), both from the practical standpoint of wanting to be able to predict the viscosity of a mixture from the properties of the pure components and from the theoretical viewpoint of wishing to gain a clearer insight into the behavior of liquid mixtures. It has long been recognized that viscosity-composition curves are not simple functions of composition. Almost never are they linear; they may have a maximum, a minimum, neither, or both.

One of the early equations, and certainly one of the most popular, relating the absolute viscosity of a liquid to temperature (*1, 2, 6*) is

$$\mu = Ae^{B/T} \qquad (1)$$

Eyring (*5*) gave the equation added theoretical significance in the following form:

$$\mu = \frac{\lambda_1 h}{\lambda_2 \lambda_3 \lambda^2} e^{\Delta G^*/RT} \qquad (2)$$

If λ is assumed equal to λ_1, and $\lambda_1\lambda_2\lambda_3$ is identified with the molecular volume, Equation (2) may be written as

$$\mu = \frac{hN}{V} e^{\Delta G^*/RT} \qquad (3)$$

or

$$\nu = \mu/\rho = \frac{hN}{M} e^{\Delta G^*/RT} \qquad (4)$$

Eyring's picture of shear between two layers of liquid involves the successive passage of individual molecules from one equilibrium position to another as indicated in Figure 1. Such a passage requires that either a hole or site be available. The production of such a site requires the expenditure of energy to push back other molecules. The movement of the molecule may be regarded as the passage of the system over a potential-energy barrier, related to ΔG^*.

DERIVATION OF THE CUBIC EQUATION

In a study of the viscosity of a mixture of molecules of types 1 and 2 a number of different encounters must be considered, some of which are shown in Figure 2.

The types of interaction considered in this case are only three bodied and are, in effect, all in one plane. If the two types of molecules are different in size (radius) by more than a factor of 1.5, it will probably become necessary to take into account other interactions involving more than three molecules and especially on a three-dimensional basis (instead of simply in one plane). The ratio of 1.5 to 1 in size is chosen arbitrarily. The three-body model shown in Figure 2 seems to describe the situation well for the methanol-toluene system; the ratio of molar volumes for this system is about 2.6, resulting in a ratio of the radii of approximately 1.39.

The type of interaction shown in Figure 2*a* would correspond to a free energy of activation of ΔG_1^*, that is for pure component 1. The interaction of Figure 2*h* would be characteristic of ΔG_2^*, or pure component 2. Interactions of types *b*, *c*, and *d* all correspond to two molecules of type 1 and one of type 2. One would expect the activation energy for types *c* and *d* to be identical; they will be referred to as ΔG_{112}^*. The free energy of activation for interaction *b* will be referred to as ΔG_{121}^*. Similarly energies of activation for types *f* and *g* would be equal and designated by ΔG_{122}^*, whereas type *e* may be designated by ΔG_{212}^*.

In any binary mixture of mole fraction x_1 the fraction of the times interactions of type *a* (Figure 2) would be x_1^3, as long as the number of molecules of types 1 and 2 was statistically large. Corresponding occurrences of the various types of interactions are listed below:

Type of interaction	1-1-1	1-2-1
Fraction of total occurrences	x_1^3	$x_1^2x_2$

The assumption made here of course is that the probability for the interactions is dependent only on the concentration and not on the free energy of activation. This might well be a point to question. Perhaps the rate of each individual interaction is proportional to the energy of activation in much the same manner as the reaction rate of a chemical reaction. It may be assumed that for the mixture there is a free energy of activation ΔG^* and further that

$$\Delta G^* = x_1^3\,\Delta G_1^* + x_1^2x_2\,\Delta G_{121}^* + 2x_1^2x_2\,\Delta G_{112}^* + x_1x_2^2\,\Delta G_{212}^* + 2x_1x_2^2\,\Delta G_{122}^* + x_2^3\,\Delta G_2^* \qquad (5)$$

Two additional assumptions are made at this point:

$$\Delta G_{121}^* \doteq \Delta G_{112}^* \equiv \Delta G_{12}^*, \text{ and} \qquad (6)$$

$$\Delta G_{212}^* \doteq \Delta G_{122}^* \equiv \Delta G_{21}^* \qquad (7)$$

Incorporating Equations (6) and (7) into Equation (5) results in

$$\Delta G^* = x_1^3\,\Delta G_1^* + 3x_1^2x_2\,\Delta G_{12}^* + 3x_1x_2^2\,\Delta G_{21}^* + x_2^3\,\Delta G_2^* \qquad (8)$$

It was necessary to make assumptions (6) and (7) because with the cubic Equation (5) it is not possible to determine four arbitrary constants. Even though ΔG_{121}^* and ΔG_{112}^* would be expected to be physically different, it is not possible to differentiate between them with viscosity-composition data alone. Equation (5) may be written

$$\Delta G^* = x_1^3\,\Delta G_1^* + x_1^2x_2\,(\Delta G_{121}^* + 2\Delta G_{112}^*) + x_1x_2^2\,(\Delta G_{212}^* + 2\Delta G_{122}^*) + x_2^3\Delta G_2^* \qquad (9)$$

in which case

$$\Delta G_{12}^* = \frac{\Delta G_{121}^* + 2\Delta G_{112}^*}{3} \qquad (10)$$

$$\Delta G_{21}^* = \frac{\Delta G_{212}^* + 2\Delta G_{122}^*}{3} \qquad (11)$$

It must be further emphasized that for certain systems the three-body, essentially planar model indicated here may have to be modified to incorporate three-dimensional, four-body (or more) interactions. The most important result of the theory proposed here is that the free energies of activation for viscosity are the additive quantity. The fact that the three-body model fits so well for several systems, as shown below, lends support to the premise that, at least for certain cases, the one-dimensional approach is sufficient. For the acetone-water system discussed below, a four-body model was used. This approaches the multibody, three-dimensional problem. For this system the four-body model is much more reasonable than the three-body model discussed here.

2-1-1, 1-1-2	2-1-2	2-2-1, 1-2-2	2-2-2
$2x_1^2x_2$	$x_1x_2^2$	$2x_1x_2^2$	x_2^3

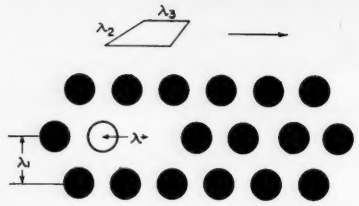

Fig. 1. Distances between molecules in a liquid (5).

The multibody model would necessitate a lengthy, if not unwieldy, equation having many constants; such an equation may be necessary for certain mixtures.

For each type of energy of activation considered here a corresponding kinematic viscosity may be assigned. For the mixture

$$\nu = \frac{hN}{M_{avg}} e^{\Delta G^*/RT} \qquad (12)$$

For pure component 1

$$\nu_1 = \frac{hN}{M_1} e^{\Delta G_1^*/RT} \qquad (13)$$

For interactions of types b, c, and d in Figure 2

$$\nu_{12} = \frac{hN}{M_{12}} e^{\Delta G_{12}^*/RT} \qquad (14)$$

For interactions of types e, f, and g in Figure 2

$$\nu_{21} = \frac{hN}{M_{21}} e^{\Delta G_{21}^*/RT} \qquad (15)$$

and for pure component 2

$$\nu_2 = \frac{hN}{M_2} e^{\Delta G_2^*/RT} \qquad (16)$$

Substituting Equation (8) into (12) results in the following expression for the kinematic viscosity of the mixture:

$$\nu = \frac{hN}{M_{avg}} e^{[x_1^3\Delta G_1^* + 3x_1^2x_2\Delta G_{12}^* + 3x_1x_2^2\Delta G_{21}^* + x_2^3\Delta G_2^*]/RT} \qquad (17)$$

Taking logarithms of Equations (13) through (17), combining to eliminate the free energies of activation, and rearranging yields

$$\ln\nu = x_1^3\ln\nu_1 + 3x_1^2x_2\ln\nu_{12} + 3x_1x_2^2 \ln\nu_{21} + x_2^3\ln\nu_2 + \ln\frac{hN}{M_{avg}} - x_1^3\ln\frac{hN}{M_1} - 3x_1^2x_2\ln\frac{hN}{M_{12}} - 3x_1x_2^2\ln\frac{hN}{M_{21}} - x_2^3\ln\frac{hN}{M_2} \qquad (18)$$

When one recalls that $x_1^3 + 3x_1^2x_2 + 3x_1x_2^2 + x_2^3 = (x_1 + x_2)^3 = 1.0$, Equation (18) may be written

$$\ln\nu = \theta(x) - \ln M_{avg} + x_1^3\ln M_1 + 3x_1^2x_2\ln M_{12} + 3x_1x_2^2\ln M_{21} + x_2^3\ln M_2 \qquad (19)$$

The various molecular weights may be assumed to be as follows:

$$M_{avg} = x_1M_1 + x_2M_2$$

$M_{12} = (2M_1 + M_2)/3$ since these interactions involve two molecules of type 1 and one molecule of type 2.

$M_{21} = (M_1 + 2M_2)/3$ since the three-body interactions involve two molecules of type 2 and one of type 1.

Substituting these quantities into Equation (19) and condensing the equation results in

$$\ln\nu = x_1^3\ln\nu_1 + 3x_1^2x_2\ln\nu_{12} + 3x_1x_2^2\ln\nu_{21} + x_2^3\ln\nu_2 - \ln[x_1 + x_2M_2/M_1] + 3x_1^2x_2\ln[(2 + M_2/M_1)/3] + 3x_1x_2^2\ln[(1 + 2M_2/M_1)/3] + x_2^3\ln[M_2/M_1] \qquad (20)$$

It is noted that the entire equation involves only two undetermined constants, ν_{12} and ν_{21}. Other features of the equation include the possibility of having a maximum, a minimum, neither, or both for ν as a function of x.

If $M_2/M_1 = 1.0$, the last four terms of the equation vanish. Every term of the equation contains the logarithm to the base e, and hence each term may be replaced by the logarithm to the base 10, with which it is often more convenient to work.

Further development of the equations may be made by using

$$\Delta G^* = \Delta H^* - T\Delta S^* \qquad (21)$$

at a given temperature. Substitution of Equation (21) into Equation (12) results in

$$\nu = \frac{hN}{M_{avg}} e^{-\Delta S^*/R} e^{\Delta H^*/RT} \qquad (22)$$

Furthermore

$$\nu_1 = \frac{hN}{M_1} e^{-\Delta S_1^*/R} e^{\Delta H_1^*/RT} \qquad (23)$$

$$\nu_{12} = \frac{hN}{M_{12}} e^{-\Delta S_{12}^*/R} e^{\Delta H_{12}^*/RT} \qquad (24)$$

$$\nu_{21} = \frac{hN}{M_{21}} e^{-\Delta S_{21}^*/R} e^{\Delta H_{21}^*/RT} \qquad (25)$$

and

$$\nu_2 = \frac{hN}{M_2} e^{-\Delta S_2^*/R} e^{\Delta H_2^*/RT} \qquad (26)$$

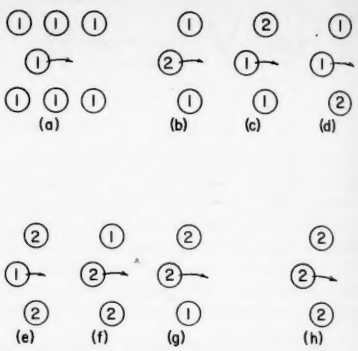

Fig. 2. Types of viscosity interactions in a binary mixture, three-body model.

Substitution of Equations (23) through (26) into Equation (20) results in an equation relating the viscosity of a liquid mixture to both composition and temperature. In such an equation the only constants not known *a priori* or not involving the pure components are ΔS_{12}^*, ΔS_{21}^*, ΔH_{12}^*, and ΔH_{21}^*. If these constants are assumed independent of temperature, a method is provided for extrapolating viscosity-composition data at two temperatures to other temperatures.

Forerunners to Equation (20) are those by Kendall (*11*); Glasstone, Laidler, and Eyring (*5*); Hirschfelder, Curtiss, and Bird (*8*); and Frenkel (*3, 4*). The latter was one of the first to consider interactions of molecules of 1 with 2. Frenkel's equation is

$$\ln\mu = x_1^3\ln\mu_1 + 2x_1x_2\ln\mu_{12} + x_2^3\ln\mu_2 \qquad (27)$$

Kendall's equation is

$$\ln(1/\mu) = x_1\ln(1/\mu_1) + x_2\ln(1/\mu_2) \qquad (28)$$

or

$$\ln\mu = x_1\ln\mu_1 + x_2\ln\mu_2 \qquad (29)$$

The similarity of Equations (27) and (29) to Equation (20) is at once apparent. For Equation (27) or (29) to hold, however, requires that the molal volumes of the mixture, component 1, and component 2 all be equal. This condition seldom obtains. Equation (27) can have a maximum or a minimum, but not both, as required by the experimental data for methanol-toluene mixtures (*7*).

Table 1. Enthalpies and Entropies of Activation for Viscosity for the Methanol-Toluene System

$\Delta H_1^* = 2.27$ kcal./g.mole	$\Delta S_1^* = -0.000369$ kcal./g.mole °K.
$\Delta H_{12}^* = 2.64$ kcal./g.mole	$\Delta S_{12}^* = -0.000511$ kcal./g.mole °K.
$\Delta H_{21}^* = 2.04$ kcal./g.mole	$\Delta S_{21}^* = -0.00246$ kcal./g.mole °K.
$\Delta H_2^* = 1.88$ kcal./g.mole	$\Delta S_2^* = -0.00364$ kcal./g.mole °K.

These constants were determined for the temperature range from 20° to 60°C.

TABLE 2. KINEMATIC VISCOSITIES FOR THE METHANOL-TOLUENE SYSTEM

	20.00°C.	25.00°C.	37.80°C.	50.05°C.	60.11°C.
ν_1, cs.	0.7373	0.6914	0.5908	0.5138	0.4590
ν_{12}, cs.	0.9093	0.8609	0.7080	0.6004	0.5359
ν_{21}, cs.	0.6420	0.5850	0.5195	0.4595	0.4159
ν_2, cs.	0.6786	0.6414	0.5621	0.5009	0.4592

DERIVATION OF THE QUARTIC EQUATION

When one considers the movement of a molecule in a mixture from one equilibrium position to another, the three-body interactions considered above may not always be realistic. This would be especially true where the size of one component molecule is much greater than the size of the other component molecule.

The four-body model approaches more nearly a three-dimensional treatment. The interactions to be considered are shown in Figure 3. Types a and p are seen to correspond to the pure components 1 and 2 respectively. Types b, c, and d would be expected to be identical, whereas type e should be different from the previous three. Since, however, types b through e all involve three molecules of component 1 and one molecule of component 2, it is not possible to differentiate between the interactions with viscosity data alone. Six interactions are involved with two molecules of each component, interactions f through k; and four interactions are discerned with three molecules of component 2 and one of component 1, types l through o.

As before, the energies of activation for the four-body interactions are added in proportion to the fraction of the total occurrences for each interaction shown in Figure 3:

$$\Delta G^\circ = x_1^4\Delta G_1^\circ + 4x_1^3x_2\Delta G_{1112}^{\circ\prime} + 6x_1^2x_2^2\Delta G_{1122}^{\circ\prime} + 4x_1x_2^3\Delta G_{2221}^{\circ\prime} + x_2^4\Delta G_2^\circ \qquad (30)$$

In this equation $\Delta G_{1112}^{\circ\prime}$ is an equivalent free energy for interactions of types b, c, d, and e and does not differentiate between the first three and the last interaction. Likewise $\Delta G_{1122}^{\circ\prime}$ and $\Delta G_{2221}^{\circ\prime}$ are combinations similar to those made in Equations (10) and (11). $\Delta G_{1122}^{\circ\prime}$ combines the free energies of activation for types f, g, and h with those of i, j, and k. $\Delta G_{2221}^{\circ\prime}$ combines the free energies of activation for type l with those of types m, n, and o.

By techniques entirely analogous to the method given above, the following equation is derived:.

$$\ln\nu_{mix} = x_1^4\ln\nu_1 + 4x_1^3x_2\ln\nu'_{1112} + 6x_1^2x_2^2\ln\nu'_{1122} + 4x_1x_2^3\ln\nu'_{2221} + x_2^4\ln\nu_2 - \ln(x_1 + x_2M_2/M_1) + 4x_1^3x_2\ln[(3 + M_2/M_1)/4] + 6x_1^2x_2^2\ln[(1 + M_2/M_1)/2] + 4x_1x_2^3\ln[(1 + 3M_2/M_1)/4] + x_2^4\ln(M_2/M_1) \qquad (31)$$

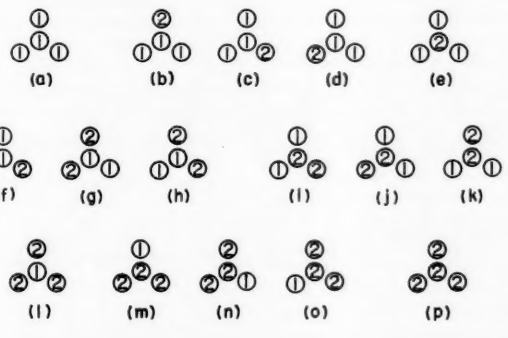

The molecule in the center of each group is considered to be moving perpendicular to the page between the other three molecules

Fig. 3. Types of viscosity interactions in a binary mixture, four-body model.

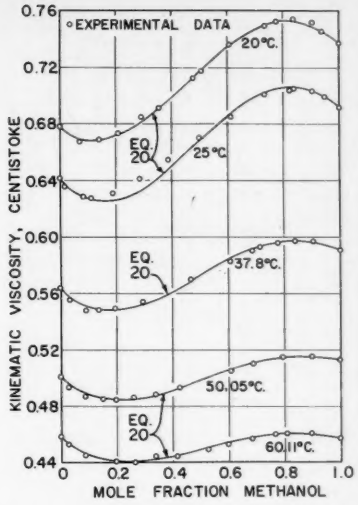

Fig. 4. Viscosity of liquid methanol-toluene mixtures.

RESULTS

Methanol-Toluene System

Equation (20) was tested first with the experimentally obtained data for the viscosity of mixtures of methanol-toluene solutions (7). The data for each temperature were used in Equation (20), and the constants ν_{12} and ν_{21} were determined by the method of least squares. Then, with these constants, $\ln\nu$ was calculated at each composition given. Noting that

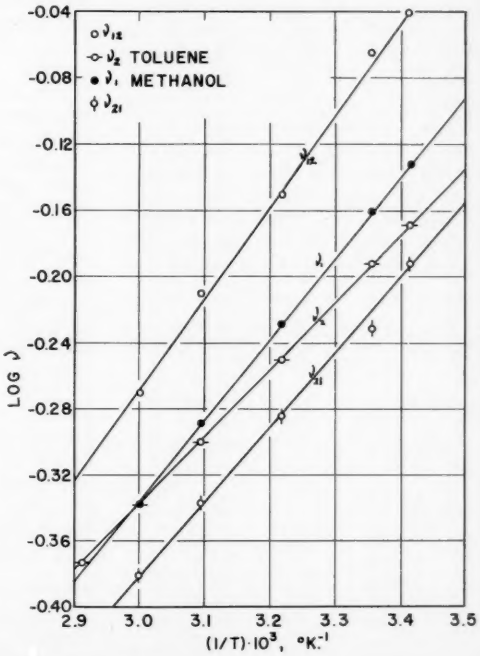

Fig. 5. Kinematic viscosity as a function of temperature.

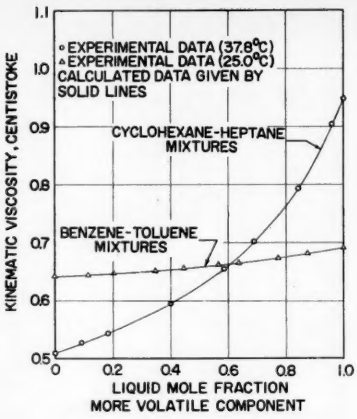

Fig. 6. Kinematic viscosities of mixtures as a function of composition.

$$\ln\nu_{calc.} - \ln\nu_{expt'l.} = \Delta\ln\nu$$

$$\doteq \frac{\Delta\nu}{\nu} = \frac{\nu_{calc} - \nu_{expt'l}}{\nu}$$

one can compare calculated and experimental viscosity determinations by calculating a percentage difference as 100 times $\Delta\ln\nu$. The average percentage difference at each temperature was calculated by averaging the absolute value of the difference at each composition without regard to sign. Except for three data points at 25°C. and one at 37.8°C., all the calculated viscosity values agree with the experimental data with a maximum difference of ± 0.5%. The average difference, again excepting the three points at 25°C., is about ± 0.2%, which is the same magnitude as the reported accuracy of the data (7). It may therefore be concluded that for the methanol-toluene system Equation (20) correlates the data with a high degree of precision. Figure 4 shows the viscosity-composition curves for the methanol-toluene system. The solid lines in Figure 4 were calculated from Equation (20) by the use of the ν_{12} and ν_{21} determined by the method of least squares. The circles represent the experimental data.

Table 3. Kinematic Viscosities of Benzene-Toluene Mixtures at 25.00°C.

Mole fraction benzene x_1	Kinematic viscosity, centistoke ν
0.0000	0.6414
0.1159	0.6439
0.2032	0.6468
0.3445	0.6509
0.4476	0.6546
0.5677	0.6608
0.6394	0.6645
0.7741	0.6730
0.8772	0.6807
1.0000	0.6915

Differentiation of Equation (22) results in

$$\frac{d\ln\nu}{d(1/T)} = \Delta H^*/R + (1/RT)\frac{d\Delta H^*}{d(1/T)} - \frac{1}{R}\frac{d\Delta S^*}{d(1/T)} \quad (32)$$

If the last two terms are negligible,

$$\frac{d\ln\nu}{d(1/T)} = \Delta H^*/R \quad (32a)$$

If both ΔH^* and ΔS^* are independent of temperature, $\ln\nu$ is a linear function of $1/T$. Figure 5 shows $\log\nu_1$, $\log\nu_2$, $\log\nu_{12}$, and $\log\nu_{21}$ as functions of $1/T$. The fact that the lines are straight over the 40-odd degrees centigrade indicates that the enthalpies and entropies of activation for viscosity are independent of temperature over this range for the methanol-toluene system.

For those systems for which $\ln\nu$ is not a linear function of the reciprocal temperature, Equation (32) must be used or else the liquid does not fit Eyring's basic model as exemplified by Equation (4). For those systems for which $\ln\nu$ is a linear function of the reciprocal temperature, Equation (32*a*) may be used to interpolate accurately the viscosity as a function of temperature. Table 1 presents the enthalpies and entropies of activation for viscosity for the methanol-toluene system calculated by the use of Equations (22) and (32*a*). Table 2 gives all the kinematic viscosities at the five temperatures listed.

Benzene-Toluene System

Precise experimental data for the kinematic viscosity of benzene-toluene mixtures at 25.00°C. are given in Table 3. The precision with which Equation (20) fits the data with a maximum difference of 0.06% and an average difference of 0.02% is certainly within the accuracy of the data. For the system at 25.00°C. ν_{12} and ν_{21} are 0.6616 and 0.6493 centistoke respectively. Figure 6 shows a line calculated from Equation (20) and gives the experimental data points (9).

Cyclohexane-Heptane System

Kinematic viscosity data are given in Table 4 for the cyclohexane-heptane system at 37.8°C. The average percentage difference is ± 0.2%, and the maximum difference is 0.5%, which is the same magnitude as the experimental accuracy of the data. For this system at 37.8°C. ν_{12} and ν_{21} are 0.6272 and 0.5782 centistoke respectively.

Acetone-Water System

One of the most nonideal systems insofar as viscosity-composition data are concerned is acetone-water. Figure 7 shows the acetone-water viscosity ex-

Table 4. Kinematic Viscosities of Cyclohexane-Heptane Mixtures at 37.8°C. (9)

Mole fraction cyclohexane x_1	Kinematic viscosity, centistoke ν
0.000	0.510
0.092	0.527
0.184	0.544
0.402	0.595
0.585	0.655
0.690	0.702
0.841	0.792
0.960	0.904
1.000	0.947

perimental data (*10*), the data calculated according to the cubic Equation (20), and the data according to the quartic Equation (31). In each case the unknown constants were determined by the method of least squares. Equation (20) fits the data with an average deviation of 6.4%; the maximum deviation is 15.8%. Equation (31), however, has an average deviation of only 2.1% and a maximum deviation of 4.8%. It is important to notice that it is in the low acetone concentrations that both Equations (20) and (31) fit the poorest.

DISCUSSION

The accuracy with which Equation (20) fits the data for the first three systems presented is encouraging. For these three systems, at least, the model proposed seems adequate. More important, however, is the indication that it is the free energy of activation that is the additive quantity in the viscosity of mixtures. Equation (31) was not used for the data of the methanol-toluene, benzene-toluene, or cyclohexane-heptane systems. Mathematically this equation must fit the data at least

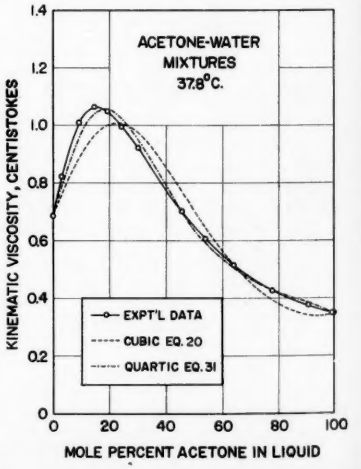

Fig. 7. Comparison of acetone-water mixtures with two theoretical models.

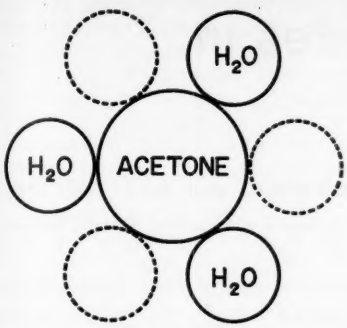

Fig. 8. Interaction of an acetone molecule with water molecules.

as well and probably better than Equation (20). Since Equation (20) already fits within the accuracy of the experimental data, nothing could be gained by applying the quartic equation.

For those systems which do not fit Equation (20) well, as for example the acetone-water systems discussed here, a more general equation is necessary. Equation (20) is concerned only with the interactions of three molecules at a time. This is rather like a flatland description of a three-dimensional occurrence. The four-body interactions are a more accurate representation of the physical facts for mixtures whose component molecules are approximately the same size. The four-body model also enjoys the three-dimensional representation of the problem. Figure 8, however, shows that even a four-body model is unrealistic for molecules differing in size as much as acetone and water. In Figure 8 the size ratio is 1.61, which is the cube root of the ratio of the molar volumes of acetone and water. The three water molecules circled with solid lines in this figure can hardly be descriptive of the interactions involved in the movement of an acetone molecule when three additional water molecules, shown as dashed circles, do not fill all the available space around the periphery of the acetone molecule. Again the illustration shows a two-dimensional representation. On a three-dimensional basis perhaps a dozen or more molecules are affected by the movement of a single acetone molecule.

Table 5. Size Ratios of Systems Studied

System	Volumetric size ratio (molal)	Volumetric size ratio
Methanol-toluene	1/2.62	1/1.38
Benzene-toluene	1/1.20	1/1.06
Cyclohexane-heptane	1/1.21	1/1.07
Acetone-water	4.16/1	1.61/1

Where such interactions are an important fraction of the total occurrences, as in the low acetone concentrations, one would expect that at least a seventh- or eighth-order equation would be necessary to describe viscosity-concentration data accurately.

For the acetone-water system it is also interesting to note that the quartic equation fits the data above 50 mole % fairly well. This might indicate that a fifth-order equation is satisfactory in this region, but an eighth-order equation might be required for the low acetone concentrations.

Not enough systems have been investigated here to indicate when it is permissible to use the cubic equation and when a more complicated equation is called for. As a rough guide, however, if the component molecules in a mixture are close to the same size, a cubic or quartic equation should adequately describe the mixtures. If the size ratio of the molecules is more than 1.5, one may expect to employ a higher order equation to describe the mixtures accurately. Table 5 gives the size ratios for the systems treated here.

The use of the kinematic viscosity in most of the equations presented here instead of the absolute viscosity has the obvious advantage of avoiding equations containing volume fractions, or volume changes on mixing, quantities which are not always known.

While it is true that many liquids do not follow Equation (3) or (4) well over the entire range of temperature possible for the liquid, there is usually some temperature range for which viscosities may be described by the methods presented here.

Many attempts have been made to relate ΔG^* to chemical structure (*12, 14*) for pure liquids. These attempts have been either unsuccessful or at best not entirely satisfactory. Prediction of ΔG_{12}^* and ΔG_{21}^* (or the corresponding ΔH^*'s and ΔS^*'s) is not possible at this time.

It is granted that the approach presented here is highly oversimplified, but the accuracy obtained for even the three systems discussed here is sufficiently good to make further examination and development of the theory worthwhile.

ACKNOWLEDGMENT

The author wishes to acknowledge the diligent assistance of Dale H. Aulbaugh in the preliminary calculations and of Neil A. Dougharty in many of the later calculations.

NOTATION

A, B = empirical constants
ΔG^* = molal free energy of activation for viscosity, cal./g.mole
R = gas constant, 1.987 cal./(g. mole)(°K.)
T = absolute temperature
N = Avogadro number, 6.023×10^{23} molecules/g.mole
h = Planck constant, 6.6240×10^{-27} erg.-sec./molecule
M = molecular weight, g./g.mole
e = base of natural logarithms, 2.71828 . . .
V = molal volume, cc./g.mole
x_i = mole fraction of component i in the liquid

Greek Letters

μ = absolute viscosity, poise or centipoise
ν = kinematic viscosity, stoke or centistoke. All numerical values given in this paper are in centistoke.
ρ = liquid density, g. mass/cc.
λ = average intermolecular distances between adjacent liquid molecules (Figure 1)

$$\theta(x) = x_1^3 \ln\nu_1 + 3x_1^2 x_2 \ln\nu_{12} + 3x_1 x_2^2 \ln\nu_{21} + x_2^3 \ln\nu_2$$

$$\Psi(x) = -\ln [x_1 + x_2 M_2/M_1] + 3x_1^2 x_2 \ln [(2 + M_2/M_1)/3] + 3x_1 x_2^2 \ln [(1 + 2M_2/M_1)/3] + x_2^3 \ln M_2/M_1$$

LITERATURE CITED

1. Andrade, E. N. da C., *Phil. Mag.*, **17**, 497, 698 (1934).
2. Arrhenius, S., *Medd. Vetenskapsakad. Nobelinst.*, **2**, 25 (1913).
3. Frenkel, Y. I., "Kinetic Theory of Liquids," Oxford Univ. Press, London (1946).
4. ———, *Petroleum (London)*, **9**, No. 2, 27 (1946).
5. Glasstone, Samuel, K. J. Laidler, and Henry Eyring, "The Theory of Rate Processes," McGraw-Hill, New York (1941).
6. Guzman, J. de, *Anales soc. espan. fis. quim.*, **11**, 353 (1913).
7. Hammond, L. W., Katherine S. Howard, and R. A. McAllister, *J. Phys. Chem.*, **62**, 637 (1958).
8. Hirschfelder, J. O., C. F. Curtiss, and R. Byron Bird, "Molecular Theory of Gases and Liquids," Wiley, New York (1954).
9. Howard, Katherine S., and F. P. Pike, Private communication.
10. Howard, Katherine S., and R. A. McAllister, *A.I.Ch.E. Journal*, **4**, 362 (1958).
11. Kendall, J., *Medd. Ventenskapsakad. Nobelinst.*, **2**, 25, 1 (1933).
12. Moore, R. J., P. Gibbs, and Henry Eyring, *J. Phys. Chem.*, **57**, 172 (1953).
13. Partington, J. R., "An Advanced Treatise on Physical Chemistry: Vol. II, The Properties of Liquids," Longmans, Green, London (1951).
14. Reid, R. C., and T. K. Sherwood, "The Properties of Gases and Liquids," McGraw-Hill, New York (1958).

Manuscript received May 11, 1959; revision received December 3, 1959; paper accepted December 3, 1959. Paper presented at A.I.Ch.E. St. Paul meeting.

Flow Patterns and Mixing Rates in Agitated Vessels

K. W. NORWOOD and A. B. METZNER

University of Delaware, Newark, Delaware

Mixing rates in agitated vessels are predicted through measurement of the flow patterns which determine them. These measurements suggest the use of a model that assumes that nearly all the mixing occurs in a small "perfectly mixed" region near the impeller, with flow throughout the remainder of the tank serving primarily to bring the fluid into this region of the impeller.

On the basis of this model, equations were developed for relating volumetric flow rates, hence the mixing rates, to the operating variables. While the theory could be checked directly only to Reynolds numbers of slightly over 600 (owing to limitations of the experimental technique employed in this part of the mixing-rate studies), the volumetric flow rates could be measured from Reynolds numbers of 36 to 1.7 $\times$ 10^4. The times required for completion of an acid-base neutralization (terminal mixing) were also measured from Reynolds numbers of 1.6 to 1.8 $\times$ 10^5.

Flat-blade, dimensionally similar turbines with diameters of 2, 4, and 6 in. were used. Tank diameters ranged from 5.76 to 15.5 in. The baffle width equaled one tenth of the tank diameter in all runs. All the data were for Newtonian fluid systems, but the extension of this work to non-Newtonian materials is discussed briefly.

The literature in the field of agitation and mixing of fluids may be subdivided into two general categories: quantitative studies of power consumption and papers dealing with observations of the rates and quality of mixing. The former area has been investigated for a number of years, with both Newtonian and non-Newtonian fluids; however little has been done in regard to quantitative determinations of mixing rates or to an understanding of flow patterns and the factors controlling them. In fact, only two studies (*2, 12*) appear to be available in which any attempt was made to define the factors controlling mixing rates. In addition, several papers (*5, 6, 7, 10, 11*) report measurements of fluid velocities near the region of the impeller or in the vessel.

In view of these facts, the purposes of the present investigation were, 1) to study the flow patterns in agitated vessels and to determine how these factors influence mixing rates, and 2) to use the above to develop design equations for predicting mixing rates in Newtonian fluids and to consider the extension of these results to non-Newtonian systems.

The first of these purposes required the development of a suitable instrument for measuring point velocities under turbulent conditions in viscous liquids.

THEORY

Probably all the operations carried out in vessels equipped with an agitator depend primarily on high rates of fluid shear, high fluid-recirculation rates, or some combination of these variables. Emulsification processes, for example, require primarily a high intensity of the shearing action to reduce droplet size, and high rates of heat transfer depend upon large flow rates of the fluid past the heated surfaces. Chemical reactions require both large flow rates to distribute reactant streams throughout the vessel and a high intensity of turbulence (at least at one place within the vessel) to aid the mixing of the reactant streams to the desired degree of completeness on a molecular level.

Metzner and Taylor (*5*) have shown that the shear rates and local rates of power dissipation in a fluid agitated inside a cylindrical vessel with flat-bladed turbines are initially very high at the impeller but decrease by several orders of magnitude within about 1 in. from the tip of a 4-in. turbine impeller. Obviously most of the power is dissipated in the immediate region of the impeller. The fluid in this region has a more thoroughly mixed condition than anywhere else in the tank, regardless of the measure or standard of quality of mixing. Under these conditions the mixing process may be described by a gross model which assumes a "perfectly mixed"[•] volume in the region of the impeller with little mixing in the rest of the tank. For clarity of expression, the equations for this model will be formulated for a specific mixing operation, the batchwise mixing of the reacting components of an infinitely fast chemical reaction. The latter restriction is introduced to eliminate any dependence on chemical kinetics (the sole controlling factor will be the rate of mixing of reactants) and should be a good assumption for most ionic reactions. The resulting equations may also be used as an approximation to the residence times required in continuous stirred-tank reactors, but these introduce the additional complication that some reactants may short-circuit to the draw-off point, especially if it is poorly located, and additional information as to the distribution of residence times would then be required.

The neutralization of a given number of equivalents of base (M_o) initially evenly distributed throughout a tank of volume V_T by the stoichiometric amount of acid introduced near the impeller[•] at time zero will be considered. The following additional assumptions are utilized:

1. Nearly all the mixing takes place in a small perfectly mixed volume of fluid near the impeller.

2. Any unreacted acid which is pumped out of this volume reacts in the other parts of the tank in localized pockets of turbulence before being recirculated to the impeller. While the intensity of such turbulence away from the impeller is low, that it is not zero at Reynolds numbers above 10 has been shown both by photographic data (*5*) and by visual observations in the present study. In particular the regions behind the baffles, above and below the impeller (near the vertical axis of the tank), and near the tank wall at the level of the impeller show appreciable turbulence at transitional and turbulent Reynolds numbers.

3. Any base which enters V is neutralized substantially instantaneously.

4. All the fluid in the tank is in recirculating motion.

Under these conditions a material balance for the unreacted acid, written over the volume, simplifies to

$$-QC_t - QC_T = V\,dC_t/dt \qquad (1)$$

The two limiting relationships between time and C_T are as follows. If the outflow from V short-circuited completely, then shortly after time zero

K. W. Norwood is with General Electric Company, Richland, Washington.

[•] Perfectly blended, but not necessarily homogeneous on a molecular scale.

[•] In continuous processes all reactants would normally be introduced into this perfectly mixed region.

C_T would equal zero and neutralization of the base would occur only by diffusion. On the other hand, if the outflow from V did not recirculate to V until all the fluid in the tank had passed through it once, then C_T could be taken as equal to M_o/V_T. In reality the value of C_T always lies somewhere between these limits, and because base is consumed in the reaction, C_T is probably a decreasing function of time. Additionally C_t and C_T have the following similar characteristics:

$$C_T(0) = M_o/V_T \qquad (2a)$$

$$C_t(0) = (M_o/V)(1 - V/V_T) \qquad (2b)$$

$$C_T(t_F) = 0 = C_t(t_F) \qquad (2c)$$

These considerations suggest that a good approximation for C_T as a function of time would appear to be

$$C_T = (V/V_T)C_t \qquad (2d)$$

which is equivalent to assuming that the concentration of base in the inflow stream to the impeller is equal to the average base concentration in the tank.

Substituting Equation (2d) in Equation (1) and integrating, one obtains

$$C_t/C_t(0)2= e^{-(Q/V)(1+V/V_T)t} \qquad (3)$$

or

$$M(t)/M_o = (1 - V/V_T)\, e^{-(Q/V)(1+V/V_T)t} \qquad (4)$$

If one ignores the short time lag between the pumping of a slug of acid out of the volume and its neutralization in the tank, $M(t)/M_o$ is equal to the fraction of the original acid or base still unreacted at t; therefore

$$\frac{1 - F(t)}{1 - V/V_T} = e^{-Q/V(1+V/V_T)t} \qquad (5)$$

The following approximate conclusions concerning the volume may be drawn from photographic data (5):

1. V is approximately independent of impeller speed.

2. $0 < V \leq 0.15$ cu. ft. for the impeller diameter range from 2 to 6 in.

The volumetric flow rate is not only of importance in Equation (5) and the problem considered here but also in almost all other mixing-rate processes. The following expression for the theoretical pumping capacity of a flat-blade turbine impeller has been derived by van de Vusse (12):

$$Q_{th} = \pi^2 ND^2w\,(1 - q^2)^{1/2} \qquad (6)$$

This derivation, based on the analogy between a turbine mixer and a centrifugal pump, assumed that loss of energy due to drag on the impeller is negligible. Entrainment of fluid by the jet stream from the impeller was also neglected. It appears reasonable to rewrite Equation (6) as

$$Q = c_1 \pi^2 ND^2w(1 - q^2)^{1/2}f(\mu) \qquad (7)$$

Fragmentary data (10) indicate, that c_1 is independent of impeller speed and is equal to 1.96 for the agitation of water by a 4-in. turbine impeller operating in the impeller speed range of 100 to 200 rev./min. in a baffled tank.

Equation (7) is a somewhat discouraging result. The factor c_1, and possibly $f(\mu)$, appear to be important enough to require careful determination. At present this must be carried out experimentally. Similar conclusions may be reached from the more recent and extensive analysis of Nielsen (7). Thus for the present the work required to obtain Q [hence the mixing rates obtained by use of Equation (5)] appears to be nearly as extensive as a direct (empirical) determination and correlation of mixing rates. This is not to say that the previous theoretical considerations are of no value, but they do not afford any very immediate prediction of mixing rates.

An empirical analysis of the terminal mixing time yields by means of dimensional considerations

$$f(ND^2\rho/\mu,\ T/D,\ y/D,\ g/N^2D,\ Nt_F = 0 \qquad (8)$$

The Froude number g/N^2D accounts for the gravitational effects on the fluid motion. In view of the fact that several investigators have shown that the Froude number is not of significance in determining power requirements in baffled tanks, one might conclude superficially that the Froude number should not affect mixing times under similar conditions. However the effect of gravity on the flow pattern, hence on mixing rates, can be shown most easily by considering the limiting case of zero gravitational force. Under these conditions the liquid would be thrown out to the sides of the vessel by the impeller and would tend to remain there, yielding no recirculation and therefore little or no mixing. Thus if the force of gravity could be changed in the laboratory, the flow pattern and therefore the mixing time would be affected unless the vessel were filled to a rigid surface.

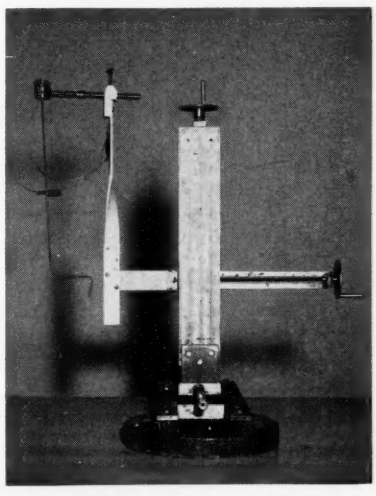

Fig. 1. Thermistor probe and probe positioner.

DESCRIPTION OF EQUIPMENT

The data were taken in baffled ($J/T = 0.1$), cylindrical, flat-bottomed, Pyrex-glass mixing vessels. The fluids were agitated with centrally positioned turbine impellers having six flat blades ($w = D/5$). Each of the various-sized impellers was mounted 35.4% of the distance from the tank bottom to the liquid surface. The impellers were geometrically similar in all dimensions. The size ranges of impeller diameter and vessel diameter which were used in the study are given in Table 1.

The probe used to measure flow rates and the probe positioner are shown in Figure 1. The probe was formed by joining a long piece of L-shaped hypodermic tubing to a short L-shaped piece by a collar-and-spring device in such a way that the short L could be rotated independently of the large L. A thermistor bead was mounted at the tip of the short L, and the leads were threaded through the tubing. The probe positioner consisted of three lathe beds arranged so that the probe might be moved independently in each of three directions, and the sides of the beds were marked at intervals to permit determination of the exact position of the probe in the tank.

The velocity-measuring probe was used as the fourth side of a Wheatstone's bridge; two 500-ohm resistors and a decade resistor comprised the other three sides. The bridge was powered by a power supply and a power amplifier; input and output voltages were measured with suitable voltmeters. The resistance of the probe was allowed to vary with flow rate, and the input to and the output from the bridge were kept constant by varying the decade box resistance. This method of operation gave a calibration curve of velocity as a function of the decade box reading and the viscosity and density of the fluid.

The test liquids, mixtures of corn syrup and water, were all single phase Newtonian liquids. Their viscosities were measured with a capillary-tube viscometer.

OPERATING PROCEDURE

Mixing times were measured by means of a slightly modified version of the method of Fox and Gex (2). The time necessary to neutralize a known amount of acid dispersed in a tank of fluid with an exact equivalent amount of base is defined as the terminal mixing time (2). Fractional mixing times were similarly measured by noting the time for some known fraction of the stoichiometric amount of acid to be neutralized. Methyl-

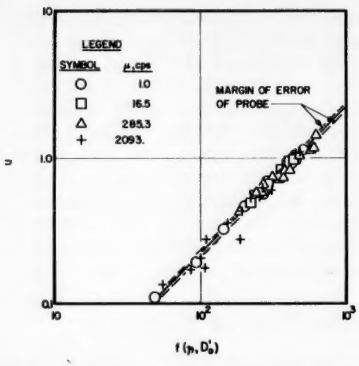

Fig. 2. Calibration of Probe, with photographic data used as the primary standard.

red indicator was used to determine the end points. At the initial neutral point the liquid had a pH such that the indicator was just on the yellow side of the red-yellow color change (pH = 6.3). Since methods of measurement involve a chemical reaction between ions, a degree of mixing close to absolutely complete mixing (homogeneity even to the molecular level) must be achieved before all the red color can be eliminated, when it is assumed that the visual observation is sufficiently acute to detect any unmixed volumes.

The thermistor probe was calibrated by means of velocity data obtained by several investigators (*5, 10, 11*) in photographic studies of the flow patterns in the region of a turbine impeller. These data were taken with mixing equipment identical to that which was used in a part of this work. The data were obtained by the use of corn-syrup–water mixtures of four viscosities: 1.0 centipoises (*10*), 16.5 and 285.3 centipoises (*11*), and 2,093 centipoises (*5*). The final calibration curve, Figure 2, shows that most of the data are within the margin of error of the probe, as determined by the sensitivity of the vacuum-tube voltmeter to decade resistance changes. The detailed function $F(\eta, D'_o)$ is not given, as it is undoubtedly restricted to the particular probe used. Figure 2 is given primarily to show that point velocities could be determined with a mean accuracy of ±5% over the entire range studied. A detailed description of the probe and its directionality and operation is available (*8*).

Total flow rates were obtained by integrating the measured velocities over the entire moving stream of fluid, from the center of the vertical vortex above the impeller to the center of the vortex below. These vortices are very well defined under conditions of good mixing (*5, 10*) and delineate completely and accurately the area over which such an integration should be carried out.

Table 1. Ranges of Variables Studied

Variable	Range	
	Mixing-time data	Velocity data
Impeller diameter	2 to 6 in.	2 to 6 in.
Tank diameter	5.72 to 15.5 in.	11.3 in.
T/D ratio	1.35 to 5.66	1.89 to 5.66
Fluid depth	6 to 12 in.	11.3 in.
y/D ratio	1.5 to 6.0	2.8
Impeller speed	40 to 4,820 rev./min.	75 to 2,300 rev./min.
Reynolds number	1.6 to 1.83 × 10^5	35.7 to 1.72 × 10^4
Viscosity	0.3624 to 7,780 centipoises	1.0 to 1,783 centipoises

All data were obtained with $J = 0.1T$.

Density terms have been included in Figures 3 and 5 since they generally accompanied changes in viscosity; however the changes in fluid density were too small to enable a highly accurate determination of the true effect of density changes alone.

RESULTS AND DISCUSSION

The study of mixing rates and flow patterns covered the major areas of industrial importance with regard to Reynolds number and geometric ratios; however the scale of equipment was smaller than would be found in industry. The 498 mixing-time measurements and twenty-five velocity traverses were taken over the ranges of variables given in Table 1.

Volumetric Flow Rate

The volumetric flow-rate data (Figure 3) were correlated by

$$Q = 9.0 \times 10^{-4}\, ND^3 w (D^{0.4}\rho/\mu)^{0.5} (1-q^2)^{0.5} \qquad (9)$$

over the entire Reynolds number range studied. The maximum deviation from the best line through the data is 33%; the average deviation of the twenty-five points is 9.7%.

Calculation of the volumetric output of an impeller for design purposes, with either Figure 3 or Equation (9) used, requires some knowledge of the term $(1-q^2)^{1/2}$. In the present work q was measured; it almost always proved to be negligible, as suggested by van de Vusse (*12*) for baffled systems. In one instance omission of this term would have resulted in an error of 7%, but in no other case was the term less than 0.99. Thus the present recommendation is to neglect it completely.

Comparison of Equations (9) and (7) shows that the product $c_1 f(\mu)$, while independent of impeller speed

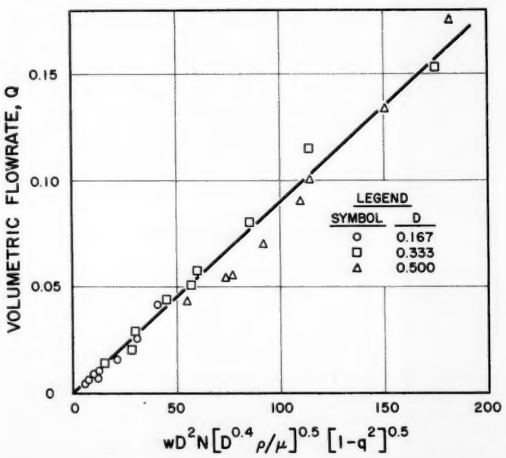

Fig. 3. Correlation of total (volumetric) flow rates.

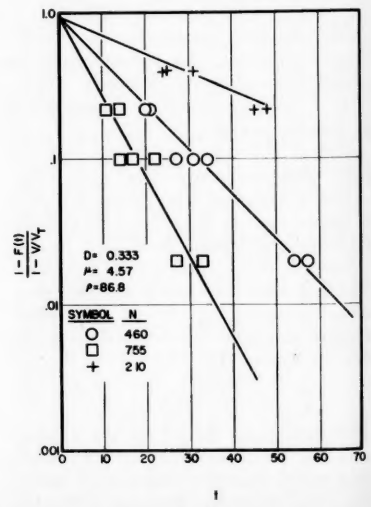

Fig. 4. Proof of model used to correlate times required for fractional completion of the mixing.

TABLE 2. SCALING EQUATIONS—TURBULENT REGION

Reference	Operating conditions	Mixing time equation	Slope of logarithmic plot of N_P vs N_{Re}	Scaling equation for geometric similarity and equal mixing times
1	General	—	—	$P_2 = K^5 P_1$
2	Propeller, unbaffled	$\frac{t_T (ND^2)^{2/3} g^{1/6}}{y^{1/2} T} \alpha \left(\frac{D^2 N \rho}{\mu}\right)^{-1/6}$	−1/6	$P_2 = K^{4.1} P_1$
3	Baffled, propellers	$t_T \alpha N^{-1}$	0	$P_2 = K^5 P_1$
12	Paddles or turbines, unbaffled	$t_T \alpha N^{-1} (N^2 D)^{-0.30 \text{ to } 0.35}$	0 to −0.15	$P_2 = K^{4.11} P_1$ to $K^{4.44} P_1$
12	Propellers, baffled and unbaffled	$t_T \alpha N^{-1.5} D^{-0.25}$	0	$P_2 = K^{4.50} P_1$
Present work	Turbines, baffled	$\frac{t_T (ND^2)^{2/3} g^{1/6}}{y^{1/2} T} = \text{const.}$	0	$P_2 = K^{5.75} P_1$

(as postulated earlier), is incorporated as a dimensional term which differs appreciably from a value of unity. Therefore extrapolation to greatly different values of the relevant variables cannot be recommended. This limitation is unimportant insofar as Reynolds numbers and viscosities are concerned, since wide ranges were covered, but the applicability of Equation (9) to large-scale equipment remains unproved. An article appearing since the present work was completed (*6*), while very carefully carried out, does not alleviate this problem, nor does it propose any general correlation of the recirculation rate Q.

Fractional Mixing Times

The times required to neutralize between 60 and 98% of the base in the tank, by addition of the appropriate percentage of the stoichiometric amount of acid, are shown in Figure 4 for three typical runs. The coordinates and scales are as suggested by Equation (5); the fact that the correlating curves are straight lines shows that Equation (5) is obeyed. Knowledge of the value of Q from the flow-rate measurements enables determination of V from these slopes*. Values of the perfectly mixed volume as obtained from twenty-five sets of runs similar to those shown on Figure 4 are correlated in Figure 5. It is evident that this volume is determined primarily by the impeller size and is only slightly dependent on the fluid properties; an 1,800-fold change in viscosity changes the value of V by only about 40%. No dependence on impeller speed was shown over the entire range studied, 75 to 2,300 rev./min.

Figure 6, with the above correlations for V and Q utilized, summarizes the applicability of Equation (5) to the prediction of the actual fractional mixing times. The maximum deviation from the theoretical line is 26.5%, and the average deviation is 10.3%; the range of Reynolds numbers covered is from 36 to 640. Higher Reynolds numbers could not be studied, because the time for fractional mixing became too short. At low Reynolds numbers not all the fluid in the tank is in motion, the theory becomes inapplicable as mixing rates approach zero, and the process is of no industrial interest. It must also be noted that the theory predicts infinite mixing times for complete or perfect mixing [$F(t) = 1.0$]. While the theory must break down as $F(t)$ approaches unity, since the diffusive processes largely neglected in the present analysis must be responsible for the ultimate completion of mixing, no deviations were noted up to 98.8% of complete mixing, the highest level studied in this phase of the program.

* Since $V/V_T << 1.0$ only a very approximate estimate suffices to define the value of the ordinate for any given measurement; the slope however is sensitive to small percentage variations in V.

Time Required for Terminal Mixing

The relationship between the dimensionless groups in Equation (8), for calculation of the time required for terminal mixing, is shown in Figure 7. The average deviation of all the points from the best curve through the data is 11.4%. The maximum deviation is

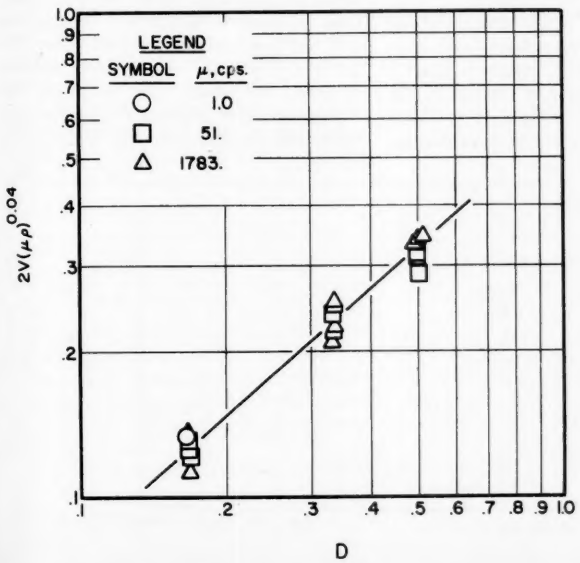

Fig. 5. Dependence of perfectly mixed volume on impeller diameter, fluid density, and viscosity.

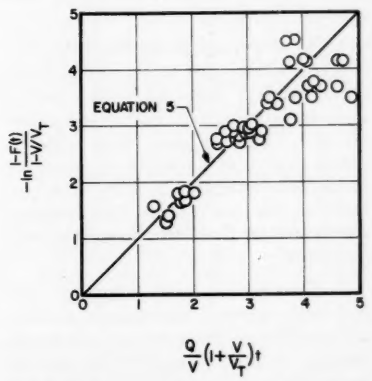

Fig. 6. Final correlation of fractional mixing times (V and Q obtained from Figures 5 and 3, respectively).

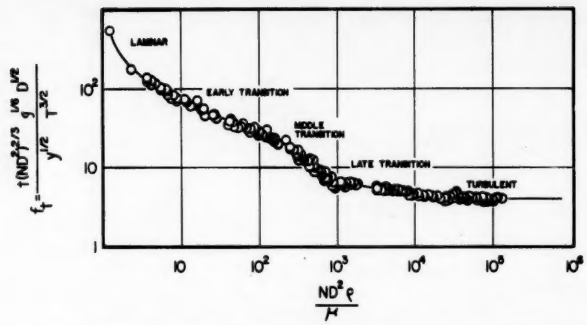

Fig. 7. Empirical correlation of time required for terminal mixing.

about 40%, but most points are within 20% of the curve.

The end of the laminar region, in which little or no turbulent mixing takes place, coincides approximately with the lowest Reynolds number at which flow at the tank wall and fluid surface may be first observed visually (*4, 5*). Photographs taken (*5*) at Reynolds numbers in the early transition region show that all the fluid in the tank is in motion, but the flow is very sluggish, largely in the tangential direction, and the mixing rates are still very low. No turbulence is evident except close to the impeller. Photographs in the middle transition region show much more turbulence, and the velocity measurements show that all the fluid is now in reasonably rapid motion; therefore the mixing times decrease rapidly with further increases in flow rate or Reynolds number.

Although mixing times, even for terminal mixing, were too short to be measured above a Reynolds number of 1.8×10^5, the turbulent region of the curve was extended after a comparison of the existing mixing-time–factor curve with the power-number–Reynolds-number curve for turbine impellers rotating in baffled tanks, in both Newtonian (*9*) and non-Newtonian (*4*) fluids. Figure 8 shows both smoothed curves. The important points to note are as follows:

1. As one proceeds up the Reynolds-number scale, the mixing-time–factor curve changes slope each time and at the same point that the power curve changes. This is only reasonable in that a change in the trend of power requirements indicates that the flow patterns in the tank must be changing, which in turn lead to changes in mixing rates.

2. The power curve flattens out, that is the power requirements become independent of viscosity, at a Reynolds number of about 2 to 4×10^4 and remains flat to a Reynolds number of 10^6, the upper limit of the power data.

In view of these facts, moderate extensions of the mixing-time–factor curve seem to be reasonable.

Comparison with Prior Art

Fox and Gex (*2*) have developed a mixing-time-factor–Reynolds number curve for Newtonian fluids agitated by marine propellers and side-entering jets in unbaffled tanks. Several differences between their work and the present study are of importance:

1. Their final correlating equation is identical in form to the present one for turbine impellers with two exceptions: the mixing-time factor used for turbines is equal to the product of the mixing-time factor for marine propellers or jets and the square root of the D/T ratio, and second the numerical values are generally different for different impellers even after the D/T term is considered.

2. The disappearance of the last wisp of color in their experiments was isolated and located at different points in the tank, whereas the disappearance of the last wisp of color with turbine impellers always occurred in the region of the impeller.

These differences between turbine mixers on one hand and jets and propellers on the other indicate that a significant portion of the mixing in the latter two systems occurs away from the region of the agitator mechanism.

At very high Reynolds numbers this factor, rather than the rate of fluid recirculation, may possibly control mixing rates, and the propeller becomes a more efficient mixer than does the turbine. Within the range of Reynolds numbers studied, however, the reverse appears to be true. For example, with a 2,000-centipoise fluid, a 3-in. impeller, and a T/D ratio of 6.0 in both systems the power consumptions are equal when the Reynolds numbers are 100 for the propeller and 60 for the turbine. The mixing time with a turbine used under these conditions is only about 6% of that required by the propeller. If a fluid having a 1-centipoise viscosity were used instead, the mixing times would be identical in both systems at equal power consumptions. In this case the Reynolds numbers are 2×10^5 for the propeller and 0.7×10^5 for the turbine. Kramers and co-workers (*3*) arrived at the opposite conclusion concerning the relative merits of propellers and turbines, but their turbines had unusually narrow blades, to which their inferior performance may have been due.

Corrsin (*1*) presented an analysis of a fluid mixer operating at high Reynolds numbers (turbulent region) in which he assumed that stationary isotropic turbulence exists throughout the tank. From this analysis he derived an equation for scaling geometrically similar mixers. This and the other scaling equations available at the present time are presented in Table 2. One may note that although all of the exponents for the scaling factor K are between 4 and 6, only the data of Kramers *et al.* (*3*), which were used by Corrsin to help support his deduction, yield an equation identical with the postulated one. However Kramers's results are not entirely conclusive in that his group carried out only a small number of tests in which the scale of the equipment was varied. While Corrsin's approach is thus left with little direct

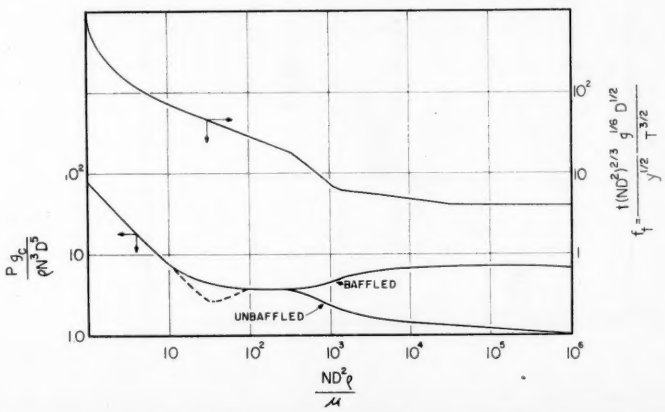

Fig. 8. Comparison of terminal mixing time and power consumption correlations.

experimental support, it should be noted that the empirically determined exponents are subject to considerable experimental error and, with the exception of the present results (on small-scale equipment), have not been determined to better than 10 to 20%.

Mixing Rates in Non-Newtonian Systems

Photographic (5) and visual (4) data on pseudoplastic non-Newtonian fluids agitated with a single flat-bladed turbine show that only a part of the fluid in the tank is in motion unless the Reynolds numbers exceed about 270 at $T/D = 3.0$, 110 at $T/D = 2.0$, 90 at $T/D = 1.5$, and 50 at $T/D = 1.3$

Therefore the mixing-time factor of Figure 7 would tend to approach very large values below these Reynolds numbers, as compared with the break at a Reynolds number of about 2 for the Newtonian data in Figure 7. In other words a series of laminar curves, each intersecting the early-transition curve of Figure 7 at the above-indicated Reynolds numbers, for various T/D ratios, might be expected. Since the photographic study (5) indicated rapid increases in fluid turnover at increasing Reynolds numbers, use of the curve of Figure 7 at higher Reynolds numbers would perhaps be conservative for pseudoplastic fluids.

Use of the curves of Figure 7 for dilatant systems is also suggested in the absence of specific data, but no estimate of the accuracy of this suggestion is possible.

CONCLUSIONS

1. A model of the mixing process, based on the assumption that the contents of the vessel consist of a small perfectly mixed volume in the region of the impeller, surrounded by unmixed fluids, was supported experimentally to Reynolds numbers of 640. This model may be used to define the extent of completion of fast, batch reactions by the equation

$$\frac{1 - F(t)}{1 - V/V_T} = e^{-Q/V(1+V/V_T)t}$$

The model probably will not apply to mixing in the fully turbulent region, since considerable mixing may then occur in other parts of the tank and the volume may cease to be a pertinent variable. All data supporting this model were taken with a flat-blade turbine in a baffled tank.

2. Data on the total volumetric flow rates were correlated over the Reynolds number range of 36 to 1.72×10^4 by

$$Q = 9.0 \times 10^{-4} NwD^2 (D^{0.4}\rho/\mu)^{1/2} \sqrt{1 - q^2}$$

3. Times required for terminal mixing, measured by carrying out an acid-base neutralization, were correlated empirically (Figure 7) for Reynolds numbers between 3 and 1.8×10^5. Each change in the character of the mixing-time curve reflects a change in the flow conditions in the tank which is also reflected in the power-number–Reynolds-number curve.

4. The mixing-time factor for the agitation of Newtonian fluids by turbine impellers in baffled tanks is found to be related to the mixing-time factor for the agitation of Newtonian fluids by jets and propellers in unbaffled tanks by the square root of the T/D ratio. The mixing-time factors and power-consumption data combined suggest that turbines are much more efficient at low Reynolds numbers than are propellers. At the highest Reynolds numbers studied in this work the two have become comparable.

5. Application of the present mixing-time data (Figure 7) to non-Newtonian systems at sufficiently high Reynolds numbers is suggested as an approximate procedure for pseudoplastic systems until data become available.

ACKNOWLEDGMENT

This work was supported by the Office of Ordnance Research, U.S. Army, and by a fellowship from the Esso Research and Engineering Company. Both sources of aid are gratefully acknowledged.

NOTATION

c_1 = entrainment factor
C_T = concentration of base, moles/cu. ft. $C_T(0)$ refers to this term at zero time
C_t = concentration of acid, moles/cu. ft. $C_t(0)$ refers to this term at zero time
D = impeller diameter, ft.
D_o = probe resistance at zero flow, ohms
D_R = probe resistance at velocity u, ohms
D'_o = $(D_R - D_o)$, ohms
e = base of Napierian logarithms
f = functional relationship
f_t = mixing-time factor (dimensionless) $f_t = t_f (ND^2)^{2/3} g^{1/6} D^{1/2}/y^{1/2}T^{2/3}$
$f\eta$, D'_o = abscissa of calibration curve
$f(\mu)$ = correction factor for viscous drag of fluid on the impeller
$F(t)$ = fraction mixed, dimensionless
g = gravitational acceleration, ft./sec.^{2}
g_c = conversion factor, ft. lb.-mass/(lb.-force)(sec.)^2
J = baffle width, ft.
K = ratio of size, prototype to model
$M(t)$ = moles of acid or base in tank at time t
M_o = moles of acid or base in tank at time zero
N = rotational speed, rev./sec. in dimensionless groups; otherwise rev./min.
N_{Re} = Reynolds number (dimensionless), $ND^2\rho/\mu$
N_P = power number (dimensionless), $Pg_c/N^3D^5\rho$
P = power, (ft.)(lb.-force)/sec. P_2 refers to the power consumption of a prototype and P_1 to that of a model.
Q = volumetric flow rate, cu. ft./sec.
Q_{th} = theoretical volumetric flow rate, cu. ft./sec.
q = ratio of (angular) fluid velocity at the blade tip to angular impeller velocity
T = tank diameter, ft.
t = time, sec.
t_T = terminal mixing time, sec.
u = velocity, ft./sec.
V = volume of perfectly mixed region, cu. ft.
V_T = total volume of fluid in tank, cu. ft.
w = impeller blade width, ft.
y = fluid depth, ft.
η = ratio of (μ/ρ) for unspecified fluid to (μ/ρ) for water, dimensionless
μ = viscosity, (lb.-mole)(ft.)(sec.)
π = 3.14 . . .
ρ = density, lb.-mass cu. ft.

LITERATURE CITED

1. Corrsin, Stanley, *A.I.Ch.E. Journal*, **3**, 329 (1957).
2. Fox, E. A., and V. E. Gex, *ibid.*, **2**, 539 (1956).
3. Kramers, H., G. M. Baars, and W. H. Knoll, *Chem. Eng. Sci.*, **2**, 35 (1953).
4. Metzner, A. B., and R. E. Otto, *A.I.Ch.E. Journal*, **3**, 3 (1957).
5. Metzner, A. B., and J. S. Taylor, *ibid.*, **6**, 109 (1960). See also Taylor, J. S., M.Ch.E. thesis, Univ. Del., Newark (1955).
6. Nagata, S., K. Yamamoto, and M. Ujihara, *Chem. Eng. (Japan)*, **23**, 130 (1959).
7. Nielsen, H. J., Ph.D. Thesis, Ill. Inst. Technol., Chicago (1958).
8. Norwood, K. W., Ph.D. Thesis, Univ. Del., Newark (1959).
9. Rushton, J. M., E. W. Costitch, and H. J. Everett, *Chem. Eng. Progr.*, **46**, 395, 467 (1950).
10. Sachs, J. P., and J. H. Rushton, *ibid.*, **50**, 597 (1954). See also Sachs, J. P., Ph.D. Thesis, Ill. Inst. Technol., Chicago (1951).
11. Tennant, B. W., Thesis, Ill. Inst. Technol., Chicago (1952).
12. van de Vusse, J. G., *Chem. Eng. Sci.*, **4**, 178, 209 (1955).

Manuscript received July 17, 1959; revision received December 1, 1959; paper accepted December 7, 1959.

Liquid, Gas, and Dense-Fluid Viscosity of Propane

KENNETH E. STARLING, BERT E. EAKIN and REX T. ELLINGTON

Institute of Gas Technology, Chicago, Illinois

Experimental data, believed accurate within ±0.5%, are presented for pressures of 100 to 8,000 lb./sq. in. abs. for nine temperatures from 77° to 280°F. One isotherm, within 1° of the critical, indicates the detail required in further investigation of the critical region. These data were combined with the available literature values to prepare a table of recommended viscosity values with maximum uncertainty of ±2% for temperatures from 70° to 460°F. Two generalized correlations and the Enskog viscosity theory for dense gases exhibit significant errors in predicting the data. Methods are suggested for extrapolation of the values to higher temperatures and pressures.

More data on the physical properties of hydrocarbon liquids and gases at elevated pressures and temperatures are needed because of the trend toward these conditions in industrial processes and the more frequent discovery of reservoirs at great depths with the resulting increased occurrence of condensate types of systems. The literature contains relatively few viscosity data for elevated pressures and temperatures for single components and very few data for mixtures. Methane, ethane, and propane are the only saturated hydrocarbons for which the effect of pressure on the viscosity behavior has been reported by more than one investigator. The reported methane viscosities are in fair agreement, but the ethane and propane data differ by as much as 10% for those conditions for which it is possible to make direct comparisons. Therefore an extensive program has been initiated to provide new viscosity data for single components, mixtures, and naturally occurring fluid systems.

Experimental data are presented for gaseous, liquid, and dense-fluid propane at pressures from 100 to 8,000 lb./sq. in. abs. for nine temperatures between 77° and 280°F. These data, which are believed to be accurate to within ±0.5%, have been compared with the data of previous investigators, and differences have been resolved. To prevent each engineer needing values for calculations from having to reevaluate the data, a table of recommended propane viscosity values is presented for four ranges of pressure and temperature: (1) liquid at 50 lb./sq. in. abs. from −300° to 10°F., with an uncertainty of ±5%; (2) gas, liquid, and dense fluid for 100 to 8,000 lb./sq. in. abs. and 70° to 280°F., with an uncertainty of ±0.5%; (3) gas and dense fluid for 100 to 8,000 lb./sq. in. abs. and 340° to 460°F., with an uncertainty of ±2%; and (4) dense fluid and liquid for 9,000 to 20,000 lb./sq. in. abs. and 100° to 300°F., with an uncertainty of ±5%.

APPARATUS AND MATERIALS

In previous viscosity studies a modified Rankine type of capillary viscometer was used (*4*), but operational difficulties limited use of this instrument to measurements on light natural gas, methane, and inert gases at low densities. An analysis (*8*) of the various types of viscometers led to the development of a new design based on the principle of the Rankine instrument, that is laminar flow of the fluid through a capillary tube, but an improved method of obtaining the pressure differential for fluid movement. This is an absolute instrument which does not require calibration with a fluid of known viscosity. A schematic diagram of the new viscometer and associated test equipment, which have been previously described in detail (*7*), is shown in Figure 1.

During an experimental run mercury flows from the reservoir into the receiver, forcing the test fluid through the capillary. The time recorded is that taken for the mercury level to rise from the lower receiver electrode to the upper electrode and involves displacement of some 7 ml. of fluid. The long electrode ends some distance above the vessel bottom and so provides an initial volume to permit flow conditions to stabilize before timing begins. The receiver is mounted rigidly, and the reservoir is free to move in an arc of radius equal to the length of the mercury flow tube. The flow tube and capillary jacket are attached to the receiver and reservoir by 0.25-in. high-pressure swivel joints. The reservoir axis remains vertical as it is raised, since the mercury flow tube and capillary-tube jacket assembly act as a parallel linkage. In this manner the pressure differential across the capillary tube (equivalent to the difference in level of the mercury surfaces in the reservoir and receiver) can be varied from 3 to 40 cm. by raising the mercury reservoir to predetermined positions.

The Pyrex capillary tube is about 0.25-mm. I.D. by 5-mm. O.D. and 91 cm. in length. Its bore was determined by the mercury-pellet method described in detail by Carr (*4*). The viscometer is mounted in an air bath designed for operation from ambient temperature to 400°F. Initially it was possible to maintain the temperature of the reservoir and receiver only within ±0.3°F. of the selected temperature. This variation was later reduced to ±0.1°F. The instrument may be operated at pressures up to 8,000 lb./sq. in. abs.

To determine the accuracy and standard deviation of the instrument, a series of thirty-one separate tests was made on nitrogen at 1,000 lb./sq. in. gauge. The 95% confidence limit (twice the standard deviation) for these experimental data was 99.4% and the absolute accuracy 99.7% [based on what are regarded as the best published data for nitrogen (*7*)]. Data were also obtained for liquid water at room temperature and 1,150 lb./sq. in. gauge; the results of fifteen measurements differed by only ±0.3% from the values reported in the literature (*7*).

The propane used was certified 99.99+ mole % pure, and a mass spectrometer analysis detected no impurities in the samples used.

EXPERIMENTAL DATA

To achieve the objectives of the investigation, it was necessary to obtain data for the gas, liquid, and dense-fluid regions and to conduct an intensive examination of the viscosity behavior in the region near the critical point. Propane was chosen for the initial investigation because its critical temperature of 206.3°F. falls near the midpoint of the operating temperature range of the instrument, permitting study of the viscosity of each phase to be made over a fairly wide temperature range. The experimental program was planned to provide sufficient data to resolve the differences between previous data and to permit a set of recommended values to be established.

Propane viscosity data were obtained for nine temperatures from 77° to 280°F., for a general range of test pressures from 100 to 8,000 lb./sq. in. abs., and are presented in Figures 2 and 3. As data were obtained, plots of isothermal values were used to indicate trends and questionable points. However because the data were obtained at progressively higher pressures at a given temperature, the isotherm plots (Figure 2) were relatively insensitive to data-point errors. For a better check on the internal consistency of the data, a cross plot (Figure 3) was prepared of the viscosity at constant pressure as a function of temperature. This made questionable data much more apparent; that is, the 220°F., 8,000 lb./sq. in. abs. point is ap-

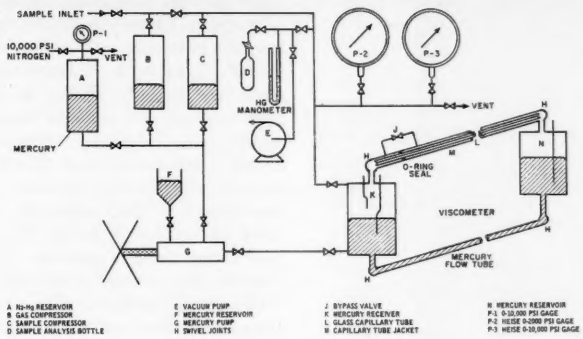

Fig. 1. Schematic diagram of IGT viscometer.

parently 2% low, based on the smooth curve through the other 8,000 lb./sq. in. abs. data.

Each point in Figures 2 and 3 represents the average value determined from three to five repeat measurements at each of at least two different pressure differentials across the capillary tube. The repeat measurements generally were reproducible to within ±0.2%, and the values calculated for the different pressure differentials generally agreed within ±0.3%. Greater deviations were observed under certain sets of conditions, particularly near the critical point. For most of these cases where greater than normal deviations were observed, the calculated average Reynolds number was higher than 1,500, and turbulent flow may have existed in the capillary tube. Detailed tables of the experimental data have been prepared and are available.[*]

An attempt was made to define the critical viscosity for propane as a part of the investigation at 206.6°F. Data were obtained at pressure intervals as close as 8 lb./sq. in. on both sides of the reported critical pressure, 617.4 lb./sq. in. abs. as shown in Figure 4. However in going from 617.4 to 625.0 lb./sq. in. abs. the viscosity increased 120 μpoises, which would indicate that the actual critical pressure for the propane sample tested might be slightly above 618 lb./sq. in. abs. Figure 4 also indicates that a very detailed investigation of viscosity behavior in the region near the critical will be required to determine an accurate critical viscosity value.

Investigation is underway to provide detailed data similar to those presented here, for ethane and *n*-butane, and to define the critical region of each in significant detail. The data for propane, ethane, and butane will permit rigorous testing of the theorem of corresponding states and the dense-gas theory as applied to viscosity.

COMPARISON WITH LITERATURE VALUES

Data on the effect of pressure on the viscosity of propane have been reported by seven groups of investigators and were used to test the new data and to develop a conviction regarding their validity. Comings, Mayland, and Egly (*6*) utilized a capillary-tube viscometer to measure gas-phase viscosity at pressures up to 600 lb./sq. in. abs. and temperatures to 220°F. Both gas and liquid viscosities were measured by three groups with rolling ball viscometers: Sage and Lacey (11) up to 2,000 lb./sq. in. abs. and 220°F.; and Bicher and Katz, (*2*) and Smith and Brown (*14*) to 5,000 lb./sq. in. abs. and 400°F. Baron, Roof, and Wells (*1*) utilized a modified capillary-tube instrument for measurement of both gas and liquid viscosities up to 8,000 lb./sq. in. abs. and 275° F. Van Wijk, van der Veen, Brinkman, and Seeder (*19*) used a falling-body viscometer for measurements at 6,000 to 20,000 lb./sq. in. abs. and 89° to 300°F. Swift, Christy, and Kurata (*16*) reported data for saturated liquid propane from −300° to 194°F. obtained by use of a falling-body viscometer.

The viscosity data reported by Sage and Lacey show significant deviations from the values reported by Comings *et al.* and those of this investigation, as shown in Figure 5 for 160° and 220°F. Comings's values and the new data were both obtained with capillary-tube viscometers where laminar flow conditions can be assured; these data differ by less than the 1 to 2% experimental uncertainty Comings ascribed to his data. The data of Sage and Lacey were obtained by use of a rolling-ball viscometer, but the density-viscosity behavior of propane in the gas phase almost precludes existence of laminar flow in this type of instrument. When turbulent flow occurs, the apparent viscosity values calculated from the measurements will be higher than the true values, and the data indicate that this may be the case.

Figure 5 illustrates the insensitivity of the plot of isotherms. Even though the three sets of data differ markedly, a smooth curve can be drawn through each set. A more rigorous test of the accuracy of the data is the plotting of isobars of viscosity as a function of temperature. Comings's values and the new data are shown in Figure 6 for 100, 200, 300, and 400 lb./sq. in. abs. Only one of the new data points is more than 0.5% from the smooth curves drawn through these points, and all but two of Comings's points lie within ±2% (their stated experi-

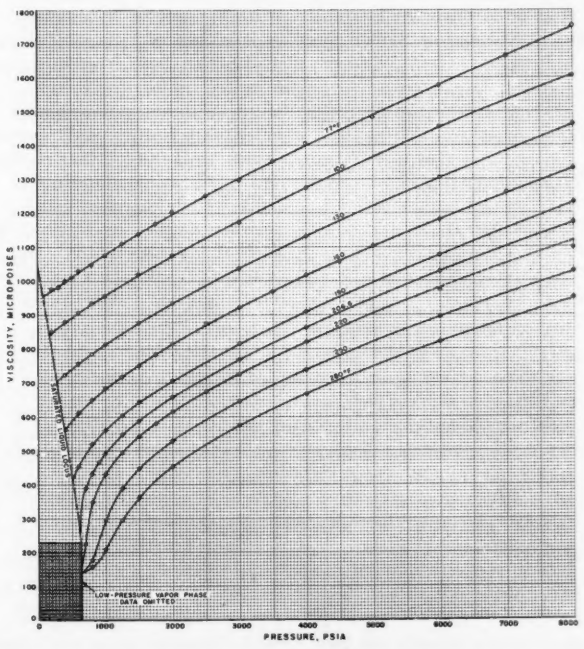

Fig. 2. Experimental propane viscosity vs. pressure.

[*] Tabular material has been deposited as document 6346 with the American Documentation Institute, Photoduplication Service, Library of Congress, Washington 25, D. C., and may be obtained for $3.75 for photoprints or $2.00 for 35-mm. microfilm.

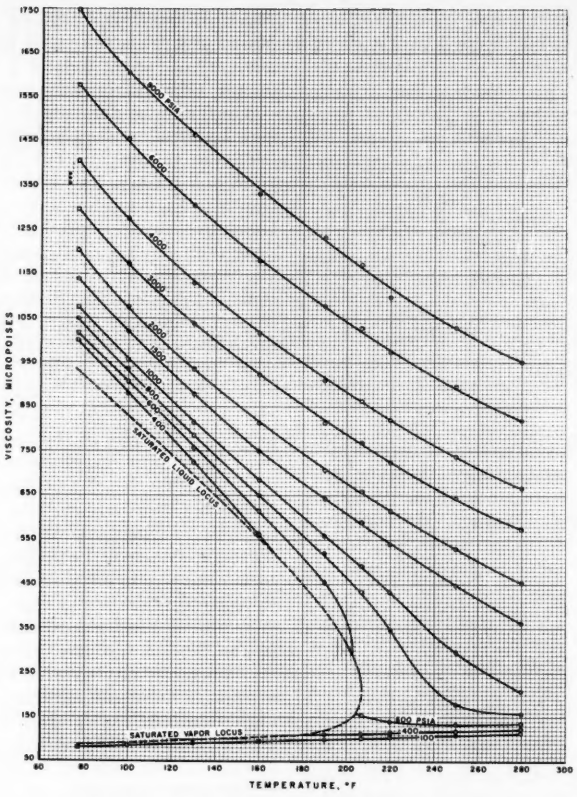

Fig. 3. Experimental propane viscosity vs. temperature.

mental uncertainty) of the curves. The data of Sage and Lacey and of Smith and Brown exhibited such scatter that a smooth curve could not be drawn through them for comparison.

Most of the available data for 1,000 lb./sq. in. abs. agree fairly well. Those of Smith and Brown and of Bicher and Katz agree with the data of this investigation within ±2%, which is within their stated experimental accuracy of ± 3 to 5%. Also the data of Baron, Roof, and Wells and Sage and Lacey, differ by less than 1% from the Institute of Gas Technology data, except at 125°F., where Baron's value is 47 μpoises less. This agreement is illustrated in Figure 7, where the data of the different investigators are compared with isobars of the recommended values at 1,000, 2,000, 3,000, 5,000, and 8,000 lb./sq. in. abs.

At higher pressures the agreement between data is not so good. When the new data are plotted as isotherms (Figure 2), the viscosity increases almost linearly with pressure above 1,500 lb./sq. in. abs. Some of the data of Sage and Lacey indicate similar behavior, but their data for 190° and 220°F. exhibit a distinct downward curvature at 2,000 lb./sq. in. abs. The plots of data for various temperatures which were used for comparing the data for pressures above 600 lb./sq. in. abs. are not shown; however the relative shape of the isotherms for pressures above 1,000 lb./sq. in. abs. can be inferred from Figures 2 and 7. The data of Bicher and Katz and of Van Wijk, et al., indicate the same near-linearity of the isotherms and general shape of isobars as the Institute of Gas Technology data. Bicher and Katz's data are only 1 to 3% higher, and those of Van Wijk et al. are less than 3% lower than the Institute of Gas Technology data. The data of Smith and Brown show definite drooping of the isotherms, with values 5 to 9% lower than Institute of Gas Technology data at 5,000 lb./sq. in. abs. This may have been caused by the calibration coefficient for the instrument not adequately compensating for pressure effects.

The best agreement was observed at 175° and 225°F. for the data of Baron, Roof, and Wells and of the present authors, where the observed differences are less than 1% over the entire pressure range to 8,000 lb./sq. in. abs. At 275°F. the data agree to within 1% for pressures up to 3,000 lb./sq. in. abs., but at the higher pressures Baron's values tend to fall below the Institute of Gas Technology values and are 3% less at 8,000 lb./sq. in. abs. The greatest difference observed between these two sets of data is at 125°F., where Baron's values are consistently 47 μpoises (3.2 to 5.9%) less than those predicted from the Institute of Gas Technology values. These low values do not follow the expected viscosity-temperature trend. Both the Institute of Gas Technology and Baron et al. data were obtained with capillary-tube viscometers.

Swift, Christy, and Kurata recently presented data for liquid propane for temperatures from −300° to 194°F. Five of the seven data points between 86° and 194°F. could be compared directly with the Institute of Gas Technology data. These exhibited differences of less than 2%; the remaining two points differed from the Institute of Gas Technology data by less than the ±5% stated possible experimental error. The data of Swift, et al., were obtained by use of a relative-value (falling-body) instrument.

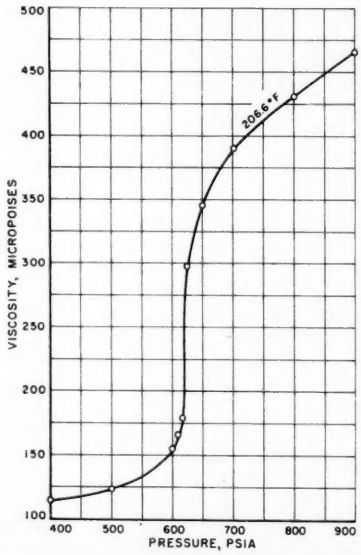

Fig. 4. Change of propane viscosity with pressure at 0.3°F. above critical temperature.

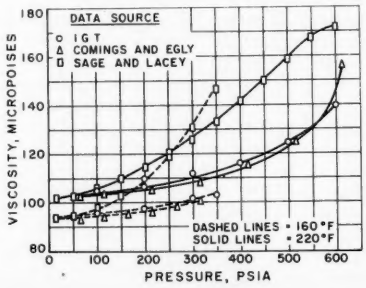

Fig. 5. Comparison of propane viscosity data at 160° and 220°F.

SELECTION OF RECOMMENDED VALUES

There is no single criterion by which the accuracy of the various data can

be determined. However on the basis of comparisons discussed and the trends indicated by kinetic theory, it was decided that for temperatures from 100° to 280°F. values read from a large-scale viscosity-temperature plot of the new data would have an estimated error of less than 0.5%. Such a plot would also permit extrapolation of the curves through the 77°F. data for estimation of viscosity values at 70°F. The values so determined were then cross plotted as isotherms on a viscosity-pressure diagram to detect any irregularities. In this manner the viscosity values for 70° to 280°F. reported in Table 1 were obtained.

It is not possible to extrapolate the experimental data to higher temperatures by use of either of the large-scale plots referred to above, owing to the scatter of the high-temperature data of Bicher and Katz and of Smith and Brown, which are the only values available. However Thodos and co-workers (*3, 13*) have proposed a method for correlation of viscosity data which has proved effective for pure mono- and di-atomic materials and would provide a basis for extrapolation to higher temperatures. Thodos defines a residual viscosity as the difference between the viscosity at a given pressure and temperature, μ, and the viscosity at 1 atm. and the same temperature μ_o. A logarithmic plot of residual viscosity vs. density resulted in a smooth continuous curve for the mono- and diatomic molecules tested. In this manner pressure and temperature are eliminated as independent variables.

A Thodos type of plot was constructed for the new experimental propane viscosity data and is shown in Figure 8. The μ_o values were calculated by use of the Sutherland (*15*) equation (with T in °R.) which represented atmospheric-pressure propane-viscosity data of Trautz and Sorg (*17*) within 0.1%:

$$\mu_o = (6.805\,T^{3/2})/(T + 502.4) \qquad (1)$$

All but two of the points on Figure 8 fall within ±1% of the smooth curve drawn through the data, which again is a good test of the consistency of the experimental results. Since this plot has correlated the experimental data from 77° to 280°F. into a single curve, it should be possible to use the plot as a means of extrapolation to higher temperatures; all the densities encountered would lie within the range of existing data.

The μ_o values were calculated with the Sutherland equation for temperatures of 340°, 400°, and 460°F. The data of Sage and Lacey (*12*) were used to determine the densities for each of the pressures at the three temperatures, and the corresponding values of residual viscosity were read from Figure 8. The viscosity values obtained by this technique formed smooth isobars which were continuations of the curves of experimental data at lower temperatures, as is shown in Figure 7; it can also be noted in Figure 7 that the predicted curves lie between the data of Bicher and Katz, and Smith

Table 1. Recommended Values for the Viscosity of Propane

Critical temperature = 206.3°F.
Critical pressure = 617.4 lb./sq. in. abs.

A. Uncertainty Less Than 2%

Temperature, °F. / Pressure, lb./sq. in. abs.	70.0	100.0	130.0	160.0	190.0	220.0	250.0	280.0	340.0	400.0	460.0
	Viscosity, μpoises										
14.7	80	85	89	93	98	102	106	110	118	126	133
100	81	86	91	96	100	105	110	114	120	128	135
200	1,010	848	93	98	102	107	112	116	122	130	137
300	1,025	863	710	102	106	110	114	119	124	132	139
400	1,040	877	725	562	112	116	119	123	127	134	141
500	1,055	891	741	588	127	125	125	129	131	137	143
600	1,070	905	755	610	454	140	134	135	135	140	146
800	1,095	932	785	650	520	345	178	157	148	149	153
1,000	1,125	956	814	682	560	432	295	208	169	162	162
1,250	1,157	987	846	718	605	495	390	297	208	185	178
1,500	1,189	1,017	877	753	643	543	447	362	253	212	197
1,750	1,218	1,045	906	785	675	580	492	412	294	242	218
2,000	1,247	1,074	935	815	705	615	530	453	335	272	240
2,500	1,300	1,126	988	870	762	675	593	518	402	329	284
3,000	1,351	1,176	1,037	922	815	725	645	575	460	379	327
4,000	1,445	1,275	1,132	1,016	910	820	740	667	555	469	405
5,000	1,538	1,367	1,220	1,102	996	903	820	748	636	546	476
6,000	1,627	1,450	1,305	1,182	1,077	981	895	822	709	615	540
7,000	1,715	1,535	1,385	1,257	1,155	1,053	964	887	777	680	602
8,000	1,802	1,610	1,463	1,333	1,231	1,120	1,028	950	841	741	660

B. Uncertainty Less Than 5%

Temperature, °F. / Pressure, lb./sq. in. abs.	-300.0	-250.0	-200.0	-150.0	-100.0	-50.0	0.0	10.0
	Viscosity, μpoises							
50	72,500	17,000	7,400	4,400	3,000	2,100	1,600	1,500
Temperature, °F. / Pressure, lb./sq. in. abs.		100.0	150.0		200.0	250.0		300.0
	Viscosity, μpoises							
9,000		1,645	1,405		1,227	1,070		948
10,000		1,725	1,485		1,300	1,138		1,005
12,000		1,880	1,625		1,420	1,245		1,117
14,000		—	1,762		1,545	1,367		1,222
16,000		—	—		1,667	1,480		1,325
18,000		—	—		—	1,592		1,430
20,000		—	—		—	1,700		1,530

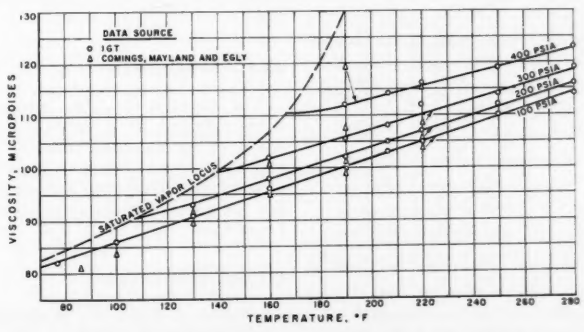

Fig. 6. Comparison of propane viscosity data at low pressure.

and Brown, and have the same general curvature. It is estimated that the viscosities reported in Table 1 for 340°, 400°, and 460°F. have an uncertainty of ±2%.

Swift, Christy, and Kurata (*16*) recently published values for the viscosity of liquid propane at low temperatures. Van Wijk, van der Veen, Brinkman and Seeder (*19*) published values for extreme pressures. The values reported in Table 1 were interpolated from these sets of data and are included to provide as complete a viscosity field as is presently possible. These values have an uncertainty of ±5%.

COMPARISON WITH CORRELATIONS

Some of the propane viscosities reported in Table 1 were compared with those predicted by two generalized viscosity correlations based on the theorem of corresponding states. The correlations of Uyehara and Watson (18) apply to both the gas and liquid phases, and the observed deviations are generally within the ±10% accuracy claimed for the chart. This correlation tends to predict viscosity values which are consistently higher than the observed values. Carr (*4*) presented a correlation for predicting the viscosity of light natural gases with a high degree of accuracy, but when applied to propane the accuracy is much less. This correlation tends to predict viscosity values which are lower than the observed data, particularly at lower temperatures. Carr's correlation appears to be the better of the two for calculating gas viscosities in regions where data are not available.

Another method of correlating viscosity behavior is by use of Enskog's (*5, 9*) viscosity theory for dense gases.

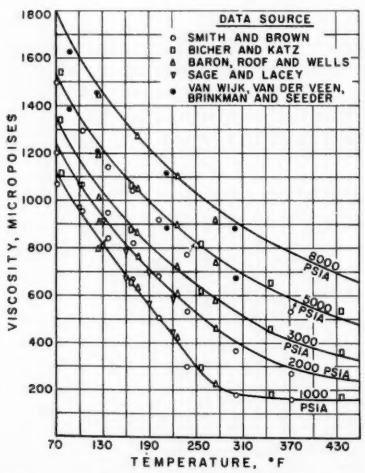

Fig. 7. Comparison of IGT recommended propane viscosity values with data of other investigators.

To test this relationship, terms in the equation were computed by the use of Enskog's equation of state; the Benedict-Webb-Rubin equation of state; the propane B-W-R constants of Opfell, Schlinger and Sage (*10*); and a plot of experimental kinematic viscosity vs. density.

Agreement between observed data and values calculated with the Enskog theory is poor, particularly at the lower temperatures. However it is apparent that the Enskog relationship does predict the effect of pressure on viscosity, since the deviations are almost constant at any one temperature. To test this hypothesis, a new value of one Enskog constant was evaluated from the experimental 2,000 lb./sq. in. abs. data for each temperature and used in calculation of the viscosities by the Enskog equation. The resulting deviations are small and consistent for the higher pressures. This would tend to indicate that if the Enskog temperature parameter were evaluated from one experimental data point, the Enskog relationship could be used with fair confidence to extend the data to higher densities at the same temperature, provided that the P-V-T data or an applicable equation of state were available.

SUMMARY

New experimental viscosity data have been presented for propane over the range of petroleum reservoir pressures and temperatures. The new data have been combined with existing literature values to present a consistent viscosity field for fluid propane from 70° to 460°F. for a wide range of pressures and for the liquid at 50 lb./sq. in. abs. down to −300°F. The Enskog dense gas viscosity theory can be used to predict accurately the influence of pressure on viscosity for propane, even for the liquid phase, but the temperature dependence of one equation parameter is not adequately predicted by the Enskog equation. The residual viscosity concept of Thodos was shown to be applicable to propane and to serve as a useful extrapolation technique.

ACKNOWLEDGMENT

The experimental data presented here were obtained as a part of a continued study of hydrocarbon physical properties supported through basic research program of the Institute of Gas Technology and by the American Petroleum Institute through Grant-in-Aid No. 77.

LITERATURE CITED

1. Baron, J. D., J. G. Roof, and F. W. Wells, *J. Chem. Eng. Data*, 4, 283 (July, 1959).

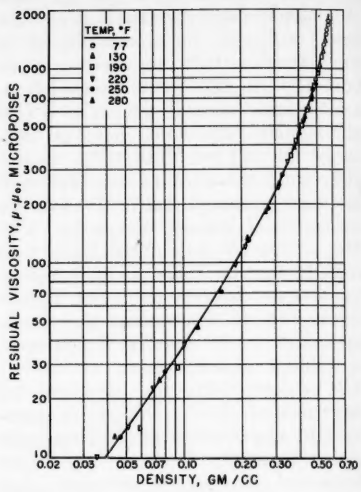

Fig. 8. Propane residual viscosity vs. density.

2. Bicher, L. B., Jr., and D. L. Katz, *Ind. Eng. Chem.*, **35**, 754 (July, 1943).
3. Brebach, W. J., and George Thodos, *ibid.*, **50**, 1095 (July, 1958).
4. Carr, N. L., *Inst. Gas Technol. Res. Bull. No.* **23** (June, 1953).
5. Chapman, S., and T. G. Cowling, "The Mathematical Theory of Non-Uniform Gases," Cambridge Univ. Press, London (1939).
6. Comings, E. W., B. J. Mayland, and R. S. Egly, *Univ. Ill. Eng. Exp. Sta. Bull. No. 354* (1944).
7. Eakin, B. E., and R. T. Ellington, *Trans. Am. Inst. Mining Met. Petrol. Engrs.*, **216**, 85 (1959), abstracted in *J. Pet. Tech.*, **11**, 71 (April, 1959).
8. ———, *Proc. Natl. Conf. on Industrial Hydraulics*, **11**, 163 (1957).
9. Enskog, D., Dissertation, Upsala, Sweden (1917).
10. Opfell, J. B., W. G. Schlinger, and B. H. Sage, *Ind. Eng. Chem.*, **46**, 1286 (June, 1954).
11. Sage, B. H. and W. N. Lacey, *Ind. Eng. Chem.*, **30**, 829 (July, 1938).
12. ———, "Thermodynamic Properties of the Lighter Paraffin Hydrocarbons and Nitrogen," American Petroleum Institute, New York (1950).
13. Shimotake, Hiroshi, and George Thodos, *A.I.Ch.E. Journal*, **4**, 257 (September, 1958).
14. Smith, A. S., and G. G. Brown, *Ind. Eng. Chem.*, **35**, 705 (June, 1943).
15. Sutherland, W., *Phil. Mag.*, **36**, 507 (1893).
16. Swift, G. W., J. A. Christy, and Fred Kurata, *A.I.Ch.E. Journal*, **5**, 98 (March, 1959).
17. Trautz, M., and K. G. Sorg, *Ann. Physik*, **10**, Series 5, 81 (1931).
18. Uyehara, O. A., and K. M. Watson, *Natl. Petrol. News*, **36**, R-714, R-716-R-720, R-722 (October 4, 1944).
19. Van Wijk, W. R., J. H. van der Veen, H. C. Brinkman, and W. A. Seeder, *Physica*, **8**, No. 1, 45 (1940).

Manuscript received May 25, 1959; revision received December 7, 1959; paper accepted December 9, 1959. Paper presented at A.I.Ch.E. St. Paul meeting.

Effect of Radial Temperature Variation on Axial Mixing in Pipes

R. D. HAWTHORN

Shell Development Company, Emeryville, California

In a pipe reactor axial mixing results in a distribution of residence times of fluid elements in the reactor. Taylor and others have discussed methods of predicting the extent of axial mixing for isothermal flow in pipes; however, in a reactor the heat of reaction and its supply or removal at the wall can cause significant radial variation of temperature and temperature-dependent physical properties. Thus the velocity profile in a reactor may differ from that in a pipe through which fluid flows at constant temperature.

This paper presents an analysis of the effects of radial temperature variations on effective axial diffusion coefficients. In laminar flow it is found that radial temperature variation may increase or decrease the effective diffusivity two- to threefold from that calculated for isothermal flow. At Reynolds numbers greater than 10,000 the diffusivity calculated for constant temperature flow does not differ significantly from that for flow through a reactor tube (with radial temperature variation) at the same Reynolds number, calculated with the viscosity evaluated at the wall temperature. In turbulent flow at Reynolds numbers less than 10,000, the effect of radial temperature variation is important but can be estimated only roughly.

The flow of fluid through a straight pipe is accompanied by mixing in the axial direction. Axial mixing results primarily from variation of the fluid velocity over the pipe cross section and is opposed by radial processes (molecular and eddy). In a pipe reactor axial mixing results in a distribution of residence times of fluid elements flowing through the reactor.

Taylor (2, 3), considering both theoretically and experimentally the process of axial dispersion in a fluid flowing through a pipe in either laminar or turbulent isothermal flow, showed that for sufficiently long pipes the dispersion may be successfully treated as apparent axial diffusion about a plane moving through the pipe with the fluid mean velocity. Tichacek, Barkelew, and Baron (4) improved upon Taylor's treatment of axial mixing in isothermal turbulent flow, using more exact experimental velocity profiles. They noted the sensitivity of the calculated apparent axial diffusivity to small changes in the fluid velocity profile.

In chemical reactors heat generation (or consumption) by the reaction(s) and cooling (or heating) of the pipe walls create significant radial temperature gradients, which in turn may result in radial variations of physical properties of the flowing fluid sufficient to cause important differences between the velocity profile in the reactor and that anticipated for isothermal flow. If the velocity profile is changed, the apparent axial diffusivity will also be affected. This paper presents the results of an investigation to determine under what flow conditions such radial temperature gradients may have an important effect on the rate of axial mixing and to formulate methods of calculating the magnitude of the effect of a temperature gradient on the apparent axial diffusivity for arbitrary flow and heat-generation conditions.

The investigation has been limited to cases in which the fluid flowing is a liquid. In such cases the primary effect of a radial temperature gradient on axial mixing is through its effect on the viscosity, since other physical properties of the liquid are much less sensitive to temperature change than the viscosity. Effects of temperature on the molecular diffusivity and the fluid density have been neglected in this study.

CALCULATION METHODS

The general method employed has been the calculation of the effective axial diffusivity for a particular flow condition in which the fluid is isothermal and subsequently the calculation of the value of E for a similar flow with radial temperature variation. The ratio of the two values calculated is a quantitative measure of the effect of the imposed temperature gradient on the rate of axial mixing under this flow condition.

The effective axial diffusivity is defined as

$$Q = -\pi a^2 E \frac{\partial C_m}{\partial x} \qquad (1)$$

The equation relating the effective diffusivity to the velocity profile and radial diffusivity

$$E = (2/a^2) \int_0^a \frac{1}{r(\epsilon+\mathcal{D})} [\int_0^r (u-V) r' dr']^2 dr, \qquad (2)$$

has been derived by Tichacek, Barkelew, and Baron (4). It is necessary to know u and ϵ as functions of r in order to evaluate E.

Laminar Flow

In pure laminar flow

$$\epsilon(r) \equiv 0 \qquad (3)$$

and if the flow is also isothermal,

$$u(r) = 2V(1 - r^2/a^2) \qquad (4)$$

With a radial variation in viscosity the radial velocity gradient is related to the wall shear stress and the viscosity:

$$-\frac{du}{dr} = \frac{\tau_w r/a}{\mu(r)} \qquad (5)$$

In the calculation of velocity profiles it was assumed that

1. The temperature is either parabolic in radius (corresponding to uniform distribution of heat source or sink due to reaction) or quartic in radius (corresponding to a parabolic distribution of sources or sinks).

2. The relationship between temperature and viscosity is of the form

$$\mu(r) = \frac{K}{B + T(r)} \qquad (6)$$

3. The temperature is independent of axial position. (The heat transfer rate at the wall was equal to the heat generation rate in the fluid.) The velocity profile could then be calculated from

$$u = \frac{\tau_w}{K}\int_r^a \frac{r}{a}\,[B + T(r)]dr \quad (7)$$

The effective axial diffusivity calculated by the use of the velocity profile generated by Equation (7) differed from that calculated for the same flow at constant temperature by a multiplicative factor involving the two constants which characterize the assumed quartic temperature profile.

The assumed viscosity-temperature relationship, Equation (6), was selected because it provided an adequate fit (with ± 0.5 % over an 80°F. range) to handbook data (5) on the viscosity of water. Subsequent comparison with viscosity data for liquids of much higher viscosity showed that Equation (6) was less satisfactory for these liquids; however, calculated effective axial diffusivities were found to be relatively insensitive to changes in radial temperature (and viscosity) profiles. Hence the temperature-viscosity relationship need not fit viscosity data well in order that axial diffusivities may be estimated satisfactorily.

Turbulent Flow

In turbulent flow the velocity gradient is related to the viscosity and momentum eddy diffusivity:

$$-\frac{du}{dr} = \frac{\tau_w r/a}{\mu(r) + \epsilon(r)\rho} \quad (8)$$

Empirical equations for $\epsilon(r)$, given by Deissler (*1*) for fully developed turbulent flow through smooth tubes, were used:

$$\epsilon = n^2 u(a-r)\left[1 - \exp\left(-\frac{n^2 u(a-r)}{\mu_w/\rho}\right)\right] \quad (9)$$

and

$$\epsilon = -N^2 \frac{\left(\frac{du}{dr}\right)^3}{\left(\frac{d^2u}{dr^2}\right)^2} \quad (10)$$

in which n and N are constants, determined by Deissler as 0.124 and 0.36 respectively.

Equation (9) applies in the region near the wall where viscosity is important in determining the velocity profile:

$$0 < y^+ < 26;\ y^+ = (a-r)\sqrt{\frac{\tau_w \rho}{\mu_w}} \quad (11)$$

Equation (10) is applicable in the central turbulent core, for y^+ greater than 26.

To calculate a velocity profile, Equations (8) and (9) were combined in form

$$-\frac{du^+}{dz} = \frac{a^+ z}{\mu(r)/\mu_w + (1-z)(n^2 u^+ a^+)\{1 - \exp[-n^2 u^+ a^+ (1-z)]\}} \quad (12)$$

Equation (11) was numerically integrated from the wall to y^+ of 26 by the use of an assumed value of a^+, and Equation (6) and a parabolic temperature profile were numerically integrated to generate values of $\mu(r)$.

For the region of y^+ greater than 26, Equations (8) and (10) were combined, dropping the effect of viscosity from Equation (8). The resulting equation, in terms of dimensionless variables, may be solved analytically for a velocity profile involving the position z_1, velocity u^+_1, and velocity gradient $(du^+/dz)_1$, at which $y^+ = 26$:

$$u^+ - u^+_1 = 1/N\left\{\sqrt{z} - \sqrt{z_1} + A\log\left[\frac{A-\sqrt{z}}{A-\sqrt{z_1}}\right]\right\} \quad (13)$$

$$A = \sqrt{z_1} - 1/2N(du^+/dz)_1 \quad (14)$$

The region at the extreme center of the pipe

$$0 < z < 0.30 = z_2 \quad (15)$$

was fitted by a parabolic velocity distribution. This eliminated subsequent difficulties which would have arisen because the eddy diffusivity corresponding to Equation (13) becomes zero when z is zero. It is justified in this calculation because the contribution of this region to the axial diffusivity is very small. In the region defined by Equation (15) the velocity profile was given by

$$u^+ - u^+_2 = \frac{z_2^2 - z^2}{4Nz_2(A - \sqrt{z_2})} \quad (16)$$

The three sections of the velocity profile, Equations (16), (13), and the integral of Equation (12), were numerically integrated to obtain the mean velocity:

$$V^+ = \int_0^1 2u^+ z dz \quad (17)$$

In the calculation of the effective axial diffusivity the assumption was made that the eddy diffusivity for mass transfer was equal to that for momentum transfer. For the three regions of the velocity profile the diffusivities for radial mass transfer were then

$$\frac{\epsilon\rho}{\mu_w} + \frac{1}{N_{Sc}} = \frac{1}{N_{Sc}} + n^2 u^+ a^+ (1-z)\{1 - \exp[-n^2 u^+ a^+ (1-z)]\} \quad (18)$$

for $0 < y^+ < 26$

in which N_{Sc} is the Schmidt group $\mu_w/\rho\mathcal{D}$:

$$\frac{\epsilon\rho}{\mu_w} = 2N a^+ z(A - z) \quad (19)$$

for $26 < y^+$ and $z > 0.3$

$$\frac{\epsilon\rho}{\mu_w} = 0.6N a^+ (A - \sqrt{0.3}) \quad (20)$$

for $0 < z < 0.3$

Equation (2) was put into the dimensionless form

$$\frac{E}{DV} = a^+ V^+ \int_0^1 \frac{1}{z\alpha}\left[\int_0^z (u^+/V^+ - 1)z'dz'\right]^2 dz \quad (21)$$

with

$$\alpha = \frac{\epsilon\rho}{\mu_w} + \frac{1}{N_{Sc}} \text{ for } y^+ < 26 \quad (22)$$

and

$$\alpha = \frac{\epsilon\rho}{\mu_w} \text{ for } y^+ > 26 \quad (23)$$

The indicated integrations were carried out numerically to obtain a value of E/DV for the value of a^+ and the temperature profile used in the calculation.

Six values of E/DV were calculated for isothermal flow with a^+ equal to 130, 260, and 650, each with Schmidt numbers of 100 and 1,000.

Deissler's values for n and N apply strictly only for fully developed turbulent flow. For the transition region some adjustment is necessary to make Equation (12) fit the known velocity profiles (*4*). n = 0.0933 and N = 0.279 were found to be suitable for a^+ = 130 and were used in all calculations for this case. Deissler's values of 0.124 and 0.36 were retained in calculations at higher Reynolds numbers.

At a^+ of 130 and 650 E/DV was calculated for flow with parabolic temperature profiles such that the ratio of the viscosity at the center line to that at the wall was 0.1 and 10.0. Each calculation was made at Schmidt numbers of 100 and 1,000.

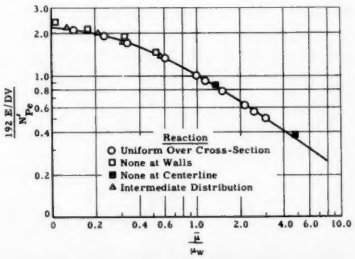

Fig. 1. Effective axial diffusivities for laminar flow of liquids in smooth tubes.

RESULTS

Laminar Flow

For isothermal laminar flow the result given by Taylor (2) may be put into the form

$$\frac{E}{DV} = \frac{DV/\mathcal{D}}{192} = \frac{N'_{Pe}}{192} \qquad (24)$$

For nonisothermal flow the ratio $(E/DV)_{\text{nonisothermal}}/(E/DV)_{\text{isothermal}}$ is conveniently expressed as a function of some characteristic of the radial viscosity profile. In Figure 1 this ratio is plotted vs. $\bar{\mu}/\mu_w$, the ratio of the viscosity of the fluid at the mixed mean temperature to the viscosity at the wall temperature. The effective axial diffusivity is relatively insensitive to the actual temperature profile. Calculated values for the extreme quartic temperature profiles (no reaction at the walls or no reaction at the center) lie within ± 10% of the curve in Figure 1 drawn through values calculated for parabolic temperature distributions (uniform heat generation or consumption over the pipe cross section).

Figure 1 shows that as the ratio $\bar{\mu}/\mu_w$ decreases, corresponding to extreme heat generation by reaction in the fluid and a high cooling rate at the walls, the effective axial diffusivity increases toward a limiting maximum approximately 2.6 times its value for comparable isothermal flow (at the same Peclet number for molecular diffusion). At the other extreme, with heat consumption in the liquid and heating at the pipe wall, E decreases toward zero as a limit.

The most important limitation on the applicability of Figure 1 is in the regions of very high or very low values of $\bar{\mu}/\mu_w$, where it is anticipated that the viscosity-temperature relationship, Equation (6), is no longer appropriate. If a value of E/DV is required for such conditions, it is recommended that it be determined by integration from Equations (2) and (5) by means of a parabolic temperature profile and an empirical viscosity-temperature relationship appropriate to the system being considered.

Turbulent Flow

Effective axial diffusivities were calculated at two values of the friction velocity Reynolds number, $a^+ = 650$ and 130. For each value E/DV was calculated for N_{Sc} of 100 and 1,000 with ratios of viscosity at the wall to viscosity at the center line of 0.1, 1.0, and 10.0. Figure 2, for $N_{Sc} = 1{,}000$, compares the values of E/DV calculated for nonisothermal flow with curves based on values of E/DV calculated by Tichacek, Barkelew, and Baron (4) for isothermal turbulent flow. The abscissa is the usual pipe-flow Reynolds number $DV\rho/\mu$, with the viscosity evaluated at the wall temperature.

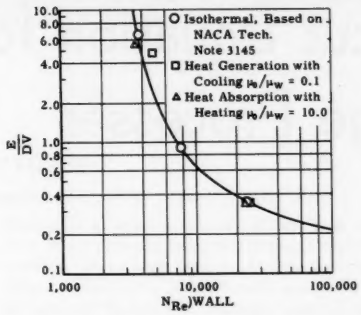

Fig. 2. Effective axial diffusivities for turbulent flow of liquids in smooth tubes at Schmidt number of 1,000.

For Reynolds numbers greater than 10,000 E/DV is not significantly affected by radial temperature gradients. The nonisothermal points in Figure 2 at N_{Re} of 20,000 to 25,000 deviate from the isothermal curve by only 3 to 6% in E/DV, much less than the 20 to 30% uncertainty associated with the calculation of E/DV for isothermal flow. Similar results were obtained for N_{Sc} of 100. Therefore Tichacek, Barkelew, and Baron's values of E/DV are recommended for turbulent flow at Reynolds numbers greater than 10,000, even though the heat generated by reaction causes significant radial variations in viscosity. In the selection of the value of E/DV the Reynolds number with the viscosity evaluated at the wall temperature should be used.

Transition Region

In flow with a radial temperature gradient it is not possible to characterize the transition between laminar and turbulent flow by a narrow range of Reynolds numbers. Temperature distributions with minimum viscosity at the wall stabilize laminar flow, and those with maximum viscosity at the wall tend to decrease the stability of laminar flow.

The points in Figure 2 at Reynolds numbers between 3,500 and 5,000 lie in a region in which either laminar flow may prevail or else the effect of the laminar sublayer region of the pipe is important in determining E/DV and thus the effect of the temperature gradient on the level of turbulence in the flow cannot be estimated accurately. These values of E/DV were calculated on the assumption that the flow is turbulent and that Equations (9) and (10) are applicable with the same values of the constants n and N that were used in calculating E/DV for isothermal flow. For the case in which heat is generated in the liquid and the walls are cooled, the calculated E/DV is larger than the true E/DV. In the alternate case the calculated E/DV is probably less than the true value.

NOTATION

A	= constant characteristic of a turbulent velocity profile
a	= pipe radius
a^+	= dimensionless pipe radius $a\sqrt{\tau_w\rho/\mu_o}$
B	= a constant
C_m	= area mean concentration
D	= pipe diameter
$\mathcal{D}$	= molecular diffusivity
E	= effective axial diffusivity
K	= a constant
n	= a constant
N	= a constant
N'_{Pe}	= Peclet number, $DV/\mathcal{D}$
N_{Re}	= Reynolds number, $DV\rho/\mu$
N_{Sc}	= Schmidt group, $\mu/\rho\mathcal{D}$
Q	= net transport of solute past reference plane moving with velocity V
r	= radial coordinate
u	= time-average velocity at a point
u^+	= dimensionless local velocity, $u/\sqrt{\tau_w/\rho}$
V	= mean velocity over pipe cross section
V^+	= dimensionless mean velocity $V/\sqrt{\tau_w/\rho}$
x	= axial distance from a reference plane moving with velocity V
y^+	= dimensionless distance from wall $(a-r)\sqrt{\tau_w\rho/\mu_w}$
z	= dimensionless radial coordinate, r/a

Greek Letters

α	= total radial diffusivity
ϵ	= coefficient of eddy transport
ρ	= density
τ_w	= wall shear stress
μ	= local viscosity
$\bar{\mu}$	= viscosity at mean fluid temperature
μ_o	= viscosity at temperature at pipe center line
μ_w	= viscosity of fluid at the wall temperature

LITERATURE CITED

1. Deissler, R. G., *Natl. Advisory Comm. Aeronaut. Tech. Note 3145* (May, 1954).
2. Taylor, G. I., *Proc. Roy. Soc. (London)*, **A219**, 186 (1953).
3. *Ibid.*, **A223**, 446 (1954).
4. Tichacek, L. J., C. H. Barkelew, and Thomas Baron, *A.I.Ch.E. Journal*, 3, 439 (1957).
5. Hodgman, C. D., ed., "Handbook of Chemistry and Physics," 31 ed. Chemical Rubber Publishing Company, Cleveland, Ohio (1949).

Manuscript received July 23, 1959; revision received December 8, 1959; paper accepted December 10, 1959.

General Short-cut Equation for Equilibrium Stage Processes

BUFORD D. SMITH and W. K. BRINKLEY

Humble Oil and Refining Company, Baytown, Texas

An equation for the prediction of the separation of a multicomponent mixture in equilibrium stage processes is presented. The equation is applicable to extraction processes with up to three feeds (an intermediate feed, a feed at the extract end, and the solvent feed at the raffinate end) and both raffinate and extract reflux. In its simplest form (simple extraction, stripping, or absorption) the equation reduces to the familiar Kremser equation. The use of the equation to solve multicomponent distillation and extraction problems is illustrated by examples.

Shortcut methods for the approximate solution of multicomponent, multistage, separation problems continue to serve useful purposes even though computers are available to provide rigorous solutions. In some problems the available equilibrium data may not be sufficiently accurate to justify the longer rigorous methods. In design studies a large number of cases can be worked quickly by a short-cut method to pinpoint the optimum conditions and then the exact solution found by some longer rigorous method. Such a procedure saves valuable computer time, since the time required for the rigorous method usually exceeds that for the short-cut method by a factor of ten or more. If a computer is not available, the designer usually must rely on the short-cut method alone.

This paper presents an analytical short-cut equation which is applicable to all equilibrium stage processes with any number of stages and handling any number of components. It is derived for an extraction column with three feeds (an intermediate feed, a feed at the extract end, and the solvent feed at the raffinate end) plus both raffinate and extract reflux, and it takes into account the degree of separation obtained for each component in the extract solvent recovery device. The complex equation for this complicated process reduces to correspondingly simpler expressions for operations which have fewer feeds and refluxes. Alders (*1*) and Tiller (*12*) have presented some of the simpler forms for extraction. In the case of a simple absorption or stripping column, the equation reduces to the familiar Kremser (*6*) equation. The forms for distillation and the more complicated extraction processes have not appeared before in the literature.

NOMENCLATURE

This section also applies to the next article in this issue.

Standard chemical engineering symbols (*11*) are used for the streams and concentrations. Standard usage requires that extract and raffinate concentrations be denoted as x and y respectively. This convention permits the same equations to be written for extraction as for distillation, absorption, and stripping.

The convention of numbering the stages from the bottom for the vapor-liquid processes (distillation, absorption, and stripping) and from the extract end for extraction is used in this paper. For the sake of uniformity an extraction column or train will always be depicted with stage 1 (extract end) at the bottom regardless of the actual direction of flow. In those extraction problems, where the extract is actually the lighter phase, the phrase stages below the feed stage should be interpreted as stages between the feed stage and the extract end.

Figure 1 is a sketch of the most complicated process considered. Note the use of N to designate the total number of stages and the use of M to denote the number of stages below the feed stage. The intermediate feed stage is designated as the $M + 1$ stage.

STATEMENT OF PROBLEM

This section also applies to the next article in this issue.

The number of design variables which must be specified by the designer of a multicomponent, multistage, separation process can be calculated by the method of Kwauk (*7*). In the solution method described in this paper the following variables are always specified: pressure in each stage; heat leak in each stage; the rate, temperature, pressure, and composition of all feed streams (including the solvent); total number of stages; and number of stages below the feed. In the case of an extraction process with extract reflux, it is also always necessary to specify g for each component in such a manner as to ensure a single phase extract product and reflux.

In addition to the variables which are always specified, it will be necessary to specify certain of the following: reflux ratios, product rates, maximum phase rates within the column or train, recovery of certain components, heat load in reboiler or condenser, and temperature at some point. Once the correct number of design variables has been specified, the complete set of product rates and compositions can be calculated.

This manner of defining the problem has the disadvantage of not permitting the direct calculation of the required solvent-to-feed ratio or the number of stages required to obtain a desired separation or product purity, but it does simplify the convergence problem when a computer is used. If a new column is being designed, several cases must be calculated with specified solvent-to-feed ratios, number of stages, and reflux ratios until the desired separation or purity is obtained. However most design problems involve the study of several cases to define the optimum conditions for economic appraisal, and therefore the reliance on the case-study approach is not a serious drawback. If desired, the short cut calculation procedure can be rearranged to give N and the solvent rate directly, but this is not covered in this paper. If the performance of an existing unit is being studied, the designer usually will have no control over the first five specifications and the above method of defining the problem is the only possible one. Also this approach eliminates the need of worrying about minimum solvent treats and minimum refluxes.

REPRESENTATION OF EQUILIBRIUM DATA

The equilibrium data is utilized in the form of the distribution coefficient $K = y/x$. In the short-cut equations the K's always appear as part of the stripping factors S_n or S_m. Ternary liquid-liquid data can be represented by plotting the K's vs. the concentration of any one of the three components. Quaternary liquid-liquid data can be represented satisfactorily by plotting the K's vs. the major solvent component (lowest K values) with concentration parameters of the component which has the next lowest K values. The correlation of the K values vs. two phase concentrations is justified by the phase rule. A four component, two phase systems (a vapor phase cannot exist if the system pressure is

Buford D. Smith is at Purdue University, Lafayette, Indiana.

greater than the vapor pressure of the liquid phases) has a variance of four. Once the temperature and pressure are specified, the specification of two-phase concentrations is sufficient to define one unique state of the system and fix all the distribution coefficients. Work is underway to develop a general correlation scheme for nonideal solution systems having more than four components, and it is hoped that the results will warrant future publication.

SHORT-CUT EQUATION*

The material presented below indicates the general method of attack.

The calculus of finite differences can be used to relate the concentration of any given component to the stage number. The distribution coefficient and the phase rates must be assumed constant within the column section under consideration if a simple analytical solution of the difference equation is desired. If these assumptions are made, the following equations can be written for each component. For the upper (or raffinate) end

$$x_n = C_1(S_n)^n + C_2 \qquad (1)$$

For the lower section (or extract) end

$$x_m = C_3(S_m)^m + C_4 \qquad (2)$$

Eliminating the constants in Equations (1) and (2) by component balances around stages N and 1 respectively, and then combining the two equations with a component balance around the feed stage, one gets the following general expression for the process pictured in Figure 1:

$$f = \frac{(1-S_n^{N-M}) + q_s(S_n^{N-M}-S_n) + R(1-S_n) + hq_{F'}S_n^{N-M}(1-S_m^{M})}{(1-S_n^{N-M}) + hS_n^{N-M}(1-S_m^{M}) + R(1-S_n) + h\left(\frac{1+R'}{1+gR'}\right)S_m^{M}S_n^{N-M}(1-S_m)} \qquad (3)$$

Equation (3) predicts the fraction of any given component which will be recovered at the lower (or extract) end of the column. The fractional recoveries of the various components will vary as their respective stripping factors vary. At $S = 1.0$, Equation (3) and all of its simpler forms take on the indeterminate form 0/0. The value of f at $S = 1.0$ is found by differentiating the numerator and denominator and evaluating the new fraction thus obtained.

For processes simpler than the one pictured in Figure 1 the applicable form of Equation (3) is correspondingly simpler. For a simple extraction or absorption process having only one feed and no refluxes, ($R = R' = F' = q_{F'} = M =$ zero and $S_n = S_m$), Equation (3) reduces to the following form of the Kremser equation:

$$f = \frac{1 - q_s S - S^N(1-q_s)}{1 - S^{N+1}} \qquad (4)$$

For a component entering only in the feed $q_s = 0$, and

$$f = \frac{1 - S^N}{1 - S^{N+1}} \qquad (4a)$$

If $q_s = 1.0$, the component enters only in the solvent, and

$$f = \frac{1 - S}{1 - S^{N+1}} \qquad (4b)$$

The expression for an extraction process with one feed and raffinate reflux is also quite simple. For $q_s = 0$

$$f = \frac{1 - S^N + R(1-S)}{1 - S^{N+1} + R(1-S)} \qquad (5a)$$

For $q_s = 1.0$

$$f = \frac{1 - S + R(1-S)}{1 - S^{N+1} + R(1-S)} \qquad (5b)$$

Casual inspection of Equations (5a) and (5b) might indicate that the use of raffinate reflux affects the recovery of a given component. However as R changes, the stripping factor must also change, and the net result is no change in f. This can be easily demonstrated for a one-stage process. The representative phase rates to be used in the calculation of the stripping factor for one stage are the equilibrium phase rates leaving the stage.

Whenever an intermediate feed is involved, S_n does not equal S_m and average stripping factors for each component must be estimated for both sections of the column. The applicable forms of Equation (3) and a method of obtaining average stripping factors for each section are illustrated in the example problems for an extraction process with extract reflux and a distillation process with total condenser and a partial reboiler.

The correct stripping factors for any given component are, of course, those which predict the correct recovery for that component under the specified column conditions. A trial-and-error procedure is required to closely approximate the correct recovery. Average K values are assumed for each component, and these are combined with a set of assumed or specified phase rates to provide the initially assumed stripping factors. The stripping factors are used with the appropriate form of Equation (3) to predict a recovery, f, for each component. The recoveries are used to calculate better approximations of product rates and compositions. A new set of K values are obtained from the new end compositions and are combined with the new stream rates to provide the stripping factors for the next trial.

Convergence is rapid, and two trials are usually sufficient if the initial assumptions are of the correct order of magnitude. If the initially assumed rates differ widely from the rates calculated in the first trial, it is necessary in some cases to repeat the first trial with the same set of K values and more reasonable rate assumptions. The extraction example presented later illustrates the effect of poor, initial product-rate assumptions on the speed of convergence. The initially assumed extract product rate was off by a factor of 20 (50 compared with 2.5), but three trials were sufficient to obtain satisfactory convergence.

In computer-logic terms the solution of Equation (3) involves two major loops. The first, or inside, loop calculates the set of stream rates and end compositions which correspond to the set of assumed K values. Complete convergence can be obtained in this loop if desired; that is there is only one set of rates and compositions for any given set of assumed K's. The second, or outside, loop uses the compositions obtained in the first loop to calculate a better set of K values and then returns the calculations to the first loop. Convergence is not so well defined in the outside loop. Each correction in the K values results in a subsequent correction in the next trial in the same direction, and if too many trials are made, the solution may gradually drift away from the correct one.

Solution time is shortened in stripping, absorption, and extraction calculation by making only one trial for each set of K values. Complete convergence in the inside loop is never desired in distillation calculations if the product rates are specified. The K values are adjusted after every trial until the rate specifications are met.

APPLICATION TO DISTILLATION

The form of Equation (3) applicable to a distillation column with a total condenser is obtained by setting $q_s = q_{F'} = R' = g = 0$ and combining the second and fourth terms in the denominator to give

* The complete derivation is available as document 6352 with the American Documentation Institute, Photoduplication Service, Library of Congress, Washington 25, D. C., and may be obtained for $1.20 for photoprints or for 35-mm. microfilm.

Table 1. Comparison with Graphical Solution Results for Two Ternary Extraction Systems

Comparison I

Process: One feed. No reflux. Eight stages.
System: Acetone (A)—Chloroform (C)—Water (S) at 25°C.
Range of K's: A = 1.8-3.7 C = 35-143 S = 0.009-0.028

Method	B	D	x_A	x_C	x_S	y_A	y_C	y_S
Graphical	204.1	52.4	0.221	0.015	0.764	0.090	0.900	0.010
Analytical	199.3	57.2	0.211	0.009	0.780	0.139	0.841	0.019

Comparison II

Process: Two feeds. No reflux. 5.4 stages.
System: Acetone (A)—Water (C)—Monochlorbenzene (S) at 25°C.
Range of K's: A = 0.93-0.99 C = 154-465 S = 0.0016-0.0027

Method	B	D	x_A	x_C	x_S	y_A	y_C	y_S
Graphical	141.2	89.6	0.140	0.006	0.854	0.010	0.989	0.001
Analytical	140.8	90.0	0.139	0.005	0.856	0.011	0.987	0.002

$$f = \frac{(1 - S_n^{N-M}) + R(1 - S_n)}{(1 - S_n^{N-M}) + R(1 - S_n) + hS_n^{N-M}(1 - S_m^{M+1})} \qquad (6)$$

Note that Equation (6) is the equation written earlier for an extraction column with one feed and raffinate reflux but with an additional term in the denominator to take into account the second section of the column present in a complete distillation column.

Equation (6) is applicable to distillation columns having either a partial reboiler or heat input to the bottom plate. The lowest equilibrium stage must always be numbered one regardless of whether it is a partial reboiler or the bottom theoretical plate. Equation (6) is not strictly applicable to a column with a partial condenser since it ignores any possible difference between the overhead and reflux compositions. However the effect of a partial condenser can be closely approximated by increasing N by 1.0.

The distillation problem, particularly if it concerns an existing column, is conveniently defined by specifying distillate rate, D/F; maximum allowable vapor rate, V/F, at some point in the column; and condenser load equal to the latent heat of condensation of V_N in addition to the first five specifications listed in Statement of Problem.

If ideal solutions are assumed, the K values are functions of temperature only at the specified tower pressures. Estimation of the K values therefore reduces to the estimation of the temperature profile. Good initial estimates of the top and bottom temperatures are obtained by splitting the feed in a reasonable manner and performing dew- and bubble-point calculations on the resulting overhead and bottom streams. The feed tray temperature can be estimated roughly by a bubble-point, dew-point, or flash calculation on the feed depending upon the thermal condition. However it is easier, and often as accurate, to read the initially assumed feed tray temperature from a straight line drawn between the assumed top and bottom temperatures.

The liquid and vapor rates are assumed to be constant within any column section, and their values are fixed by the specification of the feed, maximum vapor rate, distillate rate, and the thermal condition of the feed. Since the phase rates remain constant from trial to trial, the stripping factors can be varied only by changing the K values. This is done by adjusting the temperature profile. The top and bottom temperatures cannot be adjusted arbitrarily since they must always correspond to the dew and bubble points of the overhead and bottom streams respectively. The iteration variables therefore reduce to one, the feed tray temperature. The calculator must adjust this temperature until the vapor- and distillate-rate specifications are met. This method of calculation is analogous to the technique of a column operator who adjusts the control tray temperature until the column is loaded or until the product specifications are met.

Consider as an example the following typical plant problem. A bubble-point feed which contains 5% C_3, 15% i–C_4, 25% n–C_4, 20% i–C_5, and 35% n–C_5 is to be fed to a column with ten theoretical stages, feed on the sixth stage from the bottom, a total condenser and a maximum top vapor capacity of about 1.75 times the amount of feed to be charged. The column pressure is 120 lb./sq. in. abs. Curves which relate the losses of n–C_4 and i–C_5 in the bottom and overhead product streams respectively to the overhead rate must be developed to serve as a basis for economic calculations to pinpoint the optimum overhead rate.

Only one point on the curves (at D/F = 0.489) will be considered. Specification of D/F and the limitation of V_N/F to 1.75 fixed the phase rates per 100 moles of feed at $V = V'$ = 175, L = 126.1, and L' = 226.1 Also B = 51.1 and R = 2.581. The initially assumed temperature profile based on bubble-and dew-point calculations as described previously was 165°F. at the top, 185°F. at the feed, and 236°F. at the bottom. Average K values for each section were evaluated at the arithmetic average temperature for that section. The 165–185–234°F. (top-feed-bottom) profile resulted in calculated V_N and D rates of 162.3 and 42.5 respectively compared with the specified values of 175 and 48.9. The assumed temperature profile for the second trial was 165–210–236°F., and V_N and D rates of 177 and 49.5 were calculated. Once the specifications have been approached this closely, the calculated end compositions can be used to provide better end temperatures, by means of dew- and bubble-point calculations. The final temperature profile (third trial) was 163.5–210–234°F., and this profile met the V_N and D specifications exactly. A rigorous computer solution

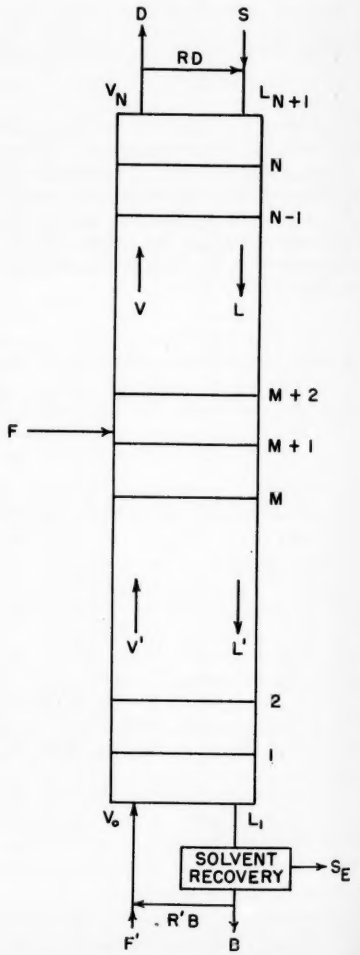

Fig. 1. Process variables and nomenclature.

of the same problem by the Thiele-Geddes method (8) provided temperatures of 166°, 202°, and 234°F. for the top, feed, and bottom stages. The rigorous solution predicted the recovery of nC_4 and iC_5 in the overhead as 92.5 and 17.9% respectively. Equation (6) predicted 90.5 and 17.9%.

The major advantage of Equation (6) over other short-cut distillation equations (3, 5) is that it provides a good estimate of the feed tray temperature as well as the end temperature. Knowledge of the intermediate temperature permits the estimation of average K values for each section rather than for the entire column. Also the three point temperature profile is helpful if the short-cut results are to be used as the initial assumptions for a rigorous computer solution. Another advantage of Equation (6) is that it makes its predictions at a specified reflux ratio rather than at total or minimum reflux. Probably the most widely used short-cut distillation method at the present time involves a combination of the Fenske total reflux equation (3), the Underwood minimum reflux equations (14), and the Gilliland (4) correlation. This method does not provide an estimate of the feed tray temperature and when applied to the above example predicts the nC_4 and iC_5 recoveries in the overhead product as 96.5 and 17.1% respectively.

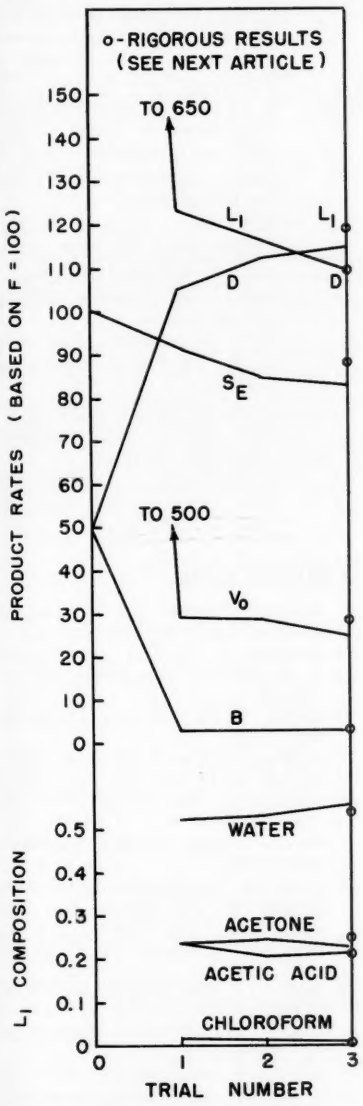

Fig. 2. Partial summary of results from short-cut solution of extraction example. Values at zero trial number are the initial assumptions. Circles at trial number three are results from rigorous method described in next article in this issue.

APPLICATION TO EXTRACTION

Immediately after its derivation the correctness of Equation (3) was checked by solving several ternary extraction problems and comparing the results with graphical solutions. To conserve space only two of the comparisons are shown in Table 1. The agreement is good and substantiates the validity of Equation (3).

In extraction calculations it is not usually convenient to specify the product rates. Therefore the rates become iteration variables and vary from trial to trial as the K values are changed. Also ideal solutions cannot be assumed, and the K values must be calculated as a function of the phase compositions. The relations between the K's and the phase compositions are not linear, and an average K for a column section should be obtained by averaging several K values evaluated at various typical stage compositions along the section.

The application of Equation (3) to extraction calculations will be illustrated by the calculation of the recovery of acetone (20 wt. %) from chloroform (80 wt. %) with a mixed solvent composed of water (65 wt. %) and acetic acid (35 wt. %). Experimental tie-line data at 25°C. for this system have been published by Brancker, Hunter, and Nash (2), and additional tie lines have been calculated by Smith (10). A five-stage column or train was specified with the feed introduced in the middle stage. A 1:1 solvent-feed ratio was used, and in order to illustrate one of the more complicated forms of Equation (3) an extract reflux ratio of $R' = 10$ was specified. It was assumed that 98% of the water and acetic acid in L_1 were recovered in S_E and that 1% of the acetone and chloroform in L_1 appeared in S_E.

The solution of this problem by graphical means (9, 10, 13) is difficult and time consuming, but it can be approximated easily through the use of Equation (3). Also Equation (3) can be applied to a system of any size, whereas graphical methods are restricted to a maximum of four components.

Since $R = F' = q_{F'} = 0$ and N and M equal 5 and 2 respectively, Equation (3) reduced to

$$f = \frac{(1-S^3{}_n) + q_s\,(S^3{}_n - S_n)}{(1-S^s{}_n) + hS^3{}_n\,(1-S^2{}_m) + h\left(\frac{1+R'}{1+gR'}\right)S^2{}_m\,S^3{}_n\,(1-S_m)} \qquad (7)$$

The individual K values for the first trial were obtained by an arithmetic average of all the experimental values available. To illustrate that the speed of convergence is little affected by the initial rates assumed, the feed was assumed to split equally between the overhead and bottom products, D and B. In all but very high solvent treat cases the extract phase rate can be assumed to vary linearly from the solvent, $S = L_{N+1}$, to L_1. The raffinate phase rates were then calculated by material balances. Average phase rates for each section were obtained by averaging the phase rates at the ends of the section. Stripping factors for each component were then calculated from the average rates and K values for use with Equation (7) to predict the various component recoveries.

The amounts of each component leaving each end of the column were calculated from the following definitions of f:

$$Bx_B + S_E\,x_{SE} = f(Fy_F + F'y_{F'} + Sx_S) \qquad (8)$$

$$Dy_D = (1-f)\,(Fy_F + F'y_{F'} + Sx_S) \qquad (9)$$

The amounts of each component in B and L_1 were then obtained from the following component balances:

$$Bx_B = \left(\frac{1-g}{1+R'g}\right)(Bx_B + S_E\,x_{SE}) \qquad (10)$$

$$L_1\,x_1 = \left(\frac{1+R'}{1-g}\right)Bx_B \qquad (11)$$

The new end rates and compositions calculated from Equations (8) to (11) permitted the estimation of better values of K, S_n, and S_m for each component for the next trial. The trials were continued until the K values obtained from the results of one trial were es-

sentially the same as those obtained from the previous trial. Some of the calculated results are shown in Figure 2. Note how erroneous the initially assumed rates were and how reasonable the results of the first trial were despite the poor assumptions. The K and K' values from trial 3 agreed well enough with those from trial 2 to end the calculations. In fact, the calculations could have been stopped after any trial without serious error. Each trial in the example required about 2 hr. calculation time.

The open circles plotted at trial 3 in Figure 2 represent the results of a more rigorous calculation method described in the next paper. Note that the results of trial 2 agree better with the rigorous method results than do those of trial 3. This illustrates the previously mentioned tendency of the short-cut method to drift away from the correct solution if too many trials are made.

The accuracy of the results shown in Figure 2 was checked by the graphical method of Powers (9). The product rates and compositions along with all the stage compositions obtained by the rigorous method were located on the projection of the two-phase surface on the water-chloroform-acetic acid face of the tetrahedron. The difference points were located, and the five stages stepped off. The rigorous method results agreed surprisingly well with the graphical construction considering the practical difficulties encountered in the accurate graphical representation of the phase-equilibrium data for a four-component system.

EXTRACTION PROBLEMS WITH HIGH SOLVENT-TO-FEED RATIOS

Two difficulties arise in problems with high solvent-to-feed ratios. First both the extract and raffinate rates undergo a large change through stage N if raffinate reflux is not used to presaturate the entering solvent. Care must be taken to ensure that the average L and V used for the raffinate end of the column are reasonable. It may be better to use V_{N-1} and L_N rather than D and S in the calculation of average rates in the raffinate end. A small error in estimating the large extract rates can cause a large percentage error in the smaller raffinate rates and a corresponding error in the stripping factors. Second a very small error in the predicted f for a solvent component (low K and large f) will result in a large percentage error in D. For example in one system studied the f predicted for component S was 0.9892 compared with the correct value of 0.9972. As a result the calculated concentration of the solvent in D was 0.30 compared with the correct value of 0.073. This difficulty can be simply corrected by checking the calculated solvent concentration in the raffinate against the solubility data and making the needed adjustment. This problem arises only with components which have low K values (solvent components), but it is, of course, possible to use the experimental solubility data to check the product concentration of any of the components.

NOTATION

A = total amount of component a entering the column

B = heavy or extract product rate, moles, weight, or volume per unit time

C_1, C_2, C_3, C_4 = constant coefficients in solutions of difference equations

D = light or raffinate product rate, moles, weight, or volume per unit time

E = operator in difference equation

f = fraction of a given component which is recovered in B (or $B + S_E$ in extraction)

F = upper feed rate, moles, weight, or volume per unit time

F' = lower feed rate if only one feed is used, $F' = 0$ and $M = 0$

g = $S_E x_{SE}/L_1 x_1$ = fraction of a given component in L_1 which is removed with S_E

h = $(L - KV)/(L' - K'V')$ if intermediate feed is similar to light or raffinate phase ($K_{M+1} = K$). Use

$$h = \frac{(L/K) - V}{(L'/K') - V'}$$

if intermediate feed is similar to heavy or extract phase ($K_{M+1} = K'$). If the column contains only one section, $h = 1.0$

K = y/x = distribution coefficient. Primes denote lower or extract section of column

L = heavy or extract phase rate, moles, weight, or volume per unit time

m = subscript referring to any stage in lower or extract end of column (stages 1 to M)

M = number of theoretical stages below the feed stage, $M + 1$

n = subscript referring to any stage in upper or raffinate end of column (stages $M + 2$ to N)

N = total number of theoretical stages including partial reboiler if any but excluding partial condenser if any

q_s = fraction of a given component which enters in the fresh solvent stream S

$q_{F'}$ = fraction of a given component which enters in the lower feed F'

q_F = $1 - q_s - q_{F'}$ = fraction of a given component which enters in the upper feed F

R = external reflux ratio at top or raffinate end of column, amount of reflux/amount of product or $(L_{N+1} - S)/D$

R' = external reflux ratio at bottom or extract end of column, amount of reflux/amount of product or $(V_0 - F')/B$

S = fresh solvent rate, moles, weight, or volume per unit time, also S is used for stripping factor when $S_n = S_m$

S_E = solvent rich material recovered in the extract solvent recovery equipment, moles, weight, or volume per unit time

S_n = KV/L = component stripping factor in upper or raffinate end of column, with K, V, and L representative averages for the section

S_m = $K'V'/L'$ = component stripping factor in lower or extract end of column, with K', V', and L' representative averages for the section

V = light or raffinate phase rate, moles, weight, or volume per unit time

x = concentration in heavy or extract phase, units consistent with units on rates

y = concentration in light or raffinate phase, units consistent with units on rates

LITERATURE CITED

1. Alders, L., "Liquid-Liquid Extraction," Elsevier, New York (1955).
2. Brancker, A. V., T. G. Hunter, and A. W. Nash, *J. Phys. Chem.*, **44**, 683 (1940).
3. Fenske, M. R., *Ind. Eng. Chem.*, **24**, 482 (1932).
4. Gilliland, E. R., *ibid.*, **32**, 1220 (1940).
5. Harbert, W. D., *ibid.*, **37**, 1162 (1945).
6. Kremser, A., *Nat. Petrol. News*, **22** (May 21, 1930).
7. Kwauk, Mooson, *A.I.Ch.E. Journal*, **2**, 240 (1956).
8. Lyster, W. N., Private communication, Humble Oil and Refining Co., Baytown, Texas (May, 1959).
9. Powers, J. E., *Chem. Eng. Progr.*, **50**, 291 (1954).
10. Smith, J. C., *Ind. Eng. Chem.*, **36**, 68 (1944).
11. Souders, Mott, Jr., *Chem. Eng. Progr.*, **52**, 255 (1956).
12. Tiller, F. M., *ibid.*, **45**, 391 (1949).
13. Treybal, R. E., "Liquid Extraction," 1 ed., p. 211, McGraw-Hill, New York (1951).
14. Underwood, A. J. V., *Chem. Eng. Progr.*, **44**, 603 (1948).

Manuscript received January 2, 1959; revision received December 17, 1959; paper accepted December 28, 1959.

Rigorous Solution of Multicomponent, Multistage Extraction Problems

BUFORD D. SMITH and W. K. BRINKLEY

Humble Oil and Refining Company, Baytown, Texas

A new rigorous calculation and convergence method for multicomponent equilibrium stage processes is presented, and the application to multicomponent, multistage extraction problems is described. The application to the vapor-liquid equilibrium stage processes is discussed briefly.

The rigorous graphical solution of multicomponent extraction problems (*2, 3, 5*) is limited to four component systems. No well-known method exists at the present time for the rigorous solution of multicomponent extraction problems with more than four components in a manner analogous to the complete solution of distillation problems by the widely used Lewis-Matheson (*1*) and Thiele-Geddes (*4*) methods.

The calculation of any equilibrium stage process involves the same basic equilibrium relationships and mass and enthalpy balances. These basic relationships however can be applied in a seemingly endless variety of ways, and a method which works well for one process may not be the most convenient method for another. For example a calculation and convergence method which functions well in distillation where the temperature profile is an iteration variable and a function of composition may not work at all for extraction problems where the temperature profile is specified and the stage temperatures cannot be adjusted to make Σy's or Σx's $= 1.0$.

This paper presents a general calculation and convergence procedure for all equilibrium stage processes. The new method is applied specifically in this paper to multicomponent, multistage extraction problems. The application of the method to distillation, absorption, and stripping calculations is under investigation.

Buford D. Smith is at Purdue University, Lafayette, Indiana.

DERIVATION OF ERROR (OR CONVERGENCE) EQUATION

The stage-to-stage calculation method described in this paper for extraction begins with the assumption of an L_1 composition and the phase-rate profiles through the column. A stage-by-stage calculation up the column provides a calculated composition of the fresh solvent based on the L_1 composition and rate profiles assumed. The differences (or errors) between the component concentrations in the calculated solvent composition and those specified in the problem statement are then used to correct the assumed L_1 composition and rate profiles for the next trial. An equation which relates the error in a calculated solvent concentration to the error for the same component in the assumed L_1 composition can be derived in the following manner.

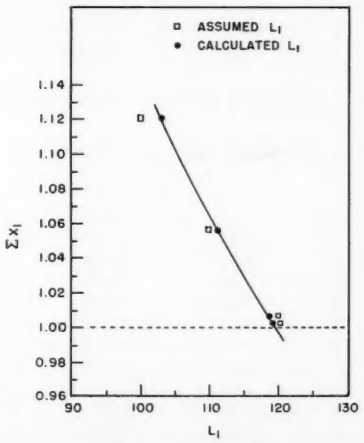

Fig. 1. Results of the four iterations. Convergence is obtained when $\Sigma\ x_1 = 1.0$ or when the calculated L_1 equals the assumed L_1.

Define y_n and x_n as the correct concentrations for the given component in the raffinate and extract phases leaving stage n. The calculated concentrations in all but the last trial will differ from these correct values. Denoting the differences between the calculated and correct values by e_{yn} and e_{xn} one can write the following equalities for each component:

Calculated raffinate concentration

$$= y_n + e_{yn}$$

Calculated extract concentration

$$= x_n + e_{xn}$$

For any given component in stage 1

$$y_1 = K_1 x_1$$

$$y_1 + e_{y1} = K_1(x_1 + e_{x1})$$

$$e_{y1} = (y_1 + e_{y1}) - y_1 = K_1 e_{x1}$$

The use of a material balance around stage 1 gives

$$e_{x2} = \left(S_1 + k\frac{L_1}{L_2}\right) e_{x1}$$

where $k = (1 + gR')/(1 + R')$.

Continuing up the column by the alternate use of equilibrium and material

balance relationships results in the following general expressions which relate the error in any stream entering or leaving a stage to e_{x1}:

$$e_{y_n} = K_n\left(S_1S_2 \ldots S_{n-1} + k\frac{L_1}{L_2} S_2S_3 \ldots S_{n-1} + \ldots k\frac{L_1}{L_{n-1}} S_{n-1} + k\frac{L_1}{L_n}\right) e_{x1} \quad (1)$$

$$e_{x_{n+1}} = \left(S_1S_2 \ldots S_n + k\frac{L_1}{L_2} S_2S_3 \ldots S_n + \ldots k\frac{L_1}{L_{n-1}} S_{n-1}S_n + k\frac{L_1}{L_n} S_n + k\frac{L_1}{L_{n+1}}\right) e_{x1} \quad (2)$$

If R' is zero (no extract reflux), k becomes 1.0. In the absence of raffinate reflux $e_{x_{n+1}} = e_{x_s}$, $L_{n+1} = S$, and Equation (2) relates e_{x_s} to e_{x_1}. If raffinate reflux is used either alone or with extract reflux, Equation (2) does not apply to the solvent stream and the following equation must be used in conjunction with Equation (1) to relate e_{x_s} and e_{x_1}:

$$S\, e_{x_s} = D\, e_{y_N} + L_1\, e_{x_1} \quad (3)$$

The number of feeds and their location have no effect on the error equation. The terms representing feed streams cancel in the derivation owing to the fact that the feed concentrations are specified and contain no errors.

Equations (1) and (2) can be applied directly to any process which involves a series of equilibrium stages. For a simple absorber $k = 1$, and Equation (2) relates an error in the calculated lean oil composition to the error for that component in the originally assumed rich oil composition. In distillation $k = 1$, and Equation (1) relates an error in the vapor leaving the top equilibrium stage (which may be a partial condenser) to the corresponding error in the assumed composition of the liquid leaving the lowest equilibrium stage (which may be a partial reboiler).

EQUILIBRIUM DATA

The representation of the equilibrium data is discussed in the previous article.

The reason for correlating the equilibrium data as a function of those components with the lowest K values is illustrated by Equations (1) and (2). A small K means a small stripping factor, and $e_{x_{n+1}}$ and e_{y_n} will not vary widely from e_{x1}. On the other hand a large K means a large stripping factor, and as the calculations proceed up the column, the errors may become very large. For example in one system studied the e_{x_0} for a component with a K value in the neighborhood of 100 varied between 10^{+8} and 10^{-8} for several trials, even though e_{x1} never exceeded $\pm$ 0.0015. If the equilibrium values are to be read as a function of the calculated phase compositions as the calculations proceed up the column, the K's must be plotted vs. the concentrations of stable components (low K values) since their stage concentrations will be reasonable even in the first trial. However if K profiles based on the corrected stage compositions from the previous trial are to be used, the K's may be correlated as a function of the concentrations of any two of the components. No matter how fantastic the calculated concentrations may be from any trial, application of the error equation provides a good, corrected set of stage compositions which can be used to select K values for the next trial.

CALCULATION PROCEDURE

The calculations begin with the assumption of phase-rate profiles and of the rate and compositon of L_1. Depending upon the number of feeds and refluxes used the following material-balance equations may be useful to calculate the end rates and compositions which correspond to the assumptions:

$$B = \frac{L_1}{1 + R'}(1 - \Sigma g\, x_1) \quad (4)$$

$$V_o y_o = F'\, y_{F'} + \frac{R'(1-g)}{1+R'} L_1 x_1 \quad (5)$$

Equation (5) must be written for each component, and the summation term in Equation (4) includes the gx_1 product for each component.

When one starts with the assumed x_1's and uses the assumed phase-rate profiles, stage-to-stage calculations are made up the column. These calculations are made in the usual manner (alternate use of the equilibrium and material-balance relationships) but with the exception that the calculated y's and x's are never normalized. Normalization of the phase compositions makes the error equation inapplicable. Also the almost correct concentrations of the stable components would be adversely affected by the large errors in the unstable component concentrations. The absence of normalization, in effect, means that each component is calculated through the column separately. The y's and x's in the various phases will sum to 1.0 in the last trial if true convergence is obtained and if the equilibrium data are correct.

The stage-to-stage calculation furnishes calculated compositions of streams V_N and L_{N+1}. If raffinate reflux is not used, $L_{N+1} = S$. If raffinate reflux is used, the calculated solvent concentration of each component is obtained from the following material balance:

$$x_s = \frac{L_{N+1}}{S} x_{N+1} - \frac{R}{R+1}\frac{V_N}{S} y_N \quad (6)$$

The e_{x_s} for each component is then

$$e_{x_s} = \text{calculated } x_s - \text{specified } x_s \quad (7)$$

Equations (1) and (2), plus Equation (3) if raffinate reflux is used, are now used to calculate the e_{x_1} for each component. The e_{x_1}'s can then be used with Equations (1) and (2) to correct all the phase concentrations throughout the column.

Once a corrected set of y_D's and x_1's are obtained, a new L_1 rate can be calculated by a simple component balance around the column. The solvent component with the lowest K value should be used in this balance since use of a less stable component may slow convergence. When extract reflux is used, the balance becomes somewhat com-

TABLE 2. CONCENTRATION PROFILES AND K VALUES FROM A TYPICAL TRIAL

System: acetone (A)—chloroform (C)—water (W)—acetic acid (H) at 25°C.

		x_A			x_C	
Stage	K_A	Calculated	Corrected	K_C	Calculated	Corrected
1	2.05	0.226	0.254	11.8	0.007	0.006
2	2.22	0.118	0.133	13.5	0.020	0.016
3	2.36	0.070	0.079	15.4	0.053	0.041
4	3.41	0.023	0.050	25.6	0.246	0.024
5	3.85	−0.073	0.036	30.8	7.41	0.021
S	—	−0.519	0.0	—	292.3	0.0
		x_W			x_H	
Stage	K_W	Calculated	Corrected	K_H	Calculated	Corrected
1	0.089	0.556	0.539	0.279	0.211	0.210
2	0.077	0.574	0.556	0.275	0.225	0.224
3	0.067	0.592	0.573	0.269	0.232	0.231
4	0.035	0.644	0.624	0.273	0.295	0.293
5	0.028	0.650	0.629	0.292	0.325	0.322
S	—	0.671	0.650	—	0.352	0.350

plicated, but the new L_1 can be calculated directly from

$$L_1 = \frac{F(y_F - y_D) + S(x_s - y_D) + F'(y_{F'} - y_D)}{x_1 \dfrac{(1+gR')}{(1+R')} + jy_D} \quad (8)$$

where $j = (R'/1 + R')(1 - \Sigma g x_1) - 1.0$. If no extract reflux is used, $R' = 0$ and the denominator reduces to $x_1 - y_D$.

Since V_0 is specified as a feed or can be calculated from the new L_1x_1's by Equation (5), it is now possible to calculate new rate profiles by means of solvent balances around the bottom end of the column (cutting V_0 and L_1). The next trial can then be made with the new rate profiles and the new rate and composition of L_1. The K values can be based on the corrected stage compositions from the previous trial or on the stage compositions obtained as the calculations move up the column.

The iteration described in the previous paragraphs converges rapidly (2 to 5 trials) to a constant set of rate profiles and to a constant L_1 rate and composition. The solution obtained however is determined by the L_1 and x_1's originally assumed. In other words repetition of the calculations with a different set of originally assumed L_1 and x_1's will produce a different solution. The correct solution is that one where the calculated x_1's and all the other stage concentrations sum to 1.0. To pinpoint the correct solution it is necessary to make three iterations with different assumed L_1 rates. The original x_1's assumed can be the same for all three iterations or they can be varied. After two of the three iterations are completed, a plot of the calculated Σx_1 vs. the calculated L_1 will indicate the L_1 at which $\Sigma x_1 = 1.0$. The third iteration with this L_1 will be close to the correct solution. It is not necessary to obtain convergence in the two preliminary iterations. One trial in each is usually sufficient to provide a Σx_1 which can be plotted to indicate the L_1 for the third trial.

The over-all convergence in distillation calculations is simpler than in extraction, absorption, or stripping. In distillation the L_1 or bottoms rate can be specified conveniently, and only one iteration is necessary. The convergence within this iteration may be slowed somewhat since in distillation there is no stream with fixed composition at the top comparable to the solvent in extraction or the lean oil in absorption. The change in the assumed overhead composition from trial to trial causes the error equation to be somewhat less effective as a convergence device and may increase the required number of trials slightly.

The time required per trial is roughly that required for any stage-to-stage distillation calculations with heat balances. For the four component, five stage extraction example presented below, the time per trial was about 5 hr. For three iterations with one trial for each of the first two iterations and two trials in the final iteration, the total calculation time for an experienced person would be about 20 hr. The number of trials required in any one iteration is independent of the number of stages and components.

EXAMPLE PROBLEM

The four component extraction example described in the previous paper was solved by the proposed rigorous method. Four iterations were made. The assumed and calculated L_1 rates and the Σx_1 for each iteration are shown in Figure 1. A plot of Σx_1 vs. the calculated L_1 rate for the first two iterations indicated an $L_1 = 120$ as the correct value. Two iterations were made at an assumed L_1 of 120 to check the effect of varying the assumed x_1's. Better values of the x_1's improve the trial results, but the L_1 rate seems to be the important iteration variable. A plot of Σx_1 vs. the calculated L_1 rate is essentially a straight line despite the two sets of assumed x_1's used.

Typical trial values of calculated and corrected stage compositions are shown in Table 1. The calculated values were the results of the stage-to-stage calculations, and the corrected values were obtained by application of the error equation. The values shown are from the first trial of the last iteration in Figure 1. Note the effect of the size of K on the reasonableness of the calculated concentrations. Note also that regardless of how unreasonable the stage concentrations become in the stage-to-stage calculation, application of the error equations furnishes reasonable corrected values. These corrected values would be the correct solution if it were not necessary to correct the rate profiles for the second trial. The second trial provided e_{x_1}'s of 0.119, −108.9, 0.0, and −0.0012 for the four components compared with the values shown in Table 2 of −0.519, 292.3, 0.021, and 0.002. It was not necessary to make a third trial since the rate profiles calculated for use in trial 3 were identical to those used in trial 2. Also the K values were essentially unchanged. The stripping factors would be unchanged for the third trial, and therefore the error equation can predict from the e_{x_1}'s from trial 2 the exact x_1's which will reduce all the e_{x_1}'s to zero in the next trial. In practical calculations the correction to x_1 necessary to make $e_{x_1} = 0$ for a component with a K as large as that of chloroform is beyond the number of decimal places carried in the calculations.

One other point warrants discussion, and that is the role played by the equilibrium data in the achievement of true convergence. The solution obtained where $\Sigma x_1 = 1.0$ will be the correct solution only if the equilibrium data and its graphical representation are exactly correct. If the K values are correct, then not only will $\Sigma x_1 = 1.0$ but also $\Sigma y_1 = 1.0$, $\Sigma x_2 = 1.0$, etc. In the example problem the K values used for chloroform were evidently too large. It was necessary to use an x_1 of approximately 0.007 to reduce the e_{x_1} of chloroform to zero. Solubility data indicate an x_1 for chloroform of approximately 0.03 based on the concentrations of the other three components. This fourfold error in the x_1 concentration of chloroform coupled with the large K value for this component caused the Σy's and Σx's to be less than 1.0 until the feed stage was reached. At that point the large amount of chloroform entering in the feed overshadowed the error in its L_1 concentration. Above the feed the phase concentrations summed to approximately 1.0. The probability of errors in the K values for chloroform is high since the concentration of chloroform in the extract phase in the tie-line determinations was usually below 0.05 wt. fraction.

The final results for the example are shown in Figure 2 of the preceding paper, where they are represented by the open circles. Comparison with the short-cut method results and the manner in which the results were checked by the graphical method of Powers (2) are described in the preceding paper.

NOTATION

- B = heavy or extract product rate, moles, weight, or volume per unit time
- D = light or raffinate product rate, moles, weight, or volume per unit time
- e = calculated stream concentration minus correct stream concentration for the component under consideration
- e_{x_n} = error in calculated value of x_n
- e_{y_n} = error in calculated value of y_n
- F = upper feed rate, moles, weight, or volume per unit time
- F' = lower feed rate, moles, weight, or volume per unit time. If only one feed is used $F' = 0$ and $M = 0$
- g = $S_E x_{sE}/L_1x_1$ = fraction of a given component in L_1 which is removed with S_E

j = $(R'/1 + R')\ (1 - \Sigma g x_1) - 1.0$

k = $(1 + gR')/(1 + R')$

K = y/x = distribution coefficient

L = heavy or extract phase rate, moles, weight, or volume per unit time

M = number of theoretical stages below the feed stage M + 1

n = subscript referring to any stage which may take on any value from 1.0 to N

N = total number of theoretical stages including partial reboiler if any but excluding partial condenser if any

R = external reflux ratio at top or raffinate end of column, amount of reflux/amount of product

R' = external reflux ratio at bottom or extract end of column, amount of reflux/amount of product

S = fresh solvent rate, moles, weight, or volume per unit time

S_E = solvent rich material recovered in the extract solvent recovery equipment, moles, weight, or volume per unit time

S_n = $K_n V_n / L_{n+1}$ = component stripping factor where the subscript n can take on any stage number from 1.0 to N

V = light or raffinate phase rate, moles, weight, or volume per unit time

x = concentration in heavy or extract phase, units consistent with units on rates

y = concentration in light or raffinate phase, units consistent with units on rates

LITERATURE CITED

1. Lewis, W. K., and G. L. Matheson, *Ind. Eng. Chem.*, **24**, 494 (1932).
2. Powers, J. E., *Chem. Eng. Progr.*, **50**, 291 (1954).
3. Smith, J. C., *Ind. Eng. Chem.*, **36**, 68 (1944).
4. Thiele, E. W., and R. L. Geddes, *ibid.*, **25**, 289 (1933).
5. Treybal, R. E., "Liquid Extraction," 1 ed., p. 211, McGraw-Hill, New York (1951).

Manuscript received January 2, 1959; revision received December 17, 1959; paper accepted December 28, 1959.

Effect of Uniformity of Fluidization On Catalytic Cracking of Cumene

ALBERT GOMEZPLATA and W. W. SHUSTER

Rensselaer Polytechnic Institute, Troy, New York

The effect of uniformity of fluidization on the catalytic cracking of cumene, with a silica-alumina catalyst, was studied in a 3-in.–diameter reactor operated at 800°F. Superficial gas velocities were varied from 0.06 to 0.24 ft./sec. for bed heights of 1.5, 3, 5, and 8 in. The percentage conversion in a fluidized bed was found to be lower than in a fixed bed and to be dependent on the type of catalyst support used. A porous plate support was up to 30% more efficient than a screen support, which is attributed to its better gas-distribution characteristics and to its ability to introduce the discontinuous phase as smaller gas bubbles. Indications are that the first few inches of bed are very effective in bringing in contact the continuous and discontinuous phase, and therefore most of the conversion due to the interaction of the two phases takes place here. This can be explained in terms of the rapid growth of gas bubbles as they proceed through the bed.

The nature of the fluid and solid flow in a fluidized bed has been investigated in many studies (*2a, 4, 5, 6, 25, 27*) and the fluidization process has been described (*8* to *13* and *18*). The general solid pattern has been established as being up the center of the column and down the sides (*4, 5, 16*) with the downward-flowing solid particles creating some back mixing of the gas along the sides (*4, 5*). The importance that the homogeneity of dispersion of fluid and particles can have on the properties of a fluidized bed has been realized, and ingenious methods have been proposed to measure bed uniformity (*1, 3, 17, 24*), but unfortunately studies have been mainly of a qualitative nature. Gilliland and coworkers (*6*) in kinetic studies of a gas-phase homogeneous reaction concluded that plug flow is a good assumption for kinetic studies and that the lowering of conversion in a fluidized bed was due mainly to gas bypassing through the gas-solid phase of the bed.

Shen and Johnstone (*23*) studied the catalytic decomposition of nitrous oxide, and Mathis and Watson (*15*) studied catalytic cumene dealkylation in both fixed and fluidized beds under isothermal bed conditions. The conversion obtained under fluidized-bed conditions was always less than for the fixed bed and was attributed to ineffective contact caused by bypassing gas. Both Shen and Johnstone (*23*) and Mathis and Watson (*15*) have proposed mathematical models to aid in the understanding of the behavior of the bed. To make mathematics manageable, quite a few assumptions have to be made and a high degree of error can be expected from such models, but as yet these two studies have not yielded enough data to make any conclusions of the general applicability of the models.

The aim of the present study was to investigate the effect of fluidization on the catalytic cracking of cumene. The cumene-cracking reaction was chosen because of its desirable cracking characteristics and because the reaction mechanism has been studied extensively (*2, 20, 21, 26*).

Special emphasis in this investigation was placed on the effect of uniformity on the cracking reaction, since it was expected that this variable would have a significant effect on the level of conversion attained in a fluidized bed.

MATERIALS AND APPARATUS

The cumene used in the kinetic study was of pure-grade quality that was purified by passing through silica gel to remove cumene hydroperoxide and other polar impurities. After purification it analyzed

Cumene	98.68%
Ethylbenzene	1.30%
Cumene hydroperoxide	0.02%

Albert Gomezplata is at present with the University of Maryland, College Park, Maryland.

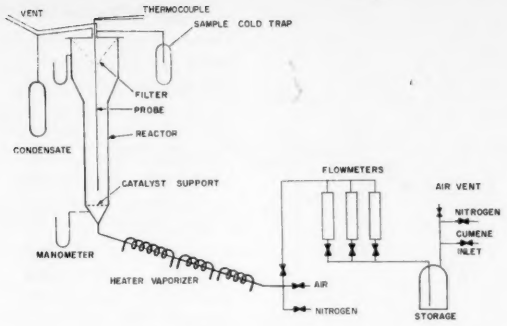

Fig. 1. Diagram of equipment.

The silica-alumina catalyst, which analyzed 13% aluminum oxide, had a surface area by B.E.T. analysis of 490 m. sq./g. The 100- to 200-mesh fraction was used after fines had been removed by fluidizing the catalyst for a period of 8 hr. at a moderate gas rate.

A flow diagram of the equipment is presented in Figure 1. Briefly, it consisted of a cumene storage tank, flow meters to measure the cumene feed, a 6-ft. heater to vaporize and preheat the cumene, and a 3-in.–diameter reactor to contact the cumene and catalyst. The reactor had a catalyst disengaging section along with a vent system designed to keep the reactor at atmospheric pressure and had provision for either a porous plate or a screen as a catalyst support. Compressed nitrogen was used to pump cumene through the system. Stainless steel was used throughout in the heater, reactor, and top assembly.

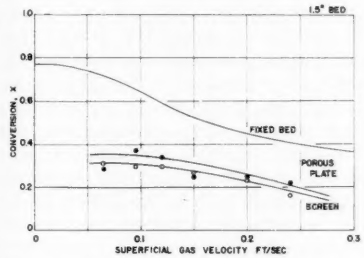

Fig. 2. Conversion vs. superficial gas velocity.

METHODS OF PROCEDURE

Before a run was started, the desired amount of catalyst was placed in the reactor and the equipment heated while air was passed through the reactor. When the apparatus reached operating temperatures, which took several hours, a 10-min. nitrogen purge was started, after which the cumene feed was applied. With practice the bed temperature could be adjusted to 800°F. within 20 min. and kept to ±5° of that temperature. A small flow of nitrogen continually flushed the sample line until a sample was taken. The normal sampling time was 10 min. After the sample had been taken, the cumene feed was stopped and the residual cumene in the boiler was allowed to evaporate. A 15-min. nitrogen purge followed, and then air was put through the reactor which caused the catalyst temperature to increase. When the temperature reached 1,000°F., the variac controlling the bed temperature was turned off until this temperature began to fall, indicating the end of the carbon burning cycle. The sample collected was transferred to a small vial and analyzed. Gas chromatography was found to be a quick and accurate method of analysis for both impurities and the fraction converted.

RESULTS

Preliminary Study

When the catalyst was fluidized with air in a plastic column, a marked difference in the uniformity of a fluidized bed was observed depending on whether a porous plate or a screen was used as a catalyst support. With a porous plate as a catalyst support, a very definite bed expansion, up to 20%, was observed even at low gas velocities. At these low gas velocities channeling does occur but usually at several places in the bed. At higher gas velocities gas passes through the dense phase in small gas bubbles that seem to be evenly distributed throughout the bed. The small bubbles at the walls combine rapidly and grow larger as they progress through the bed, and it can be inferred that a similar action takes place within the bed. From visual observations it is questionable whether the solid circulation pattern is up the center and down the sides when a porous plate is used.

With a fine-mesh screen used as the catalyst support a 60-deg. cone distributor or a 3-in. Berl saddle calming section was found necessary to obtain a symmetrical bed with gas flow through the center. Even then there was a marked difference in fluidization with a screen. At low gas velocities, channeling can be observed at only one point in the bed, with little or no bed expansion, and even at higher gas velocities, only a small percentage of bed expansion is obtained. The greater part of the gas flow was through the center of the bed, and a larger bubble size compared with that observed with a porous plate was noticed. A greater solid turbulence was evident by the considerable ejection of particles that made observation of the upper boundary of the bed impossible after a few seconds of gas flow.

The difference that supports can make was also noticed by Grohse (*17*) while determining instantaneous density profiles of fluidized beds with X-ray absorption techniques. His results indicate that a porous-plate support produces a bed that is longitudinally uniform in density and that a bed with a screen support has a greater density at the bottom, levels off in the middle, and has a lower density at the top.

It is evident that these differences in the contact of the disperse and dense

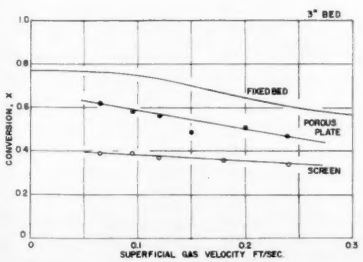

Fig. 3. Conversion vs. superficial gas velocity.

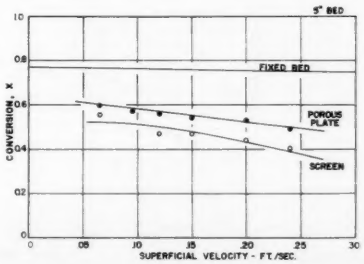

Fig. 4. Superficial gas velocity vs. conversion.

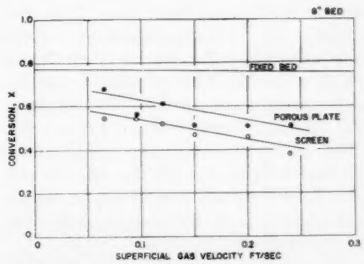

Fig. 5. Superficial gas velocity vs. conversion.

phases may lead to different reaction rates when the solid is used as a catalyst for a reaction.

Fixed-Bed Study

It was attempted to determine fixed-bed data with the same equipment as used in the fluidized-bed study; however at the low gas velocities required to reproduce the same W/F ratios used in the fluidized study, high thermal conversion was obtained (as high as 12%) and side reaction overshadowed the cracking of cumene. But the cracking of cumene by silica alumina catalyst has been studied extensively (*2, 14, 19, 20, 26*), enabling the conversion expected from a fixed bed to be calculated.

Kinetic studies have shown that the cracking of cumene is controlled by a single-site surface reaction (*2, 20*) and that the steady state reaction per unit of catalyst surface can be expressed by

$$\frac{dn}{dt} = k_s B_o \frac{Ps - 1/K_E P_m P_n}{Ps + GK_m P_m + G\Sigma K_{Ii} P_{Ii} + G} \quad (1)$$

The adsorption-equilibrium constants for cumene products and common inhibitors have been tabulated (*14*). Of special importance is cumene hydroperoxide, which is a very strong inhibitor that accumulates on storage.

The rate equation can be integrated to give an expression for the total conversion to be expected from an integral reactor (fixed-bed reactor).

$$2\frac{W}{F} k_s B_o M^s = (M^2E + C - MJ)\ln(1-x') + (M^2E + C + MJ)\ln(1-x') - 2Cx' \quad (2)$$

where

$$E = 1 + GK_I P_I + G/P$$
$$J = 2G + GK_m + GK_I P_I$$
$$C = G + GK_m - 1$$
$$M^2 = (K_E + 1)/K_E$$

Equation (2) can be used to predict the conversion expected in a fixed bed when quantitative data of the impurities of the cumene feed are available, provided that diffusion transport effects are not present and that the activity of the catalyst is assumed proportional to the B.E.T. surface area. The possibility of diffusion-transport effects was eliminated by the very fine-mesh catalyst used. The predicted conversion seems to agree with the results of the fluidized-bed study. Conversions close to equilibrium were predicted for all bed heights except the 1½-in. bed. It was at this bed height that a noticeable decrease in conversion took place in the fluidized-bed data.

The cumene cracking reaction results in a volume change and consequently an increase in gas superficial velocity with bed height. In this paper results are based on the inlet superficial velocity for simplicity.

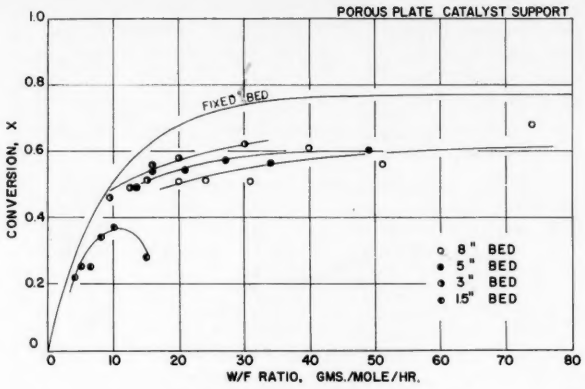

Fig. 6. Conversion vs. W/F ratio.

Fluidized-Bed Study

Thermal cracking was found to be negligible at the space velocities studied, with only 0.6% observed at low gas rates. The purified cumene cracked to benzene and propylene with very few side reaction products (compared with a 1.3% ethylbenzene impurity in the feed). Catalyst fouling was negligible over several runs made for 80 min. Reproducibility of the data was generally within 2% conversion, and frequent check runs were made. The catalyst was changed after each series of runs, although no indication was found of catalyst deactivation with time.

The results of runs made in the reactor with both a screen and porous plate, in which bed height and superficial velocity were varied, are shown in Figures 2 to 5, together with the expected conversion in a fixed bed.

The experimental results show that for the cracking of cumene over the range of conditions studied a lower conversion is obtained in a fluidized bed than in a fixed bed of similar size. This is in agreement with the results of Shen and Johnstone (*23*) and Mathis and Watson (*15*), who also obtained lower conversion in their fluidized beds. The lower conversion can be attributed to the gas that bypasses the bed in the form of bubbles or channels. The bypassing gas does contribute to the conversion in the bed, since the over-all conversion is always greater than it is for the solid-gas phase alone. It is reasonable to assume that this extra conversion is obtained from both the transfer of reactants and products between the continuous and the discontinuous phase and any reaction taking place in the discontinuous phase from catalyst entrained in that phase. It then follows that the intimacy of contact between the two phases and the distribution of the gas phase will have an effect on the conversion obtained, and the experimental results verify this conclusion. Over the range of conditions studied, up to 30% difference in conversion was noticed between a porous plate and a screen support, which have been observed to give a marked difference in bed uniformity in the plastic reactor. With a porous plate, which gave a smoother fluidiza-

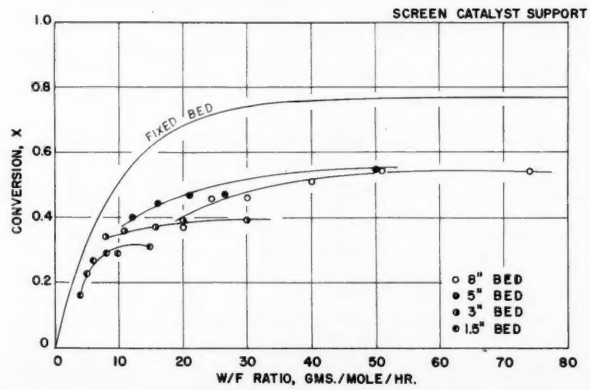

Fig. 7. Conversion vs. W/F ratio.

tion than a screen, larger conversions and greater bed efficiencies were obtained. These can be explained in terms of the smaller gas bubbles of the discontinuous phase, formed at the bottom of the bed, that expose a large surface for interaction with the continuous phase and which are distributed evenly over the total cross section of the bed. On the other hand, with a screen support larger bubbles are present in the bed, with most of the bubbling action taking place in the center; a lower conversion can thus be expected with a screen. In both cases the bubbles are observed to combine rapidly as they pass up the bed, and the subsequent influence that they have on conversion emphasizes the need for either standardizing equipment for experimental studies or finding a method to characterize the uniformity of a bed.

Mathis and Watson (*15*) proposed to characterize bed uniformity by the height-to-diameter ratio (L/D) of the bed; however this conclusion is not applicable to all beds, as is evident from Figures 6 and 7, where the same (L/D) ratio does not fix the level of conversion but is dependent on whether a screen or a porous plate is used as a catalyst support. However in view of the apparent independence of gas distribution on the inlet conditions when a porous plate is used, it may well be that in this case the (L/D) ratio would characterize the uniformity of the bed. An attempt was made to use the minute pressure fluctuations of the bed to predict bed uniformity, but the attempt was unsuccessful owing to the difficulty of isolating the pressure fluctuations in the bed from those introduced by other parts of the equipment.

The data of Mathis and Watson were obtained at a higher cracking temperature than those of the present study and cover a wider range of superficial velocities, although with relatively few points. It is difficult to compare results, even though the same reaction is involved, because of the dependence of reaction rate on the purity of the cumene used. A similar decrease in conversion with increased superficial gas velocity in the fluidized bed can be noticed, although an optimum velocity at which the fluidized bed conversion approaches the conversion in a fixed bed was not noticed. Shen and Johnstone (*25*) in their kinetic studies of catalytic decomposition of nitrous oxide did not notice an optimum velocity effect either. This velocity pinch effect is dependent on the curvature of the fixed-bed data, and in view of the extreme difficulty found in taking experimental fixed-bed data and the fact that an unusual high depression of conversion is evident in Mathis and Watson's fixed-bed results, it seems likely that their data are in error.

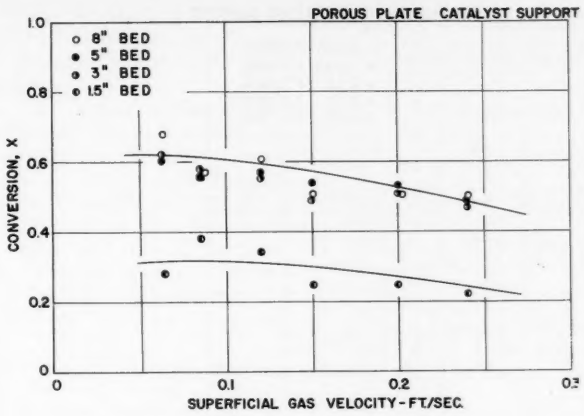

Fig. 8. Conversion vs. superficial gas velocity.

When all the runs made with a porous plate are grouped together as shown in Figure 8, very interesting results are observed. For beds of 3, 5, and 8 in., approximately the same conversion is obtained at similar superficial gas velocities, and the conversion vs. velocity curves follow similar trends. A higher conversion is obtained at low gas velocities with a leveling off at higher velocities. Similar trends are observed with a screen as shown on Figure 9, with the exception that only the 5- and 8-in. beds are similar. It should be noted that the conversion values approached in the case of a porous plate are higher than those approached in the bed with a screen and in both cases less than those predicted for a fixed bed. In this study conversion in the continuous phase closely approaches the thermodynamic equilibrium of 0.77 (*22*) conversion for all bed heights above 3 in. With this in mind, one notes that in the case of the porous plate the results indicate that essentially all the interaction between phases takes place below the first 3 in. of the bed. This is understandable in terms of the small bubbles present at the bottom and their rapid growth as they proceed up the column. With a screen, on the other hand, gas bubbles are also present at the bottom of the bed, but they are bigger and not evenly distributed, since most of the gas flow takes place up the center of the bed. A very high degree of solid turbulence results. In a bed with a screen, because of the inherently larger bubble size, lower conversions are obtained than with a porous plate. An upper limit in conversion is obtained, but a higher bed is needed to reach the maximum interaction conditions. This must be attributed to the larger percentage of catalyst entrained in the gas phase by the violent solid turbulence of the bed. Other investigators have not been able to notice these effects because their studies were not conducted under conditions where the

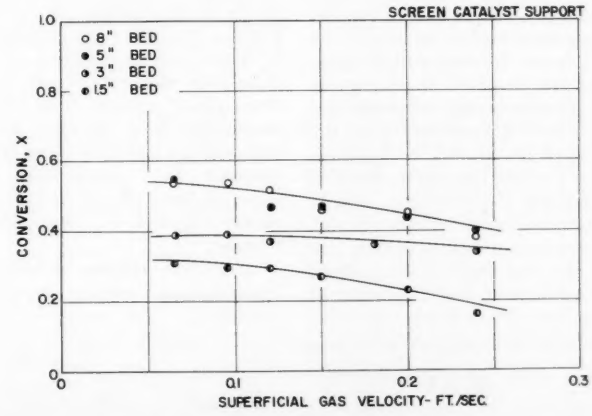

Fig. 9. Conversion vs. superficial gas velocity.

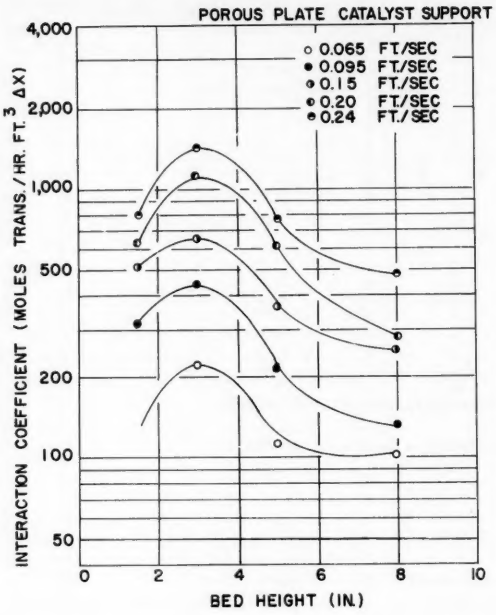

Fig. 10. Interaction coefficient vs. bed height.

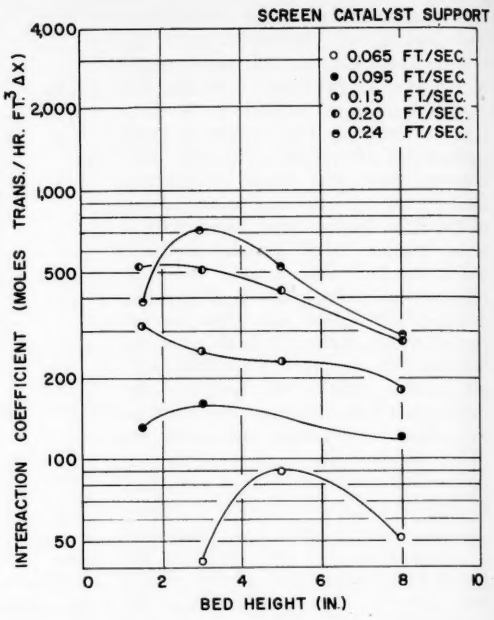

Fig. 11. Interaction coefficient vs. bed height.

conversion expected of a similar fixed bed became essentially independent of the height of the bed.

The mathematical models of fluidized beds that have so far been proposed are all based on Toomey and Johnstone's (25) theory of a discrete fluidized gas-solid mixture. The phases are assumed to constitute parallel reactors, and a mass transfer coefficient is used to account for the interaction between the phases, calculated from the difference in over-all conversion from that expected for just the gas-solid phase. The coefficient is evaluated per unit volume of bed and is assumed constant for the entire bed. Shen and Johnstone proposed two models. In one, progressive flow was assumed for both phases; in the other, progressive flow was assumed for the gas phase with complete mixing of the gas-solid phase. Mathis and Watson considered just the case of progressive flow in both phases but assumed that there was catalyst entrainment in the gas phase and introduced the back reaction in a pseudo first-order equation used to describe the cracking rate. In the present study a new simpler model, using the same approach as Mathis and Watson (15), was derived. This model except for the method of development and basic units is similar to the one proposed by Shen and Johnstone (23) for progressive flow in both phases. The refinements introduced by Mathis and Watson were not considered because of the difficulty of evaluating the extent of catalyst entrainment in the gas phase and having to account for the back reaction scheme at the high level of conversions attained with cumene.

Fluidized Reactor Model

The bed is assumed to be composed of two parallel reactors, one containing the continuous phase and the other the discontinuous phase. The discontinuous phase consists of all the bypassing gas; the continuous phase consists of the solid-gas mixture under conditions similar to those present at incipient fluidization. A pseudo mass transfer coefficient per unit bed volume is introduced to account for over-all conversion above that predicted for the dense-phase reactor. Both reactors are assumed to be at the same temperature and pressure conditions, and it is further assumed that progressive gas flow exists in both phases and that the reaction will follow a first-order kinetic scheme.

A material balance around the continuous-phase reaction element dZ results in

$$\frac{dx_A}{dZ} + \left[\frac{(K_{AB}A) + \left(\frac{kW}{L}\right)}{F_A}\right] x_A - \frac{(K_{AB}A)}{F_A} x_B = \frac{kW}{LF_A} \qquad (3)$$

A similar material balance around the discontinuous phase yields

$$\frac{dx_B}{dZ} = \frac{(K_{AB}A)}{F_B}(x_A - x_B) \qquad (4)$$

Equations (3) and (4) are simple, ordinary differential equations which can be solved by assuming progressive gas flow, constant temperature and pressure, even distribution of catalyst in phase A, and a constant interaction coefficient. The boundary conditions are $x_A = x_B = 0$ at $Z = 0$. The solutions are

$$x_A = \left[\frac{F_B g_1 + 1}{(K_{AB}A)}\right] R_1 e^{g_1 Z} + \left[\frac{F_B g_2 + 1}{(K_{AB}A)}\right] R_2 e^{g_2 Z} + 1 \qquad (5)$$

$$x_B = R_1 e^{g_1 Z} + R_2 e^{g_2 Z} + 1 \qquad (6)$$

where

$$g_1 = \frac{1}{2F_A F_B}\left[-b + \sqrt{b^2 - 4F_A F_B d}\right]$$

$$g_2 = \frac{1}{2F_A F_B}\left[-b - \sqrt{b^2 - 4F_A F_B d}\right]$$

$$b = (K_{AB}A)(F_A + F_B) + F_B \frac{kW}{L}$$

$$d = (K_{AB}A)\frac{kW}{L}$$

$$R_1 = \frac{g_1}{g_2 - g_1}$$

$$R_2 = \frac{g_2}{g_1 + g_2}$$

The over-all conversion is represented by

$$x = \frac{F_A x_A + F_B x_B}{F_A + F_B} \qquad (7)$$

Values for x_A and x_B can be substituted in the above equation and then simplified to

$$x = Q_1 e^{\theta_1 z} + Q_2 e^{\theta_1 z} + 1 \qquad (8)$$

where

$$Q_1 = R_1 \left[\frac{F_A F_B g_1 + (K_{AB}A)(F_A + F_B)}{(K_{AB}A)(F_A + F_B)} \right]$$

$$Q_2 = R_2 \left[\frac{F_A F_B g_2 + (K_{AB}A)(F_A + F_B)}{(K_{AB}A)(F_A + F_B)} \right]$$

To evaluate the interaction coefficient from experimental results, a trial-and-error solution is necessary. A value of $K_{AB}A$ is assumed, and the value of over-all conversion calculated from Equations (5) to (8). If it agrees with the experimental value, then the correct value of K_{AB} has been assumed. The interaction coefficients were calculated by a trial-and-error solution with an IBM 650 digital computer. The results are shown in Figures 10 and 11 and are plotted vs. bed height with superficial gas velocity as a parameter. In the case of a bed with a porous plate the interaction coefficient increases rapidly with bed height, goes through a maximum at approximately 3 in., and then decreases almost proportionally to bed height. With the screen the results are erratic in that some curves have an inflection at 3 in., while others just decrease with bed height. However two facts are evident: with a screen the decrease of interaction coefficient with bed height is more gradual than with a porous plate, and the coefficients are lower for the former.

The plots of interaction coefficient vs. bed height support the concept that practically all interaction between phases takes place in the first few inches of bed. The coefficients obtained with a porous plate increase quickly to a maximum and then decreases with bed height. With a screen the decrease is more gradual, and at some gas velocities no initial increase is evident. Since the coefficient is evaluated per unit of reactor volume, a coefficient decrease proportional to the bed height signifies that no more effective transfer is taking place between the phases; such a trend is noticed after the first few inches of bed height. Shen and Johnstone also found that their coefficients varied proportionally to bed height. Transfer coefficients can be transformed dimensionally to interaction coefficients by dividing the absolute pressure by the product of the gas constant, absolute temperature, and transfer coefficient. When one converts their data, interaction coefficients of 280 to 2,900 are obtained which are in the same range as those of the present study even though both systems are different. The coefficients found by Mathis and Watson on the other hand are much higher than those in the present study, and this again can be attributed to the high depression of conversion obtained in their fixed-bed data.

The greater interaction between phases at low bed heights indicates that the interaction coefficient used in the parallel reactor model is not constant over the height of the bed but is definitely higher in the lower section. These differences should be known, and studies should be started to evaluate these interaction coefficients as a function of bed height, since the parallel reactor model seems to be a practical approach to the design of a fluidized reactor from fixed-bed data.

ACKNOWLEDGMENT

The authors are indebted to Phillips Petroleum Company for providing the fellowship that made this study possible. Appreciation is extended to the Hercules Powder Company for supplying the cumene and to the American Cyanamid Company for the catalyst.

NOTATION

A	=	cross-sectional area, sq. ft., catalyst site
B_o	=	concentration of active sites per unit area, moles/m. square
D	=	reactor diameter, ft.
F	=	feed rate, moles/hr.
G	=	constant related to chemisorption of cumene
J	=	inhibitor molecule
K_E	=	equilibrium constant for reaction cumene → benzene + propylene
K_{AB}	=	interaction coefficient, moles/cu. ft./unit conversion difference
k	=	reaction-rate constant, g. moles/hr./g. catalyst
L	=	total bed height, ft.
P	=	pressure, atm.
r	=	reaction rate, g. moles reacted/hr./g. catalyst
x	=	conversion as mole fraction

Subscripts

A	=	continuous phase
B	=	discontinuous phase
I_i	=	inhibitors
m	=	benzene
n	=	propylene
s	=	cumene

Superscripts

′	=	ratio of fraction converted to fraction converted at thermodynamic equilibrium
—	=	over-all value

LITERATURE CITED

1. Baumgarten, P. K., Ph.D. thesis, Univ. Del., Dover (1956).
2. Corrigan, T. E., J. C. Garver, H. F. Rase, and R. S. Kirk, *Chem. Eng. Progr.*, **49**, 603 (1953).
2a. Yasui, George, and L. N. Johanson, *A.I.Ch.E. Journal*, **4**, 445 (1958).
3. Gerald, C. G., *Chem. Eng. Progr.*, **47**, 483 (1951).
4. Gilliland, E. R., and E. A. Mason, *Ind. Eng. Chem.*, **41**, 1191 (1949).
5. *Ibid*, **44**, 218 (1952).
6. Gilliland, E. G., E. A. Mason, and R. C. Oliver, *ibid.*, **45**, 1177 (1953).
6a. Gomezplata, Albert, Ph.D. thesis, Rensselaer Polytechnic Inst., Troy, N. Y. (1958).
7. Grohse, E. W., *A.I.Ch.E. Journal*, **1**, 358 (1955).
8. Leva, Max, Milton Grummer, Murray Weintraub, and Morris Pollchik, *Chem. Eng. Progr.*, **44**, 511 (1948).
9. *Ibid*, 619 (1948).
10. Leva, Max, Murray Weintraub, and Milton Grummer, *ibid.*, **45**, 563 (1949).
11. Leva, Max, and Milton Grummer, *ibid.*, **48**, 307 (1952).
12. Leva, Max, *Chem. Eng.*, **64**, 289 (1957).
13. Lewis, W. K., E. R. Gilliland, and W. C. Bauer, *Ind. Eng. Chem.*, **41**, 1104 (1949).
14. Maatman, R. W., R. M. Lago, and C. D. Prater, "Advances in Catalysis," 9, 531, Academic Press, N. Y. (1957).
15. Mathis, J. F., and C. C. Watson, *A.I.Ch.E. Journal*, **2**, 518, (1956).
16. Morse, R. D., *Ind. Eng. Chem.*, **41**, 1117 (1949).
17. ———, and C. O. Ballou, *Chem. Eng. Progr.*, **47**, 179 (1951).
18. Parent, L. D., Nathan Yagol, and C. S. Steiner, *ibid.*, **43**, 429 (1947).
19. Plank, C. J., and D. M. Nace, *Ind. Eng. Chem.*, **47**, 2374 (1955).
20. Prater, D. C., and R. M. Lago, *Advances in Catalysis*, **8**, 293 (1956).
21. Rase, H. F., and R. S. Kirk, *Chem. Eng. Progr.*, **50**, 35 (1954).
22. Rossini, F. D., K. S. Pitzer, R. L. Arnet, R. M. Braum, and G. C. Pimentel, "Selected Values of Physical and Thermodynamical Properties of Hydrocarbons and Related Compounds," Carnegie Press, Pittsburgh, Pa. (1953).
23. Shen, C. Y., and H. F. Johnstone, *A.I.Ch.E. Journal*, **1**, 349 (1955).
24. Shuster, W. W., and Peter Kisliak, *Chem. Eng. Progr.*, **48**, 455 (1952).
25. Toomey, Robert, and H. F. Johnstone, *ibid.*, 221 (1952).
26. Weiz, P. B., and C. D. Prater, "*Advances in Catalysis*," vol. 6, p. 143, Academic Press, New York (1954).
27. Wilhelm, R. H., and Mooson Kwauk, *Chem. Eng. Progr.*, **44**, 201 (1948).

Manuscript received May 27, 1959; revision received December 4, 1959; paper accepted December 9, 1959.

A Boundary-Layer Model of Fluid-Particle Mass Transfer in Fixed Beds

JAMES J. CARBERRY

E. I. du Pont de Nemours & Co., Inc., Wilmington, Delaware

The process of fluid-particle mass transfer in fixed beds at Reynolds numbers less than 1,000 is viewed in terms of transient molecular diffusion within a boundary layer which is developed and destroyed repeatedly as the fluid journeys through the bed. Literature data support the *j* factor derived from the premises of the model. The theory predicts a Schmidt number exponent of 2/3 for $N_{Sc} \geqq 1$; however this exponent should approach 1/2 for $N_{Sc} < 1$.

While numerous empirical correlations exist which permit the determination of mass transfer coefficients for fluid-particle exchange in fixed beds (*10, 11, 15, 22, 30*), it is nevertheless of some interest to explore these events from a theoretical point of view. To date the most interesting rationalization of fixed bed mass transfer is found in the recent work of Thoenes and Kramers (*28*) who interpreted their data in terms of mass transfer from a particle into a fluid network composed of laminar, turbulent, and stagnant regimes. The present work attempts to establish a rationale in terms of a simplified boundary-layer theory. Although this study is confined to mass transfer, the model may well be extended to heat transfer in fixed beds.

Higbie (*14*) made one of the earliest attempts to relate the average mass transfer coefficient to the species diffusivity and the average time of fluid element exposure to sink or source by

$$\bar{k} = 2\sqrt{\frac{D}{\pi\theta}} \qquad (1)$$

Higbies' theory has been verified in investigations in which the boundary conditions inherent in the model have been satisfied experimentally (*7, 21, 26*). One of the key and limiting assumptions in this model is that specifying the absence of a velocity gradient at the transfer interface. Transfer processes between a solid and flowing fluid obviously occur across a boundary at which a velocity gradient must exist; consequently the influence of velocity upon the diffusive process must be assessed. In the case of simple geometries the transfer processes may be readily predicted for an assumed velocity distribution. Heat transfer literature reveals well-known examples such as the solution of Leveque (*18*) for heat transfer between a laminar fluid and a pipe wall. Kramers (*17*) applied an analogous model to mass transfer from a wall to a laminar falling film.

In the instance of turbulent exchange Hanratty (*13*) has made a significant contribution by applying the Higbie-Danckwerts penetration model to predict the experimental concentration-profile data found in the mass transfer studies of Lin, Moulton, and Putnam (*19*). Since the data treated were obtained in the region of turbulent flow, it is apparent that the exchange involved transfer from the source to eddies, and therefore the velocity gradient in the fluid has no influence upon the diffusive process. In a comparable circumstance Johnson and Huang (*16*) found evidence to support the penetration model in their study of solids dissolution in an agitated vessel. It should be emphasized that an independent evaluation of θ is not possible in exchange events between eddies and a sink or source, and evidence for support of Higbie theory or the Danckwerts modification thereof rests upon finding a ½ power dependence of the transfer rate upon the Schmidt number.

DIFFUSION WITHIN A DEVELOPING BOUNDARY LAYER

Higbie's model follows via solution of

$$\frac{\partial c}{\partial \theta} = u\frac{\partial c}{\partial x} = D\frac{\partial^2 c}{\partial y^2} \qquad (2)$$

where the fluid velocity is invarient in x and y. It will prove fruitful however to express u as a function of these distance variables as

$$u/u_a = (Ky)^a/\left(\frac{\nu x}{u_a}\right)^b \qquad (3)$$

Thus Equation (3) becomes

$$u_a\frac{\partial c}{\partial x} = \left(\frac{\nu x}{u_a}\right)^b\frac{D}{(Ky)^a}\frac{\partial^2 c}{\partial y^2} \qquad (4)$$

Mixon and Carberry (*24*) have obtained a solution to Equation (4), expressing the average mass transfer coefficient in terms of the exponents a and b:

$$\bar{k} = \left[\frac{(a+2)}{(a+2)-(b+1)}\right]\frac{[(b+1)K]^{1/(a+2)}(a+2)^{a/(a+2)}D^{(a+1)/(a+2)}}{\Gamma[1/(a+2)](x/u_a)^{(b+1)/(a+2)}\nu^{b/(a+2)}} \qquad (5)$$

It will be recognized that the fluid velocity component in the y direction, perpendicular to flow, has been ignored in formulating the basic differential equation. The author has assumed that the term $v\,\partial c/\partial y$ is negligible relative to $u\,\partial c/\partial y$. A consideration of the perpendicular component alters the coefficient of the derived relationship [Equation (14)] by about 20%, but in no way is the indicated functionality changed (*24*).

Equation (5) reduces readily to a number of interesting cases corresponding to various value of a and b:

$a = b = o$, Higbie's model.

$$\bar{k} = 2\sqrt{\frac{D}{\pi\theta}} \text{ where } \theta = X/u_a \qquad (6)$$

$a = 1$, $b = o$, Leveque approximation

$$\bar{k} = 0.808\left(\frac{KD^2}{x/u_a}\right)^{1/3} \qquad (7)$$

Equation (7) is identical to that derived by Kramers (*17*) for solid dissolution into a falling film.

The instance of diffusion within a developing boundary layer is approximated by $a = 1$ and $b = ½$; that is

$$u/u_a = Ky/\sqrt{\frac{\nu x}{u_a}} \qquad (8)$$

Boundary-layer theory (*27*) teaches that the linear velocity approximation is

$$u/u_x = y/\sqrt{\frac{12\nu x}{u_x}} \qquad (9)$$

If the velocity at the boundary-layer edge, u_x, is expressed in terms of the average as $u_x = 2u_a$, Equation (9) reduces to

$$u/u_a = 0.815\,y/\sqrt{\frac{\nu x}{u_a}}, \quad \therefore K = 0.815 \qquad (10)$$

For $a = 1$ and $b = ½$ Equation (5) becomes

$$\bar{k} = \frac{1.15\,D^{2/3}}{(x/u_a)^{1/2}\nu^{1/6}} \qquad (11)$$

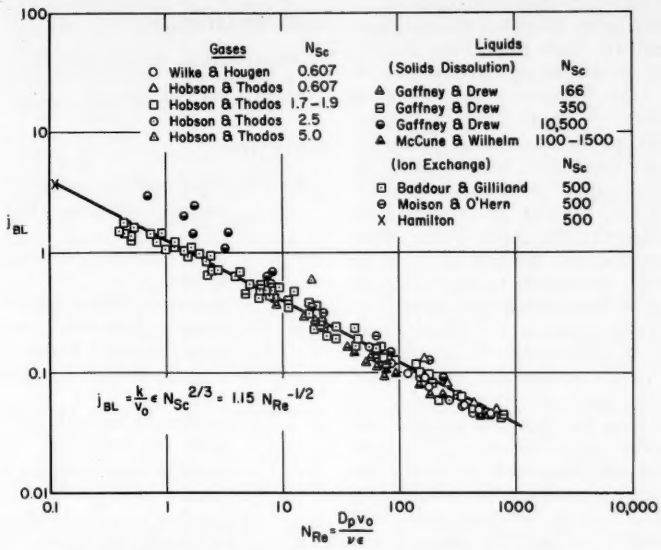

Fig. 1. Fixed bed mass transfer in terms of boundary-layer theory.

APPLICATION TO FIXED BED TRANSFER PROCESSES

The precise characterization of flowing fluid behavior in a fixed bed is hardly possible at this time. It is perhaps equally difficult to define the geometry of the fixed phase as it is seen by the flowing fluid. Nevertheless if the fixed bed is viewed as a series of discrete surfaces separated at points by void cells, it might be argued that in the flow regime below fully developed turbulence the fluid, in its journey through the bed, must experience a succession of boundary-layer developments and destructions. During a given boundary-layer development over a distance x diffusion or penetration of a species will occur between fluid and the fixed surface. If it is assumed that the velocity within the developing boundary layer at the transfer boundary can be approximated by Equation (10), then the specification of $\overline{k}$ by Equation (11) is possible if x can be defined for a fixed bed.

A specification of x is possible in the light of recently acquired axial-dispersion data for fixed beds which suggest that, for gases, mixing of a perfect nature occurs about once every particle diameter (23). Liquid-dispersion data present a more complex problem (4, 6); however if a model suggesting imperfect fluid mixing in each void cell is tolerable (5), then in terms of the developing boundary-layer notion it can be argued that the boundary layer ought to suffer destruction at the mixing points. In other words the boundary layer develops and collapses over a distance approximately equal to one particle diameter.

Thus letting

$$x = D_p = \frac{\nu N_{Re}}{u_o} \qquad (12)$$

and recalling the definition of the Schmidt number, $N_{Sc} = \nu/D$, one can reduce Equation (11) to

$$\overline{k} = 1.15\, u_o\, N_{Re}^{-1/3}\, N_{Sc}^{-2/3} \qquad (13)$$

In terms of a boundary layer j factor, bed void fraction, and the average superficial velocity based upon tube cross-sectional area

$$j_{BL} = \frac{\overline{k}}{u_o}\,\epsilon\, N_{Sc}^{2/3} = 1.15\, N_{Re}^{-1/2} \qquad (14)$$

A comparison of the theoretical relation with empirical correlations indicates that the literature j factors are usually based upon superficial velocity. Thus the derived equation can be tested against experimental data by correcting the published j factors with the void fraction encountered in the experiments and plotting the resulting j values against the Reynolds number based upon average velocity in the bed. Figure 1 displays the comparison of literature data with Equation (14). A Schmidt number variation of from 0.6 to 10,500 is represented by the data for such diverse transfer processes as vaporization, solids dissolution, dilute solution ion exchange, and chromatography. The agreement between data and theory is quite good with the exception of the low Reynolds number data of Gaffney and Drew for $N_{Sc} =$ 10,500. These authors noted however that natural-convection effects were evident in that system at low flow rates. The data of Baddour and Gilliland (1) for dilute solution ion exchange are shown in the j factor form as recalculated and presented by Moison and O'Hern (25).

Obviously not all of the literature data were considered in testing the theory. Ergun (9) has made a critical examination of fixed-bed mass transfer data, and the literature utilized in the present instance was chosen from those studies which evidenced reproducibility and absence of axial mixing effects as noted by Ergun. The latter problem was found to be a prominent one (9) and has been discussed previously (3, 8, 20).

DISCUSSION

The limits of applicability of the derived equation deserve comment. In view of the model invoked Equation (14) should be applicable until the flow rate approaches the value corresponding to turbulent boundary-layer development. The precise value of the Reynolds number at which the transition occurs in a packed bed is difficult to specify. If the character of the packed-bed friction factor-Reynolds number functionality as well as axial dispersion-flow rate relationships (4) permit an inference, then fully developed turbulent flow and therefore turbulent boundary-layer development takes place in the Reynolds number region of about several hundred. The data shown in Figure 1 would suggest that the model is valid to about N_{Re} of 1,000.

The lower flow regime limit of applicability is difficult to define in view of the natural-convection effects on one hand and the specification of x on the other. It is not inconceivable that at very low rates of flow, boundary-layer development may occur over a distance greater than one particle diameter. Thus x itself becomes a function of flow rate; that is $x \propto 1/N_{Re}$ at $N_{Re} << 1$. Such a circumstance would lead to a decrease in j with decreasing values of N_{Re}, a result verified recently by the data of Bar-Ilan and Resnick (2) and more recently by Hamilton (12).

TRANSFER RATES AT THE WALL

The recent work of Yagi (32) on heat and mass transfer at the wall of the packed bed might be interpreted in the light of the boundary-layer notion developed here. Data for mass transfer between water and the coated-tube wall of a packed bed were correlated by Yagi with the equation

$$j_D = \frac{\bar{k}}{u_o}(N_{Sc})^{2/3} = 0.60\,N_{Re'}^{-1/2};\ N_{Re'} < 40 \qquad (15)$$

When one assumes an average void fraction of 0.4, the above relationship may be written on the basis of the average fluid velocity within the bed:

$$j_D = \frac{\bar{k}}{u_o}\epsilon\,N_{Sc}^{2/3} = 0.38\,N_{Re}^{-1/2};\ N_{Re} < 100 \qquad (16)$$

While this functionality is identical to that derived above [Equation (14)], the j relations differ by a constant factor of about 3. In terms of the model suggested in this work the wall transfer data would tempt one to speculate that the boundary layer at low flow rates along the wall of a packed bed develops over a distance equivalent to several particle diameters. Thus Equation (14) is perhaps best written for both transfer at the tube wall and fluid-particle transfer at low values of N_{Re} as

$$j_{BL} = 1.15\,(nN_{Re})^{-1/2} \qquad (17)$$

An alternative model of wall-fluid heat transfer has been presented by Hanratty (*13a*).

The anomalies at low Reynolds numbers and the transfer events at the wall of a packed bed present opportunities for further experimentation designed in a manner which will confirm or deny mechanistic speculations. A quantitative specification of n and its dependence upon velocity near the wall is required to clarify the rate process at that point, while the relationship between n and the Reynolds number must be determined to rationalize particle-fluid exchange data at very low flow rates. Studies of wall-fluid transfer rates in which the inner surface of the packed tube is corrugated or coated with pellets identical to the packing should reveal the extent to which presence of a smooth exchange surface extends the boundary-layer life and thereby reduces the average exchange rate at the wall.

SCHMIDT NUMBER FUNCTIONALITY

Equation (5) states that the exponent upon the Schmidt number is governed by the value of the term $(a+1)/(a+2)$. Hence the exponent must always lie between 1/2 and 2/3 as the velocity at the transfer boundary is either a linear or less than linear function of distance ($1 \geqq a \geqq 0$). The reasoning which follows may clarify this point.

Where the diffusivity of the species is low (high Schmidt number), the region of transfer resistance most certainly lies within the hydrodynamic boundary layer. However systems characterized by high diffusivity, $N_{Sc} < 1$, present an interesting circumstance in which the concentration boundary layer becomes larger than the hydrodynamic one. In other words the hydrodynamic boundary layer tends, by reason of rapid diffusion, to become saturated in the case of transfer from the surface to the fluid. Under these circumstances the transfer rate will no longer be governed by the velocity gradient at the surface but dictated by the velocity gradient at a point closer to the hydrodynamic boundary-layer edge. To the extent that the velocity profile is nonlinear at this point, the power upon the Schmidt number will be less than 2/3. Therefore at Schmidt numbers less than unity a power dependency approaching ½ should be in evidence. Data for Schmidt numbers of about unity or less (for example 0.6 for air-water vapor) hardly provide a valid test; however Lynch and Wilke (*20*) recently presented data characterized by a Schmidt number of 0.24. Their careful analysis of these data revealed that the Schmidt exponent is close to ½. Indeed this fact was interpreted by Wilke (*31*) as perhaps being due to a concentration boundary-layer effect.

With respect to gas-liquid systems (for example absorption of a gas by a liquid flowing through a packed column) it might be expected that the Schmidt number exponent be 2/3 for the gas film, where a velocity gradient exists, and ½ for the liquid film, where for slight penetration the velocity gradient in the liquid film adjacent to the gas is probably negligible (7).

The foregoing remarks do not apply to transfer processes in turbulent flow, a topic which has been treated by Toor and Marchello (29).

CONCLUSIONS

The concept of diffusion within a boundary layer which is repeatedly developed and destroyed over a distance equal to one particle diameter is apparently supported by literature data for particle-fluid exchange in fixed beds. Additional research efforts are needed to provide data and interpretation at very low Reynolds numbers. Further studies are required in systems where the Schmidt number is significantly less than 1 to provide additional support for the contention that saturation of the hydrodynamic boundary layer results in a Schmidt exponent approaching ½.

It is possible that transfer rates in other systems, for example fluidized beds, might be interpreted in terms of an appropriately modified version of the boundary-layer model suggested here.

ACKNOWLEDGMENT

The criticisms, insights, and suggestions of Professor T. J. Hanratty were invaluable aids to the development of this work.

NOTATION

a, b	= exponents in velocity-distribution relation, Equation (3)
c	= concentration of diffusing species
D	= molecular diffusivity
D_p	= particle diameter
j_D	= mass transfer j factor
j_{BL}	= j factor defined by Equation (14)
K	= coefficient defined by Equations (3) and (10)
$\bar{k}$	= average mass transfer coefficient
n	= number of particle diameters of length, Equation (17)
N_{Re}	= Reynolds number, $D_p u_o/\nu\epsilon$
$N_{Re'}$	= Reynolds number, $D_p u_o/\nu$
N_{Sc}	= Schmidt number
u	= fluid velocity
u_o	= superficial velocity
u_a	= average velocity in a packed bed, $u_a = u_o/\epsilon$
u_x	= velocity at boundary-layer edge
v	= fluid-velocity component
x	= distance in direction of flow
y	= distance perpendicular to flow

Greek Letters

ϵ	= fractional void volume
ν	= kinematic viscosity
θ	= time
π	= 3.1416
Γ	= gamma function

LITERATURE CITED

1. Baddour, R. F., and E. R. Gilliland, *Ind. Eng. Chem.*, **45**, 330 (1953).
2. Bar-Ilan, M., and William Resnick, *ibid.*, **49**, 313 (1957).
3. Carberry, J. J., *Can. J. Chem. Eng.*, **36**, 207 (1958).
4. ———, and R. H. Bretton, *A.I.Ch.E. Journal*, **4**, 367 (1958).
5. Carberry, J. J., *ibid.*, **4**, 13M (1958).
6. Ebach, Earl, and R. R. White, *ibid.*, **4**, 161 (1958).
7. Emmert, R. E., and R. L. Pigford, *Chem. Eng. Progr.*, **50**, 87 (1954).
8. Epstein, Norman, *Can. J. Chem. Eng.*, **36**, 210 (1958).
9. Ergun, Sabri, *Chem. Eng. Progr.*, **48**, 227 (1952).
10. Gaffney, B. W., and T. B. Drew, *Ind. Eng. Chem.*, **42**, 1120 (1950).
11. Gamson, B. N., George Thodos, and O. A. Hougen, *Trans. Am. Inst. Chem. Engrs.*, **39**, 1 (1943).
12. Hamilton, P. B., Alfred I. du Pont Institute, Private Communication (1959).
13. Hanratty, T. J., *A.I.Ch.E. Journal*, **2**, 359 (1956).

13*a*. ———, *Chem. Eng. Sci.*, **3**, 209 (1954).

14. Higbie, Ralph, *Trans. Am. Inst. Chem. Engrs.*, **31**, 365 (1935).
15. Hobson, Merk, and George Thodos, *Chem. Eng. Progr.*, **47**, 370 (1951).
16. Johnson, A. I., and Chen-Jung Huang, *A.I.Ch.E. Journal*, **2**, 412 (1956).
17. Kramers, H., and P. J. Kreyger, *Chem. Eng. Sci.*, **6**, 42 (1956).
18. Leveque, J., *Ann. Mines*, **13**, 283 (1928).
19. Lin, C. S., R. W. Moulton, and G. L. Putnam, *Ind. Eng. Chem.*, **45**, 636 (1953).
20. Lynch, E. J., and C. R. Wilke, to be published, *A.I.Ch.E. Journal*.
21. Lynn, Scott, J. R. Straatemeier, and H. Kramers, *Chem. Eng. Sci.*, **4**, 58 (1955).
22. McCune, L. K., and R. H. Wilhelm, *Ind. Eng. Chem.*, **41**, 1124 (1949).
23. McHenry, K. W., and R. H. Wilhelm, *A.I.Ch.E. Journal*, **3**, 83 (1957).
24. Mixon, F. O., and J. J. Carberry, to be published, *Chem. Eng. Sci.*
25. Moison, R. L., and H. A. O'Hern, *Chem. Eng. Progr. Symposium Series No. 24*, **55**, 71 (1959).
26. Raimondi, Pietro, and H. L. Toor, *A.I.Ch.E. Journal*, **5**, 86 (1959)
27. Schlichting, Hermann, "Boundary Layer Theory," Pergamon Press, New York, (1955).
28. Thoenes, D., and H. Kramers, *Chem. Eng. Sci.*, **8**, 271 (1958).
29. Toor, H. L., and J. M. Marchello, *A.I.Ch.E. Journal*, **4**, 97 (1958).
30. Wilke, C. R., and O. A. Hougen, *Trans. Am. Inst. Chem. Engrs.*, **41**, 445 (1945).
31. Wilke, C. R., Remarks at St. Paul, Minn., A.I.Ch.E. Meeting (Sept., 1959).
32. Yagi, Sakae, and Noriaki Wakao, *A.I.Ch.E. Journal*, **5**, 79 (1959).

Manuscript received August 3, 1959; revision received December 28, 1959; paper accepted December 28, 1959. Paper presented at A.I.Ch.E. St. Paul meeting.

Entrainment and Pressure Drop in Concurrent Gas - Liquid Flow: I. Air - Water in Horizontal Flow

MOYE WICKS, III, and A. E. DUKLER

University of Houston, Houston, Texas

Experimental equipment and data are reported for entrainment and energy loss in annular, two-phase flow of water and air. Measurements were made with a sample withdrawal technique in 1- and 3-in. horizontal tubes. A knowledge of entrainment is necessary to an understanding of various mass transfer, heat transfer, and separation problems in two-phase flow. A preliminary correlation is presented.

Research in two-phase gas-liquid flow has increased steadily over the past ten years. In addition to a long-standing need for a better theoretical understanding of this type of flow the demands of a group of important industrial problems have accelerated this work.

Several investigators (*8, 17*) have demonstrated that when two phases flow together in a tube the liquid and gas streams can assume several different shapes. At high gas rates a predominant pattern is annular flow with the liquid at the wall and the gas moving in the core. This type of flow is thought to be accompanied by a dispersion or entrainment of part of the liquid in the gas phase. Entrainment is of considerable importance to an understanding of mass transfer, heat transfer, separation processes, and energy loss. This paper reports the first phase of a program to study entrainment. Equipment designed for direct measurement of entrainment and entrainment distribution is described. Experimental data on the air-water system is presented and preliminary correlation is proposed.

PREVIOUS STUDIES

Experimental data on entrainment or entrainment-measuring techniques in moving gas streams are very limited in the literature. Several studies of drop distribution from nozzles, spray chambers, and rotating disks (*16*) can be found. However in each of these cases the amount of liquid dispersed can be predetermined by the experimenter and the problems restricted to a study of drop-size distribution, spray areas, etc. In two-phase flow the entrainment is generated by the action

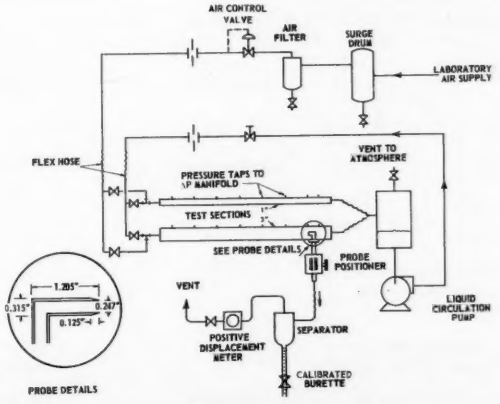

Fig. 1. Experimental equipment.

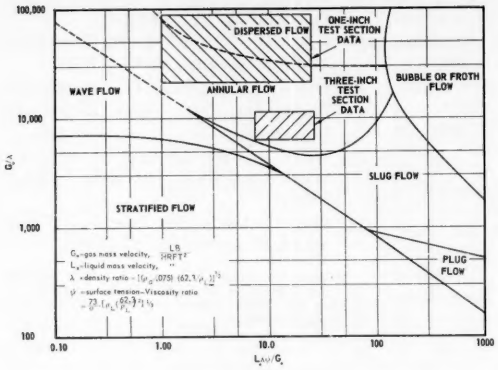

Fig. 2. Flow regimes.

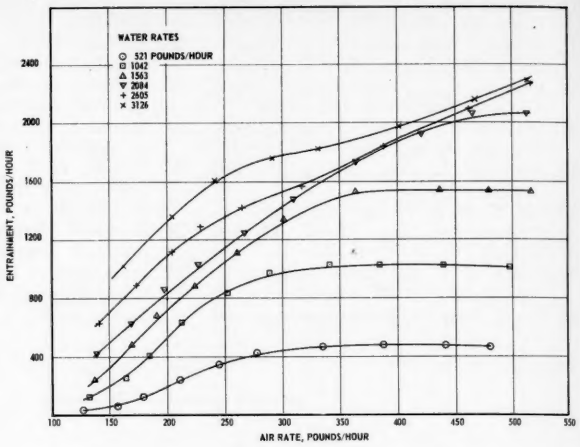

Fig. 3. Entrainment air on the tee, 1-in. tube.

of the gas on the liquid, and it is first necessary to determine how much liquid is entrained. The only source of reliable published data in the literature seems to be five points presented by Alves (2), four for air-water and one for an SAE-oil system. Entrainment data are also reported by Krasjakova (*12*). A study of these Russian data seems to indicate that the experiments were carried out in stratified flow, and flooding of the sampling tube took place. Less generally known are two studies at the University of Delaware; Fritzlen (7) and Budd (*4*) measured entrainment over limited conditions.

Closely associated studies are the work of Alexander and Coldren (*1*) who measured droplet deposition rate downstream from an atomizer spraying into a turbulent air stream and Longwell and Weiss (*15*) who measured distribution of fuel injected into high velocity air streams. In both of these cases all of the liquid was injected by some device into the gas phase and then allowed to distribute. Entrainment was close to 100%. Most recently Hanratty and Engen (*9*) report on the nature of waves formed by the flow of air across a water surface. Lane (*14*) and Hughes *et al.* (*11*) have suggested mechanisms whereby the gas moving across the surface may generate drops which are carried along in the gas phase.

EXPERIMENTAL APPARATUS

General

The system used in this study was air and water.

Figure 1 is a schematic diagram of the equipment used. After passing through control valves and calibrated metering devices the fluids entered the test section through a standard 1-in. screwed tee connection. The piping was arranged so that each phase could be injected at either the side or the run of the mixing tee.

Two-phase pressure drop can be strongly affected by mechanical vibrations transmitted to the test section (*13*). For this reason care was taken to insulate the system from such pulsations by the use of rubber-tubing connections up and downstream of the test sections. Rubber-cushioned machine bolts supported the test section at 3-ft. intervals.

A baffled 33-gal. galvanized barrel served as the water reservoir and separator. Air discharged to the atmosphere through a 3-in. gate valve on top of the barrel. Back pressure in the test section was controlled by this valve.

Table 1 shows pertinent dimensions for each test section.

Pressure Drop

When one measures two-phase pressure drop with a manometer, the lines between manometer and pressure tap must be full of one phase or the other. Preliminary experiments clearly demonstrated that the presence of two phases can cause errors in pressure drop as large as the value being measured. A purge of gas into the test section through the lead lines can be used to maintain this single-phase condition. The question arises whether this purge of itself affects the manometer reading when small differences are measured. This point was resolved by equalizing the pressure drop due to flow of purge gas in the two lead lines. The flow to each side was separately adjusted until two manometers measuring lead-line pressure drop showed the same reading. Additional details are available in reference *19*.

The technique just described was verified by excellent agreement obtained between calculated and experimentally measured pressure drop for single-phase air flow through the test section. Moreover neither pressure drop nor entrainment was measurably affected by the magnitude of the purge rate as long as it was less than 1% of the total gas rate to the test section.

Entrainment

A direct sample-withdrawal method was devised to measure entrainment. The liquid droplets and gas entered a 5/16-in. stainless steel probe with dimensions as shown in Figure 1. The probe mouth was located at the axis of the test section. Liquid and gas were separated in a small impingement separator with liquid dropping to a cali-

Table 1. Data Describing Test Sections

Test section Measurement	1-in. test section (type L copper water tube)	3-in. test section (type L copper water tube)
Outside diameter, in.	1.125	3.125
Wall thickness, in.	0.050 ± 0.004	0.090 ± 0.007
Inside diameter, in.	1.025 ± 0.008	2.945 ± 0.014
Total length, ft., in.	20′ 3¼″	20′ 6½″
Distance from entrance tee to entrainment, sampling hole, fee, in.	19′ 1⅛″	19′ 1⅜″
Distance from entrance tee to upstream pressure tap, ft., in.	6′ 4¼″	(No pressure-drop data obtained)
Distance from entrance tee to downstream tap, ft., in.	18′ 4¼″	(No pressure-drop data obtained)

TABLE 2. TYPICAL DATA

Run no.	W_L lb./hr.	t_L °F.	μ_L lb.$_M$/ ft. hr.	W_G lb./hr.	t_G °F.	μ_G lb.$_M$/ ft. hr.	ρ_G lb.$_M$/ cu. ft.	$(Re)_G$ $x10^{-5}$	f_G	$\left(\frac{dP}{dL}\right)_{TP}$ lb.$_F$/ sq. ft./ft.	m $x10^2$ ft.	$(Re)_L'$	E lb.$_M$/hr.	X	R lb.$_M$cu. ft./ lb.$_F$hr.
2,106	521	85	1.92	244	95	0.0455	0.0900	0.809	0.0190	22.9	0.569	1,320	351	0.109	2.30
2,107	521	86	1.90	211	95	0.0455	0.0891	0.705	0.0204	19.3	0.880	2,180	243	0.125	2.40
2,108	521	87	1.88	179	95	0.0455	0.0882	0.604	0.0222	15.9	1.26	3,100	130	0.145	2.03
2,109	521	87	1.88	158	95	0.0455	0.0876	0.536	0.0233	13.5	1.50	3,500	60	0.161	1.31
2,110	521	87	1.88	127	95	0.0455	0.0865	0.435	0.0230	9.21	1.95	3,820	39	0.196	1.54
2,201	1,042	86	1.91	498	95	0.0455	0.1010	1.64	0.0158	67.1	0.122	203	1,016	0.105	1.98
2,202	1,042	85	1.92	439	95	0.0455	0.0991	1.44	0.0177	59.5	0.119	154	1,022	0.118	2.82
2,203	1,042	84	1.94	384	95	0.0455	0.0972	1.26	0.0199	52.1	0.118	112	1,028	0.133	4.03
2,204	1,042	84	1.94	340	95	0.0455	0.0957	1.12	0.0220	46.0	0.126	112	1,028	0.149	5.60
2,205	1,042	85	1.92	289	95	0.0455	0.0930	0.952	0.0251	39.1	0.254	558	970	0.174	8.25

brated burette and the gas vented to the atmosphere. A schematic drawing of this sampling arrangement is shown in Figure 1.

Liquid flow through the probe was determined by measuring the time to fill a calibrated burette. Knowing probe and pipe inside diameters one could calculate total entrainment by multiplying the mass velocity through the probe by the cross-sectional area of the pipe:

$$E = G' \, x \, A \qquad (1)$$

Equation (1) is actually a special case of the general equation

$$E = \int_o^{2\pi} \int_o^{r_o - m} G(r, \theta) r dr d\theta \qquad (2)$$

which degenerates to (1) when G is independent of both r and θ and when the liquid film thickness is negligible compared with the pipe radius. To investigate this point entrainment was measured at various probe positions in both horizontal and vertical planes. Pertinent observations can be summed up as follows:

1. Variation of entrainment with probe position was greatest at low values of percentage total input liquid entrained.
2. Sensitivity to probe position decreased as completely dispersed flow was approached.
3. Even for the low percentage entrainment conditions sampling from the center of the pipe gave an averaged value for liquid loading.

Over the range of variables investigated the following factors were shown to have no significant effect on measured entrainment mass velocity when gas and liquid rates to the tube were held constant:

1. Gas flow through the probe from 9 1/2 to 1/3 of the mass velocity of gas in the test section.
2. Ratio of outside to inside probe diameter, from 1.40 to 1.02; probes of the following nominal size were tested 1/8, 3/16, 1/4, 5/16, 3/8, and 1/2, all stainless steel.
3. Length of probe along the tube axis; from 0.43 to 1.08 test-section diameters.

These measurements suggested that the capture efficiency (the ratio of the actual droplet capture rate to that if there were no interference from the sampler) was essentially 100%. Dussourd and Shapiro (*6*) suggested this capture efficiency term and related it to the dimensions of the sampler. Using their relationships one can predict the capture efficiency to be 100% for this probe system.

EXPERIMENTAL DATA

This initial series of experiments was restricted to the system water-air at low pressures. Entrainment and pressure-drop data were taken in the 1-and 3-in. test sections over the following ranges of rates: 1-in. test section; water rate: 500 to 3,100 lb./hr., air rate: 100 to 500 lb./hr., 3-in. test section; water rate: 4,000 to 8,000 lb./hr., air rate: 300 to 550 lb./hr.

Data were obtained with two basic entrance sections for all rates: (*a*) water entering along the axis of the test section with air introduced at 90 deg. and (*b*) air entering along the axis of the test section with water introduced at 90 deg. In addition the effect of absolute pressure level over the limited range of 0 to 5 in. of mercury, gauge, was explored. Two hundred and twenty-five data points were obtained for the 1-in. section and forty-four points were taken in the 3-in. section. In addition a limited number of measurements were made to determine entrainment distributions in the flow cross-sectional area.

Some picture of the flow regimes covered here can be obtained by the use of the graphical form suggested by Baker (*3*). In Figure 2 the area covered by this work is shown blocked in for the 1- and 3-in. tube. It should be noted that over the region shown for the 1-in. tube entrainment varied from less than 5 to 100% of the liquid feed to the test section. The transition from annular to dispersed flow is gradual, and no distinct boundary can be defined.

Typical plots of the raw entrainment data for the 1-in. test section appear in Figures 3 and 4 for each entrance section. In both cases shown the static pressure at the sampling point was 5 in. of mercury gauge. Similar data for the 3-in. section

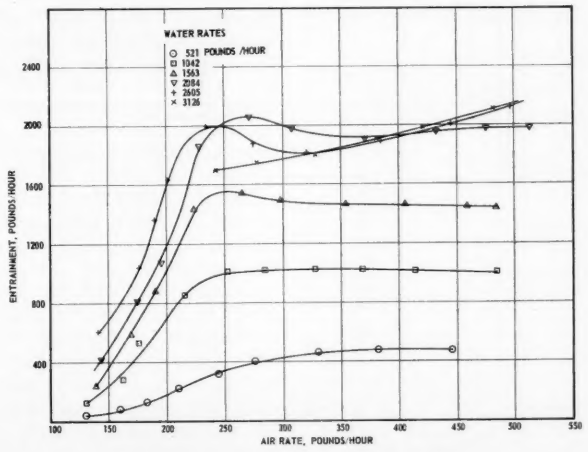

Fig. 4. Entrainment water on the tee, 1-in. tube.

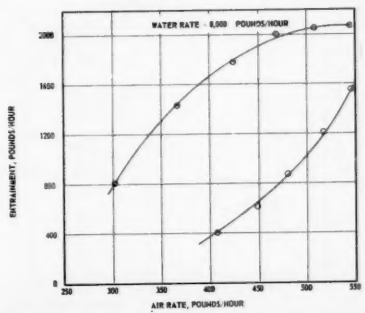

Fig. 5. Entrainment 3-in. tube, water on the tee.

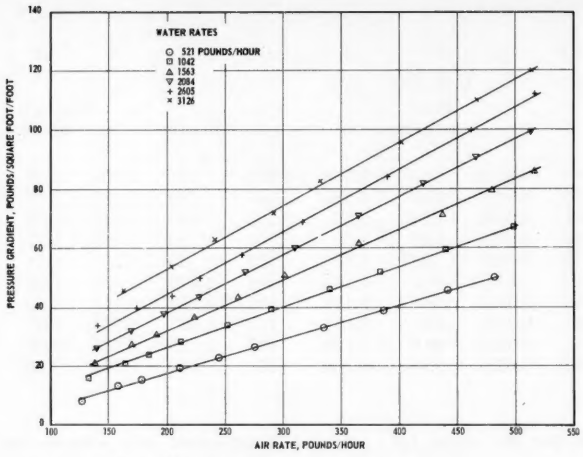

Fig. 6. Pressure drop 1-in. tube, air on the tee.

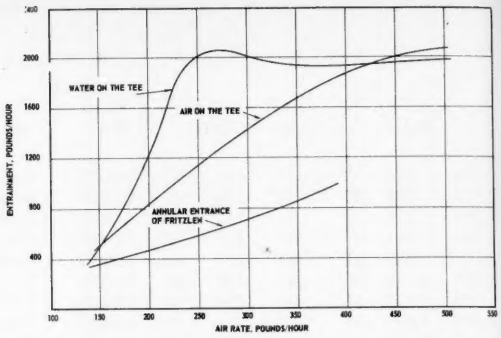

Fig. 8. Effect of entrance-section shear on entrainment.

are presented in Figure 5, where the air pressure was 2.5 in. of mercury. Typical data are shown in Table 2. Complete data may be found in reference *19*. Pressure-drop data for the 1-in. test section corresponding to data in Figures 3 and 4 are presented in Figures 6 and 7. In the 3-in. test section pressure drop was very small, and accurate values could not be obtained.

DISCUSSION OF DATA

The entrainment and pressure-drop data show consistent trends at all gas and liquid rates. The general trends are: both entrainment and pressure drop increase with water rate for a given air mass rate; both quantities increase with air mass rate for a given water rate; both entrainment and pressure drop decrease with increased total system pressure.

The influence of entrance section can be seen from Figure 8. With air on the run of the entrance tee the entrainment is higher (except at essentially completely dispersed flow) and the pressure drop is lower. Hinze (*10*) has suggested that the critical Weber number has different values depending on the manner in which the liquid mass is exposed to acceleration sources. He suggests a value of 13 for a sudden shock exposure to a fast moving gas stream and a value of 22 for gradual acceleration. It appears likely that water entering on the side of the inlet tee would behave as if it were suddenly exposed to sudden shock. On the other hand when air entered on the side into a liquid stream already filling the pipe cross section, the accelerations would be more gradual. These two entrance sections could be expected to correspond to two different critical Weber numbers. By the definition of the Weber number

$$We = \frac{\rho_A (U_A - U_W)^2 D}{\sigma_W \; g_c} \qquad (3)$$

the maximum stable drop size can be expected to be smaller for the air on the run entrance section. In accordance with the Mugele-Evans (*18*) drop size distribution theory the drop size over the entire range will be smaller. Redeposition of drops created at the entrance can be expected to be lower and therefore the measured entrainment larger, as shown in Figure 8.

A comparison of pressure drops is not nearly as clear-cut. The conditions of Figure 9 demonstrate that the two phase pressure drop is lower when entrainment is higher at equivalent phase flow rates. This seems to be generally true at the lower liquid rates and suggests that it requires less energy to transport a given amount of liquid in the gas phase rather than as a thin film adjacent to the wall. However at high liquid rates this difference seems to disappear. Further careful studies of this trend are in progress.

Further information on the effect of entrance section on entrainment appears in Figure 8 where the data of Fritzlen (*7*) are compared with those of this study for the two entrance sections. Fritzlen's entrance section was a very gradual annular entrance which contacted the two phases with minimum interaction. Figure 8 shows that as the degree of shock due to entrance section design increases, the entrainment increases. This trend is in accord with expectations, since drop size decreases as the critical Weber number decreases. Calvert and Williams (*5*) report data which also seem to support these findings. Their data for upward

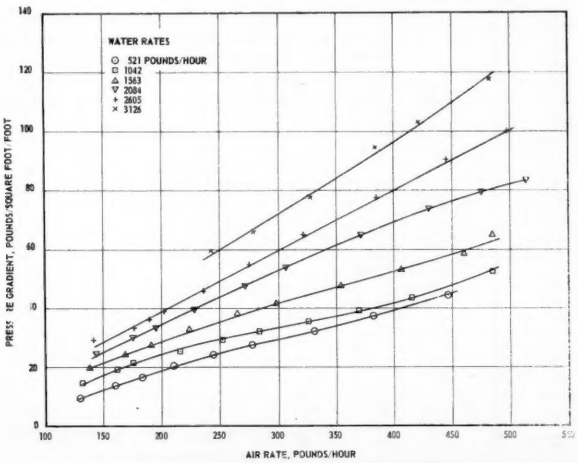

Fig. 7. Pressure drop 1-in. tube, water on the tee.

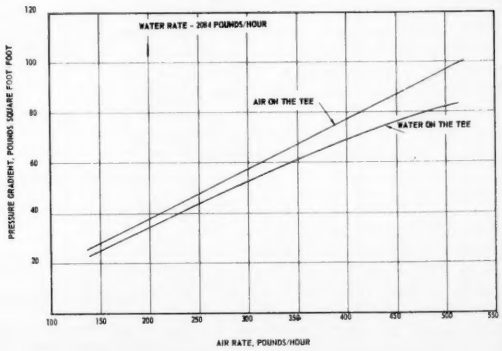
WATER RATE - 2084 POUNDS/HOUR
AIR ON THE TEE
WATER ON THE TEE
PRESSURE GRADIENT, POUNDS SQUARE FOOT FOOT
AIR RATE, POUNDS/HOUR

Fig. 9. Entrance-section effect on pressure drop.

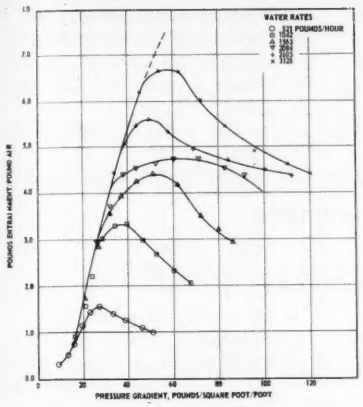

Fig. 10. Entrainment concentration, air on the tee.

concurrent two-phase flow appear to show a distinctly higher two phase pressure drop for a gradual annular entrance than for tee and ell entrances.

Figures 10 and 11 present entrainment in concentration units as a function of pressure drop. The curves for each water rate originate from a single curve at the lower gas rates. By careful observations it was found that this curve, common to all liquid rates, seemed to characterize a change in the flow pattern. As gas rate was increased and individual liquid rate lines emerged, severe manometer fluctuation seemed to be damped and a more nearly steady state flow achieved. It is suggested that this may represent the upper limit of the slug flow region, where the frequency of the slugs becomes effectively infinite and the amplitude approaches zero.

PRELIMINARY CORRELATION

Several approaches to entrainment theory have been examined, based on a study of the forces acting at the interface. As yet this method has not produced usable results. The complexity of the resulting relationships require additional experiments to define the entrainment distribution and its variation with fluid properties and channel dimensions in order to assist in arriving at suitable simplifying assumptions. Further experimental work along these lines is now in progress. However it has been possible to arrive at a semitheoretical basis for explaining the gross entrainment. This method is based on the assumption that the similarities in the mechanisms for mass and momentum transfer which have been shown to exist in single-phase flow also apply in two-phase flow. The eddies moving between the interface and the gas stream transport the liquid between the bulk liquid phase and the drop form in the gas. It thus seems likely that those external factors which determine the scale, velocity, and other characteristics of the eddy motion would influence, in a similar manner, the entrainment. Although the complete picture for energy loss and momentum transfer in two-phase flow is yet to be evolved, a preliminary relationship of entrainment can be arrived at in the following manner.

Martinelli defines ϕ as

$$\phi^2_G = \frac{\left(\frac{dP}{dL}\right)_{TP}}{\left(\frac{dP}{dL}\right)_G} \qquad (4)$$

The pressure gradient is directly proportional to the rate of momentum transfer per unit area in the direction normal to flow. Thus ϕ^2_G becomes the ratio of the rates of momentum transfer in single and two-phase flow.

Define an analogous quantity ϕ'_G such that it represents the ratio of the rate of mass transfer per unit area in two-phase flow to the mass transfer rate in a unit area for single-phase flow. Now, Martinelli has correlated the term ϕ_G with a parameter X defined by Equation (5):

$$X = \left[\frac{\left(\frac{dP}{dL}\right)_L}{\left(\frac{dP}{dL}\right)_G}\right]^{1/2} \qquad (5)$$

It is assumed that this same variable X can be used to correlate the quantity ϕ'_G, defined by Equation (6):

$$\phi'^2_G = \frac{M_{TP}}{M_G} \qquad (6)$$

It is necessary to obtain expressions for M_{TP} and M_G.

The rate of mass transfer between the liquid surface and the bulk gas is the sum of the mass of gas and liquid which is transported as the eddies change position. Under most conditions

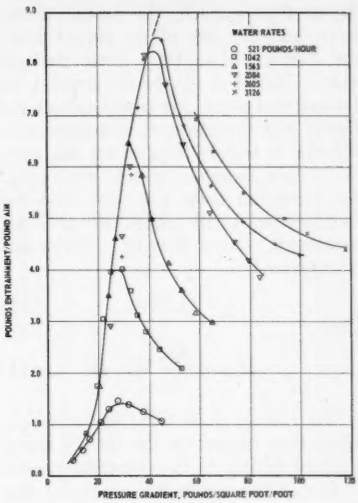

Fig. 11. Entrainment concentration water on the tee.

the liquid gas density ratio is large. For any significant degree of entrainment the mass of liquid involved is large compared with the vapor. M_{TP}, then, is uniquely related to the liquid movement. Entrainment can be pictured as a process in dynamic equilibrium. If a concentration of entrained material is defined as C_E, the rate of mass transfer can be written in the simplified expression

$$M_{TP} = kC_E \qquad (7)$$

When one defines E as the mass rate of flow of entrained liquid and Q_G as the volumetric flow of gas

$$C_E = \frac{E}{Q_G} \qquad (8)$$

$$M_{TP} = \frac{kE}{Q_G} \qquad (9)$$

Although no quantitative picture of the factors influencing k can be given now, it is possible to examine this qualitatively. The rate of shearing from the liquid surface will depend on the pro-

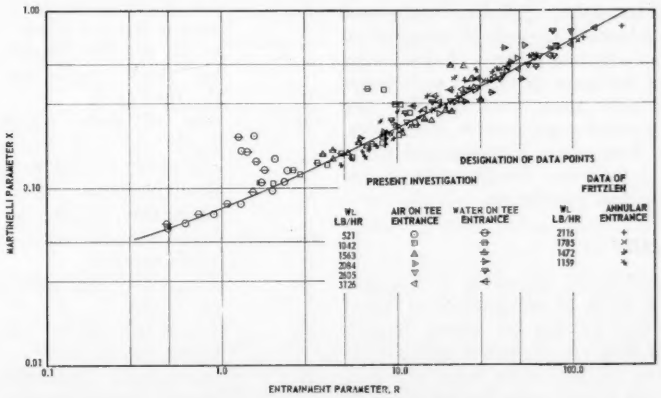

Fig. 12. Entrainment correlation.

file of that surface, the forces acting there, and the size of the liquid droplets formed when they enter the gas phase. Therefore k should depend on the external rates, the properties of the liquid, and the channel dimensions; in addition k should depend on the critical Weber number which determines the maximum drop size and drop-size distribution. Until additional data are developed, the following relationship is suggested:

$$k \sim Q_L We_c \qquad (10)$$

Thus

$$M_{TP} \sim \frac{Q_L}{Q_G} We_c E \qquad (11)$$

The rate of mass transfer for single-phase flow represents the rate of movement of eddies in the direction normal to flow. Once again it is assumed that this is proportional to the rate of momentum transfer or to the pressure gradient calculated for single-phase flow:

$$M_G = K\left(\frac{dP}{dL}\right)_G \qquad (12)$$

When one combines (11) and (12) into the definition of ϕ'_G, Equation (6) gives

$$\phi'^2_G = \frac{Q_L/Q_G\, We_c E}{K(dP/dL)_G} \qquad (13)$$

When one sets

$$R = \frac{Q_L/Q_G\, We_c E}{\left(\frac{dP}{dL}\right)_G} \qquad (14)$$

and assumes that the Martinelli parameter X will correlate ϕ'_G as it did ϕ_G, then X should also correlate the entrainment group R. Figure 12 shows all of the data of this study and the data of Fritzlen plotted on this basis. In accordance with entrance section discussions above, different critical Weber numbers could be expected for the two entrance sections used in this study and for the entrance section of Fritzlen. Based on the suggestions of Hinze a value of We_c of 22 was assumed to apply to Fritzlens equipment, with values of 13 and 16 assigned to the two entrance sections of this study. Except for some points in each series which drift away from the line, the data appear to agree within about 25% of the best curve. Experimental work, now in progress, should assist in improving this correlation.

SUMMARY

Experimental apparatus is described for the study of entrainment of liquid into a fast moving gas stream. Experimental data are presented over a wide range of air and water rates in a 1-in. tube and over a more limited range in a 3-in. tube. The influence of entrance-section design on pressure drop and entrainment is demonstrated. A preliminary correlation is presented relating an entrainment variable to the single phase pressure drops. Work is continuing with studies of entrainment distribution and property effects as well as new theoretical approaches.

ACKNOWLEDGMENT

The authors are sincerely grateful to the National Science Foundation whose financial sponsorship of the project was indispensable. The helpful suggestions of F. L. Worley, Jr., M. A. Pike, Jr., and B. W. Burke were of great assistance in the construction of the experimental equipment.

NOTATION

A = test section cross-sectional area, sq. ft.
C_E = concentration of entrained liquid, lb.$_M$/cu. ft.
D = drop diameter, ft.
$\left(\frac{dP}{dL}\right)_G$ = pressure gradient which would exist if gas flowed alone, lb.$_F$/sq. ft./ft.
$\left(\frac{dP}{dL}\right)_L$ = pressure gradient which would exist if liquid flowed alone, lb.$_F$/sq. ft./ft.
$\left(\frac{dP}{dL}\right)_{TP}$ = pressure gradient in two-phase flow, lb.$_F$/sq. ft./ft.
E = measured liquid entrainment calculated by Equation (1), lb.$_M$/hr.
G = entrainment mass velocity at any point in the pipe cross-sectional area, lb.$_M$/hr. sq. ft.
G' = entrainment mass velocity through the sampling probe measured at the pipe center line, lb.$_M$/hr. sq. ft.
g_c = 32.17 lb.$_M$ ft./lb.$_F$sec.^{2}
K = proportionality constant in Equation (12)
k = rate constant in Equation (7)
M_G = rate of mass transfer per unit area in the gas phase normal to the net flow direction during single phase gas flow, lb.$_M$/hr. sq. ft.
M_{TP} = rate of mass transfer of liquid per unit area in the gas phase normal to the net flow direction during two-phase flow, lb.$_M$/hr. sq. ft.
m = liquid film thickness, ft.
P = static pressure
Q_G = volumetric flow rate of gas, cu. ft./hr.
Q_L = volumetric flow rate of liquid, cu. ft./hr.
R = entrainment correlation parameter defined by Equation (14), lb.$_M$ cu. ft./lb.$_F$ hr.
r = internal radial distance, ft.
r_o = inside test section radius, ft.
U_A = entering air velocity, ft./sec.
U_W = entering water velocity, ft./sec.
We = Weber number defined by Equation (3)
We_c = critical Weber number

Greek Letters

θ = angle between two radius vectors, radians
π = 3.14159
ρ_A = air density, lb.$_M$/cu. ft.
σ_W = interfacial tension, lb.$_F$/ft.
ϕ = Martinelli momentum transfer parameter defined by Equation (4)
ϕ'_G = two-phase mass transfer parameter defined by Equation (6)
χ = Martinelli momentum transfer parameter defined by Equation (5)

LITERATURE CITED

1. Alexander, L. G., and C. L. Coldren, *Ind. Eng. Chem.*, **43**, 1324 (1951).
2. Alves, G. E., *Chem. Eng. Progr.*, **50**, 449 (1954).
3. Baker, O., *Oil Gas J.*, 185 (July 26, 1954).
4. Budd, J. T., III, B.Ch.E. thesis, Univ. Del., Newark (1950).
5. Calvert, Seymour, and Brymer Williams, *A.I.Ch.E. Journal*, **1**, 78 (1955).
6. Dussourd, J. L., and A. H. Shapiro, "A Deceleration Probe for Measuring Stagnation Pressure and Velocity of a Particle-Laden Gas Stream," Heat Transfer and Fluid Mechanics Inst., Univ. Calif., Los Angeles (June 23-25, 1955).
7. Fritzlen, A. F., M.Ch.E. thesis, Univ. Del., Newark (1951).
8. Gazely, C., "Co-current Gas-Liquid Flow—III, Interfacial Shear and Stability," Heat Transfer and Fluid Mechanics Inst., Univ. Calif., Berkeley (1949).
9. Hanratty, T. J., and J. M. Engen, *A.I.Ch.E. Journal*, **3**, 299 (1957).
10. Hinze, J. O., *ibid.*, **1**, 289 (1955).
11. Hughes, R. R., H. D. Evans, and C. V. Sternling, *Chem. Eng. Progr.*, **49**, 78 (1953).
12. Krasjakova, L. U., *J. Tech. Phys. (U.S.S.R.)*, **22**, No. 4, 654 to 699 (1952).
13. Laird, A. D. K., *Trans. Am. Soc. Mech. Engrs.*, **76**, 1005 (1954).
14. Lane, W. R., *Ind. Eng. Chem.*, **43**, 1312 (1951).
15. Longwell, J. P., and M. A. Weiss, *ibid.*, **45**, 667 (1953).
16. Marshall, W. R., *Chem. Eng. Progr. Monograph Ser. No. 2*, **50** (1954).
17. Martinelli, R. C., and R. W. Lockhart, *Chem. Eng. Progr.*, **45**, 39 (1949).
18. Mugele, R. A., and H. D. Evans, *Ind. Eng. Chem.*, **43**, 1317 (1951).
19. Wicks, Moye, III, M.Ch.E. thesis, Univ. Houston, Houston, Texas (1958).

Manuscript received August 4, 1959; revision received December 28, 1959; paper accepted January 4, 1960.

Performance of Packed Columns: VI. Mass Transfer Rates for Dehumidification at High Solute Concentrations

H. L. SHULMAN and R. G. ROBINSON

Clarkson College of Technology, Potsdam, New York

Air-carbon tetrachloride gas streams were dehumidified with cold liquid carbon tetrachloride in a short 4.0-in. diameter column packed with 0.5-in. Raschig rings in an attempt to explain reported unsuccessful attempts to correlate dehumidification data obtained at high solute concentration.

The data were in satisfactory agreement with a previously presented correlation if the Schmidt number was evaluated at average film conditions and interfacial conditions were employed with rigorous calculation methods to evaluate the mass transfer coefficients.

The previous paper (*10*) of this series presented a correlation for mass transfer in packed columns at low and high solute concentrations which was based on adiabatic vaporization data.

$$\left[\frac{k_G M_M P_T}{G}\right]\left[\frac{P_{BM}}{P_T}\right]^{2/3}\left[\frac{\mu}{\rho D_V}\right]^{2/3} = 1.195\left[\frac{D_P G}{\mu(1-\epsilon)}\right]^{-0.36} \quad (1)$$

Cairns and Roper (*1*) obtained a similar correlation for adiabatic vaporization data employing a wetted-wall column:

$$\left[\frac{k_G M_M P_T}{G}\right]\left[\frac{P_{BM}}{P_T}\right]^{0.83}\left[\frac{\mu}{\rho D_V}\right]^{2/3} = 0.025\left[\frac{DG}{\mu}\right]^{-0.2} \quad (2)$$

In a later attempt to test the usefulness of Equation (2) Cairns and Roper (*2*) obtained mass transfer data at high humidities for dehumidification runs in a wetted-wall column. These data however could not be correlated by Equation (2) or any other satisfactory method.

Tabular material has been deposited as document 6383 with the American Documentation Institute, Photoduplication Service, Library of Congress, Washington 25, D. C., and may be obtained for $1.25 for photoprints or 35-mm. microfilm.

Yoshida and Tanaka (*11*) on the other hand, working with columns packed with Raschig rings, were able to obtain satisfactory correlations of both vaporization and dehumidification data obtained at low humidities. There are several possible explanations for the different conclusions reached by Cairns and Roper (*2*) and Yoshida and Tanaka (*11*). The first is that correlations obtained for low solute concentrations do not apply at high concentrations for dehumidification. The second is that packed-column data lead to correlations which are not similar in form to those obtained for wetted-wall columns. The third, and most likely explanation, is that Cairns and Roper (*2*) used an oversimplified method of calculation to evaluate their data. They assumed the bulk liquid temperature was equal to the interfacial temperature and employed a logarithmic mean driving force to calculate the mass transfer coefficients. These simplifications are suitable for adiabatic vaporization work when the liquid temperature is held constant at the adiabatic saturation temperature but are not justified for dehumidification work where heat transfer takes place in the liquid phase and the interfacial temperature may be substantially different from the bulk liquid temperature. Yoshida and Tanaka (*11*) working at low humidities were able to estimate interfacial temperatures and employ a rigorous trial-and-error, graphical method of calculation to evaluate the mass transfer coefficients.

In order to test the explanations offered above and the extension of the use of Equation (1) to dehumidification work an experimental investigation was undertaken to obtain suitable dehumidification data. A short 0.5-in. Raschig ring packed column was employed to dehumidify air-carbon tetrachloride gas streams at low and high solute concentrations with cold liquid carbon tetrachloride. This system has a number of advantages over a wetted-wall column employing the air-water system. A short packed column has fluid-flow characteristics representative of all irrigated packed columns and has been shown (*9, 10*) to yield correlations in which the effects of variables such as those contained in the Schmidt and Reynolds numbers are the same regardless of column height and diameter provided the column diameter to nominal packing-size ratio is greater than 8.0.

When the air-carbon tetrachloride system is used, the physical properties of the gas stream are found to vary considerably with concentration which is not the case for the air-water system. For example the Schmidt number varies more than fivefold for air-carbon tetrachloride in the 0 to 0.70 solute mole fraction range, whereas it can be assumed constant for the air-water sys-

tem over the same concentration range. For this reason correlations developed with the air-carbon tetrachloride system are more likely to be of a sufficiently generalized nature to permit extension of their use to other systems. In addition, when physical properties vary rapidly with concentration, there is an opportunity to determine whether dimensionless groups evaluated at film or bulk conditions provide better correlations.

Short packed columns have a shortcoming however in that excellent gas and liquid distribution as well as even small end effects combine to yield much higher mass transfer coefficients than can be expected from the same packings in commercial installations. This factor limits the use of a short packed column to determining the form of a correlation and the effects of the variables. The actual prediction of mass transfer coefficients for design purposes should be based on methods which have been developed from data obtained with columns representative of those used in commercial installations. Such methods have been discussed in previous papers of this series (*6, 7, 8*).

APPARATUS

A schematic diagram of the apparatus employed in this work is shown in Figure 1.

The packed column used consisted of a 4.0-in. I. D. pyrex tube packed to a depth of 1.5 in. with 0.5-in. diameter porcelain Raschig rings. The outside of the column was heated with nichrome heating wire and insulated to avoid condensation on the walls and maintain essentially adiabatic operation. Air flow to the column, provided by a blower, was metered by a calibrated set of rotameters. Coarse adjustments of air flow were made with a variable speed drive on the blower, and valves located below the rotameters were used for fine adjustments.

The air supplied by the blower was heated to approximately 700°F. by a 4.5-kw. heater with a thermostatic temperature controller. Carbon-tetrachloride vapor was supplied by a boiler heated with a 2-kw. immersion heater with power input regulated by a variable transformer. The carbon-tetrachloride vapor was superheated by passing through a length of pipe heated by two 400-w. flexible strip heaters. The hot carbon tetrachloride vapors were then mixed with the hot air from the blower and passed through a heated, insulated pipe into the bottom of the column. The inlet gas temperature was measured just below the column by an iron-constantan thermocouple. The hot gases then passed through a gas distributor consisting of a hollow cross of brass bar stock ⅝ in. wide and ⅜ in. deep. Two grooves were cut along the underside of each arm of the cross, and six ⅛ holes were drilled along each groove from the end to the center of the cross, making a total of forty-eight discharge holes.

The gas passed upward through the packing, and its temperature above the packing was measured by a mercury thermometer placed directly in the gas stream above the liquid distributor. From the column the exit gases passed through two double pipe heat exchangers that removed by condensation most of the carbon tetrachloride remaining in the gas stream. The condensed carbon tetrachloride was returned to the boiler and the air vented to the atmosphere.

Liquid was supplied to the column by a 5-gal. steel constant head tank equipped with an overflow to assure constant liquid level. This tank was located approximately 5 ft. above the top of the column. The liquid flow was metered by a calibrated rotameter and passed into the top of the column. It was discharged directly above the packing to minimize end effects. The liquid distributor consisted of ¼-in. copper tubing forming a continuous coil of two turns. Approximately fifty holes 1/32 in. in diameter were drilled along the underside of the distributor.

The temperature of the inlet liquid was measured by a glass enclosed iron-constantan thermocouple that extended directly into the liquid distributor through the liquid inlet line. A portion of the liquid leaving the packing was collected in a shallow trough and its temperature measured by an iron-constantan thermocouple always immersed in fresh liquid from the packing in this trough. The exit liquid passed into a 5-gal. steel receiving tank located below the column. A gear pump was used to circulate the liquid. A glass wool packed filter was placed in the line between the pump and the constant head tank. Also a heat exchanger consisting of 50 ft. of coiled 0.375-in. copper tubing in a galvanized iron jacket was placed in this line to cool the liquid to the proper inlet temperature.

Inlet gas samples were taken from the inlet gas line ½ in. below the distributor. Exit-gas samples were taken through a sampling tube located just above the liquid distributor. The samples were drawn through 0.125-in. copper tubing by a slight constant vacuum, and analyses were made with a Consolidated Electrodynamics Corporation Chromatographic Analyzer, type 26-201. The analysis was made for air, and the carbon tetrachloride concentration was determined by difference. It was found that air peaks were of constant base width, so the air concentration was determined by comparing the peak height for a given sample with the peak height for pure air. The carrier gas used was helium, and a constant flow rate was used that gave sharp air peaks reproducible to within 0.2%.

PROCEDURE

The chromatographic analyzer required approximately 8 hr. to reach equilibrium, and it was turned on and set the night before runs were to be made.

The air flow was turned on first and the air heater set at 700°F. Power was supplied to the vapor line heating coils to bring the piping and insulation up to operating temperature. Then the boiler and carbon tetrachloride vapor line strip heaters were turned on, along with the column heating coil and sample line heaters. As soon as the inlet gas came up to fairly constant temperature, the liquid flow was started. A very high liquid rate was maintained for approximately ½ hr.

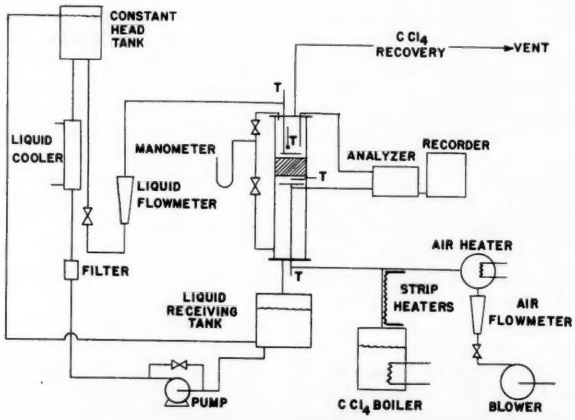

Fig. 1. Schematic diagram of apparatus.

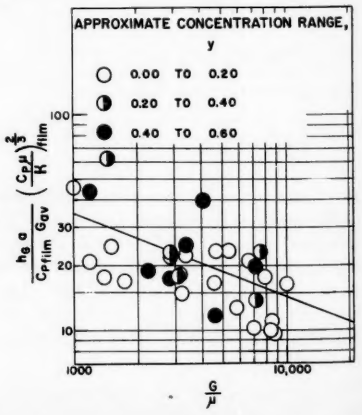

Fig. 2. Correlation of heat transfer data for vaporization runs.

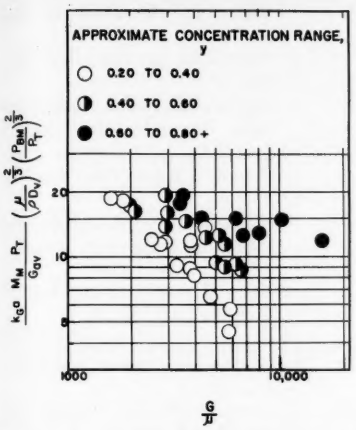

Fig. 3. Dehumidification data evaluated with bulk liquid conditions and logarithmic mean driving forces.

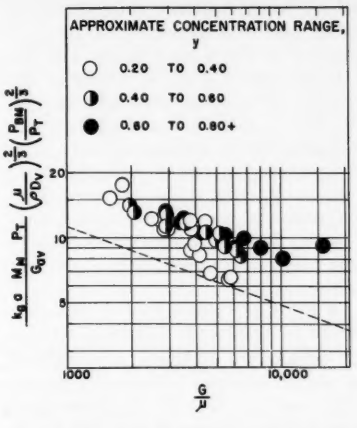

Fig. 4. Dehumidification data evaluated with interfacial conditions and the rigorous method of calculation.

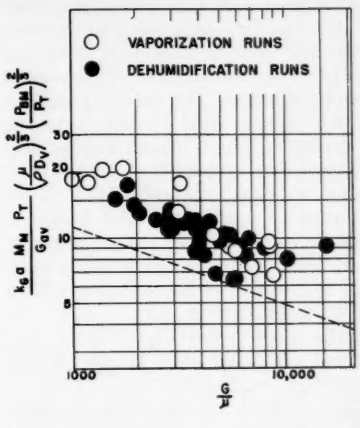

Fig. 5. Comparison of vaporization and dehumidification data obtained with the same packed column.

to thoroughly wet the packing, after which the desired flow rate was set. While the equipment was coming to equilibrium, a series of pure air peaks was taken on the chromatograph to be compared with sample peak heights.

Equilibrium conditions were determined by recording inlet and outlet gas and liquid temperatures. When all four temperatures became constant, equilibrium was attained. This condition required approximately 4 hr. from initial start-up to be fulfilled. After equilibrium had been reached, an outlet gas sample was taken for analysis. The analyzer required about 7 min. per sample, and readings of temperature, air flow, and column pressures were taken while the analysis was going on. Immediately after the outlet gas sample was taken, the inlet gas-sample line was connected to the analyzer, allowing the inlet gas about 7 min. to flush out the sample valve. The inlet gas composition remained constant for long periods and was analyzed as soon as the outlet gas analysis was complete.

When both gas samples had been analyzed, the boiler setting and air rate were changed to the next desired conditions and the column allowed to reach equilibrium once more. An average of one hour was required for the equipment to return to equilibrium under new conditions, at which time the above procedure was repeated. Pure air samples were taken before each run to assure accurate gas analysis.

In addition to the dehumidification runs a series of vaporization runs was made for comparison purposes. The procedure employed for these runs was described previously (*10*).

METHODS OF CALCULATION

Two methods of calculation were employed to evaluate the volumetric mass transfer coefficients k_Ga from the experimental data. The first is a simplified method which was employed for both the vaporization and dehumidification data, although its use can be justified only for the former. It assumes that the interfacial temperature is equal to the bulk liquid temperature for determining the driving forces, and a logarithmic mean driving force based on terminal conditions is employed as follows:

$$k_Ga = \frac{(N_Aa)}{P_T(\Delta y)_{lm}} \qquad (3)$$

where

$$(\Delta y)_{lm} = \frac{(y_i - y)_1 - (y_i - y)_2}{\ln \dfrac{(y_i - y)_1}{(y_i - y)_2}} \qquad (4)$$

and N_Aa is the pound moles of carbon tetrachloride transferred per hour per cubic foot of packing as calculated from the measured air rate and the analyses of the inlet and outlet gas streams.

The second method of calculation represents an attempt to evaluate k_Ga for the dehumidification runs by a rigorous procedure. It involves estimating the actual interfacial temperatures at several points in the column for each run. The true driving forces are then employed in a graphical integration procedure to evaluate k_Ga. An outline of the method follows; a complete calculation is available elsewhere (*4*).

The interfacial temperature can be determined by a trial-and-error procedure for any point in the column from the following transfer equation:

$$k_Ga\,P_T(y - y_i)\lambda_i + h_Ga(T_o - T_i) = h_La(T_i - T_L) \qquad (5)$$

To use this equation it is necessary to know the appropriate values of the transfer coefficients k_Ga, h_Ga, and h_La. The mass transfer coefficient k_Ga was taken from the correlation for vaporization data obtained in a similar column by Shulman and Delaney (*10*). The gas-phase heat transfer coefficient h_Ga was estimated from the line on Figure 2 which combines the vaporization data of this work with that of Shulman and Delaney (*10*). The liquid-phase heat transfer coefficient h_La for the liquid rate employed was estimated to be 13,900 B.t.u./(hr.) (cu. ft.) (°F.) from the data of Yoshida and Tanaka (*11*) corrected for differences in interfacial areas by taking the ratio of h_Ga values and for differences in liquid physical properties by taking the ratio of heat transfer coefficients in tubes under similar conditions.

To evaluate a gas composition and temperature corresponding to an intermediate bulk liquid temperature the bulk gas and liquid temperatures are taken as varying linearly with gas-phase enthalpy. Since the gas-phase enthalpy varies rapidly with composition and relatively slowly with gas temperature, it can be used to calculate a gas-phase composition corresponding to a bulk liquid temperature at an intermediate point in the column.

The calculated values are used to plot an operating line y vs. T_i and an equilibrium line y_i vs. T_i on a y–T_i diagram. Vertical differences between the two lines give the true gas-phase driving force $y - y_i$ which is employed with the following rigorous equation developed from an equation given by Sherwood and Pigford (*5*):

$$\frac{k_Ga\;P_TZ}{G'} = \int_{y_2}^{y_1} \frac{dy}{(1-y)^2(y-y_i)} \qquad (6)$$

The integral is evaluated graphically for each run.

Viscosities and diffusivities were calculated by the methods outlined by Hirschfelder, Curtis, and Bird (*3*). The reported gas rates are an average

of the inlet and outlet rates. Molecular weights and physical properties are determined from an average of inlet and outlet compositions and temperatures except as noted. The Schmidt number, which varies rapidly with changing composition but is almost independent of temperature changes, is always evaluated at film conditions, that is an average of inlet and outlet bulk and interfacial conditions. The reported values of P_{BM} are the arithmetic average of the P_{BM} at the inlet and outlet ends of the column.

The experimental results are presented as plots of $[k_G a\, M_M\, P_T/G]\,[\mu/\rho\, D_V]^{2/3}\,[P_{BM}/P_T]^{2/3}$ vs. G/μ in place of the terms shown in Equation (1). Shulman and Delaney (*10*) showed that data could be correlated equally well by either method and conclusions drawn from one applied to the other.

EXPERIMENTAL RESULTS

Dehumidification data were taken with inlet concentrations as high as 0.843 mole fraction carbon tetrachloride. To detect effects at different concentration levels an attempt was made to classify the data approximately by concentration level in some of the figures. Figure 3 shows the first attempt at correlation with the dehumidification data evaluated by the use of bulk liquid temperatures and logarithmic mean driving forces. This method was found to correlate vaporization data by both Shulman and Delaney (*10*) and Cairns and Roper (*1*). This method is no more successful in this case than it was with the dehumidification data of Cairns and Roper (*2*). The data are seen to scatter, although data at the same concentration level fall together. A simple correction for concentration level does not lead to a successful correlation because the effect of gas rate is not the one expected from Equation (1).

The second method of correlation is shown in Figure 4 with the data evaluated by means of interfacial conditions and the rigorous method of calculation. The broken line is the line of Shulman and Delaney (*10*) for vaporization data in a similar column. The data have been brought together with almost all of the separation at different concentration levels eliminated. In addition the best line through the data would show the effect of gas rate predicted by Equation (1). To explain why the data did not fall on the line given by Shulman and Delaney (*10*) for vaporization data a series of vaporization runs was made in the same column used for the dehumidification runs. Figure 5 shows both sets of data. It can be seen that both vaporization and dehumidification data come together satisfactorily when the data are obtained in the same column. The fact that the earlier data of Shulman and Delaney (*10*) lie on a parallel line below that of this work can probably be explained by the differences introduced in repacking a short column which contains as little as 1.5 in. of packing. Differences in the packing arrangement or some slight modification of end effects could easily produce the observed differences.

Of the three alternative explanations offered to explain the Cairns and Roper (*2*) results the present data indicate the use of incorrect interfacial temperatures, and the use of the logarithmic mean driving force accounts for the inability to obtain a satisfactory correlation.

SUMMARY AND CONCLUSIONS

Vaporization and dehumidification data from this and previous work at low and high solute concentrations indicate mass transfer coefficients for packings can be correlated by

$$\left[\frac{k_G\, M_M\, P_T}{G}\right]\left[\frac{P_{BM}}{P_T}\right]^{2/3}\left[\frac{\mu}{\rho D_V}\right]^{2/3} = 1.195\left[\frac{D_P G}{\mu(1-\epsilon)}\right]^{-0.36} \quad (1)$$

when the Schmidt number is evaluated at average film conditions and interfacial conditions are employed with rigorous calculations to evaluate the mass transfer coefficients.

The constant 1.195 in Equation (1) is based on the work of previous investigators who employed columns and systems for which end effects could be eliminated or evaluated rather than on the data of the present work.

The present work makes it possible to extend the use of Equation (1) and the effective interfacial areas reported previously (*6, 7, 8, 9*) to predict $k_G a$ for a wide variety of gas-liquid contacting operations when the physical properties of the system are known.

ACKNOWLEDGMENT

The authors wish to acknowledge the support of this work under Contract No. AT(30-1)-1463 of the Atomic Energy Commission.

NOTATION

a = effective interfacial area, sq. ft./cu. ft.
C_P = specific heat, B.t.u./(lb.) (°F.)
D = equivalent diameter or characteristic dimension, ft.
D_P = diameter of sphere possessing the same surface area as a piece of packing, ft.
D_V = diffusivity of solute in gas, sq.ft./hr.
G = superficial gas rate, lb./(hr.) (sq. ft.)
G' = superficial molar inert gas rate, lb. moles/(hr.) (sq.ft.)
h_G = gas-phase heat transfer coefficient, B.t.u./(hr.) (sq.ft.) (°F.)
h_L = liquid-phase heat transfer coefficient, B.t.u./(hr.) (sq.ft.) (°F.)
k = thermal conductivity, B.t.u./(hr.) (sq.ft.) (°F./ft.)
k_G = gas-phase mass transfer coefficient, lb. moles/(hr.) (sq. ft.) (atm.)
M_M = mean molecular weight of gas. lb./lb. mole
N_A = rate of mass transfer, lb. moles/(hr.) (sq.ft.)
P_{BM} = mean partial pressure of inert gas in the gas phase, atm.
P_T = total pressure, atm.
T = temperature, °F.
y = solute mole fraction
$(\Delta y)_{lm}$ = logarithmic mean driving force, mole fraction
Z = height of packing, ft.
ϵ = void fraction, cu.ft./cu.ft.
λ = latent heat of vaporization, B.t.u./lb. mole
μ = gas viscosity, lb./(hr.) (ft.)
ρ = gas density, lb./cu.ft.

Subscripts

1 = bottom of packing
2 = top of packing
i = at the interface
G = gas phase
L = liquid phase

LITERATURE CITED

1. Cairns, R. C., and G. H. Roper, *Chem. Eng. Sci.*, **3**, 97 (1954).
2. *Ibid.*, **4**, 221 (1955).
3. Hirschfelder, J. O., C. F. Curtis, and R. B. Bird, "Molecular Theory of Gases and Liquids," Wiley, New York (1954).
4. Robinson, R. G., M.Ch.E. thesis, Clarkson College of Technology, Potsdam, New York (1959).
5. Sherwood, T. K., and R. L. Pigford, "Absorption and Extraction," 2 ed., McGraw-Hill, New York (1952).
6. Shulman, H. L., C. F. Ullrich, and N. Wells, *A.I.Ch.E. Journal*, **1**, 247 (1955).
7. Shulman, H. L., C. F. Ullrich, A. Z. Proulx, and J. O. Zimmerman, *ibid.*, 253 (1955).
8. Shulman, H. L., C. F. Ullrich, N. Wells, and A. Z. Proulx, *ibid.*, 259 (1955).
9. Shulman, H. L., and J. E. Margolis, *ibid.*, **3**, 157 (1957).
10. Shulman, H. L., and L. J. Delaney, *ibid.*, **5**, No. 3 (1959).
11. Yoshida, F., and T. Tanaka, *Ind. Eng. Chem.*, **43**, 1467 (1951).

Manuscript received September 9, 1959; revision received January 21, 1960; paper accepted January 25, 1960.

Transient Response Study of Gas Flowing Through Irrigated Packing

FRANCESCO DeMARIA and ROBERT R. WHITE

University of Michigan, Ann Arbor, Michigan

The transient response of a gas phase as it flows through an irrigated packed column can be interpreted as a distribution of time spent by the elements of gas as they flow through the bed. A step function in helium concentration was introduced in the entering air stream of a column packed with Raschig rings, and the outlet concentration was recorded with time. Water was used as the liquid phase. Size of Raschig rings, depth of bed, water and gas flow rates were the main variables investigated.

The response curve for the gas reveals an increasing departure from uniform flow of the gas stream as liquid and gas rates are increased to flooding. The first and second moments of the time distribution give directly the porosity and the axial dispersion of the gas. These quantities have been found to be mainly dependent on liquid flow rates. The skewness which characterizes the weight that the various gas elements have on the dispersion about the average residence time has been found to give a convenient measurement of the uniformity of gas flow through the bed.

Recently unsteady state experimental methods have gained increased attention in chemical engineering research because the time distribution characterizes the system and may also provide a similarity criterion in the scale up of equipment.

Unsteady state experiments are based on the measurements of the response of the system to a known disturbance in experimental conditions. Work of this type has already been reported for relatively simple process systems such as single-phase flow in pipes and packed beds (*2, 6, 8, 11, 13, 26*), reactors (*7, 14, 15, 29, 34*), and heat exchangers (*3*).

An unsteady state investigation of packed gas-liquid absorption equipment appeared to be both useful and interesting for the following reasons.

1. Simplified equipment such as wetted-wall columns and disk absorption columns yields data which are not easily applicable to predictions on the performance of packed absorbers (*5*). Mass transfer data obtained from experimental columns operated at steady state conditions appear to be in wide disagreement (*27*). These difficulties are apparently due to the fact that little is known about the flow of layers of liquid and gas over discontinuous surfaces. It is possible that information on the distribution of residence times of the gas and liquid streams flowing through the column may provide a satisfactory parameter for the correlation of absorption equipment performance.

2. Unsteady state experimental techniques applied to gas-liquid flow systems present unusual problems concerning the introduction of a predetermined disturbance in one of the entering phases and the separation of the effluent phase for rapid analysis; thus work of this nature has been scarce (*18, 21*).

The problem was limited to the study of the gas-phase response to a step function in tracer concentration in the inlet stream. Complicating effects such as absorption or chemical reaction between the liquid and gas streams were eliminated. The method of introduction of the transitory disturbance permitted the measurement of the column volume occupied by the gas and the degree of longitudinal mixing as function of gas and liquid flow rates and packing sizes.

THEORY

The residence-time distribution is defined as the fraction of the entering feed flowing in the effluent per unit time which has been in the reactor between time, t, and $t + dt$. This quantity is usually indicated as $E(t)$. Danckwerts (*6*) has discussed in detail the manner in which the residence-time distribution can be determined from experiments in which the tracer is injected at the inlet either as an instantaneous pulse or as a step in its concentration.

Moments of the Residence-Time Distribution

The moments of the residence-time distribution are defined

$$\int_0^\infty t^n E(t)\,dt \qquad (1)$$

and may be used to characterize the time distribution. Table 1 lists the first four moments from the zero to the

Francesco DeMaria is with American Cyanamid Company, Stamford, Connecticut. R. R. White is now with Atlantic Refining Company, Philadelphia, Pennsylvania.

third and the corresponding relationships in terms of the effluent concentration for a step input.

The zero moment is equal to unity since the sum of all fractions of feed over all times must be equal to one. (6).

The first moment of the residence-time distribution is equal to the mean age of the gas in the system, θ. As indicated in Table 1 this quantity is equal to the average residence time calculated as $\epsilon V/q$. van der Laan (32) and later Spalding (31) have indicated that whenever there is considerable diffusional transport across the inlet and/or outlet boundary the first moment will be greater than the average residence time $\epsilon V/q$. The excess of θ over $\epsilon V/q$ is a function of the longitudinal mixing occurring in the system. The first moment is primarily a function of the throughput and is relatively insensitive to longitudinal mixing.

The second moment about the mean residence time is a measure of the dispersion of the time distribution. This quantity shown in Table 1 has dimension of sec.^{2} and is indicated by the symbol S_θ^2. Levenspiel and Smith (23) call the dimensionless second central moment a *variance* and indicated it by the symbol σ^2.

In the type of experiments discussed here the signal is introduced in such a manner that the concentration normal to the direction of flow is uniform and the dispersion about the mean exhibited by the residence-time distribution is mainly caused by the longitudinal mixing taking place in the bed. It has been shown by Levenspiel and Smith (23) that for a model in which turbulent diffusion is responsible for this longitudinal mixing the variance is equal to

$$\sigma^2 = \frac{2E}{vL} + \frac{8E^2}{v^2L^2} \qquad (2)$$

so that when the dimensionless group vL/E is sufficiently large

$$\sigma^2 \cong \frac{2E}{vL} \qquad (3)$$

Another model visualizes packed beds as made up of a series of completely mixed cells. Klinkenberg and Sjenitzer (19) have shown that the dispersion in this case is

$$\sigma^2 = \frac{1}{n} \qquad (4)$$

The similarity between the turbulent-diffusion approach and the series of completely mixed stages model has been discussed by many authors (1, 2, 18, 19, 26) who have pointed out in various ways that for equivalence of the two models

$$n \cong \frac{vL}{2E} \qquad (5)$$

for large enough values of vL/E. This result is obtained by combining Equations (3) and (4) keeping in mind that (3) is only approximately correct for large values of vL/E (23, 32).

The first moment, being essentially equal to the average residence time $\epsilon V/q$, can be used to determine the void volume or the volumetric flow rate, whichever is unknown, or as a test of consistency for the experimental data. The second moment or the variance gives directly the effective diffusion coefficient or the number of perfectly mixed stages. In those cases in which the longitudinal mixing is large however these simplified relations may not hold. van der Laan suggests more appropriate methods of obtaining the longitudinal mixing parameter (32).

Deviations from Uniform Flow

In absence of any information on the actual velocity distribution in the column the dispersion of the time distribution, while giving a measure of the degree of longitudinal mixing, yields no information about the relative weight that the various fractions of feed have on the total dispersion. The third central moment of the distribution or the skewness defined in Table 1 may provide such additional information. For a series of perfectly mixed stages the skewness is $2/n^2$ when the flow through the bed is uniformly distributed. It follows therefore that the difference between the skewness and twice the square of the dispersion should be a measure of the degree of departure from uniform flow. Should this difference be large, neither turbulent diffusion nor the series of perfectly mixed stages would be satisfactory correlation models since they both assume uniform flow velocity across the bed.

End Effects

In the event that the experimental apparatus must include entrance and/or exit sections which cannot be conveniently isolated from the test section, the mixing introduced by such end effects can be expressed by well established statistical principles (4). The moments of the time distribution for each section of a system may be added if the statistical events taking place within each section are independent. Thus for the first moment of the distribution

$$\theta = \theta_1 + \theta_2 + \cdots + \theta_n \qquad (6)$$

For the second central moment

$$S_\theta^2 = S_{\theta 1}^2 + S_{\theta 2}^2 + \cdots + S_{\theta_n}^2 \qquad (6a)$$

and for the variance

$$\sigma = \sigma_1^2 \frac{\theta_1^2}{\theta^2} + \sigma_2^2 \frac{\theta_2^2}{\theta^2} + \cdots + \sigma_n^2 \frac{\theta_2^2}{\theta^2} \qquad (6b)$$

Klinkenber and Sjenitzer have given examples of this procedure (19). When considerable diffusional transport exists at the boundary between two sections of the system, independence of the statistical events taking place in each section should not be expected.

EXPERIMENTAL

The experimental apparatus was designed to introduce a signal of helium tracer in the inlet gas stream of an absorption column of suitable dimension and record the composition of the outlet continuously and with minimum delay. The equipment therefore consists of a gas and liquid supply, a packed test column, and a gas analyzer.

Flow System

Figure 1 shows a diagram of the equipment. Compressed air at 50 lb./sq. in. is humidified in a brass column 4 in. in diameter and 4 ft., 8 in. in height. The air rate is measured through a bank of three rotameters in parallel and is adjusted and maintained constant by a pressure regulator.

Pure helium or a mixture of 15% helium and 85% nitrogen are used as tracers. The tracer flow after a primary reduction in pressure is maintained at a constant rate by means of a second pressure regulator. A three-way solenoid valve immediately before the inlet to the test column permits replacing the air flow to the column with tracer or the introduction of a pulse of tracer as slugs of short duration in the air stream.

The test column is made out of 4-in. I.D. flanged Pyrex glass pipe. The bottom section of the column is conical, and a ¾-in. I.D. liquid outlet is located at the vertex of the cone. An adjustable liquid level device is used to maintain an adequate liquid seal to allow the outgoing liquid to disengage any gas bubbles before going to the drain. The total volume of the bottom section from the three-way solenoid valve to the beginning of the packing is 0.0065 cu. ft., and it constitutes 1.5 to 2% of the total volume of the column depending on the height of the mid-section.

The upper extremity of the column is reduced in diameter to 2-in. I.D. for connection with the gas analyzer. The liquid is introduced on a side inlet and is distributed by six jets made of 1-½-mm. capillary tubing evenly spaced on a 3-in. radius. The volume of the upper section is 0.0437 cu. ft. The mid-and upper-column sections are completely filled with packing up to the gas analysis cell. Thus a portion of packing which is in the upper section remains dry during the gas-liquid runs because it is above the liquid distributor.

The column is packed with Raschig rings of ¼-⅜-and ½-in. nominal diameter. The rings were made of unglazed porcelain.

Continuous Gas Analyzer

A continuous and accurate recording of the tracer concentration in the gas stream

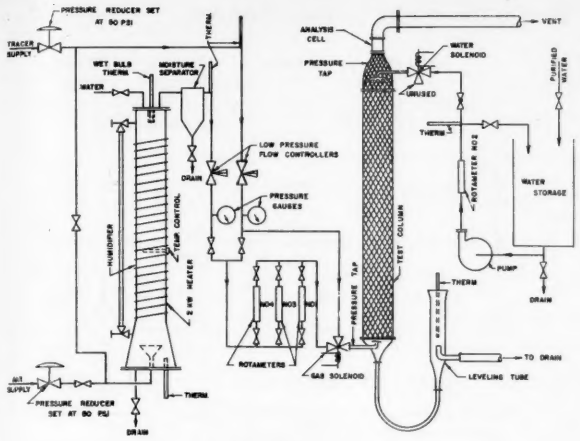

Fig. 1. Flow diagram.

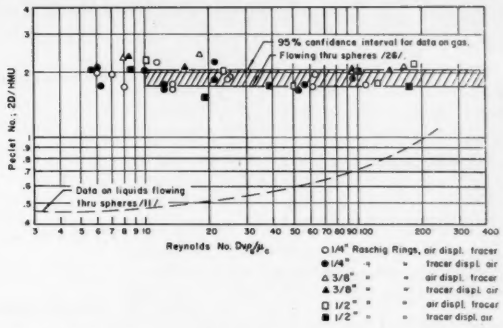
95% confidence interval for data on gas.
Flowing thru spheres /26/.
Data on liquids flowing thru spheres /11/.
Peclet No.: 2D/HMU
Reynolds No. Dvρ/μ
○ 1/4" Raschig Rings, air displ. tracer
● 1/4" " " tracer displ. air
△ 3/8" " air displ. tracer
▲ 3/8" " tracer displ. air
□ 1/2" " air displ. tracer
■ 1/2" " tracer displ. air

Fig. 3. Axial mixing through beds of spheres and Raschig rings (Peclet number vs. Reynolds number).

is obtained from an alpha particle ionization cell. Deisler, McHenry, and Wilhelm (9) used such analyzers for binary and ternary gas mixtures above atmospheric pressure. Details of the analyzer and recorder circuit are shown in Figure 2.

The electrodes of the cell are two rectangular stainless steel plates. The rectangular cell geometry was chosen to give most favorable current stability and noise characteristics. When one uses pure helium as the tracer, the output is exceedingly stable and free of stray noise. The plate used as the alpha particle emitter has on one side an active area of 1⅛-in. by 1⅛-in. covered with 100 μg. of radium 266 rolled in gold foil. The other plate is the ion collector. The plates are spaced at a distance of 1 in. within a 2-in. O.D. Teflon mount especially streamlined to minimize extraneous mixing of the gas entering the cell. The assembly is housed in a specially fabricated glass-flanged tube 3 in. long which is inserted between two 2-in. Pyrex brand pipe flanges forming the connection between the top of the test column and the exhaust pipe. The glass housing and the high impedance leads are shielded with brass foil.

A potential of about 1,000 v. across the electrodes is necessary to collect all the ions formed by the alpha particles. Thus this voltage was selected as standard throughout the experimental work. The output current of the electrodes at 1,000 v. potential varies linearly with helium concentration from a value of 1.9×10^{-8} amp. for pure helium to 9.1×10^{-8} for air.

The low output current from the electrodes is boosted by a 187 megohm resistor across the ion collector plate and the ground to a maximum potential drop of 17 v. To allow the use of 15% helium 85% nitrogen mixture as a tracer a current blocking circuit is inserted in series with the resistor. This consists of a 15-v. mercury battery connected with inverted polarity so that this constant voltage is subtracted from the high resistance circuit; the maximum output voltage corresponding to 100% air is 2 v. The high sensitivity circuit causes a certain amount of noise to be detected in the cell output; thus a 250$\mu\mu$ farad capacitor was added across the high sensitivity circuit to damp some of it out.

The increased capacitance of the high sensitivity circuit resulted in an increase in the time constant of the analyzer recorder system from 0.005 to 0.05 sec. In the experiments performed the average residence time varied from about 4 to 80 sec.; thus the lag of the analyzer recorder system was ignored since it constituted in most cases less than 1% of the total time lag.

Preliminary Tests

The manner of introduction of the tracer at the column inlet was soon limited to step changes in concentration since it was found impossible to inject an appreciable amount of tracer in a short interval of time, as compared with the contact time of the gas flowing through the column, in order to approximate an impulse signal.

Pure helium was first used as a tracer in preliminary work. It was found however that when the helium displaced the air through the column, the response curves were severely distorted especially at low flow rates. This phenomenon was attributed to the presence of convective currents due to the difference in density of the two gases.

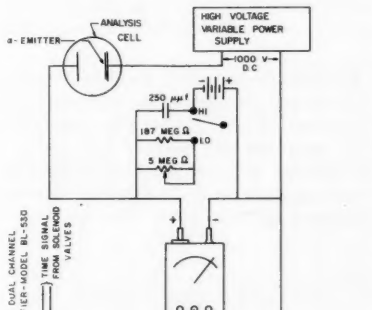

Fig. 2. Assembly of gas analyzer and accessories.

Most of the experimental work used as tracer a mixture of 15 volumes of helium and 85 volumes of nitrogen. The difference in density with air is about 16%, and the resulting response curves for the tracer displacing the air and for the air displacing the tracer were in reasonable agreement.

Standard Experimental Technique

Raschig rings of the desired size were introduced into the column by partially filling the column with water, then slowly pouring the rings from the top. The water prevented breakage and provided slow and even settling of the rings.

The porosity of the dry bed was determined by back filling the column with a known amount of water and measuring the resulting increase in liquid level.

For an irrigated packing run the packing was first thoroughly wetted by adjusting the water rate to 6,000 lb./hr./sq. ft. for about 1 hour. Then a series of runs was performed by adjusting the liquid and gas flows to the desired rates. For each liquid flow rate the column was allowed to reach equilibrium for about a half-hour. Then response curves were recorded at 15-min. intervals and compared by superposition to note if the curves were exactly congruent. If not the gas and liquid flow rates were checked and the procedure repeated until two successive sets of curves were in agreement. When flooding was reached, the flow conditions through the column were too erratic to obtain consistent response curves so that no data was obtained on or about this range of conditions. Only for run W-19 was a reasonable agreement for successive response curves obtained even though the column was flooded. The dynamic liquid holdup was measured at the end of some of the irrigated packing runs by interrupting simultaneously the gas and liquid flow and collecting the total amount of liquid drained from the column.

When a series of runs was completed and a change over of packing was neces-

Table 1. Quantities Characterizing a System in Terms of its Transient Response

Moments of the distribution of residence-times function $E(t)$	Relationships in terms of outflow concentration: Step input from 0 to C_o	Relationships in terms of outflow concentration: Impulse input (amount Q of tracer injected instantaneously)
Zero moment of $E(t)$ vs. t	$\int_o^\infty E(t)dt = 1$	$\int_o^\infty dc/C_o = 1$	$\int_o^\infty cdt = \frac{Q}{v}$
About $t = 0$ axis First moment of $E(t)$ vs. t	$\int_o^\infty tE(t)dt = \theta \simeq \frac{\epsilon V^*}{v}$	$\int_o^\infty (1\text{-}c/C_o)dt = \theta \simeq \frac{\epsilon V}{v}$	$\frac{v}{Q}\int_o^\infty tcdt = \theta \simeq \frac{\epsilon V}{v}$
About $t = 0$ axis Dispersion, second moment of $\theta E(t)$ vs. t/θ	$\sigma^2 = \int_o^\infty (t/\theta)^2\theta E(t)d(t/\theta) - 1$	$\sigma^2 = \frac{2\int_o^\infty t(1\text{-}c/C_o)dt}{\theta^2} - 1$	$\sigma^2 = \frac{\left(\frac{v}{Q}\right)^2\int_o^\infty t^2cdt}{\theta^2} - 1$
About $t/\theta = 1$ axis Skewness, third moment of $\theta E(t)$ vs. t/θ	$\nu = \int_o^\infty (t/\theta)^3\theta E(t)d(t/\theta)$	$\nu = \frac{3\int_o^\infty t^2(1\text{-}c/C_o)dt}{\theta^3}$	$\nu = \frac{\left(\frac{v}{Q}\right)^3\int_o^\infty t^3cdt}{\theta^3}$
About $t/\theta = 1$ axis	$-3\int_o^\infty (t/\theta)^2\theta E(t)d(t/\theta) + 2$	$-\frac{6\int_o^\infty t(1\text{-}c/C_o)dt}{\theta^2} + 2$	$-\frac{3\left(\frac{v}{Q}\right)^2\int_o^\infty t^2cdt}{\theta^2} + 2$

* This relationship holds only in those cases where transfer of mass at the inlet and outlet boundaries is negligible.

sary, the porosity was again checked. Then the packing was removed and weighed in such a manner as to determine the total number of particles.

RESULTS AND DISCUSSION

Dry Packing

The experimental effort was first directed to the study of the gas phase mixing through the bed in order to verify the suitability of the equipment and the method of analysis against existing data.

Consistency Checks. The consistency of the gas holdup information furnished by the transient response curve was checked by comparing θ with the average residence time computed from the known void volume and gas flow rates. For the twenty-three experiments performed (*10*) the agreement between these two quantities was found to be within ± 8%. The random deviation could be easily accounted for by considering the precision of the rotameter calibration, the reading of the recorder traces, and the subsequent handling of the data by graphical integration. It was thus concluded that for the system under study the mean age θ was for practical purposes equal to the residence time.

In accordance with the correlation models discussed previously the variance is equal to the reciprocal of the number of perfectly mixed stages in series or approximately equal to $2E/vL$. The latter quantity was estimated independently by superimposing a graph of c/C_o vs. t/θ as obtained from a given recorder trace over previously prepared graphs for the infinite column solution of the diffusion equation with increments of the group $vL/2E$ of ten units from $vL/2E = 80$ to $vL/2E = 200$. The variance and the group $2E/vL$ were found in all cases within 10% in good agreement with the theory, and Equation (5) was considered adequate for the purpose of this data analysis. Because the variance as calculated from the response curves was believed more accurate than the estimation of the group $vL/2E$, it was decided to adopt the number of mixing stages or the inverse of the variance as a measure of the extent of mixing taking place in the column.

Considerable attention was given to end effects introduced by entrance and exit sections to the test column. The correlation model, in which the packed bed is considered as made up of a series of perfectly mixed stages, gives the height of a mixed stage:

$$HMU = \frac{L}{n} \qquad (7)$$

Accordingly two bed heights 3 and 4 ft. were investigated to ascertain the presence of end effects. The average of all runs for the shorter bed gives a height of a mixed stage of 0.0247 ft. as compared with 0.0228 ft. for the longer bed.

On the assumption that the empty entrance section is equivalent to a perfectly mixed stage, the calculated variance was corrected by subtraction of the empty section contribution to the total variance in accordance with Equation (*6b*). After correction the average bed heights are 0.0228 and 0.0214 for the shorter and longer bed, respectively.

Consequently while the height of a mixed stage for the two bed lengths before correction differs by 8%, the difference is only 6% after the end correction is applied. This type of behavior is expected if the correction is real. On this basis it is presumed that the height of a mixed stage can be considered independent of column height.

It should be noted that no attempt was made to determine the actual degree of mixing taking place in the entrance section. The assumption that this section corresponds to one complete mixer leads to the largest possible correction, and as seen above this is quite small and within the precision of the data.

It may be seen from Figure 1 that the exit section varies in diameter from 4 down to 2 in. In order to take this fact into account an effective column

Table 2. Characteristic Lengths for Peclet Number Correlation

Nominal particle diameter, in.	Particle to bed diameter ratio, D/D_t	Number of runs with random packing	Mean Peclet number: $NPe = \frac{2D}{HMU}$	$NPe' = \frac{2D_p}{HMU}$	$NPe'' = \frac{2D_m}{HMU}$
¼	0.0625	22	1.87	1.73	0.331
⅜	0.0938	8	2.18	2.04	0.357
½	0.1250	10	1.89	1.82	0.335
Mean value of above numbers			1.98	1.86	0.340
Mean square deviation			0.03006	0.02543	0.00043

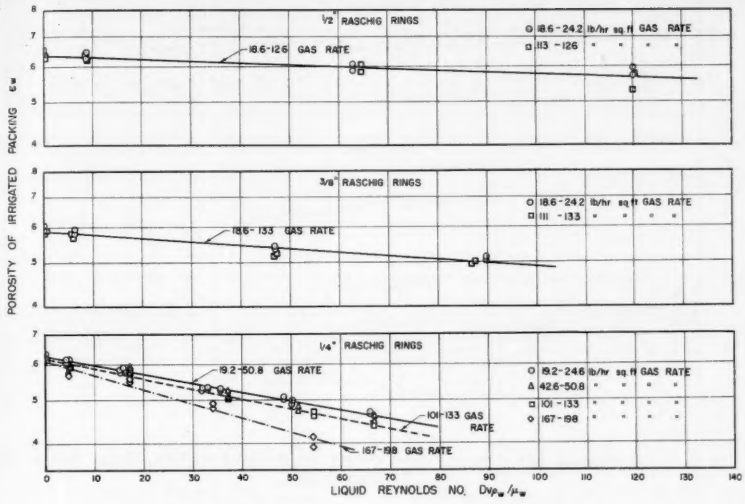

Fig. 4. Effect of liquid flow rate on porosity of irrigated packing.

length was used in the calculation of the height of a mixed stage. This was taken equal to the total volume of the equipment divided by the nominal column diameter (4 in.). To verify that this assumption was correct, runs were made with the upper section left empty and without distributor or completely filled with packing. The height of the mixed stage, computed by the use of the actual length of the test section in the first case and the effective column length in the latter case, was found in good agreement.

Comparison with Previous Investigators. An extensive study of axial mixing for gases flowing through packed beds of spheres is reported by McHenry and Wilhelm (*26*), who used a frequency-response technique. The data of these authors is represented in Figure 3 as a shaded band indicating the 95% confidence limits for the Peclet number. The data for the Raschig rings as obtained in the present work are also shown in Figure 3. The Peclet number is calculated as the ratio of twice the nominal particle diameter to the height of a perfectly mixed stage, and it is analogous to the Peclet number used by McHenry and Wilhelm except that the nominal ring diameter is used in place of the diameter of spheres. The gross agreement between the two sets of data as shown by Figure 3 may be quite fortuitous because clearly there is little hydrodynamic relationship between Raschig rings and spheres having the same diameter. However this figure serves to point out that the Peclet number is of the same order of magnitude in both sets of experimental data for both techniques of signal input, that is step-function response and frequency response.

An analogous conclusion was also obtained by Ebach (*11*) who has extensively studied axial mixing of liquids through packed beds of spheres and other packing shapes. The dotted line in the lower region of Figure 3 is representative of data obtained in his experiments with two types of unsteady state techniques, that is transient and frequency response. Other data for liquids obtained by Danckwerts (*6*) and Kramers and Alberda (*18*) also fall in the neighborhood of the dotted line.

A statistical analysis of the data obtained on Raschig rings shows that a least squares straight line through the points plotted on Figure 3 has no significant slope. Thus no apparent effect of Reynolds number in the investigated range is detectable. Therefore the Peclet number can be expressed as the true mean of forty points and is found to be equal to 1.94 ± 0.07. In statistical language the foregoing can be expressed as:

$$Pr\,(2.01 > N\,Pe > 1.87) = 95\% \quad (8)$$

These results compare well with those of McHenry and Wilhelm.

Effect of Particle Diameter. In the preceding paragraph it was tacitly assumed that the Peclet number computed as the ratio of the nominal Raschig ring diameter to the height of the mixing stage was independent of particle diameter. However this dimension is seldom used to characterize Raschig rings. More frequently the equivalent spherical diameter D_p is used (*22*). Ebach (*11*) employed this quantity in the study of axial mixing of liquid flowing through a bed of Raschig rings. For pressure drop through granular beds Kozeny (*20*) suggested as hydraulic mean diameter the quantity

$$D_m = \frac{\epsilon}{(1-\epsilon)S} = \frac{\epsilon}{a} \quad (9)$$

For spheres this quantity is

$$D_m = \frac{\epsilon D}{6(1-\epsilon)} \quad (10)$$

Since the porosity for a packed bed of spheres varies about a value of 0.4, the value of D_m is approximately 1/10 of the actual diameter of the sphere.

Table 2 was prepared to compare the suitability of each of these quantities in the correlation of the data.

On the basis of the foregoing results it is apparent that the hydraulic mean diameter is the best correlation parameter for the effect of particle size and porosity on Peclet number.

It should be noted that no attempt was made to study experimentally the hydrodynamic relationship between Raschig rings and other shapes such as spheres. No universal simple relation exists among all shapes to a common characteristic length. As the result of this work Kozeny's hydraulic mean diameter would appear to be a more general characteristic length than the nominal particle diameter. This quantity however is also a function of the packing porosity which varies according to the method of packing or with liquid and gas flow rates in the irrigated runs. For this reason the nominal diameter of the rings was preferred in the calculation of the Reynolds number which is used as the independent variable.

Irrigated Packing

Wet Porosity. The porosity of the wet packing and the extent of mixing

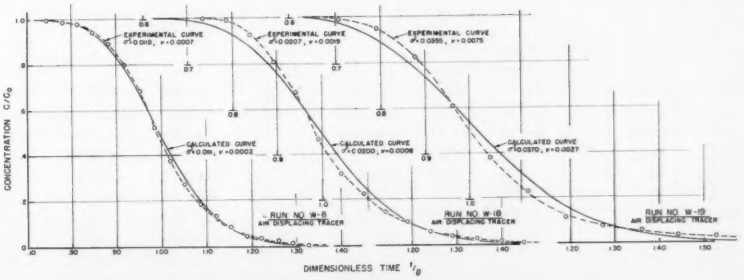

Fig. 5. Response curves showing departure from uniform flow.

taking place in the gas stream were measured in a series of forty-two runs (*10*). The variables investigated were gas and liquid flow rates and diameter of Raschig rings.

Dry-packing experiments served to verify that the mean age, as obtained from recorded concentration-time curves, can be used to calculate the volume of the bed occupied by the gas. On this basis the porosity of the irrigated bed for which no other method of direct measurement is presently known is calculated from a knowledge of the mean age of the gas θ and the corresponding volumetric flow rate. The data is shown graphically in Figure 4, where the wet porosity is plotted vs. the Reynolds number of the liquid. It can be seen here that the liquid rate is the most important variable and that the relationship between the liquid rate and the porosity is exponential in the liquid Reynolds number. Accordingly the equation

$$\frac{\epsilon_W}{\epsilon} = 0.90 \times 10^{-3.43 \times 10^{-6}\left(\frac{D}{D_t}\right)^{2.31} N_{Re_w}} \qquad (11)$$

was found to correlate the data. The statistical details of the correlation and confidence interval of the constants used in Equation (11) are reported elsewhere (*10*).

The intercept ϵ_{wo} of the wet porosity vs. liquid Reynolds number plot (Figure 4) represents the porosity of the wet packing at zero liquid flow rate; thus the difference $\epsilon_{wo} - \epsilon_w$ should correspond to the dynamic holdup. This quantity was found to be in good agreement with the amount of liquid drained from the column where both liquid and gas rates were suddenly interrupted in nine runs with ¼-in. packing (*10*). The values of $\epsilon_{wo} - \epsilon_w$ for ⅜- and ½-in. rings are also in fair agreement with operating holdup data of Shulman, Ullrich, and Wells (*30*) and Jesser and Elgin (*17*) considering slightly different packing dimensions,

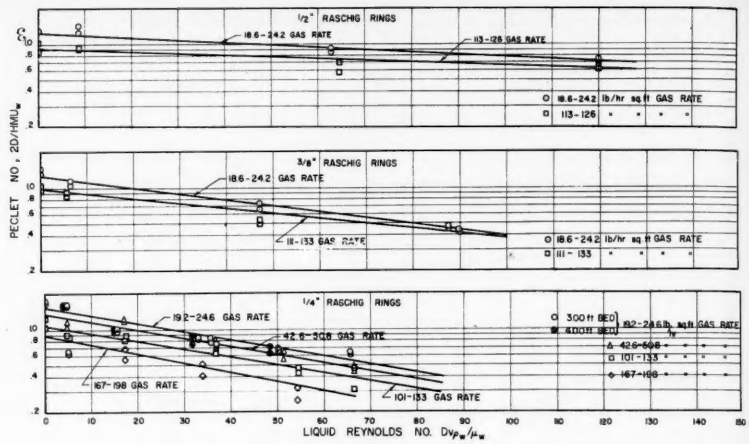

Fig. 6. Effect of liquid flow rate on Peclet number for irrigated packing (Peclet number vs. liquid Reynolds number).

differences in porosities of the dry packing, and differences in drainage time.

End Effects and Departure from Uniform Flow. For the irrigated packing experiments the packed test column was made up of three portions: a bottom empty entrance section, an irrigated section, and a section remaining dry above the liquid distributor. Again, it is assumed that the bottom section is equivalent to a complete mixer. The number of mixed stages contributed by the dry section of packing above the liquid distributor is estimated from the results of previous experiments on dry packing. The significance of the correction as applied to the variance is best understood when data on beds of different depths are compared; this is done in Table 3 where data obtained from ¼-in. Raschig ring beds having irrigated depths of 3 and 4 ft. are compared under similar operating conditions. For each run the height of a perfectly mixed stage as calculated from the variance before and after correction is reported. A more satisfactory agreement is obtained after the correction is applied. The end effects appear to be adequately accounted for on this basis, and the bed depth is no longer considered as a pertinent variable.

In the study of the gas mixing through the irrigated packing it was noted that as the liquid and gas flow rates were increased, the response of the system could no longer be correlated in terms of any of the models discussed in the theory in which uniformity of flow is assumed.

As previously suggested the difference between the skewness and twice the square of the variance was assumed to be a measure of the degree of departure from uniform flow or channeling. Figure 5 gives a graphical presentation of the distortion in the response curves by comparing a theoretical curve for which the quantity $\nu - 2\sigma^2$ is zero with an experimental curve having the same variance, but for which $\nu - 2\sigma^2$ is increasingly important.

The magnitude of the deviation from uniform flow was found to be somewhat erratic (*10*). Although this is partly due to the difference of two

Table 3. Effect of Irrigated Bed Depth on Longitudinal Mixing

					Air displacing tracer				Tracer displacing air			
Run number	Nominal packing diameter, in.	Depth of irrigated packing, ft.	Liquid flow rate, lb./hr. sq. ft.	Air flow rate, lb./hr. sq. ft.	Calculated dispersion	Height of mixed stage (uncorrected)	Corrected dispersion	Height of mixed stage (corrected)	Tracer flow rate, lb./hr. sq. ft.	Calculated dispersion	Height of mixed stage (uncorrected)	Corrected dispersion	Height of mixed stage (corrected)
W-4	¼	3	446	23.6	0.00793	0.0238	0.00854	0.0256	20.2	0.00803	0.0241	0.00869	0.0261
W-23	¼	4	447	24.2	0.00612	0.0245	0.00650	0.0260	19.3	0.00620	0.0248	0.00659	0.0264
W-1	¼	3	1,600	24.0	0.01144	0.0343	0.01383	0.0415	24.6	0.01199	0.0360	0.01466	0.0440
W-24	¼	4	1,600	24.2	0.00896	0.0358	0.01038	0.0415	19.3	0.00950	0.0380	0.01113	0.0445
W-2	¼	3	3,340	24.0	0.01330	0.0399	0.01670	0.0501	24.6	0.01324	0.0397	0.01659	0.0498
W-25	¼	4	3,340	24.2	0.01133	0.0453	0.01372	0.0549	19.3	0.00999	0.0400	0.01179	0.0472
W-3	¼	3	5,070	24.0	0.01625	0.0488	0.02156	0.0647	24.6	0.01581	0.04743	0.02080	0.0624
W-26	¼	4	5,070	24.2	0.01357	0.0543	0.01701	0.0680	19.3	0.01193	0.0477	0.01462	0.0585

Table 4. Coefficients for Mixing Correlation

Run number	Nominal particle diameter, in.	Range of liquid flow rates, lb./hr. sq. ft.	Average gas Reynolds number	Total number of points	NPe_{wo}	95% confidence interval	M	95% confidence interval
W-1 through W-7	¼	0-6,190	19.2-24.0	14	1.528	±0.030	0.0069	±0.0013
W-23 through W-26	¼	447-5,070	19.3-24.2	8	1.500	±0.064	0.0079	±0.0038
W-8, W-11, W-14, W-17 and W-20	¼	446-6,190	42.6-50.8	10	1.334	±0.038	0.0068	±0.0017
W-9, W-12, W-15, W-18, W-21, W-22	¼	0-6,190	101-133	12	1.072	±0.035	0.0067	±0.0014
W-10, W-13, W-16, W-19	¼	446-5,050	167-198	8	0.895	±0.053	0.0079	±0.0027
W-27 through W-30	⅜	0-6,200	18.6-24.2	8	1.265	±0.032	0.0053	±0.0009
W-31 through W-34	⅜	0-6,200	111-133	8	0.979	±0.045	0.0041	±0.0013
W-35 through W-38	½	0-6,200	18.6-24.2	8	1.254	±0.021	0.0020	±0.0004
W-38 through W-42	½	0-6,200	113-126	8	0.928	±0.060	0.0014	±0.0012

numbers σ^2 and ν of the same order of magnitude and subject to inaccuracy in their numerical evaluation, it is evident that the departure from uniform flow may fluctuate greatly for any one run as indicated by random variations for the same experiment when different run records are compared. Departure from uniform flow appears to be most affected by an increase in liquid flow rates. Gas flow rates appear also to have an effect, but while this is not detectable for liquid loadings below 3,000 lb./hr./sq. ft., it becomes more pronounced above this flow and is greatest when flooding is observed.

The above qualitative information gives some indication that the distortion in the response curve is perhaps due to the random occlusion of the gas flow channels by the liquid resulting in maldistribution of the gas through the bed. Consistent with this hypothesis the departure from uniform flow would increase with liquid flow rates until a point is reached in which the liquid forms a continuous phase throughout the bed (flooding). When this occurs, the gas is compelled to lift the liquid from the pores in a pulsating manner and will proceed through the column in the form of bubbles rather than a continuous stream. Consequently uniformity of gas distribution can hardly be expected.

Axial Mixing Correlation. In a manner analogous to the previous correlation for mixing of the gas through the dry packing, the axial mixing was expressed in terms of the Peclet number defined as the ratio of twice the nominal particle diameter to the height of a mixed stage.

The data in question are shown in Figure 6, where the Peclet number is plotted vs. the Reynolds number of the liquid at constant gas rate for all three different packing sizes investigated. The lines drawn through the points are calculated by the least-squares method in accordance with

$$NPe_w = NPe_{wo}\, 10^{-MNRe_w} \qquad (12)$$

The constants NPe_{wo} and M were evaluated separately for nine groups of runs during each of which the bed properties, that is particle diameter and bed porosity, were the same, and the gas flow rate varied over a narrow range so that its effect could be assumed negligible. Table 4 gives a list of the constants and the groups of runs for which they were evaluated. A statistical test shows that the average value of M for all runs having the same particle size is no different from the least squares value for individual groups of runs reported on Table 4. It can also be shown that the constants M and NPe_{wo} are power functions of the particle diameter and the gas Reynolds number, respectively (*10*).

From the foregoing the data can thus be represented by

$$NPe_w = 2.4(NRe_G)^{-0.20} \times 10^{-\left(0.013\text{-}0.088\frac{D}{D_t}\right)N_{Re_w}} \qquad (13)$$

Equation (13) can also be written in terms of the height of perfectly mixed stages:

$$HMU_w = 0.83(NRe_G)^{0.20} \times 10^{\left(0.013\text{-}0.088\frac{D}{D_t}\right)N_{Re_w}} \qquad (13a)$$

Interpretation of Mixing Data. If one uses the series of perfectly mixed stages model to interpret the results pertaining to the mixing taking place in the bed, one observes that the height of a mixed stage is smaller for dry packing than it is for wet packing. Since the height of a mixed stage is as seen in the dry packing correlation, proportional to the particle diameter, one may postulate that as the liquid descends on the packing, it envelops several packing elements to form larger aggregates thus increasing the apparent diameter of the particles, or in an equivalent manner increasing the height of a mixed stage. Consistent with this interpretation Equation (13*a*) shows that HMU increases with liquid flow rate.

An idea of the validity range of Equation (13) is given by Figure 7, where the average Peclet number for dry Raschig rings is compared with data on irrigated packing. The line for wet packing calculated from Equation (13) for a liquid flow rate equal to zero is representative of all three packing sizes used in the experiments. It is apparent that Equation (13) cannot be used to extrapolate mixing data for Reynolds numbers much less than 10 since from the preceding remarks one would expect the Peclet number for wet packing to remain always below that for dry packing. The lower line shows ¼-in. packing data for a liquid flow rate from 5,050 to 5,070 lb./hr./sq. ft. The points on the extreme right of this line are for run W-19 which was conducted under flooding conditions. Equation (13) yields higher values of the Peclet number than those observed.

A more interesting but highly speculative interpretation of the Peclet number may be given on the assumption that the ratio of hydraulic mean diameter to height of a mixed stage is a constant. As seen from Table 2 this is quite true generally for dry packing. One may assume therefore that

$$NPe'' = NPe''_w = \frac{2\frac{\epsilon}{\theta}}{HMU} = \frac{2\frac{\epsilon_w}{\theta_w}}{HMU_w} = \text{Constant}$$

Accordingly by dividing Equation (13*a*) by HMU as given by Equation (8) one finds that

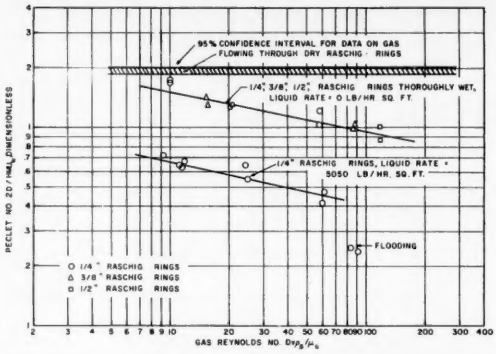
95% CONFIDENCE INTERVAL FOR DATA ON GAS FLOWING THROUGH DRY RASCHIG RINGS
1/4", 3/8", 1/2" RASCHIG RINGS THOROUGHLY WET, LIQUID RATE = 0 LB/HR SQ. FT.
1/4" RASCHIG RINGS, LIQUID RATE = 5050 LB/HR. SQ. FT.
FLOODING
○ 1/4" RASCHIG RINGS
△ 3/8" RASCHIG RINGS
□ 1/2" RASCHIG RINGS
PECLET NO 2D/HMU, DIMENSIONLESS
GAS REYNOLDS NO. $D_t p_g / \mu_g$

Fig. 7. Longitudinal mixing for gas flowing through irrigated beds of Raschig rings.

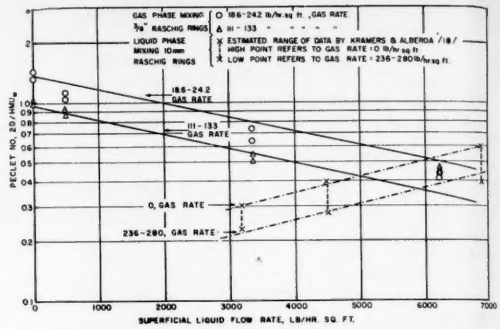
GAS PHASE MIXING
3/8" RASCHIG RINGS
LIQUID PHASE MIXING 10mm RASCHIG RINGS
○ 186-242 lb/hr.sq.ft. GAS RATE
△ 111-133 " " " "
ESTIMATED RANGE OF DATA BY KRAMERS & ALBERDA /18/
HIGH POINT REFERS TO GAS RATE = 0 lb/hr sq ft
LOW POINT REFERS TO GAS RATE = 236-280 lb/hr sq ft
186-242 GAS RATE
111-133 GAS RATE
0, GAS RATE
236-280, GAS RATE
PECLET NO. 2D/(HMU)w
SUPERFICIAL LIQUID FLOW RATE, LB/HR. SQ. FT.

Fig. 9. Peclet number for liquid and gas phase flowing countercurrently through a packed bed of Raschig rings.

$$\frac{HMU_w}{HMU} = \frac{a\epsilon_w}{a_w\epsilon} = 0.81(NRe_G)^{0.20} \cdot 10^{\left(0.013-0.088\frac{D}{D_t}\right)N_{Re_w}} \qquad (14)$$

so that the ratio of total wet packing area to dry area is obtained by dividing Equation (11) by (14):

$$\frac{a_w}{a} = 1.11(NRe_G)^{-0.20} \cdot 10^{-\left[0.013-0.088\frac{D}{D_t}-3.43\cdot10^{-6}\left(\frac{D}{D_t}\right)^{-2.31}\right]N_{Re_w}} \qquad (15)$$

Equation (15) indicates that the wetted area would decrease rapidly with liquid flow rate and at a faster rate in fact than the porosity of the wet packing. In addition the rate of decrease in area is much more pronounced for the smaller size packing than it is for larger sizes. The wetted area could also be affected but to a lesser extent, by the gas Reynolds number. This may be due to the fact that higher gas flow rates tend to make the liquid-packing aggregate more compact so that it presents less surface area to gas flow. The cumulative result of these effects is to reduce the wetted-surface area in inverse proportion to the particle size so that the area of the packed bed exposed to gas flow may, at high liquid flow rates, be larger for larger packing sizes than for the smaller packing. Figure 8 shows the relationship between the total area of the bed in contact with flowing gas as estimated by Equation (15) together with estimates of effective mass transfer area (*12, 25, 33*). The uncertainty of data on effective mass transfer area is illustrated by the low and high values reported for ½-in. Raschig rings. The data of Mayo, Hunter, and Nash (*25*) obtained by measuring the colored surface area of Raschig rings made of paper over which water containing a red dye was circulated appear in line with the total surface area as given by Equation (15). In fact one would expect that the mass transfer area is only a fraction of the total surface area exposed to gas flow and that the former increases with increasing liquid flow rates so that the two quantities approach each other asympototically.

It is possible that the area which the bed presents to liquid flow is more directly related to the effective mass transfer area. If the reasoning followed in the derivation of Equation (15) is valid, (this could be verified by obtaining mixing data on other packing shapes) then the surface area which the bed presents to gas flow could be evaluated by a study analogous to the present one for the liquid phase.

Comparison with Previous Investigators. In connection with the previous discussion it is interesting to compare the present data on the gas-phase mixing with the results reported in graphical form by Kramers and Alberda (*18*) on a number of experiments in which the mixing of water running over 10-mm. Raschig rings in an absorption column with a countercurrent air flow was measured by frequency response.

Figure 9 shows the Peclet number for the gas as measured in the present work for ⅜-in. rings (closest dimension to 10 mm.) with analogous Peclet numbers for the liquid as estimated roughly from the graphical data reported by the above authors. It is apparent from this figure that while mixing in the gas phase increases both with liquid and gas rates, in the liquid phase instead, mixing decreases with increasing liquid rates. The results on the liquid phase have to be accepted with some reservation because of their scarcity and because Kramers and Alberda do not give details about the experimental technique used. However they seem to show that according to the discussion of the previous paragraph the area which the bed presents to the flow of liquid does, indeed, behave in a similar manner to the effective mass transfer area.

Another interesting aspect of this comparison is that according to Figure 9 the Peclet number or the height of the mixing stage for both phases is of the same order of magnitude in the practical range of liquid flow rates. This fact may have some importance in greatly simplifying the interpretation of mass transfer data.

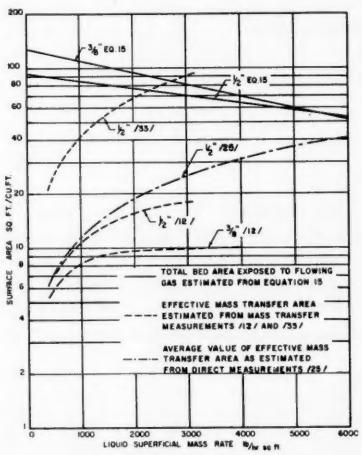
3/8" EQ. 15
½" EQ. 15
½" /33/
½" /25/
½" /12/
3/8" /12/
TOTAL BED AREA EXPOSED TO FLOWING GAS ESTIMATED FROM EQUATION 15
EFFECTIVE MASS TRANSFER AREA ESTIMATED FROM MASS TRANSFER MEASUREMENTS /12/ AND /33/
AVERAGE VALUE OF EFFECTIVE MASS TRANSFER AREA AS ESTIMATED FROM DIRECT MEASUREMENTS /25/
SURFACE AREA SQ FT/CU FT
LIQUID SUPERFICIAL MASS RATE lb/hr sq ft

Fig. 8. Total bed area exposed to flowing gas and effective mass transfer area as function of liquid flow rate.

CONCLUSIONS

The residence time distribution study presented here suggests new possibilities concerning the mechanism of gas flow through Raschig rings irrigated by liquid.

Recent methods of analysis of transient experiments (*19, 23, 32*) have been employed to correlate the data. The moments of the residence-time

distribution have in themselves a physical meaning which is not necessarily associated with a predetermined physical model.

A correlation of the first moment of the time distribution shows that the porosity of the wet packing is primarily a function of the liquid flow rate, the dry packing porosity, and the nominal packing diameter.

The variance of the residence-time distribution clearly indicates that the axial dispersion of the gas flowing through the irrigated packing is markedly greater than that for the dry packing.

The extent of mixing expressed in terms of the Peclet number appears to be a function of the following variables in order of decreasing importance: liquid flow rate, nominal diameter of the packing, and gas flow rate.

The skewness of the residence-time distribution indicates that one-dimensional diffusion models and series of perfectly mixed stages are acceptable representations of the gas flow through dry columns having packed lengths large in comparison to the nominal diameter of the packing elements. For irrigated packing instead such models appear inadequate because the flow through the column is not uniform, especially when the flooding region is approached.

On the assumption that the Peclet number for single-phase flow is a constant over a discrete range of flow rates, the area of the packing exposed to gas flow can be determined. This information may be of use in the interpretation and correlation of mass transfer data.

NOTATION

A = cross-sectional area of empty column, sq. ft.

a = total surface area of bed, sq. ft./cu. ft.

a_w = total surface area of irrigated bed, sq. ft./cu. ft.

c = tracer concentration in effluent at time t, moles/unit vol.

C_o = tracer concentration in entering stream, moles/unit vol.

$E(t)$ = distribution of residence-time function, sec.

E = effective diffusivity in the direction parallel to flow in packed bed, sq. ft./sec.

D = nominal diameter of packing element, ft.

D_m = hydraulic mean diameter ϵ/a, ft.

D_p = diameter of sphere having equal volume as packing element, ft.

D_t = diameter of packed column, ft.

HMU = height of a perfectly mixed stage L/n, ft.

HMU_w = height of a perfectly mixed stage for irrigated bed, ft.

L = length of packed bed, ft.

M = coefficient for mixing correlation for irrigated packing, dimensionless

n = number of perfectly mixed cells in series in longitudinal direction

NPe = longitudinal Peclet number, Dv/E or $2D/HMU$, dimensionless

NPe' = modified longitudinal Peclet number, $D_p v/E$, dimensionless

NPe'' = modified longitudinal Peclet number, $D_m v/E$, dimensionless

NPe_w = longitudinal Peclet number for irrigated packing, $2D/HMU_w$, dimensionless

NPe_w'' = modified longitudinal Peclet number for irrigated packing, $2D_m/HMU_w$, dimensionless

NPe_{wo} = coefficient for mixing correlation for irrigated packing, dimensionless

NRe_G = Reynolds number for gas, $Dv\rho_G/\mu_G$, dimensionless

NRe_w = Reynolds number for liquid, $Dv\rho_w/\mu_w$, dimensionless

S = specific surface of the material, sq. ft./cu. ft.

S_θ^2 = second central moment of the residence time distribution, sec.^{2}

t = time measured from introduction of signal, sec.

v = average superficial velocity, ft./sec.

V = volume of empty column, cu. ft.

q = volumetric flow rate through column, cu. ft./sec.

Greek Letters

ϵ = porosity of dry bed, volume fraction of empty column

ϵ_w = porosity of wet bed, volume fraction of empty column

ϵ_{wo} = coefficient for porosity correlation, dimensionless

θ = mean residence time $\epsilon V/q$ or L/v, sec.

μ_G = viscosity of gas lb./ft., hr.

μ_w = viscosity of the liquid lb./ft., hr.

ν = skewness, dimensionless third central moment of the distribution function

ρ_G = density of gas lb./cu. ft.

ρ_w = density of liquid, lb./cu. ft.

σ^2 = variance of the dimensionless time distribution function, dimensionless

LITERATURE CITED

1. Aris, Rutherford, and N. R. Amundson, *A.I.Ch.E. Journal*, **3**, 280 (1957).
2. Carberry, J. J., and R. H. Bretton, *ibid.*, **4**, 367 (1958).
3. Cohen, W. C., and E. F. Johnson, *Ind. Eng. Chem.*, **48**, 1031 (1956).
4. Cramer, H., "The Elements of Probability Theory," Wiley, New York (1955).
5. Danckwerts, P. V., *A.I.Ch.E. Journal*, **1**, 456 (1955).
6. ———, *Chem. Eng. Sci.*, **2**, 1 (1953).
7. ———, J. W. Jenkins, and G. Place, *Chem. Eng. Sci.*, **3**, 26 (1954).
8. Deisler, P. F., and R. H. Wilhelm, *Ind. Eng. Chem.*, **45**, 1219 (1953).
9. Deisler, P. F., K. W. McHenry, and R. H. Wilhelm, *Anal. Chem.*, **27**, 1366 (1955).
10. DeMaria, Francesco, Ph.D. thesis, Univ. Mich., Ann Arbor (May, 1958).
11. Ebach, E. A., and R. R. White, *A.I.Ch.E. Journal*, **4**, 161 (1958).
12. Fellinger, L., ScD. thesis, Mass. Inst. Technol., Cambridge (1941).
13. Fowler, F. C., and G. G. Brown, *Trans. Am. Inst. Chem. Engrs.*, **39**, 491 (1943).
14. Gilliland, E. R., and E. A. Mason, *Ind. Eng. Chem.*, **41**, 1191 (1949).
15. *Ibid.*, **44**, 218 (1952).
17. Jesser, B. W., and J. C. Elgin, *Trans. Am. Inst. Chem. Engrs.*, **34**, 277 (1953).
18. Kramers, H., and G. Alberda, *Chem. Eng. Sci.*, **2**, 173 (1953).
19. Klinkenberg, A., and F. Sjenitzer, *ibid.*, **5**, 258 (1956).
20. Kozeny, J., *Ber. Wien. Akad.*, **136A**, 271 (1925).
21. Lapidus, Leon, *Ind. Eng. Chem.*, **49**, 1000 (1957).
22. Leva, Max, "Tower Packings and Packed Tower Design," U. S. Stoneware Company, Akron, Ohio (1953).
23. Levenspiel, O., and W. K. Smith, *Chem. Eng. Sci.*, **6**, 227 (1957).
25. Mayo, F., T. G. Hunter, and A. W. Nash, *J. Soc. Chem. Ind. (London)*, **44**, 375T (1935).
26. McHenry, K. W., Jr., and R. H. Wilhelm, *A.I.Ch.E. Journal*, **3**, 83 (1957).
27. Sherwood, T. K., and R. L. Pigford, "Absorption and Extraction," McGraw-Hill, New York (1952).
28. Sherwood, T. K., G. H. Shipley, and F. A. L. Holloway, *Ind. Eng. Chem.*, **30**, 765 (1938).
29. Singer, E., D. B. Todd, and V. P. Guin, *ibid.*, **49**, 1 (1957).
30. Shulman, H. L., C. F. Ullrich, and N. Wells, *A.I.Ch.E. Journal*, **1**, 247 (1955).
31. Spalding, D. B., *Chem. Eng. Sci.*, **3**, 74 (1958).
32. van der Laan, E. Th., *ibid.*, **7**, 187 (1958).
33. Whitt, F. R., *Brit. Chem. Eng.*, **1**, 43 (1957).
34. Yagi, Sakae, and T. Miyauchi, *Chem. Eng. (Japan)*, **17**, 382 (1953).

Manuscript received February 2, 1959; revision received December 18, 1959; paper accepted December 28, 1959. Paper presented at A.I.Ch.E. St. Paul meeting.

Mass Transfer in Semifluidized Beds For Solid-Liquid System

LIANG-TSENG FAN and YUNG-CHIA YANG
Kansas State University, Manhattan, Kansas

CHIN-YUNG WEN
West Virginia University, Morgantown, West Virginia

A new fluid-solid contacting technique known as *Semifluidization* has been studied. Mass transfer data were obtained for a benzoic acid–water system, and correlations in terms of mass transfer factors and over-all void fractions (for both packed and fluidized sections) are presented. Previous mass transfer correlations for fixed and fluidized beds are critically evaluated with respect to the limitation and applicability and are discussed in relation to semifluidized-bed mass transfer correlations.

Semifluidization is a type of fluid-solid contact operation in which the expansion of a fluidized bed is partially restricted. Under such conditions the porosity of a semifluidized bed is intermediate between the rigidly packed bed and the completely fluidized bed.

Some of the characteristics of a semifluidized bed, such as the simultaneous formation of a packed section and a fluidized section in the bed, were reported in a previous communication (*9*). The purpose of this paper is to report the results of experimental work on the mass transfer aspect in a semifluidized bed of a solid-liquid system.

Aside from its practical significance in mass transfer operations, the study of rate of mass transfer is of general significance because it often leads to better understanding of other aspects of chemical engineering operations and heat transfer.

Since the mechanism of interphase mass transfer in a fluidized bed is already complicated (*4, 24*), no particular attempts were made to analyze the data in the light of the rigorous theories of interphase mass transfer. Rather, emphasis was placed on the empirical correlation of over-all mass transfer coefficients and the comparison of the correlations obtained with those of the fluidized and packed beds.

The relationships among the over-all mass transfer coefficients, the mass transfer coefficients in each individual bed, and the internal structure of the bed (that is, the relative size of the packed and fluidized sections in the bed) were carefully considered.

EXPERIMENTAL

The experimental apparatus consisted of a main test column in which granular benzoic acid particles were dissolved by a measured stream of upward flowing water. A container was provided for retention of samples of each run for analysis. Figure 1 shows the diagram of the apparatus.

Water was supplied from a 50-gal. constant-head tank (*A*) and was forced through the system by a centrifugal pump (*B*). The water was initially directed through the globe valve and a flowmeter (*C*) as a means of controlling and measuring the rate of flow. The test column consisted of two parts, a calming section (D) and a test section (F). The test section was a vertical Pyrex tube 2 in. I.D. and 24 in. high. Two brass plates clamping a filter cloth (E) were placed between the calming and the test sections to establish an even distribution of the upward flow. A rigid close-fitting sieve plate (G) was attached to a long rod which could be moved up or down to a fixed position. This was installed in the test column to adjust bed depth and prevent the complete expansion of the solid bed.

For the second series of experiments the apparatus was modified.

In the first series only the inlet and outlet concentrations were measured, whereas in the second series the axial concentration gradient of the fluid was measured. Since the samples were obtained from inlet and outlet pipes in the first series of experiments, they could be considered as the average samples across the cross section of the column. The sampling lines having 1/4-in. I.D. were employed in the second series of experiments. They were sufficiently large to assume withdrawal of uniform average samples across the cross section of the column, as evidenced by the fact that the concentration of outlet samples obtained from the sampling line just above the top of the screen was almost identical with those obtained from the outlet of the column. The apparatus used in the latter series was the same as for the former series, except the test section. This new test section was made from a 2-in. I.D. standard iron pipe with cocks attached for sampling, at 2-in. spacings. A sheet of filter cloth was cemented to the inside wall over the outlet of each cock to prevent the plugging of the solid benzoic acid particles from the sampling lines. The sizes of particles used (8 ~ 24 mesh) were much larger than the opening of the filter cloths, and the particles were freed from the dust by a washing process suggested by Evans and Gerald (*8*). No escaping of the particles from the sampling cocks was observed.

Although the solubility of the benzoic acid in water is low, in order to minimize the change of geometric shape of the particles during the experimental runs the individual runs were not permitted to exceed an 80-sec. duration. A decrease of less than 3% of the initial weight of the solid particles for a single run was experienced. Intermittent analysis of effluent liquid concentration during the run indicates that steady state operation has been achieved.

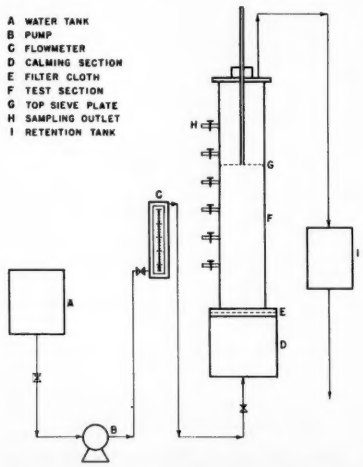

Fig. 1. Diagram of experimental apparatus.

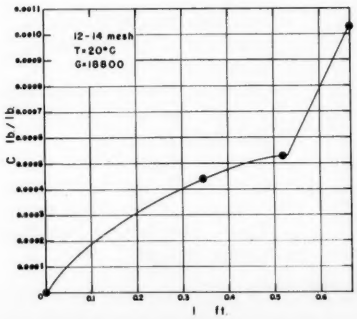

Fig. 2. Axial concentration profile.

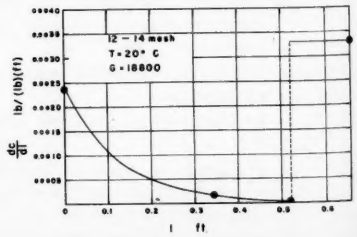

Fig. 3. Axial concentration gradient.

Table 1. Calculation of First Series of Semifluidized Data (Representative Runs)

Run no.	T, °C.	W, lb.	h_o, ft.	h, ft.	h_f, ft.
A-1	22.3	0.4916	0.5888	0.8091	0.4008
B-1	21.00	0.2533	0.2999	0.5008	0.3342
C-1	22.60	0.2645	0.3093	0.4675	0.2550

Run no.	h_{pa}, ft.	X —	R —	ϵ(over-all) —	D_p, ft.	A, sq. ft.
A-1	0.4083	0.6935	1.3732	0.6548	0.00690	10.40
B-1	0.1666	0.5555	1.6700	0.7129	0.004531	7.62
C-1	0.2125	0.6873	1.5114	0.6787	0.002610	12.50

Run no.	G, lb./(hr.)(sq. ft.)	G', lb./hr.	C_s, lb./lb.	C_2, lb./lb.	k_{lm}, lb./(hr.)(sq. ft.)(ΔC)	N_{Sc} —
A-1	16,067	350.52	0.003140	0.001640	24.90	1,120
B-1	10,610	231.47	0.003005	0.001563	22.30	1,220
C-1	4,500	98.17	0.003177	0.003051	25.38	1,110

Run no.	N_{Sh} —	N'_{Re} —	$N'_{Re}/(1-\epsilon)$ —	J_d —	$(N_{Sh}\epsilon-2)/N^{1/3}_{Sc}$ —	J'_d —
A-1	64.48	48.33	140.0	0.1670	3.87	0.1245
B-1	39.74	20.25	70.53	0.2400	2.46	0.1745
C-1	24.63	5.138	15.99	0.6045	1.61	0.4255

Table 2. Calculation of Second Series of Semifluidized Data (Representative Run)

Run no.	W, lb.	h_o, ft.	h, ft.	h_f, ft.
D-1	0.3307	0.3613	0.5717	0.3484

Run no.	h_{pa}, ft.	X —	D_p, ft.	A, sq. ft.	ϵ —	S, sq. ft.
D-1	0.2233	0.6182	0.006890	6.97	0.7004	0.023916

Run no.	Height of sampling outlet, ft. a	b	c	C, lb./lb. at a	b	c	C_1, lb./lb.	C_2, lb./lb.
D-1	0.2033	0.3700	0.5717	0.000215	0.000359	0.000943	0.00030	0.000943

Run no.	C_s, lb./lb.	$(\Delta C)_{lm}$ Packed bed	Fluidized bed	Over-all	$(\Delta C)_{lm}$ Packed bed	Fluidized bed	Over-all
D-1	0.002902	0.002271	0.002752	0.002405	0.002380	0.002752	0.002460

Run no.	G, lb./(hr.)(sq. ft.)	G', lb./hr.	k_{lm} Packed bed	Fluidized bed	Over-all	k_{lm} Packed bed	Fluidized bed	Over-all
D-1	21,524	51,477	30.83	21.08	28.97	28.68	21.08	28.32

Run no.	N'_{Re} —	$N'_{Re}/(1-\epsilon)$	N_{Sh} ΔC_{lm}	ΔC_{tm}	J_d ΔC_{lm}	ΔC_{tm}
D-1	60.88	203.30	81.00	79.3	0.1588	0.1552

Run no.	N_{Sc} —	$(N_{Sh}\epsilon-2)/N^{1/3}_{Sc}$ ΔC_{lm}	ΔC_{tm}	J_d C_{lm}	C_{tm}
D-1	1,290	5.03	4.91	0.1192	0.1167

All the experiments were carried out at room temperature, and the fluid temperature was measured at the inlet and outlet of the column. The determination of the concentration of the water sample was made by direct titration with 0.04 N. sodium hydroxide with phenolphthalein indicator. No difficulty was encountered in securing reproducible end points. The acid concentration varied from 0.0004 g. acid/g. water to 0.0030 g. acid/g. water.

Granular particles of benzoic acid employed in the present investigation were prepared in three screen ranges of 8 to 10 mesh, 12 to 14 mesh, and 20 to 24 mesh by the method of Evans and Gerald (*8*). Several tests indicated that the reproducibility of the particle characteristics by the Evans and Gerald method was excellent with deviation of less than ±1% error. Significant characteristics of the particles are summarized in the Evans and Gerald paper (*8*).

Solution saturated with the benzoic acid used in the present investigation was found by titration to be in agreement with the literature value (*22*). Also this solubility can be represented by an equation reported by Ishine (*16*) as a function of temperature:

$$C_s = 0.17 + 0.00197t + 0.00020t^2 \qquad (t: 0° \text{ to } 30°\text{C.}) \qquad (1)$$

This value was eventually used in this investigation.

The diffusivity and Schmidt number of the benzoic acid–water system were taken directly from the data of Chang (*2*), quoted by Linton and Sherwood (*19*). Values of the Schmidt number at four temperature levels were also reported by them (*2, 19*).

Since the concentrations of benzoic acid solution obtained in this work were very low, viscosity and density of water were employed to calculate the Reynolds numbers (*20*).

RANGE OF EXPERIMENT

In the first series of experiments measurements included the following variables: exit concentration, water temperature, water flow rate, and bed depth. Computed variables derived from these measurements included k, J_d, N'_{Re}, N_{Sh}, N_{Sc}, and J'_d. The ranges of major variables were as follows:

Particle diameter: 8 to 10 mesh, 12 to 14 mesh, and 20 to 24 mesh.
Water temperature: 16.8° to 24°C.
Over-all bed depth: 3 to 6 in.
Voidage: 0.65 to 0.90.
Modified Reynolds number (N'_{Re}): 5 to 130.
Sherwood number (N_{Sh}): 21 to 116.
Schmidt number (N_{Sc}): 1,020 to 1,540.

The data and calculated results of some representative runs from the first series of experiments are tabulated in Table 1.*

Table 2* contains the measured and calculated data of representative runs for the second series of experiments in which the axial concentration profile of fluid was studied in addition to those variables mentioned above. A typical axial concentration profile and concen-

* Tabular material has been deposited as document 6347 with the American Documentation Institute, Photoduplication Service, Library of Congress, Washington 25, D. C., and may be obtained for $2.50 for photoprints or $1.75 for 35-mm. microfilm.

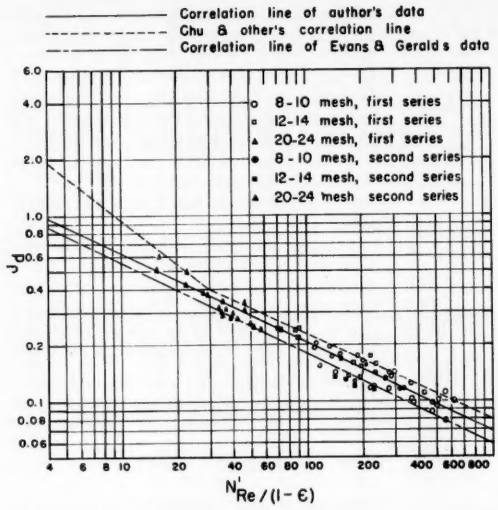
Correlation line of author's data
Chu & other's correlation line
Correlation line of Evans & Gerald's data
8-10 mesh, first series
12-14 mesh, first series
20-24 mesh, first series
8-10 mesh, second series
12-14 mesh, second series
20-24 mesh second series
Jd
N'Re / (1- ε)

Fig. 4. *Jd* factor vs. $N'_{Re}/(1-\epsilon)$ correlation of the experimental data.

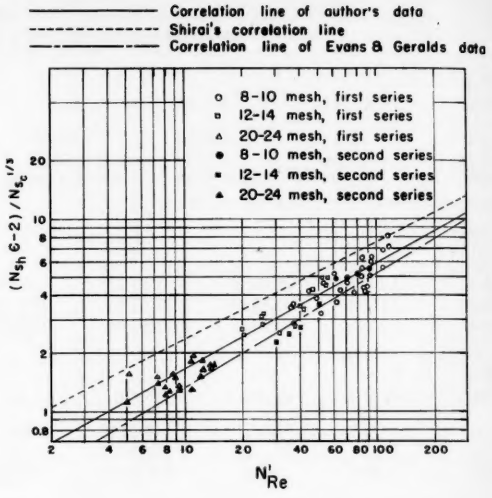
Correlation line of author's data
Shirai's correlation line
Correlation line of Evans & Geralds data
8-10 mesh, first series
12-14 mesh, first series
20-24 mesh, first series
8-10 mesh, second series
12-14 mesh, second series
20-24 mesh, second series
(Nsh ε-2) / Nsc 1/3
N'Re

Fig. 5. $(N_{Sh}\ \epsilon-2)/N_{Sc}$ 1/3 vs. N'_{Re} correlation of the experimental data.

tration gradient curves obtained in the second series of experiments are illustrated in Figures 2 and 3. The break point at 0.52 ft. of bed height corresponds to the boundary of fluidized bed section and fixed bed section at which a distinct discontinuity of concentration gradient exists.

ANALYSIS AND CORRELATION OF RESULTS

To derive the rate equation for the mass transfer between the solid particles and fluid in the semifluidized bed the following assumptions were made:

1. The concentration of the fluid in contact with the particle surface is equal to the saturated concentration.
2. The velocity distribution and concentration of fluid are uniform at any cross section of the test section.
3. The surface area of the particles per unit volume in each bed is uniform.
4. Axial turbulent diffusion coefficient, E_z, in each bed remains constant under definite flow conditions.
5. The process is isothermal.

The following material balance could be obtained for any bed height:

$$G\frac{dC}{dl} = E_z\rho_f\frac{d^2C}{dl^2} + k\,a(C_s - C) \qquad (2)$$

When one assumes that longitudinal or axial mixing in the bed can be negligible

$$E_z\rho_f\frac{d^2C}{dl^2} = 0 \qquad (3)$$

Then Equation (2) can be expressed as (*1, 5*)

$$G\frac{dC}{dl} = k\,a(C_s - C) \qquad (4)$$

Since there exists a finite discontinuity in the axial concentration gradient at the interphase of the fluidized and packed beds,

$$G\int_{C_o}^{C_1}\frac{dC}{C_s - C} + G\int_{C_1}^{C_2}\frac{dC}{C_s - C} = (k_f)_{lm}\,a_f\int_o^{l_1} dl + (k_{pa})_{lm}\,a_{pa}\int_{l_1}^{l_2} dl \qquad (5)$$

or

$$G\ln\frac{C_s - C_o}{C_s - C_1} + G\ln\frac{C_s - C_1}{C_s - C_2} = (k_f)_{lm}\,a_f h_f + (k_{pa})_{lm}\,a_{pa}h_{pa} \qquad (6)$$

But Equation (6) can be further simplified:

$$G'\ln\frac{C_s - C_o}{C_s - C_2} = (k_f)_{lm}\,A_f + (k_{pa})_{lm}\,A_{pa} \qquad (7)$$

If the weighted mean value of overall mass transfer coefficient is defined as

$$k_{lm} = (k_f)_{lm}\frac{A_f}{A} + (k_{pa})_{lm}\frac{A_{pa}}{A} \qquad (8)$$

or

$$k_{lm} = (1-X)(k_f)_{lm} + X(k_{pa})_{lm}$$

Equation (7) may be transformed into

$$G'\ln\frac{C_s - C_o}{C_s - C_2} = k_{lm}\,A \qquad (9)$$

or

$$k_{lm} = \frac{G'(C_2 - C_o)}{A(\Delta C)_{lm}} \qquad (10)$$

In order to account for the effect of axial mixing, which was neglected, k_{lm} must include a correction factor F suggested by Epstein (*7, 13*).

In case the axial concentration data are available, as in the second series of experiments, the value of k in each bed can be directly calculated by use of the integrated mean driving force as

$$(k_f)_{tm} = \frac{G'(C_1 - C_o)}{A_f(\Delta C_f)_{tm}} \qquad (11)$$

and

$$(k_{pa})_{tm} = \frac{G'(C_2 - C_1)}{A_{pa}(\Delta C_{pa})_{tm}} \qquad (12)$$

The over-all mass transfer coefficient based on integrated mean driving force may be evaluated as

$$k_{tm} = \frac{G'(C_2 - C_o)}{A(\Delta C)_{tm}} = \frac{G'(C_1 - C_o) + G'(C_2 - C_1)}{A(\Delta C)_{tm}} = \frac{(k_f)_{tm}A_f(\Delta C_f)_{tm} + (k_{pa})_{tm}A_{pa}(\Delta C_{pa})_{tm}}{A(\Delta C)_{tm}} \qquad (13)$$

Equation (13) implies that

$$k_{tm} = (1 - X)\frac{(\Delta C_f)_{tm}}{(\Delta C)_{tm}}(k_f)_{tm} + X\frac{(\Delta C_{pa})_{tm}}{(\Delta C)_{tm}}(k_{pa})_{tm} \quad (14)$$

First, the mass transfer data were correlated in terms of the J_d factor and modified Reynolds number as is illustrated in Figure 4 (*3, 14*). The mass transfer coefficients were calculated on the basis of the over-all logarithmic mean driving force, as was done by other investigators (*3, 8*) for the packed- and fluidized-bed mass transfer. The effect of natural convection on the rate of mass transfer which would become appreciable for the large particles ($D_p > 1/4$ in.) at the very low Reynolds numbers as indicated by Gaffney (*12*) was neglected, and no attempt was made to introduce Grashof number in the correlation of data. The broken line in Figure 4 represents the generalized correlation used by Chu et al. (*4*) to correlate the mass transfer data for both packed and fluidized beds. The solid line correlated all the semifluidization data with the magnitude of the deviations comparable to the correlation used by Chu et al. (*4*). The equation for the solid line was found to be

$$J_d = 1.865\left(\frac{N'_{Re}}{1-\epsilon}\right)^{-0.480} \quad (15)$$

Shirai (*23*) presented the following correlation of the mass transfer data in the particle beds as suggested by the boundary-layer theory (*10, 16*):

$$N_{Sh\epsilon} = 2.0 + 0.75\,N'^{1/2}_{Re}\,N^{1/3}_{Sc} \quad (16)$$

Figure 5 shows the similar correlation for the present data and a comparison with Shirai's equation (*23*). The regression line through the data is expressed as

$$N_{Sh\epsilon} = 2.0 + 0.46\,N'^{0.543}_{Re}\,N^{0.33}_{Sc} \quad (17)$$

To take the effect of molecular diffusion and natural convection into account the J_d factor can be modified as (*23*)

$$J'_d = \frac{N_{Sh} - 2}{(N'_{Re})(N_{Sc})^{1/3}} \quad (18)$$

The J'_d factors are also correlated as a function of $N'_{Re}/(1-\epsilon)$ in Figure 6, which yield the relationship

$$J'_d = 1.51\left(\frac{N'_{Re}}{1-\epsilon}\right)^{-1/2}$$

or

$$N_{Sh} = 2.0 + 1.51[(1-\epsilon)N'_{Re}]^{1/2}(N_{Sc})^{1/3} \quad (19)$$

The data obtained in the second series of experiments are also similarly correlated, and the results are plotted on Figures 4 to 6 again for comparison with the results of the first series of experiments.

DISCUSSION AND CONCLUSION

In order to evaluate the effect of the packed-bed formation on the mass transfer in the fluidized bed, the mechanism of the packed-bed formation should be understood. The size of the packed-bed section formed must be estimated by an equation including the independent variables of the experiment and the characteristics of ordinary fluidization under similar flow conditions. Such an equation was already reported by the authors in the previous communication (*9*).

It was also reported in the communication that the over-all mass transfer coefficients based on the over-all logarithmic driving forces can be correlated by use of J_d factor suggested by Chu and his co-workers (*3*) within the range of maximum probable deviation. Referring to Figure 4, one can see that Chu's original J_d factor correlation yields J_d values consistently higher than the present experimental data. Chu's correlation pertains only to the ordinary fluidized and packed beds. The maximum deviation of the present data based on his correlation appears to be 22% in the range of Reynolds numbers used. Evans and Gerald's (*8*) data for the benzoic acid–water system were not included in the original correlation by Chu et al. (*3*). They were recalculated in terms of J_d vs. $N'_{Re}/(1-\epsilon)$. It clearly indicates that Evans and Gerald's (*8*) data also deviate consistently from the original correlation of Chu et al. (*3*) with approximately the same magnitudes as those of the semifluidized bed data. Their packed bed data are correlated as

$$J_d = 2.132\left(\frac{N'_{Re}}{1-\epsilon}\right)^{-0.512} \quad (20)$$

and the fluidized bed data are correlated as

$$J_d = 1.340\left(\frac{N'_{Re}}{1-\epsilon}\right)^{-0.489} \quad (21)$$

The over-all correlation of Evans and Gerald's (*8*) data may be expressed as

$$J_d = 1.680\left(\frac{N'_{Re}}{1-\epsilon}\right)^{-0.490} \quad (22)$$

Comparison of Equations (22) with (15) reveals that within the range of the variables of the present investigation and the errors of experimentation the semifluidization data may be correlated as well as the data for ordinary fluidized and packed beds by use of the J_d factor vs. $N'_{Re}/(1-\epsilon)$ plot based on the over-all logarithmic mean mass transfer coefficient, k_{lm}.

The data for the benzoic acid–water system were not included in Shirai's (*23*) generalized correlation covering the data of the fluidized bed, fixed bed, and a single particle. Evans and Gerald's (*8*) data were again recorrelated by the method suggested by Shirai (*23*) as illustrated in Figure 5, which indicates that the experimental data were consistently lower than the

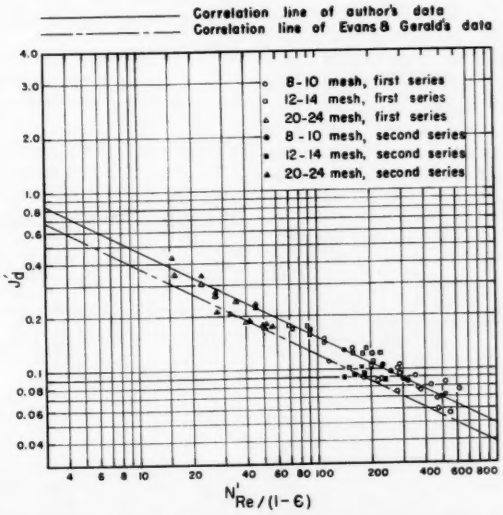

Fig. 6. $J'd$ factor vs. $N_{Re}/(1-\epsilon)$ correlation of the experimental data.

calculated values by approximately 38%. This is, however, within the range of accuracy expected from the generalized correlation of Shirai (23) for any specific system. Evans and Gerald's data are expressed as follows:

For packed bed:

$$N_{Sh\epsilon} = 2.0 + 0.424\, N'^{\,0.558}_{Re}\, N_{Sc}^{1/3} \tag{23}$$

For fluidized bed:

$$N_{Sh\epsilon} = 2.0 + 0.230\, N'^{\,0.659}_{Re}\, N_{Sc}^{1/3} \tag{24}$$

For over-all correlation:

$$N_{Sh\epsilon} = 2.0 + 0.312\, N'^{\,0.608}_{Re}\, N_{Sc}^{1/3} \tag{25}$$

The over-all correlation expressed by Equation (25) is again very similar to that for the semifluidized-bed data expressed by Equation (16) and Figure 5. These similarities of the correlation between the ordinary packed beds and semifluidized beds by use of the methods suggested by Chu et al. (3) and Shirai (23) would indicate that it is possible, at least for the purpose of correlation, to consider the semifluidized bed to possess uniform solid-density distribution. When correlations are not available for any specific system for semifluidization, the generalized mass transfer correlation of the ordinary packed and fluidized beds may be employed to estimate the mean mass transfer coefficients.

Equation (19), which was derived by modification of the J_d factor correlation to the present data, yields a mean deviation of 11.7%; Equations (15) and (17) give a deviation of 9.87% and 11.73% respectively. This implies that the use of the modified correlation as expressed by Equation (19) does not improve the correlation; however, the form of this equation would agree with the expression predicted by the boundary-layer theory (16).

Evans and Gerald's (8) data were recorrelated in the form of Equation (19). The packed-bed data are correlated as

$$N_{Sh} = 2.0 + 1.483[(1-\epsilon)\, N'_{Re}]^{1/2} (N_{Sc})^{1/3} \tag{26}$$

and the fluidized-bed data are correlated as

$$N_{Sh} = 2.0 + 1.031[(1-\epsilon) N'_{Re}]^{1/2} (N_{Sc})^{1/3} \tag{27}$$

An over-all correlation equation may be expressed as

$$N_{Sh} = 2.0 + 1.202[(1-\epsilon) N'_{Re}]^{1/2} (N_{Sc})^{1/3} \tag{28}$$

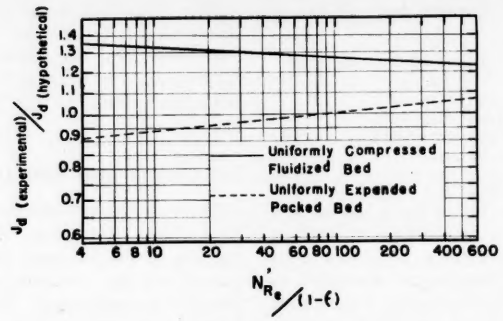

Fig. 7. Comparison of experimental value of mass transfer factor with those of hypothetical models.

In spite of the similarity and analogy as described above in correlations of the mass transfer data in the fluidized, semifluidized, and packed beds, a semifluidized bed may be considered neither a uniformly compressed fluidized bed nor a uniformly expanded packed bed as illustrated in Figure 7. The lines in Figure 7 correspond to the ratios of Equation (15) with Equations (20) and (21) respectively. The over-all mass transfer coefficients in the semifluidized bed appear greater than those of the hypothetical uniformly compressed fluidized bed with the same over-all bed porosity and smaller than those of the hypothetical uniformly expanded packed bed. As can be seen from the formation of the distinct sections of the fluidized and packed beds, which are aligned in series, the over-all mass transfer coefficients in the semifluidized beds would be expected to be a weighted average between k_f and k_{pa} obtained under the same flow conditions. This fact is expressed as Equations (8) and (14). Mass transfer coefficients calculated from these equations gave the mean deviations from the experimental values of −0.78 and −4.3% respectively. Since (9)

$$X = \frac{\rho_s S(1-\epsilon_{pa})(h_{fo}-h)}{W} \frac{(1-\epsilon_f)}{(\epsilon_f-\epsilon_{pa})} \tag{29}$$

Equation (8) can be written as

$$k_{1m} = \left[1 - \frac{\rho_s S(1-\epsilon_{pa})(h_{fo}-h)}{W} \frac{(1-\epsilon_f)}{(\epsilon_f-\epsilon_{pa})}\right](k_f)_{1m} + \frac{\rho_s S(1-\epsilon_{pa})(h_{fo}-h)}{W} \frac{(1-\epsilon_f)}{(\epsilon_f-\epsilon_{pa})}(k_{pa})_{1m} \tag{30}$$

An equation similar to Equation (30) to estimate k_{tm} can be derived by a combination of Equations (14) and (30). Equation (30) enables one to estimate the over-all mass transfer coefficients from the knowledge of ordinary packed and fluidized beds operated under the same conditions. By varying X, which in turn depends on the over-all porosity of the bed and can be arbitrarily fixed for the semifluidized bed, one should be able to obtain any value of k between k_f and k_{pa}. Since $1-\epsilon = (1-\epsilon_o)/R$, Equation (15) or (19) indicates that approximately such a change of over-all k can be controlled as inversely proportional to $\sqrt{R}$. This could be illustrated by use of the data from the experimental runs at G = 28,000 lb./(hr.)(sq.ft.) with the mean deviation of 7%. It may be desirable to point out again that under definite flow conditions the values of k_f for fluidized and k_{pa} for packed beds, unlike the corresponding k in the semifluidized bed, are fixed for any particular system.

In the first series of experiments the axial concentration profile was not determined, and the logarithmic driving force was made use of in the correlation of the data. It has already been pointed out that the k_{1m} must contain in itself the F factor of Epstein (7). The importance of the axial mixing in the solid-liquid contact process has been emphasized by various investigators recently (7, 26). However it appears that so for there is no way to predict exactly the axial mixing coefficient of a particular system under certain operating conditions with sufficient accuracy for mass transfer calculations. But there is good indication that axial mixing in the liquid-solid systems is much less extensive than in the gas-solid systems (21, 26). In Figures 4, 5, and 6 the mass transfer coefficients calculated by use of the integrated mean driving force are compared with the correlation obtained in the first series of experiments. They indicate that the deviation of the second series experimental data from the correlation are within the range of the first series of experiments. This implies that the

F factor included in the correlation of the data in the first series of the experiments were close to unity; in other words the effect of axial concentration gradient change and fluid mixing were small. Since an over-all mass transfer based on integrated mean concentration difference is employed, the radial mixing effect is not considered here. The maximum deviation of the values of F from unity for the second series of experiments was 7.65%.

As indicated in the introduction, probably no theories of interphase mass transfer based on the simple models can be adopted in the correlation of mass transfer data in the packed or fluidized bed. Danckwerts (*4*) in his review paper suggested the necessity of the theory different from either the boundary-layer theory or the surface-renewal theory to explain the behavior of gas absorption by liquid in the packed bed. The results of mass transfer investigation by Johnson and Huang (*17*) using a series of organic acids including benzoic acid suggested the applicability of the surface-renewal theory to the interphase mass transfer between solid and liquid. They too however indicated the difficulty of applying the surface-renewal theory directly to the mass transfer in packed beds because of the variation of the local conditions in the packed tower. A recent study by Bennett and Lewis (*1*) indicated that the direct applicability of the surface-renewal theory to the interphase mass transfer between the benzoic acid and water is doubtful even in the rotating-cylinder apparatus with very simple geometry. Thus further complication in application of theories to the mass transfer in semifluidized bed can be easily expected because of its complex structure. As Equation (19) indicates, 1/3 power of Schmidt numbers has been used in the present study (with a mean deviation of 11.7%), which is, as described previously, based on the boundary-layer theory (*11, 16*). Recent theory proposed by Toor and Marchello (*24*) would predict that the power for N_{Sc} should vary depending on the system and local flow conditions. It should be pointed out that in view of the relatively small range of Schmidt numbers covered in the experiments, extensive extrapolation of the empirical correlations presented in this paper must be approached with caution.

The possibility of the practical application of semifluidization has been described in the previous communication (*9*).

ACKNOWLEDGMENT

The authors express their appreciation to Henry T. Ward, Head of the Chemical Engineering Department, Kansas State University, for his advice and encouragement and also to the Kansas State University Engineering Experiment Station for financial support.

NOTATION

A = total particle surface area, sq. ft.
C = concentration of benzoic acid in water stream, lb./lb.
C_s = concentration of benzoic acid in saturated solution, lb./lb.
dl = differential bed height, ft.
D_p = equivalent spherical particle diameter, ft.
D_e = diffusivity of benzoic acid in water, (sq. ft.)/hr.
E_z = longitudinal mixing coefficient, (sq. ft.)/hr.
F = correction factor, dimensionless
f = function of
G = superficial mass velocity, lb./(hr.)(sq. ft.)
G' = mass velocity, lb./hr.
h = height of the top sieve plate or over-all depth of bed, ft.
h_o = depth of height of initial bed, ft.
h_f = height of fluidized bed section, ft.
h_{pa} = height of packed bed section, ft.
J_d = mass transfer factor, dimensionless, $[(k/G)\ N_{Sc}^{2/3}]$
J'_d = modified mass transfer factor, dimensionless
k = mass transfer coefficient, lb./hr. (sq. ft.)(unit C)
k_p = mass transfer coefficient, ft./hr.
l = distance in axial direction of bed, ft.
N'_{Re} = modified Reynolds number, dimensionless, (D_pG/μ)
N_{Sc} = Schmdit number, dimensionless
N_{Sh} = Sherwood number, dimensionless
R = bed expansion rate, dimensionless
S = cross-section area of the column, sq. ft.
T = temperature, °C.
V = over-all volume of the bed, cu. ft.
W = weight of the particle bed, lb.
X = weight fraction of particles in the packed bed section, dimensionless

Greek Letters

ϵ = void fraction or porosity in the bed, dimensionless
ρ = fluid density, lb./cu. ft.
ρ_B = bulk density of the solid, lb./cu. ft.
ρ_s = solid density, lb./cu. ft.
μ = viscosity, lb./(hr.)(ft.)

Subscript

f_o = completely fluidized bed or ordinary fluidized bed
f = fluidized bed
p = particle
pa = packed bed
0 = at bed inlet
1 = at interface between packed and fluidized beds
2 = at bed outlet
m = mean value
lm = logarithmic mean value
tm = integrated mean value

LITERATURE CITED

1. Bennett, J. A. R., and J. B. Lewis, *A.I.Ch.E. Journal*, **4**, 419 (1958).
2. Chang, S., M. S. thesis, Mass. Inst. Technol., Cambridge (1948).
3. Chu, J. C., James Kalil, and W. A. Wettereth, *Chem. Eng. Progr.*, **49**, 141 (1953).
4. Danckwerts, P. V., *A.I.Ch.E. Journal*, **1**, 456 (1955).
5. ———, and A. M. Kennedy, *Trans. Inst. Chem. Engrs.*, **32**, S 49 (1954).
6. Eckert, E. R. G., "Introduction to Heat and Mass Transfer," McGraw-Hill, New York (1950).
7. Epstein, N., *Can. J. Chem. Eng.*, **36**, 210 (1958).
8. Evans, G. C., and C. F. Gerald, *Chem. Eng. Progr.*, **49**, 135 (1953).
9. Fan, L. T., Y. C. Yang, and C. Y. Wen, *A.I.Ch.E. Journal*, **5**, 407 (1959).
10. Frossling, N., *Gerlands Beit. Geophys.*, **52**, 170 (1938).
11. Fuchs, N., *J. Phys.* (*U.S.S.R.*), **6**, 224 (1934).
12. Gaffney, B. J., and T. B. Drew, *Ind. Eng. Chem.*, **42**, 1120 (1950).
13. Galloway, L. R., W. Komarnicky, and N. Epstein, *Can. J. Chem. Eng.*, **35**, 139 (1957).
14. Garner, F. H., and R. D. Suckling, *A.I.Ch.E. Journal*, **4**, 115 (1958).
15. "International Critical Table," McGraw-Hill, New York (1926).
16. Ishine, T., T. Otake, and T. Okaka, *Chem. Eng.* (*Japan*), **15**, 255 (1951).
17. Johnson, A. I., and C. J. Huang, *A.I.Ch.E. Journal*, **2**, 412 (1956).
18. Lemlich, Robert, and Isidoro Caldes, Jr., *ibid.*, **4**, 376 (1958).
19. Linton, W. H., Jr., and T. K. Sherwood, *Chem. Eng. Progr.*, **46**, 259 (1950).
20. Perry, J. H., "Chemical Engineers' Handbook," 3 ed., McGraw-Hill, New York (1950).
21. Richardson, J. F., and A. E. Mitson, *Trans. Inst. Chem. Eng.*, **36**, 270 (1958).
22. Seidell, A., "Solubility of Organic Compounds," 3 ed., Van Nostrand, New York (1941).
23. Shirai, T., Ph.D. thesis, Tokyo Inst. Tech., Tokyo (1955).
24. Toor, H. L., and J. M. Marchello, *A.I.Ch.E. Journal*, **4**, 97 (1958).
25. Wakao, N., T. Oshima, and S. Yagi, *Chem. Eng.* (*Japan*), **22**, 780 (1958).
26. ———, *ibid.*, p. 786.

Manuscript received August 13, 1959; revision received December 7, 1959; paper accepted December 16, 1959. Paper presented at A.I.Ch.E. Atlanta meeting.

On the Steady State Activity Levels in a Reactor-Regenerator System

E. E. PETERSEN

University of California, Berkeley, California

A method is proposed for computing the steady state activity levels at various points within a reactor-regenerator system in which the residence time distribution functions in the reactor and regenerator, the permanent deactivation function, and the temporary deactivation and activation functions are arbitrarily specified. A particularly simple solution to these equations is obtained when the temporary activation and deactivation functions are of exponential form. The latter equations are used to calculate values of the mean activity in the reactor for the limiting cases of piston type of flow and complete mixing under a variety of conditions.

The activity of catalyst particles circulated in a system consisting of a fluidized reactor and a fluidized regenerator changes owing to carbon deposition on and removal from the active surface and to sintering or sealing off of active surface making parts of the catalyst surface unavailable to the reactant charge. The activity of a catalyst particle is a function of its initial properties, its history within each of the units, the extent of reaction taking place within it, the reaction temperatures, and the time of exposure to cracking conditions. After a period of residence within a reactor under cracking conditions the activity of a catalyst particle decays, and upon subsequent exposure to the environment of the regenerator the activity of the catalyst particle increases depending upon the residence time and conditions within the regenerator. However the original activity of the fresh catalyst cannot, presumably, be attained even if its residence time in the regenerator is infinite. It is therefore convenient to postulate two types of deactivation: a regenerable or temporary type which can be reactivated in a regenerator environment, and a nonregenerable or permanent type which cannot be reactivated in a regenerator environment.

The effect of each type of deactivation can be illustrated by the following description of an operating system. Consider a reactor-regenerator combination charged with fresh catalyst and operated without supplying make-up catalyst as shown in Figure 1*a*. When one assumes that only temporary deactivation occurs, the mean activity levels within the reactor and regenerator will decrease and approach some finite steady state value as the time of operation increases. The steady state value will be a function of the operation conditions and the residence-time distribution within the reactor and regenerator and the nominal residence time within each unit. The greater the catalyst recirculation rate the higher the mean activity within each unit.

Consider the operation of the reactor and regenerator again as before, except that now both temporary and permanent deactivation can occur. As operation time increases, the mean activity levels within the reactor and regenerator will not approach a steady state value but will continue to decrease and approach either a value of zero activity or some very small activity level probably independent of the mean residence time and residence-time distribution within each of the units. However if fresh catalyst is continuously introduced in the reactor, as shown in Figure 1*b*, and an equal quantity continuously withdrawn from the catalyst stream going to the regenerator, the inventory in the units remains constant and the activity levels within the reactor and regenerator again approach finite steady state values. The magnitudes of the steady state values depend on the fresh catalyst feed rate in addition to the variables mentioned for the case of temporary deactivation only.

The purpose of this paper is to predict the steady state mean level of activity in the reactor and regenerator where the residence-time distribution, the permanent deactivation functions, and the temporary deactivation and activation functions are arbitrary functions of residence time. This problem is a generalization of some work by Pigford (7) who solved for time-dependent activity within a completely mixed reactor resulting from permanent deactivation and hence did not consider the reactor and regenerator separately. Pigford assumed that the fresh catalyst feed rate was a known but arbitrarily specified function of time.

RESIDENCE TIME DISTRIBUTION FUNCTION

Assume that the reactor shown in Figure 2 contains a large number of catalyst particles and has equal catalyst feed and removal rates to maintain constant inventory within the unit. If Q tagged catalyst particles are injected into the feed stream at time $t = 0$, and the number of tagged particles $q(t)$ having left the reactor at time t is counted, a plot of the form shown in Figure 2 can be obtained. On the assumption that this function is continuous, the number of tagged particles leaving in the interval from t to $t + dt$ is represented by the time derivative of the curve in Figure 2. The residence time distribution function $T'(t)$ is defined as

$$T'(t) \equiv \frac{1}{Q}\frac{dq(t)}{dt} \qquad (1)$$

and has the property that

$$\int_0^\infty T'(t)\,dt = 1 \qquad (2)$$

Also let

$$T(t) \equiv \int_0^t T'(\gamma)\,d\gamma \qquad (3)$$

All catalyst particles entering at the same time have the same *a priori* probability of leaving the bed. The function $T'(t)$ however defines the relative probabilities of particles leaving having entered at different times.

The distribution function $T'(t)$ depends upon the type of mixing which occurs in the system. Distribution functions of engineering interest generally lie between the limits of no mixing, which corresponds to piston flow, and complete mixing; these limiting forms are shown in Figure 3. The reader is referred to the works of Danckwerts et al. (4, 5) and Singer et al. (8) for a detailed discussion of the residence time distribution function. The number of particles N remaining in the bed after an infinite time is

$$N = n\int_0^\infty [1 - \int_0^t T'(\gamma)\,d\gamma]dt \qquad (4)$$

Therefore

$$\frac{n}{N}\int_0^\infty [1 - T(t)]dt = 1 \qquad (5)$$

A particular set of residence time distribution functions of engineering interest is that obtained from m stages of equal volume in series. Complete mixing is assumed in each stage. The residence time distribution function for particles leaving the last stage in terms of the time they entered the first stage is

$$T'(\tau) = \frac{\tau^{m-1}}{(m-1)!} e^{-\tau} \qquad (6)$$

where $T'(\tau)$ is the derivative with respect to τ:

$$\tau = \frac{mnt}{N} \qquad (7)$$

When $m = 1$, the distribution function corresponds to a single completely mixed stage, and as $m \to \infty$, it approaches piston flow. The curves for several intermediate values of m are included on Figure 3.

REACTOR DEACTIVATION AND REGENERATOR ACTIVATION FUNCTIONS

The discussion is first directed to the case in which only temporary deactivation is considered and no fresh catalyst is charged (Figure 1*a*). The activity of a catalyst particle leaving the reactor depends upon its activity when entering and its residence time therein. The functions $R(\theta_1)$ and $G(\alpha)$ relate the activity of a catalyst particle and its residence time in the reactor and regenerator, respectively. These functions are characteristic of the particular operating conditions within the units, and their qualitative forms are shown in Figure 4. Consider the history of a single particle entering the reactor with an activity $R(\theta)$. After residing a time t_{r_1} in the reactor the particle leaves with an activity $R(\theta_1 + t_{r_1})$ and enters the regenerator with an activity $G(\alpha_1) = R(\theta_1 + t_{r_1})$, and after residing for a time t_{g_1} it leaves the regenerator with an activity $G(\alpha_1 + t_{g_1})$. The particle then re-enters the reactor with an activity $R(\theta_1') = G(\alpha_1 + t_{g_1})$ where in the general case $R(\theta_1) \neq R(\theta_1')$.

This is undoubtedly a simplified picture of the real behavior of catalyst particles within the system because implicit in this description are the assumptions that all particles residing a definite time in the reactor or regenerator are exposed to identical environmental conditions and that the activity is a unique function of the carbon deposition. On a statistical basis the former assumption would appear to be reasonable, whereas the latter assumption may be untrue owing to heat treating of the deposit after many cycles. However the apparent temperatures are too low for appreciable graphization to occur.

STEADY STATE ACTIVITY LEVELS WITH TEMPORARY DEACTIVATION

$F(\theta)$ and $H(\alpha)$ have properties such that

$$\int_o^\infty F(\theta)\, d\theta = 1 \qquad (8)$$

$$\int_o^\infty H(\alpha)\, d\alpha = 1 \qquad (9)$$

The mean activity of a stream of catalyst particles having an age distribution given by $F(\theta)$ is therefore

$$\overline{A}_i = \int_o^\infty F(\theta)\, R(\theta)\, d\theta \qquad (10)$$

If the age distribution of the feed does not change with time, the mean activity of the catalyst particles entering and leaving the reactor is given by Equations (10) and (11), respectively:

$$\overline{A}_o = \int_o^\infty \int_o^\infty F(\theta) R(\theta + t_r) T_R'(t_r)\, dt_r\, d\theta \qquad (11)$$

Equation (11) can be stated in words as follows. All particles entering the reactor of age θ will leave the reactor with a distribution of ages according to the distribution $T_R'(t_r)$, and a particle of age θ residing for a time t_r in the reactor will leave with an activity $R(\theta + t_r)$.

The particles leaving the reactor enter the regenreator (Figure 1*a*); therefore the average activity of the stream entering the regenerator is $\overline{A}_o$, which is also represented by

$$\overline{A}_o = \int_o^\infty H(\alpha)\, G(\alpha)\, d\alpha \qquad (12)$$

and the stream leaving the regenerator has a mean activity $\overline{A}_i$ given by

$$\overline{A}_i = \int_o^\infty \int_o^\infty H(\alpha) G(\alpha + t_g) T_G'(t_g)\, dt_g\, d\alpha \qquad (13)$$

The mean activity within the reactor and regenerator can be represented in terms of the above functions:

$$\overline{A}_R = \frac{n}{N_R} \int_o^\infty \int_o^\infty F(\theta)\, R(\theta + t_r)\, [1 - T_R(t_r)]\, dt_r\, d\theta \qquad (14)$$

$$\overline{A}_G = \frac{n}{N_G} \int_o^\infty \int_o^\infty H(\alpha) G(\alpha + t_g)\, [1 - T_G(t_g)]\, dt_g\, d\alpha \qquad (15)$$

In the general case the solution to Equations (14) and (15) can be obtained after Equations (10) through (13) have been solved simultaneously to determine the functions $F(\theta)$ and $H(\alpha)$.

Define two functions $P(\epsilon)$ and $Q(\eta)$ in such a way that $P(\epsilon)\, d\epsilon$ and $Q(\eta)\, d\eta$ are the fractions of particles leaving the reactor and regenerator respectively having ages between ϵ and $\epsilon + d\epsilon$ and $\eta + d\eta$. It follows therefore that

$$P(\epsilon) = \int_o^\epsilon F(\theta) T_R'(\epsilon - \theta)\, d\theta \qquad (16)$$

and

$$Q(\eta) = \int_o^\eta H(\alpha) T_G'(\eta - \alpha)\, d\alpha \qquad (17)$$

Furthermore

$$F(\theta)\, d\theta = -Q(\eta)\, d\eta \qquad (18)$$

$$P(\epsilon)\, d\epsilon = -H(\alpha)\, d\alpha \qquad (19)$$

Since the activity $R(\epsilon)$ of a particular group of particles leaving the reactor is equal to $G(\alpha)$, α can be functionally related to ϵ by the use of the original activity curves shown in Figure 4. Let these functions be $\alpha(\epsilon)$ and $\epsilon(\alpha)$ which are, respectively, the values of age α necessary to give the same catalyst activity as particles having an age ϵ and vice versa. Clearly θ and η are related by the functions $\eta(\theta)$ and $\theta(\eta)$ and are, respectively, identical to $\alpha(\epsilon)$ and $\epsilon(\alpha)$. From Equations (17), (18), and (19) one obtains

$$F(\theta) = \eta'(\theta) \int_x^\theta P(\epsilon)\, T_G'[\eta(\theta) - \alpha(\epsilon)]\, d\epsilon \qquad (20)$$

where $\eta'(\theta)$ is the derivative of $\eta(\theta)$ with respect to θ, and the limits have been changed to correspond to the new variable ϵ. Substituting for $P(\epsilon)$ from Equation (16) one gets

$$F(\theta) = \eta'(\theta) \int_x^\theta T_G'[\eta(\theta) - \alpha(\epsilon)] \int_o^\epsilon F(\phi) T_R'(\epsilon - \phi)\, d\phi\, d\epsilon \qquad (21)$$

Reversing the order of integration by standard procedures one obtains directly

$$F(\theta) = \eta'(\theta) \int_o^x F(\phi) \int_x^\theta T_G'[\eta(\theta) - \eta(\epsilon)]\, T_R'(\epsilon - \phi)\, d\epsilon\, d\phi - \eta'(\theta) \int_o^\theta F(\phi) \int_\theta^\epsilon T_G'[\eta(\theta) - \alpha(\epsilon)]\, T_R'(\epsilon - \phi)\, d\epsilon\, d\phi \qquad (22)$$

In more standard form Equation (22) becomes

$$F(\theta) = \eta'(\theta) \int_o^x K_1(\theta, \phi) F(\phi)\, d\phi - \eta'(\theta) \int_o^\theta K_2(\theta, \phi) F(\phi)\, d\phi \qquad (22a)$$

where

$$K_1(\theta, \phi) = \int_x^\theta T_G'[\eta(\theta) - \alpha(\epsilon)]\, T_R'(\epsilon - \phi)\, d\epsilon$$

$$K_2(\theta, \phi) = \int_\theta^\epsilon T_G'[\eta(\theta) - \alpha(\epsilon)]\, T_R'(\epsilon - \phi)\, d\epsilon$$

These Kernel functions can be evaluated provided the residence time distribution functions and the activation and deactivation functions are known.

Equation (22*a*) is a linear, homogeneous, integral equation and can be solved in general by numerical procedures. The reader is referred to the iterative method as a means of obtaining a solution.*

* See for example page 468 of reference 6.

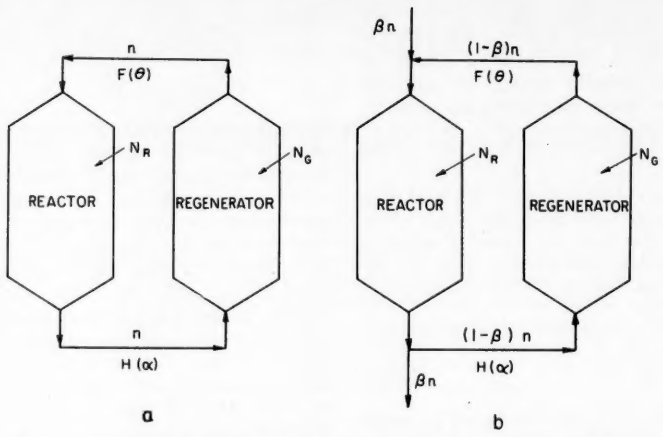

Fig. 1. Reactor-regenerator flow systems: *a*, case of temporary activation; *b*, case of temporary and permanent deactivation.

PERMANENT DEACTIVATION

When catalytic particles exhibit the property of permanent deactivation as a function of the residence time within the reactor-regenerator unit, a steady state activity level is maintained only when fresh catalyst is fed to the units. The level of activity of course depends upon the rate at which fresh catalyst is introduced. The flow diagram of the units is shown in Figure 1*b*. The recirculation is $(1-\beta)n$ particles per unit time, and the number of particles entering and leaving the reactor is n. The rate of addition of fresh catalyst particles to the system is βn. An equal number of particles is withdrawn from the stream leaving the reactor in order to keep the inventory constant.

The permanent deactivation function is given by $K(t)$ ranging in magnitude between 1 and 0 as t varies between 0 and ∞ and where t is the total residence time of catalyst particles within the reactor and regenerator units. The function $K(t)$ is assumed to be independent of the temporary deactivation functions, and $1 - K(t)$ represents a loss in activity which cannot be regenerated by exposure to the regenerator environment. The form of this function has been studied by Small et al. (9), although it is not clear at what temperature experiments should be made in order to correspond to the reacting system.

It is necessary therefore to solve for the residence-time distribution of particles in the system in terms of arbitrarily specified residence time distribution functions $T_R'(t_r)$ and $T_G'(t_g)$, and the parameters β, n, N_R, and N_G.

A schematic diagram of the system is shown on Figure 5, wherein βn untagged particles are fed and removed continuously and $(1-\beta)n$ particles are recirculated. If at time $t \geq 0$ βn tagged particles are continuously fed to the system at point A, the fraction of the tagged particles in various parts of the system will depend upon t. Let the fractions of tagged particles at points C and D be given by the functions $F(t)$ and $h(t)$, respectively. These two functions can be inter-related by the equations below in terms of the residence-time distributions in the reactor and the regenerator.

$$\beta n \int_0^t T_R'(\gamma)\, d\gamma + (1-\beta)n \int_0^t F(t-\gamma) T_R'(\gamma) d\gamma = n\,\mathcal{H}(t) \tag{23}$$

$$(1-\beta)n \int_0^t \mathcal{H}(t-\gamma) T_G'(\gamma) d\gamma = (1-\beta)n\, F(t) \tag{24}$$

The formal solution to this set of equations can be obtained in terms of the Laplace transforms (2) of the functions which are represented by small script letters:

$$\mathcal{L}\{\mathcal{H}(t)\} = h(s)$$
$$\mathcal{L}\{F(t)\} = f(s) \tag{25}$$

From Equations (3), (23), (24), and (25)

$$h(s) = \beta \mathcal{L}_R(s) + (1-\beta)\, \mathcal{L}(s) \mathcal{L}_R'(s) \tag{26}$$

$$f(s) = h(s) \mathcal{L}_G'(s) \tag{27}$$

Therefore:

$$h(s) = \frac{\beta \mathcal{L}_R(s)}{1 - (1-\beta)\mathcal{L}_G'(s)\mathcal{L}_R'(s)} \tag{28}$$

$$f(s) = \frac{\beta \mathcal{L}_G'(s)\mathcal{L}_R(s)}{1 - (1-\beta)\mathcal{L}_G'(s)\mathcal{L}_R'(s)} \tag{29}$$

The evaluation of the functions $h(t)$ and $F(t)$ has been reduced to the problem of finding the inverses of their Laplace transforms in Equations (28) and (29) for arbitrary forms of the residence time distribution functions and the fraction of the recirculation stream.

The function $F(t)$ is the fraction of tagged particles in stream C at the time t units after the introduction of tagged particles. Since no tagged particles entered the system prior to zero time, all tagged particles have resided in the system a time equal to or less than t.

Let

$$\frac{dF(t)}{dt} \equiv F'(t) \tag{30}$$

and

$$\frac{d\mathcal{H}(t)}{dt} \equiv \mathcal{H}'(t) \tag{31}$$

Consider now a reactor-regenerator system in which fresh catalyst is fed and used catalyst removed at a rate βn for a very long period of time as shown in Figure 1*b*. The residence-time distribution of the particles in streams C and D approach those given by $F'(t)$ and $h'(t)$, respectively, and the mean permanent deactivations of the streams are, respectively

$$\overline{K_c} = \int_0^\infty K(t)\, F'(t)\, dt \tag{32}$$

and

$$\overline{K_D} = \int_0^\infty K(t)\, h'(t)\, dt \tag{33}$$

Moreover the permanent deactivations of the catalyst leaving the reactor and regenerator which entered from streams C and D, respectively, are

$$\overline{K_r} = \int_0^\infty F'(t) \int_0^\infty K(t+t_r)\, T_R'(t_r)\, dt_r\, dt \tag{34}$$

$$\overline{K_g} = \int_0^\infty \mathcal{H}'(t) \int_0^\infty K(t+t_g)\, T_G'(t_g)\, dt_g\, dt \tag{35}$$

The mean permanent deactivation of the stream leaving the reactor which entered as fresh feed is

$$\overline{K_{rf}} = \int_0^\infty K(t_r) T_R'(t_r)\, dt_r \tag{36}$$

Finally the mean permanent deactivations of the particles in the reactor originating from fresh feed without recirculation and from stream C are, respectively

$$\overline{K_{Rf}} = \frac{n}{N_R} \int_0^\infty K(t_r)[1 - T_R(t_r)]\, dt_r \tag{37}$$

$$\overline{K_R} = \frac{n}{N_R}\int_0^\infty F'(t)\int_0^\infty K(t+t_r)\,[1-T_R(t_r)]\,dt_r\,dt \qquad (38)$$

and the mean permanent deactivation in the regenerator is

$$\overline{K_G} = \frac{n}{N_G}\int_0^\infty H'(t)\int_0^\infty K(t+t_g)\,[1-T_G(t_g)]\,dt_g\,dt \qquad (39)$$

STEADY STATE ACTIVITY LEVELS WITH TEMPORARY AND PERMANENT DEACTIVATION

Throughout this treatment permanent and temporary deactivation phenomena have been assumed to be independent. Permanent deactivation depends only upon residence time within the reactor-regenerator set, whereas temporary deactivation depends upon a detailed history of the residence of catalyst pellets in the reactor and regenerator. It is possible therefore to combine the treatments from the previous sections to predict the activity levels in various parts of the units for the case where fresh catalyst is fed to the units and used catalyst is removed at a rate to maintain constant catalyst inventory. The activity of catalyst for carrying out chemical reaction is given by the product of the two activities.

If the age-distribution functions of the catalyst are time independent in all parts of the unit, the equation for mean activities can be immediately written. With reference to Figure 1*b* the mean activity of catalyst entering the reactor $\overline{A_i}$ is

$$\overline{A_i} = \beta + (1-\beta)\overline{K_G}\int_0^\infty F(\theta)R(\theta)\,d\theta \qquad (40)$$

Similarly the activity of catalyst leaving the reactor $\overline{A_o}$ is

$$\overline{A_o} = \beta\overline{K_{rf}}\int_0^\infty R(t_r)T'(t_r)dt_r + (1-\beta)K_r\int_0^\infty F(\theta)\int_0^\infty R(\theta+t_r)T'(t_r)dt_r\,d\theta \qquad (41)$$

In accordance with Figure 1*b* a fraction $(1-\beta)$ of the particles leaving the reactor enter the regenerator; therefore the mean activity of the stream entering the regenerator is also $\overline{A_o}$, which can be represented also by

$$\overline{A_o} = \overline{K_D}\int_0^\infty H(\alpha)G(\alpha)\,d\alpha \qquad (42)$$

and the activity of the stream leaving the regenerator $\overline{A_i} - \beta$ is given by

$$\overline{A_i} - \beta = (1-\beta)\overline{K_G}\int_0^\infty\int_0^\infty H(\alpha)G(\alpha+t_g)T_G'(t_g)dt_g\,d\alpha \qquad (43)$$

The mean activities of particles within the reactor and regenerator are $\overline{A_R}$ and $\overline{A_G}$, respectively, where

$$\overline{A_R} = \frac{n}{N_R}\beta\overline{K_{Rf}}\int_0^\infty R(t_r)[1-T_R(t_r)]dt_r + \frac{n}{N_R}(1-\beta)\overline{K_R}\int_0^\infty F(\theta)\int_0^\infty R(\theta+t_r)[1-T(t_r)]dt_r\,d\theta \qquad (44)$$

and

$$\overline{A_G} = \frac{n}{N_G}\overline{K_G}\int_0^\infty H(\alpha)\int^\alpha G(\alpha+t_g)[1-T_G(t_g)]dt_g\,d\alpha \qquad (45)$$

If $K(t) = 1$ from $0 \leq t \leq \infty$ and β is allowed to go to zero, Equations (33) through (38) reduce to the temporary deactivation case described by Equations (10) through (15).

In the general case the mean activity in the reactor can be obtained by the use of Equations (22*a*) and (44). It is proposed however to approximate the $R(\theta)$ and $G(\alpha)$ by an exponential function in order to calculate mean activity levels under varying conditions.

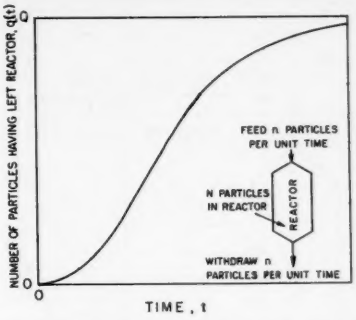
NUMBER OF PARTICLES HAVING LEFT REACTOR, q(t)
FEED n PARTICLES PER UNIT TIME
N PARTICLES IN REACTOR
REACTOR
WITHDRAW n PARTICLES PER UNIT TIME
TIME, t

Fig. 2. Residence time distribution in reactor.

ACTIVATION AND DEACTIVATION CURVES OF EXPONENTIAL FORM

Let

$$R(\theta) = e^{-k_r\theta} \qquad (46)$$

and

$$G(\alpha) = 1 - e^{-k_g\alpha} \qquad (47)$$

Substituting Equation (46) into (40) and (41) one gets

$$\overline{A_i} = \beta + (1-\beta)\overline{K_G}\int_0^\infty e^{-k_r\theta}F(\theta)d\theta \qquad (48)$$

and

$$\overline{A_o} = \beta\overline{K_{rf}}\int_0^\infty e^{-k_r t_r}T'(t_r)dt_r + (1-\beta)\overline{K_r}\int_0^\infty e^{-k_r\theta}F(\theta)d\theta\int_0^\infty e^{-k_r t_r}T_R'(t_r)dt_r \qquad (49)$$

Substituting Equation (48) into (49) one obtains

$$\overline{A_o} = \left\{\beta\overline{K_{rf}} + (\overline{A_i}-\beta)\left(\frac{\overline{K_r}}{\overline{K_G}}\right)\right\}\mathfrak{L}_R'(k_r) \qquad (50)$$

where

$$\mathfrak{L}_R'(k_r) = \int_0^\infty e^{-k_r t_r}T_R'(t_r)\,dt_r \qquad (51)$$

Substituting Equation (40) into (35) and (36) one gets

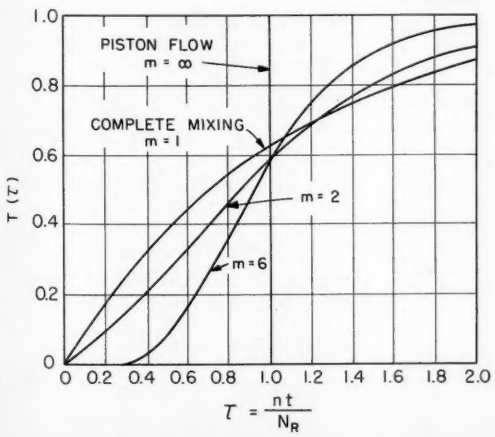

Fig. 3. Residence time distribution in reactor for piston flow, complete mixing, and intermediate cases.

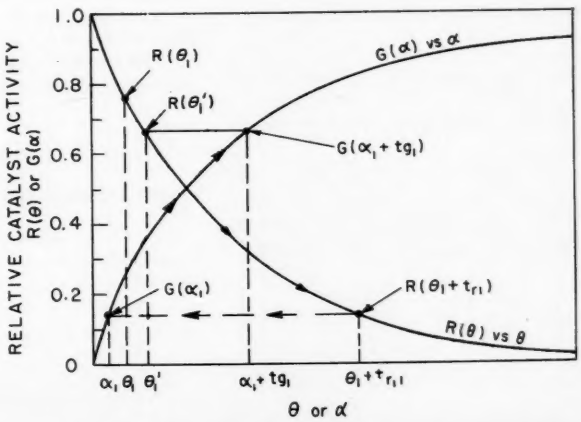

Fig. 4. Temporary reactor deactivation and regenerator activation curves.

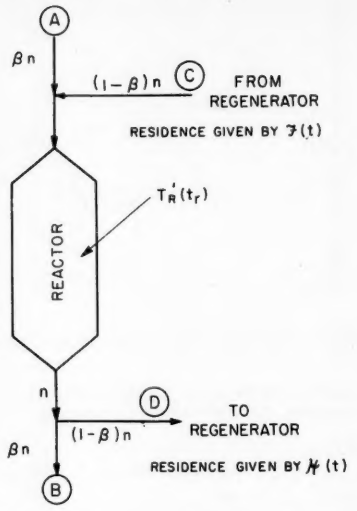

Fig. 5. Reactor regenerator flow system for case of temporary and permanent deactivation.

$$\overline{A}_o = \overline{K}_D[1 - \int_o^\infty e^{-k_g \alpha} H(\alpha)\, d\alpha] \quad (52)$$

$$\overline{A}_i - \beta = (1-\beta)\overline{K}_C \int_o^\infty \int_\alpha^\infty [1 - e^{-k_g(\alpha+t_g)}] H(\alpha) T_G'(t_g)\, dt_g\, d\alpha \quad (53)$$

When one performs the integration of Equation (53) and substitutes Equation (52)

$$\overline{A}_i - \beta = (1-\beta)\left(\frac{\overline{K}_C}{\overline{K}_D}\right)[\overline{K}_D + (\overline{A}_o - \overline{K}_D)\,t_G'(k_g)] \quad (54)$$

where

$$t_G'(k_g) = \int_o^\infty e^{-k_g t_g} T_G'(t_g)\, dt_g$$

Substituting Equation (50) into (54) and solving for $\overline{A}_i$ one obtains

$$\overline{A}_i = \beta + \frac{(1-\beta)[\overline{K}_C\overline{K}_D + \overline{K}_C(\beta\overline{K}_{rf}\,t_R'(k_r) - \overline{K}_D)\,t_G'(k_g)]}{\overline{K}_D - (1-\beta)\,\overline{K}_{rf}\,t_R'(k_r)\,t_G'(k_g)} \quad (55)$$

Finally from Equation (44) the mean activity in the reactor is computed:

$$\overline{A}_R = \frac{n}{N_R}\{\beta\overline{K}_{Rf}\int_o^\infty e^{-k_r t_r}[1 - T_r(t_r)]\,dt_r + (1-\beta)\overline{K}_R\int_o^\infty e^{-k_r\theta} F(\theta)\,d\theta \int_o^\infty e^{-k_r t_r}[1 - T_R(t_r)]\,dt_r\} \quad (56)$$

When one substitutes for $(\overline{A}_i - \beta)/(\overline{K}_C)$ from Equation (48) into (56)

$$\overline{A}_R = \frac{n}{N_R}\left[\beta\overline{K}_{Rf} + \frac{\overline{K}_R}{\overline{K}_C}(A_i - \beta)\right] \int_o^\infty e^{-k_r t_r}[1 - T_R(t_r)]\,dt_r \quad (57)$$

Expressions for $\overline{A}_o$ and $\overline{A}_G$ can be developed similarly.

The solution to the case of temporary deactivation alone can be obtained from Equations (55) and (57) if one lets $K(t) = 1$ and β go to zero. The resulting equations are

$$\overline{A}_i = \frac{1 - t_G'(k_g)}{1 - t_R'(t_r)\,t_G'(k_g)} \quad (58)$$

$$\overline{A}_R = \frac{n}{N_R}\overline{A}_i \int_o^\infty e^{-k_r t_r}[1 - T_R(t_r)]\,dt_r \quad (59)$$

Activation and deactivation functions for a particular set of operating conditions are difficult to measure accurately. Blanding (*1*) has measured activity vs. time curves and found that the activity is roughly proportional to the 0.5 power of time. Values of the mean reactor activity may be approximated by fitting an exponential function to the important range of time. However, if warranted, a solution to this problem can be obtained numerically by solving Equation (22). It should be mentioned that the problem can also be solved by a Monte-Carlo method (see reference *1*) in which the residence time that a particle spends in each unit as it cycles is determined by dice weighted according to the residence-time distributions therein.

In the following section the equations previously developed will be applied to more specific cases to illustrate their use.

ILLUSTRATIVE CALCULATIONS

When one considers only temporary deactivation, the steady state activity level within the reactor can be computed from Equations (58) and (59). These equations are easily solved for the limiting cases of complete mixing and piston flow in both the reactor and regenerator. For the first case let $N_R = N_G$ and $k_r = k_g$.

The residence time distribution function for complete mixing is

$$T_{RM}'(t_r) = \frac{n}{N_R} e^{-\frac{n}{N_R} t_r} \quad (60)$$

From Equation (58)

$$\overline{A}_{iM} = \frac{1+\epsilon}{2+\epsilon} \quad (61)$$

where

$$\epsilon = \frac{k}{\lambda};\ k = k_r = k_g;\ \text{and}\ \lambda = \frac{n}{N_R} = \frac{n}{N_G}$$

$$\overline{A}_{RM} = \frac{1}{\epsilon + 2} \quad (62)$$

For the case of piston flow through the reactor and regenerator all particles spend the same time, N/n, in each unit.

$$\overline{A}_{iP} = \frac{1 - e^{-\epsilon}}{1 - e^{-2\epsilon}} \quad (63)$$

$$\overline{A}_{RP} = \frac{(1 - e^{-\epsilon})^2}{(1 - e^{-2\epsilon})} \quad (64)$$

Figure 6 shows the activity in the reactor as a function of ϵ. Note that the highest activity of 0.50 is a result of letting $k_r = k_g$.

For the case of $k_g = 5k_r$ and $N_R = N_G$, the corresponding expressions for the activity in the reactor for complete mixing and piston flow are, respectively:

$$\overline{A}_{RM} = \frac{5}{(5\epsilon + 6)} \quad (65)$$

and

$$\overline{A}_{RP} = \frac{(1 - e^{-\epsilon})(1 - e^{-5\epsilon})}{\epsilon(1 - e^{-6\epsilon})} \quad (66)$$

where now $\epsilon = (k_r)/(\lambda)$.
The highest activity is now 5/6 which results from making $k_g = 5k_r$. Note that the highest activity levels approached in Figures 6 and 7 are discontinuous at zero; obviously when k_r is equal to zero, the activity must be 1.0. Values of the mean activity in the reactor are plotted in Figure 7 as a function of ϵ. Figures 6 and 7 show the advantages of piston flow over complete mixing.

If both permanent and temporary deactivation are considered, then $\mathcal{F}'(t)$ and $\mathcal{H}'(t)$ must be calculated in order to evaluate the mean activities $\overline{K}$'s in Equations (55) and (57). For the case of complete mixing for equal size reactor and regenerator

$$T_R'(t) = T_G'(t) = \lambda e^{-\lambda t}$$

and

$$T_R(t) = 1 - e^{-\lambda t} \quad (67)$$

Therefore from Equations (28) and (29) the Laplace transformations of the functions $'(t)$ and $'(t)$ are

$$h'(s) = \frac{\beta\lambda(s+\lambda)}{(s+\lambda)^2 - \lambda^2(1-\beta)}$$

$$f'(s) = \frac{\beta\lambda^2}{(s+\lambda)^2 - \lambda^2(1-\beta)} \quad (68)$$

Inverting the transformations by the method of partial fractions one gets

$$\mathcal{H}'(t) = \beta\lambda e^{-\lambda t}\cosh\lambda(\sqrt{1-\beta})t \quad (69)$$

$$\mathcal{F}'(t) = \frac{\beta}{\sqrt{1-\beta}}\lambda e^{-\lambda t}\sinh\lambda(\sqrt{1-\beta})t \quad (70)$$

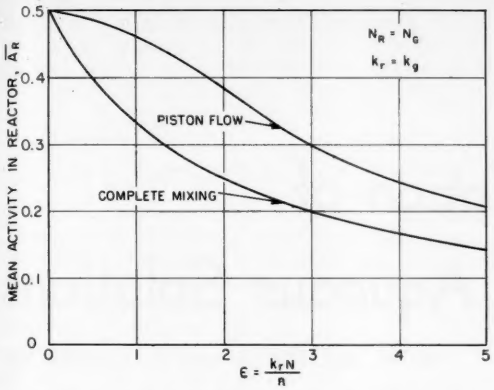

Fig. 6. Mean activity within reactor for the case of temporary deactivation.

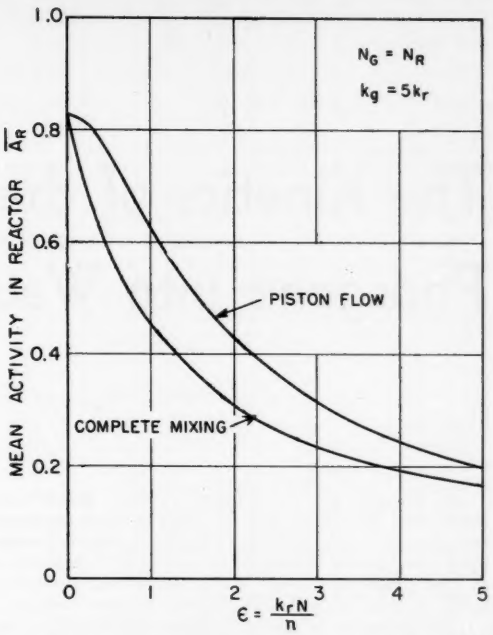

Fig. 7. Mean activity within reactor for the case of temporary deactivation.

Equations (69) and (70) may now be substituted into Equations (26) through (39) along with the appropriate function $K(t)$ to evaluate mean activities of various streams in the reactor-regenerator system.

CONCLUSIONS

This paper has dealt with a very complex subject, many details of which are not yet known. A method has been developed for calculating the mean activity levels of catalyst particles at various points within a reactor-regenerator system from arbitrarily assumed residence-time and deactivation and activation functions. The analysis developed in this paper is quite general, and although it is subject to certain idealizations regarding the temporary activation and deactivation functions, it should tentatively serve as a means of interpreting the values of mean activities and their variation with operating variables in terms of laboratory data on catalyst behavior and residence-time characteristics of reactors and regenerators.

ACKNOWLEDGMENT

The author wishes to acknowledge the helpful discussions with Professors Andreas Acrivos and Bernard Friedman during the course of this work.

NOTATION

$\overline{A}$ = mean activity
$F(\theta)$ = age-distribution function in reactor feed
$\mathcal{F}(t)$ = fraction of particles leaving regenerator having entered the system at time t or less
$\mathcal{F}'(t)$ = time derivative of $\mathcal{F}(t)$
$G(\alpha)$ = temporary activation function
$H(\alpha)$ = age-distribution function in regenerator feed
$\mathcal{H}(t)$ = fraction of particles leaving reactor having entered the system at time t or less
$\mathcal{H}'(t)$ = time derivative of $\mathcal{H}'(t)$
k = constant defined by Equations (46) and (47)
$K(t)$ = permanent deactivation function
$\overline{K}$ = mean permanent deactivation
m = number of completely mixed stages in series
n = feed rate to reactor
$P(\xi)$ = age distribution in regenerator feed
N = number of particles within reactor or regenerator
q = number of tagged particles having left reactor
$Q(\eta)$ = age distribution in reactor feed
Q = number of tagged particles introduced into reactor
$R(\theta)$ = temporary deactivation function
t = time
$T'(t)$ = residence-time distribution function
$T(t)$ = defined by Equation (3)

Greek Letters

α = catalyst age in regenerator
β = fraction of reactor feed stream which is fresh catalyst
ϵ = k/λ
λ = n/N
η = $\alpha + t_g$
θ = catalyst age in reactor
ξ = $\theta + t_r$
τ = dimensionless time

Subscripts

G and g = regenerator
i = stream entering reactor
o = stream leaving reactor
M = complete mixing
P = piston flow
R and r = reactor

Other Notation

Small letters $f(s)$, $f'(s)$, $h(s)$, $h'(s)$, $t(s)$, and $t'(s)$ represent the Laplace transforms of the corresponding capitalized functions.

LITERATURE CITED

1. Blanding, F. H., *Ind. Eng. Chem.*, **45**, 1161 (1953).
2. Brown, G. W., in "Modern Mathematics for the Engineer," E. E. Beckenbach, ed., p. 279, McGraw-Hill, New York (1956).
3. Churchill, R. V., "Modern Operational Mathematics in Engineering," p. 36, McGraw-Hill, New York (1944).
4. Danckwerts, P. V., *Chem. Eng. Sci.*, **2**, 1 (1953).
5. Danckwerts, P. V., J. M. Jenkins, and G. Place, *ibid.*, **3**, 26 (1954).
6. Kopal, Zdenek, "Numerical Analysis," Wiley, New York (1955).
7. Pigford, R. L., private communication (1955).
8. Singer, E., D. B. Todd, and V. P. Guinn, *Ind. Eng. Chem.*, **49**, 11 (1957).
9. Small, N. J. H., H. S. Kirkaldy, and A. Newton, *Proc. Fourth World Petroleum Congress*, Section III/E, Rome, Italy (1955).

Manuscript received January 30, 1959; revision received January 8, 1960; paper accepted January 11, 1960.

The Kinetics of the Absorption of Phosgene into Water and Aqueous Solutions

W. H. MANOGUE and R. L. PIGFORD

University of Delaware, Newark, Delaware

Pure phosgene gas was dissolved in short laminar jets of aqueous solution, and the results were interpreted with an unsteady state absorption-plus-reaction theory. Absorption rates of sulfur dioxide and carbon dioxide into water in the same equipment support this interpretation. The solubility of phosgene in water at 25°C. has been estimated from the absorption rates as 0.069 g.mole/(liter) (atm.). The estimated heat of solution is 6,800 cal./g.mole. At 16° and 25°C. the effect of a chemical reaction between phosgene and water on the absorption rate in a jet appears to be almost negligible, but at 45°C. a first-order reaction rate constant of 75 sec.$^{-1}$ can be derived from the absorption rates.

From absorption measurements with short jets and sodium hydroxide solutions so strong that a pseudo-first-order reaction accompanied absorption, the reaction rate constant for the bimolecular reaction between dissolved phosgene and the hydroxyl ion was estimated. A value of 1.6 x 10^4 liters/(g. mole) (sec.) was obtained at 25°C. in 1-*N* sodium hydroxide; at 35°C. in the same solution the estimated value was 2.9 x 10^4. There appears to be a slight increase in the reaction-rate constant with the ionic strength of the solution.

In chemical operations involving gaseous phosgene it is frequently desirable to remove phosgene from air, owing to its high toxicity. Scrubbing the air-phosgene mixture with a liquid absorbent is a useful technique but one for which it is difficult to design absorption equipment owing to the lack of necessary physicochemical data. It is well known that phosgene hydrolyzes in water to form carbon dioxide and hydrogen chloride in solution, but the rate constant for the reaction and concentration of dissolved phosgene at the reaction site are not known. Solubilities of unreacted phosgene in reactive solvents are of course impossible to measure by conventional methods because equilibrium cannot be established experimentally between finite quantities of gas and liquid phases. For similar reasons homogenous reaction rates cannot be observed in conventional ways. Such data are required however if the theory of diffusion and chemical reaction that has been developed in recent years (*2, 3, 22*) is to be employed for computing the effect of the irreversible reaction on the resistance to mass transfer through the liquid.

Because of the complex flow phenomena that doubtless exist in conventional gas absorption process equipment and because fluid motion has to be represented accurately in mass transport equations if valid physical constants are to be obtained from the solutions of the equations, measurements of absorption rates in large equipment are much more difficult to interpret than measurements in specially designed laboratory absorbers. If the fractional increase in the absorption rate per unit of surface can be determined in idealized apparatus, the corresponding increase in the rate per unit volume of the conventional absorber should be predictable with at least fair accuracy because the results of the laboratory experiments permit the well-established principles of physical chemistry to be employed quantitatively on the larger scale.

The most popular types of idealized absorbers employed for laboratory studies of this kind have been the short wetted-wall column (*16*), the rotating drum absorber (*4*), and the laminar liquid jet apparatus (*1, 5, 4, 14, 15, 24*). Although the first of these has been used successfully (*27*), it has been recognized recently that the end effects associated with the establishment of the parabolic velocity distribution in the liquid layer and with its disengagement from the gas introduce uncertainties. The jet apparatus seems to be more nearly free from these objections. In the thin, laminar jet the fluid velocities are everywhere nearly parallel to the axis, so that the flow pattern is very nearly rodlike. The small corrections that are required to account for the boundary-layer flow near the surface and near the nozzle and for the gradual acceleration due to gravity can be computed with accuracy, as shown by Scriven (*19*). Although the shape of the liquid surface in such apparatus is wholly different from that employed in large equipment, the possibility of giving quantitative interpretation to absorption-rate data make it ideal for laboratory investigations of mechanisms.

THEORY OF DIFFUSION COMBINED WITH FIRST-ORDER, IRREVERSIBLE REACTION

When phosgene is absorbed into a chemically reactive solvent the diffusion equation is

$$\mathcal{D}\frac{\partial^2 A}{\partial x^2} = \frac{\partial A}{\partial t} + k_1 A \qquad (1)$$

in which the last term on the right represents the effect of a first-order reaction. If the solvent is water, the reaction that destroys phosgene is the hydrolysis reaction

$$COCl_2 + H_2O \rightarrow CO_2 + 2H^+ + 2Cl^-$$

the rate of which is probably proportional to the phosgene conentration,

W. H. Manogue is with E. I. du Pont de Nemours and Company, Inc., Eastern Laboratory, Gibbstown, New Jersey.

water being in very large excess. If the solvent is an aqueous solution of an alkali like sodium hydroxide, the reaction very likely involves the direct attack of a hydroxyl ion on the dissolved phosgene molecule

$$COCl_2 + 3OH^- \rightarrow HCO_3^- + 2Cl^- + H_2O$$

and is pseudo first-order only if there is a large excess of hydroxyl ion which is essentially not depleted by reaction with phosgene in the important reaction region near the interface. (Otherwise, a second diffusion equation representing the concentration of OH^- has to be included.) The boundary conditions are

$$A(0, t) = A_i;\ A(\infty, t) = A(x, 0) = 0 \qquad (2)$$

which assume phase equilibrium at the interface and an effectively infinite depth of liquid in the direction perpendicular to the interface.

The solution of this boundary value problem has been obtained (2, 22) as

$$N_A = A_i \sqrt{k_l \mathcal{D}} \left[\frac{\exp(-k_l t)}{\sqrt{\pi k_l t}} + \text{erf}\ (\sqrt{k_l t}) \right] \qquad (3)$$

The approximate form of this result when $k_l t$ is small is of special interest in the present work. It is

$$N_A \sim A_i \sqrt{\frac{\mathcal{D}}{\pi t}} (1 + k_l t + \ldots) \qquad (4)$$

Furthermore when $k_l t$ is very large

$$N_A \sim A_i \sqrt{k_l \mathcal{D}} \qquad (5)$$

Owing to slight variations in the fluid velocity near the surface of the jet, t is not precisely the same for the fluid particles that flow near the surface and near the jet's axis. The differences are slight for jets moving at high speed however, as shown by Scriven's calculations (19, 20) for absorption without reaction. As a result,

$$t = h/U_o = \pi \overline{D}^2 h/4Q \qquad (6)$$

with good accuracy for long, slender jets.

The total rate in moles of gas per unit of time, ϕ, is obtained by summing N_A over the surface of the jet:

$$\phi = \pi \int_o^h D(h) N_A(h)\, dh$$

$$\sim \pi \overline{D} \int_o^h N_A(h) dh \qquad (7)$$

When $k_l t = 0$, that is for purely physical absorption

$$\phi = 4 A_i \sqrt{\mathcal{D} Qh} + \epsilon(h) \qquad (8)$$

where $\epsilon(h)$ is a small correction factor calculated by Scriven and Pigford (21). Similarly when $k_l t$ is small but not zero

$$\phi = 4 A_i \sqrt{\mathcal{D} Qh} \left(1 + \frac{\pi \overline{D}^2 k_l h}{12 Q} + \ldots\right) \qquad (9)$$

and when $k_l t >> 0$

$$\phi \sim \pi A_i \overline{D} \sqrt{\mathcal{D} k_l} \cdot h \qquad (10)$$

The correction term in Equation (9), accounting for deviations from rodlike flow, has not been evaluated when $k_l t \neq 0$, but it is probably smaller than the already small correction in Equation (8). The local absorption rate tends toward a constant value when $k_l t$ increases, and variations in t from one streamline to another should have decreasingly small influences on N_A.

When $k_l t$ exceeds 20, the average rate of absorption $\overline{N}_A = \phi/(\pi \overline{D} h)$ becomes independent of the jet length with an error not exceeding 2.5%. For an ideal jet having the same surface area and length as the actul jet but having a rodlike uniform velocity and a cylindrical shape it is

$$\overline{N}_A = A_i \sqrt{\mathcal{D} k_l} \qquad (11)$$

By operating experimental gas-absorption apparatus under conditions such that Equation (11) is applicable, estimates of both reaction-rate constant and equilibrium solubility can be derived from observed rates per unit surface $\overline{N}_A$, and the results can be expected to be independent of the fluid mechanical situation in the jet.

EQUIPMENT

The apparatus consisted of an absorption chamber, a jet nozzle and receiver, liquid and gas feed systems, constant-temperature baths, supporting structure and fume hood. The equipment is shown schematically in Figure 1.

The jet was produced by a piece of 6-mm. glass tubing drawn to a capillary tip (I. D. = 0.63 mm.). The capillary was slightly elliptical, the maximum range in measured diameter being about 4%. The nozzle holder was a cylindrical piece of iron which had two small packing glands for the nozzle and a thermometer. A rubber gasket permitted easy adjustment of the jet position relative to the receiver. The jet collector was a short, pointed piece of capillary tubing with an 0.78-mm. bore, a size chosen to reduce the possibility of entraining gas bubbles. Jet lengths were taken as the distance between the end of the nozzle and the top of the collector since the liquid level was maintained without fluctuation at the top of the collector during a run in order to avoid entrainment. The jet lengths were measured with a cathetometer.

The absorption chamber was a piece of 64-mm. glass tubing 180 mm. long and closed at the bottom. It was located in a constant-temperature bath. Gas entered near the bottom of the chamber through a short section of glass tubing sealed tangentially into the side. The bottom of the chamber sloped to a trapped drain line to remove any liquid spilled during start-up of the jet.

Absorbent liquid passed from the storage bottles through a constant-temperature bath into a constant-head tank. It then flowed through a rotameter and into the absorption chamber. Effluent liquid from the chamber went through the bottom of the water jacket into an overflow device that permitted adjustment of the liquid level in the capillary receiver. From there it went either to a sample bottle or to the drain.

All solutions were made with deionized water and were stored in 5-gal. Pyrex bottles, which normally held enough solution for several runs. Reagent-grade sodium hydroxide and sodium nitrate were used to prepare the salt solutions. The sodium hydroxide solutions were prepared by diluting 50% caustic, which had been decanted from the insoluble carbonate. They were stored in Pyrex bottles provided with a vent line containing Ascarite.

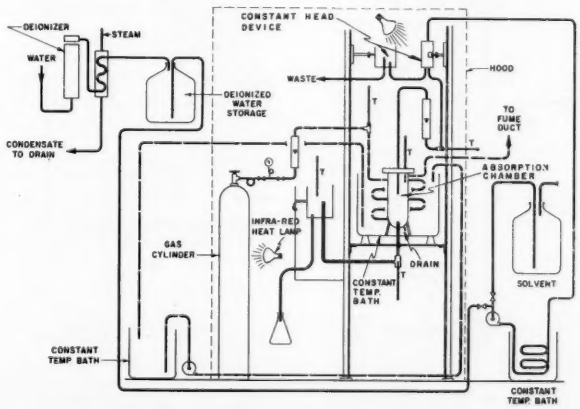

Fig. 1. Schematic drawing of apparatus.

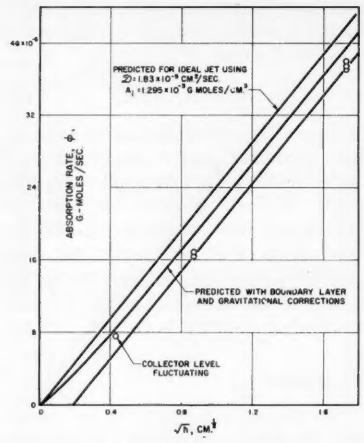
PREDICTED FOR IDEAL JET USING
$\mathcal{D}$ = 1.83 x 10^{-5} CM^2/SEC
A_i = 1.295 x 10^{-3} G MOLES/CM^3
ABSORPTION RATE, ϕ, G-MOLES/SEC
PREDICTED WITH BOUNDARY LAYER AND GRAVITATIONAL CORRECTIONS
COLLECTOR LEVEL FLUCTUATING
$\sqrt{h}$, CM$^{\frac{1}{2}}$

Fig. 2. Sulfur dioxide absorption into water at 25°C., corrected to 1.182 cc./sec. and 736 mm. Hg.

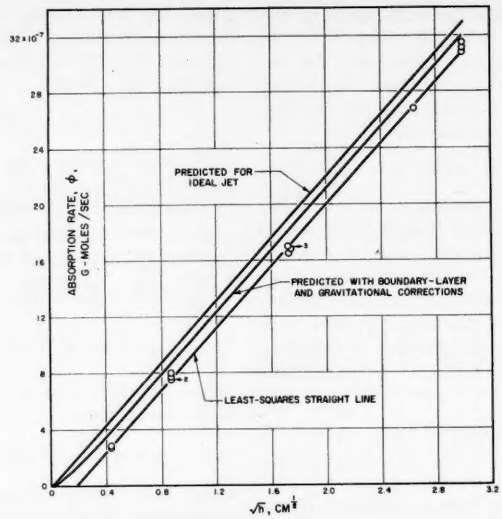

Fig. 4. Rates of phosgene absorption into water at 25°C. with 0.0628 cm. I.D. nozzle (data corrected to 1.182 cc./sec. and 736 mm. Hg).

The densities and viscosities of all solvents were obtained from the International Critical Tables.

The alkaline solutions fed to the absorber were titrated with standard hydrochloric acid to consecutive end points of 8.4 and 4.0 pH to determine both the hydroxyl ion and the amount of carbonate present. The sodium carbonate was generally less than 1% of the total alkalinity.

Special techniques were required for collecting exit liquid samples during the absorption of sulfur dioxide and carbon dioxide to minimize desorption of dissolved gas. The vapor space in the overflow chamber was made as small as possible, and the absorber effluent was fed into the bottom of a bottle containing sodium hydroxide solution. The sample bottles were purged with nitrogen prior to filling them with base. For sulfur dioxide an excess of hydrogen peroxide was added to the base. Carbon dioxide was determined by titration of the excess sodium hydroxide with standard hydrochloric acid in the presence of excess barium chloride to an end point at pH = 8.8. Sulfur dioxide was determined by titration with hydrochloric acid in the presence of an excess of hydrogen peroxide.

The absorber solutions were analyzed for chloride ion by titrating with 0.03-N silver nitrate solution. The end point was indicated by a potentiometric method which used a billet type of silver electrode with a sleeve type of mercury-mercuric sulfate reference electrode containing saturated potassium sulfate bridge solution. One ml. of concentrated nitric acid was added per 100 ml. of sample before titrating. Solutions containing sodium hydroxide were first neutralized with acetic acid. The method of analysis was checked by analyzing standard sodium chloride solutions.

Thermometers reading to 0.1°C. indicated the inlet and effluent liquid temperatures. For physical absorption the exit liquid temperature normally was maintained within 0.1°C. of the desired value. In runs where the bulk temperature of the liquid increased as a result of a chemical reaction, the average of the inlet and exit liquid bulk temperatures normally was maintained within 0.2°C. of the desired value.

Gas was taken from the top of the cylinders, fed through a rotameter into a copper coil in the constant-temperature bath surrounding the absorption chamber,

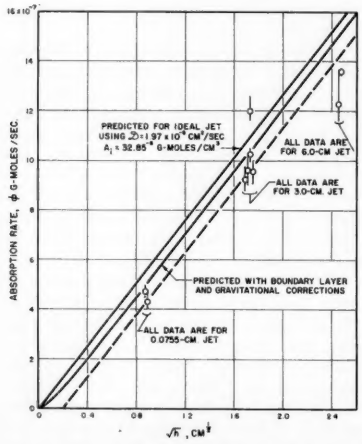
PREDICTED FOR IDEAL JET USING $\mathcal{D}$ = 1.97 x 10^{-5} CM^2/SEC
A_i = 32.85 G-MOLES/CM^3
ALL DATA ARE FOR 6.0-CM JET
ALL DATA ARE FOR 3.0-CM JET
PREDICTED WITH BOUNDARY LAYER AND GRAVITATIONAL CORRECTIONS
ALL DATA ARE FOR 0.0755-CM JET
ABSORPTION RATE, ϕ, G-MOLES/SEC
$\sqrt{h}$, CM$^{\frac{1}{2}}$

Fig. 3. Carbon dioxide absorption into water at 25°C., corrected to 1.182 cc./sec. and 736 mm. Hg.

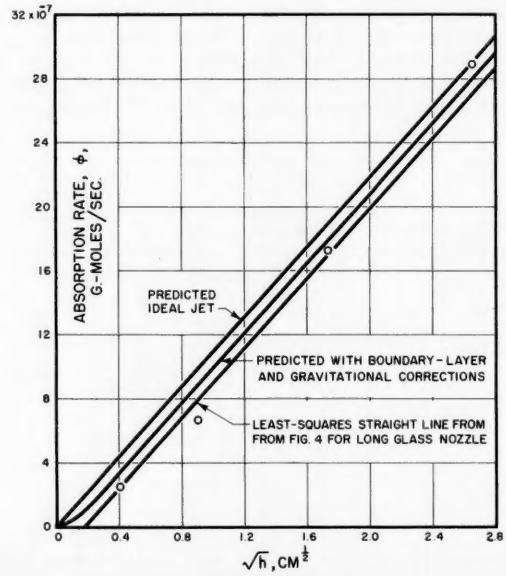
ABSORPTION RATE, ϕ, G-MOLES/SEC.
PREDICTED IDEAL JET
PREDICTED WITH BOUNDARY-LAYER AND GRAVITATIONAL CORRECTIONS
LEAST-SQUARES STRAIGHT LINE FROM FROM FIG. 4 FOR LONG GLASS NOZZLE
$\sqrt{h}$, CM$^{\frac{1}{2}}$

Fig. 5. Rates of phosgene absorption into water at 25°C., with 0.0609 cm. I.D. short glass nozzle (data corrected to 1.182 cc./sec. and 736 mm. Hg).

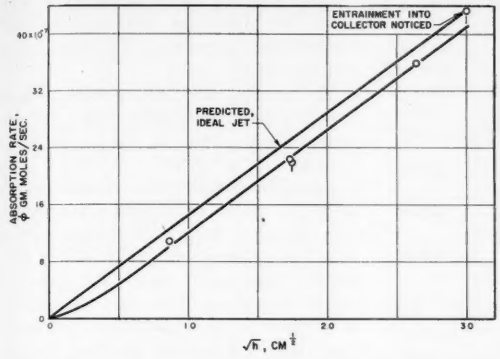

Fig. 6. Rates of phosgene absorption into water at 15°C., (corrected to 1.182 cc./sec. and 747 mm. Hg).

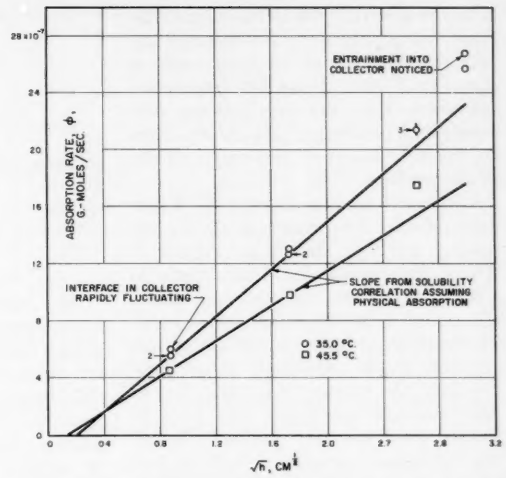
ENTRAINMENT INTO COLLECTOR NOTICED
INTERFACE IN COLLECTOR RAPIDLY FLUCTUATING
SLOPE FROM SOLUBILITY CORRELATION ASSUMING PHYSICAL ABSORPTION
O 35.0 °C.
□ 45.5 °C.
ABSORPTION RATE, ϕ, G.-MOLES/SEC.
$\sqrt{h}$, CM$^{\frac{1}{2}}$

Fig. 7. Rates of phosgene absorption into water at 35° and 45.5°C. (data corrected to 1.182 cc./sec. and 760 mm. total pressure).

and then into the chamber. The stream flowed out a side arm at the top of the chamber and was vented into the exhaust duct of the hood.

Phosgene was purchased in a 150-lb. cylinder as better than 99.5% pure. After approximately 20% of the cylinder contents were bled off, the residue gas gave constant absorption rates on check runs. An infrared analysis of this material showed no detectable hydrochloric acid, carbon monoxide, or carbon dioxide.

RESULTS

Absorption in water

Absorption rates of sulfur dioxide into water at 25°C. for several jet lengths are shown in Figure 2. Previous workers (*9, 15*) have shown that this absorption may be treated as purely physical. The data were corrected slightly by means of Equation (8) to a constant partial pressure of sulfur dioxide of 736 mm. Hg and to a constant liquid rate of 71 cc./min. Although pure gas was fed to the apparatus, it was assumed that the gas phase at the interface was saturated with water. This assumption is supported by some preliminary work in this equipment and by the more extensive work of Scriven (*19*) with carbon dioxide, which showed that presaturating the gas with water had no detectable effect on the absorption rate.

The data in Figure 2 result from five runs in which sixteen samples were taken. They are correlated by a straight line falling below the curve predicted by Equation (8), in which the correction term ϵ (h) allowing for boundary layer and gravitational corrections has been evaluated by the methods given by Scriven and Pigford (*21*). These methods require that the thickness of the boundary layer in the jet emerging from the nozzle be known; it was estimated in this work from measurements of the profile of the liquid jet actually employed. Including the correction term in Equation (8) causes the theoretical line to be displaced parallel to the line for an ideal jet, that is one having constant velocity and constant diameter. In accordance with the data the displacement from the ideal jet line should be still greater than that expected from the fluid mechanical theory. This may be due to the fact that the tip of the glass nozzle used to form the jet was wetted by the liquid, forming a stagnant pool through which dissolving gas would diffuse slowly. Alternately the lower rate of absorption may have been due to the presence of a surface-active contaminant that was present on the whole surface of the liquid, contributing an extra, constant resistance to passages of molecules through the interface.

Other authors, notably Lynn, Straatemeier, and Kramers (*10*) and Wendel (*27*) using wetted-wall columns and Cullen and Davidson (*1*) using a jet apparatus, have found that portions of their interfaces were inactive for gas absorption, evidently because of the accumulation of film at the bottom of the surfaces. Lynn et al. have shown that the subtraction of a constant area from the total interfacial area helps greatly in the correlation of data from such experiments. Scriven and Pigford (*20*) on the other hand found that the entire surface of their water jets apparently was effective in the absorption of carbon dioxide. This was probably due to the greater velocity of their interfaces. The jet design employed in this work was similar to that of Scriven, and furthermore the subtraction of a constant amount of supposedly inactive surface causes the experimental data in this work to deviate from a straight line even when conformity to a straight line would be expected. It is concluded therefore that this sort of correction is not likely to be the proper one under the experimental conditions employed. In any case however the deviations from the theoretical lines are not large. Although the magnitude of the fluid mechanical corrections is subject to some uncertainty, it is the slope of the experimental line that is most significant for the computation of the gas

Table 1. Solubility of Phosgene in Water and Aqueous Solutions

Solvent	Temp., °C.	Solubility, A_i, g.-moles / (liter)(atm.)	$\mathcal{D}$, diffusion coefficient used to calculate solubility, sq. cm./sec.	k_l, pseudo-first-order reaction rate constant, sec.$^{-1}$
Water	15	0.109	9.6×10^{-6}	3°
Water	25	0.069	12.7	6°
Water	35	0.046	16.1	22
Water	45.5	0.027	20.4	75
0.522-Molal $NaNO_3$	25	0.060	12.4	—
1.092	25	0.052	11.9	—
2.0	25	0.046	10.9	—
SO_2 in water	25	1.295 (*17*)	18.3 (*16*)	—
CO_2 in water	25	0.03285 (*17*)	19.7 (*20*)	—

° Obtained by extrapolation from the two higher temperatures.

solubility from the results, and it is believed that the properties of unstable, dissolved phosgene to be reported are reliable. The slopes of lines such as those on Figure 2 can be determined accurately from the data and are very nearly independent of any minor errors in the calculation of the true velocity of the surface.

Corrected rates of absorption of carbon dioxide into water at 25°C. for several jets are shown in Figure 3. These data result from nine runs in which twenty-nine samples were taken. The range of the observed rates as well as the average for each run are shown on the graph. Although they show considerable scatter, the data for all but one run are below the ideal-jet curve; they are also generally below the predicted curve for a real jet and may be correlated by a line parallel to the line for an ideal jet, as were the sulfur dioxide data.

The measured rates for the 6-cm. jet are farther from the predicted values than are those for other jet lengths. These data were the first taken in this investigation, when the absorption chamber was a 5-gal. battery jar which may not have been completely purged of air. Some difficulty in purging this chamber had been experienced previously, so that the presence of air may have led to the low results. The scatter of the data may be caused largely by variations in the analysis of carbon dioxide. In runs at the shorter jet lengths the blank corrections for carbon dioxide in the feed water and in the sodium hydroxide used for titration were about 20% of the titres, and these blanks showed considerable scatter from run to run.

TABLE 2

Gas	Solvent	Temperature range, °C.	Average heat of solution, cal./g.-mole
Phosgene	Water	15-45.5	6,800
Carbon dioxide	Water	15-35	4,600
Nitrous oxide	Water	15-35	5,400

The results for sulfur dioxide and carbon dioxide indicate that the method chosen to correlate the data is valid for absorption without reaction. They also show that the equations resulting from Scriven's analysis of the jet flow pattern predict the order of magnitude of deviations, ϵ, of the absorption rate in a real jet from the rates predicted for a constant-velocity jet. (The solubilities and diffusivity used in calculating the predicted rates are listed in Table 1.)

Adjusted rates of phosgene absorption in water at 25°C. are shown in Figure 4. The data result from sixteen runs in which seventy-seven samples were taken. (A run is a series of several repetitive but independent samples leading to a mean.) The results from five samples in five runs were discarded because they varied from the mean of that run by more than four times the standard deviation for the run. The standard deviations ranged from 0.2 to 2.6% of the respective means.

The absorption rate increased linearly with the square root of the jet length. This is the same dependence on the jet length which is predicted for physical absorption by Equation (8), so that the rate-determining process is probably molecular diffusion of dissolved and unreacted phosgene into water.

To compare absorption rates for different nozzles phosgene was also absorbed into water at 25°C. in a jet formed by a short 0.0609-cm. I.D. nozzle. This nozzle was constructed by sealing a piece of capillary tubing on the end of a length of 6-mm. tubing and then cutting off the capillary tubing so that only about 1.5 mm. of length remained. The data are shown in Figure 5 and are more scattered than those taken with the long nozzle. In these runs a 0.09-cm. I.D. collector was used instead of the 0.08-cm. I.D. one used with the larger nozzle. This larger collector probably is responsible for most of the scatter. However there is no apparent difference in the results obtained with the two different nozzles. The least-squares straight line through the data of Figure 4 represents the data in Figure 5 equally well.

Absorption rates of phosgene into water at 15°, 35°, and 45.5°C. are represented in Figures 6 and 7. The data scatter somewhat more than in Figure 4. The solubility of phosgene in water was calculated from the slopes of the lines in Figure 4, 6, and 7 with Equation (8) used. The term $A_i\sqrt{\mathcal{D}}$ was determined from the data, and the diffusivity was calculated by the use of the correlation of Wilke (28). This correlation predicts the diffusivity of carbon dioxide in water within 5% of the value selected by Scriven (19) after a careful study of data from several sources; it predicts the diffusivity of sulfur dioxide within 15% of Peaceman's (16) measured value. The phos-

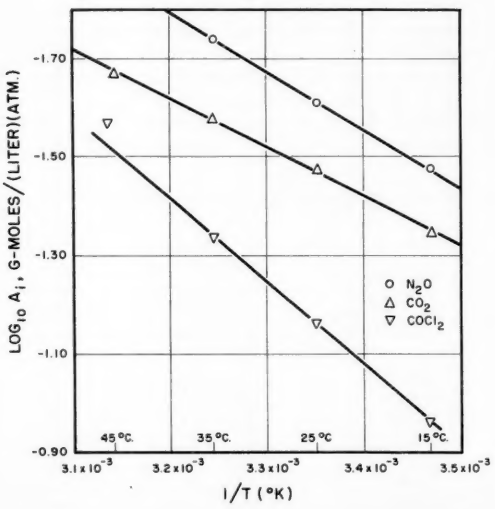

Fig. 8. Effect of temperature on the solubility of phosgene in water.

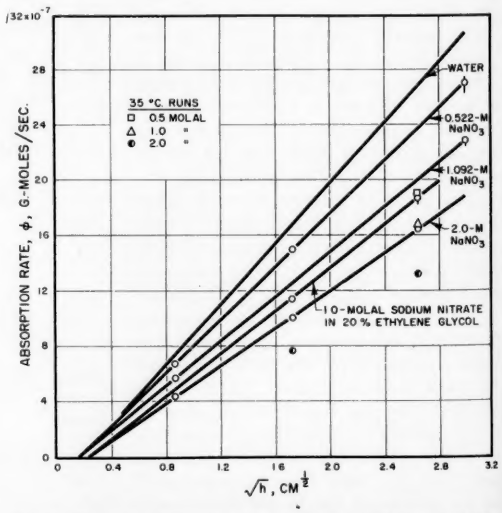

Fig. 9. Phosgene absorption into aqueous solutions of sodium nitrate at 25°C. (data corrected to 1.182 cc./sec. and 736 mm. Hg).

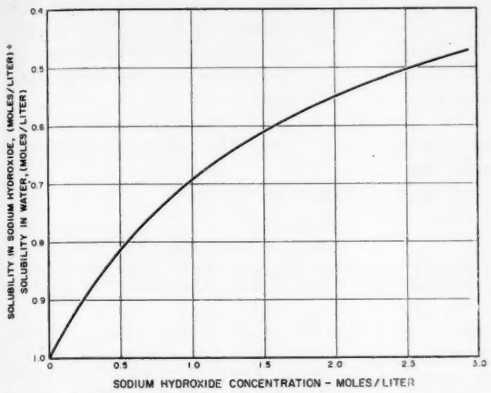
SOLUBILITY IN SODIUM HYDROXIDE, (MOLES/LITER) ÷ SOLUBILITY IN WATER, (MOLES/LITER)
SODIUM HYDROXIDE CONCENTRATION – MOLES/LITER

Fig. 10. Predicted solubility of phosgene in aqueous sodium hydroxide at 25°C. (corrected to 736 mm. Hg).

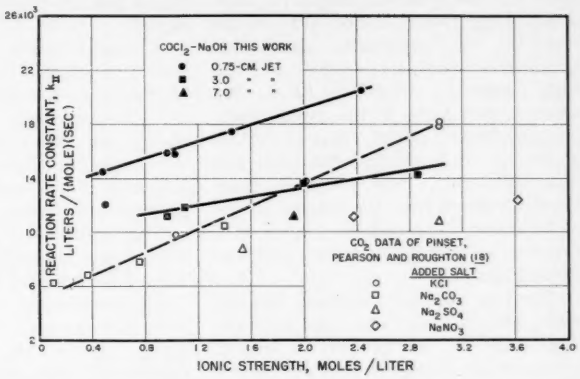

Fig. 11. Effect of ionic strength on reaction-rate constant for reaction with hydroxide ion (all measurements at 25°C.).

gene solubilities are listed in Table 1 with the estimated diffusion coefficients that were used to calculate them.

At 35° and 45.5°C. the rate of absorption into water is affected by the reaction of the dissolved phosgene, so that the second term in the parentheses of Equation (9) cannot be neglected. Its effect is greatest at the highest temperature and the largest value of jet length. On the other hand the slope of the line relating absorption rate and $h^{1/2}$ in the range where h is small is hardly affected by the reaction and gives an approximate value of $A_i\sqrt{\mathcal{D}}$. By successive trial of various values of $A_i\sqrt{\mathcal{D}}$ and k_l a pair of values can finally be computed for which the data for both short and long jets can be brought together. The values of solubility and rate constant listed in Table 1 at the two higher temperatures have been obtained by this procedure.

The logarithm of the saturation concentration of phosgene in water at equilibrium with pure phosgene gas at 1 atm. is plotted against the reciprocal of the absolute temperature in Figure 8. For comparison, data for carbon dioxide and nitrous oxide (*17*) are also shown in Figure 8. The calculated heats of solution are given in Table 2.

Figure 9 represents absorption rates of phosgene into aqueous solutions of sodium nitrate. Here again physical absorption theory correlates the data. Sodium nitrate was used for these measurements because it produced the same cation as sodium hydroxide, it was composed of monovalent ions, and its use did not interfere with the determination of absorbed phosgene by chloride ion titration.

The solubility data for the inert salt solutions are shown in Table 1. They are correlated and extrapolated with an equation similar to one proposed by Markham and Kobe (*12*):

$$\frac{S_m}{S_o} = am + \frac{1}{1 + bm} \qquad (12)$$

This equation appears to be the best one available for solution strengths above 1 molal. Neither the Setschenow (*13*) equation nor the equation proposed by van Krevelan and Hoftijzer (*25*) seems to be as accurate for concentrated solutions.

Absorption in Alkaline Solutions

In order to calculate mass transfer coefficients from rates of absorption into sodium hydroxide solutions the solubility of unhydrolyzed phosgene in these solutions is required. This may be estimated from the solubility of phosgene in aqueous sodium nitrate solutions by a method similar to that used by Markham and Kobe (*12*) which has been described in detail by Wendel (*26*). Briefly it used the fact that the salting out of gases by strong electrolytes in water has been found to depend additively on the effects of the ions present. The increased effectiveness of the hydroxyl radical over nitrate in salting out phosgene is obtained by comparing the solubilities of nitrous oxide in potassium nitrate and potassium hydroxide (*13*). Nitrous oxide is used as a reference gas because data for hydroxide solutions are available and the solubility of nitrous oxide in water is of the same magnitude as that of phosgene, so that salting out effects can be expected to be similar for the two gases. Figure 10 shows the estimated solubility of phosgene in sodium hydroxide.

A number of experiments were carried out at 25°C. in which phosgene was dissolved in sodium hydroxide solutions of varying strength up to about 3 moles/liter, with a 7.5-mm. jet used. The data are given in Table 3. It seemed probable that the change in the sodium hydroxide concentration in the reaction zone would be small enough in some of these experiments that the reaction would be pseudo-first-order; it also seemed that the rate con-

Table 3. Rates of Phosgene Absorption into Aqueous Sodium Hydroxide Solutions at 25°C.

Normality of NaOH solution	Phosgene absorption rate, g.-moles/sec. $\times 10^6$ (corr. to 760 mm. Hg total pressure)	Contact time, sec. $\times 10^2$ (with rodlike flow assumed)	k_{II} from Equation 11, liters/(g.-mole)(sec.)
	Jet length 0.75 cm., interfacial area 0.144 sq. cm.		
2.43	3.08	1.85	20,500
1.44	3.06	1.81	17,500
1.02	2.86	1.80	15,800
0.96	2.84	1.80	15,900
0.49	2.17	1.87	12,000
0.47	2.33	1.78	14,500
	Jet length 3.0 cm., interfacial area 0.575 sq. cm.		
2.86	9.74	7.78	14,200
1.99	10.4	7.57	13,600
1.09	9.94	7.40	11,800
0.96	9.48	7.20	11,200
	Jet length 7.0 cm., interfacial area 1.325 sq. cm.		
1.92	22.0	16.9	11,100

stant for this reaction might be sufficiently large that Equation (11) would represent the absorption rate. This speculation was encouraged by the high numerical values of B_o/A_i, the short contact times of the experiments, and the marked effectiveness of sodium hydroxide in increasing the phosgene absorption rate. Rate constants have been calculated from the data by means of Equation (11) and are shown as a function of sodium hydroxide normality in Figure 11.

The rate constants increase linearly with sodium hydroxide concentration. This may be interpreted in several ways: either phosgene was not hydrolyzed by a first-order reaction, or the trend in rate constants is caused by a defect in the solubility predictions or an effect of the ionic strength of the solution on the rate constant itself.

It is believed that the reaction in the short jet did not deplete the hydroxyl radical concentration appreciably and that the chemical rate is therefore pseudo-first-order. The solubility prediction is also believed satisfactory. It was assumed in the calculations that the diffusivity in Equation (11) varies inversely with the solution viscosity. Any error in this approximation is believed to be slight. A maximum error of about 2% in the estimated rate constants arises from neglecting the increase in interfacial area caused by wetting of the nozzle. This is well within the experimental error of the estimates.

The increase in the rate constants with the sodium hydroxide concentration probably results from the changing ionic strength of the solution. A similar variation in the second-order rate constant for the reaction between carbon dioxide and hydroxyl ion has been reported by Pinset, Pearson, and Roughton (*18*) and Nijsing (*15*). The data from (*18*) are reproduced in Figure 11. For ionic strengths greater than 0.3 moles/liter their data show that the rate constant increases about linearly with the ionic strength, although some ions are less effective than others. Replacing concentration with activity does not cause the results with the different salts to fall on the same line. The observed variation in the rate constant with the ionic strength is relatively slight and is about what would be expected for the reaction between a neutral molecule and an ion (*7*).

Rate constants from jets longer than 0.75 cm. are also shown in Figure 11 for comparison, although the reaction in these jets is slowed appreciably by the reduction of the hydroxyl radical concentration near the interface. Equation (11) does not apply accurately to these experiments and gives rate constants that are too small, as seen on the figure.

A value of 1.6×10^4 liters/(g.-mole)(sec.) is selected as the best estimate of the second-order rate constant in 1-*N* sodium hydroxide at 25°C. At 35°C. the only measurement which was made under pseudo-first-order conditions is in 1-*N* sodium hydroxide and gives a rate constant of 2.9×10^4.

The ratio $k_{II}(OH^-)/k_{II}(H_2O)$ at 25°C. for phosgene is 9.14×10^6. This is consistent with the values for other compounds hydrolyzing by the same mechanism (*23*), although it is lower than the value of the corresponding ratio of reaction rates for carbon dioxide, 18×10^6 (*18*).

ACKNOWLEDGMENT

This work was supported in part by the U.S. Army Chemical Corps.

NOTATION

a = constant in Equation (12), 0.01 for phosgene

A = concentration of dissolved but unreacted gas molecules; subscript i refers to the concentration at the gas-liquid interface

b = constant in Equation (12), 0.232 for phosgene

B_o = concentration of sodium hydroxide in the liquid fed to the absorber

$\mathcal{D}$ = diffusivity, sq. cm./sec.

D = jet diameter, cm.

$\overline{D}$ = average jet diameter, cm.

$\overline{D^2}$ = mean squared jet diameter, sq. cm.

h = jet length, cm.

k_I = pseudo-first-order reaction rate constant, $sec.^{-1}$.

k_{II} = second-order reaction rate constant, liters/(mole)(sec.)

m = molality of solution

N_A = instantaneous absorption rate of component A, g.-moles/(sq. cm.)(sec.)

$\overline{N_A}$ = average absorption rate of component A, g.-moles/(sq. cm.)(sec.)

Q = volumetric flow rate, cc./sec.

Sm = volume of gas at standard temperature and pressure dissolved by the quantity of solution of molality m containing 1 g. of water

So = volume of gas at standard temperature and pressure dissolved by 1 g. of water

t = elapsed time of exposure of an element of liquid surface to the gas

Uo = average velocity parallel to jet surface, defined by Equation (6)

x = distance into the liquid phase measured from the interface

ϵ = small correction factor which accounts for the effect of nozzle drag and gravitational acceleration on the absorption rate

ϕ = total absorption rate at 760 mm. Hg. pressure, moles/sec.

LITERATURE CITED

1. Cullen, E. J., and J. F. Davidson, *Trans. Faraday Soc.*, **53**, 113 (1957).
2. Danckwerts, P. V., *ibid.*, **46**, 300 (1950).
3. *Ibid.*, 701 (1950).
4. ———, and A. M. Kennedy, *Chem. Eng. Sci.*, **8**, 201 (1958).
5. Dirken, M. N. J., and H. W. Mook, *Biochem. Z.*, **219**, 452 (1930).
6. Edwards, G., R. Robertson, F. Rumford, and J. Thomson, *Trans. Inst. Chem. Engrs. (London)*, **32**, 56 (1954).
7. Frost, A. A., and R. G. Pearson, "Kinetics and Mechanisms," Wiley, New York (1953).
8. Harned, H. S., and B. R. Owen, "The Physical Chemistry of Electrolytic Solutions," 3 ed., Reinhold, New York (1958).
9. Lynn, Scott, J. R. Straatemeier, and H. Kramers, *Chem. Eng. Sci.*, **4**, 49 (1955).
10. *Ibid.*, 58 (1955).
11. Manogue, W. H., Ph.D. dissertation, Univ. Del., Newark (1957).
12. Markham, A. E., and K. A. Kobe, *J. Am. Chem. Soc.*, **63**, 449 (1941).
13. ————, *Chem. Rev.*, **28**, 519 (1941).
14. Matsuyama, T., *Mem. Fac. Eng. Kyoto Univ.*, **15**, 142 (1953).
15. Nijsing, R. A. T. O., R. N. Hendriksz, and K. Kramers, *Chem. Eng. Sci.*, **10**, 88 (1959).
16. Peaceman, D. W., Sc.D. thesis, Mass. Inst. Technol., Cambridge (1951).
17. Perry, J. H., "Chemical Engineers Handbook," 3 ed., McGraw-Hill, New York (1950).
18. Pinset, B. R. W., L. Pearson, and F. J. W. Roughton, *Trans. Faraday Soc.*, **52**, 1512 (1956).
19. Scriven, L. E., Ph.D. dissertation, Univ. of Del., Newark (1956).
20. ———, and R. L. Pigford, *A.I.Ch.E. Journal*, **4**, 382 (1958).
21. *Ibid.*, **5**, 397, (1959).
22. Sherwood, T. H., and R. L. Pigford, "Absorption and Extraction," McGraw-Hill, New York (1952).
23. Swain, C. G., and C. B. Scott, *J. Am. Chem. Soc.*, **75**, 141 (1953).
24. Uhara, I., *Bull. Chem. Soc. Japan*, **18**, 412 (1943).
25. Van Krevelen, D. W., and P. T. Hoftijzer, *Chemie et Industrie*, XXIe Congress. Intern. Chemie Ind., p. 166 (1948).
26. Wendel, M. M., M.S. thesis, Univ. Del., Newark (1954).
27. ———, and R. L. Pigford, *A.I.Ch.E. Journal*, **4**, 249 (1958).
28. Wilke, C. R., *Chem. Eng. Progr.*, **45**, 218 (1949).

Manuscript received November 3, 1958; revision received January 26, 1960; paper accepted January 29, 1960. Paper presented at A.I.Ch.E. Atlantic City meeting.

Detonation Characteristics of Hydrogen-Oxygen Mixtures at High Initial Pressures

ROY L. GEALER and STUART W. CHURCHILL

The University of Michigan, Ann Arbor, Michigan

Detonation velocities of hydrogen-oxygen mixtures were measured for initial pressures from 14.4 to 1,000 lb./sq. in. abs. and compositions from 40 to 80 mole % molecular hydrogen. Detonation and impact characteristics were computed for essentially the same range of conditions by the use of the elementary theory of detonation. Equilibrium compositions of hydrogen-oxygen mixtures at pressures from 10 to 2,000 atm. and temperatures from 3,000 to 5,000°K. were included in the computations and have been filed with the American Documentation Institute. The effect of nonideal thermodynamic properties on the computed detonation velocities was considered.

Since the velocity of propagation of a detonation wave depends upon the energy released in the combustion process, and since the net energy released is diminished by the energy consumed in dissociating the products of combustion, a decrease in the degree of dissociation of the products should result in an increase in detonation velocity. In the hydrogen-oxygen system an increase in the pressure of the system decreases the degree of dissociation of the products of combustion and thus can be expected to increase the velocity of the detonation wave.

Detonation velocities have been measured at nonambient conditions by only a few investigators. Dixon (*3*) determined detonation velocities in stoichiometric mixtures of hydrogen and oxygen at 10° and 100°C. over a pressure range from 200 to 1,500 mm. Hg. Moyle, Morrison, and Churchill (*18*) measured velocities and computed theoretical detonation characteristics over a temperature range from 160° to 480°K. and a pressure range from 0.5 to 2 atm. in various hydrogen-oxygen mixtures. Hoelzer and Stobaugh (*10*) measured velocities in hydrogen-oxygen and ethane-oxygen mixtures over a pressure range from 1 to 10 atm. for several compositions. The purpose of this investigation was to measure detonation velocities in hydrogen-oxygen mixtures over a considerably extended range of pressure.

Theoretical detonation characteristics were also computed for the experimental conditions by the use of the elementary theory of detonation. Since this work was completed, Luker, McGill, and Adler (*17*) have reported theoretical characteristics, for stoichiometric mixtures only, over the same range of pressures.

EXPERIMENTAL EQUIPMENT AND PROCEDURE

Figure 1 shows a sketch of the equipment. A 2-½-in., double-extra-heavy steel pipe was used as a mixing and pressurizing chamber. After evacuation a mixture of approximately the desired composition was proportioned into the vertical mixing pipe from the gas bottles by partial pressure. Fire resistant hydraulic fluid was pumped up through the bottom of the pipe to compress the mixture to the desired pressure. The pressurized gas was then forced out the tip of the mixing tube and into the bottom of the vertical detonation tube. Samples of each mixture were analyzed by absorbing the oxygen in a solution of alkaline pyrogallol and measuring the volumetric loss at constant pressure. Three analyses were made for each sample, and the arithmetic average was used. Samples were taken at several different times to establish the minimum time required for mixing.

The stainless steel detonation tube had a 4-in. O. D. and a ½-in. I. D. It was mounted vertically with a hot-wire ignitor near the bottom and ionization probes for velocity measurement spaced 18 in. apart, near the top. The first probe was located 53 in. from the ignitor, since the data of Dumanois and Lafitte (*4*) indicated that a fully developed wave velocity would be obtained in this distance. Velocity measurements at a series of probe locations confirmed that this distance was sufficient except in rich mixtures at low pressures as discussed later.

After the high pressure mixture of hydrogen and oxygen was charged into the detonation tube, which was closed at the top by a brass rupture diaphragm, the tube was closed off from the rest of the system and the mixture ignited. As a detonation wave passed through the tube; one ionization probe and thyratron circuit started a timer, and a second stopped it. The timer registers time intervals down to 0.1 μsec. with an accuracy of ± 0.1 μsec. The 100 kc. oscillator on the timer was standardized by beating the output against National Bureau Standards radio station WWV, the crystal being adjusted until zero beat was obtained.

The detonation tube and auxiliary equipment were located in a deep concrete-lined pit in a special test cell isolated from the laboratory area by a 1 ft.-

Roy L. Gealer is with the Ethyl Corporation, Detroit, Michigan.

thick, poured-concrete wall containing a bullet-proof glass window. All valves were operated remotely by means of flexible push-pull cable controls attached to levers on the valves, and the pressure gauges were viewed through the bullet-proof window by means of a mirror and telescope arrangement. Destruction of the charging system by an accidental explosion substantiated these precautions. Additional details concerning the equipment and work are given in reference 6.

PREDICTION OF DETONATION CHARACTERISTICS

The detonation characteristics of hydrogen-oxygen mixtures were computed for the experimental range of conditions by the use of the elementary theory of detonation. This theory postulates a planar discontinuity in pressure, temperature, and composition moving at sonic velocity relative to the burned gases (the Chapman-Jouguet condition); chemical and thermal equilibrium in the burned gases; no longitudinal energy, component, or momentum transfer except by flow; no transfer to the surroundings; and ideal gas behavior. Details and refinements of the elementary theory are presented and discussed in standard references such as Cook (*1*), Courant and Friedricks (*2*), Hirschfelder, Curtiss and Bird (*8*), and Lewis von Elbe (*15*), and therefore will not be presented here.

The chemical species which will be present must be specified to formulate the equilibrium conditions. Preliminary calculations indicated that ozone and hydrogen peroxide would be present only in negligible quantities. Therefore, only the six species molecular hydrogen, molecular oxygen, water, atomic hydrogen, atomic oxygen, and hydroxyl were assumed to be present.

When a detonation wave collides with a solid wall, a reflected wave travels back through the burned gases. This reflected wave produces a second pressure rise, and the resulting pressure is often called the *impact pressure*. The pressure behind the reflected wave was computed from the elementary theory of shock waves with the assumption of no further change in composition across the reflected wave. This assumption is discussed subsequently.

The detailed mathematical representation of the problem is presented in reference 6.

COMPUTATION PROCEDURE

In order to minimize interpolation of tabulated thermodynamic data the equations describing the elementary theory of detonation were arranged so that the following procedure could be used to compute the detonation characteristics:

1. Fix initial composition and final pressure.
2. Compute product composition and enthalpy for four assumed final temperatures.
3. Compute the final temperature corresponding to the initial composition, the final pressure, and each of the four product compositions and enthalpies.
4. Compute the error between the four calculated and assumed final temperatures.
5. Employ a Lagrangian four-point interpolation on these errors to determine that temperature for which the error is zero.
6. Employ the same interpolation factors to calculate the final molecular weight and heat-capacity ratio.
7. Calculate the detonation velocity and the initial pressure.

In order to insure that sufficient accuracy was obtained with a four-point interpolation, a single temperature was computed with a five-point interpolation. The difference in final temperature was 2°F. which is roughly a 0.05% error. The absence of scatter in the calculated points further verified the accuracy of the procedure.

An IBM-650 computer was used to compute equilibrium compositions for an initial temperature of 298°K.; initial mole fractions of hydrogen of 0.4, 0.5, 0.6, 0.6667, and 0.75; final (detonation) pressures of 10, 25, 50, 75, 100, 250, 500, 750, 1,000, 1,500, and 2,000 atm.; and product temperatures from 3,000° to 5,000°K. The details of the calculation procedure are given in reference 6. The equilibrium compositions for all of the computed conditions are given in reference 6 and have been placed on file*. Although the equilibrium compositions were obtained as an intermediary in the calculation of detonation velocities, they are of general applicability. The effect of pressure on the equilibrium composition for a stoichiometric mixture is illustrated in Figure 2 for 3,000° and 5,000°K.

THE EFFECT OF ERRORS IN PRESSURE SENSITIVE PHYSICAL PROPERTIES ON DETONATION WAVE VELOCITIES

Specific heats and enthalpies (*13*) and equilibrium constants (*9*, *12*) of the six components as a function temperature at low pressure were utilized in the computations. No data were found for the effect of pressure on these properties or on the compressibility factors and fugacity coefficients at the highest pressures for which the computations were made (final pressures of 2,000 atm.). High-pressure data which are available do not extend to the high temperatures which were attained. Even the generalized charts in terms of reduced pressures and temperatures do not extend to these conditions.

In order to determine what errors might be introduced in the computed velocities by the use of idealized properties, the equations describing the wave were reformulated in terms of compressibility factors and fugacity coefficients, and total derivatives of all of the dependent variables were formulated in terms of the partial derivative of the properties. Then the fractional and absolute errors in detonation velocity resulting from fractional and absolute errors in each of the properties were computed for a stoichiometric mixture at a final pressure of 2,000 atm. Estimates of the probable uncertainties in the properties were based primarily on the generalized reduced property charts (*11*, *19*, *20*). The initial compressibility factor was approximated as a mole average of the compressibility factors of molecular hydrogen and molecular oxygen under the initial conditions. The final reduced temperature and pressure of molecular hydrogen were beyond the range of the charts, and the critical properties of atomic hydrogen, atomic oxygen, and hydroxy are not known. Therefore the average compressibility factor of the burned mixture was assumed to be that of molecular oxygen and water, which was roughly 1.1 under the final conditions. Since the deviation of the other four components from ideality is probably less than that of molecular oxygen and water, a maximum error of −10% was attributed to the use of a compressibility factor of unity. The other property errors were similarly approximated.

The resulting negative errors in the computed velocity were found to total 9.3% and the positive errors to total 8.9%, yielding a net error of only −0.4%. In this case errors in some properties yield an appreciable error in detonation velocity, but the total positive and negative errors very nearly cancel. The detonation velocity is most sensitive to errors in the sensible enthalpies and fugacity coefficients and is quite insensitive to errors in the compressibility-factor and heat-capacity ratios. The estimated net error is very dependent on the arbitrary error attributed to the individual properties. For example the fractional errors in the fugacity coefficients of molecular hydrogen and hydroxyl were assumed to be −15%. Had they been assumed to be −10%, the net error in the theoretical

* Tabular material has been deposited as document 6378 with the American Documentation Institute, Photoduplication Service, Library of Congress, Washington 25, D. C., and may be obtained for $3.75 for photoprints or $2.00 for 35-mm. microfilm.

detonation velocity would have been −2.3% instead of −0.4%. For lower pressures and for product gases containing less water the error introduced by idealized properties would be expected to be less than the above estimate. The details of the error analysis are given in reference 6 and have been placed on file.*

RESULTS AND DISCUSSION

All experimental runs were initiated at room temperatures which varied between 70° and 80°F. The experimental and theoretical results of Moyle, Morrison, and Churchill (*18*) indicate that this small variation has a negligible effect on the detonation characteristics.

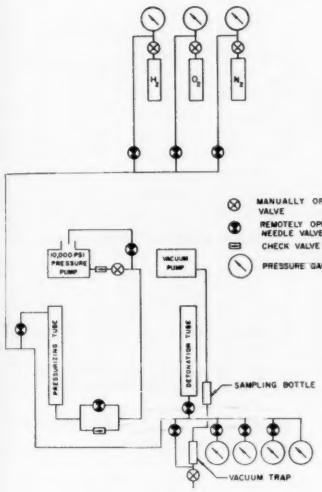

Fig. 1. Experimental apparatus.

Data were taken at initial pressures of 14.4, 25, 50, 100, 500, and 1,000 lb./sq. in. abs. Velocities at each of these pressures were measured for mixtures having nominal mole fractions of molecular hydrogen of 0.4, 0.5, 0.6, 0.667, 0.75, and 0.8. Because of the method of charging it was difficult to obtain mixtures having the exact compositions mentioned above. Only after the measurements were made and the mixtures analyzed were the initial compositions known.

In order to obtain plots at constant composition the experimental velocities were first plotted vs. mole fraction of hydrogen at the various initial pressures (Figure 3), and the experimental points were corrected for their deviation from the nominal hydrogen fraction by translation parallel to curves drawn through the raw data. Then the velocity could be plotted vs. initial pressure at discrete mole fractions of hydrogen. With this method, as opposed to cross plotting, the identity of the individual points is preserved. Since the deviations of the actual mole fractions from the nominal values were small and the slopes of the original curves were fairly constant, the uncertainty introduced by translation of the points was very slight. As the mole fraction of hydrogen approaches the limiting rich and lean values for which detonation will occur, the detonation velocity is known to fall off sharply from the almost linear dependence on composition indicated in Figure 3, and these curves should not be extrapolated.

The theoretical velocities correspond to those which would be measured in

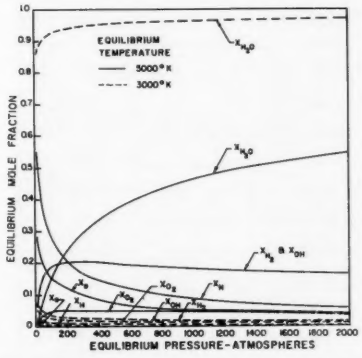

Fig. 2. Equilibrium compositions for a stoichiometric mixture of hydrogen and oxygen.

a tube of infinite diameter. Therefore in order to compare theoretical and experimental velocities it is necessary to correct the experimental measurements for the effect of a finite tube diameter. Fay (*5*) has recently presented a theoretical explanation for the observation of Kistiakowsky and Zinman (*14*) and Moyle, Morrison, and Churchill (*18*) that a plot of detonation velocity vs. the reciprocal of tube diameter results in a straight line. Furthermore Fay indicates that the velocity deficiency due to wall effects should be inversely proportional to the initial pressure.

The measured velocities in feet per second were therefore corrected by adding $30/DP$, where D is the diameter in inches, P is the pressures in atmospheres, and 30 is an empirical coefficient in ft./(sec.)(atm.)(in.) taken from the correlation of Moyle, Morrison, and Churchill for the effect of tube diameter in various hydrogen-oxygen mixtures at atmospheric pressure. This correction varied from 60 ft./sec. at atmospheric pressure to 0.9 ft./sec. at 1,000 lb./sq. in. abs. For the leanest mixture (40% molecular hydrogen) these values correspond to less than 1% and less than 0.013%, respectively, of the measured velocity and hence are negligible for practical purposes. The original and corrected data are on file.*

The theoretical and corrected experimental relationships between detonation velocity and initial pressure at various initial mixture compositions are presented in Figures 4 and 5. An inspection of these figures and of the plot of the original experimental data (Figure 3) indicates that the experimental scatter is less than 2% except for hydrogen-rich mixtures at low pressure. Experimental consistency was not attainable for 0.75 and 0.80 mole fraction hydrogen at 14.5 and 25 lb./

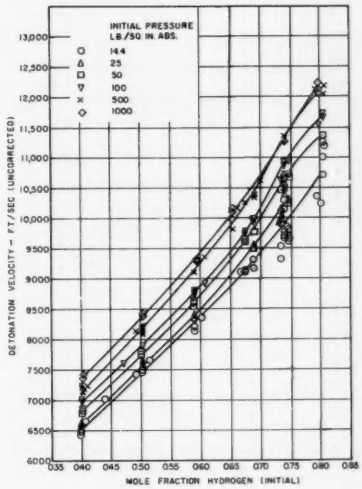

Fig. 3. Experimental detonation velocities.

sq. in. abs. initial pressure. The most probable explanation is that stable detonation did not consistently develop in the alloted distance between the ignitor wire and the first probe (58 in.) for these rich mixtures at low pressure. As the initial pressure was increased to 50 lb./sq. in. abs. and beyond, reproducible data were obtained even for the richest mixtures.

At low pressure the experimental velocities lie slightly below the theoretical curves. This discrepancy is probably due to oversimplifications in the elementary theoretical model, such as the assumption of a planar discontinuity and chemical equilibrium.

At 1,000 lb./sq. in. abs. the averages of the various groups of experimental points are about 2% above the theoretical curves. These deviations are probably due to the use of idealized properties for the computed curves. At high pressure imperfections in the ele-

* See footnote on page 501.

* See footnote in column 1.

mentary theory are probably masked by the greater effect of nonideality. Furthermore equilibrium is probably more closely approached at the high pressure because of the shorter mean free path for chemically productive collisions.

The computed ratios of detonation and impact pressures to the initial pressures are plotted vs. initial pressure in Figure 6. The ratio of pressures across the detonation wave in a stoichiometric mixture increases only from 17.7 to 21.6 as the initial pressure is increased from 8.29 to 1,362 lb./sq. in. abs. The ratio of pressures across the reflected wave is almost independent of initial composition and initial pressure and averages about 2.5. The ratio of impact to initial pressure in a stoichiometric mixture increases from 43 to 53 over the above range of initial pressure. The absolute values of the computed detonation and impact pressures for a stoichiometric mixture at an initial pressure of 1,367 lb./sq. in. abs. are thus 29, 390, and 72,260 lb./sq. in. abs. Even higher ratios and pressures are obtained if the initial temperature is lowered (*18*).

Luker, McGill, and Adler (*17*) computed detonation characteristics for the stoichiometric mixture only, over the same range of pressures, assuming the ideal gas law for the final mixture but correcting the initial density for nonideality. In addition their calculations allowed for a new equilibrium composition behind the reflected wave. Their computed wave velocities agree within 0.5% with those computed in this investigation. However their computed detonation and reflected pressure ratios are seen in Figure 6 to be 10% lower than those of this investigation at the highest initial pressures. The differences in the computed detonation pressures are apparently due to the correction of the initial density for nonideality. The differences in the computed impact pressures are due to the allowance for change in composition across the reflected wave as well as to the correction in the initial density. Taking into account nonideality at both the initial and final conditions may result in a smaller net correction than taking into account nonideality in the initial density only. Hence the relative reliability of the two estimates of developed pressure cannot be resolved until high pressure fugacities and densities are available and are incorporated in the computations. The discrepancies do establish however that the computed pressures are more sensitive than the computed wave velocity to errors in the physical properties and to oversimplifications in the theoretical model.

The excellent agreement between the measured and computed detonation velocities for a wide range of temperatures, pressures, and compositions indicates that the simplified theory of detonation used herein is adequate for the computation of velocity. Experimental data to test the computed detonation and impact pressures are very difficult to obtain, and reliable values are not yet available for even ambient conditions. Transient effects (*1*, *7*) and multiple reflections must also be considered if the failure of process equipment due to a detonation is to be predicted. Nevertheless the computed detonation and impact pressures are a first-order guide to the design of equipment in which a detonation could occur. Luker and Leibson (*16*) have indeed shown that the computed reflected pressure for conditions under which a rupture disk failed under detonation bears a constant ratio slightly greater than unity to the rated static bursting pressure, indicating that use of impact pressures for design is conservative.

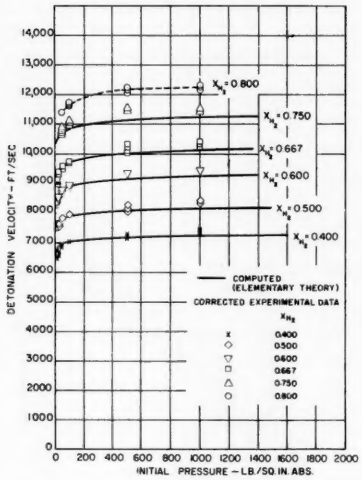

Fig. 4. Comparison of computed and corrected experimental detonation velocities, high-pressure range.

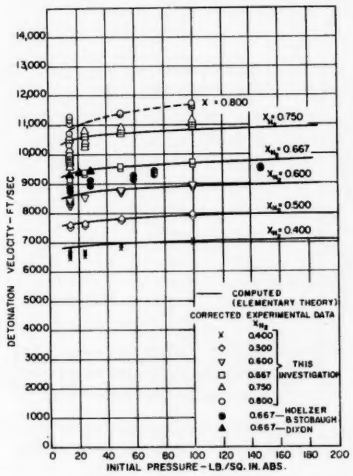

Fig. 5. Comparison of computed and corrected experimental detonation velocities, low-pressure range.

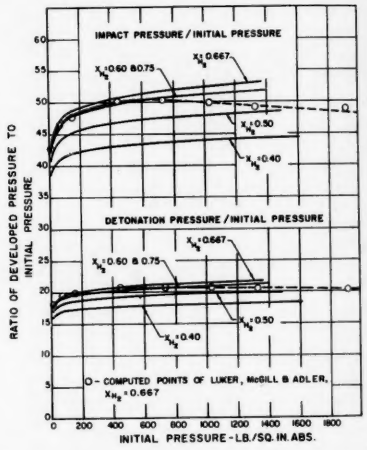
IMPACT PRESSURE / INITIAL PRESSURE
DETONATION PRESSURE / INITIAL PRESSURE
RATIO OF DEVELOPED PRESSURE TO INITIAL PRESSURE
O - COMPUTED POINTS OF LUKER, McGILL & ADLER.
INITIAL PRESSURE - LB./SQ. IN. ABS.

Fig. 6. Computed ratios of detonation and impact pressures to initial pressure.

DESTRUCTION OF EXPERIMENTAL EQUIPMENT

It was originally intended to extend the experiments to initial pressures of 10,000 lb./sq. in. abs. However as a mixture of 80% molecular hydrogen and 20% molecular oxygen was being compressed for a test at 4,000 lb./sq. in. abs., an unintended detonation occurred at 3,500 lb./sq. in. abs. The auxiliaries, which were all isolated from the detonation tube during controlled detonations and which were not designed for such a pressure, were destroyed. The detonation tube itself, which was designed for such pressures, was undamaged. The cause of this detonation is unknown. This accident suggests caution in future work with hydrogen-oxygen mixtures at high pressures.

CONCLUSIONS

This investigation indicates that velocities computed from the highly idealized theory of detonation are in reasonable agreement with experimental values throughout an extensive pressure range from 14.4 to 1,000 lb./sq. in. abs. for hydrogen-oxygen mixtures containing 40 to 80 mole % molecular hydrogen.

At the lower pressures the slight disagreement between experimental

and predicted velocities is probably due to oversimplifications in the theoretical model. Inconsistencies in the experimental data for the lowest pressures and richest mixtures are probably due to insufficient distance for wave development.

At higher pressures the slight disagreement can be rationalized in terms of the idealized properties necessarily used in the computations. The effects of errors in the different properties tend to cancel, leaving a small net error in the predicted velocity.

An important consideration for design purposes is the pressure realized when a detonation occurs. The computed ratios of the detonation and impact pressures to the initial pressure are about 20 and 50, respectively, for the conditions investigated.

ACKNOWLEDGMENT

This work was sponsored in part by Project SQUID which is supported by the Office of Naval Research, Department of the Navy, under contract Nonr 1858 (25) NR-098-038. The experimental work was carried out at the Aircraft Propulsion Laboratory of the University of Michigan. The support and advice of R. B. Morrison, T. C. Adamson, D. L. Katz, D. V. Ragone, and Alexander Weir, Jr., are appreciated.

LITERATURE CITED

1. Cook, M. A., "The Science of High Explosives," Reinhold, New York (1958).
2. Courant, R., and K. O. Friedrichs, "Supersonic Flow and Shock Waves," Interscience, New York (1948).
3. Dixon, H. B., *Phil. Trans. Roy. Soc.*, **A184**, 97 (1893); **A200**, 315 (1903).
4. Dumanois, P., and P. Laffitte, *Compt. rend*, **183**, 284 (1926).
5. Fay, J. A., *Physics of Fluids*, **2**, 283 (1959).
6. Gealer, Roy L., Ph.D. thesis, Univ. Mich., Ann Arbor (1958).
7. Gordon, W. E., A. J. Mooradian, and S. A. Harper, "Seventh Symposium (International) on Combustion," p. 752, Butterworth, London, England (1959).
8. Hirschfelder, J. F., C. F. Curtiss, and R. B. Bird, "Molecular Theory of Gases and Liquids," Wiley, New York (1954).
9. Hirschfelder, J. O., F. T. McClure, C. F. Curtiss, and D. W. Osborne, *Abs. Bib. Sci. and Ind. Reps.*, **2**, 743 (1946).
10. Hoelzer, C. A., and W. K. Stobaugh, Thesis, Air University Command, USAF Inst. Tech., Wright-Patterson Air Force Base, Ohio (1954).
11. Hougen, O. A., and K. M. Watson, "Chemical Process Principles," Part II, Wiley, New York (1949).
12. Huff, V. N., and C. S. Calvert, *Nat. Advisory Comm. Aeronaut. Tech. Note 1653* (1948).
13. Huff, V. N., S. Gordon, and V. E. Morrell, *ibid., Rept. 1037* (1951).
14. Kistiakowsky, G. B., and W. G. Zinman, "Second ONR Symposium on Detonation," p. 80, Washington, D.C., (Feb. 9-11, 1955).
15. Lewis, Bernard, and Guenther von Elbe, "Combustion, Flames, and Explosions of Gases," Academic, New York (1951).
16. Luker, J. A., and M. J. Liebson, *J. Chem. Eng. Data*, **4**, 133 (1959).
17. Luker, J. A., P. L. McGill, and L. B. Adler, *ibid.*, 136 (1959).
18. Moyle, M. P., R. B. Morrison, and S. W. Churchill, *A.I.Ch.E. Journal*, **6**, 92 (1960).
19. Nelson, L. C., and E. A. Obert, *Trans. Am. Soc. Mech. Engrs.*, **76**, 1057 (1954).
20. Perry, J. H., "Chemical Engineers' Handbook," McGraw-Hill, New York (1950).

Manuscript received August 3, 1959; revision received December 28, 1959; paper accepted January 4, 1960. Paper presented at A.I.Ch.E. San Francisco meeting.

A Scintillation Method for Determining Liquid - Liquid Interfacial Areas

GEORGE J. MITSIS, RICHARD R. PLEBUCH, and KENNETH F. GORDON

The University of Michigan, Ann Arbor, Michigan

In stirred beakers the interfacial area between xylene containing a scintillator and tritiated water was measured as a function of stirrer speed by a scintillation counting technique. Because of the 6 μ average range of the tritium betas the rate at which flashes are detected by a phototube is a function of the interfacial area. A calibration curve of count rate against known interfacial area for unstirred phases in containers of various diameters gave a numerical estimate of the interfacial area for ten configurations.

Data for mass transfer between dispersed phases in equipment such as extractors, distillation columns, and sprayers can be correlated on the basis of equations of the form

$$W = k'a(f_s - f_w) = ka(c_s - mc_w) \quad (1)$$

Because of the difficulty of obtaining interfacial areas it is usual not to attempt to separate k and a, obtaining values for each, but rather to correlate ka. Measurements of the interfacial area should contribute to a further understanding of mass transfer.

Interfacial areas have been measured

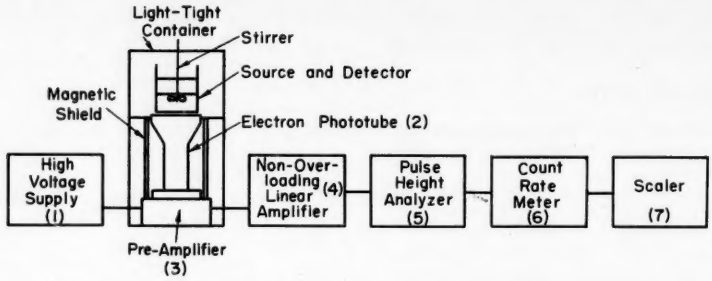

(1) Nuclear Instrument & Chemical Corp. Model 172
(2) Dumont 6363
(3) Modified A-1-A
(4) Baird Atomic's D-D-1 Model 215
(5) Radiation Control Lab, Model 2204
(6) Radiation Control Lab, Model 15
(7) Radiation Control Lab, Model 2006

Fig. 1. Detection and counting system.

previously by light-transmittance techniques (7, 8). The absorptivity of light in a highly agitated two-phase system was calibrated with the volumetric interfacial area by estimating the number and size of drops in photographs. Light transmittance has also been used to measure froth densities on a bubble-cap plate (3).

The possibility of using short range radioactive particles for measuring interfacial areas was first investigated at the Oak Ridge National Laboratory (6). Here a radioisotope emitting short-range particles was contacted with an immiscible phase capable of interacting with the particles. Because of the short range of the particles interaction was restricted to the region close to the interface. Thus the product of the interaction (such as new chemical species or radiation) will be approximately proportional to the interfacial area. Preliminary investigations with tetrachloroethylene and alpha particles from polonium-210 gave inconclusive results due to low yields of chlorine. Considerable improvement resulted at Oak Ridge when a fluorocarbon was substituted as the target phase and the neutrons produced from the nuclear interaction between the alpha particles and fluorine were detected (2). This general technique for measuring interfacial areas is limited by the necessity of high immiscibility between the phases as well as the availability of suitable isotope and target materials. The system used in the present study was tritiated water and xylene with scintillator. It satisfies both the requirement of immiscibility between the phases and of having a short particle range. In contrast to previous techniques it has a negligible health hazard. A good introduction to recent scintillation techniques may be found in a collection of papers edited by Bell and Hayes (1).

The scintillator consisted of 4 g./liter of 2, 5-diphenyloxazole with 0.05 g./liter of POPOP; 1, 4 bis-2-(5-phenyloxozolyl)-benzene, as wave length shifter, to bring the photon spectrum closer to the maximum photo tube response, and 0.01 g./liter of NPO; 2-(1-naphthyl)-5-phenyloxazole for a light restorer.

EQUIPMENT

Vessels and Stirrers

For the stirring studies and the calibration of count rate against interfacial area five beakers were used with nominal diameters of 1, 2, 3, 5, and 7 in. The beakers were 7 in. high except for the 7-in. diameter one which was 6 in. high. Shell vials 8 to 36 mm. in diameter were also used. The floors of the beakers were ground flat, and the walls were given a reflective coating of alpha-alumina while the vials were untreated. The 7-in. diameter beaker had four removable brass baffles each of beaker height and of width equal to one tenth of that of the beaker.

Detection and Counting Systems

Detection and counting of scintillations were accomplished by the single channel analyzer arrangement shown as a block diagram in Figure 1. A complete description of each component and its method of use as well as the precautions that were taken is given elsewhere (4). The phototube had a photo-sensitive surface of a 2.5-in. diameter circle. The calibration of the detection equipment indicated that a high voltage setting of 1,110 v. and a pulse height of 60 on the E Dial of the single-channel analyzer gave the maximum ratio of tritium count rate to background. The setting was used up to a count rate of 37,000 c.p.s. Above this the E dial setting was changed to a pulse height of 150 reducing the count rate by more than an order of magnitude preventing counting difficulties. The relationship between the two dial settings was established by direct calibration. While improvements could be made, such as reducing the noise by cooling the circuit and using a coincidence counter, the present method was quite adequate to demonstrate the technique.

EXPERIMENTAL

To test the equipment and settings the count rate as a function of the specific activity of the tritiated water was determined in a shell vial. When plotted on log-log paper the points fell within 10% of a straight line of unit slope from 118 counts/sec. at 0.01 mc./ml. and 11,800 counts/sec. at 1 mc./ml. The background plus noise count rate was 47 to 120 counts/sec. giving deviating points below 0.01 mc./ml. The specific activity used for the stirring results was 0.1 mc./ml. where the background and noise correction was relatively low.

Calibration of Interfacial Area

A calibration curve of the count rate in beakers as a function of interfacial area was obtained by contacting the tritium and scintillator in beakers of various cross sections. They had walls coated with alpha-alumina polishing powder as a diffuse reflector and flat ground bottoms which were optically coupled to the photocathode with silicone. The interface was a constant distance of 2 in. from the bottom in order to eliminate the effect of liquid level. Background measurements, with pure water substituted for tritiated water, were made before and after each run. The count rate increases to a maximum as the scintillator and tritium equilibrate between the phases. To insure that only counts originating at the interface were measured the count rates were taken immediately after the two liquids were contacted.

In Figure 2 it is seen that the count rate results for the two beakers smaller and one slightly larger than the photo-

Table 1. Propeller Dimensions

Number	Type	Blade dimensions (in.)	Shaft dimensions (in.)
1	Horizontal blade	2 × 0.5 × 0.025	0.25 × 14
2	Horizontal blade	3.1 × 0.75 × 0.065	0.375 × 14
3	Horizontal blade	1.15 × 0.286 × 0.020	0.130 × 14
4	Vertical blade	3.1 × 0.065 × 0.75	0.375 × 14
5	Vertical blade	1.15 × 0.020 × 0.286	0.130 × 14

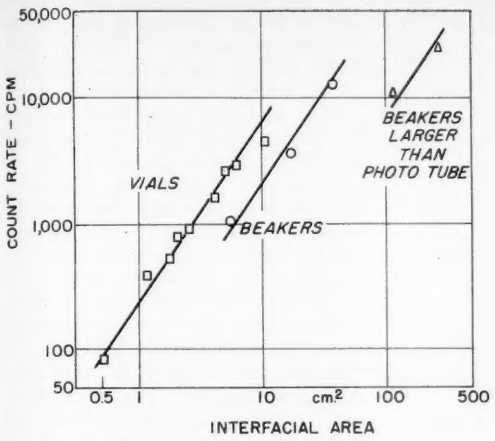

Fig. 2. Variation of count rate with interfacial area.

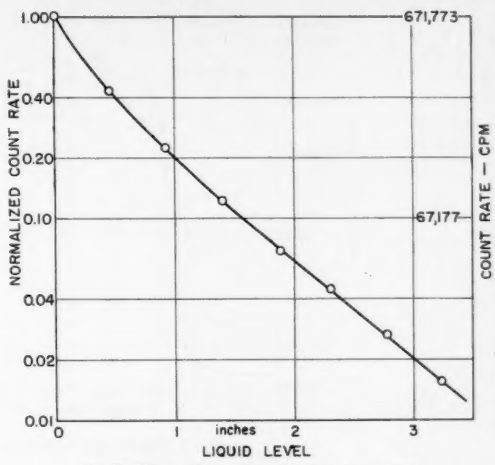

Fig. 3. Effect of interface level on count rate.

cathode fall on a straight line on log-log paper, while there is a definite effect of the geometry of the two beakers which were much larger than the photocathode. To establish conclusively that there was a direct dependence of counting rate on interfacial area a series of runs was made in uncoated vials with unground bottoms with the interface ½ in. above the bottom of the vials. Because of the effect of height of interface on the count rate, the rate for the vials has been put on the basis of that for the beakers with an interface at 2 in., as discussed below. The results are then plotted in Figure 2.

It is to be expected that the two beakers larger than the photocathode would give a lower number of counts per unit area than the smaller beakers. In the case of the large beakers the fraction of photons detected by the photocathode is reduced because of its smaller relative size. The result is that a smaller number of pulses are counted.

The effect of contamination of each phase by the other was determined by observing the difference between the initial count rate and that after steady state had been obtained as the scintillator and tritium equilibrate between the phases. The differences were within 5% of a straight line on log-log paper between 38.3 counts/sec. at 5.5 sq. cm. interfacial area and 1,210 counts/sec. at 112 sq. cm., with that for the largest beaker, 270 sq. cm., falling well below the line.

To determine the effect of liquid height a sample of used xylene and scintillator, contaminated with tritium, was placed in a 3-in. beaker and the count rate taken. Successive portions of pure water were added to raise the interface, and the count rate was measured after each addition. The ratio of count rate to that with the interface at the floor of the beaker is given in Figure 3. The count rate fell off approximately exponentially with increasing distance between the interface and the beaker floor. These results allowed a direct comparison of the calibration from the shell vials at a ½-in. level with the beakers at a 2-in. level interface as shown in Figure 2, where the data are all on the basis of a 2-in. level. The count rate for the ½-in. level was multiplied by the ratio of the normalized count rates for 2-in. and ½-in. levels, 0.055/0.432.

Because of the need for conserving tritium the more direct method of calibration with tritium and fresh scintillator was not used. In this determination some scintillations originated in the scintillator phase as well as at the interface, but as can be shown the normalized exponential curve will be the same as when all the scintillations originate at the interface. This is because below the xylene-water interface all photons will behave in the same manner independently of their place of origin.

Mixing Results

In the various combinations of beakers, propellers, and baffles the count rate was obtained as a function of stirrer speed yielding results such as those given in Figure 4. Tables 1 and 2 give the dimensions and combinations of stirrers and beakers used. Reproducibility was good with count rates obtained by increasing the stirrer speed agreeing well with those obtained by decreasing the speed.

Each plot obtained may be divided into three distinct regions. Initially there is a gradual increase in surface area as the slowly rotating propeller caused waves. As the interface is broken the area and count rate increases rapidly over a narrow range of stirrer speed. In the third region the dispersion is relatively homogeneous with the main effect being a decrease in droplet size with possibly some distortion.

CALCULATION

The effects of liquid height, insertion of propeller, and mutual contamination of the phases were observed to change the count rate considerably, and appropriate corrections were required.

Because the detected count rate is a strong function of the height from where the counts are originating, allowance must be made for the variation of efficiency of detection with position in beaker. The data of Figure 3 are used under the assumption that in the experiment the true time-average interaction or scintillation rate per unit volume of stirred beaker is constant; that is the system is homogenous. From the figure it is seen that for a given interaction rate the interactions arising near the floor of the beaker will contribute a unit count rate, while those 2 in. up will contribute a count rate of only 0.055 on the same scale. Integrating the data of Figure 3 over

Table 2. Identification of Runs

	Unbaffled								Baffled	
Run number	1	2	3	4	5	6	7	8	9	10
Beaker diam., in.	2.73	2.73	2.73	2.9	4.7	7.3	7.3	7.3	7.3	7.3
Propeller number	1	3	5	1	1	1	2	4	2	4

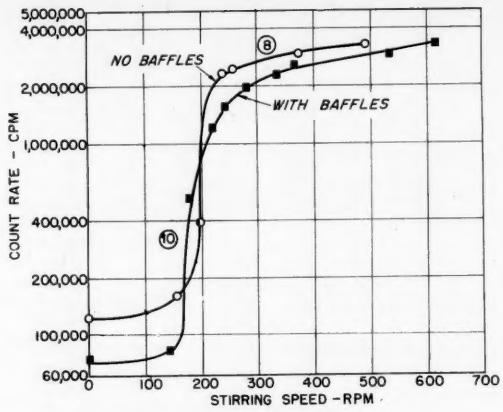

Fig. 4. Typical stirring curve.

the whole volume one can make an allowance for the detection efficiency.

The mean normalized count rate is the ratio of the count rate actually observed to that which would be observed if there were no attenuation of the scintillations between the height where they originate and the beaker floor. It is given by

$$\frac{\overline{C}}{C_o} = \left(\frac{C}{C_o}\right)_{ave} = \frac{\int_o^v C/C_o\, dv}{\int_o^v dv}$$

$$= \frac{\int_o^h C/C_o\, A dh}{Ah}$$

$$= \frac{\int_o^{h=4\text{ in.}} C/C_o\, dh}{h} = 0.153 \quad (2)$$

For the liquid levels of ½ or 2 in. used in the count rates vs. interfacial area calibration the product of the detection efficiency at the floor of the beaker and the true interaction or scintillation rate through the entire volume can be obtained from the observed interaction rate. It will be noted that $EN = C_o$:

$$C_o = EN = \frac{C_{2\text{ in.}}}{(C/C_o)_{2\text{ in.}}} = \frac{C_{1/2\text{ in.}}}{(C/C_o)_{1/2\text{ in.}}} \quad (3)$$

Calibration curves at both levels can then be placed on the same basis, say 2 in., as in Figure 3. When the system is stirred so as to be homogeneous and there is no blocking by the propeller being between a scintillation and the phototube, the count rate for the whole beaker is given by

$$C_o = EN = \frac{\overline{C}}{\overline{C}/C_o} \quad (4)$$

Not all of the count rate was due to scintillations rising at the interface. Some scintillations arose in the bulk phases because of equilibration of the tritium and the scintillator between the phases. An allowance for these two effects had to be made. The allowance was obtained by subtracting the count rate at 0 rev./min., with the propeller present and after operation and contamination, from the value obtained during calibration with fresh samples of scintillator and tritiated water where there was neither contamination nor propeller present. This correction was 38 to 69% at 0 rev./min. decreasing with increasing stirrer speed and count rate to only 0.5% at higher stirrer speeds, thus becoming negligible in the main region of interest.

At low stirrer speeds where the interface is wavy but yet essentially at a level of 2 in. the count rate yields the interfacial area directly from Figure 2, after first correcting for contamination of the phases and blocking due to the propeller, by subtracting a constant from the observed count rates.

With a high stirrer speed the contents of the beaker were homogeneous. The interfacial area was calculated by first subtracting the constant from the count rate to correct for contamination and blocking. This correction of about 0.5% is not of high accuracy because of the differing effect of the propeller yet is quite satisfactory having no appreciable effect on the results. The resulting count rate is that observed from scintillations arising throughout the whole beaker; yet the calibration curve, Figure 2, is for those arising at

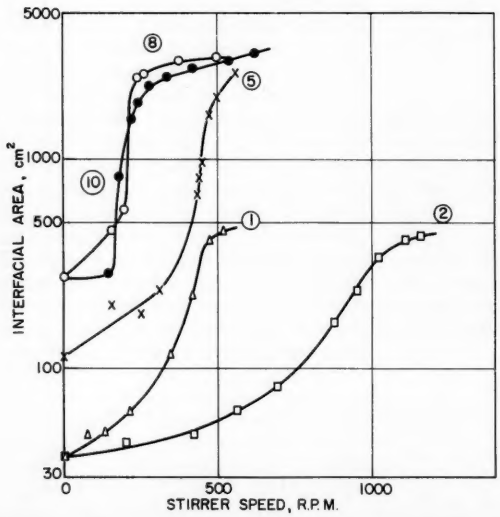

Fig 5a. Experimental values for interfacial area in stirred beaker.

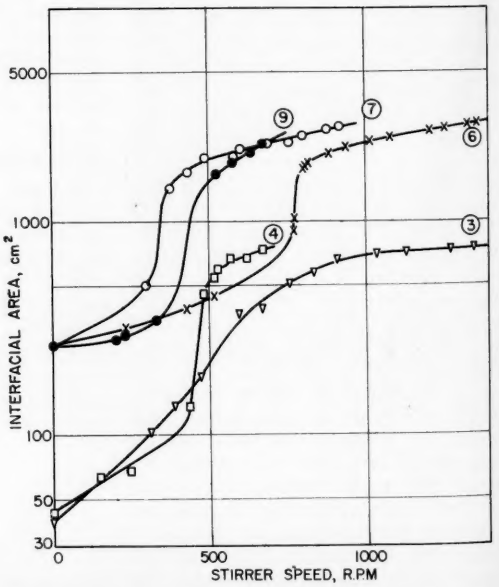

Fig. 5b. Experimental values for interfacial area in stirred beaker.

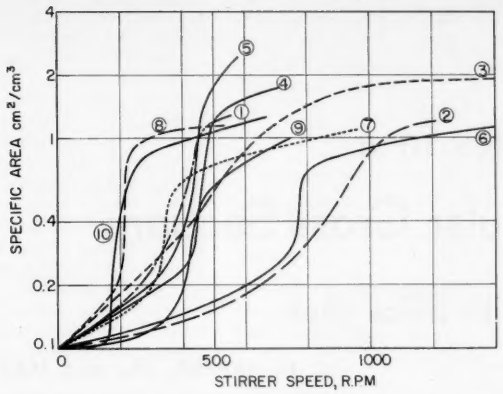

Fig. 6. Interfacial area per unit volume in stirred beakers.

a 2-in. level, $C_{2\text{in.}}$. Equation (2) gives the rate if there were no attenuation C_o by division by 0.153. The count rate must now be put on the basis of that which would be detected if the scintillations had all originated at 2 in., the height of the interface for the calibration curve. This is done by multiplying by $(C/C_o)_{2\text{in.}}$ which is 0.055 from Figure 3. The interfacial area can be read directly from Figure 2 with the resulting count rate used. This assumes that the attenuation through the xylene mixture is the same as that through water, a matter on which we do not have any information.

The interfacial area for high and low speeds is readily calculated as described above. To obtain the interfacial area at intermediate speeds it is noted that in the region of intermediate stirrer speeds the plot of count rate against stirrer speed is smooth on semi-log paper. As the interfacial area is approximately proportional to the count rate, the interfacial area for the region was drawn as a smooth line between the curves calculated for high and low stirrer speeds.

From the curves for the ten runs shown in Figure 5 it can be seen that the interfacial area is increased fifteen to fortyfold by stirring. From the identifying run number in Figures 5*a* and 5*b* and Table 2 the effect of various combinations of propellors, baffles, and beakers can be seen. While baffles may affect the critical speed where the interface breaks up, it does not seem to affect the final area greatly. The breakup of the interface could just as well be determined visually, for the speed at which it was observed to occur coincided with the rapid increase in count rate. Increasing the size of the stirrer does not seem to affect the beginning of the critical or intermediate region, but it does decrease the speed range it covers without changing the final interfacial area greatly.

From a mass transfer viewpoint the interfacial area per unit volume is of more interest than the interfacial area alone, for it relates to the efficiency of utilization of the beaker volume. This is shown in Figure 6, where it is seen that stirring increases interfacial area per unit volume fifteen to fortyfold. For the combination of beakers, baffles, and stirrers employed, the plateauing of the interfacial area occurred over a fivefold range of speed. As would be expected the vertical blades are better than horizontal ones. It is to be remembered that all the stirring results are for beakers filled to the same depth, 2 in. of water and 2 in. of xylene. No attempt was made to optimize the stirrer and baffles, for the sole aim was to demonstrate a new technique. Further work might include the determination of the attenuation, Figures 3, for mixed phases, various beakers, and a confirmation of the resulting experimental area by other techniques.

CONCLUSIONS

Interfacial areas in stirred vessels can be estimated by a scintillation technique without undue radiation hazards. The method is not expensive in expended materials, but the capital cost of the photodetection and counting circuits is high.

It is hoped that this method might prove to be a useful tool for the measurement of interfacial areas. This technique could be used in certain systems in which mass is being transferred.

ACKNOWLEDGMENT

The authors wish to thank Philip Birbara for suggesting this technique and Jack Trombka for his valuable assistance in developing the detection and counting system.

A preliminary portion of this investigation, which was taken from the thesis submitted in partial fulfillment of the requirements for the Master's degree in Nuclear Engineering, was the subject of a thirty-five line note (5).

NOTATION

A = cross-sectional area of beaker
a = interfacial area per unit volume
C = observed count rate due to volume or interfacial area element at height h above beaker floor
C_o = count rate that would be observed if volume or interfacial area element were at beaker floor
$\overline{C}$ = observed count rate due to interactions throughout the whole beaker
c = concentration
E = detection efficiency for scintillations arising on floor of beaker
f = fugacity
h = height above beaker floor
k' = mass transfer coefficient based on fugacity driving force
k = mass transfer coefficient based on concentration driving force
m = distribution coefficient
N = number of interactions occurring per unit time throughout the entire beaker volume
n = number of interactions occurring per unit time per unit thickness of contaminated scintillator
v = volume of liquid phases in beaker
W = mass transfer rate

Subscripts

s = solvent or xylene phase
w = water phase

LITERATURE CITED

1. Bell, C. G., and F. N. Hayes, "Liquid Scintillation Counting," Proc. of Conf. at Northwestern University, Pergamon Press, (1958).
2. Bressee, J. C., and C. V. Chester, The Use of Radioisotopes for the Measurement of Interfacial Area, 2nd. U.N. Int. Conf. on the Peaceful Uses of Atomic Energy (1958).
3. Crozier, R. D., Ph.D. thesis, Univ. Mich., Ann Arbor (1956).
4. Mitsis, G. J., and R. K. Plebuch, Master's thesis, Univ. Mich., Ann Arbor (1958).
5. ————, *Trans. Am. Nuc. Soc.*, **1**, No. 2, 67 (December 1958).
6. Robertson, C. S., Jr., and P. J. Birbara, "Interfacial Area by Alpha Dosimetry," Unclassified, ORNL K T-256, Unpublished.
7. Rodger, W. A., V. G. Trice, Jr., and J. H. Rushton, *Chem. Eng. Progr.*, **52**, 515 (1956).
8. Vermeulen, Theodore, G. M. Williams, and G. E. Langlois, *ibid.*, **51**, 85 (1955).

Manuscript received May 4, 1959; revision received January 20, 1960; paper accepted January 22, 1960. Paper presented at A.I.Ch.E. San Francisco meeting.

Heat Transfer and Kinetics in a Catalyst Bed of Rectangular Cross Section:

Air Oxidation of Nitric Oxide with Silica Gel

J. H. JAFFER, JR., and HARDING BLISS

Yale University, New Haven, Connecticut

The results of an investigation of heat transfer and reaction kinetics in a fixed-bed catalytic reactor of slab geometry are described. The particular reaction studied is the air oxidation of nitric oxide with silica gel. Conversions and catalyst-bed temperatures were observed in the experimental, nonisothermal slab reactor, but only a sample of these data are reported and analyzed here.

A mathematical analysis of the processes occurring in a slab reactor has been developed which leads to a design method for such reactors that permits prediction of catalyst-bed temperatures and conversions from a knowledge of specific reaction rates and the physical properties of the system. The design method involves a step-by-step procedure but requires a small number of steps. To evaluate the accuracy of the design method and to illustrate its use, the specific reaction-rate data together with published thermal-conductivity data have been used with the method to predict the results of a run on the experimental nonisothermal reactor. Good agreement between calculated and observed temperatures and conversions was obtained.

Specific reaction rates, derived from integral conversions in an experimental, isothermal reactor, are reported.

The studies of heat transfer in catalytic converters made in recent years have advanced remarkably our knowledge of this important problem in chemical engineering design. For the most part these studies have been confined to cylindrical beds, but there are certain advantages to converters of other shapes; for example, a slab bed (one of rectangular cross section with heat transfer through two opposite sides) may be enlarged greatly in an area without increasing the distance through which heat must flow, and also the mathematical analysis is somewhat simpler than for cylindrical converters. The purpose of this work was, therefore, the study of heat transfer and kinetics in a catalyst bed of rectangular cross section. The particular reaction, the air oxidation of nitric oxide with silica gel, was selected because the analysis was relatively easy and because a wide variation in reaction rates throughout the converter was anticipated. The second reason constitutes a severe test of theory and experiment.

Since conditions for the slab bed required operating in a range of temperature at which isothermal-rate data for this catalytic reaction were not available, and since the catalyst could not be assumed to be identical to that of previous investigations, it was necessary to measure such rates as well.

RANGE OF VARIABLES

For the runs in the slab bed the following were studied:

Entering gas temperatures: 81° to 136°C.
Air flow rates: 0.029 to 0.125 g. moles air/(sq. cm.)(min.)
Mole fraction nitric oxide in feed: 0.022 to 0.152

The temperature of the coolant for removal of the heat of reaction was close to that of the entering gas. The extent of conversion of nitric oxide was 42 to 82%.

The catalyst used was refrigeration-grade silica gel, 14 to 20 mesh, with a density of 0.680 g./cc.

APPARATUS, ANALYSES, AND PROCEDURE

Reactor System

Nitric oxide was generated continuously by the reaction of sodium nitrite with sulfuric acid, and air was supplied by a compressor. The reactant streams were separately purified by passage through silica gel and measured with calibrated orifice meters before being mixed in a tee upstream of the reactor. The air stream was also separately preheated approximately to the reactor coolant temperature in an electrically heated section of pipe. The flow rate of each stream was controlled with a globe valve.

Suitable thermocouples and manometers were provided so that temperatures and pressures were known at the orifices and at the entrance to the reactor. The controlled flow rates determined the composition of the gases entering the converter; no independent analyses for nitric oxide were made.

Reactor

The reactor (Figure 1) was constructed of two standard 8-in. aluminum structural channels with their plane surfaces opposed, spaced by two stainless steel bars. The web thickness of the channels was only 0.51 cm. to promote heat transfer through the walls. The stainless steel bars were 5.1 cm. in vertical dimension to minimize heat flow in this direction. Asbestos gaskets coated with gasket cement were placed between the channels and the bars, and the assembly was bolted together tightly. The resulting rectangular cross section for the catalyst was 2.26 cm. wide and 10.2 cm. high. The length was 91.5 cm., with the catalyst occupying the space between 17.6 and 74.0 cm. from the entrance. The spaces before and after the catalyst were empty. Since the position of the assembly was horizontal, the catalyst was held in place by screens. Total catalyst weight was 885 g.

Thermocouples were provided through-

J. H. Jaffer, Jr., is with Esso Research and Engineering Company, Linden, New Jersey.

out the bed to permit measurement of lateral temperature gradients at several longitudinal positions. The measurement should lie between the gas and solids temperatures, but the difference between these cannot be great under the conditions used here (later shown to be less than 1°C.). The couples were introduced through stainless steel, high-pressure tubing soldered into ¼-in. holes drilled in the top bar. Small stuffing boxes at the tops of these tubes prevented leakage of the gas where the wires entered. The couples were located in the bed with special supports to assure that movement was practically impossible and that the lead wires lay in straight, vertical (isothermal) paths.

Thermocouples were carefully located at the center of the catalyst and 0.40 and 0.80 cm. out from the center in a lateral direction. The lateral gradient thus measured was observed with such thermocouples at axial positions 3.1, 18.1, 31.8, and 48.3 cm. along the catalyst for the first forty runs. Subsequent runs all were the same except that the 18.1 position became 18.8 cm.

The whole reactor was mounted in a steel shell which contained the coolant. Water, a calcium chloride brine boiling at about 119°C., and another boiling at about 132°C. were used as coolants. The coolants were boiled slowly in the reactor shell by heat from the reactor and from two immersion heaters controlled with variable autotransformers.

The catalyst was charged to the reactor with care to insure accurate thermocouple positioning and to eliminate the possibility of subsequent catalyst-bed shrinkage.

Analyses

Continuous analysis of the reactor effluent for nitrogen dioxide was accomplished photometrically, advantage being taken of the ability of the compound to absorb blue light. Calibration of the photometer was accomplished by passing known mixtures of nitrogen dioxide and air through the apparatus, the calibrations taking the form of plots of nitrogen-dioxide concentration vs. instrument reading. Allowance for nitrogen tetroxide, present in equilibrium with nitrogen dioxide in appreciable quantity at room temperature, was made by calculation based on published equilibrium constants (5) and the fact that nitrogen tetroxide is transparent to blue light. A standardizing procedure was employed to eliminate drift.

Procedure

The catalyst was activated by passing a slow stream of dry air through the bed for 2 hr. while the catalyst temperature was maintained at 130°C. The effluent air was cooled in a glass tube immersed in a salt-ice bath, and no condensation was observed after this 2-hr period.

Prior to each day's runs fresh silica gel was charged to the reactant purifiers, the system was checked for gas leakage, reactant supply circuits were carefully purged, and the coolant was brought to the desired temperature. Air and nitric oxide flows were then begun and adjusted to the desired rates. When steady state behavior was obtained, the following readings were made:

Table 1. Representative Data, Run C-3

Gas inlet temperature	100°C.
Coolant temperature	100°C.
W_A	2.76 g. moles/min.
W_{NO}	0.383 g. moles/min.
$y°_{NO}$	0.1215
$n°_{NO}$	0.00418 moles nitric oxide/unit mass feed
X_1	0.00040 moles nitric-oxide conversion/unit mass feed
X_2	0.00242 moles nitric-oxide conversion/unit mass feed
X_3	0.00254 moles nitric-oxide conversion/unit mass feed
$X_3/n°_{NO}$	0.61
Pressure (before catalyst)	1.311 atm.
Pressure (after catalyst)	1.029 atm.

Bed temperatures, °C.

	$x = 0$	$x = 0.40$ cm.	$x = 0.80$ cm.
$y =$ 3.1 cm.	122	122	117
$y =$ 18.1 cm.	141	137	121
$y =$ 31.8 cm.	139	135	122
$y =$ 48.3 cm.	130	127	116

1. Photometer: gas inlet and outlet temperatures, pressure, instrument settings and reading.
2. Voltages of the twelve thermocouples in the catalyst.
3. Temperature of the gas stream immediately ahead of the bed.
4. Pressure in the precatalyst mixing space. In the case of those runs with boiling-water coolant this measurement was made with a separate set of runs without other observations.
5. Air flow rate.
6. Nitric oxide flow rate.
7. Ambient temperature and coolant temperature.

A detailed description of the apparatus and procedure is given by Jaffer (7).

SLAB-BED DATA

Eighty-six runs were made in the slab-bed reactor under the conditions described earlier. The temperature of the coolant except in a few cases was close to that of the entering gas.

The data of a representative run are given in Table 1. All data are reported in detail by Jaffer (7).

The homogeneous reaction before and after the catalyst was minor but could not be neglected. It is thus important to observe in Table 1 and elsewhere that the following designations were made:

X_1: conversion at bed entrance, basically a measured quantity differing from zero by a small amount

X_2: conversion at bed exit, a value calculated from X_3 and differing from it by a small amount

X_3: conversion measured at photometer.

The details of these small corrections are given in the appendix.

The reproducibility of these data was established in two ways: simple repetition of six runs and repetition after disassembly, catalyst removal and replacement, and changes in thermocouple vertical position and support construction detail for three runs. In all nine cases all temperatures were within 2°C. of the original (most were identical), and conversion was within 1% of the original. There is thus no evidence of loss of catalyst activity or movement of thermocouples in the bed.

The fact that measured catalyst bed temperatures were reproducible despite appreciable changes in vertical positioning of several thermocouples indicates that relatively little heat was transferred through the stainless steel bars; that is, slab behavior was closely approached. Similarly, no changes resulted from substantial modifications to thermocouple-support design, indicating that these supports did not affect temperature measurements.

INTERPRETATION OF DATA

For these data the concern is primarily with solving the differential equation describing the problem and with using with this solution suitable parameters for the heat transfer and heat generation quantities which appear therein. It should be noted that all mass transfer aspects of this problem have been neglected. The geometry is shown in Figure 2.

The heat balance on a differential catalyst volume may be written

$$K_f \frac{\partial^2 T_g}{\partial x^2} - Gc_p \frac{\partial T_g}{\partial y} + C_1 T_s + C_2 = 0 \qquad (1)$$

In this equation one assumes negligible axial heat conduction; negligible solids heats conductivity*; no lateral concentration gradients; conduction

* Singer and Wilhelm (9) have shown that, in heat exchangers at least, solid-to-solid conduction is important only for highly conductive particles.

through the fluid all in one plane, that is no correction for the corner; and heat generation function linear in the solids temperature, that is $C_o + C_1T_s$. The heat balance on the solid phase may be written as a simple algebraic equation when the solids conductivity is neglected:

$$C_1T_s + C_o + h_v\,(T_g - T_s) = 0 \quad (2)$$

This may be solved immediately to yield

$$T_s = \frac{C_o + h_vT_g}{h_v - C_1} \quad (3)$$

The boundary conditions are

$$T_g(x=w,0) = 0 \quad (4)$$

$$\frac{\partial T_g}{\partial x}\,(0,y) = 0 \quad (5)$$

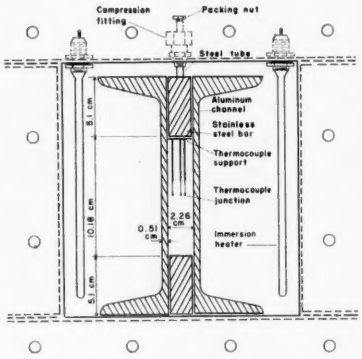

Fig. 1. End view of slab bed converter.

$$T_g(x=w,y) = T_w \quad (6)$$

The solution of this equation with the further assumption of constant properties is obtained by the Laplace transform and is

$$T_g = \frac{T_w + \frac{c}{b}}{\cos w\sqrt{b}}\cos x\sqrt{b} - \frac{c}{b} + \sum_{n=0}^{\infty}\frac{2(-1)^n}{\left(n+\frac{1}{2}\right)\pi}\left(\frac{T_w\alpha^2 + c}{b-\alpha^2}\right)\cos\alpha x\left(\exp\frac{b-\alpha^2}{a}y\right) \quad (7)$$

in which

$$\alpha = (n + 1/2)\frac{\pi}{w},\quad a = \frac{G\,c_p}{K_f},$$

$$b = \frac{C_1h_v}{K_f(h_v - C_1)},\quad c = \frac{C_oh_v}{K_f(h_v - C_1)}$$

There is no doubt that the use of this equation and others like it for catalyst beds of other shape, such as that used by Singer and Wilhelm (9), is most severely impaired by the assumption that the heat-generation function is linear in the solid temperature. This assumption is almost never a good one for extensive conversions, and it is particularly bad for the reaction here considered. In most exothermic reactions the effects of conversion and of temperature counter each other to a certain extent, at least, and so an approximation to a linear dependence on temperature may be had. In this reaction both high temperature and conversion decelerate the reaction, and the approximation to linearity is not good.

This difficulty can be overcome by limiting the application of Equation (7) to axial segments of the bed, each one of which is short enough to give a reasonably good approximation to the linearity sought. In practice, as judged by the treatment of these runs, the number of segments required is not large. Three or four should suffice in most cases. However, of course, the first boundary condition [Equation (4)] must be replaced for segments other than the first by an approximation as follows:

$$T_g(x<w,0) = \beta\cos\frac{\pi x}{2w} + \gamma\cos\frac{3\pi x}{2w} \quad (8)$$

in which β and γ are constants determined to fit the gradient of T_g at the end of the previous segment, which is found with Equation (7). This is a purely empirical correction, of course, and any convenient values of x (such as those to give easy reading of the cosines) are recommended. It should be noted that a discontinuity in T_g at the wall is permitted in the first set of boundary conditions. This discontinuity can give some difficulty if the value of T_w is large with this new boundary condition because it would distort the gradient. It is thus recommended that T_w be small, and in the cases applied T_w was 0.

This adds two terms to the previous equation, and so this final equation expressing the behavior of a slab bed is

$$T_g = \frac{T_w + \frac{c}{b}}{\cos w\sqrt{b}}\cos x\sqrt{b} - \frac{c}{b} + \sum_{n=0}^{\infty}\frac{2(-1)^n}{\left(n+\frac{1}{2}\right)\pi}\left(\frac{T_w\alpha^2 + c}{b-\alpha^2}\right)\cos\alpha x\left(\exp\frac{b-\alpha^2}{a}y\right) + \beta\cos\frac{\pi x}{2w}\exp\frac{b-\frac{\pi^2}{4w^2}}{a}y + \gamma\cos\frac{3\pi x}{2w}\exp\frac{b-\frac{9\pi^2}{4w^2}}{a}y \quad (9)$$

in which α, a, b, and c have the same meanings as before. This equation applies to all segments, even the first, if β and γ are taken to be zero for this one.

The results of the application of this equation to run C-3, the data for which are given in Table 2, will be described. Since the modified Reynolds number for this run is 31, the results of Singer and Wilhelm (9) and of Argo and Smith (1) lead to an estimate of K_f = 0.0223 cal./(min.)(cm.)(°C.) for the particle size and flow conditions involved. The heat transfer studies of Baumeister and Bennett (3) lead to an estimate for h_v of 9.85 cal./(min.)(cc.)(°C.), which is consistent with the mass transfer studies of Wilke and Hougen (12). The value of ΔH for this reaction is −13,562 cal./g. mole nitric oxide according to Giauque and Kemp (5). This figure, reversed in sign for the heat-generation function, was taken as constant over the temperature range involved. The heat of reaction per mole must be multiplied by the appropriate rate of reaction (read from one of figures in the appendix) to yield the heat-generation function. This was re-evaluated for each segment, and the segments used corresponded to those used in the experimental measurements. The details of the calculation method are best considered as a method of design and will be thus described in a subsequent section. The columns in Table 2 headed $T_{g_{AVG}}$ have bearing on the design method only, since no such measurements were made.

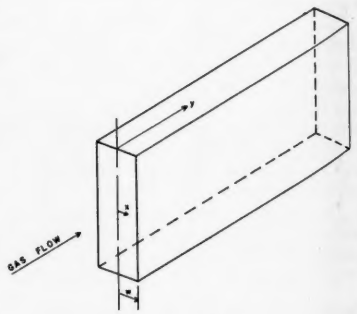

Fig. 2. Geometry of slab bed converter.

When one considers the complexity of the system involved, the results ap-

Table 2. Calculated Behavior of Run C-3 and Comparison with Measured Figures Given in Parentheses*

Segment	Length from entry, cm.	Assumed $T_{g\,Avg}$	Calc. $T_{g\,Avg}$	Conv. %	$T_g(x=0)$	$T_g(x=0.40)$	$T_g(x=0.80)$
1	3.1	113	112.7	16	115.3 (122)	115.1 (122)	112.5 (117)
2	18.1	132	130	36	142 (141)	138 (137)	125 (121)
3	31.8	132	129	47	141 (139)	137 (135)	123 (122)
4	48.3	123	124	55	138 (130)	135 (127)	124 (116)
End	56.4	123	126	59 (61)			

* It should be remembered that measured temperatures should lie between T_g and T_s and thus would be expected to be a little higher than the calculated values of T_g. However the difference between T_g and T_s cannot be large under the conditions here considered. A simple consideration of Equation (3) with the parameters for the conditions here met indicates that T_s and T_g are about 1°C. apart at most.

pear to be good. The conversion result is particularly so, although this is not so severe a test as it might first be considered, since the reaction is very slow at high conversion.

DESIGN METHOD

Equations (7) and (9) may be used as the basis of a design method for a slab reactor in the following sequence. (The description is based on an exothermic reaction.) The rate data for this particular case are described in the appendix.

1. With the specification of all entrance conditions, calculate from suitable data the reaction rate at the entrance.
2. Considering only the first axial segment, assume (a) an average T_g, (b) a maximum T_g, and (c) the extent of conversion for the end of this segment.
3. Calculate rate of reaction, defined by assumed average T_g and conversion at end of segment. Using average rate (entrance and end), calculate the conversion. Repeat 3 and 2(c) until a check is obtained.
4. Calculate the heat-generation function at entrance and lowest temperature and at the exit and highest temperature.
5. Evaluate C_o and C_1 for the segment. Note that this involves T_s, which can be solved with Equation (3) from the values of T_g.
6. Assuming knowledge of the parameters K_f, h_v, G, and c_p, evaluate a, b, and c.
7. Calculate the integral average value of T_g from the appropriate operation on Equation (7). Repeat steps 2(a), 2(c), 3, 4, 5, and 6 until a check with the assumed values is found.
8. Calculate T_g at $x = o$ using Equation (7). This should also check, but an exact agreement is not essential. A serious disagreement will require a repeated trial to this point.
9. Calculate T_g at one intermediate value of x and use this and T_g at $x = o$ to evaluate β and γ of Equation (8).
10. Proceed to the next axial segment and use Equation (9) instead of Equation (7).

It should be noted that conversion calculations are based on a mean rate in which the rates at entrance average temperature and exit average temperature are considered. The heat-generation function, however, is evaluated with rates at the entrance conversion and entrance wall temperature and the exit conversion and maximum temperature. This was done in an attempt to get the extremes of the rates, since the rate is fastest (with this reaction) at the lowest temperature and lowest conversion and slowest at the highest temperature and highest conversion. This is a refinement which may not be necessary; it is probably satisfactory to use average temperatures throughout, which would simplify the design method. Despite the necessity of assuming three items, the calculation is fairly fast after some practice.

The calculated figures in Table 2 were computed with this method.

CONCLUSIONS

The apparatus and procedure described proved to be effective in permitting the observations of temperature distributions and conversions for the catalytic oxidation of nitric oxide in a slab bed. Eighty-six runs were made, although only one is described in detail here.

A mathematical analysis led to equations describing the distribution of temperatures throughout the catalyst bed as functions of fundamental properties, flow conditions, and the rate of heat generation. These equations may be adapted to the formulation of a design method with which the temperature distributions and conversions may be predicted. This method requires the consideration of axial segments of the bed, but the number of such segments is small and thus the method is a relatively fast one.

The design method was used in conjunction with isothermal rate data given in the appendix to predict with good accuracy the results observed, although those of only one run are described.

ACKNOWLEDGMENT

J. H. Jaffer, Jr., gratefully acknowledges the financial assistance of E. I. du Pont de Nemours and of the Research Corporation.

NOTATION

a = $G\,c_p/K_f$, constants in Equations (7) and (9), cm.$^{-1}$

b = $C_1 h_v/K_f(h_v - C_1)$, constant in Equations (7) and (9), cm.$^{-3}$

C_o = constant in catalyst-bed heat-generation function, cal./(min.)(cc.)

C_1 = constant in catalyst-bed heat-generation function, cal./(min.)(cc.)(°C.)

c = $C_o h_v/K_f(h_v - C_1)$, constant in Equations (7) and (9), °C./sq. cm.

c_p = heat capacity of gas phase at constant pressure, cal./(g.)(°C.)

F = reactor feed rate, g./min.

G = superficial mass velocity of gas in catalyst bed, g./(min.)(sq. cm.)

h_v = volume-based coefficient of heat transfer between solid particles and gas in catalyst bed, cal./(min.)(cc.)(°C.)

K_f = effective thermal conductivity of gas phase in catalyst bed, cal./(min.)(cm.)(°C.)

k_h = reaction-rate constant for uncatalyzed oxidation of nitric oxide g. moles nitric oxide converted/(min.)(cc.)(atm.^{2})

n^o = total moles of reactor feed per unit mass of feed, dimensionless

n^o_{NO} = moles of nitric oxide in reactor feed per unit mass of feed, dimensionless

$n^o_{O_2}$ = moles of oxygen in reactor feed per unit mass of feed, dimensionless

p = absolute pressure, atm.

R = specific rate of oxidation of nitric oxide over silica gel, g.-moles nitric oxide converted/(min.)(atm.^{2})(cc.)

r = rate of oxidation of nitric oxide over silica gel, g. moles nitric oxide converted/(min.)(cc.)

T_g = temperature of gas phase in catalyst bed, °C. above reactor wall temperature at inlet end

$T_{g\,avg}$ = average temperature of gas phase (averaged in the lateral direction). °C. above reactor wall temperature at inlet end

T_s = temperature of solid phase in

catalyst bed, °C. above reactor wall temperature at inlet end

T_w = gas temperature at reactor wall, °C. above reactor wall temperature at inlet end

V = volume, cc.

V_B = total catalyst-bed volume, cc.

W_A = air flow rate, g. moles/min.

W_{NO} = nitric oxide flow rate, g. moles/min.

w = half width of slab catalyst bed, cm.

X = extent of conversion, moles nitric acid converted per unit mass of reactor feed, dimensionless

X_1 = value of X at catalyst-bed entrance

X_2 = value of X at catalyst-bed exit

X_3 = value of X at point of analysis

x = lateral distance from central plane of slab-shaped bed, cm.

y = axial distance through catalyst bed, cm.

y°_{NO} = mole fraction nitric acid in reactor feed, dimensionless

α = $(n + 1/2)\ \pi/w\ \ n = 0, 1, 2,$ cm.$^{-1}$

β = constant in Equation (8), °C.

γ = constant in Equation (8), °C.

LITERATURE CITED

1. Argo, W. B., and J. M. Smith, *Chem. Eng. Progr.*, **49**, 443 (1953).
2. Baker, R. W., H. N. Wong, and O. A. Hougen, *Chem. Eng. Progr. Symposium Ser. No. 4*, **48**, 103 (1952).
3. Baumeister, E. B., and C. O. Bennett, *A.I.Ch.E. Journal*, **4**, 69 (1958).
4. Burdick, C., *Ind. Eng. Chem.*, **14**, 308 (1922).
5. Giaque, W., and J. Kemp, *J. Chem. Phys.*, **6**, 41 (1938).
6. Glasstone, S., K. Laidler, and H. Eyring, "The Theory of Rate Processes," p. 279, McGraw-Hill, New York (1941).
7. Jaffer, J. H., Ph.D. thesis, Yale Univ., New Haven (1956).
8. Kurin, N., and I. Blokh, *J. Appl. Chem. (U.S.S.R.)*, **11**, 734 (1938); *Chem. Abs.*, **33**, 1885 (1939).
9. Singer, Emanuel, and R. H. Wilhelm, *Chem. Eng. Progr.*, **46**, 343 (1950).
10. Szego, L., *Gazz. Chim. ital.*, **60**, 217 (1930); *Chem. Abs.*, **24**, 2409 (1930).
11. U. S. National Bureau of Standards Circular 510 (1951).
12. Wilke, C. R., and O. A. Hougen, *Trans. Am. Inst. Chem. Engrs.*, **41**, 445 (1945).

Manuscript received July 7, 1958; revision received February 17, 1960; paper accepted February 18, 1960.

APPENDIX

A-I. Observations on the Homogeneous Reaction

The homogeneous oxidation of nitric oxide which occurs in the empty space before the catalyst and between the catalyst and the photometer is not negligible and must be taken into account in interpreting both the slab-reactor data and the isothermal-bed data discussed below. The rate equation for the third-order homogeneous reaction in a flow system is

$$\frac{dV}{F} = \frac{(n^\circ - \frac{1}{2}X)^3}{p^3 k_h\,(n^\circ_{NO} - X)^2\,(n^\circ_{O_2} - \frac{1}{2}X)}\,dX \qquad \text{(A-1)}$$

The rate constants as listed by Glasstone, Laidler, and Eyring (*6*) and the U.S. Bureau of Standards (*11*) were used in calculations based on this equation.

The photometer was located downstream of the catalyst bed, of course, and its measured value is the reported X_3 of the tables. The conversion at the exit of the catalyst bed, X_2, was obtained by successive application of Equation (A-1) in integrated form over portions of the volume between the catalyst-bed exit and the photometer. This procedure was employed to allow for the fact that the gas left the catalyst bed at temperatures as high as 172°C., although the photometer was close to room temperature. The temperature in the photometer chamber was, of course, known. Since the precise pattern of temperature change between the converter and photometer was not known and had to be estimated, there are errors in this procedure. However the over-all contributions of such errors are small because the differences between X_2 and X_3 are small; it is a correction to a correction.

With regard to precatalyst conversion in the slab reactor, it was recognized that large errors could result from direct application of Equation (A-1) because of incomplete mixing of the reactants early in the unpacked volume upstream of the catalyst. Consequently a number of runs were made in which the gas mixture immediately upstream of the catalyst bed was bypassed around the catalyst and sent directly through the photometer. The conversions read at the photometer were then adjusted to those at the catalyst-bed entrance by means of the integrated form of (A-1). Details are given by Jaffer (7). Some error was undoubtedly involved in the use of these data; however, again, it is only a correction to a correction.

The geometry of the reactor system used to obtain isothermal rate data was such that virtually perfect mixing in the precatalyst unpacked volume could be safely assumed. Hence precatalyst conversion was computed directly with the integrated form of Equation (A-1).

A-II. Determination of Isothermal Rates

Isothermal rate data for the oxidation of nitric oxide over silica gel have been reported (*2, 4, 8, 10*) for different temperatures than used here and with silica gel preparations which may well be different. Hence isothermal rate measurements were undertaken with the present catalyst and in the higher temperature region of interest here.

The range of variables for the isothermal conversion data were

Temperature	96° to 172°C.
Air flow rates	0.029 to 0.17 g. moles/(min.) (sq.cm.)
Mole fractions, nitric oxide	0.0177 to 0.146
Conversions	9 to 89%

Isothermal Reactor System. This system was similar to the slab-reactor system except for the following: air was supplied from a compressed air tank rather than a compressor, reactant stream flow rates were controlled with needle valves and measured with rotameters, and both air and nitric oxide streams were separately preheated.

Isothermal Reactor. (Figure A-1) The catalyst was contained in four parallel copper tubes, each 3/16 in. O.D., 0.314 cm. I.D., and about 61 cm. long. The packed length of each tube was 58.4 cm., resulting in a total catalyst volume of 18.0 cc., including voids, and a catalyst weight of 12.0 g. Such small tubes were used to ensure relatively fast heat transfer, and the parallel arrangement was used to give total flow rates which could be measured accurately. Loss of catalyst was prevented by tightly rolled cylinders of wire mesh inserted into fittings which connected the above tubes to a manifold. The catalyst density was 0.655 g./cc.

Thermocouples were placed along the length of these tubes, the couple junctions being located as near as possible to the

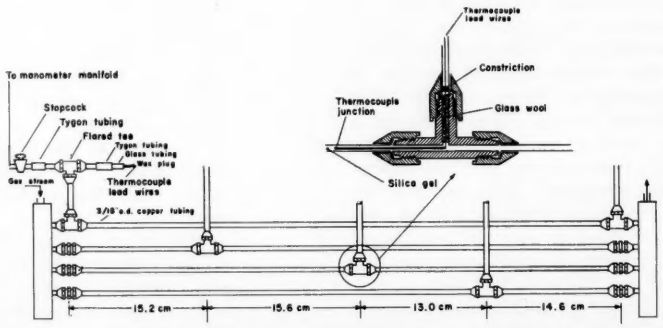

Fig. A1. Isothermal reactor.

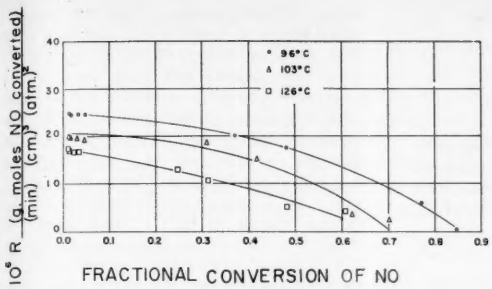

Fig. A2. Specific rate of oxidation of nitric oxide over silica gel $n^{\circ}_{NO} = 0.001$.

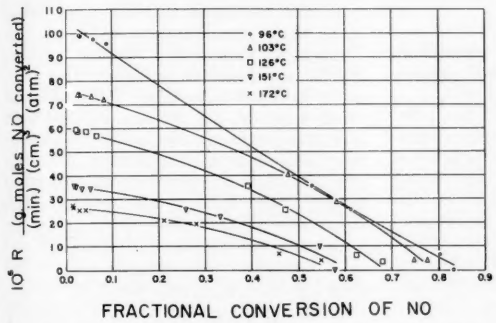

Fig. A3. Specific rate of oxidation of nitric oxide over silica gel $n^{\circ}_{NO} = 0.002$.

axes of the tubes. (See Figure A-1.) The lead wires were removed through legs of tees inserted in the tubes, care being exercised to avoid leakage of gas and to bring the leads out through an isothermal zone. These tees also led to a manometer for pressure measurement. The whole assembly was immersed in an agitated oil bath which was heated by an immersion heater.

Isothermal Runs. The catalyst was activated in the same manner as in the nonisothermal runs, and operation of the unit was essentially the same. The following data were recorded:

1. Photometer, same as for slab converter.
2. Air flow rate.
3. Nitric oxide flow rate.
4. Ambient temperature.
5. Pressures at four positions along the reactor (one connection proved sluggish).
6. Temperatures at five points along the catalyst bed.
7. Temperature of the cooling bath.

More details of the apparatus and procedure are given by Jaffer (7); however, the analytical procedure was basically the same as described before.

Isothermal Data. Eighty-five isothermal runs were made at the conditions described earlier.

The data of a representative run are given in Table A-1. All the data are given in reference (7).

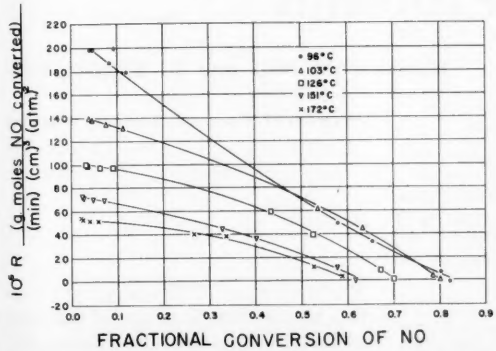

Fig. A4. Specific rate of oxidation of nitric oxide over silica gel $n^{\circ}_{NO} = 0.003$.

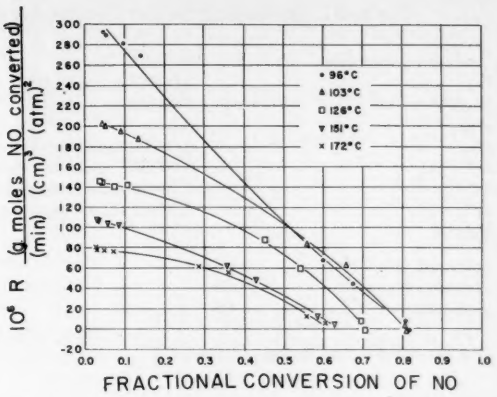

Fig. A5. Specific rate of oxidation of nitric oxide over silica gel $n^{\circ}_{NO} = 0.004$.

For all practical purposes isothermal conditions were, indeed, maintained. In some cases the temperature of one station differed from the others or from the bath by 1°C., in four cases by 2°C., and in one case by 3°C.

A pair of runs at essentially identical conditions but at quite different times were made for each of the five temperatures. The worst disagreement in any of these was 57.5 vs. 58.1% conversion; the others were in considerably better agreement. It is thus clear that there is no evidence of loss of catalyst activity.

Interpretation of the Isothermal Data. The basic relationship by which specific reaction rates were obtained from the isothermal data is

$$X_2 - X_1 = \int_0^{V_R/F} r d(V/F) \quad \text{(A-2)}$$

The fact that the feed rate, rather than catalyst volume, was varied experimentally introduced a complication. Both X_1 and X_2 varied with feed rate: X_1 because of varying residence time available for homogeneous reaction in the precatalyst volume and X_2 because of changes in X_1 and varying residence time in the catalyst bed. A mathematical analysis (7) was developed to take these factors into account.

Since total pressure varied over the length of the isothermal bed as well as from run to run, and since the effect of

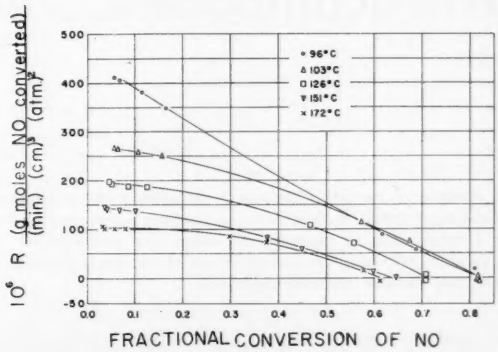

Fig. A6. Specific rate of oxidation of nitric oxide over silica gel $n^{\circ}_{NO} = 0.005$.

Table A-1. Representative Data of Isothermal Runs, Run I—14

Coolant temperature	96° to 97°C.				
W_A	0.00887 g. moles/min.				
W_{NO}	0.00152 g. moles/min.				
y°_{NO}	0.146				
n°_{NO}	0.00500 moles nitric-oxide converted/unit mass feed				
X_1*	0.000807 moles nitric-oxide converted/unit mass feed				
X_2*	0.00401 moles nitric-oxide converted/unit mass feed				
X_3*	0.00421 moles nitric-oxide converted/unit mass feed				
X_3/n°_{NO}	0.843				
Station through bed	1	2	3	4	5
Pressure, atm. abs.	1.029	—	1.020	1.013	1.007
Temperature, °C.	96	96	96	96	96

* X_3 is a measured quantity; X_2 is calculated from it as a correction for the homogeneous reaction. X_1 is calculated for the homogeneous reaction.

pressure was not specifically studied in this investigation, it was necessary to assume a pressure dependence on the basis of available data. Although there is little agreement in the literature in this regard, proportionality of the rate to the square of absolute pressure represents a reasonable compromise between reported correlations (*2, 4, 8, 10*). This relationship was assumed in deriving the reaction rates reported here.

Rates of Isothermal Reaction. The calculated rates of isothermal reaction are plotted in Figures A-2, 3, 4, 5, and 6. The ordinate is R, for use in the equation

$$X_2 - X_1 = \frac{1}{F}\int_0^{V_R} R\, p^2\, dV \qquad \text{(A-3)}$$

The abscissas are fractional conversions and the parameter temperature. A separate curve is given for each value of n°_{NO}.

Tabulated values are given by Jaffer (*7*). No empirical or semitheoretical equation has been found to correlate these rates, although there is evidence for strong adsorption of nitrogen dioxide in the practically zero rates at high conversions. Negative rates shown in some curves and in the tables at very high conversions reflect slight errors, of course. Such rates are, for all practical purposes, zero. The absence of a significant effect of gas-phase diffusion on this catalytic reaction has been reported by Baker *et al.* (*2*); accordingly any effect of velocity of flow has been neglected in interpreting these rate data.

Comparison of these results with those of others is difficult because conditions were not at all comparable. While the temperature range is considerably different from that used by Baker, Wong, and Hougen (*2*), their results and these seem to be consistent. For $n^\circ_{NO} = 0.003$, a conversion of 0.578, and a temperature of 60°C., the equation given by Baker, Wong, and Hougen predicts a rate of 0.000065 g. moles nitric oxide converted/(min.)(cc.) at 1 atm. An extrapolation of the present results to 60°C. yields a rate of 0.000075. The temperature dependence of this reaction is the same in direction as that observed by all previous workers. The decrease of the temperature dependence at higher temperatures conforms to the observations of Kurin and Blokh (*8*) and the theoretical treatment of Glasstone, Laidler, and Eyring (*6*).

It will be noted that for high initial nitric oxide concentrations and high conversion of nitric oxide, reaction rates at 103°C. are shown to be higher than those at 96°C. Such a reversal of the effect of temperature on the reaction has not been reported previously. No successful attempt has been made in the present investigation to explain this phenomenon; the effect is not large and occurs only at high conversion of nitric oxide.

A good verification of the method and of the accuracy of these rate data is that they can be used to reproduce by calculation the integral conversion data observed with excellent agreement. In run I-14 the measured value of X_2 was 0.00401; when one integrates Equation (A-3) with these rate data, the calculated value is 0.00412. The absolute magnitude of the rate in this calculation varied thirty-fold from entrance to exit of bed.

Multicomponent Diffusion Problems

HSIEN-WEN HSU and R. BYRON BIRD

University of Wisconsin, Madison, Wisconsin

Analysis of four three-component diffusion problems by means of the Stefan-Maxwell equations is presented. In three of these problems heterogeneous chemical reactions are occurring at a catalytic surface. Characteristic curves are presented for the better understanding of the analytical solutions. The results of one of the exact solutions are compared with those by the effective diffusion-coefficient approach.

The equations describing the diffusion in a ν-component mixture of gases are the Stefan-Maxwell equations (*1*):

$$\nabla x_i = \sum_{j=1}^{\nu} (c\,\mathcal{D}_{ij})^{-1}(x_i\vec{N}_j - x_j\vec{N}_i) \qquad i = 1, 2, \cdots, \nu \qquad (1)$$

The derivation of Equation (1) from the kinetic theory of gases has been given by Curtiss and Hirschfelder (*3*). Only $\nu - 1$ of these equations are independent because $\Sigma x_i = 1$.

Specific solutions to the Stefan-Maxwell equations have been given by Gilliland (4), Hoopes (5), Benedict and Boas (2), Keyes and Pigford (8), and Toor (10) for multicomponent systems. It is the purpose of this publication to extend the "dictionary" of solutions for steady state multicomponent diffusion, particularly those with chemical reactions involved. The latter are of course interesting in connection with the study of diffusion-controlled heterogeneous reactions.

DIFFUSION OF A THROUGH A STAGNANT FILM OF B AND C OF KNOWN AVERAGE COMPOSITION

Gas A is diffusing in steady state through a stagnant film of thickness δ, which consists of species B and C, as shown in Figure 1*a*. If no A were present, the film would contain B and C in concentration x_B° and x_C° (with $x_B^\circ + x_C^\circ = 1$). The authors select as the two independent equations those for B and C:

$$\frac{dx_B}{d\zeta} = \nu_{AB}\, x_B \tag{2}$$

$$\frac{dx_C}{d\zeta} = \nu_{AB}\, x_C \tag{3}$$

which are to be integrated with the boundary conditions: at $\zeta = 0$, $x_A = x_{A0}$, and at $\zeta = 1$, $x_A = x_{A\delta}$. Integration of Equations (2) and (3) gives the following concentration profiles:

$$x_B = \frac{(1 - x_{A0})\,\alpha_{AC} - (1 - x_{A\delta})}{(\alpha_{AC} - \alpha_{AB})}\,\alpha_{AB}{}^{\zeta} \tag{4}$$

$$x_C = \frac{(1 - x_{A0})\,\alpha_{AB} - (1 - x_{A\delta})}{(\alpha_{AB} - \alpha_{AC})}\,\alpha_{AC}{}^{\zeta} \tag{5}$$

in which $\alpha_{ij} = \exp\,[N_A\,\delta/c\,\mathcal{D}_{ij}]$ and $\zeta = z/\delta$.

An expression for $\vec{N}_A$ in terms of x_{A0}, $x_{A\delta}$, x_B°, and $r = \mathcal{D}_{AB}/\mathcal{D}_{AC}$ may be obtained by calculating x_B° from the above concentration profiles:

$$x_B^\circ = \frac{\int_0^\delta x_B\, dz}{\int_0^\delta (x_B + x_C)\, dz} \tag{6}$$

Inserting Equations (4) and (5) and performing the integrations one gets

$$x_B^\circ = \left[\; 1 - \frac{1}{r}\left(\frac{\alpha_{AB}{}^r - 1}{\alpha_{AB}{}^r - Q}\right)\left(\frac{\alpha_{AB} - Q}{\alpha_{AB} - 1}\right)\;\right]^{-1} \tag{7}$$

in which $Q = (1 - x_{A\delta})/(1 - x_{A0})$.

Equation (7) has been used to calculate the values of α_{AB} in terms of Q, x_B°, and r by an IBM 650 digital computer. The results are presented in graphical form in Figure 2 and in tabular form in Table 1*. The tabulated values of α_{AB} are reported to five significant figures with the range of $Q = 1.2 \rightarrow 80$, $r = 0.10 \rightarrow 0.95$ with 0.10 intervals to 0.90, and $x_B^\circ = 0.00 \rightarrow 1.00$ with 0.05 intervals. From this table the mass transfer rate can be calculated. This table has been used by Huebner in connection with studies on psychrometry in three-component systems (7).

It can be seen both from the table and the figure that α_{AB} increases with increasing Q, with decreasing r, and with decreasing x_B°.

DIFFUSION OF A THROUGH A STAGNANT FILM OF B TO FORM A_n AT A CATALYTIC SURFACE

Gas A is diffusing in steady state through a stagnant film of B to a catalytic surface, where A disappears by an irreversible chemical reaction of order h (see Figure 1*b*). The surface reaction whereby A disappears may be described stoichiometrically as

$$nA \rightarrow A_n \tag{8}$$

Note that n and h do not necessarily have to be the same. Values of $n = 2, 3, 4 \ldots$ correspond to polymerization reactions, whereas values of $n = 1/2, 1/3, 1/4, \ldots$ correspond to depolymerization at the catalytic surface. The relative molar fluxes are determined by the stoichiometry of the reaction (and not by the order of the chemical reaction); that is $N_A = -nN_{A_n}$. For this case the Stefan-Maxwell equations for A and B are

$$\frac{1}{\nu_{A_nB}} \cdot \frac{dx_A}{d\zeta} = r_{A_n}\left(1 - \frac{1}{n}\right) x_A + (r_{A_n} - r_B)x_B - r_{A_n} \tag{9}$$

$$\frac{1}{\nu_{A_nB}} \cdot \frac{dx_B}{d\zeta} = \left(r_B - \frac{1}{n}\right) x_B \tag{10}$$

in which $\nu_{A_nB} = [N_A\delta/c\,\mathcal{D}_{A_nB}]$, $r_B = \mathcal{D}_{A_nB}/\mathcal{D}_{AB}$, and $r_{A_n} = \mathcal{D}_{A_nB}/\mathcal{D}_{AA_n}$. These equations may be integrated with the boundary conditions that $x_A = x_{A0}$ and $x_B = x_{B0}$ at $\zeta = 0$. The integration of the x_B equation is done first; the result is then substituted into Equation (9), and the resulting first-order linear differential equation is integrated:

$$x_B = x_{B0} \exp\,[R\,\nu_{A_nB}\,\zeta] \tag{11}$$

$$x_A = [x_{A0} - N^{-1} + M^{-1}x_{B0}] \exp\,[Nr_{A_n}\,\nu_{A_nB}\,\zeta] + N^{-1} - M^{-1}\,x_{B0} \exp\,[R\,\nu_{A_nB}\,\zeta] \tag{12}$$

in which

$$N = 1 - \frac{1}{n},\quad M = 1 - \frac{1}{n}\left(\frac{1 - r_{A_n}}{r_B - r_{A_n}}\right),$$

$$\text{and}\quad R = r_B - \frac{1}{n} \tag{13 a, b, c}$$

The condition that there be an hth order reaction at the catalytic surface is that at $\zeta = 1$

$$N_A = k_h\,x_A{}^h \quad \text{or} \quad \nu_{A_nB} = K\,x_A{}^h \tag{14}$$

where $K = [k_h\,\delta/c\,\mathcal{D}_{A_nB}]$. Applying this condition to Equation (12) one gets the following transcendental equation for ν_{A_nB}:

$$\sqrt[h]{\frac{\nu_{A_nB}}{K}} = [x_{A0} - N^{-1} + M^{-1}\,x_{B0}] \cdot \exp\,(N\,r_{A_n}\,\nu_{A_nB}) + N^{-1} - M^{-1}\,x_{B0} \cdot \exp\,(R\,\nu_{A_nB}) \tag{15}$$

Equations (12) and (15) do not hold for several special cases. For these cases the mass transfer rate ν_{A_nB} is calculated from the following formulas:

Case I

$r_{A_n} = r_B$; the binary diffusivities $\mathcal{D}_{AA_n}$ and $\mathcal{D}_{AB}$ are equal. In this case the $(r_{A_n} - r_B)x_B$ term in Equation (9) disappears, and the solution is independent of the concentration x_{B0} at the outer edge of the film:

$$\nu_{A_nB} = \frac{1}{Nr_{A_n}} \ln \frac{1 - N\sqrt[h]{\nu_{A_nB}/K}}{1 - Nx_{A0}} \tag{16}$$

Case II

$n = 1$; a unimolecular rearrangement is taking place at the catalytic surface. In this case the $r_{A_n}(1 - 1/n)x_A$ term in Equation (9) disappears, and the solution gives

$$\sqrt[h]{\frac{\nu_{A_nB}}{K}} = x_{A0} - \left(\frac{r_B - r_{A_n}}{r_B - 1}\right) \cdot x_{B0}\{\exp[\nu_{A_nB}(r_B - 1)] - 1\} - r_{A_n}\,\nu_{A_nB} \tag{17}$$

Case III

$nr_B - 1 = r_{A_n}(n - 1)$; in this special case the solution is

$$\sqrt[h]{\frac{\nu_{A_nB}}{K}} = \left[\; x_{A0} - N^{-1} + x_{B0}\left(\frac{r_B - 1}{n - 1}\right)\nu_{A_nB}\;\right] \cdot \exp\,(R\,\nu_{A_nB}) + N^{-1} \tag{18}$$

* Tabular material has been deposited as document 6266 with the American Documentation Institute, Photoduplication Service, Library of Congress, Washington 25, D. C., and may be obtained for $7.50 for photoprints or $2.75 for 35-mm. microfilm.

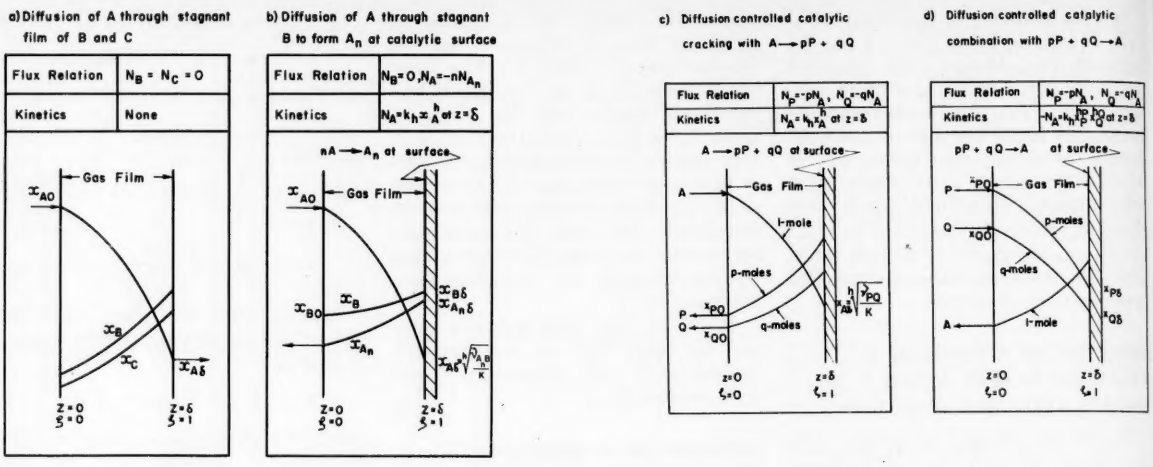

Fig. 1. Three component diffusion problems.

Equations (15), (16), and (18) have been used to tabulate ν_{A_nB} for various values of n, r_B, r_{A_n}, x_{A0}, and x_{B0} for $K = \infty$ by an IBM 650 digital computer. The results are presented in tabular form in Table 2*, and some of the characteristic results are plotted in Figure 3. The tabulated results are reported to four significant figures with the following parameters:

$n = 2, 3, 4, 1/2, 1/3, 1/4$
$r_{A_n}, r_B = 0.4, 0.8, 1.2, 2.0, 4.0, 6.0$
$x_{A0} = 0.3, 0.4, 0.5, 0.6, 0.7$
$x_{B0} = 0.1, 0.2, 0.3, 0.4$

In Figure 3 ν_{A_nB} is plotted against r_{A_n} for the following cases:

$n = 2$, $x_{A0} = 0.3$, $x_{B0} = 0.1$: for various values of r_B

$n = 2$, $x_{A0} = 0.3$, $r_B = 1.2$: for various values of x_{B0}

$n = 2$, $x_{B0} = 0.1$, $r_B = 0.4$: for various values of x_{A0}

$x_{A0} = 0.3$, $x_{B0} = 0.1$, $r_B = 0.4$: for various values of n

This figure shows the dependence of ν_{A_nB} on the main variables.

DIFFUSION-CONTROLLED CATALYTIC CRACKING WITH A → pP + qQ

Substance A diffuses through a gas film of thickness δ containing A, and the reaction products (see Figure 1c). At the catalytic surface A disappears by an irreversible chemical reaction of order h. Stoichiometrically the reaction is represented by the cracking reaction:

$$A \rightarrow pP + qQ \qquad (19)$$

The relative molar fluxes are determined by the stoichiometry (and not by the order of the reaction); that is, $pN_A = -N_P$ and $qN_A = -N_Q$. For this problem the Stefan-Maxwell equations for components P and Q are

$$\frac{1}{\nu_{PQ}} \cdot \frac{dx_P}{d\zeta} = A_P x_P + B_P x_Q + C_P \qquad (20)$$

$$\frac{1}{\nu_{PQ}} \cdot \frac{dx_Q}{d\zeta} = A_Q x_Q + B_Q x_P + C_Q \qquad (21)$$

in which

$$A_P = (1-p)r_P - q, \quad B_P = (1-r_P)p,$$
$$\text{and} \quad C_P = pr_P \qquad (22\,a, b, c)$$

and

$$r_P = \frac{\mathcal{D}_{PQ}}{\mathcal{D}_{AP}} \quad \text{and} \quad r_Q = \frac{\mathcal{D}_{PQ}}{\mathcal{D}_{AQ}} \qquad (22\,d, e)$$

The quantities A_Q, B_Q, and C_Q are defined analogously by interchanging all p and q and P and Q. Equations (20) and (21) are to be solved with the boundary conditions that at $\zeta = 0$, $x_P = x_{P0}$ and $x_Q = x_{Q0}$.

When the (s multiplied) Laplace transform of both equations is taken, two algebraic equations result, which may be solved for the transform functions $\bar{x}_P(s)$ and $\bar{x}_Q(s)$:

$$\bar{x}_P(s) = \frac{[x_{P0}]s^2 + [-A_Q x_{P0} + B_P x_{Q0} + C_P]s + [B_P C_Q - C_P A_Q]}{s^2 - [A_P + A_Q]s + [A_P A_Q - B_P B_Q]} \qquad (23)$$

and an analogous expression for $\bar{x}_Q(s)$ obtained by interchanging all p and q and all P and Q.

In order for Equation (23) to be inverted, the denominator has to be factored into $(s - s_+)(s - s_-)$, in which

$$s_\pm = \frac{1}{2}\left[(A_P + A_Q) \pm \sqrt{(A_P - A_Q)^2 + 4\,B_P B_Q}\,\right] \qquad (24)$$

One now has to consider three cases, namely $s_+ \neq s_-$, $s_+ = s_- = s_0$, and $s_+ = s_0$ when $s_- = 0$.

Case 1

Unequal roots, $s_+ \neq s_-$ In this case the inversion of Equation (23) yields

$$x_P(\zeta) = \frac{1}{(s_+ - s_-)}\left\{\begin{array}{c}[x_{P0}][s_+ \exp(s_+ \nu_{PQ}\zeta) \\ - s_- \exp(s_- \nu_{PQ}\zeta)] + [-A_Q x_{P0} \\ + B_P x_{Q0} + C_P][\exp(s_+ \nu_{PQ}\zeta) \\ - \exp(s_- \nu_{PQ}\zeta)] + [B_P C_Q - C_P A_Q] \\ \cdot\left[\dfrac{\exp(s_+ \nu_{PQ}\zeta) - 1}{s_+}\right. \\ \left. - \dfrac{\exp(s_- \nu_{PQ}\zeta) - 1}{s_-}\right]\end{array}\right\} \qquad (25)$$

with a similar expression for $\bar{x}_Q(\zeta)$. The condition that there be an hth-order reaction at the catalytic surface which is similar to Equations (14) is that at $\zeta = 1$

$$N_A = k_h x_A^h \quad \text{or} \quad \nu_{PQ} = K_h x_A^h \qquad (26)$$

where $K_h = [k_h \delta / c\,\mathcal{D}_{PQ}]$. Thus when

* See footnote on page 517.

one sets $x_P + x_Q = 1 - x_A$ at $\zeta = 1$, one obtains

$$[Xs_+ + Y + Zs_+^{-1}]\exp(s_+\nu_{PQ}) - [Xs_- + Y + Zs_-^{-1}]\exp(s_-\nu_{PQ}) = (s_+ - s_-)\left[1 - \frac{Z}{s_+s_-} - \sqrt[h]{\nu_{PQ}/K_h}\right] \quad (27)$$

in which

$$X = x_{P0} + x_{Q0} \quad (28)$$

$$Y = x_{P0}(p + q - r_Q) + x_{Q0} \cdot (p + q - r_P) + (pr_P + qr_Q) \quad (29)$$

$$Z = pq(r_P + r_Q) - r_Pr_Q(p + q) + (p^2r_P + q^2r_Q) \quad (30)$$

$$s_\pm = \frac{1}{2}\left\{ \frac{(1-p)r_P + (1-q)r_Q - (p+q)}{\pm\sqrt{\{(1-p)r_P - (1-q)r_Q + (p-q)\}^2 + 4pq\,(1-r_P)(1-r_Q)}} \right\} \quad (31)$$

[Equation (31) is the simplified form of Equation (24).]

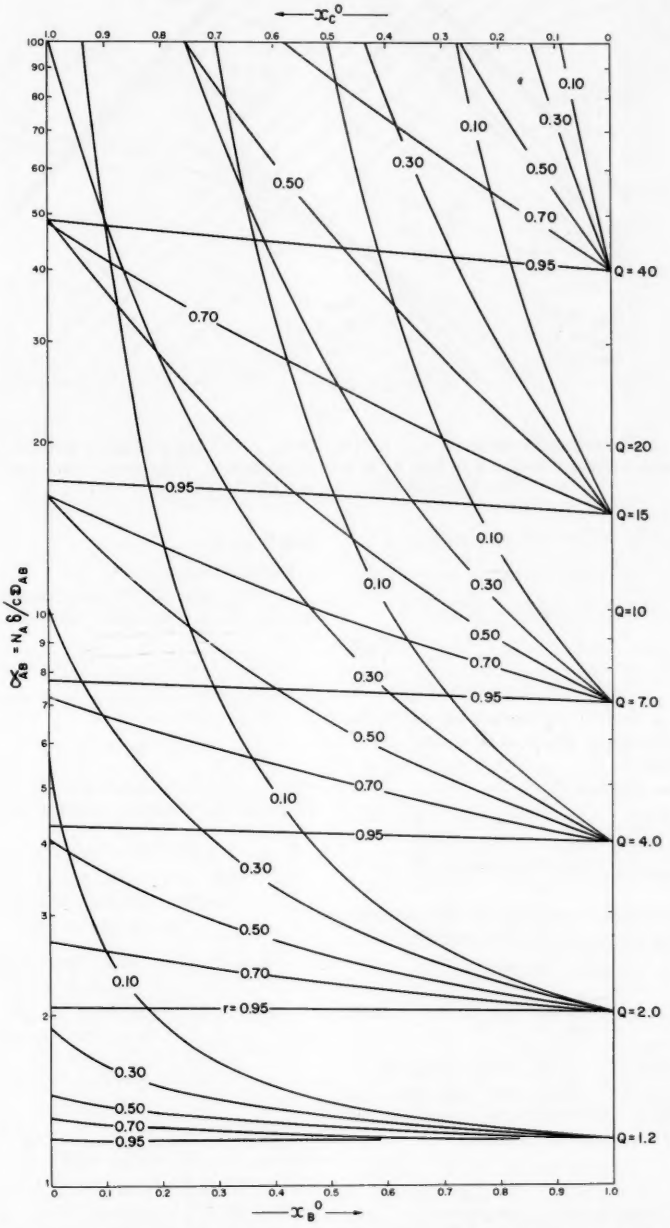

Fig. 2. The calculated values of $\alpha_{AB} = \exp[N_A\,\delta/c\,\mathcal{D}_{AB}]$ for the problem of diffusion of *A* through stagnant *B* and *C*. These curves were calculated from Equation (7). To find a value of α_{AB}, first select the value of *Q* at the right of the chart and the curve appropriate for a given value of *r*. Then move along this curve to the left until the value of x_B^0 is located. For example for $Q = 2$, $r = 0.3$, $x_B^0 = 0.5$, one finds that $\alpha_{AB} = 2.95$.

Case II

Equal roots, $s_+ = s_- = s_e$

In this case the inversion of Equation (23) leads to

$$x_P(\zeta) = [x_{P0}]\,[1 + s_e\,\nu_{PQ}\,\zeta] \cdot \exp(s_e\,\nu_{PQ}\,\zeta) + [-A_Qx_{P0} + B_Px_{Q0} + C_P]\,\nu_{PQ}\zeta\exp(s_e\,\nu_{PQ}\,\zeta) + [B_PC_Q - C_PA_Q](s_e\,\nu_{PQ})^{-2}[s_e\,\nu_{PQ}\,\zeta\exp(s_e\,\nu_{PQ}\,\zeta) - \exp(s_e\,\nu_{PQ}\,\zeta) + 1] \quad (32)$$

with a similar expression for $x_Q(\zeta)$. Then application of the conditions that $x_P + x_Q = 1 - x_A$ at $\zeta = 1$ gives

$$[X + Ys_e^{-1} + Zs_e^{-2}]s_e\,\nu_{PQ}\exp(s_e\,\nu_{PQ}) + [X - Zs_e^{-2}]\exp(s_e\,\nu_{PQ}) = 1 - Zs_e^{-2} - \sqrt[h]{\nu_{PQ}/K_h} \quad (33)$$

in which *X*, *Y*, *Z* are defined in Equations (28) to (30) and $s_e = (1/2) \cdot [(1-p)r_P + (1-q)r_Q - (p+q)]$.

Case III

One root is zero; $s_\pm = s_0$ when $s_\mp = 0$

In this case the inversion of Equation (23) gives

$$x_P(\zeta) = [x_{P0}]\exp(s_0\,\nu_{PQ}\,\zeta) + [-A_Qx_{P0} + B_Px_{Q0} + C_P]s_0^{-1} \cdot [\exp(s_0\,\nu_{PQ}\,\zeta) - 1] + [B_PC_Q - C_PA_Q]s_0^{-2}[\exp(s_0\,\nu_{PQ}\,\zeta) - 1 - s_0\,\nu_{PQ}\,\zeta] \quad (34)$$

with a similar expression for $x_Q(\zeta)$. At $\zeta = 1$ it is known that $x_P + x_Q = 1 - x_A$, so that

$$[X + Ys_0^{-1} + Zs_0^{-2}]\exp(s_0\,\nu_{PQ}) - Zs_0^{-1}\,\nu_{PQ} = [1 + Ys_0^{-1} + Zs_0^{-2}] - \sqrt[h]{\nu_{PQ}/K_h}$$

in which *X*, *Y*, *Z* are defined in Equation (28) to (30) and $s_0 = (1-p)r_P + (1-q)r_Q - (p+q)$.

Equations (27), (33), and (35) have been used to tabulate ν_{PQ} for various values of p, q, x_{P0}, x_{Q0}, r_P, and r_Q for $K = \infty$ by an IBM 650 digital computer. The results are presented in tabular form in Table 3*, and some

* See footnote on page 517.

of the characteristic results are plotted in Figure 4. The tabulated data are reported to four significant figures with the following parameters:

$p, q = 1, 2$
$r_P, r_Q = 1.0, 1.5, 3.0, 4.5, 6.0$
$x_{P0} = 0.2, 0.3, 0.4, 0.5, 0.6, 0.7$
$x_{Q0} = 0.2, 0.3, 0.4$

In Figure 4 the values of ν_{PQ} are plotted against r_Q for the following cases: $p = 1$, $q = 1$, $r_P = 1.5$, $x_{Q0} = 0.2$: for various values of x_{P0}; $p = 1$, $q = 1$, $x_{P0} = 0.2$, $x_{P0} = 0.2$: for various values of x_P; $x_{P0} = 0.2$, $x_{Q0} = 0.2$, $r_P = 6.0$: for various values of p and q.

DIFFUSION-CONTROLLED CATALYTIC COMBINING WITH pP + qQ → A

Species P and Q are diffusing through a gas film of thickness δ, containing P and Q and the reaction product, toward a catalytic surface on which the $(h_P + h_Q)$ order irreversible chemical reaction occurs, as shown in Figure 1*d*:

$$pP + qQ \rightarrow A \qquad (36)$$

Thus the Stefan-Maxwell equations for components P and Q with the stoichiometric requirements and the boundary conditions are exactly the same as the problem of $A \rightarrow pP + qQ$ discussed previously [that is, the Stefan-Maxwell equations are Equations (20) and (21), and the boundary conditions are $x_P = x_{P0}$ and $x_Q = x_{Q0}$ at $\zeta = 0$]. Therefore the solutions of $x_P(\zeta)$ and $x_Q(\zeta)$ are exactly the same as $A \rightarrow pP + qQ$ problem. Similarly, there are also three cases which have to be considered, namely $s_+ \neq s_-$, $s_+ = s_- = s_e$, and $s_\pm = s_0$ when $s_\mp = 0$.

Case I

Unequal roots, $s_+ \neq s_-$

In this case $x_P(\zeta)$ can be rewritten from Equation (25):

$$x_P(\zeta) = \frac{1}{s_+ - s_-}$$

$$\{[X_P s_+ + Y_P + Z_P s_+^{-1}]\exp(s_+ \nu_{PQ}\,\zeta)$$

$$-[X_P s_- + Y_P + Z_P s_-^{-1}]\exp(s_- \nu_{PQ}\,\zeta)\}$$

$$+ \frac{Z_P}{s_+ s_-} \qquad (37)$$

in which

$$X_P = x_{P0} \qquad (38)$$

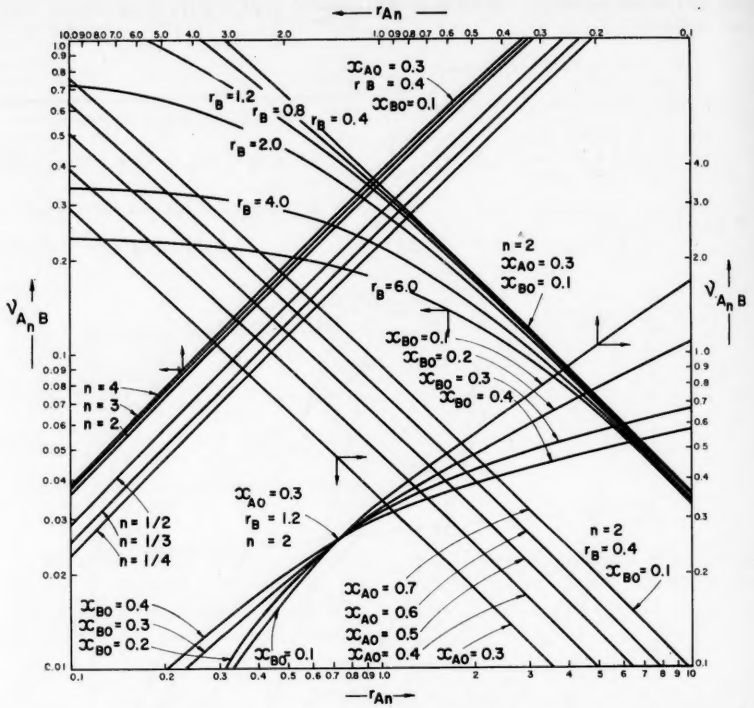

Fig. 3. The calculated values of $\nu_{A_nB} = [N_A\,\delta/c\mathcal{D}_{A_nB}]$ for the problem of diffusion of A through a stagnant film of B to form A_n at a catalytic surface. These curves were calculated from Equations (15), (16), and (18) for $K = \infty$.

$$Y_P = [p - (1-q)r_Q]x_{P0} + p(1-r_P)x_{Q0} + pr_P \qquad (39)$$

$$Z_P = pq(1-r_P)r_Q - pr_P[(1-q)r_Q - p] \qquad (40)$$

$s_\pm$ is defined in Equation (31) with a similar expression for $x_Q(\zeta)$ by interchanging all p and q and all P and Q.

One may see that

Equation (28) $X = X_P + X_Q$
Equation (29) $Y = Y_P + Y_Q$
Equation (30) $Z = Z_P + Z_Q$

The kinetic equation at the catalytic surface ($\zeta = 1$) for this problem is

$$-N_A = k_h\, x_P^{h_P}\, x_Q^{h_Q}$$

$$\text{or} \quad -\frac{\nu_{PQ}}{K_h} = x_P^{h_P}\, x_Q^{h_Q} \qquad (41)$$

in which $k_h = k_P/p = k_Q/q$ and $K_h = [k_h\,\delta/c\mathcal{D}_{PQ}]$. Thus one will get the following transcendental equation of ν_{PQ} at the catalytic surface:

$$h_P \ln\left[\frac{1}{s_+ - s_-}\left[\begin{array}{c}[X_P s_+ + Y_P + Z_P s_+^{-1}]\exp(s_+ \nu_{PQ}) \\ -[X_P s_- + Y_P + Z_P s_-^{-1}]\exp(s_- \nu_{PQ})\end{array}\right] + \frac{Z_P}{s_+ s_-}\right]$$

$$+ h_Q \ln\left[\frac{1}{s_+ - s_-}\left[\begin{array}{c}[X_Q s_+ + Y_Q + Z_Q s_+^{-1}]\exp(s_+ \nu_{PQ}) \\ -[X_Q s_- + Y_Q + Z_Q s_-^{-1}]\exp(s_- \nu_{PQ})\end{array}\right] + \frac{Z_Q}{s_+ s_-}\right]$$

$$- \ln[-\nu_{PQ}/K_h] = 0 \qquad (42)$$

Case II

Equal roots, $s_+ = s_- = s_e$

In this case $x_P(\zeta)$ may also be rewritten from Equation (32):

$$x_P(\zeta) = [X_P - Z_P s_e^{-2}]\exp(s_e \nu_{PQ}\,\zeta) + Z_P s_e^{-2} + [X_P + Y_P s_e^{-1} + Z_P s_e^{-2}]\, s_e \nu_{PQ}\,\zeta \exp(s_e \nu_{PQ}\,\zeta) \qquad (43)$$

with a similar expression for $x_Q(\zeta)$. Thus at the catalytic surface one gets

$$h_P \ln\left[\begin{array}{c}[X_P - Z_P s_e^{-2}]\exp(s_e \nu_{PQ}) \\ + Z_P s_e^{-2} \\ +[X_P + Y_P s_e^{-1} + Z_P s_e^{-2}] \\ \cdot\, s_e \nu_{PQ} \exp(s_e \nu_{PQ})\end{array}\right]$$

$$+ h_Q \ln\left[\begin{array}{c}[X_Q - Z_Q s_e^{-2}]\exp(s_e \nu_{PQ}) \\ + Z_Q s_e^{-2} \\ + [X_Q + Y_Q s_e^{-1} + Z_Q s_e^{-2}] \\ \cdot\, s_e \nu_{PQ} \exp(s_e \nu_{PQ})\end{array}\right]$$

$$- \ln[-\nu_{PQ}/K_h] = 0 \qquad (44)$$

in which X_P, X_Q, Y_P, Y_Q, Z_P, and Z_Q are defined in Equations (38) to (40), and $s_e = (\frac{1}{2})[(1-p)r_P + (1-q)r_Q - (p+q)]$.

Case III

One root is zero, $s_\pm = s_0$ when $s_\mp = 0$

In this case $x_P(\zeta)$ is rewritten from Equation (34):

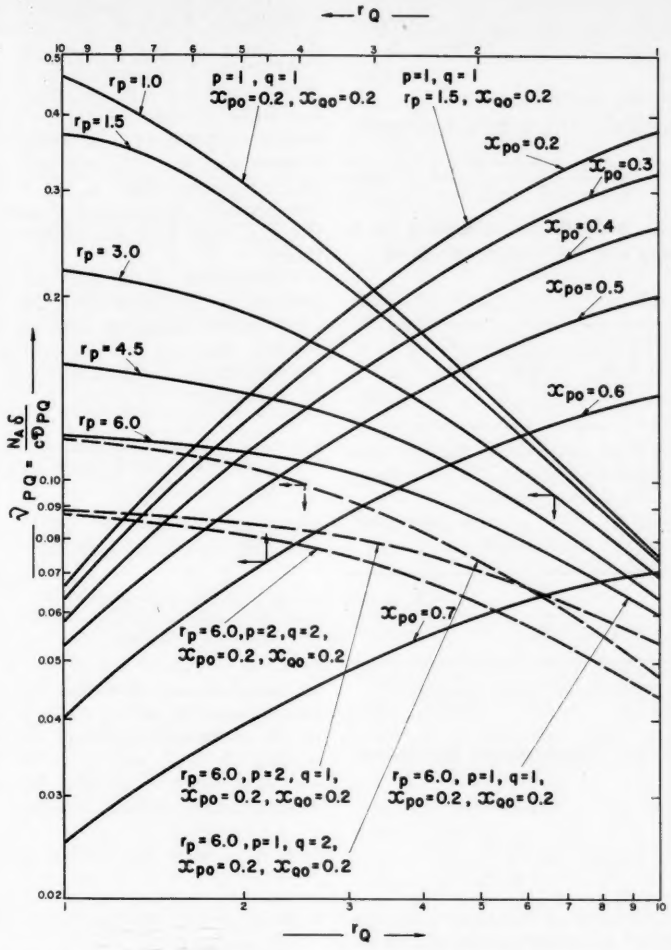
r_Q
r_p = 1.0
p = 1 , q = 1
x_{po} = 0.2 , x_{Qo} = 0.2
p = 1, q = 1
r_p = 1.5, x_{Qo} = 0.2
r_p = 1.5
x_{po} = 0.2
x_{po} = 0.3
x_{po} = 0.4
r_p = 3.0
x_{po} = 0.5
r_p = 4.5
x_{po} = 0.6
r_p = 6.0
$\nu_{PQ} = \frac{N_A \delta}{c \mathcal{D}_{PQ}}$
x_{po} = 0.7
r_p = 6.0, p = 2, q = 2,
x_{po} = 0.2, x_{Qo} = 0.2
r_p = 6.0, p = 2, q = 1,
x_{po} = 0.2, x_{Qo} = 0.2
r_p = 6.0, p = 1, q = 1,
x_{po} = 0.2, x_{Qo} = 0.2
r_p = 6.0, p = 1, q = 2,
x_{po} = 0.2, x_{Qo} = 0.2
r_Q

Fig. 4. The calculated values of $\nu_{PQ} = [N_A \delta/c\mathcal{D}_{PQ}]$ for the problem of diffusion-controlled catalytic cracking with $A \rightarrow pP + qQ$. These curves were calculated from Equations (27), (33), and (35) for $K = \infty$.

$$x_P(\zeta) = [X_P + Y_P s_0^{-1} + Z_P s_0^{-2}] \exp(s_0 \nu_{PQ} \zeta) - Z_P s_0^{-1} \nu_{PQ} \zeta - Y_P s_0^{-1} - Z_P s_0^{-2} \quad (45)$$

with a similar expression for $x_Q(\zeta)$. Then at the catalytic surface one obtains

$$h_P \ln \left[\begin{array}{c} [X_P + Y_P s_0^{-1} + Z_P s_0^{-2}] \\ \cdot \exp(s_0 \nu_{PQ}) \\ - Z_P s_0^{-1} \nu_{PQ} - Y_P s_0^{-1} - Z_P s_0^{-2} \end{array} \right] + h_Q \ln \left[\begin{array}{c} [X_Q + Y_Q s_0^{-1} + Z_Q s_0^{-2}] \\ \cdot \exp(s_0 \nu_{PQ}) \\ - Z_Q s_0^{-1} \nu_{PQ} - Y_Q s_0^{-1} - Z_Q s_0^{-2} \end{array} \right] - \ln [-\nu_{PQ}/K_h] = 0 \quad (46)$$

in which X_P, X_Q, Y_P, Y_Q, Z_P, and Z_Q are defined in Equations (38) to (40), and $s_0 = (1 - p)r_P + (1 - q)r_Q - (p + q)$.

Equation (42), (44), and (46) are to be used for the calculation of ν_{PQ} for the various values of p, q, and x_{Po}, x_{Qo}, r_P, r_Q, and K_h.

It is important to note that the values of $x_P(\delta)$ and $x_Q(\delta)$ can be evaluated from the value of ν_{PQ}. These values of $x_P(\delta)$ and $x_Q(\delta)$ determine which of the following conditions holds at the catalytic surface:

(i) $qx_{Ps} - px_{Qs} = 0$
no excess reactant at the catalytic surface

(ii) $qx_{Ps} - px_{Qs} > 0$
xP is the excess reactant at the catalytic surface

(iii) $qx_{Ps} - px_{Qs} < 0$
xQ is the excess reactant at the catalytic surface

When $K_h = \infty$, Equations (42), (44), and (46) do not hold. For this case a special consideration has to be made for the calculation of ν_{PQ} because Equation (41) becomes

$$x_P^{h_P} x_Q^{h_Q} = 0 \quad (47)$$

Hence one cannot tell whether $x_P = 0$ or $x_Q = 0$ at the catalytic surface. In this case one may arbitrarily select $x_P(\delta) = 0$ and proceed with the calculation of ν_{PQ}. Then after the calculation one has to substitute this ν_{PQ} into the expression for $x_Q(\delta)$ to verify its sign, for $x_Q(\delta)$ cannot be a negative value. If by using the ν_{PQ} obtained from $x_P(\delta) = 0$ one gets $x_Q(\delta) < 0$, then it is obvious that the assumption made (that is $x_P(\delta) = 0$) is incorrect and that instead one has to use $x_Q(\delta) = 0$ for the calculation of ν_{PQ}.

In other words if one obtained $x_Q(\delta) = 0$ by use of the ν_{PQ} calculated from $x_P(\delta) = 0$, it is seen that this is case (i), in which there is no excess reactant at the catalytic surface. If $x_Q(\delta) > 0$, this is the case (iii), where x_Q is the excess reactant at the catalytic surface. If $x_Q(\delta) < 0$, this is the case (ii). It is obvious that x_Q is the limiting reactant; thus one has to use $x_Q(\delta) = 0$ for the calculation of ν_{PQ}.

There are also three cases, the same as previous ones, which have to be considered when $K_h = \infty$, namely, $s_+ \neq s_-$, $s_+ = s_- = s_e$, and $s_\pm = s_0$ when $s_\mp = 0$.

Case I

Unequal roots, $s_+ \neq s_-$

The transcendental equation of ν_{PQ} at the catalytic surface is

$$[X_P s_+ + Y_P + Z_P s_+^{-1}] \exp(s_+ \nu_{PQ}) + Z_P (s_+ - s_-) s_+^{-1} s_-^{-1} = [X_P s_- + Y_P + Z_P s_-^{-1}] \exp(s_- \nu_{PQ}) \quad (48)$$

Case II

Equal roots, $s_+ = s_- = s_e$

In this case at the catalytic surface one obtains

$$[X_P - Z_P s_e^{-2}] \exp(s_e \nu_{PQ}) + Z_P s_e^{-2} + [X_P + Y_P s_e^{-1} + Z_P s_e^{-2}] \cdot s_e \nu_{PQ} \exp(s_e \nu_{PQ}) = 0 \quad (49)$$

Case III

One root is zero, $s_\pm = s_0$ when $s_\mp = 0$

In this case at the catalytic surface one will obtain

$$[X_P + Y_P s_0^{-1} + Z_P s_0^{-2}] \exp(s_0 \nu_{PQ}) - Z_P s_0^{-1} \nu_{PQ} = [Y_P + Z_P s_0^{-1}] s_0^{-1} \quad (50)$$

Equations (48), (49), and (50) hold only with the condition that the substitution of ν_{PQ}, which is calculated from one of these equations, to $x_Q(\delta)$ gives $x_Q(\delta) \geq 0$. Otherwise, with similar expressions for the above three equations obtained by interchanging, all p and q and all P and Q have to be used for the calculation of ν_{PQ}.

METHODS OF USING EFFECTIVE DIFFUSIVITY

In this section the authors compare the results of diffusion-controlled cata-

lytic cracking with $A \rightarrow pP + qQ$ with those obtained by using an effective diffusivity and the usual binary formulas. Such methods have previously been proposed by Hougen and Watson (6), Wilke (11), and Stewart (9). The method used here is essentially that of Stewart but written up in a form similar to the development given by Hougen and Watson so that comparison between the various approaches can be made. The authors suggest a method of modifying the effective-diffusivity approach by allowing the effective diffusivity to vary linearly with either composition or distance.

$$\mathcal{D}_{Am} = \frac{1 - \Xi_A}{\left[\frac{x_B}{\mathcal{D}_{AB}} + \frac{x_P}{\mathcal{D}_{AP}} + \frac{x_Q}{\mathcal{D}_{AQ}} + \frac{x_I}{\mathcal{D}_{AI}} - \frac{x_A}{a}\left(\frac{b}{\mathcal{D}_{AB}} - \frac{p}{\mathcal{D}_{AP}} - \frac{q}{\mathcal{D}_{AQ}}\right)\right]} \tag{56}$$

Assumption of Constant Effective Diffusivity

For the general gaseous reaction $aA + bB \rightleftharpoons pP + qQ$ proceeding in contact with a solid catalyst in the presence of an inert gas I the stoichiometric requirements are

$$N_B = (b/a)N_A, \quad N_P = -(p/a)N_A, \text{ and}$$

$$N_Q = -(q/a)N_A \quad (51\,a, b, c)$$

Hence the Stefan-Maxwell equation for component A is

$$-\frac{dx_A}{dz} = \frac{N_A}{c}\left[\frac{x_B}{\mathcal{D}_{AB}} + \frac{x_P}{\mathcal{D}_{AP}} + \frac{x_Q}{\mathcal{D}_{AQ}} + \frac{x_I}{\mathcal{D}_{AI}} - \frac{x_A}{a}\left(\frac{b}{\mathcal{D}_{AB}} - \frac{p}{\mathcal{D}_{AP}} - \frac{q}{\mathcal{D}_{AQ}}\right)\right] \tag{52}$$

Thus the expression for N_A becomes

$$N_A = -c\left[\frac{x_B}{\mathcal{D}_{AB}} + \frac{x_P}{\mathcal{D}_{AP}} + \frac{x_Q}{\mathcal{D}_{AQ}} + \frac{x_I}{\mathcal{D}_{AI}} - \frac{x_A}{a}\left(\frac{b}{\mathcal{D}_{AB}} - \frac{p}{\mathcal{D}_{AP}} - \frac{q}{\mathcal{D}_{AQ}}\right)\right]^{-1}\frac{dx_A}{dz} \tag{53}$$

Thus far no assumptions have been made, except that the system consists of ideal gases at constant temperature and pressure.

Next Equation (53) can be rewritten in an alternative form simply for the purpose of obtaining a relation which resembles the expression for binary diffusion of A into stagnant I in a two-component system:

$$N_A = -(c\,\mathcal{D}_{Am})(1 - \Xi_A x_A)^{-1}\frac{dx_A}{dz} \tag{54}$$

In this expression

$$\Xi_A = [N_A + N_B + N_P + N_Q]\,N_A^{-1} = \frac{a + b - p - q}{a} \tag{55}$$

and $\mathcal{D}_{Am}$ is an effective diffusivity for A diffusing into the mixture, given by

It should be emphasized that the step from Equation (53) to (54) is nothing more than a rearrangement.

Equation (54) is next integrated with respect to z to give

$$N_A = (c\,\mathcal{D}_{Am})\delta^{-1}(x_{A0} - x_{A\delta})(x_f)_A^{-1} \tag{57}$$

in which x_f for component A is defined as

$$(x_f)_A = \Xi_A(x_{A0} - x_{A\delta}) \cdot \left\{\ln\frac{1 - \Xi_A x_{A\delta}}{1 - \Xi_A x_{A0}}\right\}^{-1} \tag{58}$$

The integration of Equation (54) was performed by assuming that $\mathcal{D}_{Am}$ is independent of composition and hence of position. This assumption is clearly made just to effect a simplification.

Equation (57) is the same result which Stewart has given. For B, P, and Q stationary Equation (57) reduces to the result of Wilke; also Equation (56) is then his expression for effective diffusivity. Note, however, that Wilke's expression for diffusivity is the same as that in equation (17) of Hougen and Watson if all their $\mathcal{D}_{ij}$ are replaced by $\mathcal{D}_{ij}^{-1}$. Equation (57) is the same as that given by Hougen and Watson, but the $\mathcal{D}_{Am}$ used here are different from theirs.

The solution of the $A \rightarrow pP + qQ$ problem by Equations (56), (57), and (58) is now compared with the exact solution obtained previously. For this problem the $\mathcal{D}_{Am}$ of Equation (56) can be written as

$$\mathcal{D}_{Am} = \frac{(1 - \Xi_A)\mathcal{D}_{PQ}}{(x_P + p\,x_A)r_P + (x_Q + q\,x_A)r_Q} \tag{59}$$

Then from Equations (57), (58), and (59) ν_{PQ} can be obtained:

$$\nu_{PQ} = \frac{N_A\delta}{c\mathcal{D}_{PQ}} = \frac{[1 - \Xi_A x_A]\ln[(1 - \Xi_A x_{A0})/(1 - \Xi_A x_{A\delta})]}{\Xi_A[(x_P + px_A)r_P + (x_Q + qx_A)r_Q]} \tag{60}$$

In order to use Equation (60) the quantities x_A, x_P, and x_Q are to be taken as the arithmetic mean of the mole fraction of A, P, and Q at the inner and outer edges of the film. Hence for instantaneous surface reaction one takes x_A to be $\frac{1}{2}x_{A0}$. Further one takes x_P to be $\frac{1}{2}[x_{P0} + \{x_{P0}/(x_{P0} + x_{Q0})\}]$ and an analogous expression for x_Q; this is tantamount to assuming that the ratio of concentrations of P and Q at $z = \delta$ is exactly the same as that at $z = 0$.

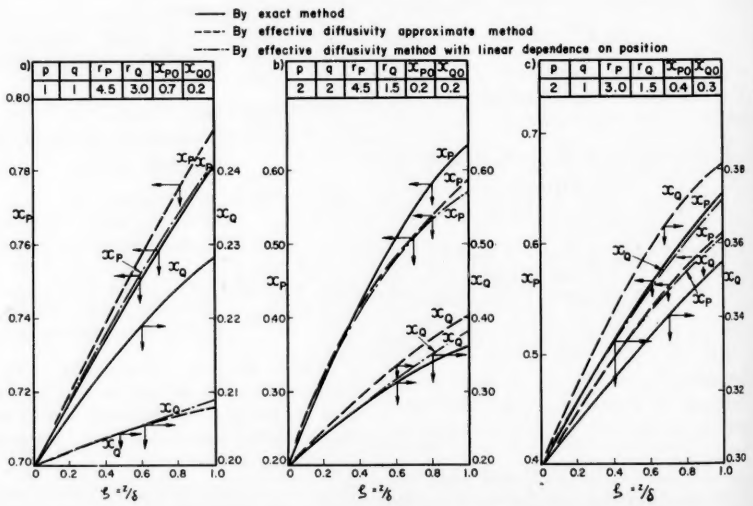
By exact method
By effective diffusivity approximate method
By effective diffusivity method with linear dependence on position
a)
b)
c)
p q rP rQ xP0 xQ0
1 1 4.5 3.0 0.7 0.2
2 2 4.5 1.5 0.2 0.2
2 1 3.0 1.5 0.4 0.3
ξ = z/δ

Fig. 5. Comparison of the concentration profiles for the $A \rightarrow pP + qQ$ problem (for $K = \infty$) as calculated by the exact method and by two effective diffusivity methods.

Assumption of Linear Effective Diffusivity

From Equation (56) it is known that the effective diffusivity $\mathcal{D}_{Am}$ is dependent on composition and hence on position. Hence the authors suggest a method for modifying the effective-diffusivity approach so as to make the effective diffusivity linearly dependent on either composition or distance.

Method I

$\mathcal{D}_{Am}$ linearly dependent on distance

In this case Equation (54) for the $A \rightarrow pP + qQ$ problem can be written as

$$N_A = -c\mathcal{D}_{Am0}\left[1 + \beta\left(\frac{z}{\delta}\right)\right] \cdot [1 - x_A(1-p-q)]^{-1}\frac{dx_A}{dz} \quad (61)$$

In this expression $\mathcal{D}_{Am0}$ is $\mathcal{D}_{Am}$ evaluated at $z = 0$ and is obtained from Equation (59) by replacing x_A, x_P, and x_Q by their corresponding values at $z = 0$, namely x_{A0}, x_{P0}, and x_{Q0}. The quantity β is a constant and can be expressed as follows by use of Equation (59):

$$\beta = \frac{1 - x_{A\delta}(1-p-q)}{1 - x_{A0}(1-p-q)}$$

$$\cdot \frac{r_P(x_{P0} + px_{A0}) + r_Q(x_{Q0} + qx_{A0})}{r_P(x_{P\delta} + px_{A\delta}) + r_Q(x_{Q\delta} + qx_{A\delta})} - 1 \quad (62)$$

Equation (61) is next integrated with respect to z to give

$$\nu_{PQ} = \frac{N_A\delta}{c\mathcal{D}_{PQ}} = \frac{1 - x_{A0}(1-p-q)}{[r_P(x_{P0}+px_{A0}) + r_Q(x_{Q0}+qx_{A0})](1-p-q)} \cdot \frac{\beta}{\ln(1+\beta)} \cdot \ln\left[\frac{1-x_{A\delta}(1-p-q)}{1-x_{A0}(1-p-q)}\right] \quad (63)$$

When $K_h = \infty$, $x_{A\delta} = 0$, and Equation (62) becomes

$$\beta = \frac{1}{1 - x_{A0}(1-p-q)} \cdot \frac{r_P(x_{P0} + px_{A0}) + r_Q(x_{Q0} + qx_{A0})}{x_{P\delta}(r_P - r_Q) + r_Q} - 1 \quad (64)$$

In order to make use of Equation (64) one takes $x_{P\delta} = \frac{1}{2} \cdot [x_{P0} + \{x_{P0}/(x_{P0} + x_{Q0})\}]$ provided $r_P - r_Q < 0$; when $r_P - r_Q > 0$, Equation (64) must be modified by interchanging all p and q and all P and Q. When $r_P = r_Q$, Equation (64) reduces to $\beta = 0$, and hence $\mathcal{D}_{Am} = \mathcal{D}_{Am0}$.

Method II

$\mathcal{D}_{Am}$ linearly dependent on composition

In this case an expression similar to Equation (61) can be written as

$$N_A = -c\mathcal{D}_{Am0}\left[1 + \beta\left(\frac{x_{A0} - x_A}{x_{A0}}\right)\right] [1 - x_A(1-p-q)]^{-1}\frac{dx_A}{dz} \quad (65)$$

$\mathcal{D}_{Am0}$ and β are exactly the same as defined in Method I for the case $K_h = \infty$.

Integration of Equation (65) with respect to z gives

$$\nu_{PQ} = \frac{N_A\delta}{c\mathcal{D}_{PQ}} = \frac{1 - x_{A0}(1-p-q)}{[r_P(x_{P0} + px_{A0}) + r_Q(x_{Q0} + qx_{A0})](1-p-q)} \cdot \left[\left(1 - \frac{\beta}{x_{A0}(1-p-q)}\right) \cdot \ln\left[\frac{1-x_{A\delta}(1-p-q)}{1-x_{A0}(1-p-q)}\right] - \beta\left(\frac{x_{A0} - x_{A\delta}}{x_{A0}}\right)\right] \quad (66)$$

When $\beta = 0$, Equations (63) and (66) reduce to Equation (60) which is the method of assuming constant effective diffusivity.

Discussion of Results

A few values of ν_{PQ}, calculated from Equations (60), (63), and (66), along with the corresponding exact values from Table 3, are summarized for the $A \rightarrow pP + qQ$ problem (with infinitely fast surface reaction) in Table 1. Additional comparisons are given in Table 4*.

From Table 1 one sees that an effective-diffusivity approach to a multicomponent diffusion problem gives acceptable results. The method is simple, and the formula is similar to that of the binary case. In this method the authors suggest that when the ratio of r_P to r_Q is close to unity, the constant effective-diffusivity approach is preferable; when the ratio of r_P to r_Q is far from unity, the modified effective-diffusivity approach (either linearly dependent on position or linearly dependent on concentration) should be used.

It is important to note that although good agreement for ν_{PQ} is obtained by the effective-diffusivity method, there is quite a discrepancy between the exact concentration profile and that obtained by this method. A few concentration profiles obtained by the exact method, by the constant effective-diffusivity method, and by the method of

Table 1. Sample Comparison of the Values of $\nu_{PQ} = N_A\delta/c\mathcal{D}_{PQ}$ by the Effective Diffusivity Methods with Those from the Exact Solution, for the $A \rightarrow pP + qQ$ Problem (with $K = \infty$)

(In each square the first number is the exact value, the second number is the value calculated from the constant effective diffusivity method [by Equation (60)], the third number is the value calculated from the linearly position-dependent effective-diffusivity method [by Equation (63)], and the fourth number is the value calculated from the linearly concentration-dependent effective-diffusivity method [by Equation (66)].

	r_P \ r_Q	1.0	1.5	3.0	4.5	6.0
$p = 2$			0.0801	0.0597	0.0474	0.0396
$q = 1$	1.0		0.0815	0.0618	0.0498	0.0417
$x_{P0} = 0.7$			0.0810	0.0604	0.0476	0.0401
$x_{Q0} = 0.2$			0.0808	0.0603	0.0481	0.0400
		0.0647	0.0603	0.0485	0.0402	0.0343
	1.5	0.0660	0.0608	0.0491	0.0412	0.0355
		0.0658	0.0608	0.0486	0.0402	0.0344
		0.0659	0.0608	0.0484	0.0402	0.0344
		0.0361	0.0346	0.0307	0.0271	0.0243
	3.0	0.0361	0.0345	0.0304	0.0272	0.0246
		0.0359	0.0343	0.0304	0.0270	0.0242
		0.0359	0.0343	0.0304	0.0270	0.0244
		0.0248	0.0240	0.0220	0.0203	0.0187
	4.5	0.0248	0.0241	0.0220	0.0203	0.0188
		0.0243	0.0239	0.0219	0.0203	0.0187
		0.0246	0.0239	0.0221	0.0203	0.0187
		0.0188	0.0184	0.0172	0.0162	0.0152
	6.0	0.0189	0.0185	0.0172	0.0164	0.0152
		0.0186	0.0184	0.0172	0.0162	0.0152
		0.0190	0.0184	0.0172	0.0161	0.0152

* See footnote on page 517.

Table 2. Comparison of the Concentration Profile by the Effective Diffusivity Methods and that by the Exact Method for the $A \rightarrow pP + qQ$ Problem for $K = \infty$

$p = 1$ $q = 1$ $r_P = 4.5$ $r_Q = 3.0$ $x_{P0} = 0.7$ $x_{Q0} = 0.2$	by the exact method: $x_P(\zeta) = 0.9998 + 0.3793 \exp(0.038\zeta) - 0.6791 \exp(-0.084\zeta)$ $x_Q(\zeta) = 0.9998 - 0.2865 \exp(0.038\zeta) - 0.5133 \exp(-0.086\zeta)$ by the constant effective diffusivity method: $x_P(\zeta) = 1.0000 - 0.3000 \exp(-0.316\zeta)$ $x_Q(\zeta) = 1.0000 - 0.8000 \exp(-0.012\zeta)$ by the linearly position dependent effective diffusivity method: $x_P(\zeta) = 1.0000 - 0.3000(1-0.0221\zeta)^{14.29}$ $x_Q(\zeta) = 1.0000 - 0.8000(1-0.0221\zeta)^{0.528}$
$p = 2$ $q = 2$ $r_P = 4.5$ $r_Q = 1.5$ $x_{P0} = 0.2$ $x_{Q0} = 0.2$	by the exact method: $x_P(\zeta) = 0.6665 + 0.4189 \exp(-0.212\zeta) - 0.8854 \exp(-0.871\zeta)$ $x_Q(\zeta) = 0.6665 - 0.2715 \exp(-0.212\zeta) - 0.1950 \exp(-0.871\zeta)$ by the constant effective diffusivity method: $x_P(\zeta) = 0.6667 - 0.4667 \exp(-1.544\zeta)$ $x_Q(\zeta) = 0.6667 - 0.4667 \exp(-0.515\zeta)$ by the linearly position dependent effective diffusivity method: $x_P(\zeta) = 0.6667 - 0.4667(1-0.1304\zeta)^{11.35}$ $x_Q(\zeta) = 0.6667 - 0.4667(1-0.1304\zeta)^{3.44}$
$p = 2$ $q = 1$ $r_P = 3.0$ $r_Q = 1.5$ $x_{P0} = 0.4$ $x_{Q0} = 0.3$	by the exact method: $x_P(\zeta) = 1.0000 + 0.1042 \exp(-0.122\zeta) - 0.7042 \exp(-0.453\zeta)$ $x_Q(\zeta) = 0.5000 - 0.0711 \exp(-0.122\zeta) - 0.1289 \exp(-0.453\zeta)$ by the constant effective diffusivity method: $x_P(\zeta) = 1.0000 - 0.6000 \exp(-0.448\zeta)$ $x_Q(\zeta) = 0.5000 - 0.2000 \exp(-0.565\zeta)$ by the linearly position dependent effective diffusivity method: $x_P(\zeta) = 1.0000 - 0.6000(1+0.1081\zeta)^{-4.135}$ $x_Q(\zeta) = 0.5000 - 0.2000(1+0.1081\zeta)^{-4.370}$

effective diffusivity linearly dependent on position are shown in Table 2. These profiles are plotted in Figure 5. Because profiles calculated by the method of effective diffusivity, linearly dependent on concentration, cannot be expressed explicitly, they are not shown in Table 2.

Certainly the expressions used here for the heterogeneous reaction rates at the wall are idealized expressions. More general expressions should take into account the adsorption and desorption mechanisms which occur at the surface.

ACKNOWLEDGMENT

The authors wish to thank the Wisconsin Alumni Research Foundation for financial support of H. W. Hsu during this project, and R. Byron Bird wishes to acknowledge support of the Guggenheim Memorial Fund during a portion of this work. Acknowledgments are also due to the staff of the University of Wisconsin Numerical Analysis Laboratory for assistance and advice in the operation of the IBM 650 computer. In addition, the authors wish to express their thanks to O. A. Hougen, W. E. Stewart, and F. Yoshida for an extended conversation regarding the approximate methods discussed in the last section of this paper.

NOTATION

a, b = number of moles

A_P, B_P, C_P = dimensionless constants defined in Equations (22 *a, b, c*)

c = molar density (moles cm.$^{-3}$); $c = p/RT$

$\mathcal{D}_{ij}$ = binary diffusion coefficient for the gas pair *i-j* (cm.^{2} sec.$^{-1}$)

$\mathcal{D}_{im}$ = effective binary diffusion coefficient for *i* into a mixture of the other components (sq. cm. sec^{-1})

h = order of chemical reaction

k_h = reaction rate constant for *h*th order reaction (mole cm.$^{-2}$ sec.$^{-1}$)

K = dimensionless quantity defined in Equation (14) = $k_h\delta/c\mathcal{D}_{A_nB}$

K_h = dimensionless quantity defined in Equation (26) = $k_h\delta/c\mathcal{D}_{PQ}$

M, N, R = dimensionless constants defined in Equations (13 *a, b, c*)

N_A = mass transfer rate

N_i = mole flux of the *i* component with respect to stationary axes (mole cm.$^{-2}$sec.$^{-1}$)

n = number of moles

p = total pressure

p, q = number of moles

P, Q = components *P* and *Q*

Q = dimensionless quantity = $(1 - x_{A\delta})/(1 - x_{A0})$

r_i = ratio of binary diffusivity defined in each case

R = gas constant

s_+ = dimensionless constants defined in Equations (24) and (31)

T = absolute temperature

X, Y, Z = dimensionless constants defined in Equations (28), (29), and (30)

x_i = mole fraction of the *i*th component

z = distance into film, (cm.)

Greek Letters

α_{ij} = dimensionless quantity = $\exp \nu_{ij}$

β = constant defined in Equation (62)

δ = thickness of gas film

Ξ_i = constant defined in Equation (40)

ζ = z/δ = dimensionless distance coordinate

ν = total number of chemically distinct species in a multicomponent gas mixture

ν_{ij} = dimensionless quantity = $N_A\delta/c\mathcal{D}_{ij}$

Subscripts

$A, A_n, B, C, P, Q,$ = quantities pertaining to components in multicomponent mixture

i = quantity pertaining to the *i*th species in multicomponent mixture

0 = quantity evaluated at $z = 0$

δ = quantity evaluated at $z = \delta$

0 = zero root (with *s*)

e = equal root (with *s*)

+ = positive root (with *s*)

− = negative root (with *s*)

Superscript

0 = the known average quantity

LITERATURE CITED

1. Bird, R. B., W. E. Stewart, and E. N. Lightfoot, "Transport Phenomena," chap. 18, Wiley, New York (1960).
2. Benedict, Manson, and Arnold Boas, *Chem. Eng. Progr.*, **47**, 51 (1951).
3. Curtiss, C. F., and J. O. Hirschfelder, *J. Chem. Phys.*, **17**, 550 (1949).
4. Gilliland, E. R. "Absorption and Extraction," 1 ed., pp. 11-14, McGraw-Hill, New York (1937).
5. Hoopes, J. W., Jr., Ph.D. Thesis, Columbia Univ., New York (1951).
6. Hougen, O. A., and K. M. Watson, "Chemical Process Principles," Part III, pp. 977-982, Wiley, New York (1947).
7. Huebner, G. W., M. S. Thesis, Univ. Wisc., Madison (1957).
8. Keyes, J. J., Jr., and R. L. Pigford, *Chem. Eng. Sci.*, **6**, 215 (1957).
9. Stewart, W. E., Unpublished Analysis referred to in *Natl. Advisory Comm. Aeronaut., Tech Note 3208*, p. 9 (July, 1954). (See also Reference *1*, chap. 18, 21.)
10. Toor, H. L., *A.I.Ch.E. Journal*, **3**, 198 (1957).
11. Wilke, C. R., *Chem. Eng. Progr.*, **46**, 95 (1950).

Manuscript received May 19, 1959; revision received October 30, 1959; paper accepted November 2, 1959.

Turbulent Diffusion and the Multicomponent Reynolds Analogy

H. L. TOOR

Carnegie Institute of Technology

An understanding of mass transfer in a turbulent multicomponent fluid necessitates some knowledge of turbulent diffusion in such a fluid. In this paper equations for turbulent diffusion in a multicomponent fluid will be developed and used to derive the multicomponent Reynolds analogy.

TURBULENT DIFFUSION

Consider transfer in a highly turbulent fluid where the flux due to molecular diffusion is negligible compared with the turbulent flux. The flux with respect to a fixed coordinate system may be written as the flux with respect to a coordinate system moving at the mean molar velocity plus the convective flux due to the moving coordinate. The flux with respect to the moving coordinate is caused by the turbulent mixing and, as in a binary system, may be assumed to be minus the product of a turbulent diffusivity, which is a function of the local conditions of turbulence, and the local gradient of the time mean concentration (*1*). For one dimension

$$N_i = Ny_i - \epsilon_i C \frac{dy_i}{dx}, i = 1,2. . .n \quad (1)$$

One of the above equations is not independent, and all the quantities used here are the usual time-averaged ones.

If Equation (1) is summed over all components, one obtains

$$\sum_{i=1}^{n} \epsilon_i C \frac{dy_i}{dx} = 0 \quad (2)$$

so the two turbulent diffusivities in a binary system are always equal and any interaction between the molecular and turbulent diffusivities [of the type considered by Jenkins (*4*) for example] merely makes the single turbulent diffusivity a function of the single molecular diffusivity. In a multicomponent system in which the molecular diffusivities are unequal, however, any interaction between the molecular and turbulent diffusivities would not only make the turbulent diffusivities functions of molecular diffusivities but would make the turbulent diffusivities unequal.

If transfer takes place entirely by turbulent mixing, as assumed for example in mixing-length theories, then the ϵ_i are independent of molecular diffusivity and are all equal. Since this condition is approximately realized in binary systems where experiment and theory indicate that the effect of molecular Schmidt or Prandtl number on turbulent diffusivity is not large (*7*), it seems reasonable, at least as a first approximation, to assume that the same condition holds in multicomponent systems, $\epsilon_i = \epsilon$, for all i.

If it is further assumed that the presence of the flux N does not affect ϵ (this is equivalent to assuming that the velocity N/C is small enough so that its effect on the turbulence is negligible), then ϵ is fixed by the ordinary hydrodynamics and is independent of the number of species.

With $\epsilon_i = \epsilon$, Equation (1) becomes

$$N_i = Ny_i - \epsilon C \frac{dy_i}{dx}, i = 1,2. . .n-1 \quad (3)$$

There are of course other ways in which the eddy diffusivity could be defined, in terms of the mean mass velocity instead of mean molar velocity for example (*1*). However in dilute systems all definitions are essentially equivalent, and in concentrated systems the differences among the conclusions obtained by use of different definitions are probably less than the unknown coupling of the diffusion equations with the equations of motion. The present choice of a molar frame of reference leads to the simplest equations for gases, and the assumption that ϵ in Equation (3) has the same values as in a dilute binary fluid should give, at the worst, the correct magnitude of the transfer. In dilute mixtures the assumption should be very reliable.

Equation (3) is the same as the Maxwell-Stefan diffusion equation (*5*) for a system in which all the binary diffusion coefficients are equal to ϵ; therefore the solutions to Equation (3) also apply to the nonturbulent system in which all the diffusion coefficients are equal.

In equimolal transfer N is zero and from Equation (3) the flux of each component in an n component mixture follows the same equation as in binary equimolal transfer, so none of the multicomponent molecular diffusion phenomena which have been described earlier occur here (*10*).

When one gas is stagnant, species n for example in an n component mixture, it follows by summing Equation (3) over the nonstagnant species that the total flux is given by

$$N = \frac{\epsilon C}{y_n} \frac{dy_n}{dx} \quad (4)$$

which is a generalization of the equivalent binary equation. In the binary case N is the flux of the single nonstagnant species, but in an n component system N is the sum of $n-1$ fluxes.

Combining Equation (4) with Equation (3) yields an explicit equation for the separate fluxes:

$$N_i = -\epsilon C\, y_n \frac{d(y_i/y_n)}{dx}, i = 1,2. . .n-1 \quad (5)$$

In the general case y_n is of course the sum of the mole fractions of all the nonstagnant gases.

INTEGRATED FORMS FOR STEADY STATE TRANSFER

In the following development the molar density is taken as constant. For one-dimensional steady state transfer, when there is no flow normal to x, all the fluxes are independent of x and Equation (3) can be directly integrated. A more general integration can be carried out if one considers the case where the fluxes all vary with x in the same manner:

$$\frac{N_i}{N_{iw}} = f(x) \qquad (6)$$

Cases in which Equation (6) may hold will be discussed later. Combining Equation (6) with Equation (3) and integrating from 0 to L, one obtains

$$N_w = \frac{\bar{\epsilon}C}{L} \ln\left(\frac{N_w y_{iL} - N_{iw}}{N_w y_{io} - N_{iw}}\right), i = 1,2\ldots n \qquad (7)$$

where

$$\frac{L}{\bar{\epsilon}} = \int_o^L \frac{f(x)dx}{\epsilon} \qquad (8)$$

Equation (7) is indeterminate, and one more condition is required to allow solution for N_{iw}. When there is equimolal transfer, $N_w = 0$ and the solution is

$$N_{iw} = \frac{\bar{\epsilon}C}{L}(y_{io} - y_{iL}), i = 1,2\ldots n \qquad (9)$$

which is the same equation as obtained in a binary mixture.

When one or more components are stagnant, the total flux integral obtained from Equation (4) is

$$N_w = \frac{\bar{\epsilon}C}{L} \ln \frac{y_{nL}}{y_{no}} = \frac{\bar{\epsilon}C}{L} \frac{(y_{nL} - y_{no})}{(y_n)_m} \qquad (10)$$

and if this is combined with Equation (7), the separate fluxes are obtained:

$$N_{iw} = \frac{\bar{\epsilon}C}{L} \frac{y_{no}}{(y_n)_m}(\delta_T y_{io} - y_{iL}), \quad i = 1,2\ldots n-1 \qquad (11)$$

where

$$\delta_T = \frac{y_{nL}}{y_{no}} \qquad (12)$$

The above results indicate that reverse diffusion and related phenomena which occur in multicomponent gaseous diffusion (*10*) can occur in turbulent multicomponent diffusion when there is a stagnant species but not in equimolal transfer. For a binary mixture Equation (11) reduces to the well-known form, and the effect of the bulk merely introduces the $(y_2)_m$ term (*8*).

It is important to note that the predicted interaction effects in turbulent diffusion are generally smaller than in molecular diffusion and are due to the bulk flow caused by the diffusion; therefore they disappear in equimolal transfer. In molecular diffusion the interactions, when one gas is stagnant, are a combination of interactions caused by differences in diffusion coefficients and flow interactions, and in this case, even in equimolal transfer, the interactions remain (*10*).

REYNOLDS ANALOGY

Mass transfer to a turbulent fluid is described by the combination of Equation (3) (suitably generalized) with a differential material balance, but most binary analogy calculations have avoided the necessity of solving the resulting equation by assuming the manner in which the flux varies with radial position. Since the absolute value of the radial flux must vary from a maximum at the wall of, say, a tube to zero at the center, a linear approximation to $f(x)$ in Equation (6) is correct in the limits,

$$\frac{N_i}{N_{iw}} = \left(1 - \frac{2x'}{d}\right) \quad i = 1,2 \qquad (13)$$

It can be shown for the binary case that for a constant flux at the wall this linear form is a good approximation (*3*). (Since binary equimolal and dilute binary transfer with the nondilute gas stagnant are both equivalent to heat transfer, results will be quoted without necessarily making any distinction.) Furthermore it has also been shown that away from the tube inlet and for all but the lowest Schmidt numbers (and consequently for all binary mass transfer) the wall concentration distribution has little effect on the mass transfer coefficient (*9*). Thus the multicomponent mass transfer problem will be attacked by considering mass transfer to a turbulent fluid moving in a tube under such conditions that there is a constant wall flux for all species.

The question immediately arises as to whether Equation (13) is as valid in a multicomponent system as in a binary one. In equimolal transfer, where there is no difference between multicomponent and binary transfer, the binary results are valid for each species, and so Equation (13) should be a good approximation for all components, This argument breaks down near the wall, where molecular diffusion is controlling, but can be replaced there by the argument that the flux cannot vary significantly in a thin film.

A more rigorous and more general argument, similar to that used by Churchill and Balzhiser (*3*) for heat transfer, is possible. For steady state transfer in a tube with radial symmetry, a material balance with axial diffusion neglected yields

$$C\frac{\partial(u(x'')y_i)}{\partial Z} + \frac{1}{x''}\frac{\partial}{\partial x''}(x''N_i) = 0, i = 1,2\ldots n \qquad (14)$$

If the system is relatively dilute in diffusing species, then u can be taken as approximately constant with Z, and in the limit of a long tube with a constant wall flux for all species (the limit considered, usually implicitly, in binary systems) the concentration profiles change slowly; so $\partial y_i/\partial Z$ can be taken as independent of x'' and equal to dy_i/dZ. With these assumptions Equation (14) is similar to the analogous heat transfer problem, and integration and substitution of a material balance which neglects variations in axial velocity yields

$$\frac{N_i}{N_{iw}} = \frac{4}{x''d}\int_o^{x''} x \frac{u(x)}{V} dx, i = 1,2\ldots n \qquad (15)$$

which is essentially the same equation as obtained for heat transfer (*3*). Consequently for fluids which are not too concentrated the variation of N_i/N_{iw} with radius depends only upon the velocity profile, is the same for all species, and is the same as in heat transfer or in binary mass transfer. This variation is found to be close to linear (*3*) when a normal turbulent velocity profile is substituted into Equation (15).

By earlier assumptions the eddy diffusivity of mass has the same values in a multicomponent system as in a binary system when the hydrodynamics are the same in both cases. Since the eddy diffusivity of mass in a binary system is approximately equal to the eddy diffusivity of momentum, Equation (8) with the linear flux variation, the normal shear-stress relationship, and a force balance becomes

$$\frac{L}{\bar{\epsilon}} = \frac{\rho}{\tau_w}\int_{L_1}^{L_2} du \qquad (16)$$

and $L_2 - L_1 = L$.

The Reynolds analogy is obtained when the turbulence is assumed to extend to the wall so the velocity at L_1 is zero, when L_2 is taken as the radial position where the local velocity has the same value as the mean velocity, and when it is further assumed that at this latter point all the local concentrations have the same values as the bulk mean concentrations. Then

$$\frac{\bar{\epsilon}}{L} = \frac{\tau_w}{\rho V} = \frac{f}{2} \qquad (17)$$

Subscript L now refers to the bulk concentration, subscript o becomes subscript w, and subscript w refers to the flux at the wall. Equation (7) becomes, for example,

$$N_w = \frac{f}{2} G_m \ln\left(\frac{N_w \bar{y}_i - N_{iw}}{N_w y_{iw} - N_{iw}}\right), \quad i = 1,2\ldots n \qquad (18)$$

and this is the multicomponent Reynolds analogy.

Even though the Reynolds analogy neglects the molecular diffusion which takes place adjacent to the boundary between a turbulent fluid and another phase, it is a good approximation for mass transfer in a binary gas because the Schmidt number in gases is close to 1 and the molecular diffusion equation in a binary gas is of the same form as the turbulent-diffusion equation. In multicomponent gases the molecular-diffusion equations can differ considerably from the above turbulent-diffusion equations, and so if molecular diffusion is significant, Equation (18) cannot in general be nearly so good an approximation for mass transfer in a multicomponent gas as in a binary one. Further developments, which include the effect of molecular diffusion, will be presented in a later paper.

Few concrete generalizations are possible in the case of liquids because of the paucity of data concerning multicomponent liquid diffusion. However in a liquid in which there are negligible cross-diffusion effects, Equation (1) describes molecular diffusion, and if the molar density does not vary too greatly and the various molecular diffusion coefficients are approximately equal (all these conditions may be satisfied in many systems), then, as in a binary system (2), Equation (18) can be used for mass transfer if the righthand side is corrected for the effect of Schmidt number by multiplying by the average Schmidt number to the $-2/3$ power:

$$N_w = \frac{f}{2} G_m (N_{Sc})^{-2/3} \ln\left(\frac{N_w \bar{y}_i - N_{iw}}{N_w y_{iw} - N_{iw}}\right) \qquad i = 1,2\ldots n \qquad (19)$$

NOTATION

C = molar density, moles/cu. ft.
d = diameter, ft.
f = Fanning friction factor
$f(x)$ = function of x
G_m = molar mass velocity, moles/(hr.)(sq. ft.)
L = length of diffusion path, ft.
n = number of species
N = total molar flux with respect to a fixed coordinate, moles/(hr.)(sq. ft.)
N_i = molar flux of species i, with respect to a fixed coordinate, moles/(hr.)(sq. ft.)
N_{Sc} = Schmidt number
u = axial velocity, ft./hr.
V = mean axial velocity, ft./hr.
x = distance coordinate, ft.
x' = distance from wall, ft.
x'' = radial distance from tube center, ft.
y = mole fraction
Z = axial distance, ft.
δ_r = interaction term
ϵ = turbulent diffusivity, sq. ft./hr.
$\bar{\epsilon}$ = mean diffusivity which reduces to ϵ when the diffusivity is constant
ρ = mass density, lb.-mass/cu. ft.

Subscripts

i = species i
m = log mean
n = species n
w = position w or wall
o,L = positions in x coordinates
L_1,L_2 = positions in x' coordinates

LITERATURE CITED

1. Bird, R. B., W. E. Stewart, and E. H. Lightfoot, "Notes on Transport Phenomena," Wiley, New York (1958).
2. Chilton, T. H., and A. P. Colburn, *Ind. Eng. Chem.*, **26**, 1183 (1934).
3. Churchill, S. W., and R. E. Balzhiser, *Chem. Eng. Progr. Symposium Ser. No. 29*, **55**, 127 (1959).
4. Jenkins, R., "Heat Transfer and Fluid Mechanics Institute," Stanford Univ. Press, Palo Alto, Calif. (1951).
5. Maxwell, J. C., "Scientific Papers," **2**, Dover, New York (1952).
6. Reichardt, H., *Natl. Advisory Comm. Aeronaut. Tech. Memo 1047* (1943).
7. Sherwood, T. K., *Chem. Eng. Progr. Symposium Ser. No. 25*, **55**, 71 (1959).
8. ———, and R. L. Pigford, "Absorption and Extraction," McGraw-Hill, New York (1952).
9. Sleicher, C. A., Jr., and Myron Tribus, *Trans. Am. Soc. Mech. Engrs.*, **79**, 789 (1957).
10. Toor, H. L., *A.I.Ch.E. Journal*, **3**, 198 (1957).

SAVE THOSE BACK ISSUES!

Every so often an unprecedented demand for a particular issue, or an unexpected influx of new subscribers and members puts the editor in the embarrassing position of running out of copies of A.I.Ch.E. Journal. This has happened several times in our short history and if members have copies of any of the following issues, we would be glad to purchase them.

The issue which we need and for which we will pay $1.50 each is: March 1960.

All these issues were overprinted to the usual extent, but because popular features spurred single copy sales, our reserves are exhausted.

Help fellow members by sending your back numbers of the issues specified above to:

Mrs. E. PLATTNER
A.I.Ch.E. Journal
25 West 45 St.
New York 36, N. Y.

IMPORTANT NOTICE

If your address has changed, please fill out this form and mail to A.I.Ch.E. JOURNAL, 25 West 45th Street, New York 36, New York.

EFFECTIVE DATE OF NEW ADDRESS _____ DATE OF THIS NOTICE _____

PREVIOUS ADDRESS

STREET NUMBER, STREET NAME, POST OFFICE BOX NUMBER _____

NAME OF CITY OR TOWN _____ ZONE NO. _____ NAME OF STATE _____

NEW ADDRESS

STREET NUMBER, STREET NAME, POST OFFICE BOX NUMBER _____

NAME OF CITY OR TOWN _____ ZONE NO. _____ NAME OF STATE _____

PRINT NAME & MEM. REF. NO. _____ SIGN NAME HERE _____

Join an A. I. Ch. E. Division!

Formed so that members with common interests may meet and work together within the framework of the Institute, two A.I.Ch.E. divisions catering to specific fields have been created so far: the Heat Transfer and the Nuclear Engineering Divisions.

Among other activities, the Heat Transfer Division sponsors the Joint A.I.Ch.E.-A.S.M.E. Heat Transfer Conference held each August. The Nuclear Engineering Division is similarly responsible for the A.I.Ch.E.'s part in the biennial Nuclear Congress. Specifically the purposes of the divisions are as follow:

The Heat Transfer Division of A.I.Ch.E. encourages investigations and fosters the dissemination of knowledge in the science and art of heat transfer. It provides opportunities for engineers and scientists to exchange ideas, experiences and evaluations through meetings and conferences. The Division coordinates the Institute's activities in the field of heat transfer and cooperates with other societies in this field.

The Nuclear Engineering Division has responsibility for coordinating the activities of the Institute in the field of nuclear energy. The Division plans symposia, attempts to foster Local Section activities in this field and has accepted the Institute's responsibilities in the development of nuclear standards. Members receive a nuclear newsletter three times a year.

Stuart W. Churchill is chairman of the Heat Transfer Division and W. A. Rodger of the Nuclear Engineering Division.

Interested members should fill in the form below and send it with $2.00 annual dues to the Secretary-Treasurer of either division: Raymond F. Fremed, Heat Transfer Division, A.I.Ch.E., Post Office Box 213, Far Rockaway 91, New York; Charles E. Dryden, Nuclear Engineering Division, A.I.Ch.E., Ohio State University, Columbus, Ohio.

Name

Company

Preferred Address

Dear Editor:

Baer and McKelvey claim to have proved that the lower condensation coefficients obtained with air present are the result of a higher resistance at the interface, rather than the result of a diffusional resistance [*A.I.Ch.E. Journal*, **4**, 218 (1958)]. The authors supported this conclusion by showing that their data could be represented by straight lines on the appropriate type of graph. However a typical set of data may appear to give straight lines on several plots, particularly if the data scatter slightly and do not cover a wide range. A straight line for the plot testing one theory does not rule out other theories.

The authors said that diffusion effects were negligible in their work because straight lines and not curves were obtained on Figures 5 and 6, the plots drawn to test their theory. However with only 6 to 8 points for each line, only a 1.5-fold range of abscissa values, and with an average error of about 10% of the range of ordinate values, it is possible that a slightly flexed curve would fit the data just as well or better. Rather than basing their conclusions on whether or not the graphs seemed linear, the authors should have prepared separate plots based on a linear form of the equation which did allow for diffusion.

To test the diffusion theory the interfacial resistance would be assumed small and the heat flux expressed as

$$\frac{q}{A} = h(t - t_s)$$

$$= h_N(t_i - t_s) = \lambda\, k_g(p - p_i)$$

If the mass transfer coefficient is constant, and if the driving force for diffusion, $(p - p_i)$, is assumed proportional to the temperature difference, $(t - t_i)$, the equation becomes

$$h(t - t_s) = h_N(t_i - t_s) = b(t - t_i)$$

or

$$\frac{1}{h} = \frac{1}{h_N} + \frac{1}{b}$$

Since $h_N = C(q/A)^{-1/3}$, a plot of $(1/h)$ vs. $(q/A)^{1/3}$ is suggested, but this is exactly the same plot as the authors' graph of $(\Delta T_1/\Delta T_2)$ vs. $(\Delta T_2)^{1/3}$, which was used to test for interfacial resistance! The mass transfer coefficient would actually not be constant because the natural convection would increase with increased heat flux, though this effect would be partially cancelled by the increase in the logarithmic mean pressure of the air in the diffusion layer. [For one-way diffusion, the Nusselt number becomes $(k_g P_{BM} D)/(RT D_v)$.] Even if the exact variation of k_g with (q/A) were known, it would not be much help here; because of the scatter of the data the assumption of either a slight increase or a slight decrease in k_g with (q/A) would still give apparently straight lines on the corresponding graphs. The conclusion is that the relative importance of diffusion and interface effects cannot be determined by graphical manipulation unless extremely accurate data and a more exact expression for the mass transfer rate are available.

Effect of Air on Coefficients for Film Condensation
Steam at 1 atm. condensing on a horizontal 3-in. cylinder

		Theory		Data of Othmer	
Δt	% Air	h	h/h_o	h	h/h_o
10°F.	0	2,390	1.0	2,200	1.0
	2		0.19		0.32
	4		0.14		0.21
	6		0.10		0.15
40°F.	0	1,500	1.0	1,300	1.0
	2		0.30		0.44
	6		0.19		0.25

There is a reliable way to show that diffusion must be at least partly responsible for the low condensing coefficients obtained with air. The mass transfer coefficient is predicted from the correlations for natural convection, with a trial-and-error method used to estimate the interface temperature. A calculation for methanol condensing at atmospheric pressure shows that the presence of 1% air could lower the apparent film coefficient to 40% of the normal value. The turbulence created by the injection of vapor into the condenser would generally make the mass transfer rate slightly higher than for natural convection, but not enough higher to eliminate the diffusion resistance completely. Since the authors did not include their complete data for methanol, the coefficients of Othmer for steam-air mixtures (taken from McAdams, "Heat Transmission") were used for a detailed comparison of theoretical and experimental coefficients.

The measured coefficients are about 50% higher than those predicted, with published correlations for mass transfer by natural convection used. Therefore the primary effect of air is probably a result of a diffusion resistance; this could easily be demonstrated experimentally by comparing the coefficients for natural and forced convection. To measure the interfacial resistance in the presence of air would require elaborate apparatus designed to minimize both the diffusional resistance and the resistance of the condensate film.

Very truly yours,

Peter Harriott
Cornell University
Ithaca, New York

Entrainment and Extraction Efficiency of Mixer-Settlers

C. A. SLEICHER, JR.

Shell Development Company, Emeryville, California

In mixer-settler extraction systems the settlers are seldom completely effective. Usually there occurs some entrainment of light phase in the heavy one and of heavy phase in the light one. This entrainment is analogous to axial mixing in continuous columns, which has been treated in the literature (3, 4). In this note a theoretical analysis is made of the effect of entrainment on the efficiency of countercurrent extractors consisting of multiple mixer-settler stages with finite rates of mass transfer.

The effect of entrainment on efficiency of extractors has been analyzed by Felix and Holder (2) for the case of mixers which operate at 100% efficiency, that is, infinite mass transfer rate. Their results however are unrealistic since their Equation (21) yields zero extraction for infinite internal entrainment rate. Such an extractor is actually equivalent to one stage. The difficulty can be traced to their boundary condition, which should be replaced by a balance around the first stage.

The present problem is closely related to that of the effect of entrainment on the efficiency of plate absorption towers and distillation columns, which was investigated in the 1930's by several authors (1). The problem of entrainment in extractors differs principally in that there is entrainment of two phases rather than one. Furthermore the solution presented here is for the effect of entrainment on the overall efficiency of extractors, whereas the distillation work concerned the efficiency of individual plates.

C. A. Sleicher, Jr., is now with the University of Washington, Seattle, Washington.

DESCRIPTION OF EXTRACTOR MODELS

Figure 1 shows the extractor schematically and identifies symbols. The liquids leaving the first and last settlers go to after settlers or to purification equipment of some kind which returns entrained liquid to streams entering the mixers. Solute is transferred from a raffinate phase that passes countercurrent to the solvent phase. Each of the phases from a settler is contaminated with entrainment of the other phase. Note that f is expressed as a fraction of Q_f; similarly s is a fraction of Q_s. In this note "entrainment", when used quantitatively, refers to f and s and not to entrainment holdups.

From each settler at very high entrainment rates the concentrations of solute in the solvent leaving in the solvent phase and leaving as entrainment in the raffinate phase from each settler would be about the same. Similarly the concentration of solute in the raffinate phase entrained with the solvent stream would be equal to that in the raffinate leaving in the raffinate stream. At very low rates of entrainment however the entrained drops would be small and nearly in equilibrium with the entraining phase. Because of this difference calculations have been made for two models. The model for high entrainment rate is called *Model 1*, and the principal assumptions for it are the following:

1. The amount of entrainment in a given phase is the same from each settler.

2. The solvent and solute-free raffinate are immiscible (or their solubility does not vary with solute concentration and hence stage number).

3. The volume rates of solvent and feed phases do not change from stage to stage.

4. The distribution coefficient (equilibrium ratio) is constant; that is it is not a function of concentration.

5. Coalescence and redispersion of the dispersed phase and mixing of the continuous phase in the mixer is so rapid that the solute concentration is uniform throughout each phase.

6. The rate of mass transfer in the mixer is given by $Kav\ (x_n - my_n)$. Kav is assumed to be the same for every mixer.

7. All mass transfer takes place in the mixer.

For Model 2 all assumptions are the same as for Model 1 except assumption 7. At the low rates of entrainment ascribed to Model 2 enough mass transfer is assumed in the settlers to allow the drops to reach equilibrium with the entraining phase. For this model, then, assumption 7 is the entrainment that leaves with each bulk phase from the settler is in equilibrium with that bulk phase.

This condition means that some mass transfer takes place in the settlers and that therefore the composition of the feed that leaves as entrainment with the solvent stream is different from the bulk concentration of the feed or raffinate stream from any settler.

THE ANALYSIS AND ITS RESULTS

The extractor models can be described by the difference equations formed from appropriate material balances. These equations and their end conditions can be written in terms of the dimensionless variables f, s, N, F, t, Ψ_n, and Γ_n.

As in reference 4 the solution is expressed in terms of Ψ_n. It varies from 0 at the feed inlet stream to a possible maximum at the outlet of 1, which occurs when the raffinate is in equilibrium with the incoming solvent.

The solution of the difference equation for Model 1 is

$$\Psi_n = C_0 + C_1\lambda_1^n + C_2\lambda_2^n + C_3\lambda_3^n \quad (1)$$

where the λ are the roots of

$$f(1+s)\lambda^3 - [(1+s)(1+t) + f(2+3s+Ft)]\lambda^2 + [(1+f)(1+Ft) + s(2+3f+t)]\lambda = s(1+f) \quad (2)$$

Table 1. Representative Results of Model 1

$N = 6$

F	f	s	t	ψ_S/ψ_{S0}	E_e	E_o
0.25	0.1	0.1	1	0.9926	0.95	0.32
0.25	0.1	0.1	10	0.9989	0.87	0.72
0.25	0.1	0.1	∞	0.9994	0.83	0.83
0.25	0.1	0.4	∞	0.9958	0.62	0.62
0.25	0.4	0.1	∞	0.9988	0.76	0.76
0.25	0.4	0.4	∞	0.9943	0.58	0.58
1	0.1	0.1	1	0.980	0.95	0.47
1	0.1	0.1	10	0.979	0.87	0.80
1	0.1	0.1	∞	0.978	0.86	0.86
1	0.1	0.4	∞	0.948	0.72	0.72
1	0.4	0.4	∞	0.923	0.63	0.63

The four constants of Equation (1) are determined from four end conditions, which are found by writing material balances for each phase at each end of the column. In writing these end conditions the after settlers are designated 0 and $N+1$. Observe that from the viewpoint of Mixer 1 the influent feed has composition x_0, and for Mixer N the influent solvent has composition y_{N+1}. The end conditions are then

Dimensional form	Dimensionless form	
$x_N = x_{N+1}$	$\Psi_N = \Psi_{N+1}$	(3)
$x_1 + f x_1 = (1+f) x_0$	$f\Psi_1 = (1+f)\Psi_0$	(4)
$y_0 = y_1$	$\Gamma_0 = \Gamma_1$	(5)
$y_1 + s y_N = (1+s) y_{N+1}$	$s\Gamma_N = (1+s)\Gamma_{N+1}$	(6)

Equations (3) and (5) specify that no mass transfer takes place in the after settlers, and Equations (4) and (6) specify the composition of the feed to stage 1 and of the solvent to stage N, respectively.

Substitution of Ψ from Equation (1) into Equations (3) through (6) yields four linear algebraic equations that can be solved for the constants C_m. These equations will be designated by the numbers (7) through (10).

For special cases the solutions are much simpler than the general solution represented by Equations (1), (7), (8), (9), and (10). Listed below for reference are solutions for particular cases of interest.

For equilibrium in the mixer

$$\Psi_n = \frac{F\lambda^n - \lambda}{F^n\lambda^N - \lambda} \tag{11}$$

where $\lambda = (F + fF + s)/(1 + fF + s)$

and when $F = 1$

$$\Psi_n = \frac{f + s + n}{2(f + s) + 1 + N} \tag{12}$$

With no entrainment

$$\Psi_n = \frac{\lambda^n - 1}{F\lambda^N - 1} \tag{13}$$

where $\lambda = (1 + Ft)/(1 + t)$

and when $F = 1$,

$$\Psi_n = \frac{tn}{1 + t + tN} \tag{14}$$

With no entrainment and equilibrium in the mixer

$$\Psi_n = \frac{F^n - 1}{F^{N+1} - 1} \tag{15}$$

and when $F = 1$,

$$\Psi_n = \frac{n}{1 + N} \tag{16}$$

For infinite entrainment of both phases

$$\Psi_1 = \Psi_2 = \ldots = \Psi_N = \frac{Nt}{1 + Nt + FNt} \tag{17}$$

The equations for the general case were solved on a digital computer for about 800 combinations of the five parameters in the following range: $3 \leq N \leq 10$, $0.25 < F < 4$, $0.3 < t < \infty$, $0 < f$ and $s < 0.8$. Table 1 gives some representative results. The settler efficiency E_e is defined by N_e/N, where both N_e and N reflect the same t, F, and Ψ_N. It was found that the settler efficiency is only weakly dependent on N and F and is more strongly dependent on t at low F. The magnitude of E_e is of particular interest. For example with $F = 1$ and $N = 6$, 10% entrainment of each phase yields a settler efficiency of 0.86 to 0.95, and 20% entrainment yields 0.77 to 0.89. These entrainment rates are quite high, and yet the efficiency is decreased by at most 23%. It is not until the entrainment of each phase reaches 0.4 that the stage efficiency falls below 60%. The over-all efficiency is of course strongly dependent on the rate of mass transfer (expressed by t) as well as entrainment. Throughout most of the studied range of parameters the settler efficiency is correlated within 5% by the following empirical equation:

$$E_e = \frac{\log F + (N-1)\log\lambda'}{N \log F} \tag{18}$$

where

$$\lambda' = \frac{F + E_m(Ff + s)}{1 + E_m(Ff + s)}$$

For $F = 1$ this simplifies to

$$E_e = \frac{N + E_m(f + s)}{N + NE_m(f + s)}$$

Here E_m is the efficiency of a single mixer, $Ft/(1 + Ft)$. It is easily shown that this expression for the mixer efficiency is equivalent to the Murphree plate efficiency of a distillation column. Equation (18) is exact for the case of $t = \infty$ and is proposed in place of Equation (22) of reference 2.

For the over-all efficiency it was found that multiplying the settler efficiency by an over-all mixer efficiency gives an adequate correlation. The over-all efficiency of an extractor with no entrainment is equal to the mixer efficiency only when the extraction factor is unity. In general

$$E_{mo} = \frac{\log \dfrac{1 + Ft}{1 + t}}{\log F} \tag{19}$$

This equation multiplied by the settler efficiency correlates the over-all efficiency within 10% throughout most of range of parameters investigated; that is

$$E_o = E_e E_{mo} \tag{20}$$

Equations (18), (19), and (20) afford a means of calculating the number of actual stages of a mixer-settler extractor from the entrainment and mass transfer rates.

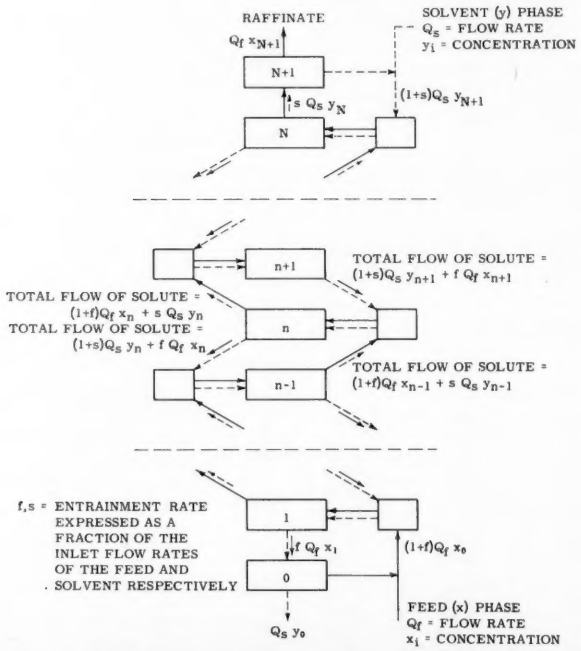
RAFFINATE
$Q_f\ x_{N+1}$
SOLVENT (y) PHASE
Q_S = FLOW RATE
y_1 = CONCENTRATION
N+1
N
$s\ Q_S\ y_N$
$(1+s)Q_S\ y_{N+1}$
n+1
n
n-1
TOTAL FLOW OF SOLUTE = $(1+s)Q_S\ y_{n+1} + f\ Q_f\ x_{n+1}$
TOTAL FLOW OF SOLUTE = $(1+f)Q_f\ x_n + s\ Q_S\ y_n$
TOTAL FLOW OF SOLUTE = $(1+s)Q_S\ y_n + f\ Q_f\ x_n$
TOTAL FLOW OF SOLUTE = $(1+f)Q_f\ x_{n-1} + s\ Q_S\ y_{n-1}$
f,s = ENTRAINMENT RATE EXPRESSED AS A FRACTION OF THE INLET FLOW RATES OF THE FEED AND SOLVENT RESPECTIVELY
1
0
$f\ Q_f\ x_1$
$(1+f)Q_f\ x_0$
$Q_S\ y_0$
FEED (x) PHASE
Q_f = FLOW RATE
x_1 = CONCENTRATION

Fig. 1. Nomenclature for staged extraction, Model 1.

Model 2

The difference equation for Model 2 is of second rather than fourth order. Its solution is

$$\Psi_n = \frac{FH\lambda^n - J}{F^2H\lambda^N - J}$$

where

$$H = 1 + fF + s$$

$$J = F + fF + s$$

$$\lambda = \frac{H[F(1+f)(1+f+s)+J(Ft+fFt+st+s+2fs)]}{J[t(1+fF+s)^2+f^2F(1+2s)+(1+s)^2(1+2f)]}$$

Only a few calculations were made for Model 2 because it became evident that at entrainment rates in the range of validity of the model (probably f and s of 0.1 or less) the entrainment has little effect on extraction. When equilibrium is reached in the mixer, both models give the same result. For other cases the extent of extraction is always greater for Model 2 because of the mass transfer in the settler.

USE OF THE ANALYSIS AND CONCLUSIONS

This analysis will find utility in the design of settlers, for it suggests that settlers other than after settlers are sometimes over-designed. If there are no complicating consequences of entrainment, such as the formation of stable emulsions, entrainment rates as high as 10% are rarely consequential.

The results will also be useful for interpreting experimental data. In particular if an extractor has low efficiency, measurements of entrainment from the settlers will establish whether the low efficiency is caused by the entrainment or by poor mass transfer in the mixers.

The major conclusion to be drawn from this work is that high entrainment rates have relatively little effect on the efficiency of mixer-settler extractors. When such extractors have poor efficiency, it is therefore more likely to be caused by low mass transfer rate than by entrainment from the settlers. This suggests that efficiency of some mixer settlers might be improved by operating the mixers at higher rates provided that (1) there occurs no deleterious effect such as the formation of stable emulsions and (2) the capacity of the after settlers is adequate. If after settlers are not used, then improvement might be obtained without excessive entrainment in the effluents by increasing the mixing rates in all but the first and last mixers.

NOTATIONS

E_e = entrainment or settler efficiency, N_o/N

E_m = Murphree efficiency in distillation or mixer efficiency in extraction, $Ft/(1 + Ft)$

E_{mo} = over-all efficiency of a column with no entrainment [see Equation (19)]

E_o = over-all efficiency, N_t/N

F = extraction factor, mQ_f/Q_s

f = fraction of Q_f entrained in the solvent phase from a settler

Kav = product of a mass transfer coefficient and the interfacial area per mixer

N = number of actual stages

N_o = number of stages to effect a given extraction with no entrainment

N_t = number of theoretical stages

Q_f = flow rate of feed phase to extractor

Q_s = flow rate of solvent phase to extractor

s = fraction of Q_s entrained in the feed phase from a settler

t = Kav/Q_s

x = concentration of solute in feed or raffinate phase

y = concentration of solute in solvent phase

Ψ_n = dimensionless concentration of feed phase, $(x_1 - x_n)/(x_1 - my_1)$

Ψ_N/Ψ_{No} = $\Psi(s, f, F, t, N)/\Psi(0, 0, F, t, N)$

Γ_n = dimensionless concentration of solvent phase, $(y_n - y_1)Q_s/(x_1 - my_1)Q_f$

LITERATURE CITED

1. Colburn, A. P., *Ind. Eng. Chem.*, **28**, 526 (1936).
2. Felix, J. R. and C. H. Holder, *A.I.Ch.E. Journal*, **1**, 296 (1955).
3. Miyauchi, T., *USAEC*, UCRL-3911 (1957).
4. Sleicher, C. A., Jr., *A.I.Ch.E. Journal*, **5**, 145 (1959).

CHEMICAL ENGINEERING PROGRESS SYMPOSIUM SERIES ABSTRACTS

The Chemical Engineering Progress Symposium Series is composed of papers on specific subjects conveniently bound in individual books, which are published at intervals. The books are 8½ by 11 inches, paper covered, and cost $3.50 to members, $4.50 to nonmembers. They may be ordered from the Secretary's Office, the American Institute of Chemical Engineers, 25 West 45 Street, New York 36, New York.

The *A. I. Ch. E. Journal* will publish, from time to time, abstracts of the articles appearing in the Symposium Series volumes. Recently published volumes are abstracted below.

CHEMICAL ENGINEERING EDUCATION —ACADEMIC AND INDUSTRIAL, Vol. 55, No. 26, 1959.

Evolution of the Unit Operations, Warren K. Lewis. The technological achievements of the profession in America during the last half century have been impressive. No small part of the credit is due to the training the young engineer has received. The emphasis on basic science has given the understanding of inner mechanisms and the analytical ability to foresee and plan for ultimate results. The unit operations approach has stimulated technical imagination and has shown the way to the transfer of experience acquired in one area to others which sometimes seemed unrelated. Moreover, making it possible to reduce coverage of detail without sacrifice in breadth has resulted in training in greater depth. The foundations laid by the educational pioneers have proved sound and dependable. **Development of Chemical Engineering at the University of Michigan,** Donald L. Katz. The sixty years of chemical engineering education are surveyed for the influences that have dominated the curriculum. As in most schools, at Michigan the birth of this new branch of engineering was due largely to teachers of chemistry. The association of the faculty with industrial processes drew the teacher into research on engineering problems and provided the stimulus for new engineering courses. The evolution of the

curriculum is traced from one consisting primarily of chemical technology through the development of engineering science to the current program, characterized as the era of design. New concepts now under discussion are likely to be introduced very soon. **Present Status of the Unit Operations,** William Licht. The concept of the unit operations is a unique American contribution to the development of the chemical engineering profession. The coinage of the neat phrase *unit operations* about 1915 served to distinguish concisely the area of activity of this kind of engineer in industry, helped him to become freed of his earlier identification as a composite mechanical-engineer-chemist, and speeded recognition of the new young branch of engineering as an independent discipline in its own right. It also became the focal point around which the teaching of chemical engineering was organized for many years. **A Definition of Chemical Engineering and a Few Implications Regarding Chemical Engineering Education,** Seymour Calvert and H. Benne Kendall. With a definition of engineering and a concept of the process of thinking and learning, a few implications have been drawn as to the nature of the "average" engineer and the most effective method for teaching him. The essential parts of an undergraduate curriculum have been considered and a conclusion drawn that not much significant variation can be made in its content. **The Engineering-Science Approach in the Teaching of Chemical Engineering,** W. H. Corcoran. The goal of the engineering-science curriculum is to prepare the chemical engineer for the broadest approach to his professional career. After training in engineering science the chemical engineer should have the ability to begin fruitful work in research, development, or production in any industry concerned with physical and chemical changes. The broadest foundation will be found in mathematics, physics, and chemistry; engineering-science training may be considered as directed primarily toward the development of facility in the application of those sciences to the basic problems of chemical engineering. **Graduate Work in Chemical Engineering,** Kenneth A. Kobe. The only quantitative measure of graduate work in chemical engineering in the United States is the number of degrees granted. The approximate ratio of 19:4:1 for B.S.:M.S.:Ph.D. degrees shows the extent to which engineers enter graduate work. The fact that five sixths of the engineering schools give the master's degree and half give the doctorate makes it worthwhile to examine the requirements that the various schools have for their graduate degrees. **Chemical Engineering Education at the Graduate Level,** A. B. Metzner. This paper is based on the hypothesis that graduate education should not consist of simply an extension of undergraduate work to mask any deficiencies therein, but instead should provide a rigorous and mechanistic analysis of the fundamental scientific factors underlying the processes of engineering interest. Proper analysis of a research problem would constitute the core around which the program would be built. Recognizing the diversity of the industrial opportunities to which chemical engineers may be attracted, a well-rounded department offering graduate education must be able to provide research opportunities in a number of different areas. Work in these specialties, however, should never degenerate to descriptive discussions of present (or past) industrial processes and should consist primarily of instruction offered by the appropriate science departments rather than by engineering instructors. **A Look into the Future–Technical Study Course Sponsored by the Local Section,** A. G. Gibson, W. R. Manning,

(*Continued on page 6S.*)

Wiley BOOKS

TRANSPORT PHENOMENA

By R. B. Bird, W. E. Stewart, *and* E. N. Lightfoot, *all at University of Wisconsin.* Treats transport phenomena as a distinct subject in engineering science. Gives parallel coverage to three analogous transport processes: momentum transport (flow of viscous fluids); energy transport (flow of heat); mass transport (flow of chemical mixtures in species). *1960. 780 pages. $13.75.*

PRINCIPLES OF UNIT OPERATIONS

By A. S. Foust, L. A. Wenzel, C. W. Clump, L. Maus, *and* L. B. Andersen, *all of Lehigh University.* Offers a new presentation of unit operations. They are presented as unified groups of operations stemming from identical fundamentals. *1960. 578 pages. $15.00*

THE ANALYSIS OF VARIANCE

By Henry Scheffe, *University of California.* The only unified presentation of theory, including the geometry. It is a true key to practical use of the subject, requiring only a limited background in mathematics and statistics. *1960. 447 pages. $14.00*

THEORY OF THERMAL STRESSES

By B. A. Boley *and* J. H. Weiner, *Columbia University.* A primer on thermal stresses in various structural situations, from principles to practical analyses. Includes: elastic, inelastic problems; heat transfer theory as an element of thermal stress analysis; approximate analytical methods in the light of more exact theory; theory of heat conduction. *1960. 586 pages. $15.50*

THE NATURE AND PROPERTIES OF ENGINEERING MATERIALS

By Z. D. Jastrzebski, *Lafayette College.* Much more basic than the usual treatment, this book stresses materials from the engineering viewpoint, with realistic and practical applications. *1959. 571 pages. $11.00*

Send now for on-approval copies

JOHN WILEY & SONS, Inc.

440 PARK AVENUE SOUTH
NEW YORK 16, N. Y.

now available . . . . A.I.Ch.E.'s second Computer Program Manual

. . . describes a program that essentially will completely design, including sizing the nozzles, a shell-and-tube heat exchanger or cooler, with liquid on both the shell and tube sides. It can also be used to calculate the pressure drops and over-all coefficient in checking an existing exchanger for a new service. The program uses standard methods.

The program listing is given for a basic IBM 650 computer; however the complete description of the calculation procedure and the logic diagram included will facilitate its translation for use on other computers

Price: $50.

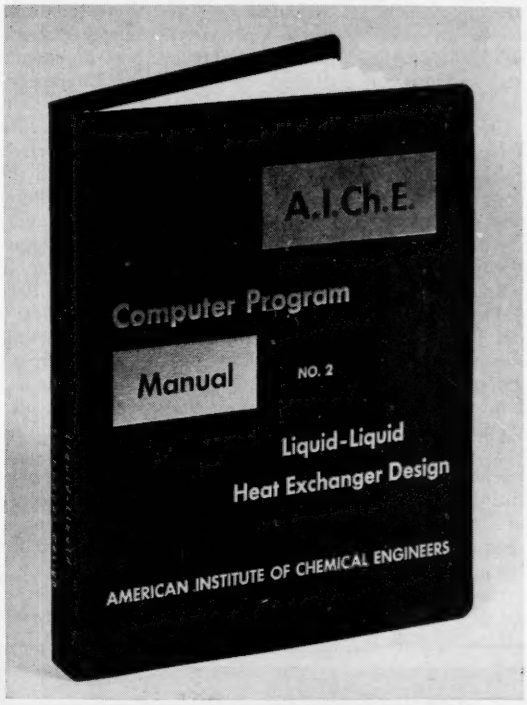

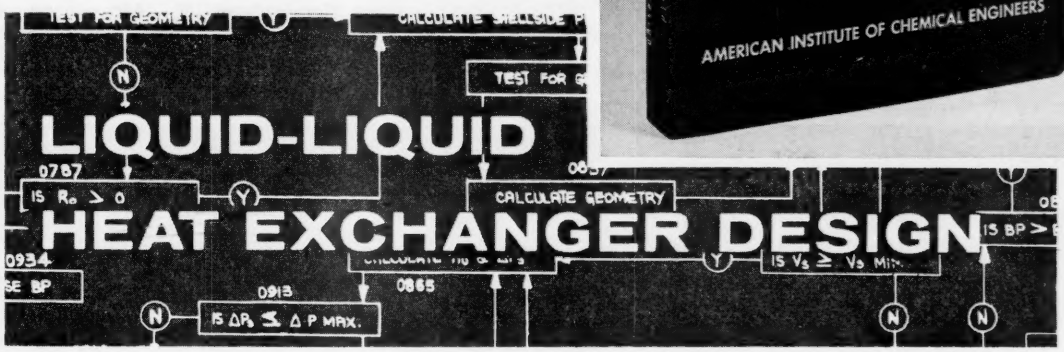

CONTENTS

- Description of program
- Diagrammatic flow chart
- Program details and operation
- Notation
- Literature cited
- Deck listing
- Sample problem—new exchanger
- Sample problem—existing exchanger
- Process engineering interpretive coding system

Send today for your copy of the Liquid–Liquid Heat Exchanger Design Manual. Also available is the first A.I.Ch.E. Computer Program manual, on Line Sizing.

American Institute of Chemical Engineers
25 West 45 Street
New York 36, New York

Please send me ——— copies of the following manuals:

☐ No. 1. Line Sizing ($30) ☐ No. 2. Liquid–Liquid Heat Exchanger Design ($50) ☐ Enclosed is my check for $———
(Add 3% for delivery in New York City.)

☐ Please send me the manual(s) checked above for a 10-day free examination. I will return it (them) at the end of 10 days, or you may bill me.

Name_____

Position_____

Company_____

Street_____

City_____ State_____

(*Continued from page 4S.*)
and R. E. Pyle. The study-course program is a practical method of stimulating the engineer to continue his education. It offers the section member a low-cost medium whereby the chemical engineer can continue his professional development throughout his industrial career. **A Curriculum Organized by an Industry and a University,** David H. Morgan. One notes today a great and growing interdependence of American social institutions. Industry, business, labor, education, government, all have a common concern—lifeblood in the form of new personnel to move forward in a rapidly changing social order. As a case in point, this paper submits curricula organized, built, and operated by the joint efforts of industry and education. **An Advanced Training Program of a Specialized Industry,** John J. Merrill and Harrison M. Lavender. Three principal areas for continuing education in chemical engineering in industry are discussed: the technical, supervisory, and management areas. Each of these areas is presented in terms of its functions, its educational needs, and the methods used for providing the necessary education. From this description of the present situation the authors go on to discuss trends and to forecast briefly future requirements for continuing education. Much of the material presented is developed directly from successful practices of the Standard Oil Company of California and its research subsidiary, California Research Corporation. It is believed that the material presented applies quite generally to most large oil companies and with some limitations to most other processing industries employing large numbers of chemical engineers. **Education for Engineers—Training for Mobility,** Carl H. Elliott. The story of Socony Mobil's continuing education of chemical engineers is one which varies from location to location. The laboratory story is different from the story in the refineries, and the story in the research and development laboratories varies from that in the technical service laboratory. A look into the future reveals the complex and increasingly broad role that engineers will play in a scientifically oriented, industrial society. The author's beliefs in this direction stem from his recent experiences, first on the staff of the technical extension division of a major engineering school where the work was quasiinstructional and quasiconsultative in the fields of management organization, human relations, and industrial psychology, and second from present observations of the engineer in field locations and also from the over-all Socony Mobile view.

INDEX OF ADVERTISERS

Computer Systems, Inc. 354
Hevi-Duty Electric Company 2S
Stearns-Roger Mfg. Co., The 6S
Vulcan-Cincinnati, Inc. Outside Back Cover
Wiley & Sons, Inc., John 4S

Advertising Officers

New York 36—Paul A. Jolcuvar, Adv. Sales Mgr., Carl G. Lassen, Asst. Adv. Sales Mgr., Donald J. Stroop, Dist. Mgr., Robert S. Bugbee, Dist. Mgr.; 25 W. 45th St., COlumbus 5-7330.

Philadelphia—Lee W. Swift, Jr., Dist. Mgr.; 1207 Broad-Locust Bldg., PEnnypacker 5-5560.

Chicago 4—Martin J. Crowley, Jr., Dist. Mgr.; Robert Kliesch, Dist. Mgr.; 53 West Jackson Blvd., Room 504, HArrison 7-3760.

Cleveland 15—Harry L. Gebauer, Dist. Mgr., 1501 Euclid Ave., SUperior 1-3315.

Pasadena 1, Calif.—Richard P. McKey, Dist. Mgr., 465 Converse Place, MUrray 1-0685.

Dallas 18—Richard E. Hoierman, Dist. Mgr., 9006 Capri Drive, DIamond 8-1229.

Birmingham 9, Ala.—Fred W. Smith, Dist. Mgr., 1201 Forest View Lane, Vesthaven, TRemont 1-5762.

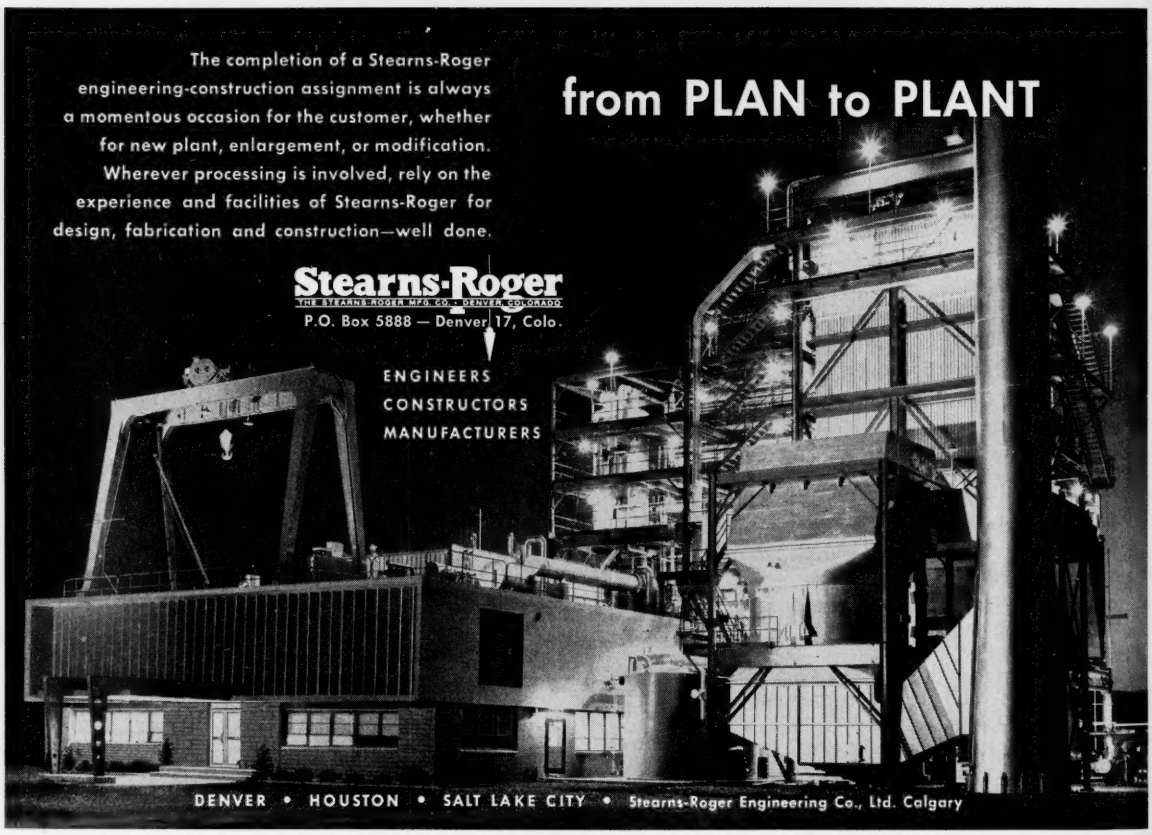
The completion of a Stearns-Roger engineering-construction assignment is always a momentous occasion for the customer, whether for new plant, enlargement, or modification. Wherever processing is involved, rely on the experience and facilities of Stearns-Roger for design, fabrication and construction—well done.
from PLAN to PLANT
Stearns-Roger
THE STEARNS-ROGER MFG. CO. • DENVER, COLORADO
P.O. Box 5888 — Denver 17, Colo.
ENGINEERS
CONSTRUCTORS
MANUFACTURERS
DENVER • HOUSTON • SALT LAKE CITY • Stearns-Roger Engineering Co., Ltd. Calgary

RS
354
2S
6S
Cover
4S
uvar,
ssen,
ald J.
rt S.
45th
, Jr.,
ocust
y, Jr.,
Dist.
Blvd.,
0.
auer,
Ave.,
d P.
Con-
85.
rman,
Drive,
W.
Forest
mont